

**“Elucidating the role of histone
acetylation in regulating chromatin
dynamism in *Saccharomyces
cerevisiae*”**

Thesis submitted for the Degree of
Doctor of Philosophy (Science) in
Biotechnology

By

Preeti Khan

Post Graduate and Research Department of Biotechnology

St. Xavier's College (Autonomous), Kolkata

Affiliated to the University of Calcutta

2024

Dedicated to my parents.....

ACKNOWLEDGEMENT

Embarking on the path to finalize the research encapsulated in this thesis proved to be a rollercoaster ride for me. There were many exciting moments, but also times when things got tough. The moments of elation and despair have effectively equipped me with the resilience needed to transition to the subsequent phase of my academic pursuits. None of this would have been achievable without the support and guidance of a multitude of individuals, and for their contributions, I am sincerely thankful.

First and foremost, I want to express my sincere gratitude to my Ph.D. mentor, Dr. Ronita Nag Chaudhuri, for her invaluable guidance, encouragement, and academic inspiration. Throughout the entire journey, she has been an incredible source of support. During moments when I harboured uncertainty about certain scientific approaches, she consistently bolstered my confidence with logical insights and provided encouragement. She has consistently motivated me to strive for new heights in my academic journey, demonstrating unwavering confidence in my abilities. Her disciplined approach, scientific insights, and methodologies have played a pivotal role in shaping my Ph.D. research and, consequently, influencing my career path. Dr. Nag Chaudhuri was instrumental in introducing me to the field of epigenetics, for which I am immensely grateful. The rigor and dedication she brings to this scientific domain have inspired and motivated me to pursue further studies in the field of epigenetics and I hope that I can make her proud one day.

I extend my gratitude to the Council for Scientific and Industrial Research (CSIR) for their support in funding my Ph.D. fellowship. Additionally, my appreciation goes to the Science and Engineering Research Board (DST-SERB) and the DBT-Boost to University Interdisciplinary Lifescience Departments for Education and Research (DBT-BUILDER) for their generous funding of my Ph.D. research.

I express my gratitude to the faculty and staff of the Department of Biotechnology at St. Xavier's College, Kolkata, for providing me with essential infrastructure and fostering a friendly work environment.

I extend my appreciation to the administrative authority of St. Xavier's College, Kolkata, for ensuring a conducive research environment.

I want to thank Prof. Shubho Chaudhuri from Bose Institute, Kolkata, for the tremendous help and support that he has always provided throughout this journey. I'm also grateful to his lab members, Dr. Dipan Roy, Dr. Amit Paul, Dr. Rwitie Mallick, Dr. Pratiti Dasgupta, Mrs. Jinia Chakraborty, Ms. Sonal Sachdev, and Ms. Ruby Biswas, for their invaluable help and for consistently being welcoming and accommodating whenever needed.

I express my heartfelt appreciation to my fellow lab mates, including Dr. Sonia Bedi, Dr. Anagh Ray, Dr. Sourabh Sengupta, Mrs. Drishti Mandal, Mr. Saptarshi Datta, Mr. Sicon Mitra, Mr. Priyabrata Singha, and Mr. Swarnavo Chakraborty. Their invaluable contributions have transformed my research career into a joyful and enriching experience. I am deeply grateful for their unwavering support, as without them, navigating the challenges of my work in this lab would have been difficult.

My gratitude would be incomplete without acknowledging the significant contribution of my lab seniors, who not only immersed me in the lab culture but also lived by example to make me understand the hard realities of life. A special mention goes to Dr. Sonia Bedi, Dr. Anagh Ray, and Dr. Sourabh Sengupta for their encouragement and invaluable suggestions during my research period. I extend sincere thanks to Dr. Anagh Ray, my senior, for the academic help provided in the early stages of my Ph.D. journey.

I extend my gratitude to my fellow lab mates and seniors at St. Xavier's College, Department of Biotechnology, including Dr. Aheli Majumder, Dr. Puja Ghosh, Dr. Shubhangi Agarwal, Mrs. Peeali Mukherjee, Dr. Shrestha Chakraborty, Mrs. Indrila Saha, Ms. Ruchira Das, Mr. Arnab Pal, Mr. Anirban Roy, Ms Indira Chakraborty, Ms Sushmita Nandy, and Ms. Aparajita Mondal. Engaging in numerous academic and informal discussions with them has been instrumental in maintaining my enthusiasm throughout my Ph.D. research journey. I appreciate their contributions in fostering a competitive and supportive work environment, and I am thankful for their role in uplifting my spirits during this phase of my academic career.

I take a moment to extend my heartfelt appreciation to the members and my fellow comrades of Bharat Soka Gakkai, an organization committed to disseminating the teachings of Buddha.

Their steadfast support and encouragement have served as a guiding light, offering solace and preserving my mental well-being during the demanding stages of my Ph.D. Their unwavering guidance has instilled in me the courage to surmount every obstacle encountered on my doctoral journey, and for this, I am deeply thankful.

I wish to express my sincere and heartfelt gratitude to every individual who, in various capacities, has contributed to making my Ph.D. journey meaningful. My appreciation extends to each and every one of them.

Most importantly, I am eternally grateful to my parents, Mr. Barun Kumar Khan and Mrs. Rumi Khan for their unconditional support and perseverance. While they may not have been directly involved in my benchwork, their genuine celebration of my successes and shared sorrow in each failure have been invaluable. Their emotional and mental support is beyond limits and no amount of words are enough to describe their contribution in this journey. In moments marked by failure and despair, they have been the pillar of strength, helping me rise resiliently. Their unmatched support and unwavering faith in my capabilities, has been a source of unparalleled encouragement. Without them, my research and my thesis would undoubtedly have been impossible. I also want to convey my deepest gratitude to my extended family, my in-laws, Mr. Arun Kumar Sengupta and Mrs. Sushmita Sengupta for their incredible support and encouragement throughout my research journey.

Above all, I want to express my infinite gratitude to my first friend in the lab, a supportive senior, and my partner for life, Dr. Sourabh Sengupta. He has been my rock, offering unwavering emotional and moral support throughout every stage of my Ph.D. journey. His unwavering belief in my abilities is unmatched, and I feel incredibly fortunate to have such an understanding and loving partner for life. Sourabh has stood by me through every highs and lows of my Ph.D. journey, never judging or questioning me. His unconditional support has played a pivotal role in making my thesis and research a reality, and I will forever be thankful to him.

Preeti Khan

7th of February, 2024

CONTENTS

TOPIC	PAGE
<u>Abstract</u>	7-9
<u>Literature Review</u>	10-41
<u>Background study</u>	42-47
<u>Origin of this work</u>	48
<u>Objectives of the work</u>	49
<u>Materials and Methods</u>	50-105
<u>Chapter 1: Understanding the role of H3K56 acetylation in regulating chromatin dynamics during Nucleotide Excision Repair</u>	
<u>Introduction</u>	108-111
<u>Results</u>	112-126
<u>Discussion</u>	127-133
<u>Chapter 2: Understanding the role of H3K56 acetylation in transcription regulation.</u>	
<u>Introduction</u>	136-138
<u>Results</u>	139-159
<u>Discussion</u>	160-165
<u>Summary at a glance</u>	166
<u>Bibliography</u>	167-186
<u>Publications</u>	187-252



ABSTRACT

In eukaryotes, the compaction of DNA into chromatin creates barriers to accessibility during crucial DNA processes, such as replication, transcription, and repair. However, far from being static, the fluid nature of chromatin exhibits a continuous dynamism between compact and relaxed structures. Such dynamicity is intricately governed by several factors, including histone post-translational modifications that ensure precise regulation of DNA templated processes. Notably, histone lysine acetylation, which neutralizes the positive charge on specific histone residues, emerges as the most widespread and significant amongst the post-translational modifications. This study delves into the influence of histone acetylation on chromatin dynamics during specific DNA-templated processes such as Nucleotide Excision Repair (NER) and transcription. The work specifically explores the impact of acetylation on the 56th lysine residue of histone H3 (H3K56) during NER and transcription. H3K56 acetylation is a unique residue present in the globular core of histone H3 that is recognized for weakening the association of DNA with the histone octamer thus critically influencing DNA unwrapping and accessibility. In eukaryotes efficient NER relies on a substantial stretch of naked DNA for large repair protein complexes to access the DNA damage site. This study demonstrates that acetylation of H3K56 is crucial for DNA accessibility during NER occurring in a chromatin milieu. Utilizing H3K56 mutants, H3K56Q and H3K56R, mimicking constitutively acetylated and unacetylated lysine it was revealed that H3K56 acetylation regulates early NER events. H3K56 acetylation is found to be a pre-requisite for recruitment of crucial repair factor, Rad16, with constitutive acetylation facilitating Rad16 recruitment independently of UV exposure. Additionally, H3K56 acetylation is crucial for UV-induced hyperacetylation of H3 N-terminal tail residues, specifically H3K9 and H3K14. Therefore, the absence of H3K56 acetylation impedes UV-induced recruitment of Rad16 and compromises NER efficiency by affecting H3K9 and H3K14 hyperacetylation. Notably, the UV-induced oscillation of chromatin architecture between compact and relaxed states, characteristic of NER, is distinctly absent in the absence of H3K56 acetylation. In vitro studies using cell extracts from H3K56 mutants further emphasized the involvement of H3K56 acetylation in nucleosome modulation and DNA accessibility during NER. Besides NER, the study also demonstrates that H3K56 acetylation is crucial in regulating RNAPII-dependent transcription within active gene regions. The "histone code" hypothesis proposes that the complex interplay of histone modifications is a key determinant that shapes the chromatin landscape. The findings of this study uncover an intricate interplay between H3K56 acetylation and deacetylation of the H4 N-terminal tail residue H4K16, that collectively facilitate the progression of RNA polymerase II through the gene body of active genes. The results indicate a sequential relationship where H4K16

deacetylation precedes and induces H3K56 acetylation. Significantly, the recruitment of Rtt109, the histone acetyltransferase responsible for H3K56 acetylation, is found to be essentially dependent on H4K16 deacetylation. In strains with Hos2 deletion, where H4K16 deacetylation is impaired, both H3K56 acetylation and RNA polymerase II recruitment are significantly compromised. Remarkably, the dynamic interplay of H4K16 deacetylation and H3K56 acetylation was found to be intricately linked to active transcription. Thus, H4K16 deacetylation serves as a driver for H3K56 acetylation, and the collaborative action of these two modifications is essential for the efficient functioning of RNA polymerase II during active transcription.

In summary, this study highlights the importance of H3K56 acetylation, emphasizing its impact in the establishment of a histone code that intricately governs chromatin accessibility during the process of NER as well as its broader role in moulding the chromatin environment that distinctly influences the outcomes of processes such as transcription.



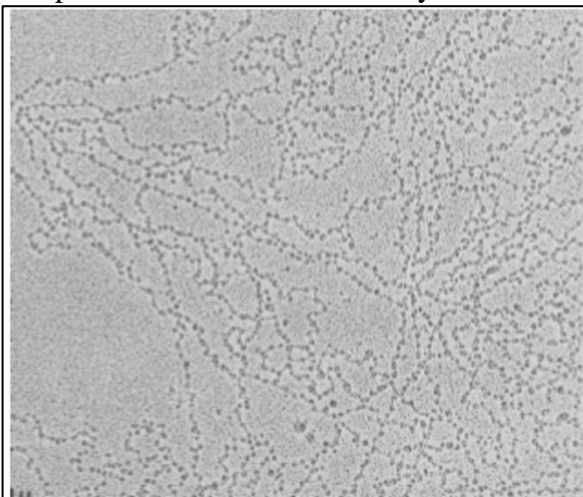
LITERATURE REVIEW

CHROMATIN IS DYNAMIC IN NATURE

The intricacies of life, governed by the genetic code entrusted in DNA, unfolds within the confines of a eukaryotic cell's nucleus, a space with dimensions measured in mere microns. Yet, this microscopic space must accommodate a vast repository of genetic information, a remarkable feat achieved through the complex orchestration of DNA compaction into chromatin. Chromatin's intrigue lies in its dual role- it not only serves to compact the DNA but also orchestrates our body's control over DNA's reading and utilization. This control extends to the "central dogma," where DNA's transcription to RNA and RNA's translation to protein is governed, as proposed by Francis Crick in 1970¹. Chromatin compaction inhibits this process requiring spontaneous remodeling for accessibility to factors regulating crucial cellular functions. Remarkably, chromatin does not impose a uniform blockade; rather, it selectively governs the accessibility of distinct portions of the DNA sequence. This selectivity forms the foundation for the finely tuned control over the activation or repression of specific gene expressions. This pivotal regulation dictates the intricate orchestration of when, how, and which DNA segments are transcribed and translated, crucially influencing the cell's behavior and function. The dynamic nature of chromatin, essential for such precise regulation, is intricately governed by a cadre of regulatory factors. Post-translational histone modifications, chromatin remodelers, histone chaperones and histone variants collaborate in a meticulously coordinated manner^{2,3}. These molecular players, either in isolation or concert, contribute to the nuanced modulation of chromatin structure. The orchestration of these regulatory mechanisms is a topic that will be explored in greater depth in a subsequent section.

Within the nucleus, chromatin is strategically organized into specific chromosomal territories. These territories confine the overall mobility of chromatin, establishing a structured landscape within the cellular nucleus. Despite this confinement, the dynamic nature of chromatin allows for both intra and inter-chromosomal associations, facilitating a sophisticated regulatory framework for gene expression⁴. Traditionally chromatin is divided into two major forms of structure: Heterochromatin which is considered to be of two types: constitutive heterochromatin which contains repeats of DNA sequences bound in nucleoprotein complexes like telomeres and centromeres that never completely decondense⁵⁻⁷ and facultative heterochromatin which contains genetic elements that are silenced beyond a certain point of developmental stages like the inactive X chromosome of mammalian males⁸. Genes that are more easily transcribed and undergo de-condensation during interphase are part of the active '**euchromatin**'. Though euchromatic regions are more open, it is the high gene density of these regions that define the open chromatin state as even gene poor regions within the euchromatin

are compactly packaged like heterochromatin⁹. Thus, it becomes clear that chromatin architecture within the nucleus allows for a 3D spatial organisation of the genome in such a way that despite being restricted to chromosomal territories, chromatin is dynamic in nature. The key advantage of this dynamic chromatin structure lies in its ability to maintain a degree of DNA accessibility despite the overall compact organization. This delicate balance between compaction and an accessible chromatin structure is vital for proper regulation of essential DNA-templated processes¹⁰. Processes such as transcription, where genetic information is transcribed into RNA, and replication, where DNA is duplicated, rely on the availability of DNA as a substrate for large protein complexes. Similarly, mechanisms involved in repair of DNA damage as well as recombination pathways also necessitate a level of DNA accessibility within the compact structure of chromatin. Particularly the mechanisms underlying the compaction of chromatin into chromosomes and the reverse process remain a complex enigma, even as we delve into the details of chromatin architecture. Initially, the prevailing notion was that the primary actors in chromatin compaction were the interactions between DNA and histone proteins. This traditional view suggested a straightforward relationship between DNA winding around histones, forming nucleosomes—the basic packaging units of chromatin—and the subsequent folding into higher-order structures, ultimately leading to the formation of chromosomes. However, a paradigm shift occurred with the ground-breaking discovery by Adolph and colleagues in 1977^{11,12}, revealing that non-histone proteins act as scaffolds during metaphase chromosome assembly. This revelation underscored the complexity of chromatin



Electron microscope image of chromatin from the early developmental stage of a fruit fly (*Drosophila*), which shows the chromatin looking like 'beads on a string'. The width of this image represents 1.6 micrometers as seen in the actual microscope view. (taken from Baldi et al., NSMB 2020)

compaction, challenging the simplistic DNA-histone interaction model.

The most fundamental unit in the hierarchy of chromatin is the 'beads-on-a-string' fiber, a structure with a diameter of 10 nm composed of DNA-wrapped histones to form nucleosomes. The dynamic nature of chromatin, crucial for accommodating the accessibility requirements of nuclear factors during different stages of the cell cycle, hinges on understanding how this 10 nm fiber structure compacts into chromatin.

Historically, it was hypothesized that the 10 nm fiber condenses further into 30 nm fibers

through the interaction of DNA-wrapped histone beads with 'linker' histones outside the beads^{13,14}. These 30 nm fibers were then thought to coil up into thicker fibers, forming coil-within-coil structures called 'chromonema' fibers, as later proposed¹⁵. However, the existence of such a complex structure during interphase would require an equally intricate mechanism of continuous chromatin folding and unfolding, potentially hindering the proper functioning of nuclear processes.

Considering that various DNA metabolic processes often require simultaneous and coordinated access to distinct parts of the genome; it becomes evident that the regulation of chromatin structure is a critical determinant of DNA accessibility. If this regulation involves a complex folding and unfolding process, it could potentially become a rate-limiting step, impeding the seamless functioning of the cell during interphase. Fortunately, advancements in various microscopy techniques have contributed to an improved understanding of the hierarchical organization of chromatin. Alternative theories have emerged, suggesting that chromatin can exist in a more easily accessible hierarchy without the need for complex folding and unfolding processes. These evolving perspectives offer new avenues for unravelling the mysteries of chromatin dynamics and its role in facilitating essential cellular processes. The inability to detect the 30 nm chromatin fiber consistently across various cell types through electron microscopy, small-angle X-ray scattering studies and light microscopy has raised doubts about its significance in chromatin hierarchy¹⁶. In vitro investigations have unveiled two potential modes of compaction for the fundamental 10 nm chromatin fibers. The well-known 30 nm fiber is one option, but there is also a "polymer melt" structure where 10 nm oligomers self-assemble into a mesh-like conformation, distinct from a higher-order fiber structure. Instead, it forms a globular organization^{17,18}.

This globular organization of 10 nm fibers can be conceptualized as "liquid droplets" or domains that merge to create larger chromatin structures during interphase. These structures, molded by chromatin-associated proteins or macromolecules, serve as dynamic and functional units^{10,19,20}. When considering the three-dimensional organization of the genome, this perspective allows us to envision the coexistence of active and inactive domains in a dynamic manner without overly complicating the processes of chromatin folding and unfolding.

ORGANIZATION OF CHROMATIN

The nucleosome core particle

The nucleosome, which forms the most fundamental structural unit of chromatin comprises a central nucleosome core particle (NCP) enveloped by DNA of varying linker lengths . At the heart of the NCP is a histone octamer, around which DNA of approximately 147bp in length is intricately wound in left-handed orientation approximately 1.65 times²¹.

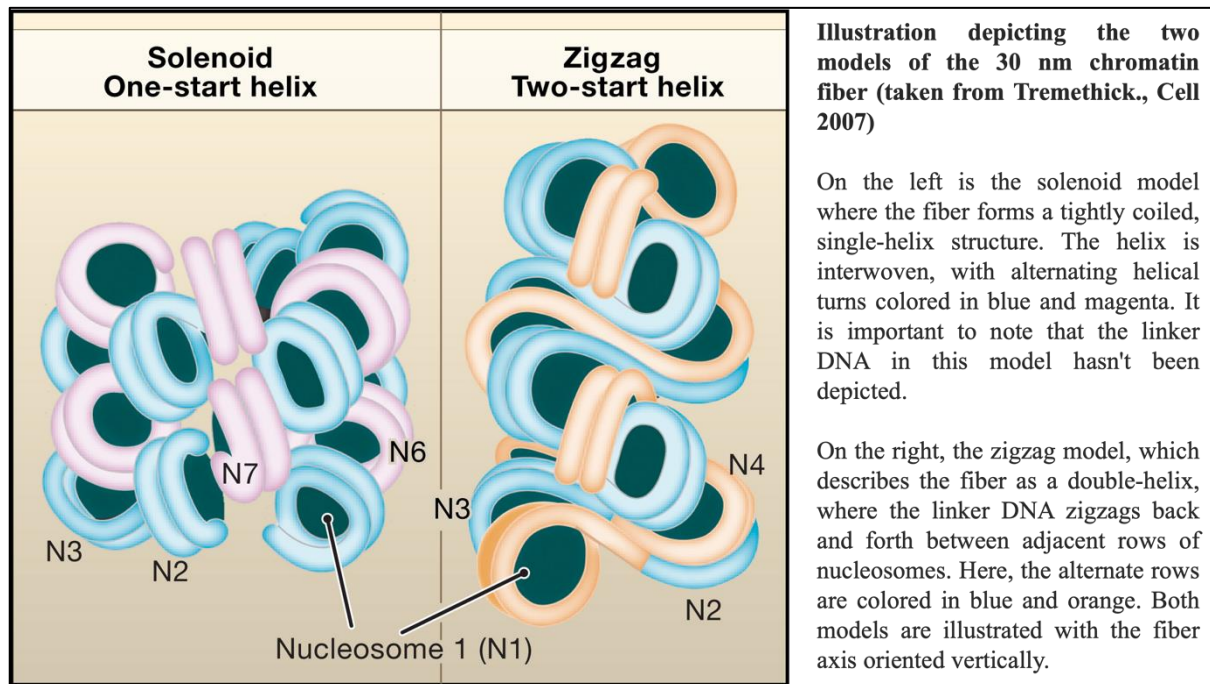
The octamer of histones comprises four core histones in two copies of each. These histones are highly conserved and are called as H2A, H2B, H3, and H4. These histones share a common structural motif consisting of a region termed as the histone fold and an N-terminal tail that is flexible²². The octamer is formed when two pairs of the dimer of H2A/H2B assembles with that of one H3/H4 tetramer.

Within the nucleosome structure, the interaction between the H2A/H2B dimers and the H3/H4 tetramer is a critical determinant of stability. This interaction is facilitated by a four-helix bundle that forms between histone H2B and histone H4, as well as through the dynamic interplay between the H2A docking domain and the H3/H4 tetramer. These mechanisms are discussed in detail in a later section.

The 30nm fibre- a higher order structure of chromatin

The winding of DNA around nucleosomes represents an essential first step of compaction, but it alone is insufficient to accommodate the entire length of cellular DNA, which can exceed 2 meters, within a nucleus of average size, typically less than 10 micrometers. Nucleosomes, connected by the linker DNA, collectively form a structural motif known as the 'beads on a string,' creating a 10-nanometer chromatin fiber, a configuration readily observable through electron microscopy²³. However, to achieve further compaction and organization, the binding of linker histones to nucleosomes becomes pivotal. This interaction, coupled with the subsequent arrangement of nucleosomal arrays, contributes to the formation of a higher-order secondary structure known as the 30-nanometer fiber. This advanced level of chromatin packaging has been elucidated through studies conducted by Robinson and colleagues in 2006^{24,25}, providing insights into the intricate and multi-tiered organization of chromatin within the nucleus. Studies based on electron microscopy have given rise to two prevailing models for the structure of 30-nanometer fibers, namely the one-start solenoid model and the two-start Zig-Zag model. These models provide hypothetical frameworks to comprehend how nucleosome arrays organize themselves at a higher level of chromatin structure. In the one-

start solenoid model, it is proposed that the arrays of nucleosomes compact into a single-start helix structure. In this helical configuration, nucleosomes that are adjacent to each other are linked by a linker DNA present in a bent conformation. This model envisions a continuous helical arrangement of nucleosomes, creating a cohesive structure within the chromatin fiber^{26,27}.



On the other hand, the two-start Zig-Zag model suggests an arrangement where nucleosomes adopt a Zig-Zag pattern. In this model, nucleosomes are organized into two stacks, and straight linker DNA connects them. The linker DNA criss-crosses between each stack, forming a pattern reminiscent of a Zig-Zag. This model, proposed by Woodcock et al. in 1984 and further developed by Williams et al. in 1986, envisions a distinct structural arrangement with a different geometry compared to the one-start solenoid model^{13,28}. Despite these theoretical predictions based on EM studies, the actual portrayal of the secondary chromatin structure under normal physiological conditions within a cell remains elusive. Interestingly, "hierarchical helical folding" model proposes that the 30 nm fiber achieves further compaction and stepwise folding into successively larger structures, specifically around 100 nanometers and subsequently around 200 nanometers^{15,29}. This intricate folding process culminates in the formation of the ultimate mitotic chromosomes. The prevailing "radial loop model" has gained wider acceptance in understanding the intricate dynamics of chromatin organization. This model proposes that 30-nanometer chromatin fibers attach themselves to a central non-histone protein scaffold or matrix, composed of Condensin and Topoisomerase II alpha protein

complexes. Consequently, chromatin loops are formed around this central scaffold, as outlined by Adolph et al. in 1977 and further elucidated by Maeshima and Laemmli in 2003^{11,12,30}.

In the decondensed state, chromatin domains, which typically compact into radial loops attached to the nuclear matrix, are referred to as Scaffold/Matrix Associated Regions (S/MARs). This concept, introduced by Strukov et al. in 2003 and explored by Narwade et al. in 2019, emphasizes the dynamic nature of chromatin and its association with non-histone proteins^{31,32}. This model contrasts with the notion of sequential chromatin fiber formation seen in other models. Instead, the radial loop model suggests a macromolecular aggregate structure that condenses into chromosomes by attaching to protein matrices. Hancock in 2012 and Maeshima et al. in 2014 have contributed to the understanding of this structural arrangement^{19,20}. A quaternary structure has also been identified where 300-nanometer fibers form chromatidal loops, undergoing further plectonemic coiling to generate fibers measuring 600–700 nanometers in length, as described by Banfalvi in 2008³³.

While there is limited information available on these intermediate levels of chromatin compaction between the tertiary 300-nanometer structure and the visible metaphase chromosomes, which have a fiber length diameter of approximately 1.4 micrometers, it is evident that a complex hierarchy of chromatin structures exists.

Chromatin domains

An alternative theory of chromatin organization challenges classical models. It posits that chromatin is organized into repeating domain-like units that form 10-nanometer fiber aggregates resembling 'liquid drops' with distinct epigenetic signatures, acting as functional genomic units. Chromatin domains are dynamic, compact, and may span chromosomal territories, regulating access for nuclear machineries and influencing nuclear processes, as suggested by Hansen et al. in 2018 and Maeshima et al. in 2019^{10,18}. Chromatin domains, classified by physical or functional separation, fall into three types. **Lamina Associated Domains (LADs)** are regions at the nuclear periphery linked with the nuclear lamina, often gene-poor with silenced or repressed genes³⁴. **Nucleolus Associated Domains (NADs)**, constituting around 4% of chromatin, reside near the nucleolus, housing gene-poor or low-transcribing regions^{35,36}. **Topologically Associating Domains (TADs)** are sub-megabase-sized regions grouped by chromatin conformation capture techniques. TADs, physically separated by active chromatin or nucleosome-free regions, serve as dynamic units influencing genome organization within regulatory landscapes^{37,38}.

NUCLEOSOMES: THE CENTRAL REGULATORS OF CHROMATIN DYNAMICS

The intricate organization of the chromatin architecture underscores the complexity of genetic information processing within eukaryotic cells. However, despite this organized framework, the primary determinant for the seamless functioning of nuclear processes lies at the level of nucleosomes, where accessibility remains paramount.

In-depth reviews by Woodcock and Ghosh (2010) and Li and Reinberg (2011) meticulously explore the complexities of chromatin architecture^{14,39}. While the 30-nanometer fiber is acknowledged to be less favorable for transcription compared to the 10-nanometer structure, these reviews propose a potential solution—local unfolding of chromatin. This unfolding could enable the accessibility of large multi-subunit complexes to essential DNA segments, overcoming potential hindrances posed by higher-order chromatin structures.

Micrococcal Nuclease (MNase), a compact enzyme capable of uniformly accessing diverse chromatin regions, has further fueled speculation. Schwartz et al.'s work in 2019 highlights MNase's ability to navigate and access DNA templates in transcriptionally active, repressed, and heterochromatic domains, even in densely packed chromatin regions⁴⁰.

This perspective emphasizes that the most crucial adjustments and structural modifications for DNA access occur at the 10-nanometer chromatin fiber level. Despite the presence of organized chromatin domains, accessibility at the nucleosomal level remains unimpeded, forming the cornerstone of nuclear process functionality^{41,42}. Confocal laser microscopy studies, such as those by Hihara et al. in 2012, provide additional insights into chromatin's dynamic nature. These studies reveal that dynamic chromatin character offers substantial accessibility to densely packed regions, regardless of the cell's interphase or mitotic stage⁴³. Notably, experiments inhibiting local nucleosomal dynamics through crosslinking-based methods demonstrate impaired accessibility to densely packed chromatin regions⁴³.

Thus, the orchestration of genetic information processing in eukaryotic cells relies on the finely tuned interplay between chromatin dynamics and nucleosomal behavior. Nucleosomal dynamics provide adaptability and accessibility, enabling regulatory factors to traverse densely packed chromatin domains. Understanding these intricacies unveils fundamental principles of genome regulation and provides crucial insights into the molecular choreography governing essential cellular processes.

For an in-depth understanding of nucleosomes dynamics it is vital to study the architecture of nucleosomes.

Nucleosome architecture

The nucleosome core, a foundational architectural unit of chromatin, manifests an extraordinary degree of evolutionary conservation spanning from yeast to metazoans^{44,45}. As expounded earlier, this core component encapsulates a 147-base pair segment of DNA intricately enfolded by two copies each of four core histone proteins, namely H2A, H2B, H3 and H4⁴⁴. These core histones, integral constituents of this molecular ensemble, autonomously arrange themselves into a spool-like configuration, collectively sculpting a compact disc characterized by dimensions of approximately 5.5 nm in height and diameter of 11nm⁴⁶. Histone H1, referred to as the linker histone, is distinct from the nucleosome core particle (NCP). Instead of being within the NCP, it is positioned at the entry/exit site of the nucleosomal DNA. The linker histone attaches to the NCP through an added 20 base pairs of DNA that winds in a different conformation from the 146 base pairs of DNA bound to the NCP. This entire complex is termed the 'chromatosome,' as coined by Simpson in 1978⁴⁷. Another variant, histone H5, discovered in chicken erythrocytes, is recognized for its stronger binding to the nucleosome compared to H1. This enhanced binding is attributed to its higher basicity resulting from an increased presence of lysine and arginine residues⁴⁸. It's noteworthy that lower eukaryotes, such as yeast, known for their actively transcribing genome, do not possess the linker histone H1^{49,50}. While the baker's yeast *Saccharomyces cerevisiae* does have an H1 analogue known as Hho1p, the fission yeast *Schizosaccharomyces pombe* lacks any form of linker histone^{51,52}.

A pivotal facet distinguishing the nucleosome core resides in the meticulous wrapping of the core DNA around the histone spool, a process consummated through approximately 1¾ left-handed superhelical turns. Within this structural marvel, a nexus of 14 critical points of contact emerges, where remarkably conserved arginine residues located on the histones, colloquially denoted as 'superhelix locations' (SHL), intricately engage with the DNA molecule^{21,53,54}. The SHL serves as a blueprint, designating specific locations where the DNA major groove faces inward toward the core of histones. Notably, the central base pair of the nucleosomal DNA, coined as SHL position 0, marks the nucleosomal 'dyad.' This dyad, with an imaginary axis of symmetry passing through it, influences the wrapping of the histone core by the two DNA gyres, attaching at SHL positions ± 7 . This architectural arrangement imparts stability to the nucleosome core, creating a squat yet highly organized structure. The association between the core DNA and histones is so intimate that the former is shielded from nuclease digestion,

highlighting the robustness of this interaction. In contrast, the linker DNA, which connects nucleosomes, is digested rapidly. Interestingly, the term "nucleosome core particle" originated from the extensive digestion of native chromatin by micrococcal nuclease⁵⁵. This process revealed the resistant and protected nature of the core DNA, solidifying the concept of the nucleosome core as a distinct and resilient entity within the chromatin landscape. For dynamic nucleosome behavior, a delicate balance is maintained through the release of histone-DNA interactions, primarily orchestrated by transient post-translational modifications (PTMs) of histone residues. Remarkably, PTMs at residues situated farther from the dyad, specifically at SHL ± 3 near the DNA entry-exit points, play a pivotal role in facilitating the unwrapping of the NCP. Meanwhile, PTMs in proximity to the dyad contribute to histone release during the disassembly of nucleosomes but do not influence the unwrapping process itself^{56,57}. In essence, these histone modifications at specific SHL positions delicately regulate the dynamic interplay between histones and DNA, unveiling a sophisticated mechanism essential for nucleosome dynamics and contributing to the broader understanding of chromatin remodeling processes.

The four core histones, modest in size (11-15 kDa), emerges as a cornerstone in chromatin architecture, exhibiting high conservation among eukaryotic species. A distinctive feature of these histones is the presence of an N-terminal 'tail' domain, constituting about 25% of their mass, which remains unstructured in the absence of any DNA or any kind of interactions with macromolecules. The predominant portion of histone mass resides in the C-terminal domain a large proportion of which is α -helical forming a critical interface for histone-histone interactions that culminate in a structure that resembles an octamer like column serving as the scaffold for DNA wrapping. A remarkable and conserved motif known as the 'histone fold' dominates each C-terminal domain, showcasing two α -helices which are shorter namely $\alpha 1$ and $\alpha 3$ that flank a longer central α -helix named $\alpha 2$. This motif, characterized by what is termed as 'handshake' interaction, orchestrates the heterodimerization of H2A and H2B as well as H3 with H4, underscoring its significance in histone assembly⁵⁸. Despite limited primary sequence homology, the histone fold motif epitomizes a ubiquitous dimerization interface, transcending evolution and manifesting in diverse protein complexes, even those unrelated to DNA association⁵⁹. The interaction between histone dimers is a sophisticated process primarily facilitated through the formation of 4-helix bundles at the interfaces of dimer-dimer connections, resulting in the creation of a symmetrically arch-shaped structure. Notably, the H3/H4 dimer exhibits a fascinating ability to self-associate, giving rise to a structurally robust tetramer. On either end of this tetramer, an H2A/H2B dimer is strategically positioned via an H4:H2B 4-helix bundle²¹. This intricate arrangement of histone components, akin to a

symmetrical string of tetramers, intricately assembles to form a helical ramp of DNA contact sites, underscoring the intricate orchestration necessary for the histone octamer formation.

The histone octamer stability is notably contingent upon specific factors, such as the wrapping of DNA around it or exposure to solutions characterized by elevated salt concentrations, attributable to the inherent positive charge carried by its constituent proteins. The arc-shaped structure, housing the dimers of H2A with H2B and H3 with H4, strategically positions three DNA binding sites along the curved edge on the outer side⁶⁰. These sites, characterized by the presence of paired structural elements from each dimer, including β -loops that are paired and central α -helical ends, intricately engage the DNA backbone at strategic intervals⁶⁰. This structural configuration forms the basis for the intricate interactions between nucleosomes and DNA, unveiling a molecular choreography essential for genomic organization.

Noteworthy research findings bring to light the intriguing observation that, *in vivo*, the removal of H2A-H2B dimers transpires with greater frequency compared to H3-H4 dimers. This intriguing phenomenon serves as a prerequisite for subsequent events involving the removal or exchange of H3 or H4 histones⁶¹. These revelations contribute to a deeper understanding of the dynamic and finely tuned processes governing histone dynamics and nucleosome stability in the intricate landscape of chromatin architecture. The rationale behind this observed phenomenon lies in the relative stability of histone dimers. Specifically, H2A-H2B dimers exhibit higher stability than H3-H4 dimers. However, the robustness of the interface of H3 between the two H3/H4 dimers surpasses that of the strength of the H2B-H4 interface, rendering the tetramer of H3/H4 a more stable core. This structural arrangement not only ensures stability but also facilitates the easy removal of dimers of H2A/H2B, contributing to the dynamic nature of chromatin⁶².

The tail domain interaction of core histones, conventionally perceived as "unstructured," assume configurations resembling random coil conformations when existing freely in solution, devoid of DNA interaction, or subjected to high salt environments. Comprising an array of amino acids, including lysines, arginines, and others, these tail domains are categorized as intrinsically disordered peptides, a classification derived from meticulous sequence analyses. While these domains predominantly exhibit a tight association with nucleosome binding sites under physiological conditions, periodic dissociation events do transpire^{63,64}.

Contrary to expectations, the contribution of these tail domains to the stability of mononucleosomes in terms of thermal stability is minimal⁶⁵, and their removal amplifies the proportion of DNA that is unwrapped, enhancing accessibility to DNA-binding factors⁶⁶⁻⁶⁸. Notably, the susceptibility of these tail domains to protease action and their reported mobility

on the Nuclear Magnetic Resonance (NMR) timescale predominantly arises from the approximately 2-4% of time during which the tails undergo dissociation, adopting random coil conformations within the milieu of physiological salt conditions. Within the intricate landscape of chromatin, crosslinking evidence lends credence to the proposition that tail domains assume well-defined structures and engage in specific interactions^{69,70}. Measurements conducted using Circular Dichroism (CD) spectroscopy reveal that, within physiological salt concentrations, these tail domains exhibit a considerable amount of α -helical conformation. Intriguingly, tail domain hyperacetylation enhances their α -helical content, adding a layer of complexity to the regulatory landscape of histone tail dynamics⁷¹.

Accessible to enzymes for posttranslational modifications crucial for epigenetic signaling, tail domains play a pivotal role in mediating internucleosomal interactions within condensed chromatin structures^{72,73}. Their primary function involves organizing higher-order chromatin structures, crucial for nucleosome array compaction. Tail domains interact with multitude of proteins and specific DNA sites in chromatin. For instance, the histone H4 tail binds to an acidic patch within the dimer of H2A/H2B of an adjoining nucleosome^{17,74}. The tail domain of H3 extensively contacts DNA present within the nucleosome arrays, engaging exclusively in condensed chromatin the DNA of neighboring nucleosomes. Both H3 and H4 tails participate in contacts between adjacent nucleosomes to facilitate the folding of chromatin fiber, additionally, for higher order chromatin structures, the tails engage in contacts over long ranges between chromatin fibers^{17,75-77}. Specifically certain posttranslational modifications occurring within histone tails likely induce varied chromatin states by altering tail interactions⁷⁸⁻⁸⁰. For instance, H4K16 acetylation a residue present on the N-terminal tail residue of histone H4, critically reduces the interaction of the H4 tail with an acidic binding pocket present on the surface of the nucleosomes, contributing to the stability of condensed chromatin structures⁸¹⁻⁸³. Acetylation generally restricts nucleosome arrays from undergoing folding or oligomerization in presence of salts, directly altering interactions of tails with protein or specific DNA⁸⁴⁻⁸⁶.

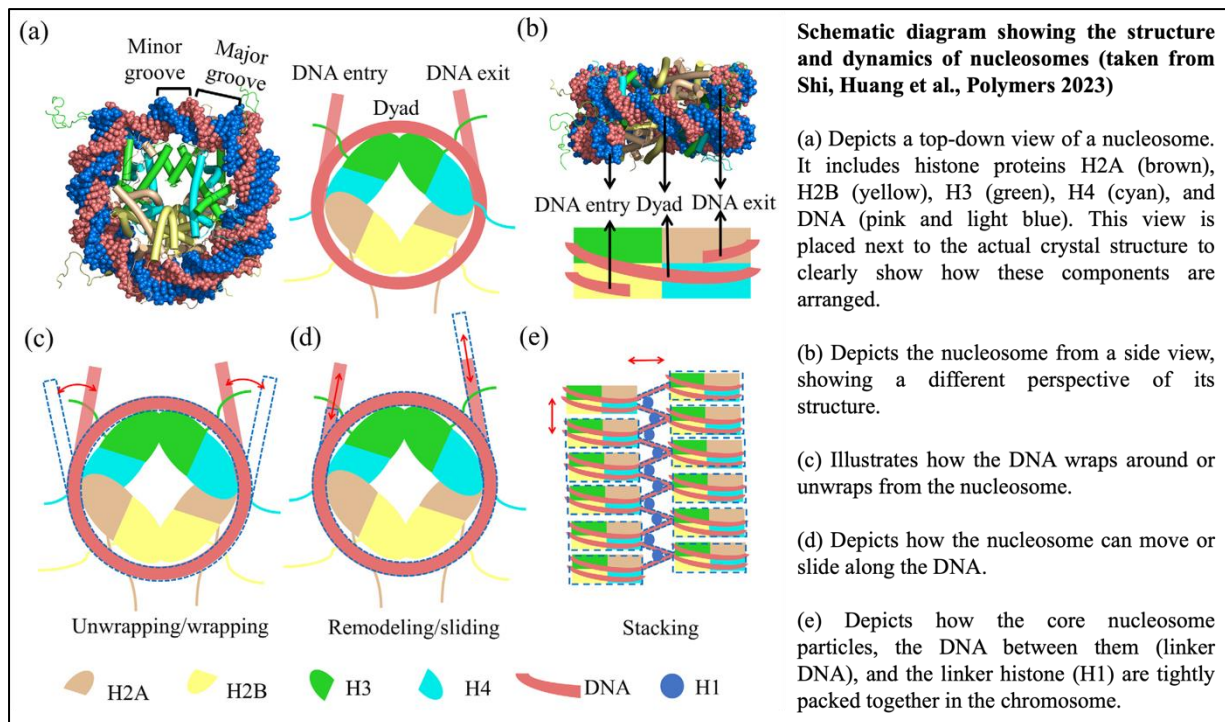
Nucleosome dynamics

As previously described, the incorporation of DNA into nucleosomes provides a protective shield against nucleases and imposes constraints on the binding of trans-acting factors. Despite the predominant uniform structures observed in X-ray crystal studies, nucleosomes exhibit dynamic behaviours, deviating from these static conformations. Notably, nucleosome DNA displays transient unwrapping or breathing rebinding to the nucleosome surface at rates that

permit access to DNA binding factors. Nucleosome breathing is a spontaneous process where a segment of nucleosomal DNA relaxes from the histone core, increasing the linker length and thereby revealing a potential DNA binding site for trans-acting factors^{87,88,89}.

There are other modes of nucleosome dynamics that can be categorized into mechanisms that are dependent or independent of ATP. These dynamics, modulated by histone and DNA composition, create a rich and intricate landscape for genome regulation.

One prominent example of ATP-dependent nucleosome dynamics involves the sliding of nucleosomes facilitated by chromatin remodelers dependent on ATP. In this process, the histone octamer shifts from its bound DNA to the neighboring DNA segment, covering a distance of approximately 100 base pairs, resembling a "rolling over" mechanism⁹⁰. Additionally, ATP-independent processes, such as the reconfiguration of nucleosomes by RNA polymerases, play a significant role in transcription and its regulation.



Recent advancements in experimental techniques, including FRET, NMR, cryo-EM, cross-linking studies as well as mass spectrometry, have revealed more nuanced and sophisticated modes of nucleosome dynamics detected and utilized by chromatin proteins.

For instance, twist-defects in DNA within the nucleosome core provide a pathway FOR nucleosome remodeling in a manner dependent on ATP⁹¹. Intrinsically the dynamics as well as the plasticity of core histones has also been linked to these processes, albeit with some debate. Suppression of these dynamics, achieved through the introduction of cross-links at

specific disulfide bonds within individual dimers of H3/H4, has been shown to inhibit the sliding of nucleosomes, increase the eviction of octamers and impair chromatin compaction. These findings suggest that the octamer of histones may take up alternative conformations beyond those generally captured in traditional X-rays⁹²⁻⁹⁴.

Thus, the intricate interplay between ATP-dependent and independent nucleosome dynamics, influenced by DNA and histone composition, contributes to a dynamic and versatile regulatory chromatin landscape. These dynamic modes of nucleosome behavior, ranging from sliding to more subtle conformational changes, provide the cellular machinery with diverse tools for modulating gene expression and maintaining the intricate balance required for proper cellular function.

HISTONE PTMS- VITAL REGULATORS OF NUCLEOSOME DYNAMICS

The intricacies of nucleosome dynamics unfold as a precisely orchestrated interplay involving a myriad of molecular participants. This ensemble features post-translational histone modifications, chromatin remodelers, histone chaperones and histone variants each intricately engaged in an isolated or concerted manner to meticulously orchestrate modulation of DNA accessibility. At the heart of this complex interplay, histone post-translational modifications emerge as pivotal conductors, not only shaping the immediate chromatin structure but also guiding the actions of histone variants, chaperones, and remodelers. Strategically positioned within the interfaces of DNA–histone and histone–histone interactions, post-translational histone modifications (PTMs) are crucial regulatory elements. Specific enzymes covalently modify histones inducing alterations in amino acid side chains within these interfaces, prompting a consequential shift in the energy landscape of nucleosomes. This transformative shift, as elucidated by Bowman and Poirier in 2015, sets the platform for recruitment of histone chaperones and chromatin remodelers⁹⁵. These recruited entities play a pivotal role in orchestrating the accessibility of chromatin to DNA-binding factors, forming a nuanced regulatory network within chromatin dynamics. Modifications of histones play crucial role in regulating precisely the dynamics of nucleosomes through three distinct mechanisms. Firstly, they influence intra-nucleosomal interactions among histones and between histones and DNA. Secondly, they impact inter-nucleosomal interactions, and thirdly, they govern the recruitment of essential factors and modifiers crucial for chromatin regulation. Lysine and arginine residues, characterized by their elongated basic side chains, primarily mediate histone-DNA contacts, contributing to the stabilization of chromatin's compact organization. The

introduction of negatively charged acetyl groups to these side chains disrupts the charge-dependent interactions of histones. Concurrently, the addition of methyl groups governs the spatio-temporal interactions of these residues.

In a three-dimensional context, the combinations of histone modifications across adjacent nucleosomes create a landscape conducive to the formation of favorable binding sites. These sites serve as recognition points for competing motifs or domains associated with different proteins. Notably, acetyl and methyl groups added to lysine and arginine residues enable their recognition by proteins containing bromodomains and chromodomains, respectively. These regulatory proteins govern various cellular processes by either repositioning nucleosomes or recruiting other factors, such as chaperones, as needed. Additionally, these modifications often mark specific gene regions, such as promoters, thereby differentially regulating the transcription process by recruiting either transcription machinery or inhibitory components^{96,97}. One of the remarkable features of these PTMs is their reversibility. In addition to the introduction of modifications, the active removal of histone modifications by histone-demodifying enzymes complements the dynamic regulation of chromatin-based processes. This allows for the spatial and timely establishment of highly specialized chromatin environments that govern dynamic processes such as gene expression and DNA damage repair, as discussed by Kouzarides in 2007⁹⁸. Beyond acetylation and methylation, which have been extensively studied and are integral to our comprehension of gene regulation, a multitude of novel PTMs have been unearthed. These newer additions include butyrylation, crotonylation, malonylation, citrullination, and more⁹⁹. While these modifications hold immense promise, their precise functions and roles in gene regulation remain enigmatic, awaiting further investigation and deciphering. Four prominent PTMs have captured the spotlight due to their prevalence and well-established functions: acetylation, methylation, phosphorylation, and ubiquitylation.

- **Acetylation**, for instance, neutralizes positive charges on lysine residues and weakens histone-DNA interactions. It involves the transfer of an acetyl group from acetyl CoA to the ϵ -amino group of lysine side chains. This process results in the neutralization of the positive charge on lysine and a reduction in the strength of the interaction between histones and DNA, contributing to an open and accessible chromatin structure. Histone Acetyl Transferase enzymes (HATs) play a crucial role in catalyzing this reaction, using acetyl CoA as a cofactor. In contrast, Histone Deacetylases (HDACs) are enzymes that counteract the actions of HATs by reversing lysine acetylation. This reversal process

helps to restore the positive charge of histone lysine residues and significantly increases the stability of the local chromatin structure.

- **Methylation**, on the other hand, carries diverse functions depending on the context, including both gene activation and repression. It is orchestrated by enzymes called Histone Methyl Transferases (HMTs) that comprises of protein arginine methyl transferases (PRMT) and histone lysine methyltransferases (HKMT). This process primarily targets lysine and arginine side chains, involving the transfer from S-Adenosyl Methionine (SAM) one or more methyl groups to lysines and arginines, respectively. Methyl group removal is catalyzed by histone demethylases, with only a few identified so far. Prominent examples include JMJD6, which can demethylate arginines H3R2 and H4R3, and lysine-specific demethylase 1 (LSD1), which relies on nitrogen that is protonated as well as FAD as a cofactor and is compatible with mono/dimethylated histone lysine substrates. These dynamic modifications critically fine-tune the expression of genes and chromatin structure.
- **Phosphorylation**, catalyzed by kinases, serves as a rapid switch for regulating gene expression by influencing the interactions between histones and other regulatory proteins. Phosphorylation can occur place threonine (T), serine (S) and tyrosine (Y) residues. The addition and removal of these phosphorylation marks are orchestrated by enzymes known as kinases and phosphatases, respectively.
- **Ubiquitylation**, typically associated with gene silencing, tags histones for degradation or recruits chromatin remodelers to alter chromatin structure. It is a large covalent modification involving the attachment of a polypeptide comprising of 76 amino acids called ubiquitin to specific lysine residues on histones. This process is orchestrated by a series of three enzymes: the activating enzyme E1, the conjugating enzymes E2, and the ligating enzyme E3. These enzyme complexes play a crucial role in determining which lysine residues are targeted for ubiquitylation and whether it results in mono- or polyubiquitylation. Despite its considerable size, ubiquitylation remains a highly dynamic modification. It can be reversed through the action of isopeptidases known as de-ubiquitinating enzymes, which are essential for regulating both gene activation and silencing.

Crosstalk among PTMs: an Additional Layer of Complexity in regulation of chromatin dynamics

The meticulous arrangement of chromatin structure is guided by a rich repertoire of potential histone modifications, providing a sophisticated mechanism for intricately fine-tuned control. Yet, delving deeper into the regulation of chromatin dynamics reveals an added layer of complexity. This complexity arises not only from the individual impact of histone post-translational modifications (PTMs) but also from their intricate interplay with modifications found on other histone residues. The foundational "histone code" hypothesis proposes that the interplay of multiple histone modifications or the sequence in which they are added serves as a decipherable code, transmitting unique signals that act as cues in the recruitment of synergistic or antagonistic chromatin factors and remodeling enzymes^{79,100}.

A prominent example is the chromodomain-containing proteins, such as CMT3 and Chd1, which exhibit a preference for doubly-modified histones: CMT3 prefers H3K9me3-K27me3, while Chd1 prefers H3R2me2-K4me3. Intriguingly, these proteins do not bind to either individual methylation state alone, underscoring the importance of specific PTM combinations^{101,102}. BPTF, a protein involved in ATP-dependent chromatin remodeling, features both a plant homeodomain (PHD) and a bromodomain in close proximity. In vitro studies have demonstrated that the PHD-Bromo module of BPTF exhibits increased affinity for H3K4me3/H4K16ac mono-nucleosomes compared to nucleosomes lacking either the H4K16ac or H3K4me3 mark¹⁰³. The presence of H3K4me3 is particularly noteworthy, as it is associated with transcriptional activity, serving as a docking site for the recruitment of TFIID, a key general transcription factor essential for assembling during transcription the RNAPII pre-initiation complex (PIC)¹⁰⁴.

Additionally certain histone PTMs may have contrasting effects depending on where in the genome these modifications are present. The phosphorylation of H3S10 plays a dynamic role in chromatin regulation, exhibiting distinct functions during different phases of the cell cycle. In interphase, H3S10ph is intricately associated with acetylation at H3K9 and H3K14. This co-occurrence is linked to the relaxation of chromatin structure, creating a more accessible environment for various transcription factors. In stark contrast, during mitosis, the phosphorylation of H3S10 takes on a different role, now linked to an augmented methylation at H3K9. The collaborative effect of phosphorylation at H3S10 and increased methylation at H3K9 serves to condense chromatin¹⁰⁵. This mitotic chromatin compaction contributes to the orderly segregation of genetic material during cell division^{106,107}. The phosphorylation event at H3S10 thus acts as a regulatory switch, modulating chromatin structure in a cell cycle-

regulated manner to meet the distinct functional requirements of interphase and mitosis. This exemplifies how a single histone modification can elicit contrasting functions contingent on the chromatin context and its intricate crosstalk with associated histone modifications. The ultimate functional outcome is thus determined by the dynamic and multifaceted interplay of these signals, highlighting the complexity inherent in the regulation of chromatin dynamics.

Mechanisms of histone PTM crosstalk

The intricate binding of proteins to specific histone modifications can be subject to disruption by neighboring modifications. A notable example is the mitotic interference with HP1 binding to H3K9me_{2/3} due to the phosphorylation of H3S10, a phenomenon commonly referred to as a “phospho switch”¹⁰⁸. Another instance involves the impeding effect of H3K4 methylation on the binding of certain proteins equipped with PHD-Bromo cassettes, such as TRIM24, to H3K23ac¹⁰⁹. Additionally, this modification hinders the binding of proteins containing ADD domains, including ATRX, Dnmt3, and Dnmt3L, to H3K9me₃ or me₂¹¹⁰⁻¹¹². Another intriguing example involves the interaction between the unmodified H3R2 residue and the PHD finger of the Uhrf1 protein. Uhrf1, crucial for maintaining CpG DNA methylation, can accommodate any of the three methylation states of H3K4 while binding to H3R2¹¹³. However, the methylation of either H3R2 or the trimethylation of H3K4 negatively impacts Uhrf1's binding to the H3 tail. Uhrf1, acting as a molecular bridge between histone methylation at H3K9 and the DNA methylation maintenance during replication of DNA, demonstrates sensitivity to specific histone methylation states¹¹⁴. It is noteworthy that DNA methylation, known as a silencing mark, and H3K4me₃, recognized as an activation mark, are intricately linked in their regulatory interplay. The recruitment of ADD domain-containing proteins and Uhrf1, both associated with DNA methylation, occurs only in the absence of a methyl group at H3K4¹¹⁴. This underscores the nuanced and context-dependent nature of histone modifications in influencing the targeting and activity of epigenetic regulatory proteins.

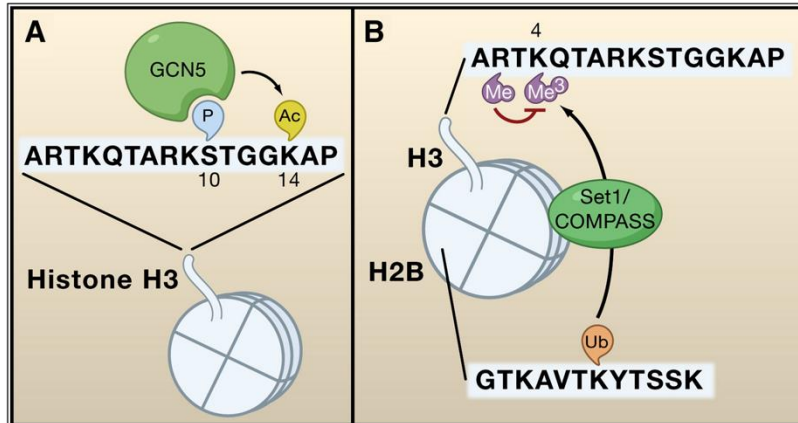


Illustration depicting examples of histone cross talk (taken from Lee et al., Cell 2010)

- The first example is where the prior phosphorylation (P) of serine 10 stimulates GCN5 to add acetyl groups (Ac) to the histone H3 tail.
- The second example is where histone modifications communicate across different histones. Adding a single ubiquitin to histone H2B on lysine 120 can lead to the trimethylation of lysine 4 on the histone 3 tail (H3K4) by Set1/COMPASS. However, if the nearby arginine of H3 is already methylated, COMPASS and COMPASS-like complexes may be blocked from adding methyl groups to H3K4.

Combinations of PTMs can also act sequentially to direct crosstalk between PTMs themselves or factors they recruit to regulate chromatin structure and function during processes. A notable example is in yeast where the prior ubiquitylation of H2BK123 by scRad6/Bre1 is necessary for scCOMPASS mediated H3K4 methylation and the methylation of H3K79 by scDot1^{115,116}. The histone

acetyltransferase MORF demonstrates a strong preference for acetylating histone H3 at the lysine 23 (H3K23) residue. Within the native MORF complex, the double PHD finger (DPF) domain exhibits an affinity for histone H3 acylated at Lysine 14 (H3K14). The interaction between the DPF domain and crotonylated H3K14 actively promotes the acetylation activity of the MORF complex¹¹⁷. Active genes exhibit a simultaneous presence of trimethylation on H3K4 and histone H3 and H4 acetylation at their promoters and transcription start sites (TSS). There are various HAT complexes that have been identified with readers for H3K4me3. For instance, the tandem tudor domain of SGF29, found in the HAT complex SAGA, binds H3K4me3 at the promoters of genes¹¹⁸. Deleting SGF29 that can bind to trimethylated or demethylated H3K4 results in the loss of SAGA complex as well acetylation of H3K9 at target sites¹¹⁸. Similar examples include yeast NuA3 and NuA4, as well as mammalian HBO1, which contain PHD fingers capable of binding H3K4me3¹¹⁹⁻¹²¹. The turnover of the acetylation of lysine residues of histone H3, orchestrated by the interplay between the HATs like p300/CBP and HDACs, occurs dynamically on histone H3 tails with pre-existing H3K4me3¹²². In higher eukaryotes, including flies, mice, and humans this phenomenon is highly conserved. Deletion of CFP1, leading to the loss of trimethylated H3K4, results in the loss of CpG island-associated H3K9ac in Embryonic Stem Cells (ESCs)¹²³. Studies in the model system Dictyostelium discoideum demonstrate that SET1 knockout and loss of trimethylation of H3K4 result in the loss of dynamic H3 acetylation¹²⁴.

H3K36me3, akin to H3K4me3, reveals its influence on histone acetylation dynamics. In transcribing loci this mark allows the recruitment of HDACs as studied in yeast, where the bromodomain-containing EAF3 complex recognizes H3K36me2/3, thereby recruiting the HDAC RPD3S complex¹²⁵⁻¹²⁷.

Additionally, competitive antagonism arises when multiple modification pathways target the same lysine residues. This phenomenon is particularly evident in lysines susceptible to acetylation, methylation, or ubiquitination, leading to a dynamic interplay of modifications vying for occupancy at specific sites. For instance, the transcriptional repressor protein namely Polycomb Repressive Complex 2 or PRC2 is intricately associated with cell fate development regulation. When PRC2-dependent H3K27me3 is lost, there is a consequential rise in H3K27Ac levels, which, in turn, augments gene activity. Essential to the transcriptional repression orchestrated by PRC2 is the prevention of H3K27 acetylation, specifically mediated by the histone acetyltransferases CBP/p300. This mechanism promotes the establishment of H3K27me3, a repressive histone mark crucial for PRC2's regulatory role¹²⁸.

Furthermore, cooperation between modifications also emerges as a pivotal regulatory mechanism. For instance, the strength of the interaction of the protein PHF8 via the PHD finger to H3K4 trimethylated histones is enhanced when the 9th and 14th lysine residue of histone H3 are concurrently acetylated on the same H3 tail¹²⁹.

Coordination of PTMs, Histone Variants, Chaperones, and Remodeling Activities in Orchestrating Nucleosome Dynamics

The interplay among post-translational histone modifications (PTMs), histone chaperones, ATP-dependent remodelers and histone variants at the nucleosome interface takes center stage in chromatin structural and functional regulation. **Histone variants**, serve as markers for specific chromatin regions and are distinguished by their sequence and structural differences from canonical histones. They are integrated into chromatin with the assistance of specialized histone chaperones. This results in the formation of homotypic (two variants) or heterotypic (one variant) nucleosomes alongside canonical core histones¹³⁰ that can have several significant impacts: They can modify the chromatin structure by influencing the stability of nucleosomes. This occurs through their distinct interactions with core histones, which can lead to variations in nucleosome stability¹³¹. They can introduce unique patterns of post-translational modifications, further diversifying the chromatin landscape¹³². Furthermore, they play a pivotal role in demarcating particular regions in the genome. A prominent example is CENP-A a variant of histone H3, which is particularly introduced at the centromere. CENP-A serves as a

binding platform for the kinetochore, facilitating the coordination of chromosome segregation¹³³. Other histone variants are actively involved in marking sites associated with transcriptionally active genes or DNA repair, recruiting specific factors essential for these processes¹³⁴. For instance, several investigations have provided intriguing insights into the role of H2A.Z, particularly when associated with H3K27me3, shedding light on its impact on chromatin compaction both in vitro and within the stem cells of mouse embryos¹³⁵. The interaction between H2A.Z and the N-terminal tail of histone H4 plays a vital role in this process, as H2A.Z creates an extended acidic patch at the interface of H2A/H2B, thus enabling the formation of higher-order chromatin structures in vitro¹³⁶.

Notably, the genomic distribution of H2A.Z exhibits interesting patterns, with lower levels detected genome-wide. However, its occupancy is notably higher in regions associated with active promoters and transcription start sites, as evidenced by studies¹³⁷. In vivo studies have reinforced these observations, revealing that enhancers enriched with H2A.Z tend to be more accessible and are marked by acetylation at H3K122, serving as an indicator of active gene promoters¹³⁸.

The intricate interplay of histone modifications further extends to H3K56 acetylation, a post-translational modification associated with nucleosome unwrapping and histone deposition. In actively transcribing loci or regions that are poised for activation, H3K56 acetylation significantly influences H2A.Z deposition by modulating the activity of SWR1, an ATPase dependent chromatin remodeler¹³⁹. SWR1 collaborates synergistically with another remodeler, INO80, in a sophisticated regulatory network. Their concerted efforts serve to evict H2A.Z and restore canonical H2A, establishing a delicate equilibrium between H2A.Z deposition at active gene promoters by SWR1 and H2A.Z eviction by INO80. This dynamic interplay is further regulated by the processes of acetylation and deacetylation¹³⁹.

Histone chaperones, characterized by their high acidity, play a vital role in stabilizing basic histones, especially in the absence of DNA. They achieve this by shielding the surfaces of histones that interact with DNA and other histones within the nucleosome. Beyond their conventional role in nucleosomal contexts, such as during processes like replication and transcription, where histone-free DNA is required, histone chaperones are essential for preventing histone aggregation and unwanted interactions with DNA.

These molecular chaperones are central to various facets of histone metabolism, encompassing histone storage, transport, post-translational modifications (PTMs), and turnover. Their crucial involvement extends to pivotal roles in nucleosome assembly and disassembly, as outlined in the work by Hammond et al. in 2017¹⁴⁰.

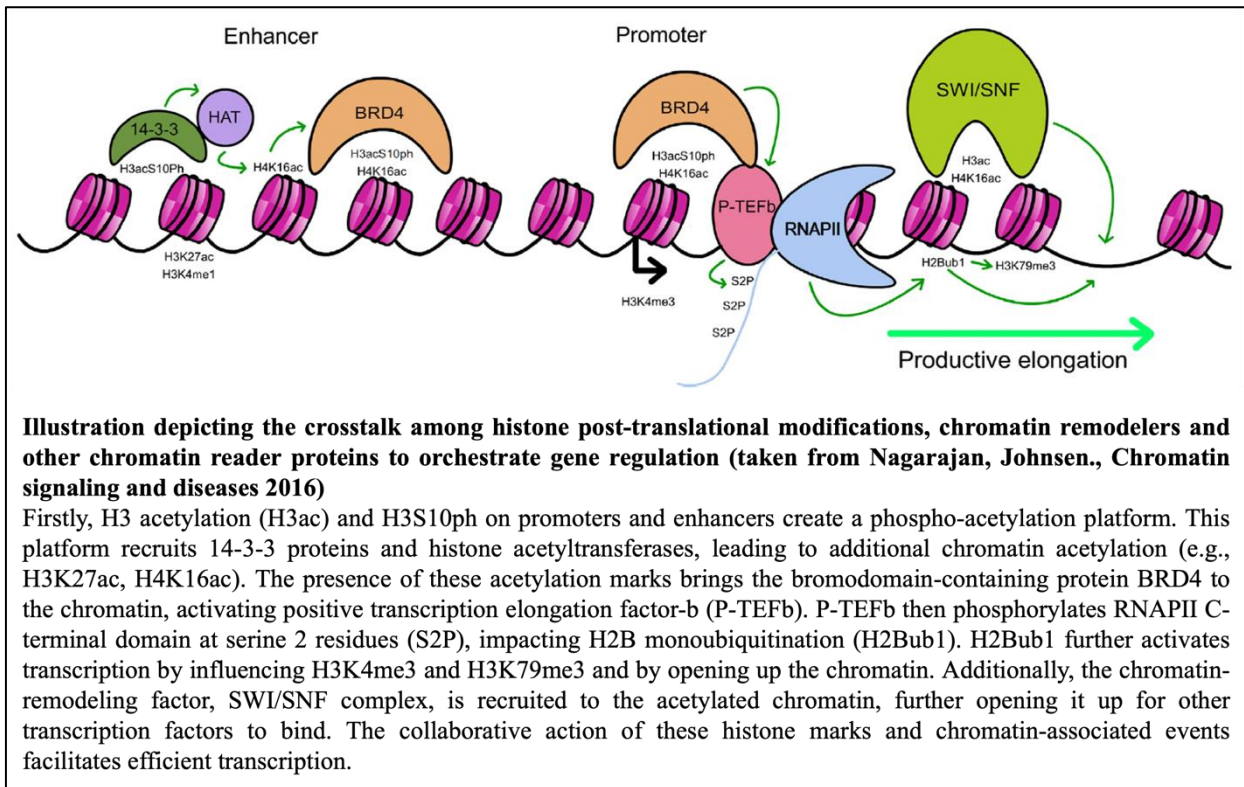
The impact of post-translational modifications (PTMs) on chaperone binding has been extensively studied, with H3K56 acetylation serving as an illustrative example. H3K56 acetylation facilitates the process of chaperone mediated chromatin assembly in yeast. The histone chaperone Chromatin Assembly Factor 1 (CAF1) exhibits enhanced binding to tetramers containing H3K56 acetylation that enables it to deliver H3/H4 tetramers to the site of nucleosome assembly and, leading to more efficient deposition of histones onto DNA and, consequently, nucleosome formation¹⁴¹. On the other hand, Regulator of Transposition Ty1 106 (Rtt106), another histone chaperone that participates in nucleosome assembly may not directly be influenced by the acetyl group but a pleckstrin homology domain (PH) domain of Rtt106 binds preferentially to a conformation of the tetramer of H3/H4 induced by H3K56 acetylation¹⁴².

Furthermore, other PTMs, such as a novel type of methylation at a glutamine residue (Q105) within yeast H2A histone, have been linked to chaperone binding sites. Specifically, this methylation is associated with the chaperone complex FACT (Facilitator of Active Chromatin Transcription)¹⁴³.

Chromatin remodelers play a crucial role in altering DNA accessibility by repositioning nucleosomes. They directly impact how genes and regulatory elements are accessed and influence gene expression patterns^{144,145}. Some remodeling complexes go even further by enabling the exchange of histones with histone variants and assisting histone chaperones in the de novo assembly of nucleosomes¹⁴⁶. Consequently, chromatin remodelers exert dynamic control over access to specific chromatin regions, inducing changes in chromatin topology in a spatially and temporally restricted manner¹⁴⁷.

The key to the DNA translocation reaction performed by chromatin remodelers lies in the RecA-like ATPase domain, which is an integral component of these enzymes¹⁴⁸. Additionally, chromatin remodelers contain various DNA-binding and regulatory domains and subunits, often forming multi-subunit complexes¹⁴⁶. These domains and subunits define the specific actions of distinct chromatin remodeling complexes by influencing their recruitment to genomic locations, such as regions rich in specific histone modifications, and by modulating the outcomes of nucleosome sliding, which can include nucleosome eviction or histone exchange¹⁴⁴. Furthermore, the binding of accessory reader domains to specific DNA structures or post-translational modifications triggers a conformational change, allowing for the activation of the chromatin remodelers in an allosteric manner^{149,150}.

One noteworthy example of this regulatory mechanism involves the Swi2/Snf2 protein, which features a bromodomain facilitating its recognition of acetylated histones. This interaction allows the chromatin remodeling complex SWI/SNF to bind and ultimately facilitate the 'opening' of chromatin structures¹⁵¹. In the context of yeast, H3K56 acetylation has been identified as a key modification that allows the binding of SWI/SNF a chromatin remodeler to the chromatin. This in turn facilitates the expression of specific genes¹⁵². Furthermore, recent

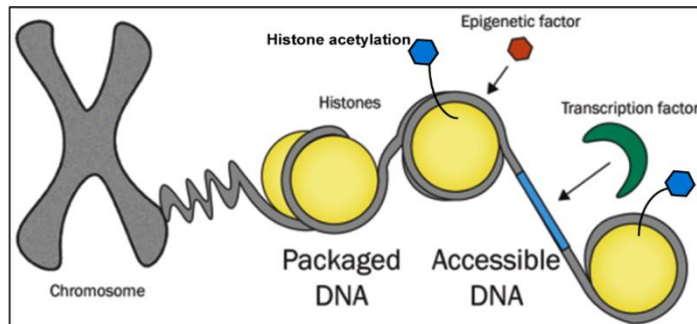


research has shed light on the role of PHD fingers in recognizing acetylated histones. An illustrative example is DPF3b which is an integral component of the chromatin-remodeling complex BAF that has a tandem PHD finger responsible for allowing the BAF complex to associate with histones that are acetylated, thereby influencing chromatin structure¹⁵³. Another vital chromatin-remodeling complex in yeast is the RSC remodeling complex, which is known to play a critical role in regulation of transcription and DNA repair. H3K14Ac emerges as a critical modification that enhances the retention of RSC on nucleosomes and amplifies its remodeling activity¹⁵⁴.

Moreover, the recognition of histone modifications extends to H3K4 trimethylation. This modification allows the chromodomain of the ATP-dependent remodeler CHD1 to bind to and reposition nucleosomes¹⁵⁵. Additionally, JMJD2A which is a histone demethylase contains a tandem tudor domain that specifically recognize tri-methylated H3K4¹⁵⁶. In both cases, H3K4me3 serves as a direct recruiter of chromatin-modifying enzymes.

HISTONE ACETYLATION- A UBIQUITOUS POST-TRANSLATIONAL MODIFICATION

Among the various modifications that histones undergo, the processes of acetylation and deacetylation targeting histone lysine residues stand out as the most pervasive and one of the most extensively studied post-translational modifications within the realm of histones. The pre-eminence of these modifications can be attributed to the multifaceted impact of histone acetylation on chromatin processes. Notably, Histone acetyltransferases (HATs) are enzymes that transfer an acetyl group from acetyl-Coenzyme A (acetyl-CoA) to the ϵ -amino group



Depicting the effect of histone acetylation on DNA accessibility Adapted from Gehlenborg et al., Medicine and Biology 2019

of side chains of lysines present within histones. This process neutralizes the positive charge of lysine residues in the lysine-rich histone tails and core domains. Since these tail and core domain residues interact with nucleosomal DNA which is negatively charged, the presence of acetylation weakens the strength of the interaction between histone and DNA, facilitating alterations in chromatin structure. Furthermore, histone acetylation also serves as a signaling mechanism, facilitating the recruitment of effector proteins on chromatin thereby altering chromatin functions. Owing to its dynamic properties acetylation-deacetylation of histone lysine residues is linked to all DNA-templated functions.

The central focus of this thesis resides in unraveling the effects of histone acetylation on chromatin functions. Subsequent sections will delve into the specific roles played by histone acetylation in the structural regulation of chromatin and its broader implications on chromatin function.

Effect of histone tail and core acetylation on nucleosome dynamics

Research indicates that histone acetylation serves as a key determinant in enhancing DNA site accessibility within nucleosomes. Studies employing restriction enzyme accessibility have shown that acetylation can double DNA accessibility at a particular site¹⁵⁷. This implies that acetylation facilitates a more open and permissive environment within the nucleosomal structure, allowing for greater interaction between regulatory factors and the underlying DNA.

The influence of histone acetylation on the mechanical properties of nucleosomes has been elucidated through advanced techniques such as single-molecule force spectroscopy which demonstrate how histone acetylation can significantly reduce the force that is required for the mechanical unwrapping of nucleosomes¹⁵⁸. In simpler terms, acetylation renders the nucleosomal structure more flexible and less resistant to unraveling, indicating a direct correlation between acetylation and the physical dynamics of nucleosome unwrapping.

Furthermore, complementary findings from FRET based studies have provided additional evidence proof of the influence of acetylation of histones on unwrapping of nucleosomes. Specifically, the involvement of the Piccolo NuA4 complex in histone acetylation has been implicated in increasing the degree of nucleosome unwrapping¹⁵⁹. This suggests that acetylation, particularly facilitated by specific molecular complexes, actively promotes the exposure of DNA within the nucleosome, further emphasizing the regulatory role of histone acetylation in chromatin dynamics.

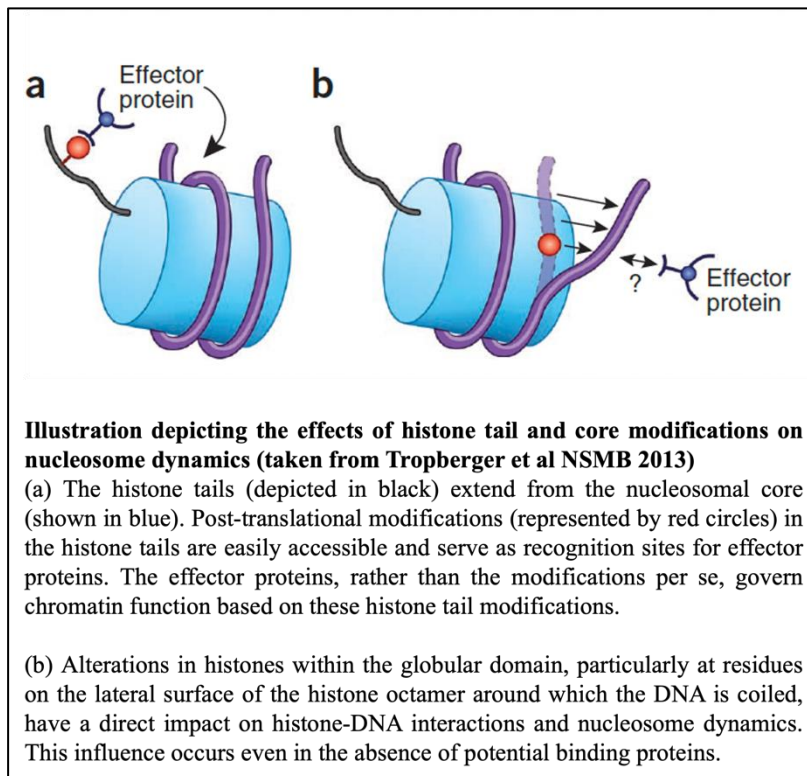
Histones, exhibit a structural and functional duality through their two distinct domains: the globular domains comprising the nucleosomal core, where DNA is intricately wound, and the unstructured tails extending from this core. The histone N-terminal tails that extending from the nucleosomal core particle on the outside, have long been recognized as crucial sites for acetylation that play a critical role in dynamically regulating chromatin structure¹⁶⁰. Over several years, extensive research has focused on understanding how these modifications, by recruiting or excluding specific "reader" proteins, influence various DNA-dependent processes¹⁶¹.

Hyperacetylation of histone tails, introduces a disruptive element to nucleosome array folding¹⁶². This modification not only perturbs the structural organization of nucleosome arrays but also correlates with an enhancement in RNA transcription^{86,163,164}. Investigations utilizing recombinant histones have pinpointed the specific involvement of residues between 14th and the 19th in the tail of histone H4 in the compaction of nucleosome arrays⁷⁴. This underscores the nuanced and region-specific influence of histone tails to the overall chromatin structure. Intriguingly, a subsequent study reinforced these observations by demonstrating how the modification of a single residue on the N-terminal tail of histone H4, H4K16 prevents nucleosome array compaction⁸¹. This highlights the intricacy of histone tail acetylation and their precise influence on the three-dimensional organization of chromatin.

A substantial body of research has been dedicated to unraveling the detailed roles of histone tails and their profound impact on chromatin compaction. Numerous reviews delve into the molecular intricacies of histone tail modifications and their consequences for chromatin

structure, providing a comprehensive understanding of the regulatory mechanisms governing this fundamental aspect of cellular function^{165,39,166-168}.

Up until a very recent period, the immediate influence of histone post-translational modifications (PTMs) on the structure of nucleosomes and, by extension, on the functionality of chromatin remained largely correlated with the modification of residues situated within the histone globular core domain, particularly those present on the histone octamer lateral surface. Being in close proximity to the DNA molecule they hold significant structural importance and can exert a direct influence on chromatin function, challenging the traditional focus on N-terminal tail acetylation^{3,169}. The histone octamer scaffold which is formed collectively by the globular core domains of all the four histones, creating a structural foundation around which DNA is tightly wound. This assembly is crucial for maintaining the integrity of nucleosomal architecture. The outer surface of this histone octamer, known as the



lateral surface, directly interfaces with DNA. Nucleosomal DNA, in a state that is tightly associated to this lateral surface, is conventionally considered largely inaccessible to regulatory factors. However, experiments involving single nucleosomes have unveiled a dynamic behavior wherein nucleosomal DNA unwraps spontaneously followed by a subsequent

rewrapping onto the lateral surface. This dynamic process offers a plausible explanation for the observed phenomenon *in vivo*, where a significant proportion of the binding of transcription factors still occurs on nucleosomal DNA^{87,88,170}. The rate of localized unwrapping of nucleosomal DNA emerges as a critical regulatory mechanism governing various DNA-dependent processes. The significance of interactions between histones and DNA is underscored by the finding that single amino acid mutation of histone residues present on the histone octamer lateral surface present a greater likelihood of resulting in lethality compared

to a mutation on the histone tail or surface free of DNA binding. Intriguingly, a major proportion of acetylation that is known to occur within the globular domains of histones map to the lateral surface¹⁷¹. Acetylation on the lateral surface of histone octamer have the potential to influence profoundly the binding dynamics of histone with DNA. Given the highly positive charge of the lateral surface, essential for binding the negatively charged DNA backbone, PTMs that alter the charges of the side chains of amino acids, for instance acetylation, are particularly influential. Supporting this notion, in yeast, mutations that occur on lateral-surface of the histone octamer that change the charges of the side chains of amino acids have been shown to affect ribosomal DNA silencing¹⁷². Notably, a quantitative modeling study has validated that neutralizing single positive charges, as seen in the acetylation of lysine residues on the lateral surface of histones, significantly weakens the interaction of DNA with the histone octamer, directly influencing nucleosome dynamics and transcription¹⁷³.

Influence of histone acetylation on chromatin functions- DNA damage response and transcription

The cellular ramifications of histone acetylation are closely intertwined with transcriptional regulation. Acetylation induces a transition in chromatin from a tightly packed state to a more relaxed state^{174,175}. This structural change renders DNA more accessible to various transcriptional machinery components, including RNAPII, as well as proteins associated with initiation and elongation of transcription¹⁷⁶. A pivotal histone acetyltransferase in this context is p300, a transcriptional coactivator that plays a key role in gene enhancers by acetylating histones and thereby promoting expression of genes¹⁷⁷.

In vivo, p300 acetylates all four core histones, displaying a stronger preference for histones H3 and H4^{178,179}. The dysregulation of p300 has been implicated in cancer, as it can alter the expression of numerous oncoproteins and tumor suppressor proteins^{180,181}. Histone acetylation at H3K9, a tail residue, emerges as a very important player in promoting the release of RNAPII from paused states. This process is facilitated by the direct recruitment of the super elongation complex (SEC) to chromatin. H3K9ac serves as a crucial substrate for SEC binding, and is essential for maximizing pol II pause release through SEC activity¹⁸². Loss of H3K9ac results in an increased pol II pausing index on specific genes in HeLa cells, highlighting the functional impact of this histone modification on transcriptional regulation¹⁸². The presence of acetylation at histone H3 lysine 122 (H3K122ac), a globular core domain modification, has been observed to closely associate with various marks indicative of active gene regions, including H3K4me3, H2A.Z, and H3.3, as well as enhancers marked by H3K4me1 and H3K27ac¹⁸³. Notably,

genomic regions marked by H3K122ac exhibit a scarcity of nucleosomes, and this modification is particularly enriched around the transcriptional start sites of genes. H3K122ac actively promotes the eviction of nucleosomes, facilitating increased accessibility for the transcriptional machinery¹⁸³. A relatively recent addition to the repertoire of globular domain modifications is histone H3 lysine 64 acetylation (H3K64ac)¹⁸⁴. Notably, H3K64ac exhibits a distinctive spatial distribution, being prominently present at the active gene start sites, and its abundance correlates directly with the mRNA output of the associated gene. This modification is also notably found on active enhancers, underscoring its association with regions crucial for transcriptional regulation. During embryonic stem cell (ESC) differentiation, H3K64ac exhibits dynamic behavior. Initially concentrated at pluripotency-associated gene promoters, its distribution subsequently shifts towards genes linked to differentiation. This pattern suggests that H3K64ac serves as a reliable indicator of the transcriptional state during cellular differentiation. Its preferential association with the active transcription-associated H3.3 histone variant further underscores its functional relevance¹⁸⁴. The enzymes responsible for H3K64 acetylation are primarily p300/CREB-binding protein (CBP), key players in histone acetylation cascades¹⁸⁴. This suggests a potential co-localization of H3K64ac with other histone acetylation marks regulated by p300/CBP, highlighting the interconnected nature of various acetylation events in chromatin regulation. Functional studies reveal that H3K64ac has a direct impact on chromatin structure. It decreases nucleosome stability, indicating a role in modulating chromatin's structural integrity¹⁸⁴. In vitro assays further demonstrate that H3K64ac enhances nucleosome eviction, implicating its involvement in rendering genes more accessible to the cellular transcriptional machinery.

The acetylation of H3K115 a residue situated within the histone globular core, has garnered attention. This modification has been found to localize near the active promoters and coincides with the binding of transcription factors at enhancers¹⁸⁵.

Beyond its role in transcriptional regulation, there is a growing body of evidence suggesting the involvement of histone acetylation in DNA damage repair pathways¹⁸⁶⁻¹⁸⁹. Given that chromatin structure dictates DNA accessibility, acetylation plays a crucial role in facilitating the repair of DNA damage repair by regulating the accessibility of protein complexes associated with DNA damage with chromatin.

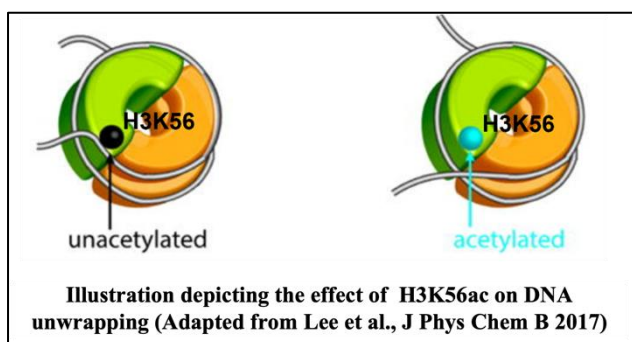
The acetylation of H3K18 and H3K27 for instance modulates the activity of UDG and APE1 two enzymes associated with base excision repair¹⁹⁰. Furthermore, acetylation of H4K16 has been identified as a facilitator of the repair of double-strand break by the homologous recombination pathway¹⁹¹. Additionally, binding of Ku70/80 a protein associated with

nonhomologous end joining is enhanced by p300 mediated acetylation of H3 and H4 at sites of DNA damage¹⁹². These intricate molecular interactions highlight the multifaceted role of histone acetylation in cellular processes, ranging from transcriptional regulation to the maintenance of genomic integrity through repair of damage on DNA.

The activation of ATM in response to ionizing radiation (IR) requires H4K16 acetylation which is the substrate for the HAT MOF¹⁹³. In mice, H4K16 acetylation can be recognized by PA200, a proteasome activator, via its bromodomain-like region. This allows it to target core histones for degradation by proteasomes in an acetylation dependent manner upon DNA double-strand breaks that ultimately leads to chromatin relaxation and facilitating DNA repair¹⁹⁴. Tip60 in humans or its homolog in yeast, Esa1 induces acetylation of histones around DNA damage sites during double strand break repair, promoting chromatin relaxation and the recruitment of repair proteins^{195,196}. The acetylation of histones is a dynamic process during DNA repair, and proper regulation of the balance between histone acetyltransferases and histone deacetylases is vital for the process of repair and maintenance of genome integrity. For example, in MEFs, DNA damage is induced if the histone deacetylase HDAC3 is lost; this ultimately activates the checkpoint during S phase, emphasizing the significance of HDAC3 in the maintenance of genomic stability during DNA replication¹⁹⁷. H4K16 deacetylation in yeast by Sin3p is vital for the binding of 53BP1 to H4K20 methylated histones that enables proper NHEJ repair¹⁹⁸. Histone deacetylation mediated by HDACs such as Rpd3, Sir2, and Hst1 during homologous recombination at sites of double strand breaks is vital for maintenance of cell viability¹⁹⁹. In yeast, the regulation of H4K16 acetylation-deacetylation dynamics is vital for proper functioning of Nucleotide Excision Repair (NER)²⁰⁰.

H3K56 acetylation – A unique PTM of the histone H3 globular core

The histone tails, extend from the surface of the nucleosome to a stretch of approximately 20 to 30 amino acids and primarily undergo modifications at the region towards the N-terminal which is inherently accessible. However, lysine 56 is a very unique residue, encompassing approximately the last 10 bases of DNA entering and exiting the nucleosome⁴⁴. Furthermore, at this site H3K56 is the only lysine residue that can be acetylated. H3K56 residue forms water-mediated contacts with the phosphate backbone of DNA, positioning it strategically to



enhance accessibility of the DNA to a large number of proteins²⁰¹. In line with this, K56 acetylation weakens DNA association with the histone octamer, significantly impacting DNA unwrapping, increases the fraction of nucleosomes with unwrapped DNA at the end position and influences the unwrapping internally to it almost 4 times^{56,202}. Notably, the accessibility of enzymes such as micrococcal nuclease increases upon H3K56 acetylation, and it reduces the strength of binding of DNA with tetramers acetylated at H3K56 almost 15-fold compared to tetramers lacking the modification^{203,204}. Single-molecule FRET distribution measurements showed a remarkable 7-fold increase in DNA unwrapping from the histone octamer at the entry/exit site of DNA upon H3K56ac²⁰². Another study, utilizing H3K56ac prepared through sequential NCL, reported a threefold increase in transcription factor occupancy that extends approximately 27 base pairs within the nucleosome as a result of increased DNA unwrapping²⁰⁵. These findings suggest that nucleosomes can unwrap from the entry or exit region of the nucleosomal DNA, and a fall in the free energy of unwrapping at the edge of the nucleosome can enhance accessibility of DNA further within. This property of nucleosomes results in binding of transcription factors in a cooperative manner to adjacent sites within the nucleosome^{206,207}. Notably, the use of H3(K56Q) that mimics the acetylation of lysine increases the occupancy of a transcription factor at similar level, indicating that this mimic can capture the impact on nucleosome unwrapping mediated by acetylation²⁰⁵. Contrary to expectations as revealed by X-ray crystallography based studies nucleosomes that bear the H3K56Q mutation mimicking acetylation are unable to distort the interface of histone-DNA. Thus, while H3K56 acetylation does not impede the formation of a completely wrapped nucleosomes, this modification tips the equilibrium of site exposure toward a partially unwrapped state, significantly enhancing the accessibility of nucleosomal DNA¹⁷⁰. In *Saccharomyces cerevisiae*, acetylation of H3K56 is catalysed by the HAT Rtt109 together with the histone chaperone Asf1²⁰⁸⁻²¹². Being the last residue of the N-terminal alpha helix on H3, H3K56 normally remains embedded in nucleosomal DNA and is thought to be acetylated on free histones prior to their deposition onto chromatin²¹³. Therefore, presence of this modification mark on chromatin is often an indication of newly synthesized histones deposited in a replication dependent or independent way^{141,204}. What is unique about H3K56 is that it has a dual role in regulating nucleosome dynamics in a context-dependent manner. During replication, H3K56 acetylation has a non-redundant role with other H3 acetylation on the newly synthesized histones. H3K56 acetylation can promote the process of nucleosome assembly by enhancing the affinity of H3/H4 tetramer binding to downstream chaperones that participate in histone deposition. H3K56 acetylation, it increases the affinity with which the histone

chaperone known as CAF-1 associates with tetramer of H3/H4 that allows it to deposit histones onto chromatin during replication coupled nucleosome assembly¹⁴¹. Furthermore, research utilizing NMR and isothermal titration calorimetry (ITC) techniques demonstrated that the acetylation of H3K56 enhances significantly the affinity with which RTT106 associates with H3/H4 tetramers by its double pleckstrin-homology (PH) domain during the process of nucleosome assembly during replication^{142,214}. These findings collectively suggest that the acetylation of H3K56 exerts its influence on nucleosome assembly and disassembly by affecting interactions of tetramers of H3/H4 with histone chaperones. H3K56 acetylation generally peaks during S phase and as cells progress into G2/M phase of the cell cycle, H3K56 is rapidly deacetylated by the balanced action of the HDACs Hst3 and Hst4^{204,215}. However, if cells encounter any DNA damage during replication H3K56 acetylation is persistently maintained to activate checkpoint proteins via the DNA damage response pathway^{204,216}. However, after the damage repair if H3K56 acetylation is not removed it causes defects in cell cycle^{217,218}. Thus, the dynamic regulation of H3K56 acetylation is vital for proper cellular functions. Interestingly, H3K56 acetylation also regulates transcription coupled nucleosome dynamics. The acetylation of H3K56 has been found to profoundly influence the unwrapping kinetics of nucleosomal DNA that could influence transcription elongation^{219,220}. In heterochromatin regions acetylation of H3K56 promotes the elongation of transcription without affecting higher order chromatin structure formation²²¹. H3K56 acetylation colocalizes with transcribing loci and has been strongly correlated with the processes of both transcription initiation, elongation and transcription-coupled histone exchange^{208,222,223}. Presence of H3K6 acetylation during transcription is suggested to tip the balance of nucleosomes towards a disassembled state thus allowing an accessible chromatin architecture for gene expression²²⁴. As H3K56 acetylation can increase accessibility of linker DNA it can help keep chromatin a more poised architecture that allows recruitment of chromatin remodelers such as SWI/SNF and thereby promotes gene expression²²⁵. Furthermore, the unfolding of DNA wrapped around nucleosomes induced by acetylation of H3K56 aids helps in diminishing the RNAPII pause duration²²⁰. Infact, in mESCs, hyperacetylated H3K56 is known to enable RNAP II pause release at the promoter proximal site allowing RNAPII to subsequently progress through the genes²²⁶. Additionally, histone H2A/H2B dimer dissociation from chromatin as well as nucleosome assembly/disassembly by the histone chaperone FACT is critically influenced by acetylation of H3K56^{227,228}. Furthermore, H3K56 acetylation influences the activity of SWR1, an ATPase dependent chromatin remodeler responsible for the deposition of H2A.Z to regions associated with and poised for active transcription¹³⁹.

SWR1 collaborates synergistically with another remodeler, INO80, in a sophisticated regulatory network. Their concerted efforts serve to evict H2A.Z and restore canonical H2A, establishing a delicate equilibrium between H2A.Z deposition at active gene promoters by SWR1 and H2A.Z eviction by INO80. This dynamic interplay is further regulated by the processes of H3K56 acetylation and deacetylation¹³⁹. Besides transcription and replication, impairments in H3K56 acetylation render cells more susceptible to agents that are genotoxic, indicating that this modification is crucial for the cellular response to DNA damage^{204,229}. Furthermore, during DNA double strand break repair, the acetylation of H3K56 is thought to be a prerequisite for the inactivation of checkpoint proteins associated with DNA damage thus ensuring the survivability of cells^{141,229}. These findings underscore the significant role played by this modification in orchestrating the DNA damage response. Furthermore, molecular simulation studies have shown that lesion sensing by damage repair proteins can increase several folds in the presence of H3K56 acetylation indicating a role of this residue in DNA damage accessibility²³⁰. H3K56ac regulates critically the stability of advancing replication forks²³¹. The lack Rtt109 and Asf1 results in an increase in the frequency of recombination as evidenced by an increased exchange of sister chromatid²³². During replication, the fine balance between acetylation as well as deacetylation of H3K56 is essential as it allows efficient homologous recombination (HR) by facilitating the machinery involved in recombination to select the appropriate sister chromatid²³³. In essence, the critical regulation of H3K56 acetylation, characterized by precision, timeliness, and dynamic adjustments, proves to be a crucial element for promoting cell survival when confronted with DNA damage. In *Saccharomyces cerevisiae*, H3K56 acetylation status is not only crucial for replication, transcription and repair but has also been implicated in telomeric silencing²³⁴. Thus, the impact of acetylating a single residue within the histone H3 core domain (H3K56) becomes apparent when considering its profound influence on the dynamics of chromatin structure and function.

BACKGROUND STUDY

Acetylation of lysine residues in the H3 and H4 N-terminal tails as well as in the core region plays a critical role in the intricate regulation of chromatin. However, a comprehensive understanding of the precise mechanisms governing these modifications in various cellular processes remains yet to be explored. To understand how histone modifications regulate chromatin dynamics, previously the acetylation of H4K16, a residue of the histone H4 N-terminal was studied. On the N-terminal tail of histone H4, there are four residues of lysine which can regulate inter-nucleosomal interactions based on their acetylation status. However, amongst this, acetylation of H4K16 has unique functions.

To grasp the significance of H4K16 acetylation, it is essential to comprehend the interaction of the H4-N terminal tail with the dimer of H2A/H2B. Within the H4-N-terminal tail, the 17th and 19th residues are particularly significant, forming what is referred to as an arginine hook or anchor motif⁶⁰. This motif holds notable importance, as it is universally utilized by chromatin-binding proteins for direct nucleosome attachment. The arginine anchor engages with a deep acidic groove, comprised of six aspartate and two glutamate residues, situated at the interface of the H2A-H2B dimer. Consequently, any motif featuring the arginine anchor can directly bind to the nucleosome disc face through the H2A-H2B interface. The 15th to 20th residues of the N-terminal tail of histone H4 exhibit a propensity to form structures that are α -helical. This configuration positions the H4K16, H4R17, H4R19, and H4K20 residues on one face of the α -helix²³⁵. Notably, the H4 R17-R19 arginine anchor hook associates with the acidic groove on the H2A-H2B interface. In its deacetylated state, H4K16 is the first H4 N-terminal residue to interact with the acidic patch of the dimer of H2A/H2B, establishing an inter-nucleosomal contact between the tail of histone H4 and the nucleosome via an arginine anchor motif.

Acetylation of H4K16 introduces a structural shift, disrupting formation of the H4 tail α -helix and destabilizing its interaction with H2A-H2B. This disruption leads to the loss of local chromatin compaction²³⁶⁻²³⁸. The structural significance of H4K16 is further emphasized by its capacity to regulate nucleosomal contact between the N-terminal tail of histone H4 and the H2A-H2B dimer. Moreover, the acetylation status of H4K16 serves as a regulatory switch for the recruitment of different proteins²³⁹. On one hand, acetylation of H4K16 disrupts the binding of the N-terminal tail of histone H4 to the nucleosome core, allowing for competitive binding of other proteins containing the arginine anchor motif to the same site. On the other hand,

H4K16 acetylation engages in an intricate interplay with the acetylation of three other residues on the N-terminal tail of histone H4 that include H4K5, H4K8 and H4K12 to regulate chromatin dynamics.

In the realm of eukaryotes, where all nuclear processes unfold within a chromatin milieu, the accessibility of nuclear factors to DNA hinges on nucleosome dynamics. Such dynamic behaviour empowers the fine-tuning of local chromatin structure. Given its strategic location within the H4-N-terminal tail, understanding how H4K16 acetylation-deacetylation regulates chromatin dynamics seemed imperative. To explore this, two significant DNA metabolic pathways were chosen as investigative tools: Nucleotide Excision Repair (NER) and transcription.

To explore the effects of the dynamic interplay of acetylation and deacetylation at H4K16 in orchestrating chromatin structural and functional regulation during nuclear processes, two structurally distinct mutants of H4K16 were strategically employed. Specifically, yeast strains were meticulously engineered to harbour mutations in the N-terminal tail of histone H4, where the 16th amino acid, a lysine residue (H4K16), was substituted either by an arginine residue (H4K16R) or a glutamine residue (H4K16Q). The choice of these mutants was driven by their unique characteristics. The guanidino group in arginine, unlike lysine, precludes its acetylation. On the other hand, the acetamide group in glutamine closely mimics the charge and structure of an acetylated lysine, allowing it to function as an acetylated lysine both in vitro and in vivo^{240,241}. Consequently, the H4K16R and H4K16Q mutants lack the regulatable nature of lysine acetylation present in the wild type (WT) strain, instead embodying a constitutively deacetylated (K16R) or acetylated (K16Q) state of lysine, respectively.

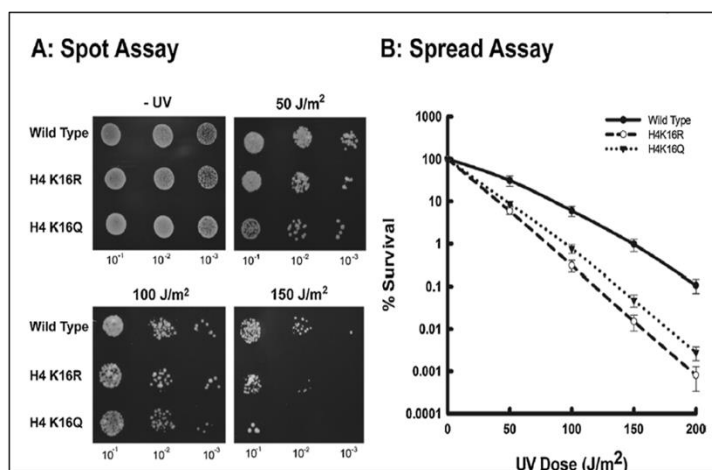
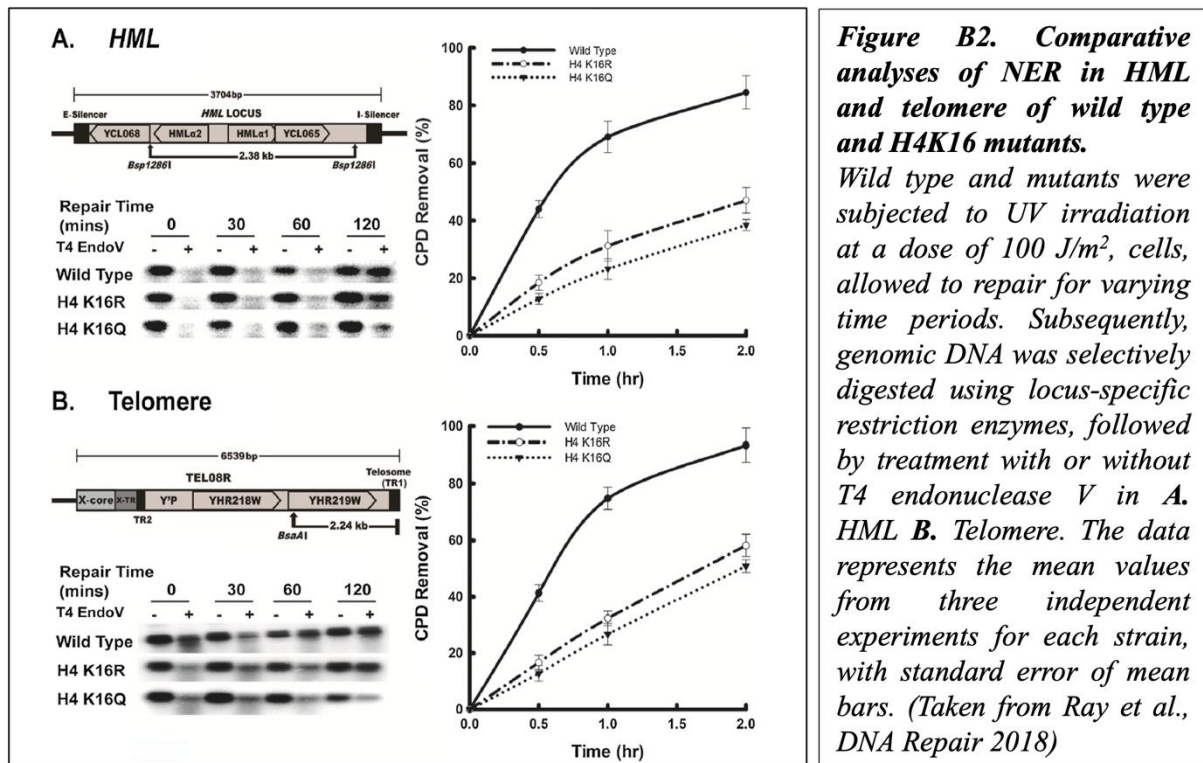


Figure B1. UV-sensitivity assay of wild type and mutants of H4K16. Ten-fold serial dilutions of control or UV-treated cells of wild type and H4K16 mutants were **A.** spotted and **B.** spread on YPA plates. For spread assay the colony forming units from triplicate sets were plotted. The data presented represents the average values derived from three separate and independent experiments, with error bars indicating the standard error of the mean. (Taken from Ray et al., DNA Repair 2018)

The functional consequences of disrupting H4K16 acetylation-deacetylation dynamics through these mutations were profound. Both mutants exhibited compromised chromatin functions, with heightened UV sensitivity and a diminished Nucleotide Excision Repair (NER) rate

compared to the wild type (Figure B1 & B2). Remarkably, the locked acetylation or deacetylation states of H4K16 substantially impeded chromatin regulation, illustrating the



critical role of H4K16 dynamics in processes such as NER, which rely on the inherent plasticity of chromatin.

In summation, the findings underscored the indispensable nature of the dynamic regulation of H4K16 deacetylation and acetylation for the efficient execution of Nucleotide Excision Repair in *Saccharomyces cerevisiae*.

The regulatory impact of H4K16 on transcriptional outcomes has been previously delineated, demonstrating that its deacetylation induces changes in the expression patterns of gene clusters²⁴². As transcription is a fundamental and essential DNA templated process, the effects of disrupting H4K16 regulation on transcription was also investigated. In this context, the study delved into the impact of mutation on H4K16 on the expression of six constitutively active genes namely, *PYK1*, *RPB2*, *ACT1*, *TFC1*, *UBC6*, and *TAF10*, chosen for their involvement in housekeeping pathways, ensuring their constant expression under normal growth conditions.

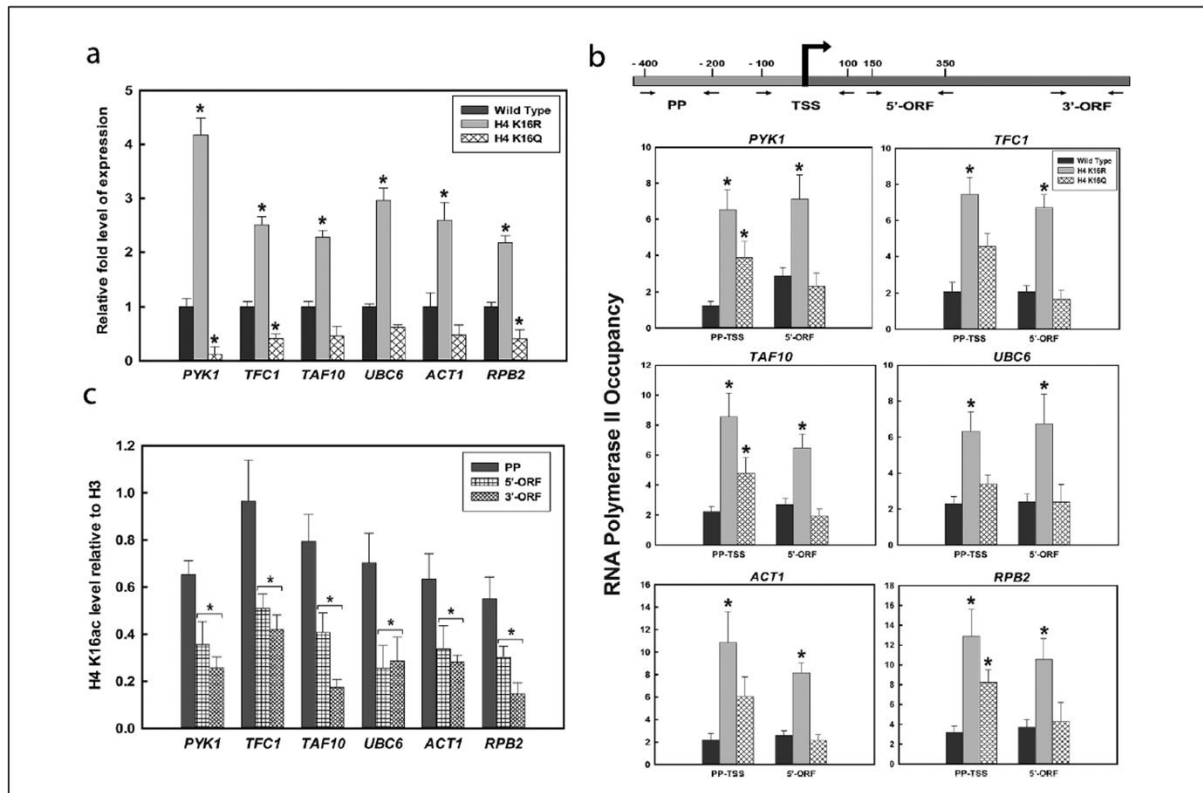


Figure B3. Analyses of gene expression levels, RNAPII occupancy in wild type and mutants and H4K16 acetylation levels during transcription. **A.** RNA was extracted from both wild-type and H4K16 mutant strains, and subsequent RT-qPCR was performed to assess the expression levels of six constitutively active genes: PYK1, TFC1, TAF10, UBC6, ACT1, and RPB2. **B.** ChIP analyses were conducted using (b) RNAPII antibody to examine recruitment at the promoter, transcription start site (PP-TSS), and 5' end (5'-ORF) and **C.** anti-acetyl H4K16 antibody in wild-type cells to evaluate the acetylation status at the promoter-proximal region (PP), 5' end (5'-ORF), and 3' end (3'-ORF) of the consistently transcribing genes mentioned above. The levels of H4K16 acetylation were normalized to the ChIP data of the same regions with anti-H3 antibody and graphically represented. The data represents the mean of three independent experiments with standard error of mean bars. Statistically significant values (*, $P < 0.05$) are indicated. (Taken from Ray et al., *Epigenetics* 2020)

Upon analysing the expression levels of these six constitutively active genes in H4K16 mutants, a noteworthy trend emerged. Deacetylation of H4K16 was found to enhance gene expression, while the presence of H4K16 acetylation led to reduced expression levels (Figure B3 A). This aligns with existing literature that establishes an anticorrelation between H4K16 acetylation and transcriptional activity^{239,243}. Moreover, an examination of RNA Polymerase II (RNAPII) recruitment in both mutants provided additional insights. RNAPII recruitment decreased over the gene body in H4K16Q and remained at higher levels in H4K16R. This indicated that in H4K16Q cells, lacking deacetylation of H4K16, the chromatin landscape did not favour the elongation of RNAPII in the coding region of the genes, resulting in reduced gene expression (Figure B3 B).

Further analyses of the acetylation status of H4K16 at the six constitutively transcribing genes in wild type cells revealed an intriguing pattern. Specifically, the promoter-proximal (PP)

regions of these active genes exhibited H4K16 acetylation, while the 5' and 3' ends of the coding open reading frames (ORFs) were deacetylated at H4K16 (Figure B3 C). This spatial acetylation pattern suggested a nuanced regulation of H4K16 during the transcriptional processes. Collectively, the findings underscore that H4K16 dynamics is important not just for a specific process such as NER but also in shaping the chromatin environment and influencing transcriptional outcomes.

In the course of this study, a fascinating observation emerged: the deacetylation of H4K16 led to higher acetylation levels of H3K56, a crucial H3 core residue (Figure B4). H3K56 acetylation is recognized for its role in promoting chromatin remodeling by SWI/SNF and facilitating histone exchange associated with transcription^{223,225}. This heightened acetylation of H3K56 in presence of H4K16 deacetylation during transcription, suggested an intricate crosstalk between the H4 tail and H3 core modifications, dynamically shaping nuclear processes.

It is worth noting that other studies have revealed a reciprocal relationship: in the DNA damage response pathway, the impact of H3K56 hyperacetylation can be mitigated by reducing H4K16

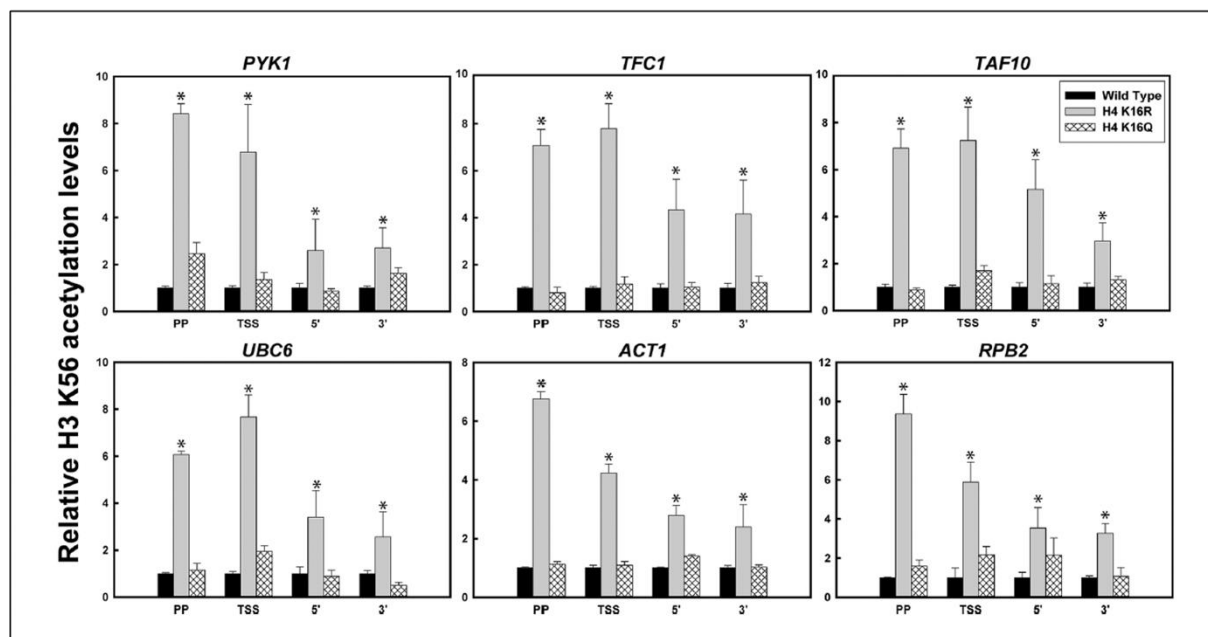


Figure B4. Comparative analyses of H3K56 acetylation levels between wild type and H4K16 mutants in constitutively active genes. ChIP-qPCR analyses were performed using an anti-acetyl H3K56 antibody to examine the acetylation pattern of H3K56 in transcriptionally active loci, including the promoter proximal region (PP), transcription start site (TSS), 5' end (5'-ORF), and 3' end (3'-ORF) of the ORFs of constitutively active genes. The obtained values were normalized to the ChIP data of the corresponding regions with an anti-H3 antibody and were graphically presented to illustrate the levels of H3K56 acetylation in H4K16 mutant cells relative to the wild type. The data represents the mean of three independent experiments with standard error of mean bars. Statistically significant values (*, $P < 0.05$) are indicated. (Taken from Ray et al., *Epigenetics* 2020)

acetylation levels²⁴⁴. Collectively, these intriguing observations indicate the existence of a vital interplay between the deacetylation of H4K16 and H3K56 acetylation in regulating DNA metabolic functions.

Notably, the fact that H4K16 acetylation status which was important for NER and transcription as evidenced from the background studies, could affect H3K56 acetylation, warranted an exploration into the effects of H3K56 acetylation during these processes, constituting a significant aim of the present thesis.

Furthermore, the research outlined in this thesis aims to delve into the complexities of the crosstalk between H3K56 and H4K16 acetylation. Such investigations holds the potential to offer more profound insights into the fundamental mechanisms through which histone modifications interact, ultimately enriching our understanding on finely tuned regulation of chromatin dynamics.

ORIGIN OF THIS WORK

In a previous study, the role of a histone H4-N terminal tail residue, H4K16 in regulating chromatin dynamics during DNA metabolic processes was investigated. H4K16 is a unique residue having a very tight regulation of its own acetylation-deacetylation status. From the studies it was found that a dynamic regulation of H4K16 acetylation and deacetylation is indispensable for efficient Nucleotide Excision Repair as well as regulation of gene expression^{200,245}. Interestingly, during the above studies it was observed that deacetylation of H4K16 could influence the acetylation status of H3K56 residue and effectively promote gene expression²⁴⁵. H3K56 is a unique residue whose acetylation is known to influence the dynamics of nucleosomal DNA unwrapping, a process that critically influences DNA accessibility. As NER and transcription critically depend on DNA accessibility, my work was aimed towards understanding the role of H3K56 acetylation in regulating chromatin dynamics during Nucleotide Excision Repair pathway and transcription. The study also delved into understanding the crosstalk between acetylation of H3K56 with H4K16 deacetylation and how they contribute to generate a chromatin environment suitable for DNA templated processes in *Saccharomyces cerevisiae*.

OBJECTIVES OF THE WORK

- ✓ Generation of structural mutants of histone H3 lysine 56 (H3K56) namely H3K56R and H3K56Q in the wild type background that mimic the constitutively deacetylated and constitutively acetylated states of histone H3K56, respectively.
- ✓ To investigate the NER proficiency of H3K56 mutants compared to wild type.
- ✓ To understand the acetylation status of H3K56 during Nucleotide Excision Repair pathway.
- ✓ To understand the differences in chromatin accessibility and DNA unwrapping/rewrapping dynamics between wild type and H3K56 mutants during a DNA metabolic process such as Nucleotide Excision repair.
- ✓ Gene expression analyses to check for the effect of histone mutation on transcription in wild type and H3K56 mutant strains.
- ✓ ChIP based analyses to understand the crosstalk between H3K56 acetylation and modification of other histone residues known to be important for gene expression.



MATERIALS AND METHODS

INDEX

1. <u>Generation of yeast strains</u>	52-54
1.1 <u>Isolation of yeast shuttle vectors</u>	54-56
1.2 <u>Site-directed mutagenesis</u>	56-59
1.3 <u>Sequencing of mutated vectors</u>	59-60
1.4 <u>High-efficiency transformation of shuttle vectors into yeast</u>	60-64
1.5 <u>High-efficiency transformation of PCR product (linear DNA cassette) in yeast</u>	64-71
2. <u>Yeast genomic DNA isolation</u>	71-72
3. <u>Whole genome NER analyses</u>	72-75
4. <u>UV-sensitivity assays</u>	75-77
5. <u>Plasmid supercoiling assay</u>	77-81
6. <u>Yeast RNA isolation</u>	82-86
7. <u>Chromatin accessibility assay</u>	86-89
8. <u>Chromatin Immunoprecipitation (ChIP)</u>	89-94
9. <u>Transcription inhibition assays</u>	94-97
10. <u>Immunoblot analysis</u>	97-100
11. <u>Real time (qPCR) and data analysis</u>	100-105

1. Generation of yeast strains:

In order to unravel the intricate effects of dynamic acetylation and deacetylation of H3K56 on the control of chromatin structure and its effect on various nuclear processes, two distinct structural mutants of H3K56 were generated. Specifically, the 56th amino acid in H3 globular core domain, which is a lysine residue (H3K56), was substituted with either an arginine residue (H3K56R) or a glutamine residue (H3K56Q). Arginine (R) and glutamine (Q) were chosen as substitutions because they possess side chain structures that are similar to lysine, albeit with subtle differences. Arginine features a slightly longer basic side chain, with a guanidino group at the end, in contrast to the amide group present in lysine. This structural dissimilarity renders arginine incapable of being acetylated, as the guanidino group prevents this modification, unlike lysine. On the other hand, glutamine boasts a shorter polar uncharged side chain, but intriguingly, the acetamide group at the end of glutamine closely resembles the charge and structure of an acetylated lysine to such an extent that it can function as an acetylated lysine both *in vitro*²⁴⁶. The significance of these H3K56R and H3K56Q mutants lies in their ability to mimic the lysine acetylation status without the capacity for regulation, which is present in the wild type (WT) strain. Essentially, the H3K56R mutant replicates a constitutively deacetylated state, while the H3K56Q mutant mimics a constitutively acetylated state of lysine at position 56. This experimental design enabled to explore the precise consequences of locking H3K56 in either an acetylated or deacetylated state and how this modification status, or lack thereof, influences the structure of chromatin and, by extension, diverse processes unfolding within the cellular nucleus such as Nucleotide Excision Repair (NER) and transcription.

As previously described, to create the various mutant strains used in this study, *Saccharomyces cerevisiae* strain WY121, generously provided by Dr. John Wyrick of Washington State University, served as the foundational parent strain.^{200,245,247-249} The genomic Histone H3 (*HHT*) and Histone H4 (*HHF*) genes are exceptionally compact, each spanning approximately 350 base pairs, and they are closely situated on the yeast chromosomes. This proximity makes it impossible to individually modify either of these genes without affecting the other. Both copies of these genes are present on chromosome II (*HHT1-HHF1*) and chromosome XIV (*HHT2-HHF2*), and to create any H3 or H4 mutants, both copies have to be eliminated. Hence, in WY121 the two copies of the histone H3-H4 genes present within the genome are eliminated^{200,245,247-249}. The parent strain harbors a plasmid, designated as pJL001, housing the *HHT2-HHF2* cassette as the sole supplier of H3/H4 histones. Additionally, it encompasses the *URA3* gene, serving as a marker for counter-selection^{200,245,247,249}.

To incorporate the targeted H3K56R and H3K56Q mutations, as well as to establish a wild-type (WT) control, plasmids were utilized. Specifically, the plasmids pEMH129 (H3K56R) and pEMH108 (H3K56Q) were employed, each carrying mutations in the HHT2 gene responsible for histone H3. Additionally, a control WT plasmid (pEMH7), lacking any mutations in HHT2, was used. These plasmids were generously provided by Professor J. D. Boeke from the John Hopkins University School of Medicine, USA^{247,249}. These plasmids, each carrying a set of H3/H4 genes and a marker TRP1 for counter selection, were employed to replace the pJL001 plasmid that provided the original copy of H3-H4^{200,245,247,249}. This process led to the creation of strains bearing either the H3K56R or H3K56Q mutations or no mutations (WT).

Firstly, the desired plasmids bearing point mutations in HHT2 were isolated from bacteria. Following this, the WY121 cells were transformed with these plasmids (see Section 1.4). It was ensured that, when cultured in SC medium devoid of uracil and tryptophan, the yeast cells harbored both pJL001 and pEMH7 plasmids.^{200,245,247,249} To eliminate the pJL001 plasmid from the yeast strains, the transformed cells were cultured in tryptophan-deficient SC medium supplemented with 5'-Fluoroorotic Acid (5'-FOA). (detailed in section 1.4). This compound induces the formation of a toxic product in the uracil synthesis pathway, specifically targeting the URA3 marker on the pJL001 plasmid. Consequently, yeast transformants that were originally URA3+ became URA3-, thereby ensuring that the only histone H3 and H4 source for the three strains would be the pEMH plasmids carrying the TRP1 marker^{200,245,247,249}.

After the selection process, the plasmids were extracted from the yeast cells (see section 1.1). Subsequently, sequencing was conducted (see section 1.3) to verify the presence or absence of mutations in the working strains.

In a comparable fashion, to generate double mutants, the pEMH33 and pEMH35 plasmids, which carry HHT2 point mutations H4K16R and H41K6Q, respectively, underwent site-directed mutagenesis (elaborated in section 1.2). This process was employed to introduce H3K56Q point mutations as well as H3K56R point mutations into the HHT2 cassette encoding histone H3 present in the corresponding plasmids. A sequencing was performed for confirming the presence of the correct mutation i.e. H4K16QH3K56Q, H4K16RH3K56Q, H4K16QH3K56R and H4K16RH3K56R. Following confirmation, the plasmids were introduced by transformation into the parent strain, WY121. Subsequently, shuffling of plasmid was initiated by cultivating the cells in 5'-Fluoroorotic Acid (5'-FOA), facilitating the development of the corresponding double mutant strain²⁴⁹.

The method for generation of $\Delta Sas2$ strain has been described previously²⁴⁵. Similarly, in this investigation, the $Hos2\Delta$ and $Hos2\Delta H3K56Q$ strains were generated employing a homologous recombination-based gene deletion strategy utilizing PCR (explained in detail in section 1.5). The deletion mutant was constructed using the KANMX4 antibiotic resistance module contained in the plasmid pFA6-KANMX4, generously provided by Prof. Shubho Chaudhuri from Bose Institute, Kolkata, India²⁴⁹. The module was strategically introduced to the genomic locus of the gene to be deleted either in wild type or H3K56Q mutant background, resulting in the cells acquiring a $\Delta hos2$ genotype. This genetic alteration endowed the cells with resistance to the antibiotic geneticin (G418) (detailed in section 1.5).

To add a myc tag at the C-terminal end of RTT109 in wild-type cells and cells of H4K16 mutants namely, H4K16R and H4K16Q strains, a similar method relying on a PCR mediated homologous recombination was employed (as detailed in section 1.5). A stretch of linear DNA, housing the KANMX6 module, and flanked by sequences homologous to the immediate upstream as well as downstream regions of the RTT109 gene stop codon, underwent amplification. This amplification process utilized pFA6A-13myc-KANMX6, a shuttle vector as the template (procured from addgene # 39294; <http://n2t.net/addgene:39294> ; RRID: Addgene_39294). Subsequently, this cassette was utilized for transformation of cells of wild type and of H4K16 mutants namely, H4K16R and H4K16Q strains. The transformed strains were cultivated on antibiotic G418 for the selection of positive transformants. Confirmation of RTT109 tagging by myc at the C-terminal end in both wild-type and H4K16 mutants was achieved through western blot²⁴⁹.

1.1 Isolation of yeast shuttle vectors: The isolation of yeast shuttle vectors (pEMH plasmids) was followed based on the technique outlined in Sobanski et al., Biotechnology techniques 1995 with minor modifications²⁵⁰. This technique involves the use of glass beads to disrupt yeast cells and employs reagents commonly utilized in bacterial mini-preps. The outcome is the isolation of plasmid DNA, free from chromosomal impurities, in quantities suitable for direct visualization on agarose gels. It's important to highlight that yeast cells naturally carry a 2 μ plasmid, which is also acquired during plasmid isolation using the glass bead method. Consequently, after extracting plasmid DNA from yeast, it's crucial to transform it into bacteria. This step aids in selecting the shuttle vectors containing antibiotic resistance markers. These

shuttle vectors can then be isolated from bacteria and further modified to create different mutations.

Buffers and solutions:

Solution I	100mM NaCl, 10mM Tris-Cl pH 8.0, 1 mM EDTA, 0.1% SDS
Solution II	0.2N NaOH, 1% Triton X-100
Solution III	3M Sodium acetate pH 4.8
Tris-equilibrated phenol (SRL)	
Acid washed glass beads (SIGMA-425-600µm)	sterilized by autoclaving
Chloroform (Merck)	
Isoamyl alcohol (SRL)	
RNAse A	Used at a stock concentration of 10 mg/ml
Isopropanol (Merck)	
ammonium acetate	Used at a stock concentration of 7.5M
Ethanol	70%
1XTE Buffer	prepared with 1M Tris pH 8.0, 0.5M EDTA

Methodology:

- Here, exponentially growing yeast cells were collected and resuspended in 200µl of **solution I**.
- 200µl of acid-washed glass beads (425-600µm, sterilized by autoclaving) were incorporated and the cells were subjected to agitation at maximum speed (30 seconds x 8 times).
- Following this, solution II (ice-cold) was incorporated into the mixture. After a thorough mixing process by inversion, solution III (ice-cold) was added, followed by a comprehensive mixing of the sample. Subsequently, the mixture was placed on ice, allowing it to incubate for a period of 5 minutes.
- After the cold incubation, an equivalent volume of phenol-chloroform: isoamyl alcohol (25: 24: 1) was introduced. The sample underwent a vortexing procedure lasting 2

minutes, followed by centrifugation at 13,500 rpm for a duration of 15 minutes. The upper aqueous phase was collected and subjected to treatment with 20 µg RNase A for 1 hour at 37°C.

- The phenol: chloroform procedure described above was done again, and the top layer which is the aqueous phase was retrieved after centrifuging the samples for a duration of 15 minutes at 13,500rpm.
- The precipitation of nucleic acids was done with isopropanol at 0.7 volumes and ammonium acetate (7.5M). The samples were subjected to ice incubation for no longer than 10 minutes (to avoid salt contamination) and DNA pellets were retrieved by centrifuging the samples at 13,500 rpm for 15 minutes at RT.
- Pellet of DNA was subsequently subjected to washing with 70% ethanol, dried followed by dissolution in TE buffer.

1.2 Site-directed mutagenesis:

Site-directed mutagenesis (SDM) is a method employed to alter specific sequences of nucleotide at a particular location and allows to study the effect of alteration of specific genes on DNA metabolic functions. In this study, SDM was employed based on the technique outlined in Zheng et al., NAR 2004²⁵¹. 56th lysine of histone H3 encoded in HHT2 cassette of the pEMH plasmid was mutated to either arginine or glutamine.

To perform Site-Directed Mutagenesis (SDM), it is crucial to use a double-stranded plasmid DNA that originates from bacteria. This choice is essential because, after the SDM process, a step involving DpnI digestion is employed to remove the original, unmutated template. The reason for this requirement lies in the mechanism of action of DpnI, an enzyme that selectively digests DNA that is either fully methylated or hemi-methylated. This characteristic is present in the parent plasmid DNA template, which is originally obtained from bacteria. However, it is absent in the amplified plasmid DNA resulting from the SDM process. By using a bacterial origin template, DpnI can effectively target and eliminate the unmutated parent DNA, leaving only the desired mutated DNA for subsequent use.

Primers:

Typically, primers have a length of 45-50 base pairs. The 5' ends of both primers bind to the same region of the template, creating a complementary overlap region. This overlap region, usually spanning 15-20 base pairs, contains the residue to be mutated. The 3' ends of both primers, although non-complementary to each other, are complementary to the template. The non-overlapping segments of the primers are approximately 25-30 base pairs long. This specific approach to primer design serves the dual purpose of minimizing the likelihood of primer dimer formation and enhancing the efficiency of the PCR process. Additionally, the primers are oriented away from each other such that they can amplify the entire plasmid DNA by inverse PCR. In this study SDM was used for the generation of double mutants namely, H4K16QH3K56Q, H4K16RH3K56Q, H4K16QH3K56R, H4K16RH3K56R. The plasmids pEMH33 as well as pEMH35 that bore point mutation H4K16R and H41K6Q in HHT2 gene, respectively were used as template for PCR utilizing the following primers to create subsequent mutation in HHT2 gene coding for histone H3.

The lysine at position 56 of histone H3 in the *HHT2* gene cassette of the pEMH plasmids is represented by AAA. A point mutation was introduced such that AAA was mutated to AGA or CAA representing H3K56R and H3K56Q mutation, respectively.

For H3K56R mutation primers used were as follows:

FP- 5'

GAAGATTCCAAAGATCTACTGAACTGTTGATCAGAAAGTTACCTTTCC -3'

RP- 5'-

CAGTAGATCTTTGGAATCTTCTAATTTCTCTCAAGGCAACAGTACCTG -3'

For H3K56Q mutation primers used were as follows :

FP- 5'-

GAAGATTCCAACAATCTACTGAACTGTTGATCAGAAAGTTACCTTTCC-3'

RP- 5'-

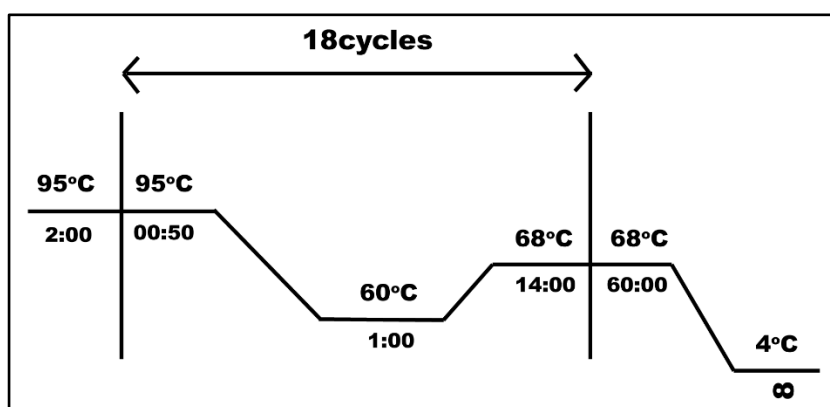
CAGTAGATTGTTGGAATCTTCTAATTTCTCTCAAGGCAACAGTACCTG-3'

PCR conditions

For SDM PCR, a 50 μ l reaction was set-up as follows:

Components	Amount in 50 μ l
10X Pfu Buffer	5 μ l
Forward Primer (10 μ M)	1 μ l
Reverse Primer (10 μ M)	1 μ l
dNTPs (10mM)	1 μ l
plasmid template (50 ng/ μ l)	1 μ l
Pfu turbo (2.5U/ μ l)	1 μ l
dH ₂ O	40 μ l

The PCR reaction cycle is demonstrated below:



DpnI digestion:

- At the end of the SDM PCR reaction 15 μ l of PCR product was aliquoted into a separate tube. The remaining 35 μ l of PCR product was treated with 1 μ l of DpnI endonuclease (10U/ μ l, Agilent) in a thermal cycler at 37°C for 1-2 hours that specifically digests the parental DNA template, rendering mutation containing synthesized DNA.
- 5 μ l of the DpnI untreated and treated PCR products were electrophoresed on a 1% agarose gel and visualized. [Note: If the parent template is successfully digested by DpnI then there will be a slight difference in the band intensity between the DpnI untreated and treated products on the agarose gel].
- In a subsequent step, 10 μ l of the DpnI digested PCR product is transformed into competent XLI-B cells.

- The plasmids were extracted from the transformed bacterial cells, and sequencing was conducted to verify the presence of the intended mutation in the plasmid cassette.

1.3 Sequencing of mutated vectors (pEMH plasmids):

To confirm the presence of the desired mutation in the pEMH plasmids, a sequencing process was conducted. Initially, plasmid DNA was extracted using the QIAprep Spin Miniprep kit according to the manufacturer's instructions. This purified plasmid DNA was then subjected to sequencing using the Big Dye Terminator Automated Sequencer (Applied Biosystems).

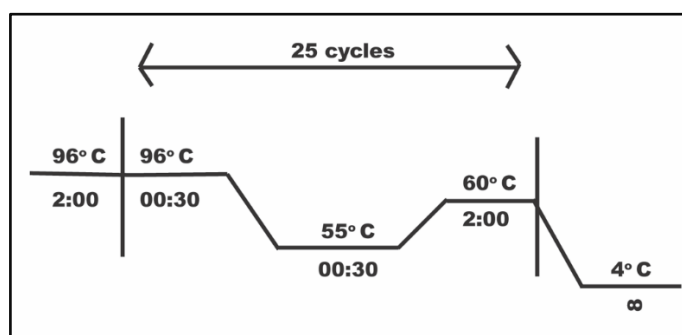
For the sequencing procedure, specific primers were employed, either the M13 forward (M13F) or M13 reverse primers (M13R). It's important to note that pRS414 serves as the vector backbone for the pEMH plasmid. The HHT2-HHF2 cassette is inserted into pRS414 in a specific orientation, which is crucial for the sequencing results. When using the M13F primer, the sequence reads correspond to the HHF2 cassette, whereas when using the M13R primer, the sequence reads pertain to the HHT2 cassette. The choice between M13F and M13R primers is determined by the location of the mutation within the histone H3 or H4 regions.

PCR reaction conditions:

For the sequencing reaction a 10 μ l reaction was set-up as follows:

Components	Volume in 10 μ l
5X Buffer	2 μ l
Primer (M13F/M13R)(3pmole)	1 μ l
Ready reaction (RR) mix	1 μ l
DNA	1 μ l
H ₂ O	5 μ l

The PCR cycle was set-up as follows:



Clean-up of the PCR products for sequencing:

- 10µl of nuclease-free water was added to the PCR products to bring the final volume to 20µl. These samples were then transferred into 0.5 ml microcentrifuge tubes.
- Next, to each sample tube 1µl of 125mM EDTA (pH 8.0) and 2µl of 3M Na-Acetate (pH 5.2) was added. These components were thoroughly mixed.
- To these prepared samples, 50µl of 100% ethanol was added, and they were left in the dark at RT for 20 minutes.
- The samples were then subjected to centrifugation at 13,000 rpm for 30 minutes, followed by a wash step with 70% ethanol at 13,000 rpm for 5 minutes.
- The resulting DNA pellet was air-dried and subsequently dissolved in 12µl of Hi-Di Formamide.
- Following this, the samples were heated at 95°C for 5 minutes, snap-chilled on ice for 5 minutes, and then loaded into an automated sequencer machine for the actual sequencing process.
- Plasmids that confirmed the presence of the desired mutation by sequencing were utilized for transformation into yeast, thereby generating the desired strains.

1.4 High-efficiency transformation of shuttle vectors (pEMH plasmid) into yeast:

Yeast shuttle vectors (pEMH plasmids) bearing point mutations in *HHT2* and/or *HHF2* were introduced into WY121 strains using a high-efficiency transformation protocol based on the method described by Gietz et al. in "Methods in Enzymology" in 2002²⁵², with slight modifications. In this procedure, cells intended for transformation were collected, rinsed with sterile water, and then resuspended in a Transformation Mix comprising PEG, LiAC, SS-Carrier DNA, and plasmid DNA, all without any prior treatment. Subsequently, they were immediately exposed to a heat shock at 42°C.

The efficiency of transforming yeast with foreign DNA is heavily contingent on the duration of this heat shock at 42°C, primarily governing the success of the transformation process. Typically, yeast cells in the logarithmic growth phase are preferred for transformation, as they are more amenable to manipulation compared to stationary phase cells, which necessitate nearly 2 hours of heat shock for efficient transformation. In this study, a standardized approach was established, enabling yeast cells with an optical density

at 600nm of approximately 0.7 ($\sim 1 \times 10^7$ cells per/ml) to be effectively transformed with plasmid DNA using a 25-minute heat shock at 42°C.

Media and reagents:

1M Lithium Acetate (LiOAc) (SRL)	sterilized by autoclaving
50% w/v Polyethylene glycol (PEG-3350) (SIGMA)	Dissolve 1g in 1ml of warm water, incubate, and then make up the volume to 2ml. Vortex vigorously for thorough mixing. Always prepare fresh.
Single stranded herring sperm DNA (35µg/µl)	The carrier DNA is denatured by boiling in water-bath for 10 min and snap-chilled for 2 min in ice immediately before use.
YPD	1% yeast extract, 2% peptone, 2% dextrose
SC^{-URA-TRP}	0.17 % YNB, 0.072% SC ^{-URA-TRP} mix, 2% dextrose, 2% agar, 0.5% (NH ₄) ₂ SO ₄ , pH adjusted to 5.6 with 10N NaOH.
SC^{-TRP} 5FOA	0.67 % YNB, 0.2% SC ^{-URA-TRP} mix, 2% dextrose, 50mg uracil, 0.1% 5FOA volume made up with H ₂ O and filter-sterilized. In a separate conical, 2% agar is mixed separately in appropriate amount of distilled H ₂ O and sterilized by autoclaving. After the agar mix cools down to $\sim 50^\circ\text{C}$, the two solutions are mixed and poured into petri-dishes.
100% DMSO (NEB)- B0515A	

Methodology:

- Yeast strains (WY121) were inoculated into 3ml of yeast extract-peptone-dextrose (YPD) medium and incubated overnight on a rotary shaker at 30°C.
- The next day sufficient inoculum from the 3ml saturated cultures were introduced into 15 ml pre-warmed YPD medium such that starting O.D. was 0.2.
- The culture was then incubated at 30°C for 5 to 6 hours till the O.D₆₀₀ reached ~ 0.7 .
- Once the desired O.D was reached, cells were collected by centrifugation at 3000 rpm for 5 minutes at RT.
- Supernatant was discarded and pellet was resuspended in 1ml sterile water by gentle tapping.
- Cells were centrifuged at 2500 rpm for 5 minutes at RT.
- Supernatant was discarded and pellet was subsequently resuspended in 100 µl of 0.1M LiOAc by gentle tapping followed by a spin for 5 seconds at max speed.

- Supernatant was discarded and the pellet was again resuspended in 100µl 0.1M LiOAc by gentle tapping and split into two 50µl aliquots and cells were collected by spinning at max speed 5 seconds.
- To each 50µl aliquot of cells, 360µl of T mix (containing the pEMH plasmids) was added along with 1%DMSO and the mixture was vortexed vigorously and immediately placed in a water-bath at 42°C for 25 minutes.
- Following heat shock, cells were collected by centrifugation at 8000 rpm for 15 seconds and the supernatant was removed.
- Cells were then resuspended in 500µl sterile water; 200µl aliquots of transformed cells were then spread on SC^{-URA-TRP} and incubated for 2 days at 30°C. At this stage transformed cells bearing both plasmid pJL001 bearing counter-selectable marker URA3 and pEMH plasmid with TRP 1 marker would survive on SC^{-URA-TRP} plates.

Composition of Transformation mix (T mix)

Reagents	No. of transformations
	1
PEG 3350 (50% w/v)	240µl
1M LiOAc	36µl
Boiled SS-herring sperm DNA (35µg/µl)	4.5µl
Plasmid DNA plus sterile water	79.5µl
Total volume	360µl

- **5'-FOA shuffling and generation of yeast strains** - To create yeast strains, both wild type and mutant variants, the transformed colonies from the step above were subsequently grown in SC^{-TRP} medium, which contained an additional component, 5'-FOA (5'-Fluoroorotic acid). The incorporation of 5'-FOA serves a specific purpose in the selection process during the generation of yeast strains. This compound is employed to isolate mutant cells that are incapable of using orotic acid as the primary source for synthesizing the pyrimidine ring, which is an

essential component of DNA and RNA. Generally, strains in which *URA5* and *URA3* genes, each of which plays a role in processing 5'-FOA are active; they can convert 5-FOA into 5-fluorouridine monophosphate. However, the product, fluorodeoxyuridine, which eventually forms as a result of this conversion, happens to be a potent inhibitor of an enzyme called thymidylate synthetase. Thymidylate synthetase is an essential enzyme involved in the production of thymidine, a crucial building block of DNA. When it is inhibited, DNA synthesis is disrupted, rendering the cell unable to replicate its DNA. As a consequence of this inhibition, the fluorodeoxyuridine formed is toxic to the cell, as it hampers DNA replication. Consequently, the *Saccharomyces cerevisiae* strain WY121 containing a functional *URA3* gene encoded by plasmid pJL001, is inevitably driven out in the presence of 5-FOA. This strategic removal of pJL001 plasmid is a key step in the process. Once the pJL001 plasmid is eliminated, only the pEMH plasmids remain. These pEMH plasmids serve as the only histone H3 and H4 source in the yeast strains. Consequently, this process culminates in the generation of both wild type and mutant yeast strains.

Reagents:

SC^{-TRP} 5FOA-	0.67 % YNB, 0.2% SC- ^{URA-TRP} mix, 2% dextrose, 50mg uracil, 0.1% 5FOA volume made up with H ₂ O and filter-sterilized. In a separate conical, 2% agar is mixed separately in appropriate amount of distilled H ₂ O and sterilized by autoclaving. After the agar mix cools down to ~ 50°C, the two solutions are mixed thoroughly and poured into petri-dishes.
--------------------------------	--

Methodology:

- A single colony from the transformed plates in SC-^{URA-TRP} was streaked onto SC-^{TRP} 5FOA along with a control colony of WY121 and incubated for 5-6 days at 30°C. [WY121 was employed as a control to validate the effectiveness of 5-FOA selection. Since WY121 bearing *URA3* marker, cannot survive in the presence of 5-FOA, its inability to persist confirms the efficacy of 5-FOA as a selection agent.]
- After 5-6 days, cells that could shuffle out *URA3* containing plasmids survived. A single colony from these plates was subsequently re-streaked onto SC-^{TRP} as well as SC-^{URA-TRP} plates.

- At this stage cells that have effectively removed the pJL001 plasmid, carrying the URA3 selection marker, would be incapable of thriving on SC-URA-TRP plates. Instead, they would only flourish on SC-TRP plates. This growth pattern serves as confirmation that the plasmids have been successfully shuffled out of the cells.
- To provide additional validation that the colonies growing on SC-TRP plates in the previous step, which carry the plasmids, indeed harbor the intended mutations, these colonies were isolated and subsequently subjected to sequencing. This enabled to verify the creation of either wild type or mutant yeast strains.

1.5 High-efficiency transformation of PCR product (linear DNA cassette) into yeast:

For the purpose of generating deletion mutants and tagged strains a high efficiency transformation method was employed based on the protocol by Gardner et al with modifications²⁵³. Here, gene deletion and tagging are primarily accomplished using PCR based homologous recombination method. A linear DNA cassette is amplified from a plasmid vector, typically encompassing around 40 to 60 base pairs (bp) of flanking sequences with similarity to the target gene and incorporating a selectable marker. When this cassette is introduced into yeast cells it allows homologous recombination. Depending on the homology sequences present in the cassette either gene deletion or tagging can be achieved. The distinguishing feature of these cassettes, often referred to as modules, is the inclusion of a dominant drug resistance marker flanked by the *Ashbya gossypii* TEF promoter and terminator. This design enables the marker to be expressed in *S. cerevisiae* while significantly reducing the risk of random integration into the yeast genome. This reduction in random integration arises from the absence of any homologous sequences between the marker and the yeast genome. Two vectors were employed for gene deletion and tagging, specifically pFA6-KANMX4 and pFA6a-13Myc-KANMX6, respectively. Both KANMX4 and KANMX6 modules carry the eukaryotic antibiotic selection marker G418, also known as Geneticin.

For gene deletion, the KANMX4 module was employed. The PCR primers were designed with specificity to the 3' end of the KANMX4 module. Additionally, these primers included 5' overhangs that contained approximately 40 base pairs of sequences that were homologous to the regions bordering the gene that was slated for deletion. In

the context of C-terminal tagging, the KANMX6 module was amplified using primers that had 5' overhangs designed to match sequences situated at the 5' and 3' regions of the stop codon of the gene to be tagged. When this module is introduced into yeast cells, it allows the replacement of the stop codon of the gene with the KANMX6 module which contains a stop codon within it. This allows for the generation of a fusion protein with a C-terminal tag.

Primers for gene deletion:

For generating deletion mutants, pFA6-KANMX4 was used as a template with the following primers:

FP-

5'TACGTTAAAATCAGGTATCAAGTGAATAACAACACGCAACATGCGTACG
CTGCAGGTCGAC-3'

RP-

5'AAAAAAAAACGGGAGATTAACCGAATAGCAAACCTCTTAACTAATCGA
TGAATTCGAGCTCG- 3'

The PCR product generated with the following primers were then used to transformed wild type and H3K56Q mutants with the high-efficiency transformation protocol (discussed below) to generate *Hos2Δ* and *Hos2ΔH3K56Q* mutants, respectively.

Primers for gene tagging:

For generating tagged strains, pFA6a-13Myc-KANMX6 was used as template for PCR with the following primers:

FP-

5'GCTAAAACCGCGTAAAAAAGCTAAAGCCTTGCCTAAAACTCGGATCCCC
GGGTTAATTAA-3'

RP-

5'ATGCTACATACGTGTACTAAATAATAAATATCAATATGTAGAATTCGAG
CTCGTTTAACTGG-3'

The PCR product generated with the following primers was used to tag the H3K56 HAT, Rtt109 in wild type as well as the H4K16 mutant strains H4K16R and H4K16Q using the high-efficiency transformation protocol (discussed below)

The deletion module, when amplified from pFA6-KANMX4, has an approximate length of 1.5 kilobases (kb), while the tagging module, obtained from pFA6a-13Myc-KANMX6, is approximately 2.3 kb in size. Consequently, even though the subsequent steps for transforming the deletion and tagging modules are the same, there is a crucial divergence in the initial step. For the transformation of deletion modules, yeast strains were typically cultivated in YPD medium. In contrast, when the tagging module was transformed, yeast strains were cultured in double-strength YPD medium containing adenine hemisulfate. Repeated attempts were made to transform the tagging module by culturing cells in YPD medium, but the procedure gave no positive transformants. This inefficiency of transformation is attributed to the larger size of the tagging module, which cannot be readily incorporated into yeast cells through conventional means. In a nutrient-rich environment such as the 2XYPAD medium which contains the amino acid adenine, yeast cells undergo changes in their cell membranes, inducing invaginations that can facilitate the capture of DNA into endocytic vesicles²⁵⁴. Using this procedure, successful introduction of the tagging module into yeast cells could be achieved. The procedure for transformation of PCR products for gene deletion and tagging is mentioned below.

Media and Reagents:

YPD	1% yeast extract, 2% peptone, 2% dextrose.
2XYPAD	For 1 litre, yeast extract 20g, dextrose 40g, peptone 40g, adenine hemisulfate (SRL) 0.08g.
10X TE	For 10ml solution, add 1ml of 1M Tris pH 8 and 200µl of 0.5M EDTA, volume makeup with sterile water.
10X LiOAc	1M LiOAc adjusted to pH 7.5 with acetic acid.
TEL buffer	For 20ml, 2ml 10XTE, 2ml 10X LiOAC, 16ml sterile H ₂ O.
50% w/v Polyethylene glycol (PEG-3350) (SIGMA)	For 2ml, dissolve 1g in 1ml freshly incubate in warm water, once dissolved volume makeup to 2ml, vortex vigorously to mix. Always prepared fresh.

Media and Reagents:

TEL-PEG	For 1.5ml, mix 1.2 ml 50% PEG 3350 with 150 μ l 10X TE and 150 μ l 10X LiOAC.
ss-herring sperm DNA (35μg/μl)	The carrier DNA is denatured by boiling in water-bath for 10 min and snap-chilled for 2 min in ice immediately before use.
100% DMSO (NEB)- B0515A	
0.9% NaCl	
40mg/ml G418 (SIGMA)	prepared by dissolving 40mg of G418 in 1ml of sterile H ₂ O
YPA+G418 plates-	500 μ l of G418 (40mg/ml) added to 100ml of YPA medium, mixed thoroughly and plated.

Methodology:

- Yeast strains were inoculated into 3ml of yeast extract-peptone-dextrose (YPD) or 2XYPAD medium and incubated overnight on a rotary shaker at 30°C.
- The next day sufficient inoculum from the 3ml saturated cultures were introduced into 15 ml pre-warmed YPD or 2XYPAD medium such that starting O.D. was 0.2.
- The culture was then incubated at 30°C for 5 to 6 hours till the O.D₆₀₀ reached ~ 0.7.
- Once the desired O.D was reached, cells were collected by centrifugation at 3000 rpm for 5 minutes at RT.
- Supernatant was discarded and the pellet was resuspended in 1ml 1XTE by gentle tapping.
- Cells were collected by centrifugation at 3000 rpm for 5 minutes (RT) and resuspended in 1ml TEL buffer.
- Cells were centrifuged again 3000 rpm for 5 minutes (RT), cells were collected and resuspended in 200 μ l TEL buffer.
- For each transformation: In a fresh sterile 1.5ml tube, 5 μ l of ss-herring sperm DNA (35 μ g/ μ l) and 30 μ l PCR product (linear DNA cassette) were mixed by gentle tapping. [Prior to use an aliquot of herring sperm DNA was boiled for 10 minutes and snap-chilled on ice for 2-5 minutes]

- To the above mixture, 700µl of TEL-PEG was added and mixed thoroughly by vortexing. Finally, 150µl competent cells were added and mixed by pulse vortexing pulse.
- The tube was immediately incubated at 30°C incubator for 30 minutes with occasional shaking. Following incubation, 70µl DMSO was added to the tube and mixed by inversion.
- The tube was immediately placed for heat shock at 42°C water bath for 1 hour. After heat shock, tube was snap chilled on ice for ~1 minute.
- Cells were centrifuged at RT for 1min at 5000 rpm and supernatant was discarded.
- The pellet was resuspended in 500µl 0.9% NaCl by slow pipetting and the cells were collected by centrifugation at RT for 1 minute at 3000 rpm.
- After discarding the supernatant, cells were washed with 500µl sterile water and collected by centrifugation at 3000 rpm for 1 minute at RT.
- After the water wash cells were finally resuspended in 200µl YPD medium and spread on YPD agar medium followed by incubation for ~ 2 days at 30°C until confluent growth was obtained.
- Subsequently, for positive selection, cells were transferred from YPA plates to antibiotic medium (YPA+G418) by replica plating method and incubated for ~ 3 to 4 days at 30°C.
- In a subsequent step, the positive transformants obtained on YPA+G418 plates were screened for deletion or tagging.

Screening of deletion mutants: For the screening of *Hos2Δ* and *Hos2ΔH3K56Q* strains firstly genomic DNA was isolated using a crude method as described in Gardner et al., 2004²⁵³.

Genomic DNA, obtained through the rapid isolation protocol as mentioned below , was subjected to PCR amplification using two distinct sets of primers. In the first primer pair, the aim was to achieve positive selection. The forward primer was designed to bind to a region located 200 base pairs upstream of the gene's start codon that was targeted for deletion. In contrast, the reverse primer was designed to bind 150-200 base pairs downstream within the KANMX4 module.

Conversely, the second primer pair was employed for a negative selection. While the forward primer remained the same as in the positive selection primer pair, the reverse primer was designed to be complementary to a region +100bp downstream within the gene slated for deletion. Consequently, if the deletion process was successful, a PCR band would be visible with the first primer pair, while no bands would appear when the second primer pair was used. In contrast, when genomic DNA from a wild type strain was subjected to PCR amplification with both primer pairs, a positive band would be obtained with the second primer pair, while no bands would emerge with the first primer pair. This configuration served as the negative control in the experiment, providing a basis for comparison.

Rapid genomic DNA isolation

1. Cultivate the strain to a state of saturation using the preferred growth medium.
2. 1.5 ml of the overnight culture is harvested in a screw-cap microfuge tube
3. Cell pellets are resuspended in 200 µl of TSENT by vigorous vortexing.
4. 0.3 grams of acid-washed glass beads (SIGMA) are added into the resuspended cells, roughly equivalent to 150 µl in volume.
5. 200 µl of phenol/chloroform/IAA is added (25:24:1).
6. The tubes are vigorously vortexed for 5 minutes.
7. The mixture is centrifuged for 5 minutes at maximum speed in a microfuge.
8. Carefully the upper aqueous phase is transferred to a new Eppendorf tube.
9. 10 µl of 3M NaOAc at pH 5.2 and 500 µl of 100% room temperature ethanol is added to precipitate DNA. The solution is mixed by vortexing.
10. The DNA pellet is collected by centrifugation for 5 minutes at maximum speed in a microfuge.
11. The pellet is washed with 500 µl of cold 70% ethanol and centrifuged for 5 minutes at maximum speed in a microfuge.
12. The pellet is allowed to air dry for 5-15 minutes and resuspended in 50 µl of TE.

Primers for screening of *Hos2Δ* mutants:

Positive selection primer pair (Primer pair 1)

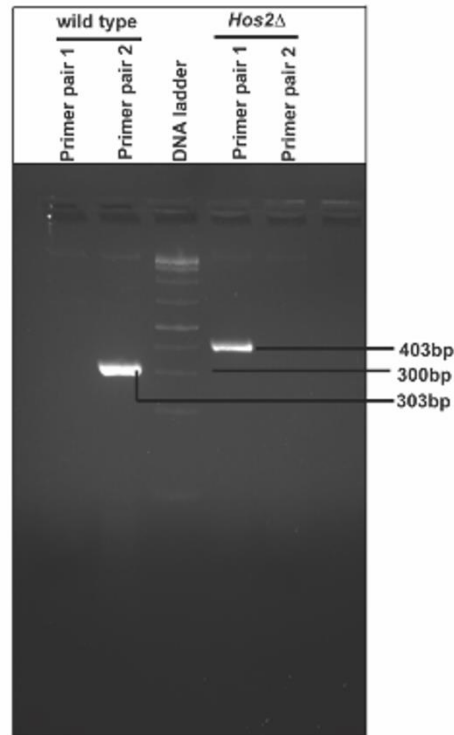
-200Hos2FP-5'-GTAGAATGCCCTGTTTATAC-3'

KANMX4RP- 5'-GGATGTATGGGCTAAATG-3'

Negative selection primer pair (Primer pair 2)

-200Hos2FP-5'-GTAGAATGCCCTGTTTATAC-3'

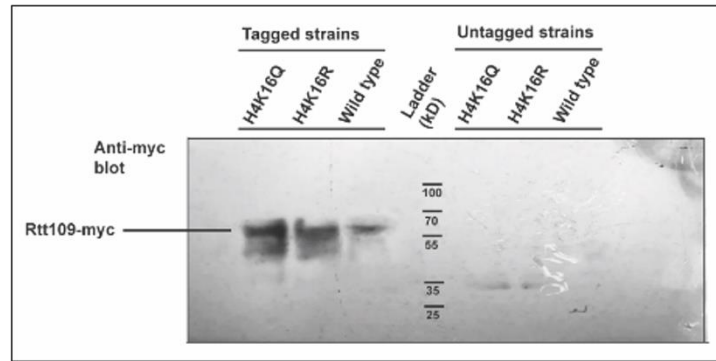
+100Hos2RP-5'-GTTAAAATGATACGATACCC-3'



Representative gel picture for Hos2 deletion screening. The gel image depicts the results of screening for the deletion of the Hos2 gene using two primer pairs, referred to as Primer Pair 1 and Primer Pair 2. Primer Pair 1 involves a forward primer binding to a region located 200 base pairs upstream of the Hos2 gene and 200 base pairs downstream within the KANMX4 module. This binding results in the amplification of a band approximately 403 base pairs in size, indicative of a positive selection. Meanwhile, Primer Pair 2 utilizes a forward primer binding to a region 200 base pairs upstream of the Hos2 gene and 100 base pairs downstream within the Hos2 gene itself, producing a band of approximately 303 base pairs. This band serves as an indicator of negative selection in the screening process.

Screening of tagged strains:

For the screening of tagged strains, cell extracts were prepared from the cultures of positive transformants (see Materials and Methods section 10). Simultaneously, cell extracts were also prepared of the respective untagged strains to serve as control. 20ug of the cell extracts were electrophoresed on 10% SDS-PAGE gel and subjected to western blot analysis (see Materials and Methods section 10) with anti-myc antibody (abcam # ab32) at a dilution of 1:1000. Tagging was confirmed by visualization of a specific band around 65kD in an autoradiographic film. [Note: In this study C-terminal end of Rtt109 was fused to 13 myc tags; Rtt109 is a 50kD protein and each myc tag is ~ 1.2kD thus making the tagged protein ~ 65kD in size)



Screening of Rtt109-myc tagged strains. 10µg whole cell extracts electrophoresed on a 10% SDS-PAGE gel and immunoblotted with anti-myc antibody at a dilution of 1:1000

2. Yeast Genomic DNA isolation:

Buffers and reagents:

10X PBS	1.37M NaCl, 0.027M KCl, 0.1M Na ₂ HPO ₄ , 0.018 M KH ₂ PO ₄
Nuclei isolation buffer (NIB)	17% glycerol, 50mM MOPS pH 8.0, 150mM K-acetate, 2mM MgCl ₂ , 0.5mM spermine, 0.15mM spermidine
10% SDS	
Acid-washed glass beads (SIGMA-425-600µm)	sterilized by autoclaving
1XTE- 1X TE pH 8.0	10mM Tris pH 8.0, 1mM EDTA
RNase A	Used at a stock concentration of 10 mg/ml
Tris-equilibrated phenol (SRL)	
Saturated NaCl	A saturated solution of NaCl was created by vigorously stirring a specific volume of water while adding NaCl until the point at which the NaCl ceased to dissolve in the solution
Chloroform (Merck)	
Na-acetate pH 5.2	Used at a stock concentration of 3M
Isopropanol (Merck)	
Ethanol (Merck)	

Methodology:

- Yeast cell pellets (washed once in 1X PBS) was dissolved in 500-600µl of NIB and transferred to tubes containing 1.5ml of acid-washed glass beads.
- Yeast cells were disrupted by vortexing at max speed (30 seconds x 12 times)
- 500-700µl of 10% SDS was added, and the samples were incubated at 65°C water-bath for 3.5 hours.
- Samples were allowed to cool, followed by the addition of 1 ml 1XTE and 2.5 ml saturated NaCl (to precipitate SDS, proteins and cell debris), mixed by vortexing and incubated for another 10 minutes at 65°C water-bath.
- Samples were allowed to cool and subsequently subjected to centrifugation at 9000 rpm for 20 minutes at RT.
- The supernatant was collected, and an equal volume of isopropanol was added to precipitate nucleic acids. The samples were mixed and incubated for 15 minutes at RT followed by centrifugation at 10,000rpm for 15 minutes at RT.
- DNA pellet was washed with 70% ethanol, partly dried, dissolved in 400-500µl 1XTE and incubated with 40ug RNase A for 4-5 hours at 37 °C to completely remove RNA.
- Phenol: chloroform extraction was done twice followed by extraction with chloroform once. The DNA was precipitated with 2.5 vol of ice-cold ethanol and 0.1 volume of 3M sodium acetate pH 5.2 and incubated overnight at -20 °C.
- The next day the DNA pellet was obtained by centrifugation at 13500 rpm for 15 minutes at RT, the pellet was subsequently washed with 70% ethanol and dissolved in 1XTE.

3. Whole genome NER analyses:

Cyclo-butane pyrimidine dimers (CPDs) are bulky helix distorting DNA lesions formed upon exposure to UV radiation, impeding vital processes such as replication and transcription, potentially leading to mutagenesis and cancer. Two mechanisms mitigate their impact: photolyase-mediated direct repair, triggered by blue-light-activated enzyme photolyase, and nucleotide excision repair (NER) which is also known as dark repair. Higher eukaryotes and placental mammals like us, often UV-exposed due to ozone depletion, lack photolyase and rely solely on NER.

A technique utilizing T4 endonuclease V (T4 Endo V), sourced from T4-infected *E. coli*, aids in quantifying CPD removal via NER^{200,247}. UV-irradiated cells, undergoing repair at various

intervals, are sampled and their genomic DNA extracted. Digesting equal DNA amounts with T4 Endo V and comparing their fragmentation patterns to un-repaired UV-irradiated DNA serves as a gauge. Initially, T4 Endo V cleaves DNA into smaller fragments, reflective of heightened CPD presence post-UV exposure. As NER progresses, CPDs diminish, generating larger fragments. CPDs are formed by intrastrand cross-links of adjacent pyrimidines. As T4 Endo V cleaves 5'-end of a CPD, it consequently triggers the formation of single-strand breaks wherever CPDs are situated on the DNA strand. This implies that conventional electrophoresis of double-stranded DNA digested by T4 Endo V will not yield fragment separation according to their sizes. To achieve the separation of single stranded DNA fragments created by T4 Endonuclease V digestion, electrophoresis must be conducted under denaturing conditions. In this study, conducted in yeast cells housing photolyase, the assay was conducted in the dark to ensure that NER was the sole repair mechanism. In contrast, yeast cells possessing photolyase enable CPD elimination through both photolyase and NER pathways. Through this approach, the impact of NER on CPD removal was precisely deciphered.

Buffers and Enzymes:

10X PBS- 10X T4 Endonuclease Buffer- #M0308S (NEB)	1.37M NaCl, 0.027M KCl, 0.1M Na ₂ HPO ₄ , 0.018 M KH ₂ PO ₄
T4 endonuclease V enzyme-	#M0308S (NEB)- For the assay, the enzyme was diluted to a ratio of 1:25 in 1X T4 Endonuclease V buffer.
Alkaline gel polymerizing buffer	0.5 M NaCl, 0.01M EDTA
Alkaline gel running buffer (4X)	0.05 N NaOH, 0.01M EDTA.
Alkaline sample loading buffer	0.2 M NaOH, 0.004M EDTA, 15% (w/v) Ficoll 400, 0.25% (w/v) Xylene Cyanol and a pinch of bromophenol blue
Alkaline gel neutralization buffer	1M Tris pH 7.6, 1.5M NaCl

Methodology:

- Yeast cells, measuring O.D₆₀₀ of 0.7 (~ 1 x 10⁷ cells/ml) in a 50 ml volume, were collected, washed with PBS at a dilution of 1X, and then exposed to UV-irradiation at a dose of 100J/m² (254nm).

- After subjecting yeast cells to UV-irradiation, the cells were collected, suspended in pre-warmed YPD medium, and provided the opportunity to engage the NER pathway for CPD repair. This repair process was allowed in the dark for different time points (0 min, 30 min, 60 min, 120 min) at 30°C.
- Extraction of genomic DNA was performed from these cells following established procedures as described in Materials and Methods section 2. Following this, a reaction was formulated using equal proportions of genomic DNA extracted at different times of repair, as mentioned below.

Components	Amount in reaction mix
DNA	40 µg
10X Buffer	4 µl
	Volume makeup with H ₂ O to 37µl

- The above reaction mixture was divided equally into two reaction tubes (18µl in each tube). To each of the two tubes either 2µl of water or 2µl of T4 Endonuclease V was added and mixed. The samples with or without T4 Endonuclease V were subsequently incubated for a period of 2 hours at 37°C.
- Following the incubation at 37°C, 1X alkaline sample loading buffer was added to the sample tubes, mixed, and subsequently loaded onto a 1.2% alkaline agarose gel and electrophoresed with alkaline gel running buffer at 25V for 16-17 hours at RT.
- To allow subsequent visualization by EtBr, the alkaline gel was neutralized twice with 200 ml neutralization buffer with gentle agitation at RT for 30 minutes.
- The gel was subsequently stained with EtBr for 5-10 min, washed several times with distilled water and then visualized using Gel-docTM EZ Imager (Bio-Rad).
- The gel was scanned by densitometry using Image LabTM Software to quantify intensities of T4 Endonuclease V digested single stranded DNA fragments for each repair time point.
- An adaptation of the DNA CPD quantification technique as described^{200,247,255} was employed to estimate the approximate CPD count at various repair time points. Signal intensities of the T4 Endo V digested samples were adjusted to the signal intensity of the T4 Endo V mock-treated samples, yielding a ratio indicative of digested DNA content at each repair interval. Subsequently, this ratio was normalized to the ratio of digested DNA content at the 0-minute repair time point. Consequently, this gave the

approximate CPD quantity at each sequential repair time point. The percentage of CPD removal at each repair time point was calculated using the formula $100 - 100 * [-\ln (\text{CPD no. at repair time-point X}) / -\ln (\text{CPD no. at repair timepoint 0})]$ and graphically represented.

4. *UV-sensitivity assay:*

The UV sensitivity assay described previously in Khan et al., DNA Repair 2022²⁵⁶ is a technique employed to evaluate the vulnerability of microorganisms, commonly yeast or bacteria, to ultraviolet (UV) radiation. This assay relies on the fundamental concept that exposure to UV radiation can inflict damage to the DNA of these microorganisms, resulting in mutations, cell mortality, or inhibited growth. Here, cultures of the desired yeast strain are grown to a certain density under normal conditions. A portion of the cultured cells is prepared as a suspension in sterile water. The suspension containing the yeast cells is subjected to UV irradiation at varying doses. The UV-exposed cells and unexposed cells are serially diluted to obtain varying concentrations. These diluted cell suspensions are then either spotted or evenly spread onto suitable growth medium. Both the UV-exposed and non-exposed cultures are subsequently incubated in a dark environment for a specified duration. For assays involving spreading on agar plates, the number of colony-forming units (CFUs) in both the UV-treated and untreated cultures is quantified and compared after the incubation period. This allows the comparison and assessment of the impact of UV radiation on the viability and growth of wild type and mutant yeast strains and to draw conclusions about their sensitivity to UV-induced DNA damage.

Methodology:

- *Spot assay*

- A colony of the suitable yeast strain was introduced into 3 ml of yeast extract-peptone-dextrose (YPD) medium, then left to incubate overnight under agitation at 30°C.
- The next day an appropriate amount of inoculum from the saturated cultures were added to fresh 5ml of YPD medium such that the starting O.D. was 0.2. The culture was then incubated at 30°C for 5 to 6 hours till the O.D₆₀₀ reached ~ 0.7 (~ 0.9×10^7 cells/ml).
- Upon reaching the specified optical density, the cultures were harvested through centrifugation, and then reconstituted in a precise volume of sterile water to achieve a final suspension with a concentration of 0.9×10^7 cells/ml.

- Subsequently, the suspension of yeast approximately 300 μl at a concentration of 0.9×10^7 cells/ml in sterile water was applied onto a sterile watch glass. This setup was then subjected to UV irradiation at 254 nm, with exposure doses ranging from 50 to 150 J/m^2 .
- Post UV treatment, a series of 10-fold dilutions of the cells were prepared. In parallel, another set of 10-fold serial dilutions of cells that had not undergone UV treatment were prepared. Subsequently, these serial dilutions were spotted onto YPD plates. The entire process was carried out in the dark to prevent activation of photolyase mediated repair.
- The plates were wrapped in Al foil to prevent light exposure and carefully incubated in a light-restricted environment at 30°C for 48 to 72 hours. The UV- untreated control plates were incubated for 48 hours while the UV-treated plates were incubated for 72 hours.

-Spread assay:

In the case of the spread assay, Steps 1 to 5 remain consistent with the previously described procedure under spot assay. However, a modification was introduced in the selection of dilutions for plating on YPD plates to facilitate the growth of individual colonies. This modification involved establishing a standardized cell-to-UV dose ratio, wherein the least diluted samples were exposed to higher UV doses, while more diluted samples were utilized for lower UV doses. This strategy is illustrated in the table below:

UV dose	Serial dilution for spreading
No UV	10^{-3}
50 J/m^2	10^{-3}
100 J/m^2	10^{-2}
150 J/m^2	10^{-1}

- Serially diluted samples corresponding to the various UV doses and the control plate without UV exposure were evenly spread in triplicates for each strain. Subsequently, the plates were kept in dark and incubated at 30°C for a period of 48 to 72 hours.
- Post incubation, the colony forming unit numbers were counted and subsequently the dilution factor was considered for the respective UV doses to get the exact number of colony forming units. Subsequently, the CFUs of the UV treated samples were

normalized by the UV untreated control and the ratio was plotted as a percentage of survival.

5. *Plasmid Supercoiling assay*

The plasmid supercoiling assay is a multi-step process which as described in Khan et al., DNA Repair 2022²⁵⁶ was utilized to investigate the change in supercoiling state of plasmid DNA or more precisely the DNA wrapping/unwrapping dynamics when incubated with cell extracts of wild type and mutant yeast strains that been previously subjected to UV-induced NER. The assay was divided into four fundamental steps:

- **Large-Scale Plasmid DNA Preparation:** In this initial phase, a substantial quantity of plasmid DNA is isolated from a significant batch of bacterial culture. The objective is to enrich the population of plasmids in their supercoiled state. This step ensures that there is a substantial amount of supercoiled plasmid DNA available for subsequent analysis.
- **Topoisomerase I Assay standardization for relaxation of plasmids:** The supercoiled plasmid DNA obtained in the previous step is then subjected to the action of an enzyme called Topoisomerase I. This enzyme plays a critical role in facilitating the transition of supercoiled plasmids to their relaxed state. Various concentrations of Topoisomerase I were used to establish a standardized enzyme-to-DNA ratio that ensures the relaxation of the entire population of supercoiled plasmids.
- **Cell extract Preparation:** Following the standardization of the Topoisomerase I assay; cell extracts were prepared from both wild-type and mutant yeast strains previously treated in presence or absence of UV irradiation and permitted to undergo repair in the dark for various time periods. These cell extracts contain the necessary cellular components, including histone proteins, that would be used in the supercoiling experiments.
- **Supercoiling Assay-** In the final step, the previously relaxed plasmid DNA from Step 2 and the cell extracts prepared in Step 3 are combined and incubated together. This incubation allows for protein-DNA interactions to take place. Any alterations or changes in the conformation of the plasmid DNA due to these protein interactions are then visualized through electrophoresis on an agarose gel.

The detailed procedure for each of the steps is described below.

Large-scale isolation of supercoiled plasmid from bacteria:

Buffers and solutions:

Solution I	50mM glucose, 25mM Tris-Cl pH 8.0, EDTA pH 8.0
Solution II	0.2N NaOH, 1% SDS (freshly prepared)
Solution III	3M K-acetate, pH adjusted with glacial acetic acid to 5.5

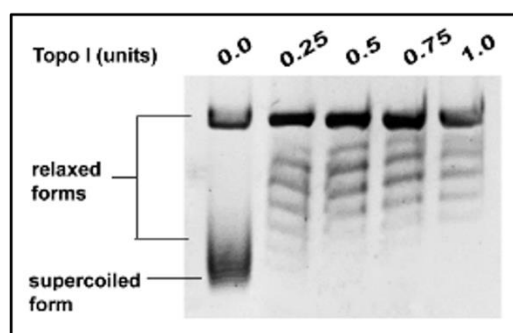
For successful plasmid supercoiling assay, the first step was to maximize the yield of negatively supercoiled plasmids isolated from bacteria which would be further subjected to Topoisomerase I to allow relaxation of the supercoiled plasmid. Hence, a large -scale plasmid isolation method was employed.

- Here, 200ml cells cultured overnight in Luria-broth (LB) with appropriate antibiotic at 37°C were collected in two oakridge tubes by centrifugation at 6000 rpm for 4 minutes at 4 °C.
- In about 10ml of solution I, 20µl RNase A (125µg/µl) was added, mixed and then 4ml of this RNase A containing solution I was added to each of the two oakridge tubes containing bacterial cell pellets.
- Pellets were resuspended in solution I and subsequently 8ml of freshly prepared solution II was then added to the resuspended cells. The tubes were mixed by inversion, followed by the addition of 6ml of solution III. The samples were mixed and incubated on ice for 10-15 minutes. The samples were then subjected to centrifugation at 10,000 rpm for 15 minutes.
- To the supernatant 0.7 volumes of isopropanol was added and centrifuged at 10,000 rpm for 10 minutes. The pellet was then washed with 2ml 70% ethanol by swirling (no centrifugation); supernatant was discarded, and pellet was allowed to dry.
- The dried pellet was then resuspended in 4ml TE and 10µl of this sample was loaded onto 0.8% agarose gel to check for the presence of RNA. To remove remnant RNA 5 µl of RNase A (125 µg/µl) was added to the sample and incubated for 45 minutes at 37 °C.

- Plasmid DNA was extracted using equal volumes of phenol: chloroform and the supernatant was collected by centrifugation at 10,000 rpm for 10 minutes at 4°C. The supernatant was collected and extracted again by chloroform only.
- The supernatant was subsequently transferred to siliconized corex tube (prevents nucleic acids from absorbing to the wall of the tube so that maximum amount of DNA can be collected). The DNA was precipitated with 0.25 volumes of isopropanol and 0.1 volumes of 3M sodium acetate pH 5.2 and collected by centrifugation at 10,000 rpm for 10 minutes at 4°C.
- The DNA pellet was dissolved in 300-500µl TE (no more than 500 µl TE) and 2µl of the undiluted plasmid was electrophoresed onto a 0.8% agarose gel and the remaining plasmid was stored in aliquots at -20°C.

Standardization of Topoisomerase assay for plasmid DNA relaxation:

- 2µg of large-scale plasmid was treated with or without increasing concentrations of Topoisomerase I (5U/µl) (NEB) ranging from 0.25-1.0U at 30°C for 1 h.
- The topoisomerase reaction was terminated by the addition of 10mM EDTA and SDS at a percentage of 0.05% followed by an incubation at 37°C for 30 minutes. The sample volume was made up to 220µl with water.
- The DNA was extracted with equal volumes of phenol: chloroform at 13,500 rpm for 15 minutes (RT). To the supernatant 2.5 volumes of ethanol and 0.1 volumes of 3M sodium acetate was added and the mixture was incubated overnight at -20°C. The next day DNA pellet was obtained after centrifugation and washing with 70% ethanol at 13,500 rpm for 15 minutes at RT. The pellet was dissolved in 1XTE, and the entire sample was electrophoresed in 1X TBE buffer at 25V for 18-20 hours at 4°C in a 1.2% agarose gel without EtBr. The next day, gel was stained with EtBr for 10 minutes at RT followed by washing several times with distilled water and subsequently visualized using Gel-docTM EZ Imager (Bio-Rad).



Standardization of Topoisomerase I assay with 2ug of plasmid DNA and increasing concentrations of Topoisomerase I

Cell extract preparation for supercoiling assay:

Buffers and solutions:

Yeast Lysis buffer	100mM Hepes-KOH pH 7.9, 245mM KCl, 1mM EDTA, 2.5mM DTT, 1mg/ml PIC (SRE0055), 1mM PMSF
Yeast Dialysis buffer	20mM Hepes-KOH pH 7.9, 50mM KCl, 0.5mM EDTA, 1mM DTT, Glycerol 20% (v/v), 0.1mM PMSF

To prepare cell extracts for the supercoiling assay, the following protocol was followed, based on Li et al., 2016²⁵⁷, with slight modifications:

- Cells from wild-type and mutant yeast strains, at their mid-logarithmic phase with an OD₆₀₀ of around 0.7 (~1 x 10⁷ cells/ml) underwent UV irradiation at a dose of 100J/m². Subsequently, they were allowed to undergo repair in the absence of light for different durations. Following this, the cells were collected and washed with ice-cold distilled H₂O.
- The cell pellet was re-suspended in 200µl of yeast lysis buffer containing protease inhibitors. To allow cell lysis, 700µl of acid-washed glass beads were added to the mixture. The samples were then vigorously vortexed at maximum speed for a period of 30 seconds. This step was repeated 7-8 times, with a 1-minute resting period on ice between cycles.
- After the lysis steps, the samples were centrifuged at 4°C for 3 minutes at 2500 g. This step helped to separate cellular debris and intact cells from the lysate. The resulting supernatant, which contained the soluble cell components, was carefully

transferred to a fresh microfuge tube. This supernatant was further centrifuged at 4°C for 10 minutes at 10,000 rpm to remove any debris.

- The cleared supernatant was then subjected to dialysis for 4 hours at 4°C using yeast dialysis buffer. After dialysis, the protein concentration in the cell extract was determined using Bradford Reagent. The remaining cell extract was divided into aliquots and stored at -20°C.

Supercoiling assay:

For the supercoiling assay, a 30µl reaction was set up in a microfuge tube, which involved the following steps:

- Initially, negatively supercoiled plasmid DNA was incubated at 30°C in the presence of Topoisomerase I for 1 hour. [Note: Here 2µg of plasmid DNA was incubated with 1U of Topoisomerase I as standardized in a previous step].
- After the 1 hour incubation, 20µg cell extracts prepared as described in a previous section were introduced into the reaction mixture. The assembly reaction was allowed to continue at 30°C for an additional 1.5 hours. This phase of the assay allowed for protein-DNA interactions to occur.
- To halt the supercoiling reaction, 10mM EDTA and 0.05% SDS were added to the mixture, and it was incubated at 37°C for 30 minutes. Following the termination step, the samples underwent a 30µg RNase A treatment at 37°C for 1 hour. Subsequently, Proteinase K treatment was carried out at 55°C for 1 hour in the presence of 0.1% SDS. [Note: Proteinase K activity is enhanced in the presence of SDS]. The sample volume was made up to ~ 220µl with water.
- In the next step, DNA extraction involved equal volumes of phenol and chloroform and subsequent centrifugation at 13,500 rpm for 15 minutes at RT. To the resulting supernatant, 2.5 volumes of ethanol and 0.1 volumes of 3M sodium acetate were added, and the mixture underwent an overnight incubation at -20°C to precipitate the DNA.
- After centrifugation, washing with 70% ethanol at 13,500 rpm for 15 minutes at RT yielded a DNA pellet. This pellet was re-suspended in 1X TE buffer, and the entire sample was electrophoresed in a 1.2% agarose gel without EtBr using 1X TBE buffer at 25V for 18-20 hour at 4°C. The following day, the gel was stained with EtBr for 10 minutes at RT, washed with distilled water multiple times, and subsequently visualized using the Gel-doc™ EZ Imager (Bio-Rad).

6. *Yeast RNA isolation:*

TRIzol reagent, a monophasic solution combining of guanidine isothiocyanate and phenol, serves a crucial role in yeast cell wall lysis. In this process, TRIzol preserves RNA integrity while simultaneously disrupting cells and dissolving cellular components. The nomenclature of the reagent reflects its methodology, as it facilitates the isolation of RNA, DNA, and proteins into distinct phases. Upon adding chloroform and subsequent centrifugation, the facile partitioning of DNA, RNA, and proteins occurs, resembling the process of a phenol:chloroform extraction. Through TRIzol chloroform extraction, proteins are extracted into the organic phase, DNA resides in the interface, and RNA is found in the aqueous phase. To recover RNA from the aqueous phase, precipitation with isopropanol can be done with ease.

Reagents and solutions:

Liquid N₂	
TRIzol Reagent (Invitrogen)	
Chloroform (Merck)	
DEPC treated water	0.1 % DEPC (SRL) stirred in water for 5h-overnight and double autoclaved.
DEPC treated glass beads	Acid-washed glass beads (SIGMA) soaked in DEPC treated water overnight, dried, and double autoclaved.
75% Ethanol	prepared with DEPC treated water.
Isopropanol (Merck)	
Gel loading dye	prepared with double autoclaved glycerol (70%), DEPC treated water (30%) and a pinch of bromophenol blue.
1% agarose gel	prepared with DEPC treated water

Reagents and solutions:

DNase I enzyme (Thermo Scientific) 1U/ μ l	
EDTA (Thermo Scientific)	50mM
Revert-aid Reverse Transcriptase enzyme (Thermo Scientific)	
Oligo (dT)₁₈	
dNTP	(10mM stock)

Methodology:

- 50 ml of mid-log phase yeast cells with an O.D₆₀₀ of ~ 0.7 ($\sim 1 \times 10^7$ cells/ml) were harvested by centrifugation at 4500 rpm for 2 minute at 4 °C.
- Cell pellets were rapidly frozen in liquid nitrogen. This was followed by the addition of 1 ml of TRIzol reagent to the frozen cell pellets, and the cells were thawed on ice.
- The cells after resuspension in TRIzol were moved to 1.5 ml Eppendorf tubes containing 200 μ l DEPC treated- glass beads (acid-washed) (425-600 μ m). The yeast cell wall was disrupted by vortexing (30 seconds X 12times) with a rest of 1 minute on ice between each cycle.
- The disrupted cells were centrifuged at 12,000 rpm for 15 minutes at 4 °C to pellet debris. To the supernatant, 200 μ l of chloroform was added and mixed vigorously by shaking (no vortexing) and incubated at RT for 5 minutes.
- After the 5-minute incubation in presence of chloroform, the samples were subjected to centrifugation at 13,500 rpm for 15 minute at 4 °C, and the aqueous phase containing RNA was collected.
- To this, 500 μ l of isopropanol (per ml of TRIzol) was added and mixed by inversion followed by incubation on ice for 5 minutes.
- RNA pellet was precipitated after a centrifugation step at 13500 rpm for 15 minutes at 4 °C. The RNA pellet was washed twice with 1 ml of 75% Ethanol (made with DEPC treated water) at 13500 rpm for 5 minutes at 4 °C. [**Note:** Washing was done by placing the tube 180° relative to its position in the first spin].

- The pellet was allowed to air-dry for 5-10 minutes (care should be taken to not over-dry the pellet as it drastically reduces RNA solubility). The dried pellet was then dissolved in DEPC treated water and incubated at 65 °C for 10-20 minutes to dissolve the RNA pellet (occasional gentle tapping or pipetting was done to allow proper dissolution of the RNA pellet). 2µl of the isolated RNA was electrophoresed on a 1% agarose gel to visualize RNA bands.
- To eliminate DNA contamination, the extracted RNA samples were subsequently subjected to DNase I treatment. A 50 µl reaction was set-up as illustrated in the table below.

Component	Amount in 50µl reaction
RNA	Up to 20 µg
10X DNase I Buffer	5µl
DNase I enzyme	5µl
RNase-free H ₂ O	Up to 50µl

- The DNase I reaction was conducted at a temperature of 37°C for a duration of 1 hour. To terminate the reaction, 5mM EDTA was introduced, and the mixture was then incubated at 65°C for 5 minutes.
- After the stop, appropriate amount of DEPC- treated water was added to the tubes such that the final volume of sample in each tube was made up to 200µl.
- To the above samples equal volumes of TRIzol: chloroform (1:1) was added. The solution was mixed vigorously by shaking and centrifuged at 13,500 rpm for 15 minutes at 4 °C to recover RNA from the aqueous phase.
- To precipitate RNA, 0.75 volumes (~300µl) of isopropanol was added, samples were mixed by inversion and allowed to stand on ice for 5 minutes followed by centrifugation.
- Post centrifugation at 13500 rpm for 15 minutes at 4 °C, the pellet was washed twice with 75% ethanol by centrifugation at 13,500 rpm for 10 minutes at 4 °C [Note: Washing was done by placing the tube 180° relative to its position in the first spin].
- The air-dried RNA pellet was subsequently dissolved in ~ 30µl of DEPC- treated water and incubated at 65 °C for 10-20 minutes to dissolve the RNA pellet.
- The concentration of isolated total RNA was checked using a spectrophotometer using the following formula:

$$\text{RNA concentration } (\mu\text{g}/\mu\text{l}) = [\text{O.D}_{260} * 40(\mu\text{g}/\text{ml} * \text{dilution factor})]/1000$$

- The total RNA that was obtained was reverse transcribed using the RevertAid Reverse Transcriptase enzyme. In each PCR tube the following reaction was set-up:

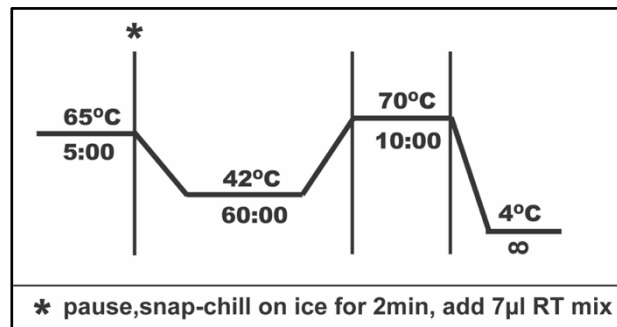
Component	Amount in 13 μ l
RNA	Up to 5 μ g
Oligo dT	1 μ l
Nuclease free H ₂ O	Up to 13 μ l

- The PCR tubes containing the components mentioned in the table above were incubated at 65 °C for 5 minutes in a thermal cycler and quickly snap-chilled on ice for 2 minutes. [Note: Same amount of a particular RNA sample was added to two separate PCR tubes, one to serve for the Reverse transcriptase reaction (+RT) and the other to serve as a control without any Reverse Transcriptase (-RT)].
- Post ice incubation, 7 μ l of Reverse Transcriptase (+RT) mix (described in the table below) was added to each tube. [Note: Simultaneously, to serve as the control (-RT), RNA containing PCR tubes were mixed with nuclease free H₂O instead of Reverse Transcriptase enzyme]. Both the +RT and -RT tubes were mixed gently and incubated at 42 °C for 60 minutes in a thermal cycler.

Reverse Transcriptase mix

Component	Amount in 7 μ l
RevertAid Reverse Transcriptase	1 μ l
dNTP	2 μ l
5X RevertAid Reverse Transcriptase buffer	4 μ l

- The reaction was terminated by incubating the mixture at 72 °C for 10 minutes.
- The resulting first strand cDNA obtained was used for gene expression studies.
- The Reverse transcriptase reaction is illustrated below.



7. *Chromatin accessibility assay:*

Micrococcal nuclease (MNase) is an endonuclease extensively employed to evaluate the degree of chromatin compaction within living cells. Its small size endows MNase with the capacity to infiltrate densely packed chromatin regions and cleave DNA segments devoid of protective histone proteins. This cleavage action yields DNA fragments that occur in multiples of nucleosome sizes. Each nucleosome, composed of roughly 150 base pairs of DNA coiled around a core histone octamer, safeguards this section of DNA from MNase's enzymatic shearing, exclusively permitting the cleavage of linker DNA. Consequently, digestion of chromatin by MNase gives an idea of the extent of nucleosomal DNA accessibility and hence the overall accessibility of chromatin architecture. Regions highly amenable to MNase yield predominantly mononucleosomal DNA fragments (~150 base pairs), with dinucleosomal (~300 base pairs), trinucleosomal (~450 base pairs), tetranucleosomal (~600 base pairs), and so forth, fragments appearing proportionally as chromatin accessibility diminishes. The extent of MNase digestion can be controlled by adjusting the reaction conditions, including the enzyme concentration and digestion time. Keeping the digestion time constant, chromatin can be exposed to different MNase concentrations, producing a spectrum of nucleosomal fractions. Alternatively, a fixed MNase concentration can be applied to chromatin samples at various digestion time points to gauge accessibility. Nonetheless, it is crucial to standardize the optimal MNase digestion conditions for a given quantity of nuclear chromatin extract. This standardization is necessary because with mild digestion conditions, MNase will preferentially cleave linker DNA regions, leaving the nucleosomal DNA intact. However, as the digestion progresses or under more stringent conditions, MNase can start to digest the nucleosomal DNA as well, generating sub-nucleosomal fractions.

A digestion time of 10 minutes was established as optimal for treating nuclear chromatin derived from yeast cells with an O.D₆₀₀ of ~0.8 (~1x 10⁷ cells/ml). Keeping the time constant MNase enzyme concentrations were varied (ranging from 5 to 15 units) to assess chromatin accessibility. To facilitate the penetration of MNase it is essential to disrupt yeast cell walls.

This is achieved through enzymatic digestion with Zymolyase (extracted from *Arthrobacter Luteus*). Enzymatic digestion with Zymolyase is often preferred over mechanical shearing as it specifically targets the components of the cell wall without affecting the integrity of other cellular structures. This selectivity ensures that the cell wall is disrupted while leaving the nuclear and cytoplasmic components intact, which is crucial for the accuracy of a MNase assay. However, it is crucial to control the incubation time and enzyme concentration as over-sphaeroplasting of yeast cells often allow MNase to completely digest the DNA resulting in inaccurate representation of chromatin organization within the cell. For the current study, a 25 min incubation time at RT was optimized for effective sphaeroplasting using yeast cells with an O.D₆₀₀ of ~0.8 (~1x 10⁷ cells/ml).

Reagents and buffers:

1M Sorbitol	(prepared from 2M stock)
YLE Buffer	Zymolyase enzyme from <i>Arthrobacter luteus</i> (MP Biomedicals) at a concentration of 10 mg/ml in 1 M Sorbitol along with β-ME at a concentration of 5mM.
Sphaeroplast Digestion Buffer (SDB)	1M Sorbitol, 50mM NaCl, 10mM Tris-Cl pH 7.5, 5mM MgCl ₂ , 1mM CaCl ₂ , 1mM β-mercaptoethanol, 0.5mM Spermidine, 0.075% NP-40
MNase- (Worthington, USA, LS004798)	25U/μl
Stop solution (5% SDS, 250mM EDTA)	freshly prepared by adding equal volumes of 10% SDS and 500mM EDTA stocks. Prior to use the solution is kept at 37 °C to allow proper dissolution of SDS.
Proteinase K (Thermo Scientific)	
RNase A	(10mg/ml)
7.5M ammonium acetate	
Isopropanol (Merck)	
70% ethanol	

Methodology:

- 100ml of exponentially growing yeast cells with an O.D₆₀₀ of ~0.8 (~1x 10⁷ cells/ml) were harvested by centrifugation at 4500 rpm for 2 minutes at RT. The cell pellets were washed twice with sterile water and collected by centrifugation at 4500 rpm for 2 minutes at RT.
- The cell pellets were quickly resuspended in YLE buffer to digest the cell wall. This digestion step was carried out for 25 minutes at RT to generate sphaeroplasts. Subsequently, the cells were centrifuged at 13,500 rpm for 5 minutes at RT to remove YLE buffer.
- To eliminate any remnants of YLE buffer, in a subsequent step the cells were washed twice with 1ml of 1M sorbitol (no resuspension of cells) at 13,500 rpm for 2 minutes at RT. [**Note:** During the second wash the tube was rotated 180° relative to its position during the first spin].
- Following the wash step, sphaeroplasts were resuspended in 1.3ml of SDB and 200µl aliquots of this suspension were transferred to 1.5ml Eppendorf tubes containing 0, 5, 10, 15 units of MNase (25U/µl). The samples were mixed quickly by inversion and immediately incubated at 37 °C water-bath for 10 minutes to allow enzymatic digestion.
- The MNase reaction was terminated by adding 0.1 volumes of stop solution and mixed vigorously by vortexing. [**Note:** At this step, the digests should turn from opaque sphaeroplasts to clear lysates].
- The lysates were subsequently subjected to 1.5µl of Proteinase K overnight at 55 °C water-bath.
- Post-proteinase K treatment equal volumes of phenol: chloroform was added, and the supernatant (aqueous phase) was collected after centrifugation at 13500 rpm for 15 minutes at RT.
- To the supernatant, 4µl of RNase A was added and the sample was incubated at 37°C water-bath for 4 hours.
- The sample was subjected to phenol: chloroform extraction again and the supernatant was collected. To precipitate DNA, to the supernatant 40µl of 7.5M ammonium acetate and 260µl of isopropanol was added, mixed and the sample was centrifuged at 13500 rpm for 15 minutes at 4 °C. [**Note:** At this step, a translucent DNA pellet is obtained].

- The DNA pellet was washed with 1ml of 70% ethanol and centrifuged at 13500 rpm for 10 minutes at 4 °C. [**Note:** At this step, DNA pellet turns white].
- The pellet is subsequently dried and dissolved in 25µl TE overnight. The MNase digested fragments are subsequently resolved in a 1.2% agarose gel and visualized using Gel-doc[™] EZ Imager (Bio-Rad).
- To analyze chromatin accessibility the gels were scanned densitometrically using Image J software.

8. Chromatin Immunoprecipitation (ChIP):

Chromatin Immunoprecipitation (ChIP) is technique used to investigate the interactions between proteins and specific regions of DNA within a cell or tissue. The principle behind ChIP is to selectively enrich and isolate DNA fragments associated with a particular protein of interest, to facilitate the determination of where that protein binds to the genome. The first step in ChIP involves cross-linking proteins to DNA within the cell or tissue of interest. It helps to preserve the native protein-DNA associations and prevents them from being disrupted during subsequent steps. This is typically achieved by incubation of cells with a cross-linking agent (e.g., formaldehyde) for a defined period, which forms covalent bonds between proteins and DNA, effectively "freezing" the protein-DNA interactions in place. Maintaining standard fixation time in presence of formaldehyde is crucial to avoid over-fixing as this could lead to diminished immunoprecipitation and DNA recovery in the subsequent steps. Hence, post cross-linking the cells are thoroughly washed in presence of appropriate buffer to remove excess formaldehyde. Subsequently, the cross-linked cells or tissues are then lysed to break open the cells and release the chromatin, which consists of DNA and associated proteins. This step is essential for accessing the chromatin and making it available for immunoprecipitation. Subsequently, the chromatin is enzymatically or mechanically sheared into smaller fragments, typically not more than 200-500 base pairs in length. This step ensures that the DNA fragments are small enough to be effectively immunoprecipitated. Furthermore, this process helps to selectively immuno-precipitate specific protein-DNA complexes of interest. This selectivity is vital because when DNA fragment sizes exceed 500 bp, there is an elevated risk of capturing proteins located farther from the targeted DNA region. This can lead to inaccurate results by including unintended protein interactions. To immuno-precipitate protein-DNA complexes, antibodies specific to the protein of interest are added to the chromatin mixture. Prior to the addition of antibodies, a pre-clearing step is included to eliminate non-specific protein-DNA

interactions that can occur between chromatin fragments and the Protein A Sepharose beads used for immunoprecipitation. These non-specific interactions can lead to high background noise in ChIP data. After the immunoprecipitation step, the beads containing these complexes are typically collected by centrifugation. The pellet containing the immunoprecipitated material is gently resuspended in a low-salt buffer or washing buffer. This buffer is designed to maintain the stability of the complexes while facilitating the removal of unbound or non-specifically bound material. The supernatant, containing unbound contaminants, is discarded. This is followed by washing with high-salt buffers to further reduce non-specific interactions. After the completion of washing steps, the beads containing the purified, specific protein-DNA complexes are subjected to a final wash with a buffer compatible with subsequent downstream applications. Subsequently, in the elution step protein-DNA complexes are recovered from beads and subjected to a cross-linking reversal followed by Proteinase K digestion. This step is essential because it allows for the separation of DNA from the bound proteins, enabling downstream analysis of the isolated DNA fragments. The DNA fragments are then extracted and purified and represents the specific genomic regions bound by the protein of interest. The isolated DNA is then subsequently analyzed using quantitative polymerase chain reaction (qPCR) to determine the precise DNA sequences associated with the target protein. Primers used for PCR are generally used to amplify 200-300bp of DNA as larger amplicon sizes can result in the amplification of DNA regions bound by nucleosomes adjacent to the region of interest. This occurs because each nucleosome typically encompasses only approximately 150 base pairs of DNA.

Reagents, buffers, and enzymes:

1X TE pH 8.0	10mM Tris pH 8.0, 1mM EDTA
RNase A	10mg/ml
IP elution solution	1% SDS, 0.1 M NaHCO ₃
NaCl	4M
Proteinase K (Thermo Scientific)	
3M sodium acetate pH 5.2	
Glycogen (Thermo Scientific)	
Ethanol (Merck)	

Reagents, buffers, and enzymes:

37% formaldehyde	
1M Sorbitol buffer	prepared from 2M stock
YLE Buffer	Zymolyase enzyme from <i>Arthrobacter luteus</i> (MP Biomedicals) at a concentration of 10 mg/ml in 1 M Sorbitol along with β -ME at a concentration of 5mM
Sphaeroplast Digestion Buffer (SDB)	1M Sorbitol, 50mM NaCl, 10mM Tris-Cl pH 7.5, 5mM MgCl ₂ , 1mM CaCl ₂ , 1mM β -mercaptoethanol, 0.5mM Spermidine, 0.075% NP-40
MNase (Worthington, USA, LS004798)	25U/ μ l
Stop solution	5% SDS, 250mM EDTA
PMSF	250mM
Pre-treated protein A agarose beads	50% slurry pre-adsorbed with 0.1% BSA and 100 μ g herring sperm DNA.
Lysis Buffer	50 mM HEPES (pH 7.5), 140 mM NaCl, 1mM EDTA, 1% Triton X-100, 1mM PMSF, 0.1% DOC
Wash Buffer I	50 mM HEPES (pH 7.5), 500 mM NaCl, 1mM EDTA, 1% Triton X-100, 1mM PMSF, 0.1% DOC
Wash Buffer II	10 mM Tris pH 8.0, 250mM LiCl, 1mM EDTA, 0.5% NP-40, 0.5% DOC

Methodology:

- Yeast cells in logarithmic growth phase, exhibiting an OD₆₀₀ of approximately 0.8-0.9 (equivalent to around 1.2×10^7 cells/ml), underwent initial cross-linking with 1% formaldehyde for a duration of 30 minutes at RT. [**Note:** 50ml cells were collected for each IP]
- These cross-linked cells were then harvested and washed with 1M sorbitol wash buffer. The washed cells were subsequently resuspended in 650 μ l of SDB (per IP)
- To achieve DNA fragments ranging from 200-500bp, 600 μ l of SDB resuspended cells from Step 2 were then digested with 75 units of MNase for 15 minutes at 37°C.

- The reaction was then terminated with 0.1 volumes of Stop solution and vortexed vigorously.
- The digestion reaction was diluted with sterile water to a volume containing <0.3% SDS (~ 1.2ml per IP) and 1mM PMSF was added to it. The total volume obtained was the Whole Chromatin Extract (WCE) which would be used in the subsequent steps for immunoprecipitation with a particular antibody. The components and their respective amounts added to the SDB resuspended cells in Step 3-5 are illustrated in the order of addition in the table below:

Components	Amount in 600µl of SDB resuspended cells
MNase (25U/µl)	3µl
Stop solution	60µl
PMSF	4.8µl
H ₂ O	540µl
Total volume	~1.2ml

- Prior to immunoprecipitation, to the WCE 70µl of pre-treated beads (see section 8.1) per IP (50% slurry) was added and the mixture was rotated 4-5 hours at 4°C.
- The beads were subsequently discarded and the pre-cleared WCE was collected by centrifugation at 6000 rpm for 2 min at 4°C. A 1% portion of the pre-cleared WCE was reserved and stored at -20°C as Input DNA to serve as control.
- The remaining WCE was divided into equal aliquots to facilitate individual immunoprecipitation (IP) reactions.
- Each IP reaction was incubated with 2 – 3 µg of antibody overnight at 4°C.
- After the overnight incubation, the immunocomplexes were subjected to precipitation using 20µl pre-treated Protein A-Sepharose beads as described in Section 6.1.
- The precipitation was allowed to occur for a duration of 1.5-2 hours at 4°C.
- Immunocomplex-bound beads were collected by centrifugation at 6000 rpm for 2 minutes at 4°C.
- The beads were subsequently washed twice with Lysis Buffer, followed by washing twice with Wash Buffer I and Wash Buffer II for 5-10 minutes with agitation at 4°C.
- The beads were finally washed once with 1X TE pH 8.0 and collected by centrifugation at 6000 rpm for 2 minutes at 4°C. The beads were subsequently suspended in 100µl 1X

TE to which 3µl of RNase A was added and the mixture was incubated at 37°C for 45 minutes.

- Following incubation, 1ml 1X TE was added to each IP sample, mixed, and the beads collected by centrifugation at 6000 rpm for 2 min at 4°C.
- For elution of the immunocomplexes from the beads, 250µl of IP elution solution was added, and the samples were incubated at RT for 45-60 minutes with occasional vortexing. 250µl of the eluted samples was collected in a fresh tube by spinning the beads at 6000 rpm for 2 minutes at RT. 250µl of fresh IP elution solution was again added to the tubes containing the beads and the process was repeated. The two eluted samples were combined giving a final volume of 500µl. To the input samples that were kept aside at - 20°C in step 7, 500µl of sterile water was added and mixed.
- Both eluted IP samples and input samples were subjected to reverse cross-linking by the addition of 25µl of 4M NaCl and incubation overnight at 65°C water-bath.
- Following this step, samples were allowed to cool and 1.5µl of Proteinase K was added, and the samples were incubated at 55°C water-bath for 3-4 hours.
- Subsequently, samples were allowed to cool to RT and DNA was extracted with equal volumes of phenol: chloroform.
- The phenol: chloroform added samples were vortexed vigorously and centrifuged at 13500 rpm for 15 minutes at RT.
- The upper aqueous phase was collected to a fresh tube to which 1µl glycogen, 0.1 volumes of 3M Sodium acetate pH 5.2 and 3 volumes of absolute ethanol was added. The samples were mixed and incubated overnight at - 20°C.
- The DNA pellet was collected by centrifugation at 13500 rpm for 15 minutes at 4°C. The supernatant was discarded, and the pellet was washed with 70% ethanol followed by centrifugation at 13500 rpm for 10 minutes at 4°C.
- To the dried DNA pellet, 25µl of 1X TE was added and samples were analyzed by qPCR.

8.1 Pre-treatment of beads:

- a) Take 750 µl of Protein A agarose beads in a 2 ml Eppendorf tube.
- b) Centrifuge the tube at 6000 rpm for 2 minutes at 4°C and discard the supernatant.
- c) Add 1 ml of TE and gently mix the beads by inversion.
- d) Centrifuge again at 6000 rpm for 2 minutes at 4°C.
- e) Repeat step c & d two to three more times.
- f) In a final step, add 1ml 1X TE and resuspend them.
- g) Combine the resuspended beads with 100 µg of BSA (Bovine Serum Albumin) and 100 µg of hsDNA (herring sperm DNA) [**Note:** Herring sperm DNA is boiled in water-bath for 10 min, snap-chilled on ice for 2 min and then added to the beads.
- h) Incubate the beads overnight at 4°C with gentle agitation.

9. *Transcription inhibition assay:*

- **6-Azauracil sensitivity assay:** 6-Azauracil (6-AU) is a pyrimidine analog known to inhibit two enzymes involved in de novo pyrimidine nucleotide biosynthesis: IMP dehydrogenase and orotidylate decarboxylase. Inhibition of these enzymes by 6-AU leads to a reduction in the cellular levels of guanine and uracil nucleotides, which are essential building blocks for RNA synthesis²⁵⁸. During transcription, RNA polymerase II (RNAPII) synthesizes RNA molecules using nucleotides as substrates. When nucleotide pools are reduced due to 6-AU treatment, RNA polymerase II may experience challenges in obtaining a sufficient supply of nucleotides for efficient transcription. Deletion or mutation of factors associated with RNAPII elongation machinery may lead to a compromised RNA polymerase complex that is less efficient in elongating transcripts. Under normal conditions with ample nucleotide availability, these mutations might have minimal effects on transcription. However, when nucleotide levels are reduced by 6-AU treatment, transcriptional elongation becomes more dependent on a fully functional RNA polymerase.

Therefore, the primary objective of a 6-AU sensitivity assay in yeast is to evaluate how wild type and mutant yeast strains respond to 6-AU, thus helping in understanding their role in transcription elongation. To effectively apply selective pressure in this assay, it's crucial to maintain precise control over the yeast's nutrient environment. This can be easily achieved when allowing cells to grow in agar plates containing Synthetic Complete (SC) medium with

or without 6-AU instead of Yeast Peptone Dextrose (YPD) medium containing agar plates. SC medium is a precisely defined synthetic medium with a known and controllable composition of nutrients, including amino acids, sugars, and salts. Conversely, YPD medium is nutrient-rich and contains complex components like yeast extract and peptone, which can exhibit batch-to-batch variability and lack precise definition. This variation in YPD medium can obscure the effects of 6-AU and potentially lead to inaccurate assay results.

Media and other components:

Synthetic Complete Supplement Mixture (SC medium)- Himedia	
6-AU (Sigma)	10 mg/ml stock prepared in 1M NH ₄ OH

Methodology

- Yeast single colony cultures were grown overnight in YPD medium at 30°C until saturation.
- Inoculum from these saturated cultures was introduced into fresh pre-warmed YPD, and the cultures were incubated for 4-5 hours until reaching an OD₆₀₀ of 0.6 - 0.7 (~ 1 x 10⁷ cells/ml)
- After the desired O.D was reached, 10-fold serial dilutions of these cells were prepared in SC medium.
- The serial dilutions were applied as spots on SC medium, both with and without 100 µg/ml 6-AU, and then incubated at 30°C.
- Plates lacking 6-AU were kept for incubation for a duration of 2 days, whereas plates containing 100 µg/ml 6-AU were subjected to a prolonged incubation period of 4 days at 30°C.

-1,10-phenanthroline treatment:

1,10-Phenanthroline, often referred to simply as phenanthroline, is a chemical compound known for its broad-spectrum inhibitory effects on transcription initiation and elongation primarily by interfering with metal-dependent processes and disrupting the coordination of metal ions within the transcription machinery²⁵⁹⁻²⁶¹. It is a metal chelator that can form stable complexes with transition metals like zinc, iron and copper that are essential for RNA

Polymerase II (RNAPII) activity. Therefore, it is widely used to study the effects of transcription inhibition on histone modification patterns as well as the association of factors with the transcribing RNAPII. As described in Khan et al MCB 2023²⁶², yeast cells were subjected to a concentration of 200µg/ml of phenanthroline for various time periods (15min, 30 min, 60 min) to study the effects of transcription inhibition on histone acetylation and the association of particular HATs with active RNAPII. The method for phenanthroline treatment is illustrated below.

Media and other components:

Yeast-extract peptone dextrose medium (YPD)	1% yeast extract, 2% peptone, 2% dextrose
1,10-phenanthroline (Sigma)	100 mg/ml stock prepared in 100% ethanol.

Methodology:

- Single colony cultures of the appropriate yeast strains were grown overnight in YPD medium at 30°C until saturation.
- Inoculum from these saturated cultures was introduced into fresh pre-warmed YPD, and the cultures were incubated overnight in YPD medium at 30°C until reaching an O.D₆₀₀ of 0.8-0.9 (~1.2 x 10⁷ cells/ml)
- Upon achieving the target optical density, a fraction of the cell population was collected, which was the untreated control (0-minute time point).
- The remaining cell population was split into two equal portions. In one set, phenanthroline, dissolved in 100% ethanol, was introduced to achieve a final concentration of 200 µg/ml. In the second set, an equivalent volume of 100% ethanol was added, excluding phenanthroline. Both sets of cells were concurrently subjected to incubation for durations of 15 min, 30 min, and 60 min, respectively at 30°C.
- These cells underwent processing for either Chromatin Immunoprecipitation or immunoblot. In the case of immunoblot, the cells were collected post-treatment through centrifugation at 4500 rpm for 2 minutes at 4°C. After a single wash with sterile water, the cells were rapidly chilled in liquid nitrogen and then subjected to processing following the procedure outlined in the Materials and Methods Section 10. For

Chromatin Immunoprecipitation, after phenanthroline treatment in step 4, cells were immediately cross-linked with 1% formaldehyde and processed as per the protocol described in Materials and Methods Section 8.

10. Immunoblot analysis:

- **Protein isolation:** To assess the levels of histone modifications in cellular extracts, whole cell extracts of yeast (WCE) were prepared based on the procedure outlined in the subsequent protocol.

a. Preparation of yeast whole cell extracts:

Reagents and buffers:

1X PBS (prepared from 10X stock)	0.137M NaCl, 0.0027M KCl, 0.01M Na ₂ HPO ₄ , 0.0018 M KH ₂ PO ₄
Liquid N₂	
250mM PMSF (SIGMA)	
Protease Inhibitor Cocktail (SRE0055)	Used at a concentration of 1mg/ml
Acid-washed glass beads (Sigma)-425-600µm	

Methodology:

- Yeast cells with an O.D₆₀₀ of 0.8-0.9 (~1.2 x 10⁷ cells/ml) were harvested by centrifugation at 5000 rpm for 5 minutes at 4°C.
- The cell pellets were resuspended in 1ml ice-cold 1XPBS containing protease inhibitors and transferred to a 2ml Eppendorf tube.
- The cells were collected after centrifugation at 14500 rpm for 1 minute at 4°C. The supernatant was discarded, and the cell pellet was immediately snap-freezed in liquid N₂.

- To the frozen cell pellet, 200µl of acid-washed glass beads and 500µl of ice-cold lysis buffer was added. The tubes were kept on ice through all the steps.
- The cells were vortexed at full speed (30 seconds x 8 times). The tube was kept on ice for 1 minute between cycles.
- The lysate was cleared by centrifugation at 14500 rpm for 15 minutes at 4°C. The debris was discarded, and the supernatant (whole cell extract) was collected in a fresh tube. Aliquot of samples was collected for Bradford assay to measure the protein concentration and the remaining whole cell extract (WCE) was stored in aliquots at -20°C. For Bradford assay, a standard curve was plotted by measuring the absorbance of known concentrations of BSA (Bovine Serum Albumin).

- **Protein quantification via Bradford assay**

Yeast whole cell extracts were quantified by the Bradford assay as follows:

Sample Name	(Bradford reagent + H ₂ O) µl	Sample amount (µl)
Blank	(500 + 500) µl	-
0.25 mg/ml BSA standard	(500 + 497) µl	3µl
0.5 mg/ml BSA standard	(500 + 497) µl	3µl
1.0 mg/ml BSA standard	(500 + 497) µl	3µl
2.0 mg/ml BSA standard	(500 + 497) µl	3µl
Unknown	(500 + 497) µl	3µl

For the Bradford assay, a set of known concentrations of Bovine Serum Albumin (BSA) standards ranging from 0.25mg/ml- 2mg/ml, as presented in the table above, was utilized. After a 10-minute incubation period in the dark, optical density (OD) readings were taken at 595nm. To determine the concentration of unknown protein samples, a standard curve was constructed

using the values obtained from the BSA standards, and the concentration of the unknown samples was determined by extrapolating from this standard curve.

Gel electrophoresis, immuno-blotting, and detection:

Reagents, gels, and buffers-

5% stacking gel	30% acrylamide mix 330µl, 1.5 M Tris-Cl (pH 6.8) 250µl, 10% SDS 50µl, 10% APS 50µl, TEMED 2µl and water up to 2ml.
10% resolving gel	30% acrylamide mix 1.7ml, 0.5 M Tris-Cl (pH 8.8) 1.3ml, 10% SDS 50µl, 10% APS 50µl, TEMED 2µl and water up to 5ml.
16% resolving gel	30% acrylamide mix 2.66ml, 0.5 M Tris-Cl (pH 8.8) 1.3ml, 10% SDS 50µl, 10% APS 50µl, TEMED 2µl and water up to 5ml.
SDS running buffer-	Glycine 14g, Tris base 3g, SDS 1g water up to 1 litre.
Sample loading buffer (2X)-	For 1ml, 125µl Tris-Cl pH 6.8, 400µl 10% SDS, 100µl β-ME, 200µl glycerol and 0.0001g bromophenol blue
Transfer Buffer (Towbin's)-	Glycine 14.4 g, Tris base 3g, methanol 200ml and water up to 1litre.
10X TBS-	Tris 30g, NaCl 80g, KCl 2g, adjust pH with HCl to 7.4 and volume makeup with water to 1 litre.
0.1 % TBST-	1X TBS mixed with 0.1% Tween-20

Methodology:

- For the detection of histone modifications at the cellular levels, 10µg of whole cell extracts (WCE) were boiled for 5 minutes at 100°C in 2X loading buffer and subjected to electrophoresis on a 16% SDS-PAGE gel. These samples were then transferred to a PVDF membrane using a protein wet transfer apparatus with Towbin's Buffer.
- After the electrophoresis, the gel was left in Towbin's buffer for approximately 5-10 minutes. The PVDF membranes were cut to match the size of the gel, and blotting

papers were prepared accordingly. To activate the PVDF membrane, it was briefly immersed in 100% methanol for 30 seconds. Both the PVDF membrane and blotting paper were then moistened with transfer buffer.

- The PVDF membrane and gel sandwich was assembled within mini trans-Blot gel holder cassettes (Bio-Rad). These cassettes were positioned in electrophoresis tanks containing chilled transfer buffer. The histone proteins were transferred onto the PVDF membranes at a constant current of 70mA (~40V) for 45 minutes at 4°C.
- After the protein transfer, the PVDF membrane was subjected to a blocking step with a solution containing 5% (w/v) non-fat dry milk (NFDM) in 1X Tris-buffered saline (TBS) for 45 minutes at RT. Following this blocking step, the membrane was washed twice with 1X TBS solution. Subsequently, the PVDF membrane was incubated overnight at 4°C with primary antibodies, including anti-histone H4 Acetyl K16, anti-histone H3 acetyl K56 and anti-histone H3 (#Cell Signaling Technology – E2B8W; #abcam – ab195478; #BB-AB0055). The primary antibodies were used at dilutions of 1:2500, 1:10,000, and 1:5000, respectively, and these dilutions were prepared in 1X TBS. The membrane was gently shaken during this overnight incubation.
- Following the incubation with the primary antibodies, the membrane was washed twice with 0.1% Tris-buffered saline with Tween (TBST), with each wash lasting for 10 minutes.
- Next, the PVDF membrane was probed with a secondary antibody, specifically a goat anti-rabbit IgG, at a dilution of 1:5000. This secondary antibody incubation lasted for 1.5 hours. Post-secondary antibody incubation, the membranes were washed six times, with each wash lasting for 10 minutes, using 0.1% TBST.
- To visualize the protein bands, the membrane was developed using a chemiluminescent substrate, SuperSignal® West Pico from Thermo Scientific™.

11. Real time PCR (qPCR) and data analysis

In the current study, real time PCR (qPCR) was employed to assess variations in the amplification of specific DNA regions during both ChIP (Chromatin Immunoprecipitation) and gene expression analysis. The detection method in this research relies on a fluorescent dye known as SYBR green, which is included in the DyNAmo Colour Flash SYBR® Green qPCR Kit from Thermo Scientific™ (# F416L) that was utilized for the study. This dye binds to double-stranded DNA.

During PCR, as the number of amplification cycles progresses, the number of DNA fragments produced increases exponentially. This exponential growth follows the formula 2^n , where 'n' represents the cycle number. As amplification proceeds and more DNA fragments are generated, a real-time thermal cycler system is used to monitor the increase in fluorescence signal.

To accurately measure and quantify the amplification, these systems are carefully calibrated. They establish a threshold fluorescence value below which the signal generated by amplification is considered insignificant. The cycle at which the intensity of the amplified DNA crosses this threshold fluorescence level is referred to as the threshold cycle (C^T) value. Notably, a lower C^T value indicates a higher level of amplification, as it means that the signal intensity of the amplified products surpassed the threshold fluorescence at an earlier stage.

The Applied Biosystems 7500 Fast Real-Time PCR System, developed by Thermo Scientific™, was used in the current study to conduct these analyses.

For qPCR analysis of immunoprecipitated DNA or cDNA the following reaction was set-up.

Components	Amount in 20µl
DNA	2µl
SYBR with buffer	7µl
Primer (2.5µM)	1µl
H ₂ O	10µl

[Note: Prior to the preparation of the PCR mix, 0.3X of passive reference dye (ROX) is added to 1ml of SYBR green and mixed thoroughly]

In ChIP-qPCR analysis, both immunoprecipitated DNA and a control sample called 'input' DNA were analysed through qPCR to determine their C^T values. In the ChIP process, the entire cell extract is sonicated, and before the immunoprecipitation, a small portion (1%) of this extract is reserved as 'input' DNA for experimental control.

As previously described in Ray et al., DNA Repair 2018; Epigenetics 2020; Khan et al DNA Repair 2022; MCB 2023^{200,245,256,262} the C^T values from the 'input' DNA samples were adjusted to represent 100% of the DNA content and the percentage input of protein occupancy on target DNA region was calculated using the formula:

$$100 * 2^{(C_{T(\text{Input})} - C_{T(\text{IP})})}$$

For calculating acetylation level of specific histone residues at different regions, antibodies against acetylated histone residues and H3 were used for ChIP-qPCR. For the NER based studies, the amount of acetylated histone was normalized to the amount of H3 at that region and graphically represented. For the transcription-based studies, the amount of acetylated histone was normalized to the amount of H3 at a particularly transcribing region. Simultaneously, the amount of acetylated histone was normalized to the amount of H3 also at a non-transcribing control region. Following that, the levels of histone modifications at the transcribing loci were depicted graphically in relation to the non-transcribing control region. As previously described in Khan et al DNA Repair 2022; MCB 2023^{256,262}, the statistical significance of the difference in histone modification levels between wild type and mutant strains for both NER and transcription-based studies was tested using two-tailed independent student's t-test and the results having a *P* value of < 0.05 were significant.

In the RT-qPCR analysis, quantification by absolute method of template molecules was carried out using the standard curve method as previously described in Ray et al., Epigenetics 2020; Khan et al MCB 2023^{245,263}. This approach relies on C^T values obtained from qPCR to accurately determine the actual amount of template molecules (cDNA), allowing for a precise assessment of gene expression levels.

To generate the standard curve, cDNA was synthesized and subsequently diluted serially at ratios spanning from $1/10^1$ to $1/10^9$. The aforementioned dilutions were employed for qPCR as templates, utilizing primers specific to the constitutively active genes employed in this investigation. The C^T values obtained from these qPCR experiments were used to create a standard curve for gene expression. This standard curve followed the equation: $y = m \ln(x) + c$, where "y" represented the C^T value, and "x" represented the amount of amplicon (double-stranded DNA) present in nanograms (ng).

Following the creation of the standard curve, undiluted cDNA was employed in subsequent qPCR analyses. Subsequently, the C^T values acquired for the genes used for expression analysis were applied to the standard curves, enabling the determination of the actual count of transcripts expressed for each gene. As previously described in Ray et al., Epigenetics 2020; Khan et al., MCB 2023^{245,262}, this computation was executed using a predefined formula.:

$(\text{dsDNA amount in ng} * \text{Avogadro No.}) / (\text{size of dsDNA in base pair} * (2 * \text{D.F} * 330))$

where 330 g/mol is the average mass of a single base and D.F is the dilution factor 10^9 . The actual number of mRNA transcripts (copy number of transcripts) being produced in histone structural mutants and wild type cells were graphically represented. The statistical significance in the expression level differences between wild-type and mutant strains was assessed through

a two-tailed independent Student's t-test. Results with a *P*-value less than 0.05 were deemed significant.

The primers used in this study for ChIP and gene expression analysis are listed in the table below:

ChIP qPCR primers used for NER studies	Sequence
<i>HML (YCL065)</i>	F- 5'-CATCGTCTTGCTCTTGTT-3' R-5'-GTATATAGACAATGCAATCGTAC-3'
Telomere (<i>YHR218</i>)	F-5' GGTAATAATTCAGAACTGGTGC-3' R-5'CTTGAAACAACGTGTAGACCA-3'
<i>GAL10</i>	F-5' GGTAATTGACTGCTGGTGA-3' R-5' AAAGTGGGGATTTTGGG-3'
<i>RPB2</i>	F-5' TGGTCACACAGGTAAAAAACT-3' R-5' AAAATCTCTCTCGAACGATCGG-3'

ChIP qPCR primers for transcription studies	Sequence
<i>PYK1</i> Promoter (PP) 5'ORF 3'ORF	F- 5'- TTGAGTTGAGTGAGTGCTTTG-3' R-5'-CTGGAAAAAAGAGGTTCTTG-3' F- 5'-CTCATTAAACGTTGTTGCTGG-3' R-5'-ACCTGGGTACAATTCTTCGGA-3' F-5'-ATGCCCAAGAGCTGCTAGATT-3' R-5'-ACTTGCAAAGTGTTGGAGTGA-3'
<i>RPB2</i> Promoter (PP) 5'ORF (FPRP4) 3'ORF (FP3revRT)	F- 5'- TGCTTGGCGTTCAAAATG-3' R-5'-TCTGTAAACCTGAGGAGAAGG -3' F- 5'- TCAAGTCAAGCTTTATGGTCG-3' R-5'-AAGCATTTCCAGCATTTGCC -3' F-5'-TGGTCACACACAGGTAAAAAACT -3' R-5'-AAAATCTCTCGAACGATCGG-3'
<i>ACT1</i> Promoter (PP) 5'ORF 3'ORF (scACTF3'R)	F- 5'- CCGTTTTGAAACCAAACCTCG-3' R-5'-GCGTGAAAAATCTAAAAGCTG-3' F- 5'-GGTTGCTGCTTTGGTTATTGA-3' R-5'-TTCCATATCGTCCCAGTTGGT-3' F-5'-TGCTGAAAGAGAAATTGTCCG-3' R-5'-CGACATCACACTTCATGATGG-3'

ChIP qPCR primers for transcription studies		Sequence
<i>TFC1</i>	Promoter (PP)	F- 5'- CGACCTCATTATCACATTTT-3' R-5'-ACCAAAAGCGAAGAAGCGAA-3'
	5'ORF	F- 5'-CGTCCAATTTGGGTAAAAGA-3' R-5'-GGTGGTGGCTTTGGTACATT-3'
	3'ORF	F-5'-GACGCTGCTTTGGAAAATGA -3' R-5'-TCATCAACAAATCCCTTGAGC-3'
<i>UBC6</i>	Promoter (PP)	F-5'-TAAACTAGCCAACTCGCCATC-3' R-5'-ATCACGGCTCCTAAAGTGTGA -3'
	5'ORF	F- 5'-TACAAGGGCGGTCAATATCA-3' R-5'-GGCTTCATCACTGGTCATGAA-3'
	3'ORF	F-5'-AGGTGATGAAACAGAAGACCC -3' R-5'-AAGGCCAACCAAAAACAAAA-3'
<i>TAF10</i>	Promoter (PP)	F-5'-AATGGGTCGGATTAATAG -3' R-5'-AATCTGCAGCTTCTTTA -3'
	5'ORF	F- 5'-CGATGATGGGGACAATGAT-3' R-5'-ACCCGTTTTTGGTTAAATAGT-3'
	3'ORF	F-5'-TTCCGTAGCGGTATCTAATGC -3' R-5'-AACGATAAAAGTCTGGGCGA-3'
<i>PMA1</i>	Promoter (PP)	F-5'-GCTCCCCTCCATTAGTTTC -3' R-5'-TTCTTTCTTTTCAATGTGTGTAT-3'
	5'ORF	F- 5'-CTGCTGTTGTTATCAGAGA -3' R-5'-CCAACGAAAGTGTTGTAC-3'
	3'ORF	F-5'-CTATGTTCTTACCAAAGGG -3' R-5'-CGGACGACAGTAACAATAT-3'
<i>PHO84</i>	Promoter (PP)	F-5'-GTCGTGTGAAAGGCTTTCC -3' R-5'-TTATACAAGAGATGAGGATGAGC -3'
	5'ORF	F- 5'-GGTACTGTTATTGGTCAATT -3' R-5'-CATTTGGTAGTGGCAAATTC-3'
	3'ORF	F-5'-TGGTGAGTGTTTCCCAACT -3' R-5'-CTGGGATCAACAAGGTTGTG-3'
<i>ADH1</i>	Promoter (PP)	F-5'-GATGGAAGACACTAAAGGA -3' R-5'-CAGGTCTATTTATACTTGATAGC -3'
	5'ORF	F- 5'-ACGAAGGTGCCGGTGTCTG -3' R-5'-GGTACCTTGAGGAATGTGA-3'
	3'ORF	F-5'-TTAGAGCTAACGGTACCAC -3' R-5'-CGTAAATTTCTGGCAAGGTAG-3'

ChIP qPCR primer for non-transcribing locus (control)	Sequence
Telomere (TELO8RYP)	F-5'-GTGTTAGACAAGGCCGTAG -3' R-5'-CCCTTTTGGCGTACCTAC-3'
Primers for gene expression studies	
<i>PYK1</i> (3')	F-5'-ATGCCCAAGAGCTGCTAGATT-3' R-5'-ACTTGCAAAGTGTGGAGTGA-3'
<i>RPB2</i> (FP3revRT)	F-5'-TGGTCACACACAGGTAAAAAACT -3' R-5'-AAAATCTCTCGAACGATCGG-3'
<i>ACT1</i> (scATF3'R)	F-5'-TGCTGAAAGAGAAATTGTCCG-3' R-5'-CGACATCACACTTCATGATGG-3'
<i>TFC1</i> (3')	F-5'-GACGCTGCTTTGGAAAATGA -3' R-5'-TCATCAACAAATCCCTTGAGC-3'
<i>UBC6</i> (3')	F-5'-AGGTGATGAAACAGAAGACCC -3' R-5'-AAGGCCAACCAAAAACAAAA-3'
<i>TAF10</i> (3')	F-5'-TTCCGTAGCGGTATCTAATGC -3' R-5'-AACGATAAAAGTCTGGGCGA-3'
<i>PMA1</i> (3')	F-5'-CTATGTTCTTACCAAAGGG -3' R-5'-CGGACGACAGTAACAATAT-3'
<i>PHO84</i> (3')	F-5'-TGGTGAGTGTTTCCCAACT -3' R-5'-CTGGGATCAACAAGGTTGTG-3'
<i>ADH1</i> (3')	F-5'-TTAGAGCTAACGGTACCAC -3' R-5'-CGTAAATTTCTGGCAAGGTAG-3'



CHAPTER I

Understanding the role of H3K56
acetylation in regulating chromatin
dynamics during
Nucleotide Excision Repair



Introduction

The stability of the genome is under constant threat from both internal and external factors that can cause various types of DNA damage, including lesions to DNA bases or the DNA backbone. A complex system of DNA repair mechanisms actively strives to inhibit the transformation of this DNA damage into mutations or chromosomal irregularities. This protective system is crucial for averting genetic diseases, premature aging, cancer, and other chronic health conditions. A particular DNA repair mechanism, termed nucleotide excision repair (NER), is dedicated to eliminating DNA adducts that are usually larger and more intricate than regular nucleotides. Prominent instances of these bulky lesions, commonly found in the genome, encompass crosslinks of di-pyrimidines induced by ultraviolet (UV) light exposure and DNA adducts resulting from exposure to chemical carcinogens. Among environmental factors, UV radiation emerges as a prevalent cause of DNA damage and significantly contributes to the onset of skin cancer. The generation of numerous covalent crosslinks between neighboring pyrimidine bases in each skin cell is a consequence of exposure to shortwave sunlight. This occurrence varies based on factors like geographic location, time of day, type of season, type of weather conditions, and the exposure duration. These crosslinks predominantly take the form of cyclobutane pyrimidine dimers (CPDs) and pyrimidine-pyrimidone (6-4) photoproducts (6-4PPs). CPDs lesions form between adjacent thymine-thymine (T-T) or thymine-cytosine (T-C) bases and 6-4 Photoproducts (6-4PPs) that are pyrimidine adducts that develop between adjacent pyrimidine pairs with specific configurations, including 5'-T-C-3', 5'-C-C-3', and 5'-T-T-3', but not 5'-C-T-3' pairs²⁶⁴. These bulky lesions are principally removed by the process of NER through the coordinated action of approximately 30 genes. The process begins with the recognition of photolesions and the unwinding of the double-stranded DNA, a task performed by a DNA helicase. This coordinated effort is accompanied by the cutting of the DNA strand containing the lesion at the nucleotides positioned at the 5' and 3' ends of the lesion. Subsequently, a new DNA strand is synthesized by DNA polymerase, the damaged strand is excised, and DNA ligase closes the gap in the newly synthesized strand where the nick was present.

NER encompasses two distinct pathways that share almost the same set of proteins responsible for these functions, namely, Global Genome NER (GG-NER) and Transcription-coupled NER (TC-NER). The primary difference between these two pathways lies in how NER is initiated: GG-NER is initiated by the recruitment of specific damage recognition proteins to photolesions found throughout the genome. These lesions can be present in non-transcribing DNA strands of active genes or in regions that are transcriptionally silent and repressed. On the other hand, in transcription-coupled nucleotide excision repair (TC-NER), the presence of RNA

polymerases stalled at DNA lesions serves as a recruitment signal for additional NER proteins to act. Thus, GG-NER serves as a global surveillance mechanism to preserve genomic integrity and respond to DNA damage throughout the genome while TC-NER preserves the integrity of active genes. It is noteworthy that beyond the initial damage recognition step, both NER pathways share the same set of NER factors, which include Xeroderma pigmentosum (XP) proteins in mammals and radiation-sensitive (Rad) proteins in yeast. When it comes to rectifying UV-induced cyclobutane pyrimidine dimers (CPDs) and 6-4 photoproduct (6-4PP) lesions, there are essentially two pathways available: photoreactivation, or "light repair," and NER, or "dark repair." Photoreactivation is a relatively swifter and simpler process, involving the reversion of damaged pyrimidines back to their original forms. This reversion is catalysed by an enzyme called photolyase. CPD photolyases are found in a wide range of organisms, including bacteria, fungi, plants, invertebrates, and many vertebrates. Meanwhile, 6-4PP photolyases have been identified in species like *Drosophila*, silkworm, *Xenopus laevis*, and rattlesnakes. However, notably, these photolyases are not functionally present in organisms such as *E. coli* or yeast.

For placental mammals, including humans, neither of these photolyases is known to be functionally active. As a result, "dark repair" (NER) becomes the sole DNA damage response (DDR) pathway responsible for the repair of photolesions induced by UV radiation from sunlight. In these organisms, defects in the NER pathway can lead to a significantly heightened risk of skin cancer because unrepaired DNA photolesions created by UV irradiation possess mutagenic properties. Furthermore, deficiencies in NER-related genes can give rise to three distinct genetic disorders in humans, all of which share a predisposition to sun sensitivity and an increased risk of cancer. These disorders are Xeroderma pigmentosum (XP), Cockayne's syndrome (CS), and trichothiodystrophy (TTD). Notably, NER-responsive genes show similarities between humans and yeast. Given the crucial role of NER in humans, this study therefore focuses on investigating chromatin dynamics during the NER process in yeast as a model system. In order for effective NER within a chromatin setting, the repair machinery must have access to nearly 100 base pairs of DNA devoid of nucleosomes. Consequently, when addressing UV-induced DNA damage, the critical bottleneck lies in the dynamic reorganization of chromatin, serving as the limiting factor in the repair process. The chromatin dynamics during NER is carefully coordinated by histone modifications and chromatin remodellers, ensuring that chromatin remains accessible and that nucleosomes are rearranged at the site of DNA damage^{265,266}.

Prior research has indicated that histone acetylation, particularly at the N-terminal lysine residues of histone H3 and H4 has a stimulating effect on the repair of UV-induced DNA damage²⁶⁷⁻²⁶⁹. Additionally, background studies as mentioned previously have underscored the critical role of the H4K16 acetylation in governing chromatin dynamics during NER²⁰⁰. While extensive research has revealed the impact of histone tail acetylation on regulation of NER, influence of histone core residue acetylation like that of H3K56, in the context of NER has not been thoroughly investigated. Notably, the acetylation of the H3K56 residue has been associated with the DNA damage response pathway in prior studies²⁷⁰⁻²⁷³. Despite this, its precise role in the NER pathway has remained ambiguous. Given this background, part of my research was focused on elucidating the role of H3K56 acetylation in the regulation of chromatin dynamics during the NER process.



Results

Efficient NER in *Saccharomyces cerevisiae* necessitates the acetylation of H3K56

To comprehend the role of H3K56 acetylation in governing the dynamics of chromatin during the NER pathway in yeast, two distinct mutants were generated, namely H3K56R and H3K56Q. These mutants were designed to mimic two contrasting states of H3K56 acetylation. H3K56R mutant mimics the constitutively deacetylated state of H3K56. In this mutant, the lysine residue at position 56 on histone H3 is substituted with arginine (R), rendering it incapable of undergoing acetylation. As a result, H3K56 remains in a non-acetylated or deacetylated form continuously. Conversely, the H3K56Q mutant is constructed to emulate the constitutively acetylated state of H3K56. In this mutant, the lysine at position 56 is replaced with glutamine (Q), which closely mimics the acetylated lysine in terms of its chemical properties. Consequently, H3K56 is locked in a perpetually acetylated state. Using these mutants, the first objective was to understand whether H3K56 acetylation had a role specifically during NER. To address this, a cell survivability assay was performed in presence or absence of UV-irradiation. Cell survival assays, which evaluate the growth, adaptability, and resilience of cells following exposure to external agents, serve as effective means to compare the viability of cellular functions between mutant cells and wild type control cells. In the context of this study, yeast cells were subjected to ultraviolet (UV) radiation and the survival of H3K56 mutants were examined to determine whether changes in the acetylation status of this particular histone residue had any impact on cell functions during an adaptive response. Yeast cells have the capability to employ one or both of the pathways of “light” and “dark” repair to rectify UV-induced DNA damage. This makes it challenging to assess the effect of H3K56 mutation on cell adaptability to UV irradiation when both pathways are active in these cells. In the process of photoreactivation, the presence of 'blue' light photons (~380 - 440 nm) enables a chromophore within an enzyme called photolyase to directly reverse UV-induced pyrimidine-dimer lesions back to their undamaged, monomeric DNA form. To isolate the impact of H3K56 on DNA damage response (DDR) specifically through the NER pathway, the "light repair" pathway is deactivated by incubating UV-irradiated cells in the dark. Any observed defects in the survival of H3K56 mutants under these conditions would imply a direct influence of H3K56 particularly on the NER pathway.

Yeast cells were subjected to UV irradiation at 254 nm, with varying doses of exposure (50 J/m², 100J/m² and 150J/m²) and subsequently introduced onto YPD plates by either spotting or spreading followed by an incubation simultaneously with no UV treated control plates in the

dark at 30°C for a period of 48-72h (detailed in Materials and Methods section). Notably, the entire procedure was conducted in presence of yellow light to prevent the activation of repair mediated by photolyase. The findings distinctly demonstrated a substantial decline in cell survival for the H3K56R mutant, lacking H3K56 acetylation, especially under UV exposures of 100 and 150 J/m². This contrasted markedly with the results witnessed in both wild-type as well as H3K56Q mutant, (Figure C1 A & C1 B).

To elucidate the precise cause of this increased UV sensitivity in H3K56R mutant, it was imperative to investigate whether the lack of H3K56 acetylation could impact the rate at which

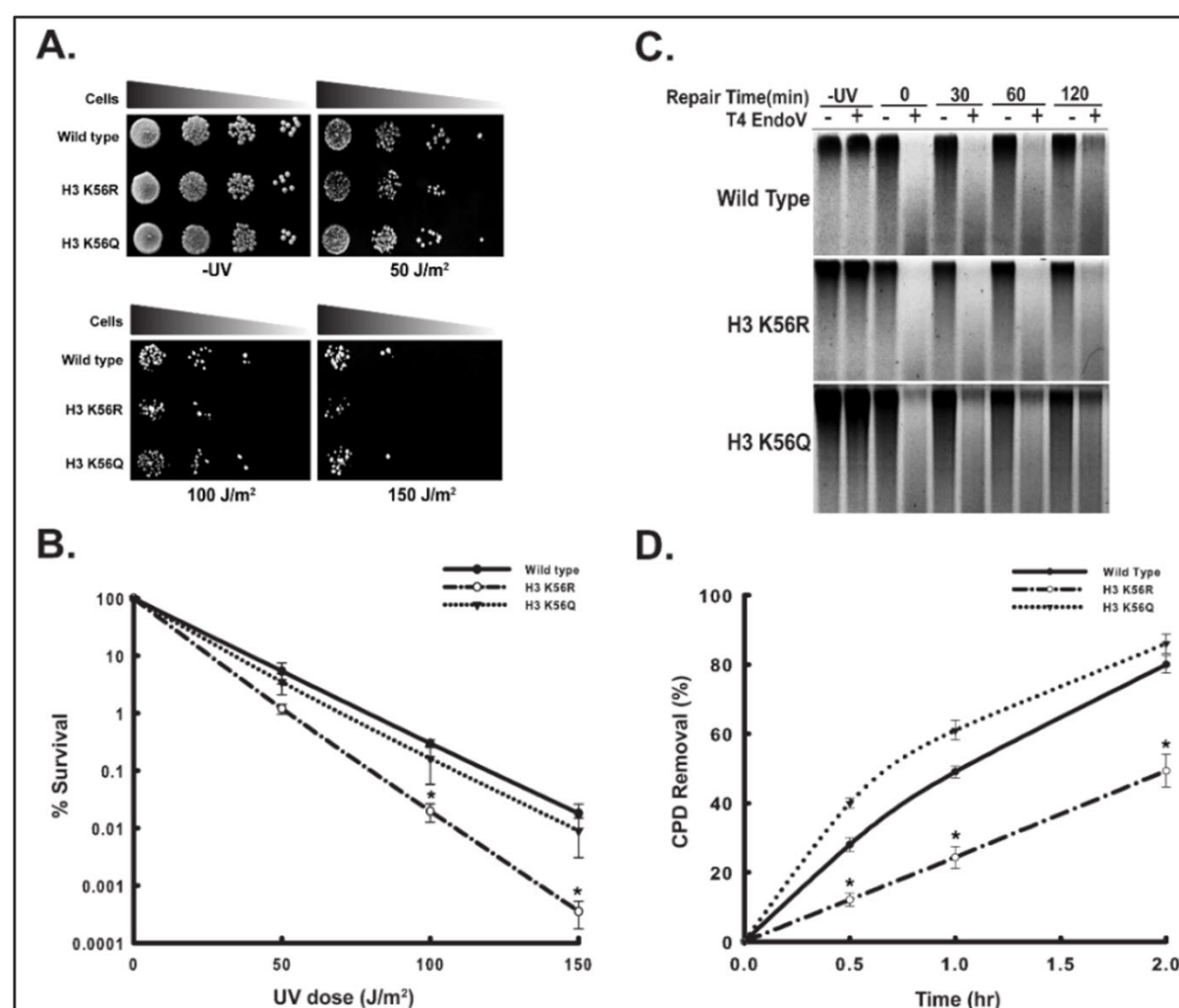


Figure C1. H3K56 acetylation is required for efficient NER. Ten-fold serial dilutions of control or UV-treated cells of wild type and H3K56 mutants were **A.** spotted and **B.** spread on YPA plates. For spread assay the colony forming units from triplicate sets were plotted. **C.** T4 Endonuclease V Assay followed by alkaline gel electrophoresis of genomic DNA isolated from wild type and H3K56 mutants treated with or without 100 J/m² of UV irradiation **D.** CPD removal rate of wild type and H3K56 mutants graphically plotted. Data represent the mean for three independent experiments with standard error of mean bars and asterisks indicate *t*-test significant *P* values < 0.05. (Taken from Khan et al., DNA Repair 2022)

damage is removed through the NER pathway. To conduct this investigation, yeast cells were subjected to UV at a dose of 100 J/m². The choice of a 100 J/m² UV dose was based on the findings depicted in Figure C1 B. At a higher dose of 150 J/m² a drastic decrease in cell survivability was observed especially in the H3K56R mutant cells (Figure C1 B). Consequently, conducting experiments at this higher dose became impractical. Therefore, an intermediate UV dose of 100 J/m², which demonstrated distinct sensitivity variations between wild type cells and that of mutants, was selected for this and subsequent experiments. In this experiment, yeast cells were exposed to a UV dose of 100 J/m² and permitted to undergo repair in dark. Subsequently, genomic DNA was extracted from these cells and subjected to the T4 Endonuclease V assay. Subsequently, the DNA samples underwent electrophoresis in an alkaline gel, maintaining denaturing conditions, and were subsequently utilized for the quantification of Cyclobutane Pyrimidine Dimers (CPDs). The determination of the CPD removal rate was subsequently computed. (see Section 3 under Materials and Methods) . The results unequivocally indicated a significant reduction in the rate of CPD removal in H3K56R cells, lacking acetylation at H3K56, compared to the wild-type cells (Figure C1 C & C1 D). Conversely, the presence of constant H3K56 acetylation (H3K56Q) facilitated CPD removal in H3K56Q mutants, exhibiting efficiency comparable to wild-type cells. Interestingly, H3K56Q mutants showed a slightly elevated rate of CPD removal during the early phases of repair compared to the wild type (Figure C1 C & C1 D).

To gain further insight into whether the observed UV sensitivity and NER deficiency in H3K56R cells were indeed linked to the lack of H3K56 acetylation, the pattern of H3K56 acetylation during NER was checked. For this, wild type cells were subjected to UV irradiation at a dose of 100J/m² and allowed to repair in the dark for varying time periods. Subsequently, the chromatin was isolated and subjected to immunoprecipitation with anti-H3K56ac antibody and the levels of H3K56 acetylation in response to UV induced NER was checked by qPCR. To determine whether H3K56 acetylation during NER was pervasive throughout the genome or limited to specific chromatin loci, four distinct chromatin loci were chosen to represent diverse chromatin states. These loci included *HML* and telomeres, representing

transcriptionally silent regions; *GAL10*, a locus under transcriptional repression; and *RPB2*, a locus actively engaged in transcription.

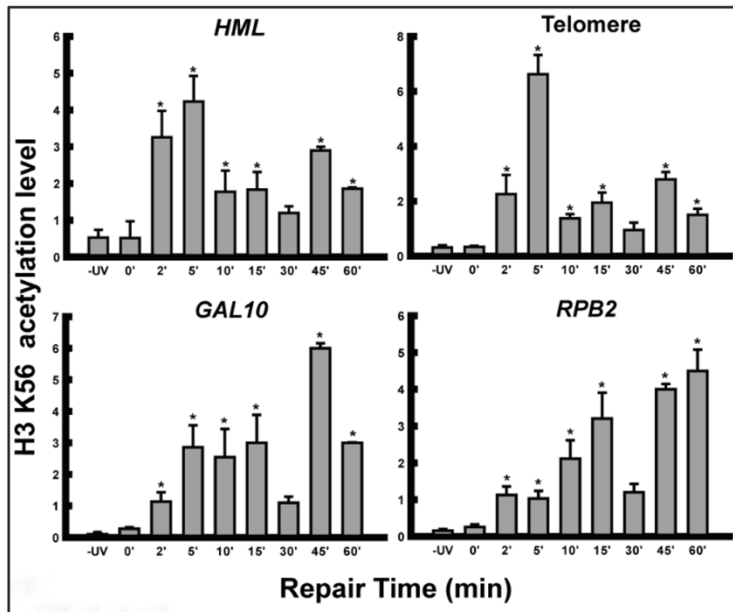


Figure C2. Acetylation status of H3K56 during NER. ChIP qPCR analyses using anti-acetyl H3K56 antibody of chromatin isolated from wild type cells treated with or without 100J/m² of UV followed by repair for varying time periods as indicated. H3K56 acetylation levels were normalized to histone H3 and checked using qPCR primers in HML, telomere, GAL10 and RPB2 loci. Data represent the mean for three independent experiments with standard error of mean bars and asterisks indicate t-test significant *P* values < 0.05. (Taken from Khan et al., DNA repair 2022)

The results obtained from all tested genomic loci provided clear evidence that significant levels of H3K56 hyperacetylation occurred within the first few minutes in response to UV exposure (Figure C2). Moreover, such acetylation was maintained at least till the first 60 min of repair in all the genomic loci tested. The cumulative results substantiated the assertion that H3K56 acetylation is an essential requirement in the process of NER. This elucidated the rationale behind the compromised NER observed in mutants devoid of H3K56 acetylation (H3K56R), thereby emphasizing the pivotal role of this acetylation in the remediation of UV-induced DNA damage.

H3K56 acetylation is necessary for the recruitment of repair factor Rad16 during NER

Histone modifications may function either during initial chromatin accessibility and/or during chromatin restoration step post NER. Therefore, it was important to understand the exact stage that requires H3K56 acetylation. In this investigation, it was noted that hyperacetylation of H3K56 induced by UV takes place rapidly, occurring within a brief timeframe of 2 minutes during NER (Figure 2). Furthermore, mutants with constitutive acetylation of H3K56 (H3K56Q) also exhibited slightly increased CPD removal rate compared to wild type cells during the early time points of repair (Figure C1 D). Together, these findings led to the question whether H3K56 acetylation was essential for regulating initial events in the NER pathway. Some of the important events associated with the initial phases of NER include the recruitment

of repair factors and chromatin accessibility. Therefore, initially the effect of H3K56 acetylation on recruitment of crucial NER factor Rad16 was monitored.

NER in yeast is orchestrated by a group of 10 well-known radiation-sensitive (Rad) genes: RAD1, RAD2, RAD3, RAD4, RAD7, RAD10, RAD14, RAD16, RAD23, and RAD25.

In yeast, the Rad proteins form complexes referred to as Nucleotide Excision Repair Factors (NEFs). These NEFs are pivotal in recognizing DNA lesions, performing precise incisions at the 5' and 3' regions flanking the lesion, and unwinding the DNA strands to facilitate the removal of the damaged segment²⁷⁴. There are four distinct NEFs formed by Rad protein complexes, each playing a unique role in NER:

1. NEF1, consisting of Rad1, Rad10, and Rad14.
2. NEF2, composed of Rad4 and Rad23.
3. NEF3, a complex involving Rad2, Rad3, Rad25, TFIIH, and other factors.
4. NEF4, comprising Rad7 and Rad16.

Within the NEF4 complex, Rad16 possesses its own ATPase activity, which plays a critical role in the repair process. Interestingly, this ATPase activity is sensitive to the presence of UV-induced DNA damage. As a result, NEF4 tracks along the DNA, utilizing ATP as an energy source, until it reaches the specific site of the DNA lesion.

At the site of the lesion, a noteworthy shift occurs: the UV-induced DNA damage inhibits the ATPase activity of Rad16. This inhibition leads to the stable binding of the NEF4 complex to the damaged DNA site²⁷⁵. This model of NER initiation represents a swifter and highly crucial step for the repair of lesions located on non-transcribing DNA strands and in transcriptionally silent regions of the genome^{276,277}. It's worth noting that the deletion of NEF4 factors, namely Rad7 and Rad16, has a severe impact on NER in the genomic regions²⁷⁷, underscoring the pivotal role of NEF4 in facilitating efficient repair of DNA lesions in such regions. Additionally, Rad16 is characterized as a member protein of the Swi/snf family that is required to generate DNA superhelical torsion, a function that is thought to be indispensable for efficient damage removal through the GG-NER pathway²⁷⁸. Moreover, Rad16 serves a dual role by inducing superhelical torsion in DNA and playing an essential role in Histone Acetyltransferase (HAT)-mediated UV-induced hyperacetylation of histone H3. This hyperacetylation, in turn, creates a chromatin structure that is accessible, facilitating the recruitment of downstream factors in the NER pathway. Consequently, this process promotes the efficacy of GG-NER^{279,280}. The significant role of Rad16 in the GG-NER pathway, coupled with the impact of H3K56 acetylation on the rate of NER, prompted the exploration of the correlation between H3K56 acetylation and Rad16 recruitment during NER.

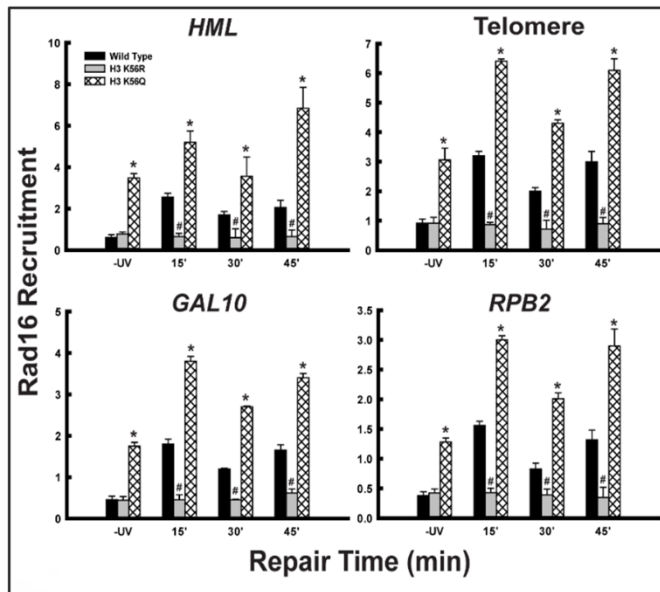


Figure C3. Rad16 recruitment during NER requires H3K56 acetylation. Comparative analysis of Rad16 recruitment was done on chromatin isolated from wild type and H3K56 mutants treated with or without 100J/m² of UV followed by repair for varying time periods as indicated. Chromatin immunoprecipitated samples were subjected to qPCR using primers specific to HML, telomere, GAL10 and RPB2 loci. Data represent the mean for three independent experiments with standard error of mean bars, * and # indicate t-test significant *P* values < 0.05. (Taken from Khan et al., DNA repair 2022)

In this investigation, the wild-type cells and mutant strains of H3K56 underwent UV irradiation at a dose of 100 J/m² and were permitted to undergo repair in dark for varying durations. Subsequently, chromatin was isolated and subjected to immunoprecipitation using antibodies targeting Rad16. PCR amplification was carried out using primers specific to distinct regions of the *HML*, telomere, *GAL10*, and *RPB2* loci, respectively. Notably, the results revealed a substantial increase in Rad16 recruitment in the H3K56Q mutant compared to the wild type across all tested genomic loci, both in the presence and absence of UV exposure (Figure C3). Remarkably, in wild-type cells, the recruitment of Rad16 is primarily reliant on NER. However, this UV-dependence can be nullified in the presence of continuous acetylation of H3K56. Conversely, the lack of H3K56 acetylation in the H3K56R mutant substantially hinders Rad16 recruitment, persisting as an obstruction even after 45 minutes of the repair process. The results unequivocally demonstrate that H3K56 acetylation is a necessary condition for the recruitment of Rad16 in the context of NER. Moreover, it appears plausible that H3K56 acetylation plays a regulatory role in the UV-dependent recruitment of Rad16, and the continuous acetylation of H3K56 mitigates this regulatory effect. It is known that when UV-induced DNA damage is absent, the ATPase activity of Rad16 remains inactive, and the protein stays immobilized in a complex with Rad7 at specific genome regions known as GG-NER complex binding sites (GCBs). This immobilization is aided by barrier nucleosomes. Earlier speculation posited that a chromatin event responsive to UV triggers the elimination of obstructive nucleosomes, thereby facilitating the redistribution of the complex of Rad7 and Rad16 to the precise locations of DNA damage²⁸¹.

What is particularly noteworthy is the observation of a higher recruitment of Rad16 in H3K56Q cells even in the absence of damage on DNA (Figure C3). This finding strongly implies an essential, damage-inducible response which triggers the loss of the barrier nucleosomes and subsequent redistribution of Rad16 to sites of damage remains unrestrained in the presence of constant H3K56 acetylation. This further underscore the intricate regulatory role of H3K56 acetylation in modulating the cellular response to UV-induced DNA damage.

Acetylation of H3K56 influences acetylation of N-terminal tail residues of H3 during NER

Prior research has indicated that histone acetylation, particularly at the N-terminal lysine residues of histone H3 and H4 are some of the initial events of the NER pathway that stimulate the repair of DNA damage incurred upon UV exposure primarily with the help of their ability to promote the recruitment of chromatin remodellers²⁶⁹. Studies conducted on a genome-wide scale have revealed that histone hyperacetylation, specifically involving H3K9 and/or K14, occurs in response to UV exposure during the repair of a transcriptionally silenced yeast locus^{200,282}. Furthermore, it has been established that UV-induced hyperacetylation of H3K9 and H3K14, is reliant on the activity of Rad16^{268,280}. Considering the reliance of Rad16 recruitment on H3K56 acetylation, the subsequent aim was to investigate potential interplay between the acetylation of H3K56 and that of residues K9 and K14 on histone H3 during the process of NER.

To delve into this inquiry, a ChIP protocol was utilized to track the fluctuations in H3K9 and H3K14 acetylation levels following UV-induced DNA damage. In this experimental setup, both wild-type cells and cells with H3K56 mutation underwent treatment with or without UV at a dose of 100 J/m². Subsequently, these cells were allowed to undergo repair for different durations, and the ensuing chromatin was isolated. Immunoprecipitation was then performed using antibodies specific to H3K14 and H3K9 acetylation, respectively. PCR was done to check the levels of H3K14 and H3K9 acetylation in response to UV-induced NER in *HML*, telomere, *GAL10*, and *RPB2* loci, respectively. Under conditions without UV-induced DNA damage, notable differences emerged, with H3K56R mutant cells exhibiting significantly elevated levels of H3K14 acetylation compared to both the wild type and H3K56Q mutant counterparts (Figure C4A). Conversely, in the presence of UV, both wild-type and H3K56Q cells displayed pronounced hyperacetylation of H3K14, primarily in a UV-dependent manner. Additionally, in wild-type cells, H3K14 hyperacetylation manifested within the initial 10

minutes of the repair process, while H3K56Q cells exhibited nearly immediate hyperacetylation (0 minutes). Intriguingly, H3K56R mutant cells demonstrated no discernible UV-dependent hyperacetylation of H3K14, at least until the initial 40 minutes of the repair process (Figure C4A). These findings culminated in the deduction that, in normal

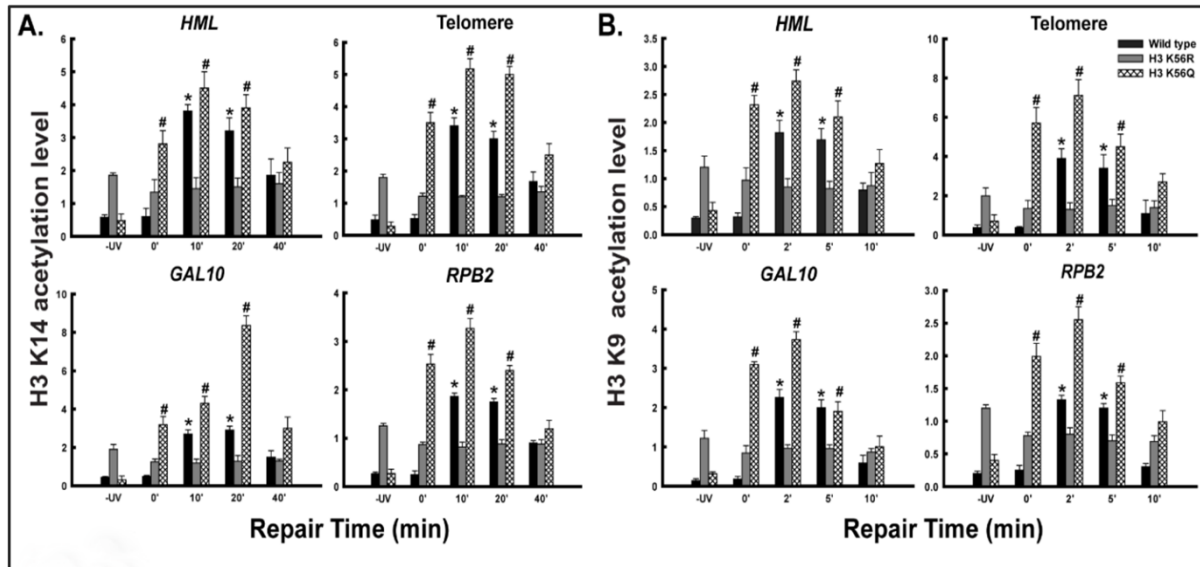


Figure C4. H3K56 acetylation promotes H3 N-terminal tail residue acetylation during NER. ChIP q-PCR analyses using **A.** anti-acetyl H3K14 and **B.** anti-acetyl H3K9 antibody on chromatin isolated from wild type and H3K56 mutant cells treated with or without UV irradiation at 100 J/m² followed by repair incubation for different time periods as indicated. qPCR analysis was done using primers specific to HML, GAL10, RPB2 and telomere regions. Data represent the mean for three independent experiments with standard error of mean bars, * and # indicate t-test significant P values < 0.05. (Taken from Khan et al., DNA repair 2022)

circumstances, the acetylation of H3K14 operates independently of H3K56 acetylation. Nevertheless, during the NER process, the UV-induced H3K14 acetylation necessitates prior acetylation of H3K56. Furthermore, this correlation is reinforced by a noteworthy observation: the constitutive acetylation of H3K56, as observed in H3K56Q cells expedites the acetylation of H3K14 immediately following UV exposure, transpiring even before cells of wild type. In a following ChIP assay utilizing an H3K9ac antibody, a parallel acetylation pattern emerged, mirroring that observed for H3K14 in the H3K56 mutants when compared to the wild type. In the absence of UV-induced DNA damage, acetylation of H3K9 in mutants lacking H3K56 acetylation (H3K56R) was conspicuously elevated in contrast to both the wild type strains and cells of H3K56Q mutant. (Figure C4 B).

However, upon irradiation with UV, distinctive hyperacetylation of H3K9 specifically during NER was identified in wild-type strains and cells with H3K56Q mutation, yet no corresponding

elevation in acetylation was noted in the H3K56R mutant. Mirroring the observed trend in H3K14 acetylation, in H3K56Q cells, acetylation of H3K9 surged immediately after cells had been irradiated with UV (0 minutes), whereas wild type cells exhibited noticeable hyperacetylation from 2 minute onwards during the repair process. (Figure C4 B).

In summary, the aforementioned outcomes are distinctly indicative of the fact that in the absence of UV irradiation, H3K9 and H3K14 acetylation remains unaffected by the acetylation status of H3K56. Conversely, subsequent to irradiation with UV, H3K9 and H3K14 hyperacetylation induced upon NER shows dependency on prior acetylation at H3K56.

Lack of H3K56 acetylation compromises chromatin accessibility during NER

When it comes to repairing DNA damage, particularly through the NER pathway, which involves complex multiprotein assemblies, the assembling of DNA into chromatin can create barriers that impede the accessibility of the NER factors to the damaged site. The "Access-Repair-Restore" model outlines the fundamental steps involved in DNA repair pathways like NER. These steps include manipulating the chromatin architecture to enable access of the repair factors to the damaged site removing the damage itself, and ultimately restoring the chromatin to its pre-damaged state²⁸³. It is essential to highlight that beyond the initial chromatin accessibility and reorganization promoting the recruitment of repair factors, such as Rad16, these factors have been observed to actively assist in recruiting Histone Acetyltransferases (HATs). This recruitment leads to heightened histone acetylation, subsequently fostering a more open and accessible chromatin structure crucial for the subsequent binding and localization of downstream repair proteins during NER.

Given that recruitment of Rad16 as well as H3 tail residue acetylation during NER was promoted in presence of constant H3K56 acetylation (H3K56Q), this raised a compelling question: what impact does H3K56 acetylation have on the chromatin structure during the NER process?

To explore the impact of H3K56 acetylation on accessibility of chromatin during the process of NER, a digestion assay employing the enzyme micrococcal nuclease (MNase) was performed using both wild type and cells with H3K56 mutations, both in the presence and absence of UV irradiation.

MNase enzyme is an endonuclease that selectively targets the linker DNA regions situated between two nucleosomes. It subsequently digests the free DNA ends that extend towards the core nucleosomes. DNA that is tightly wound around histone proteins within nucleosomes is

protected from MNase digestion. Digestion of chromatin by MNase leads to the generation of a series of digested chromatin fractions corresponding to mono, di, tri or tetra-nucleosomal DNA and so on based on the level of chromatin accessibility. Therefore, by subjecting chromatin to MNase digestion, we can assess the degree of accessibility of nucleosomal DNA and, consequently, gain insights into the overall accessibility of the chromatin architecture. The results obtained from the MNase digestion profiles in the absence of UV exposure (-UV) provided a clear depiction of chromatin structure differences. Notably, H3K56Q cells exhibited a more accessible chromatin structure when compared to the wild type cells. This observation was particularly evident in the gel panels showing the effects of 10 units of MNase digestion (Figure C5 A). In the case of H3K56Q cells, the nucleosomal DNA bands appeared less prominent, signifying that the DNA wrapped around the histones in nucleosomes was more susceptible to enzymatic digestion. This increased susceptibility to digestion suggests that in H3K56Q cells, the chromatin structure is more open and accessible, making nucleosomal DNA readily available for enzymatic cleavage. In contrast, the wild type and H3K56R mutant cells displayed a comparatively more compact chromatin structure, as indicated by the more distinct nucleosomal DNA bands. (Figure C5 A). Furthermore, nucleosomal DNA bands (10 units of MNase) were scanned by densitometry and individual nucleosomal DNA bands were represented as peaks, where peak heights reflected the intensity of nucleosomal DNA. Therefore, greater peak heights as observed in wild type strains and cells with H3K56R mutation under control conditions further indicated that the chromatin was less accessible to digestion by MNase. On the other hand, in H3K56Q cells a lower peak height indicated that the chromatin was more susceptible to MNase digestion leading to a loss of distinct bands of nucleosomes (Figure C5 B). Thus, from the above result it could be concluded that existence of constitutive H3K56 acetylation renders chromatin more amenable or accessible. To decipher the influence of H3K56 acetylation on governing chromatin dynamics in the context of NER, cells of wild type, H3K56R, and H3K56Q variants underwent exposure to 100 J/m² of UV. Subsequently, these cells were permitted to undergo repair for different durations, and a comparative MNase digestion profile was subsequently generated. MNase profiles clearly demonstrated distinct differences in chromatin structure with or without UV. The MNase digestion profiles, coupled with their corresponding scans, distinctly illustrate that within the first 30 minutes of the repair process, wild-type cells undergo intricate rearrangements in chromatin, resulting in the formation of higher-order structures resilient to MNase digestion (Figure C5 A). By 60-min of the repair process, a noticeable transformation occurred. The higher-order chromatin structures, which were previously dominant, began to diminish, giving

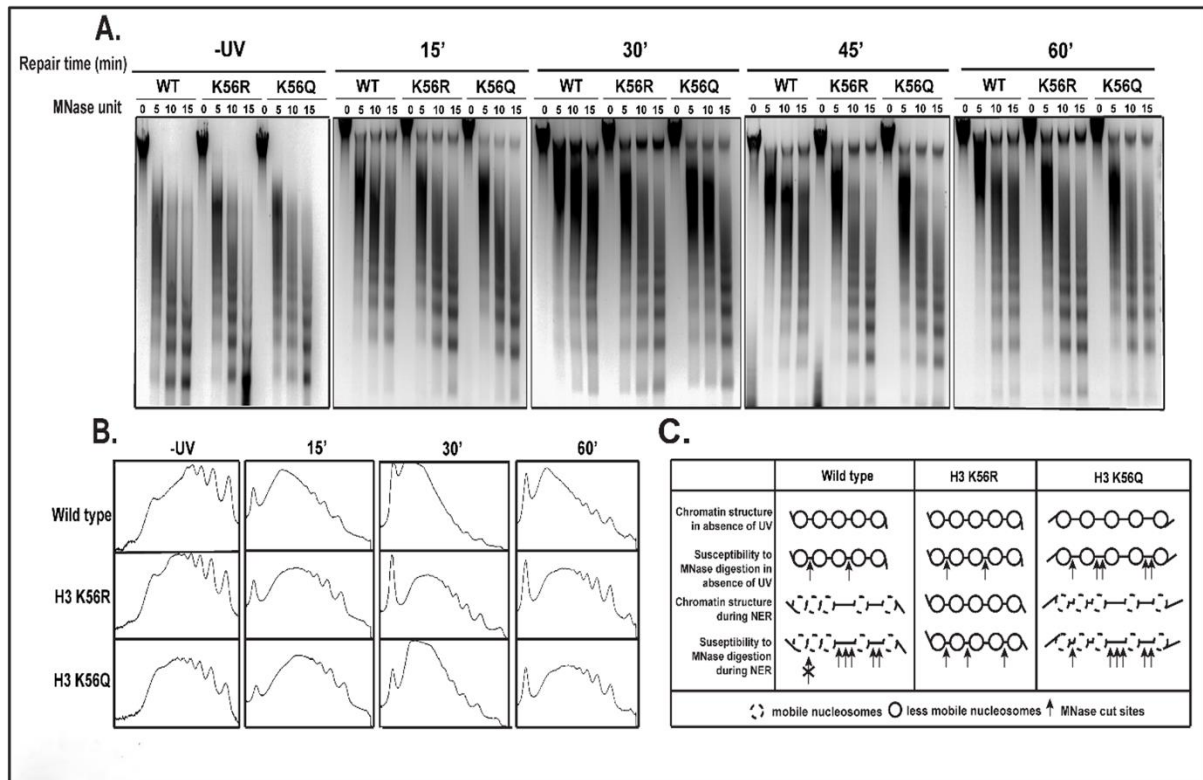


Figure C5. H3K56 acetylation promotes chromatin accessibility. Wild type and H3K56 mutants treated with or without 100 J/m² followed by repair incubation for indicated time periods was subjected to varying concentrations of MNase, genomic DNA isolated and electrophoresed on 1.2% agarose gel. **A.** Representative gels showing digestion profile of bulk chromatin, stained with ethidium bromide **B.** Corresponding scans of 10 units of MNase (25 U/μl) digest gel lanes **C.** Schematic representation depicting the influence of constitutive acetylation of H3K56 in making chromatin more susceptible to MNase digestion, that in presence of UV induced DNA damage provides an environment more conducive for chromatin switching between compacted and relaxed states, a phenomenon that in wild type essentially occurs in a NER-responsive manner. (Taken from Khan et al., DNA repair 2022)

way to the emergence of lower-order chromatin structures. This dynamic transition between higher-order and lower-order chromatin states as observed in wild type cells appeared to be a distinctive characteristic of effective NER. What is particularly intriguing is that this oscillation between compact and relaxed chromatin states appeared to be more pronounced in the presence of constitutive H3K56 acetylation (H3K56Q) (Figure C5 A). The corresponding scans (Figure C5 B) further confirmed this observation. Specifically, H3K56Q cells exhibited a more relaxed chromatin state compared to wild type cells by 60 min of NER. Conversely, the lack of acetylation of H3K56 in H3K56R mutant cells markedly impeded the dynamics of chromatin structure during NER. Higher-order chromatin conformations were less evident, and the observable interplay between compaction and relaxation, as seen in cells of wild-type and H3K56Q cells, was conspicuously absent in cells with H3K56R mutation. This was apparent

from the gel profiles and corresponding scans (Figure C5 A & C5 B). The profile of MNase digestion obtained during 15 min of the NER process and during 60 min of NER in H3K56R cells were evidently similar and exhibited no variation. Collectively, these observations strongly suggest that, under conditions of UV-induced DNA damage, wild-type cells undergo intricate rearrangements of chromatin, dynamically alternating between compaction and relaxation at distinct regions to enable effective access to the damaged sites. The presence of a constant acetylation of H3K56 (as seen in H3K56Q), facilitates the attainment of such a chromatin state as effortlessly as in wild-type cells. In contrast, the absence of acetylation of H3K56 (as in H3K56R) significantly hampers these chromatin dynamics, resulting in a deficiency in proficient NER.

H3K56 acetylation regulates DNA unwrapping dynamics during NER

The MNase digestion assays provided clear evidence of the dynamic nature of nucleosomes during NER. A crucial factor in regulating nucleosome dynamics is the ability of DNA to partially unwrap from the ends of nucleosomes. Previous studies have highlighted the importance of transient DNA unwrapping to facilitate the accessibility of lesions located within the buried regions of the genome²⁸⁴.

Given the fact that the presence of H3K56 acetylation at the entry/exit sites of DNA in the nucleosome promotes DNA unwrapping, the next objective was to investigate how H3K56 acetylation affects the dynamics of DNA unwrapping during NER. To do this, plasmid DNA supercoiling technique was employed which allowed the investigation of the impact of H3K56 acetylation on the unwrapping dynamics of DNA during the repair process.

Within nucleosomes, as DNA winds around a histone octamer, it induces negative supercoiling. In this study, the experiment began with the isolation of plasmid DNA that was initially negatively supercoiled (see Materials and Methods section 5). Next, the negatively supercoiled plasmid DNA was relaxed using an enzyme called Topoisomerase I. This relaxed plasmid DNA was then incubated in the presence of Topoisomerase I with whole cell extracts derived from wild type, H3K56R and H3K56Q mutant cells. These cell extracts were derived from cells that had been treated with or without UV at a dose of 100 J/m², and subsequently permitted to undergo NER for varying durations.

The underlying rationale of this experiment was to assess whether the population of histones present in the cell extracts had the capacity to modulate the wrapping/unwrapping dynamics of

DNA. If histones within the cell extracts were capable of inducing DNA wrapping, the initially relaxed plasmid would undergo transition into its supercoiled or wrapped state. Conversely, if the histones within the cell extracts were unable to initiate DNA wrapping, the relaxed plasmid would remain in its relaxed configuration.

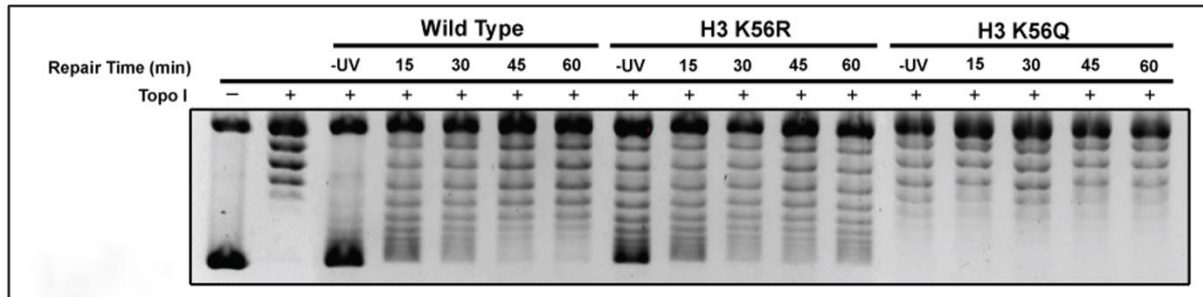


Figure C6: Plasmid supercoiling assay with wild type and H3K56 mutant cell extracts. Cell extracts prepared from wild type and H3K56 mutants treated with or without 100 J/m² of UV followed by repair incubation for indicated time periods was incubated with negatively supercoiled plasmid DNA previously relaxed with Topoisomerase I, plasmid DNA isolated after protein removal, resolved on an agarose gel, and stained with ethidium bromide. (Taken from Khan et al., DNA repair 2022)

When the relaxed plasmid DNA was treated with extracts of cells from wild type that had not been exposed to UV radiation, it indeed promoted DNA wrapping. This, in turn, caused the initially relaxed plasmid to transition into its supercoiled form (Figure 6). Such a supercoiled state could not be achieved with cell extracts of H3K56Q mutants that maintained the plasmid primarily in the relaxed conformation. Notably, extracts from H3K56R cells displayed diverse conformations of plasmid DNA spanning from supercoiled to relaxed states. Consequently, the absence of H3K56 acetylation resulted in an inability to fully achieve either the supercoiled or relaxed configurations of plasmid DNA. This contrasted with the more open conformation of plasmid DNA that was maintained in the presence of H3K56 acetylation. (Figure C6).

Intriguingly, during the NER process, the cell extracts from wild type cells induced a significant transition in plasmid DNA structure from a supercoiled towards a more relaxed state by 60 min of repair. Strikingly, this relaxed DNA conformation resembled the conformation of plasmid DNA that had been incubated with H3K56Q cell extracts, regardless of whether UV exposure was involved. This observation underscores the role of H3K56 acetylation in promoting a more open and relaxed DNA conformation. Such a conformation could be particularly advantageous during processes like NER, especially when they occur within a chromatin environment. On the contrary, plasmid DNA incubated with H3K56R cell extracts clearly displayed an inability to oscillate between compact and relaxed states. Consequently, no distinctive alteration in the conformation of the plasmid was observed in the presence of

UV (Figure 6). This observation was in consonance with the MNase results which demonstrated that absence of acetylation of H3K56 inhibits NER- associated modulations of chromatin structure (Figure 5). In summary, these findings imply that H3K56 acetylation plays a fundamental role in governing nucleosome dynamics and the accessibility of chromatin throughout the NER process. Conversely, the absence of H3K56 acetylation substantially obstructs these dynamics, resulting in a consequential decrease in NER efficiency..



Discussion

The process of Nucleotide Excision Repair (NER) is highly intricate, particularly when it occurs within a chromatin framework. Successful NER involves a sequence of coordinated events, encapsulated by the fundamental NER essentials: "Access-Repair-Restore". In addition to the apparent necessity for factors specific to NER during the repair phase, the steps involving accessibility and restoration demand the coordinated activity of histone chaperones, histone modifiers, and chromatin remodeling proteins.. Among the various modifications of histones, previous studies have highlighted the involvement of several N-terminal tail residues of histones H3 and H4 in NER^{200,269,282,285-287}. Notably, H3K56, located at a critical position near the entry-exit point of the nucleosome, plays a vital role in the dynamics of DNA wrapping and unwrapping around nucleosomes. Acetylation of this core histone residue alters the charge and weakens the interaction between the ends of DNA and the histone octamer at the core of the nucleosome. This acetylation promotes the unwrapping of nucleosomal DNA, leading to remodelling and eventual disassembly of the nucleosome.

In the context of a process like NER, where a large repair complex must access the site of DNA damage, gaining access to nucleosomal DNA represents a critical and often rate-limiting step. Consequently, the requirement for acetylation of H3K56, which maintains chromatin in a state that is more poised and enhances nucleosomal DNA accessibility, was a compelling hypothesis. The observations in this study revealed that the absence of H3K56 acetylation, denoted by the H3K56R mutation, renders cells more susceptible to the damaging effects of UV exposure in comparison to their wild type counterparts. The increased sensitivity was notably evident, especially under higher doses of UV of 100 and 150 J/m². Intriguingly, certain previous investigations have indicated an absence of substantial influence from mutations on H3K56 on the sensitivity to UV, particularly when UV irradiations were conducted at lower doses, such as 50 or even as minimal as 5 J/m²^{270,288}. Nevertheless, in the course of the experiments conducted within this investigation, the heightened sensitivity to UV observed in cells with H3K56R mutation, in contrast to the wild type, remained consistently apparent at irradiation doses of UV of 100 and 150 J/m². On the other hand, constant H3K56 acetylation (H3K56Q) did not result in significant changes in the sensitivity of cells to UV, when compared with cells of wild type. As a result the findings of this study indicate that a lack thereof of H3K56 acetylation has a notable impact on the cellular response to DNA damage induced by UV, resulting in increased sensitivity towards UV radiation. Additionally, the results highlighted that mutants with constant H3K56 acetylation (H3K56Q) displayed a markedly improved efficiency in CPD removal, particularly in the initial phases of the repair process (30 minutes, 1 hour). It is noteworthy that despite the improved rate of CPD removal, the existence

of constant H3K56 acetylation in cells with H3K56Q mutation actually resulted in slightly higher sensitivity to UV-induced damage compared to the wild type cells. This UV sensitivity of H3K56Q cells has been attributed to the well-established cell cycle-regulated pattern of H3K56 acetylation. H3K56 acetylation exhibits distinct dynamics throughout the cell cycle. It reaches its peak during the S phase, where DNA replication takes place, and is rapidly removed as cells progress into the G2/M phase. This removal is mediated by HDACs such as hst3 and hst4, facilitating proper cell division. In response to DNA damage, H3K56 acetylation tends to persist, serving as a signal for cell cycle arrest. This pause in the cell cycle allows for the timely removal of DNA damage before cell division proceeds to prevent the inheritance of damaged DNA by daughter cells²¹⁶. However, if the acetylation of H3K56 is not appropriately removed following the repair of DNA damage, it can lead to cell cycle defects^{217,218}. Thus, the most plausible explanation for the observed UV-sensitivity is that the constitutive acetylation of H3K56, which persists post-repair, interferes with the normal progression of the cell cycle. Importantly, there were no observed defects in the NER pathway in the presence of constitutive H3K56 acetylation, emphasizing that the slightly sensitivity of UV of H3K56Q cells in comparison to wild type cells is likely attributed to disruptions in the cell cycle due to the inability to remove H3K56 acetylation post-repair.

The observation that UV-induced H3K56 hyperacetylation manifested within a remarkably short span of 2 min following UV irradiation provided a clear indication that this modification occurs during the early phases of NER. This strongly suggested that H3K56 acetylation is a critical factor in inducing the initial events of NER in response to UV-induced DNA damage. Prior research has established that UV-induced hyperacetylation of histone H3 is essential for effective DNA repair in both yeast and mammals^{200,269,282,285-287}. More specifically, the significance of acetylation on specific residues on the tail of histone H3, such as H3K9 and H3K14, in response to UV damage has been well-documented in yeast and is considered as one of the initial events during NER. Considering the observations regarding H3K56 hyperacetylation during NER, it raised the possibility of a correlation between this modification and the histone H3 N-terminal tail residue acetylation. In simpler terms, the hyperacetylation of H3K56 might be closely linked to the acetylation of other regions within the H3 histone, particularly the tail residues K9 and K14, which are known to play a crucial role in the early stages of NER. Indeed, the results revealed that the hyperacetylation tail residues of histone H3 upon UV exposure, specifically H3K9 and K14, was contingent upon the acetylation of H3K56. What is particularly intriguing is that the presence of continuous acetylation of H3K56, as seen in the H3K56Q mutants, provided cells with an additional advantage. This advantage

became evident as the N-terminal H3 tail residue acetylation occurred instantly after irradiation with UV, essentially giving the process of NER an advantage. Previous research has indicated an enhanced recruitment of Gcn5 enzyme, the major HAT for H3K9ac and H3K14ac, to the silent *MFA2* locus within 0 minutes following UV irradiation²⁸². Interestingly, UV-induced Gcn5 recruitment is known to be dependent on Rad16 activity^{280,289}. As Rad16 activity was dependent on prior H3K56 acetylation it is therefore plausible that the existence of constant H3K56 acetylation promotes recruitment of Gcn5 immediately after UV irradiation thereby facilitating the acetylation of H3 tail residues.

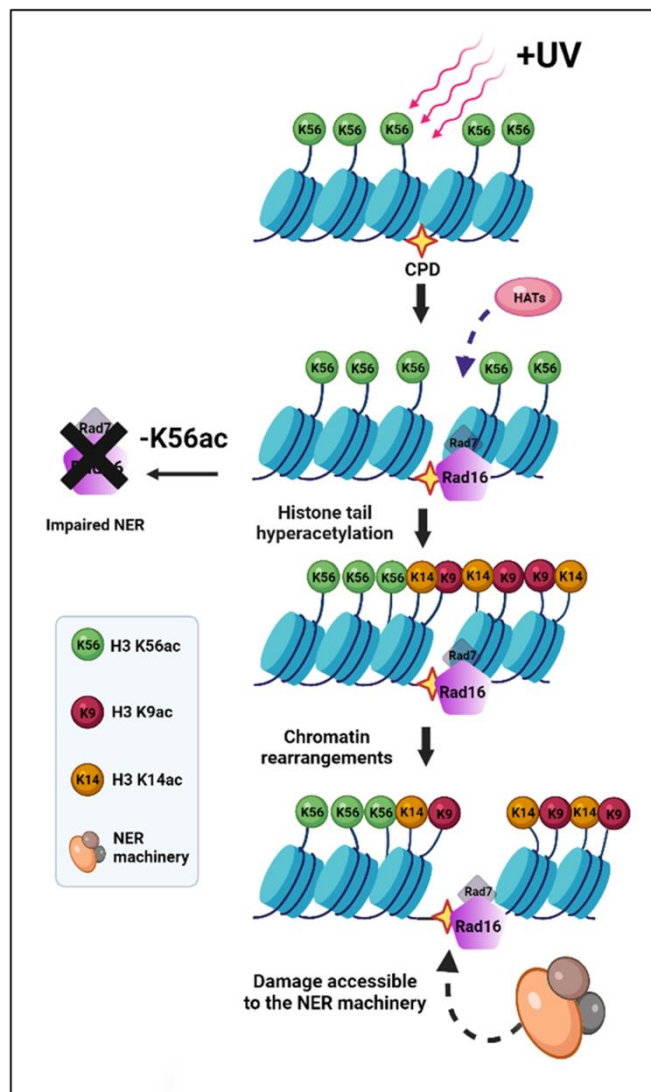
The above observation holds substantial significance, as it implies a crosstalk of acetylation of H3K56 which is a core H3 residue with acetylation of N-terminal H3 tail residues, K9 and K14, in response to DNA damage incurred upon irradiation with UV. In essence, the acetylation of H3K56 appears to act as a trigger that sets off a cascade of histone modifications in the H3 N-terminal region, thereby facilitating the early stages of NER in a coordinated manner. A notable finding in this study was that, in the absence of DNA damage induced by UV, the acetylation status of H3K56 did not exert an influence on H3K9 and K14 residue acetylation. Interestingly, without UV, the lack thereof of acetylation on H3K56, as observed in cells with H3K56R mutation, appeared to enhance the acetylation of H3K9 and K14. A promising avenue for future investigations would be to ascertain whether this heightened N-terminal H3 tail residue acetylation in the absence of acetylation of H3K56 relies on the HAT enzyme Gcn5, which is a major contributor to H3K9 and H3K14 acetylation, or if it operates independently. Notably, previous reports have indicated that when there is no UV-induced NER, Gcn5 activity is independent of Rad16. Thus, it is plausible that Gcn5 may not show a preference for H3K56 acetylation in such conditions. Previous studies have indicated that the acetylation status of specific lysine residues of histone H3 lysine can influence the selectivity of complexes of HATs such as Rtt109-Vps75, which acetylate H3K9 and H3K14²⁹⁰. In the absence of damage induced by UV, it is plausible that other HATs, such as Rtt109-Vps75, may preferentially acetylate H3K9 and H3K14 in H3K56R cells.

Surprisingly, even with elevated levels of H3K14 and K9 acetylation in the lack of damage induced by UV, H3K56R cells demonstrated a less proficient rate of NER. This inefficiency may be likely due to the incapacity of H3K56R cells to promote UV induced hyperacetylation at sites of DNA damage. Recent findings indicate that the complex of GG-NER, specifically Rad7 and Rad16, plays a role in the Gcn5 redistribution following UV exposure²⁸⁹. While persistent H3 hyperacetylation can circumvent the necessity for Rad16 and Rad7 in Global Genome-Nucleotide Excision Repair (GG-NER), this occurrence appears to be constrained to

specific chromatin contexts²⁸⁰. When considering the entire genome, deletion of Gcn5 has a negligible impact on NER while the absence of Rad16 significantly reduces the efficiency of NER compared to wild type²⁹¹. Furthermore, Rad16 plays a crucial role in generating essential superhelical torsion, which is indispensable for the elimination of damaged oligonucleotides from DNA²⁷⁸. When we consider all these pieces of evidence collectively, it becomes apparent that the inability to recruit Rad16 when H3K56 remains unacetylated as is the scenario with H3K56R cells makes it detrimental for the process of NER. Previous studies have highlighted the importance of the process of unfolding of nucleosomal DNA to make DNA damage accessible in genome regions that are typically concealed^{284,285}. The findings of this study underscore the critical role of H3K56 acetylation in facilitating an accessible chromatin in response to DNA damage induced upon UV irradiation. Devoid of H3K56 acetylation, yeast cells exhibit a deficiency in the dynamic chromatin transformations witnessed in wild-type cells throughout Nucleotide Excision Repair (NER). Upon UV irradiation, cells of wild-type manifest noteworthy reconfigurations of chromatin, giving rise to the development of intricate higher-order chromatin conformations and less conspicuous lower-order conformations during the initial phases of NER. As NER progresses, structures of lower-order reappear, suggesting the requirement for a substantial modulation of chromatin between compaction and relaxation to ensure proper repair. The observed findings align with an earlier study that reported a loss of regularly spaced nucleosomes in response to UV during the initial phases of NER, resulting in nucleosomes becoming more closely spaced²⁸¹. This implies that significant levels of nucleosome rearrangement is an important step in providing access for subsequent repair proteins to the region of DNA damage during NER. An *In vitro* investigation has provided further insights by demonstrating that acetylation of H3K56 plays a crucial role in exposing bulky lesions that distort the helical structure in nucleosomal DNA²³⁰. This is achieved by facilitating the repositioning of nucleosomes. The essential nature of acetylation of H3K56 in nucleosome remodeling and chromatin rearrangement during NER is reinforced by the observations in this study using plasmid supercoiling experiments. These observations strongly suggest that H3K56 acetylation sustains DNA in a state of relaxation and openness, a crucial condition for proficient NER. This phenomenon is apparent not only in wild-type cells but also in H3K56Q cells following exposure to UV. A compelling piece of evidence comes from comparing the plasmid conformation profiles before and after UV exposure in wild type cells. The transition from a state of extreme supercoiling to a state of relaxation during the progression of NER closely mirrors the plasmid state observed in H3K56Q cells both in presence and absence of UV. This favorable chromatin configuration, crucial for NER, remains

unattainable when H3K56 remains constantly unacetylated. This deficiency stands as a pivotal factor contributing to the diminished efficiency of NER in H3K56R cells. Consequently, the results strongly support the notion that yeast cells, in response to UV-induced NER, heavily depend on H3K56 hyperacetylation as a critical early event to establish a chromatin configuration conducive for efficient repair.

Recent discoveries have shed light on the initiation of GG-NER at the boundaries of higher order chromatin domains, from where GG-NER complexes, including Rad16 and Rad7, are redistributed in response to UV irradiation^{281,289}. This redistribution creates a stage that further promotes hyperacetylation of histone H3, exchange of histones, and remodelling of chromatin



A schematic illustrating the sequential steps initiated by H3K56 acetylation, leading to the establishment of chromatin accessibility, and facilitating the process of nucleotide excision repair (NER). (Taken from Khan et al., DNA repair 2022)

by complexes such as SWI/SNF or RSC at sites of DNA damage during the process NER. The cumulative results from this investigation propose that when lacking H3K56 acetylation (H3K56R), cells exhibit a deficiency in recruiting Rad16 in response to UV, resulting in a hindrance to the hyperacetylation of H3 tail residues and impaired modulation of chromatin during NER.

Overall, as depicted in the model (left), the acetylation of H3K56 plays a pivotal role in orchestrating several key early events during NER. The rapid onset of substantial hyperacetylation at H3K56 upon UV irradiation plays a pivotal role in orchestrating the redistribution of Rad16, the H3 tail residue hyperacetylation, and subsequently, the establishment of a histone modification code. This intricate interplay is instrumental in rendering chromatin accessible for the efficient execution of NER. These findings illuminate the complex dynamics of H3K56 acetylation

and its crucial role in regulating DNA metabolism within the intricate landscape of chromatin, offering valuable insights into the intricacies of the histone code.



CHAPTER II

Understanding the role of H3K56
acetylation in transcription
regulation



Introduction

Transcription is the key mechanism that enables a cell to translate the genetic code stored in its DNA into functional instructions for the synthesis of proteins essential for carrying out life sustaining tasks. During this universal nuclear process, RNA polymerases use DNA as a template to transcribe a wide range of RNA molecules. Eukaryotic cells employ three distinct RNA polymerases: RNAPI, RNAPII, and RNAPIII. Each of these polymerases serves a specific role in RNA production, contributing to various cellular processes. RNAPII, a complex consisting of multiple subunits, is the polymerase primarily involved in transcribing messenger RNA (mRNA). These mRNA molecules contain the code for synthesizing proteins, making them a key player in the central dogma of molecular biology. Furthermore, RNAPII is also responsible for transcribing numerous non-coding RNAs, which, unlike mRNA, are not translated into proteins but serve important regulatory functions within cells. However, much like other DNA-templated processes such as replication and repair, transcription is not immune to the complexities introduced by the compact packaging of DNA within chromatin. DNA compaction within nucleosomes is a contributory factor at every stage, from the early pre-initiation steps to the actual elongation of the transcript and eventually, the termination of transcription. Therefore, sustained research efforts have been dedicated to understand how the transcription machinery, essential for gene expression, navigates the obstacle posed by nucleosomes.

Recent *in vitro* studies emphasize that the hindrance posed by nucleosomes to the efficiency of transcription by purified RNAPII complexes is influenced by the strength of local interactions between histones and DNA, as well as the specific positions of these interactions within the nucleosome structure²⁹². *In vitro*, Pol II faces challenges of traversing through nucleosome-bound template, calling for complete removal of nucleosomes, or necessitating the displacement of at least a dimer of H2A/H2B to translocate through a nucleosome²⁹³⁻²⁹⁵. *In vivo* experiments, in contrast, reveal a distinct scenario. Most transcribed genes maintain intact nucleosomes, with nucleosomal loss observed primarily in highly transcribed genes²⁹⁶. This highlights the resilience of nucleosomes during transcription within the cellular environment, emphasizing their critical role in cellular survival. Alterations in chromatin structure during transcription elongation exert significant effects on transcription accuracy, and even a partial depletion of nucleosomes can result in anomalous initiation of transcription within gene bodies.²⁹⁷⁻²⁹⁹. The question then arises: how does RNAPII overcome the nucleosome barrier during transcription?

Surprisingly, Pol II transcript elongation rates *in vitro* on bare DNA are comparable to rates observed in living cells on genes, even when nucleosomes theoretically obstruct the

transcription process³⁰⁰. Additionally, nucleosomes with DNA sequences creating a directional barrier to transcription in vitro do not seem to significantly affect transcription when integrated into the genome in a living cell³⁰¹. These findings suggest that cells employ mechanisms to overcome the inherent obstacle presented by nucleosomes during RNAPII transcription, enabling efficient gene expression. To facilitate necessary access to the DNA template, a complex series of mechanisms come into play involving the repositioning of nucleosomes and the modification of the chemical structure of histones. Nucleosomes can be shifted to create open regions allowing for the binding of transcription factors, while histones can be exchanged with variants more favourable for transcription^{298,302}.

The alteration of local chromatin structure through repositioning or composition changes of nucleosomes is closely linked to post-translational modifications (PTMs) of histone residues. These PTMs, encompassing acetylation, methylation, phosphorylation, ubiquitination, and more, serve as marks on histones that either directly stimulate chromatin structural changes or act as cellular signals directing the chromatin environment to the transcriptional machinery^{98,160}. The regulation of these PTMs is crucial as they mediate the recruitment and activity of transcriptional factors, ensuring effective interaction with their corresponding cis regulatory elements during the transcription process. The fundamental question of how post-translational modifications (PTMs) regulate nucleosome dynamics to facilitate RNAPII in overcoming nucleosomal barriers during transcription is thus a pivotal area of investigation. Given the critical role of H3K56 acetylation in regulating nucleosome dynamics during Nucleotide Excision Repair (NER), the subsequent objective of this study was to explore its impact on a generalized chromatin event such as regulation of transcription, a process that heavily relies on the dynamism of nucleosome architecture.



Results

Hyperacetylation of H3K56 is associated with transcription of constitutively expressed genes in *Saccharomyces cerevisiae*.

For this study, nine genes were selected namely *PYK1*, *RPB2*, *ACT1*, *TFC1*, *UBC6*, *TAF10*, *PMA1*, *ADH1*, *PHO84*. These genes are constitutively expressed hence their transcription regulation can be easily monitored under normal growth conditions. Furthermore, the constitutive genes were selected from different chromosomal locations based on their unique functions in various housekeeping pathways. *PYK1* (*YAL038W*), located on chromosome I, encodes pyruvate kinase, an enzyme that catalyses the last step in glycolysis, which involves converting phosphoenolpyruvate to pyruvate^{303,304}. *RPB2* (*YOR151C*), located on chromosome XV, contains the genetic information for the second-largest subunit of the RNAPII core enzyme. Its lack or mutations can result in the failure of the core transcriptional complex to assemble³⁰⁵. *ACT1* (*YFL039C*), on chromosome VI, is responsible for encoding yeast actin, an essential protein vital for diverse cytoskeletal functions, functions critically in cell growth polarization³⁰⁶. *TFC1* (*YBR123C*), situated on chromosome II, contains the genetic information for Tau, a transcription factor. It is a component of the transcription initiation complex of RNAPIII, specifically referred to as TFIIC^{307,308}. *UBC6* (*YER100W*), situated on chromosome V, contains the genetic information for E2 a ubiquitin-conjugating enzyme located on the endoplasmic reticulum (ER) cytosolic membrane. Its principal role involves engagement in the ER-mediated degradation of proteasomes, a process dedicated to the disposal of proteins that are misfolded through degradation^{309,310}. *TAF10* (*YDR167W*), located on chromosome IV, encodes a TBP-associated factor, acting as a component in both the SAGA and TFIID complexes. These complexes play a crucial role in the assembly of the transcription initiation complex of RNAPII^{311,312}. Chromosome VII houses the *PMA1* gene (*YGL008C*), responsible for encoding the Plasma membrane P2-type H⁺-ATPase. This enzyme actively expels protons from the cell^{313,314}. *ADH1* (*YOL086C*), situated on chromosome XV, encodes alcohol dehydrogenase, an enzyme that operates as either homo- or heterotetramers. Its function is vital in reducing acetaldehyde to ethanol, marking the final step in the glycolytic pathway³¹⁵. *PHO84* (*YML123C*), situated on chromosome XIII, is a high-affinity transporter of inorganic phosphate (Pi) that also functions as a low-affinity transporter of manganese. It is under the regulation of Pho4p and Spt7p^{316,317}.

During transcription, the effect on gene expression is not solely determined by the presence or absence of a particular PTM; it also hinges on the spatial distribution of a given modification across a gene region. Different positions along the gene can exhibit distinct PTM patterns,

influencing transcription in a context-specific manner. This is most clearly demonstrated by the various states of H3K4 methylation. At the transcription start site (TSS) of a gene, nucleosomes are typically marked with trimethylated H3K4 (H3K4me3). As we move away from the TSS, either towards the distal promoter region or the coding open reading frame (ORF) region, a different PTM state is observed—namely, a di- or monomethylated state of H3K4 (H3K4me2 or H3K4me1)^{243,318}. This region-specific variation in PTMs also extends to H3K36 methylation, where di- or trimethylation (H3K36me2 or H3K36me3) is commonly found over the coding ORF of genes. This PTM pattern is closely associated with the transcription elongation process and, in particular, with the presence of an actively elongating RNA polymerase II³¹⁹. Hence, in order to comprehend the function of H3K56 acetylation in transcription, an analysis was conducted on the distribution pattern of H3K56 acetylation within the promoter and coding regions of the nine constitutively active genes under normal growth conditions. For this, Chromatin Immunoprecipitation (ChIP) analyses with antibody specific to acetylated H3K56 was conducted using wild type yeast cells. To gauge the levels of acetylated H3K56 qPCR was utilized. For this assessment, primers were used that amplified

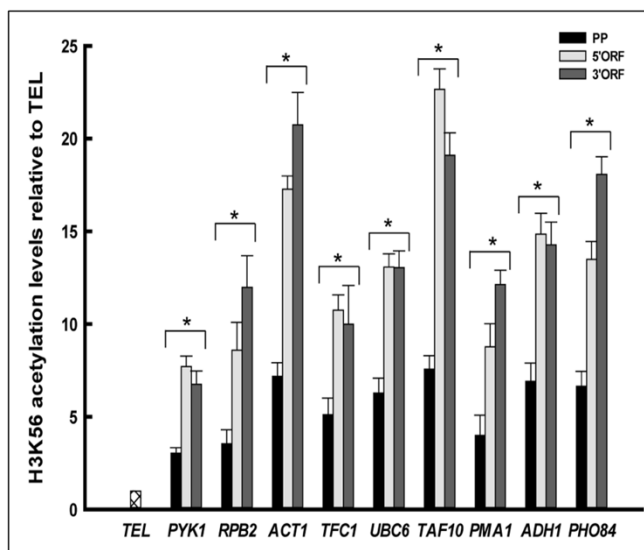


Figure C8. Acetylation status of H3K56 in constitutively active genes. ChIP qPCR analyses were conducted to assess the levels of H3K56 acetylation at the promoter (PP), 5'ORF, and 3'ORF regions of the *PYK1*, *RPB2*, *ACT1*, *TFC1*, *UBC6*, *TAF10*, *PMA1*, *ADH1* and *PHO84* loci. H3K56 acetylation levels were normalized against ChIP data obtained with anti-H3 antibody for the corresponding regions. The results were graphically depicted relative to a non-transcribing control region, *TELO8R* (designated as TEL). The data presented here represents the average of three independent experiments, with error bars indicating the standard error of the mean. Statistical significance, as determined by t-test analysis, is denoted by * and # for $P < 0.05$. (Adapted from Khan et al., MCB 2023)

a region proximal to the promoter (PP), the 5' coding region (5'-ORF), and the 3' coding region (3'-ORF) within the chosen genes. In order to ensure that the H3K56 acetylation in the various gene regions of the active genes was transcription targeted, qPCR of the ChIP DNA was also done with primers specific to a non-transcribing region of telomere (*TELO8R*) to serve as the control. The amount of acetylated H3K56 was normalized relative to the quantity of H3 present at these respective regions and the H3K56 acetylation levels in the transcribing loci were represented relative to telomere (*TELO8R*). The findings suggested a notable increase in

H3K56 acetylation within the ORF in contrast to the promoter region of the examined constitutively active genes (Figure C8).

To correlate whether the hyperacetylation of H3K56 in the gene bodies of the active genes was associated with active transcription, a comparative analysis of gene expression levels was done of wild type, H3K56R and H3K56Q. For this cDNA prepared from wild type cells and H3K56 mutant cells was subjected to RT-qPCR analysis using an absolute quantification method as

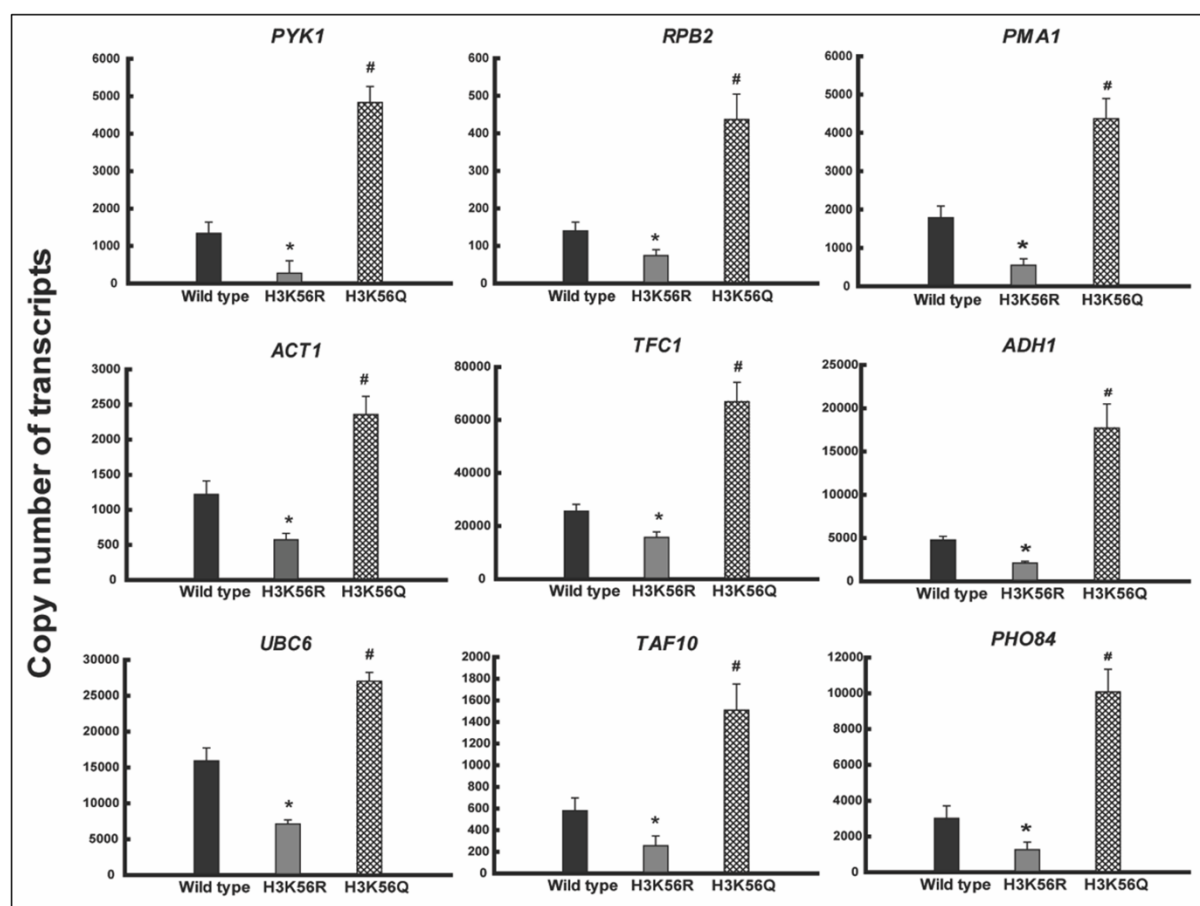


Figure C9. Comparative analysis of gene expression profiles between the wild type and H3K56 mutants. The procedure involved the extraction of RNA from both the wild type and H3K56 mutants, followed by RT-qPCR analyses utilizing the absolute quantification method outlined in the Materials and Methods section. The graphical representation depicts the copy numbers of transcripts for the specified genes in both the wild type and mutant samples. The results represent the mean values from three independent experiments, with error bars indicating the standard error of the mean. Significance levels are denoted by * and #, indicating t-test results with P values < 0.05 . (Adapted from Khan et al., MCB 2023)

detailed in Materials and Methods section. Using this method, the absolute values of the transcript copy numbers for all the genes under investigation could be obtained, which reflected the mRNA levels and gave a more conclusive understanding of the expression profiles of constitutive genes both in wild type cells and mutant cells. The outcomes revealed a substantial decrease in transcript copy numbers upon lack of H3K56 acetylation (H3K56R) compared to the wild type. This suggests that the deficiency in H3K56 acetylation hampers the expression

of constitutive genes. Conversely, with the presence of constant acetylation of H3K56 (H3K56Q), mRNA levels exhibited a noteworthy increase in comparison to wild type cells (Figure C9). This suggests that the constitutive acetylation of H3K56 promotes the expression of constitutive genes.

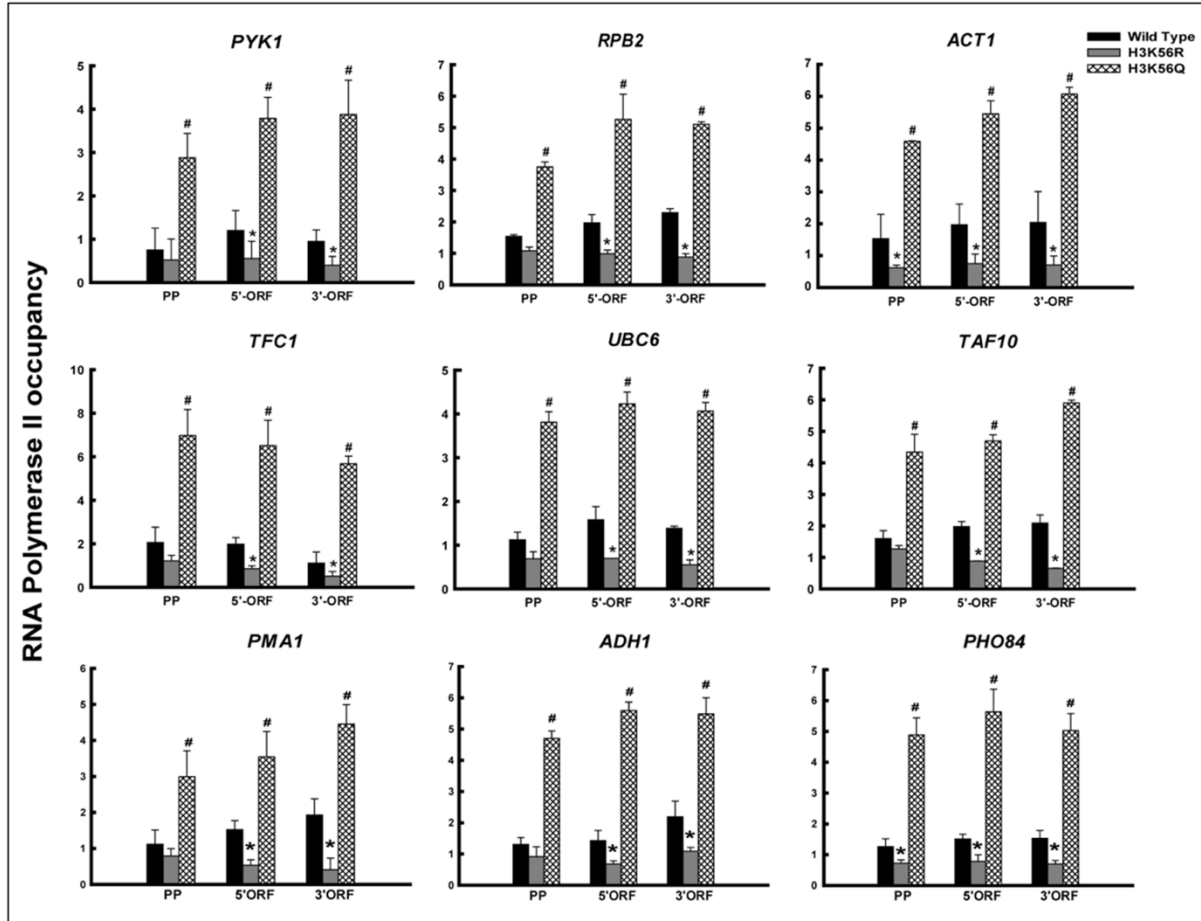


Figure C10. Comparative analysis of RNAPII occupancy between wild type and H3K56 mutants. ChIP assays were conducted using the anti-RNAPII (8WG16) antibody to assess occupancy levels at the promoter (PP), 5' ORF, and 3' ORF regions of *PYK1*, *RPB2*, *ACT1*, *TFC1*, *UBC6*, *TAF10*, *PMA1*, *ADH1* and *PHO84* loci. The obtained data, normalized by 1% input, has been graphically presented. The results represent the mean values from three independent experiments, with error bars indicating the standard error of the mean. Significance levels are denoted by * and #, indicating t-test results with *P* values < 0.05. (Adapted from Khan et al., MCB 2023)

To further substantiate the gene expression data, RNAPII occupancy of wild type cells and mutant cells of H3K56 were checked. qPCR analyses of samples immunoprecipitated with antibody specific to acetylated RNAPII (8WG16) was conducted in wild type cells and mutants of H3K56. For qPCR, primers for the genes under investigation were used to target the region proximal to the promoter designated as PP, the 5' coding region designated as 5'-ORF, and the 3' coding region designated as 3'-ORF (Figure C10). Occupancy of RNAPII was estimated as a percentage of input DNA and depicted graphically. In consonance with the gene expression profiles, it was observed that RNAPII occupancy in the constitutive genes was higher in

H3K56Q cells in comparison to wild type cells. Contrastingly, lack of acetylation of H3K56 (H3K56R) significantly impaired RNAPII recruitment in comparison to wild type cells (Figure C10). Collectively, the findings suggested that H3K56 acetylation aids RNAPII recruitment and consequently the transcription of genes that are constitutively active.

In light of the results that clearly demonstrated the regulatory function of H3K56 acetylation in the transcription of genes that are constitutively active, regardless of their specific functions within housekeeping pathways, the experiments were further streamlined. To facilitate the study, six out of the nine genes were randomly chosen for further in-depth analysis. These selected genes include *PYK1*, *RPB2*, *ACT1*, *TFC1*, *UBC6*, and *TAF10*.

Interplay of H3K56 acetylation and H4K16 deacetylation regulates RNAPII-mediated transcription of constitutively expressed genes

Histone modifications rarely act in isolation rather the way in which they are deposited, recognized and influence various functions of chromatin rely on an intricate interplay between modifications on various residues of histones. This interplay between different histone marks is vital for the precise control of gene expression and associated chromatin dynamics.

For instance, in mammals, the combination of H3K27 acetylation and H3K4 trimethylation is required for active transcription, and H3K4 trimethylation alone is insufficient to enable gene expression when H3K27ac is lacking³²⁰. Presence of H4K16 deacetylation in conjunction with H3K36me3 serves as a signal for transcription elongation. In contrast, when H4K16 is deacetylated alongside H3K4me3, it functions to suppress transcription initiation³²¹.

This intricate interplay emphasizes the concept that a particular histone modification can manifest both functions of activation and repression, contingent on the interactions and crosstalk it has with correlated modifications of histones. The context in which these modifications occur and the specific combinations in which they are found play a pivotal role in determining their ultimate impact on gene expression and chromatin regulation. This intricate network of histone modifications is a central mechanism for fine-tuning gene regulation and maintaining the dynamic balance between activation and repression of genes. Thus, investigating the interplay of histone modifications serves as a crucial mode of understanding proper mechanisms of gene regulation. In a prior investigation (refer to Background study), a notable observation had emerged: there was a positive correlation between deacetylation of H4K16 and transcription of constitutive genes. Furthermore, this study revealed that the presence of H4K16 deacetylation promoted acetylation of H3K56 in

these constitutive gene loci²⁴⁵. Given the understanding that histone modifications often act in a combinatorial fashion to regulate gene expression, it became crucial to delve deeper into the intricate relationship between H4K16 deacetylation and H3K56 acetylation. Understanding this interplay was essential for unravelling the exact role of H3K56 acetylation in the context of transcription and its impact on gene expression dynamics.

Within the euchromatin regions of the genome, which are predominantly abundant in constitutive genes, the enzyme Sas2 plays a pivotal role as the major histone acetyltransferase (HAT) responsible for acetylating H4K16. To shed light on the relationship between H4K16 deacetylation and the acetylation of H3K56 the gene encoding Sas2 was deleted. Firstly, it was important to validate the Δ Sas2 mutant. For this, a ChIP based analyses was employed with antibodies specific to acetylated H4K16 to compare the H4K16 acetylation levels in wild type and mutants lacking Sas2 (Δ Sas2). For the constitutively active genes chosen for investigation, qPCR was conducted using primers that amplified a region proximal to the promoter (PP), the 5' coding region (5'-ORF), and the 3' coding region (3'-ORF). Simultaneously, qPCR was also done with primers specific to the non-transcribing region of telomere (*TELO8R*). H4K16 acetylation levels in Δ Sas2 mutants were graphically represented relative to wild type. The

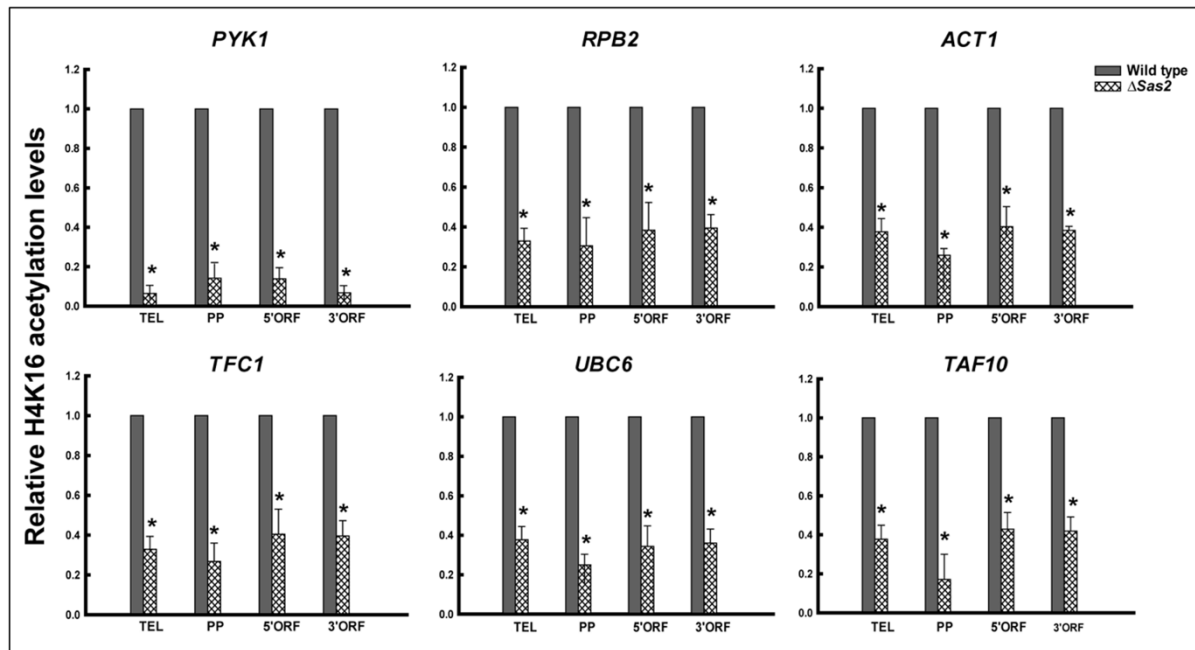


Figure C11. Comparative analyses of H4K16 acetylation levels in wild type and Δ Sas2 mutant. ChIP qPCR analyses were executed to evaluate H4K16 acetylation levels in the promoter (PP), 5'ORF, and 3'ORF regions of *PYK1*, *RPB2*, *ACT1*, *TFC1*, *UBC6*, *TAF10* loci, alongside a non-transcribing region of *TELO8R* as a control (TEL). The levels of H4K16 acetylation were normalized to ChIP data obtained with an anti-H3 antibody for the corresponding regions. The results were graphically presented to depict the relative levels of H4K16 acetylation in Sas2 Δ mutants compared to the wild type. The data represents the mean of three independent experiments, with error bars indicating the standard error of the mean. Symbol (*) has been used to highlight t-test significant P values of <0.05. (Adapted from Khan et al., MCB 2023)

findings substantiated the role of Sas2 in acetylating H4K16 within the examined constitutive genes. In cells that lacked Sas2, the acetylation levels of H4K16 were markedly diminished in comparison to wild type (Figure C11). Notably, H4K16 acetylation levels were also reduced in the telomere region of the Δ Sas2 mutant. This observation is in consonance with the known function of Sas2 as a global HAT for H4K16 acetylation functioning both in euchromatin as well as heterochromatin regions to acetylate H4K16. Once the Δ Sas2 mutant was validated, both the wild type and Δ Sas2 mutant samples were subjected to immunoprecipitation using an antibody targeting H3K56 acetylation to check the impact of deletion on levels of H3K56 acetylation in the genes that are active constitutively. qPCR was conducted using primers to amplify a region proximal to the promoter (PP), the 5' coding region (5'-ORF), and the 3' coding region (3'-ORF) of the six constitutive genes mentioned earlier (Figure C12). Simultaneously, qPCR was also done with primers specific to the non-transcribing region of telomere (*TELO8R*) to serve as the control. The levels of H3K56 acetylation were subjected to normalization by histone H3 levels and depicted on a graph in comparison to telomere (*TELO8R*). In all the examined constitutive genes, there was a distinct elevation in H3K56 acetylation observed in the Δ Sas2 mutant as compared to the wild-type cells (Figure C12).

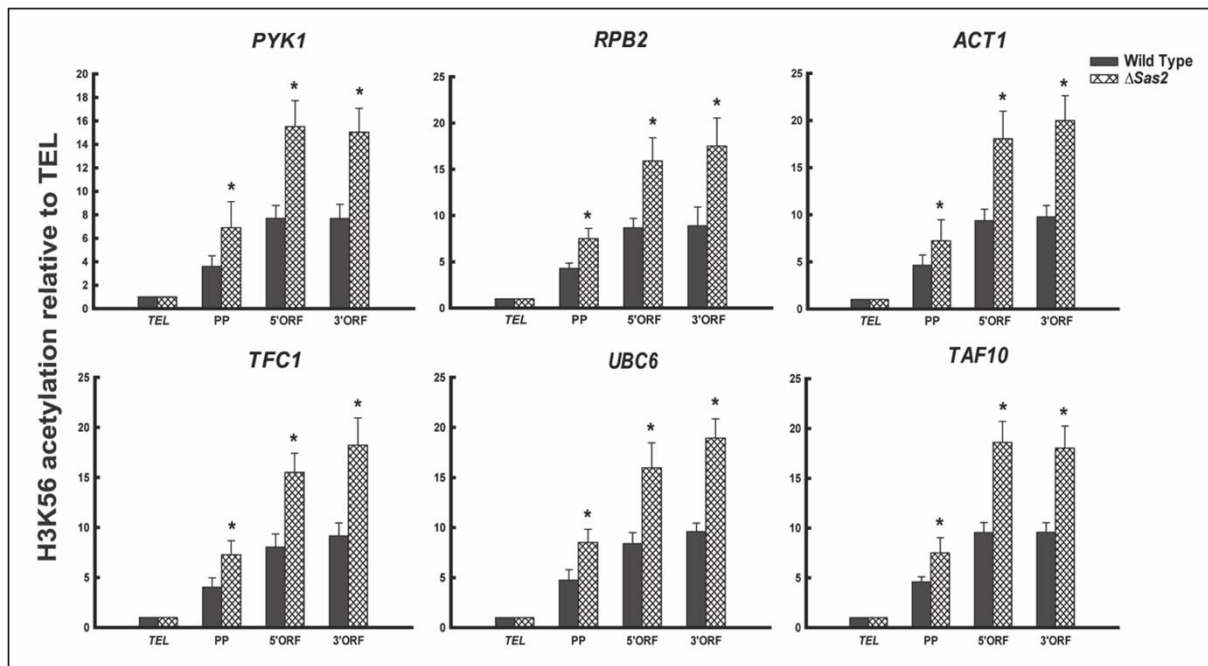


Figure C12. Comparative analyses of H3K56 acetylation levels in wild type and Δ Sas2 mutants. Chromatin from both wild-type and Δ Sas2 mutant samples was subjected to immunoprecipitation using anti-H3K56ac antibody. The resulting H3K56 acetylation levels were normalized to ChIP data obtained with an anti-H3 antibody for the corresponding regions. The graphical representation illustrates the relative H3K56 acetylation levels, with comparison to a non-transcribing control region denoted as *TELO8R* (TEL). The presented data represents the mean of three independent experiments, with error bars indicating the standard error of the mean. The symbol (*) is used to highlight t-test significant P values of <0.05. (Taken from Khan et al., MCB 2023)

To explore the connection between this elevated H3K56 acetylation and transcription, the next aim was to check the occupancy of RNAPII in both the wild type and Δ Sas2 mutant samples. To accomplish this, ChIP was conducted on samples from both wild-type and Δ Sas2 strains, utilizing an antibody targeting RNAPII (8WG16) followed by qPCR analyses. For the genes under examination, qPCR was conducted using primers that amplified a region proximal to the promoter (PP), the 5' coding region (5'-ORF), and the 3' coding region (3'-ORF). RNAPII occupancy was estimated as a percentage of input DNA and graphically represented. Notably, the findings revealed a significant increase in occupancy of RNAPII in the Δ Sas2 mutant. (Figure C13). This heightened recruitment of RNAPII was especially noticeable within the open reading frame (ORF) of the examined constitutive genes. The coexistence of elevated RNAPII levels in gene bodies and the heightened acetylation of H3K56, especially in the absence of H4K16 acetylation, strongly implies a collaborative mechanism. This mechanism suggests that the deacetylation of H4K16 and the subsequent acetylation of H3K56 likely work together to promote RNAPII- mediated transcription of genes that are constitutively active.

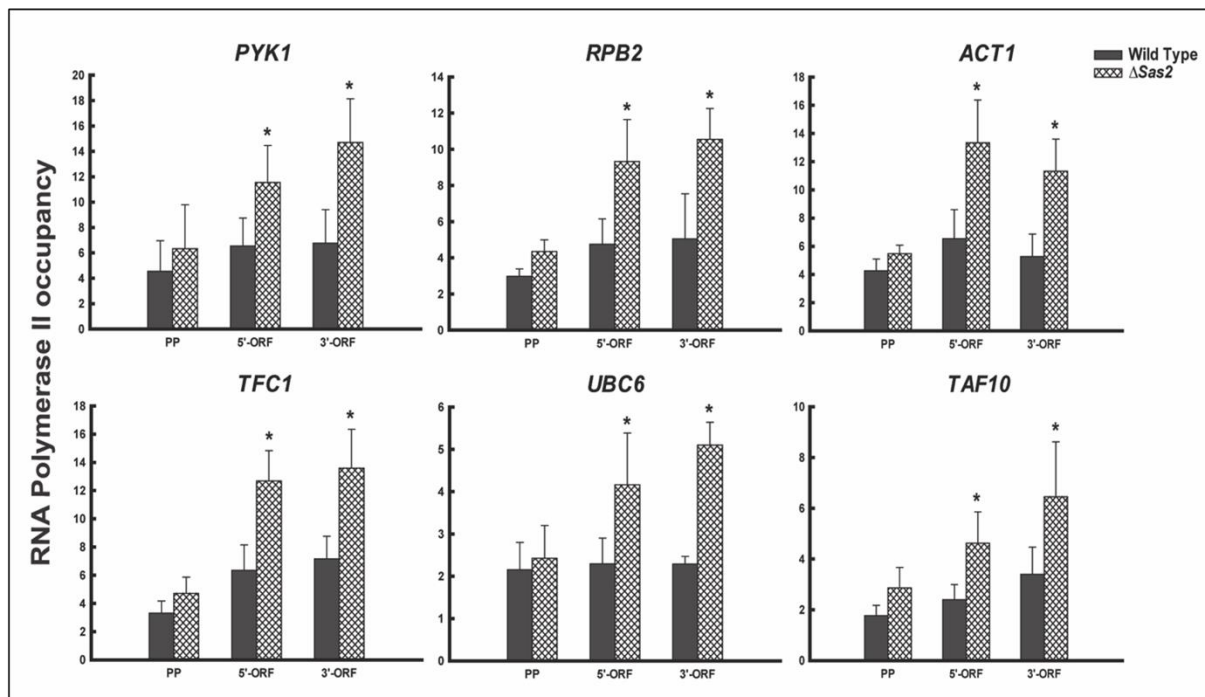


Figure C13. Comparative analyses of RNAPII occupancy in wild type and Δ Sas2 mutants. Immunoprecipitation of chromatin from both wild type and Δ Sas2 mutant samples was performed using the anti-RNA Polymerase II (RNAPII) antibody (8WG16). Subsequently, the occupancy of RNAPII was assessed by qPCR at the promoter (PP), 5'ORF, and 3'ORF regions of PYK1, RPB2, ACT1, TFC1, UBC6, and TAF10 loci. The RNAPII occupancy values were normalized by input (1%) and presented graphically. The data represents the mean of three independent experiments, with standard error of the mean bars included, and asterisks (*) denote t-test significant P values of <0.05. (Taken from Khan et al., MCB 2023)

In regions of active transcription within the genome, the deacetylation of H4K16 is predominantly regulated by the HDAC Hos2. Deleting the gene responsible for encoding Hos2 was undertaken to delve further into the direct implications of H4K16 deacetylation on H3K56 acetylation and its subsequent influence on the transcription elongation process. Hereafter, it was important to validate whether Hos2 functions to deacetylate H4K16 in the constitutively active genes. For this, a ChIP based analyses was employed with antibodies specific to acetylated H4K16 to compare the H4K16 acetylation levels in wild type cells and mutant cells lacking Hos2 (*Hos2Δ*). For the six constitutively active genes under examination, qPCR was conducted using primers that amplified a region proximal to the promoter (PP), the 5' coding region (5'-ORF), and the 3' coding region (3'-ORF). Simultaneously, qPCR was also done with primers specific to the non-transcribing region of telomere (*TELO8R*). H4K16 acetylation levels in *Hos2Δ* mutants were graphically represented relative to wild type. The results confirmed that Hos2 is responsible for removing H4K16 acetylation in the active genes tested

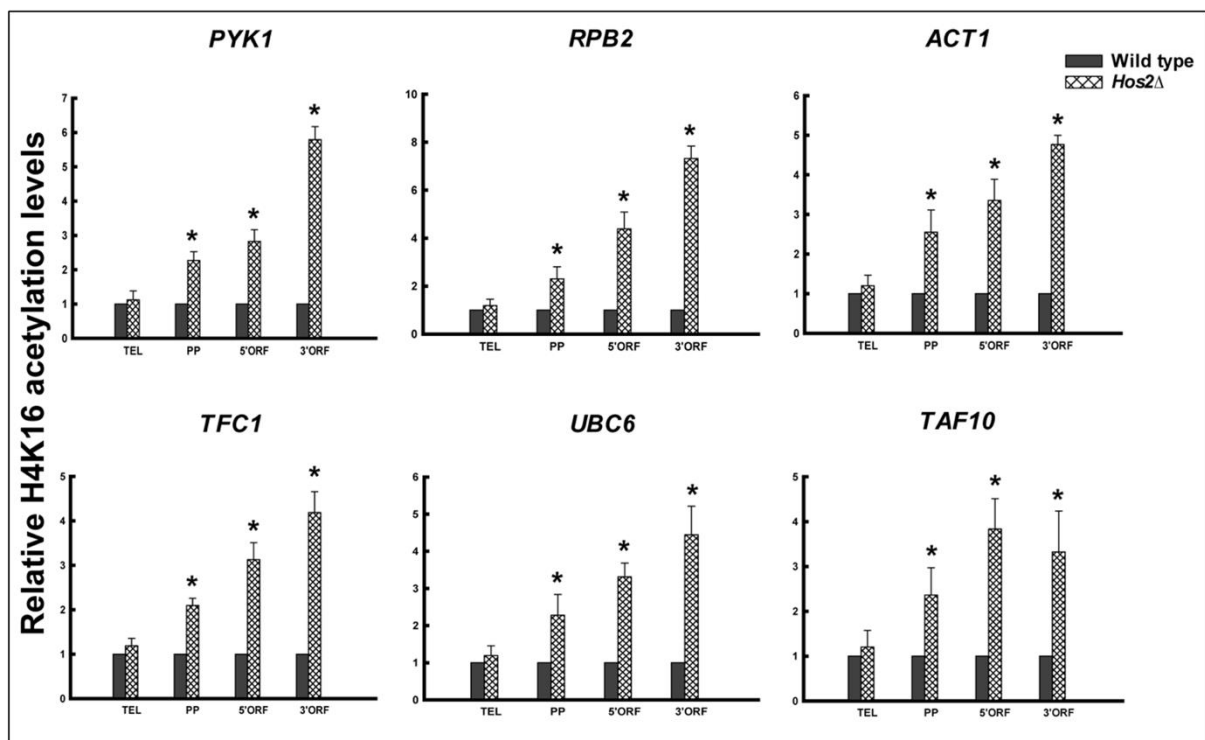
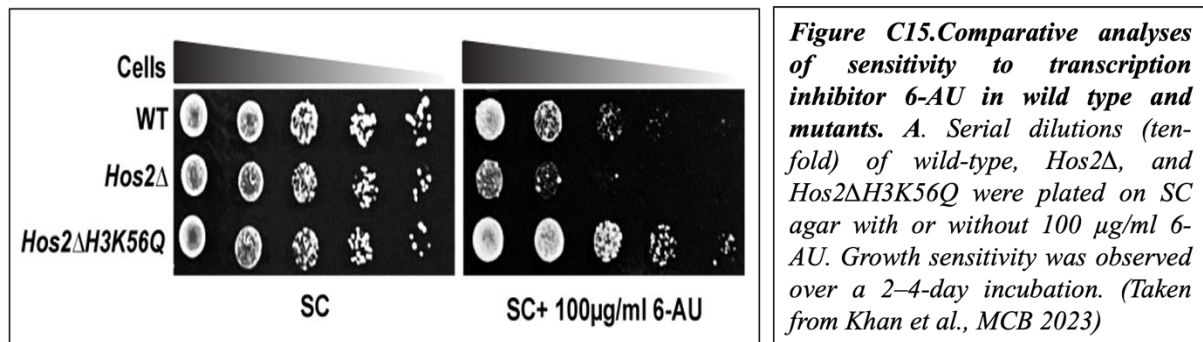


Figure C14. Comparative analyses of H4K16 acetylation levels in wild type and *Hos2Δ* mutant. ChIP qPCR analyses were executed to evaluate H4K16 acetylation levels in the promoter (PP), 5'ORF, and 3'ORF regions of *PYK1*, *RPB2*, *ACT1*, *TFC1*, *UBC6*, *TAF10* loci, alongside a non-transcribing region of *TELO8R* as a control (TEL). The levels of H4K16 acetylation were normalized to ChIP data obtained with an anti-H3 antibody for the corresponding regions. The results were graphically presented to depict the relative levels of H4K16 acetylation in *Sas2Δ* mutants compared to the wild type. The data represents the mean of three independent experiments, with error bars indicating the standard error of the mean. Symbol (*) has been used to highlight t-test significant *P* values of <0.05. (Adapted from Khan et al., MCB 2023)

as, in cells that lacked Hos2 H4K16 acetylation levels were significantly heightened in comparison to wild type (Figure C14).

The subsequent objective was to examine the impact of H4K16 deacetylation mediated by Hos2 on the process of transcription elongation. To achieve this, a cell survivability assay was carried out, comparing wild-type cells with the *Hos2Δ* mutant, both in the presence and absence of 6-AU which is an inhibitor of transcription elongation. 6-AU is a pyrimidine analog that depletes the intracellular UTP and GTP levels in yeast cells and subsequently impairs elongation by RNAPII. Therefore, when yeast cells are grown in presence of 6-AU, it impedes RNAPII elongation and consequently affects growth. Intriguingly, if yeast cells carry mutation or deletion in factors associated with RNAPII elongation, their transcription is impaired more rapidly than in wild type cells. Consequently, these cells display heightened sensitivity to 6-AU^{258,322}.

It was first important to check, whether Hos2 deletion had any general impact on cell survivability. Hence, wild type and *Hos2Δ* mutant were first grown in absence of 6-AU and cell survivability was compared. The results indicated that cell growth under control conditions was comparable between wild type cells and *Hos2Δ* mutant cells. However, when subjected to the presence of 6-AU, *Hos2Δ* mutant exhibited heightened sensitivity compared to wild type, suggesting that Hos2 may play a role in stimulating elongation by RNAPII (Figure C15).



Intriguingly, when H3K56 acetylation was constitutively present in a Hos2 deleted background (*Hos2ΔH3K56Q*), it could alleviate the sensitive phenotype exhibited by the *Hos2Δ* mutant, specifically in presence of 6-AU (Figure C15). This finding further indicated that a crosstalk exists between H4K16 deacetylation mediated by Hos2 and acetylation of H3K56. To strengthen the findings, ChIP based assay was carried out to assess the H3K56 acetylation levels in both wild type cells and *Hos2Δ* mutants. Antibody against acetylated H3K56 was used for immunoprecipitating the samples, qPCR was conducted using primers that amplified a region proximal to the promoter (PP), the 5' coding region (5'-ORF), and the 3' coding region

(3'-ORF). Concurrently, qPCR was also conducted using primers designed for a non-transcribing region within the telomere (*TELO8R*), which served as the control for comparison. Like previous experiments, H3K56 acetylation levels were subjected to normalization by histone H3 levels and depicted graphically in comparison to telomere (*TELO8R*). Clearly, the H3K56 acetylation levels exhibited a decrease in the *Hos2Δ* mutant in comparison to wild type cells across all examined loci. (Figure C16).

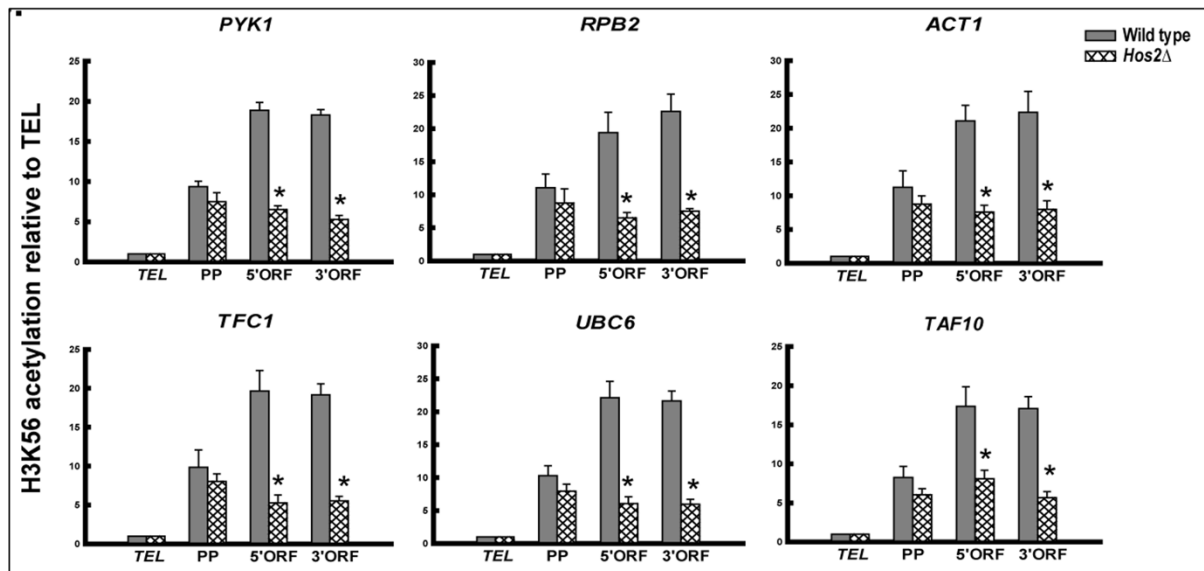


Figure C16. Comparative analysis of H3K56 acetylation levels in wild type and *Hos2Δ* mutants. Chromatin from wild type and *Hos2Δ* was immunoprecipitated with anti-H3K56ac to evaluate H3K56 acetylation levels at the PP, 5'ORF, and 3'ORF of *PYK1*, *RPB2*, *ACT1*, *TFC1*, *UBC6*, and *TAF10* loci. H3K56 acetylation levels were normalized to ChIP data with anti-H3 antibody for the same regions and depicted relative to a non-transcribing control region of *TELO8R* (TEL). The data represents the mean of three independent experiments, with error bars indicating the standard error of the mean. Symbol (*) has been used to highlight t-test significant *P* values of <0.05. (Taken from Khan et al., MCB 2023)

To further correlate these observations with transcription, wild type cells and *Hos2Δ* mutants were subjected to immunoprecipitation with antibodies specific to RNAPII (8WG16) and qPCR was conducted using primers that amplified a region proximal to the promoter (PP), the 5' coding region (5'-ORF), and the 3' coding region (3'-ORF). Occupancy of RNAPII was estimated as a percentage of the input DNA and depicted graphically.

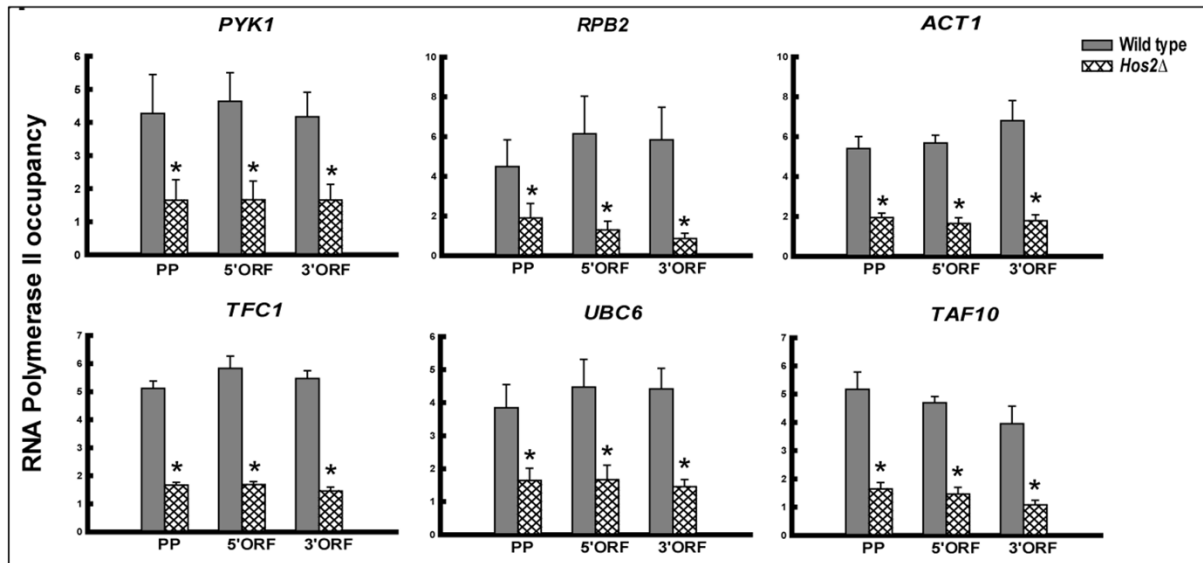


Figure C17. Comparative analysis of RNAPII occupancy in wild type and *Hos2Δ* mutants. Chromatin from wild type and *Hos2Δ* was immunoprecipitated with anti-RNAPII (8WG16) antibody, and occupancy at the PP, 5'ORF, and 3'ORF of the mentioned loci was assessed. The normalized data (1% input) was graphically presented. The data represents the mean of three independent experiments with standard error of mean bars, and * indicates *t*-test significant values $P < 0.05$. (Taken from Khan et al., MCB 2023)

The deletion of *Hos2* was noted to markedly hinder the association of RNAPII throughout the promoter as well as gene bodies of the examined constitutive loci. This underscored the essential role of H4K16 deacetylation mediated by *Hos2* in facilitating RNAPII translocation within the coding region (Figure C17). In summary, the findings imply a dependence of H3K56 acetylation on H4K16 deacetylation and suggest a crucial interplay between the two modifications for mediating elongation by RNAPII.

Constitutive H3K56 acetylation can circumvent the need for H4K16 deacetylation during transcription of constitutively expressed genes

Regulation of transcription is a highly intricate process, where not only the specific combination of histone modifications but also the sequence in which they occur plays a pivotal role. This sequential arrangement of histone modifications has been well-documented in various studies. For instance, one prominent example is the Set1-mediated trimethylation of H3K4, a widely recognized marker of active transcription. This modification is contingent upon a preceding event - the ubiquitination of H2B³²³. In *Drosophila*, another noteworthy sequence of histone modifications has been elucidated. In this context, the phosphorylation of histone H3 at Serine 10 (H3S10) by JIL-1 serves as an upstream event that facilitates the recruitment of 14-3-3 reader protein. In actively transcribing loci, the phosphorylation of

H3S10 and consequent recruitment of 14-3-3 is required for the downstream acetylation of H3K9 to allow RNAPII elongation³²⁴. These findings underscore the significance of not only the specific types of histone modifications but also the precise order in which they occur in orchestrating the dynamics of transcription.

In the present study, co-presence of deacetylation on H4K16 and acetylation on H3K56 emerged as a critical histone code in promoting the transcription of constitutively expressed genes. What is particularly noteworthy is the observation that if H3K56 is constitutively acetylated, it can effectively circumvent the requirement for H4K16 deacetylation mediated by Hos2 during transcription (Figure C15). This observation prompted speculation that H3K56 acetylation could potentially operate as an event occurring subsequent to H4K16 deacetylation and may be involved critically in facilitating the transcription process.

To further elucidate the mechanism and significance of the cross talk between H4K16 deacetylation and H3K56 acetylation four double mutants were generated namely, H4K16RH3K56Q mimicking the constant H4K16 deacetylated state and constant H3K56 acetylated H4K16QH3K56Q mimicking the constitutively acetylated state of H4K16 and constitutively acetylated state of H3K56, H4K16RH3K56R mimicking the constitutively deacetylated state of H4K16 and constant H3K56 deacetylated state and H4K16QH3K56R mimicking the constant H4K16 acetylated state and constitutively deacetylated state of H3K56, respectively. Next, using wild type, single and double mutants, a growth sensitivity assay was performed in presence or absence of 6-AU.

Under control conditions, wild type and mutants showed comparable growth while H3K56R bearing double mutants exhibited moderately reduced growth. Interestingly, in presence of 6-AU, H4K16Q cells exhibited maximum growth sensitivity compared to wild type and single mutant which indicates that transcription is obstructed when H4K16 is acetylated (Figure C18-

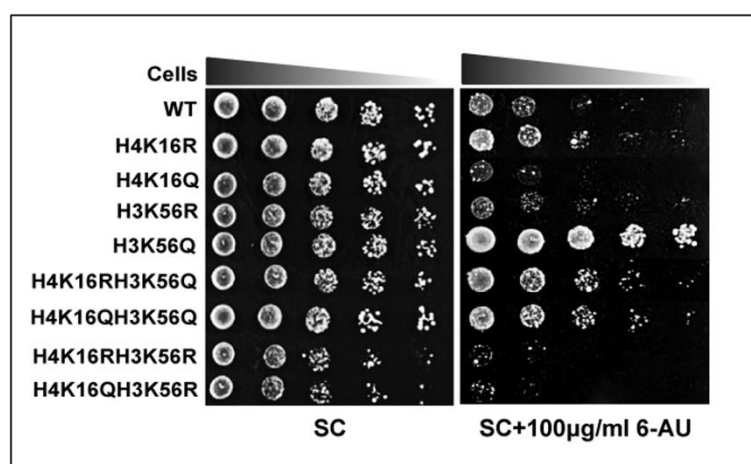


Figure C18. Comparative analyses of sensitivity to transcription inhibitor 6-AU in wild type and mutants. A. Serial dilutions (ten-fold) of wild-type and mutants were plated on SC agar with or without 100 µg/ml 6-AU. Growth sensitivity was observed over a 2–4-day incubation. (Taken from Khan et al., MCB 2023)

right panel). Contrastingly, presence of constant H3K56 acetylation (H3K56Q) conferred least sensitivity to growth in 6-AU in comparison to wild type, suggesting a positive role of H3K56 acetylation in mediating transcription elongation by RNAPII. Notably, any mutant, whether single or double, carrying the H3K56Q mutation displayed heightened resistance when grown in 6-AU (Figure C18-right panel). Thus, maintaining consistent H3K56 acetylation levels proved to alleviate growth sensitivity to 6-AU, regardless of whether H4K16 was consistently acetylated or deacetylated. To further reinforce these observations, RT-qPCR-based study was conducted to directly compare the expression profiles of genes between wild type cells and double mutants. In this study, an absolute quantification method was employed (see Section 11 under Materials and Methods) to precisely quantify and represent the exact copy numbers of transcripts, providing a clear measure of mRNA levels in both wild type cells and double mutants. The findings indicate that the double mutants carrying the H3K56Q mutation, denoted as H4K16RH3K56Q and H4K16QH3K56Q, exhibited significantly elevated expression levels of genes in comparison to wild type, regardless of whether H4K16 had glutamine (Q) mutation or arginine (R) mutation (Figure C19). On the contrary, the double mutants featuring constitutive deacetylation of H3K56, represented as H4K16RH3K56R and H4K16QH3K56R,

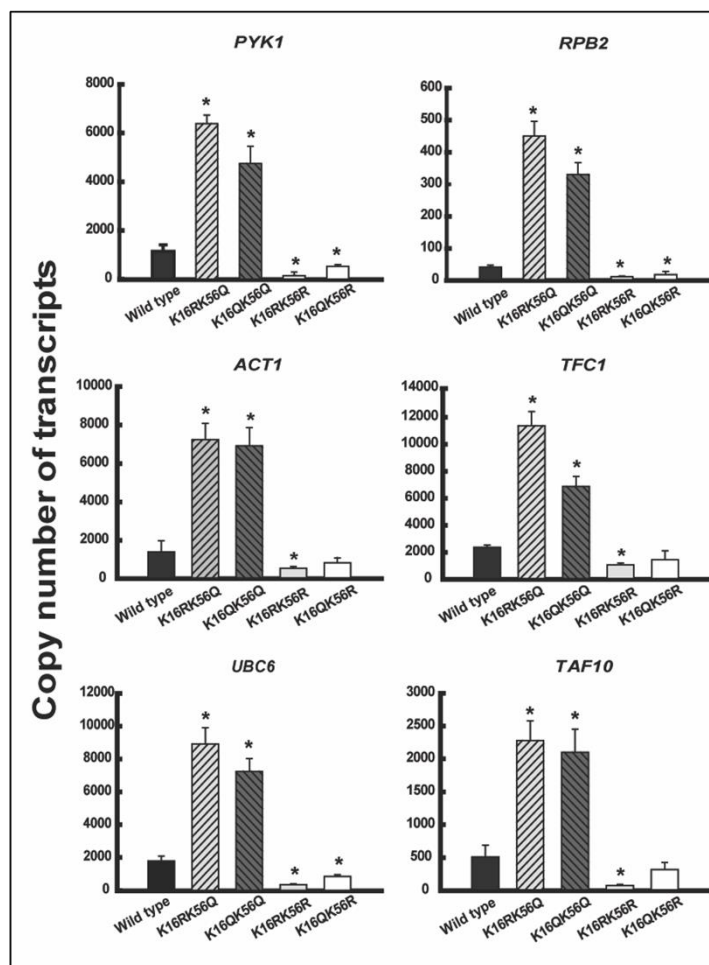


Figure C19. Comparative analysis of gene expression patterns in wild type and mutants. RNA extraction was carried out from both wild-type and mutant samples, followed by RT-qPCR analyses utilizing the absolute quantification method outlined in the Materials and Methods section. The copy numbers of transcripts for PYK1, RPB2, ACT1, TFC1, UBC6, and TAF10 in both wild-type and mutant samples were graphically plotted. The presented data represents the mean of three independent experiments, with standard error of the mean bars included. The asterisks (*) indicate t-test significant P values of <0.05. (Taken from Khan et al., MCB 2023)

significantly dampened expression of genes in comparison to wild type, regardless of the status of H4K16 acetylation (Figure C19).

To further correlate these observations, RNAPII occupancy was assessed in wild type cells and double mutant cells. ChIP- qPCR analysis was done with antibodies against RNAPII (8WG16) and the occupancy was monitored using primers that amplified a region proximal to the promoter (PP), and the 5' coding region (5' ORF) of the constitutive genes. Similar to previous experiments, RNAPII occupancy was graphically represented as a percentage of Input DNA. In consonance with the gene expression profiles, it was evident that any double mutant carrying the H3K56Q mutation exhibited significantly higher RNAPII occupancy in comparison to wild type, regardless of whether H4K16 had glutamine (Q) mutation or arginine (R) mutation (Figure C20). Conversely, in comparison to wild type cells the double mutants with constant deacetylation of H3K56 exhibited markedly reduced occupancy of RNAPII, regardless of the acetylation status of H4K16 (Figure C20). Collectively, these observations suggest the pivotal role of H3K56 acetylation during transcription. What's particularly noteworthy is that H3K56 acetylation was found to drive transcription independently of H4K16's acetylation or deacetylation status. This implies that H3K56 acetylation occurs downstream of H4K16 deacetylation and functions critically in governing the transcription process.

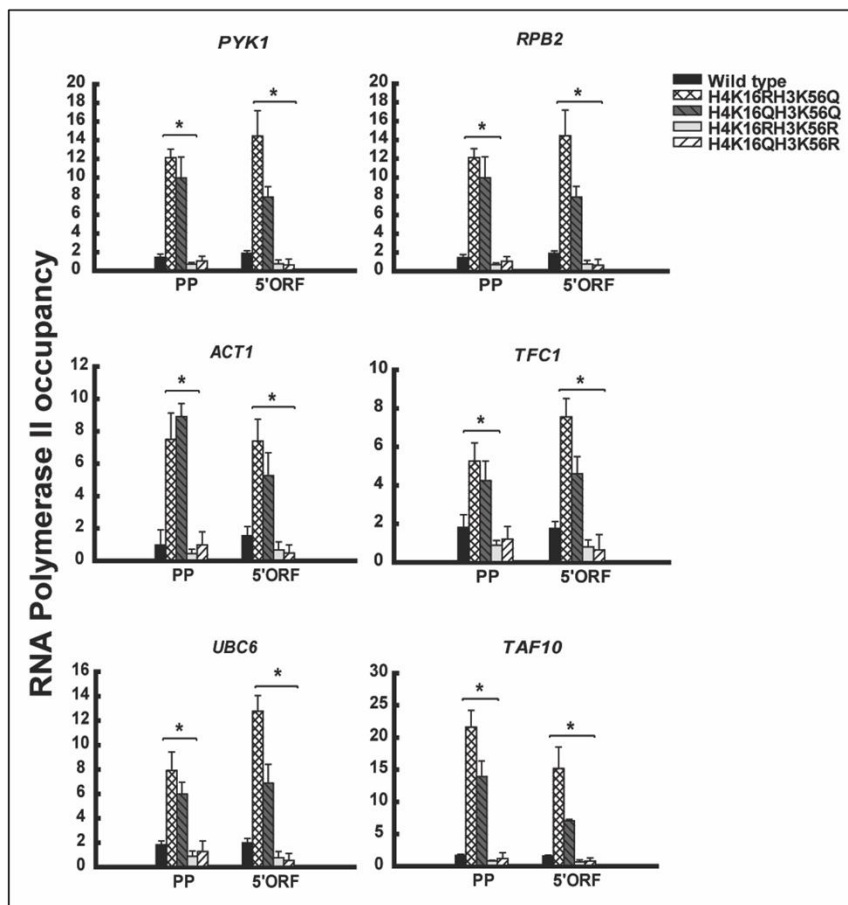


Figure C20.
Comparative analysis of RNAPII occupancy in wild type and mutants. Chromatin from wild type and mutants was immunoprecipitated with anti-RNAPII (8WG16) antibody, and occupancy at the PP, 5'ORF of the mentioned loci was assessed. The normalized data (1% input) was graphically presented. The data represents the mean of three independent experiments with standard error of mean bars, and * indicates t-test significant values $P < 0.05$. (Taken from Khan et al., MCB 2023)

Recruitment of Rtt109, the H3K56ac HAT, requires H4K16 deacetylation

Based on the aforementioned observations, it became evident that H3K56 acetylation served as a critical modification mark for effective transcription. This naturally raised questions about the necessity for H4K16 deacetylation. Multiple modes govern the interplay between two histone modifications, contributing to the intricate phenomena of gene regulation. One such mode involves indirect readout via binding proteins, where a modification interacts indirectly with another modification. Simultaneously, direct cross talk occurs when mutagenesis of a particular residue hinders the modification of another residue, as the modifying enzyme (e.g., HAT) fails to recognize the mutated substrate. These mechanisms are detailed in the literature review sections, and it is noteworthy that they may coexist without exclusivity. From the present observations, a key insight emerged: the absence of H3K56 acetylation in H4K16RH3K56R cells markedly downregulated gene expression and RNAPII occupancy. This implies that deacetylation of H4K16 can enhance the process of transcription only when H3K56 is adequately acetylated. Moreover, the observation indicated that the transcriptional deficiency observed in cells with persistent H4K16 acetylation (H4K16Q) was rectified when H3K56 was continually acetylated (H4K16QH3K56Q). This not only strengthens the crucial involvement of H3K56 acetylation in constitutive gene transcription but also underscores that the deacetylation of H4K16 primarily plays a role in facilitating H3K56 acetylation throughout this process. To further elucidate the observations, a PCR-based homologous recombination method was employed to myc-tag the major HAT responsible for acetylating H3K56, Rtt109, in wild type cells and H4K16 single mutant cells i.e., H4K16R and H4K16Q (see Materials and Methods). Next, in wild type strains and H4K16 mutant strains, ChIP assay was conducted with antibodies against myc tag to test the occupancy of Rtt109 in the constitutively active genes using primers that amplified a region proximal to the promoter (PP), the 5' coding region (5'-ORF) and 3' coding region (3'-ORF). The findings unequivocally demonstrated that in cells with the H4K16Q mutation, where H4K16 deacetylation was absent, the recruitment of Rtt109 was markedly hindered in the constitutively expressed loci, in contrast to the wild-type cells. (Figure C21). On the flip side, the existence of continuous H4K16 deacetylation (H4K16R) positively influenced the recruitment of Rtt109 in comparison to the wild type. Taken together, these outcomes imply the essential role of H4K16 deacetylation in facilitating the chromatin association of Rtt109 and subsequently H3K56 acetylation. Consequently,

hyperacetylation of H4K16 impairs Rtt109 recruitment to the promoter and gene bodies of the examined constitutive genes, leading to impaired transcription regulation.

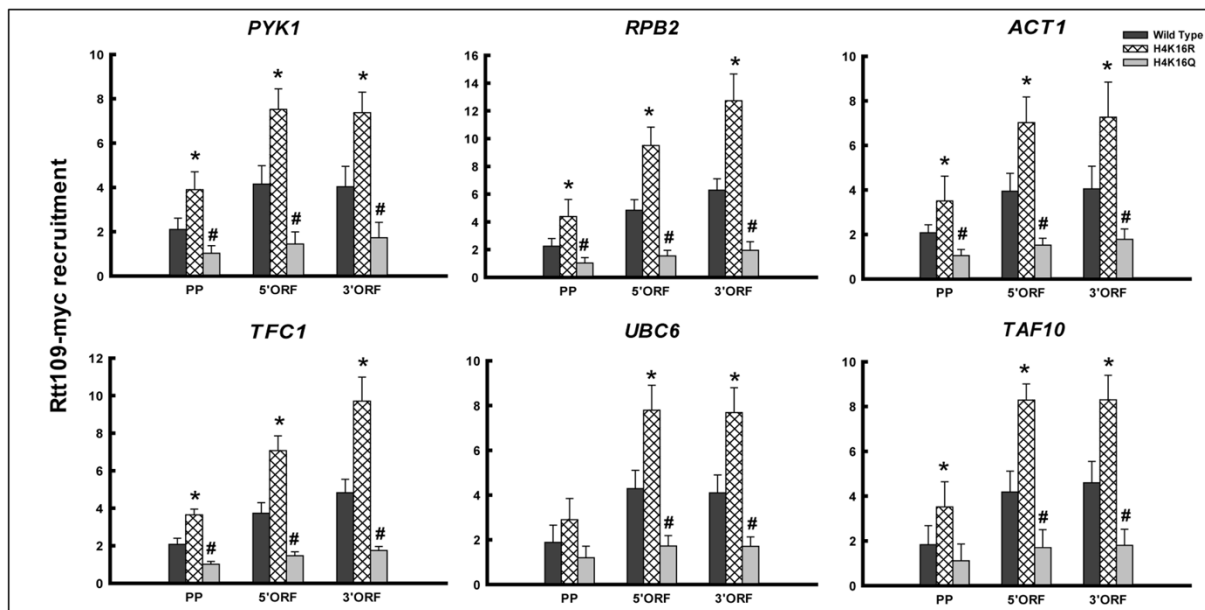


Figure C21. Comparative analysis of Rtt109 recruitment in wild type and H4K16 mutants. Chromatin extracted from wild-type and H4K16 mutants was subjected to immunoprecipitation with an anti-myc antibody to capture myc-tagged Rtt109. Subsequently, the occupancy was assessed through qPCR analyses at the promoter (PP), 5'ORF, and 3'ORF of PYK1, RPB2, ACT1, TFC1, UBC6, and TAF10 loci. The normalized data (1% input) was graphically plotted. The data represents the mean of three independent experiments with standard error of mean bars. Statistically significant values (* and #, $P < 0.05$) are indicated. (Taken from Khan et al., MCB 2023)

RNAPII regulates H3K56 acetylation to facilitate transcription of constitutively expressed genes

In addition to the well-documented role of histone modifications in governing the recruitment of "readers" and "writers" on chromatin, there is compelling evidence that the actively transcribing form of RNAPII plays a pivotal role in orchestrating a diverse array of chromatin modifiers at active loci. This generates an intricate network of histone crosstalk that serves as a crucial mechanism facilitating smooth progression of RNAPII through the gene body. For instance, the Set2 methyltransferase is directed to coding regions during elongation to methylate histone H3K36 by interacting with the phosphorylated Ser2 (Ser2P) of the RNAP II C-terminal domain (CTD)^{319,325,326}. Interestingly, the H3K36me2/3 mark serves as a signal, triggering the HDAC activity of Rpd3C(S) to promote deacetylation of H3 and H4 tail residues within coding regions, ultimately facilitating RNAPII elongation³²⁵. Notably, the phosphorylation of Serine 5 in the RNAPII CTD is instrumental in recruiting the HDAC

Rpd3C(S) to transcribed coding sequences³²⁷. This, in turn, enables the Eaf3 and Rco1 subunits of Rpd3C(S) to establish stable interactions with H3-K36Me2/3 nucleosomes³²⁷. This intricate interplay between active RNAPII and histone modifications underscores the crucial function of RNAPII in regulation of the process of transcription in a chromatin milieu.

In fact, it is well-established that Hos2, the histone deacetylase responsible for H4K16 deacetylation, is directed to active genes by phosphorylated RNAPII³²⁷⁻³²⁹. This linkage suggests that H4K16 deacetylation is contingent upon active transcription. Given the necessity of Hos2-dependent H4K16 deacetylation for H3K56 acetylation, it became crucial to explore the influence of RNAPII activity on H3K56 acetylation. In this investigation, an alternative transcription inhibitor, specifically 1,10-phenanthroline or PH, was utilized to hinder transcription. PH functions as a metal chelator, directly impacting the catalytic activity of RNAPII. This property makes it a potent and versatile transcription inhibitor, often employed for general transcription inhibition purposes^{259,261,330-332}. Wild type cells were treated with or without 200 µg/ml of phenanthroline and total cellular extracts were prepared from these cells (see Materials and Methods). Subsequently, total cellular extracts were immunoblotted with antibodies specific for acetylated H4K16 and acetylated H3K56. Additionally, equal quantities of cell extracts were subjected to immunoprecipitation with an anti-H3 antibody for the purpose of evaluating the cellular H3 levels present within the extracts. The results revealed a marked rise in H4K16 acetylation levels when transcription was inhibited (Figure C22). This observation further confirmed the anti-correlation between H4K16 acetylation and

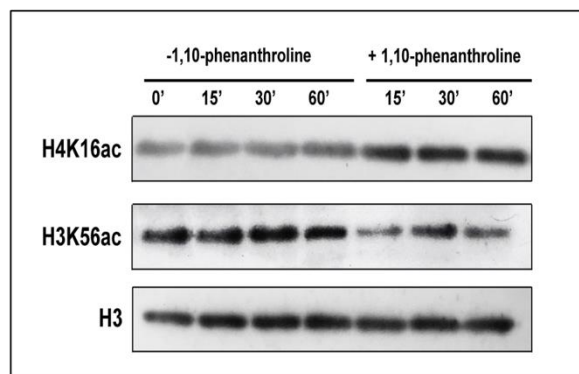


Figure C22. Immunoblot analysis of H4K16 acetylation and H3K56 acetylation levels with or without transcription inhibition in whole cell extracts of wild type. Whole cell extracts from wild type cells treated with or without 1,10-phenanthroline for varying time periods were separated on 16% SDS-PAGE and immunoblotted with anti-H4K16ac, anti-H3K56ac, and anti-H3 antibodies. (Taken from Khan et al., MCB 2023)

transcription. Notably, suppressing transcription via PH treatment led to a noteworthy decrease in the levels of H3K56 acetylation, contrasting with samples that did not undergo PH treatment suggesting that acetylation of H3K56 positively correlates with transcription contrary to H4K16 acetylation. Consequently, abrogation of transcription leads to a decrease in acetylation of H3K56 at cellular levels (Figure C22). Building upon this observation, the next inquiry focused on whether association of Rtt109 with chromatin was dependent on RNAPII activity.

For this, wild type cells were exposed to PH treatment for varying durations and concurrently subjected to immunoprecipitation with antibodies against myc-tag and RNAPII (8WG16) to monitor the occupancy of RNAPII and Rtt109-myc, respectively, with PH or without PH.

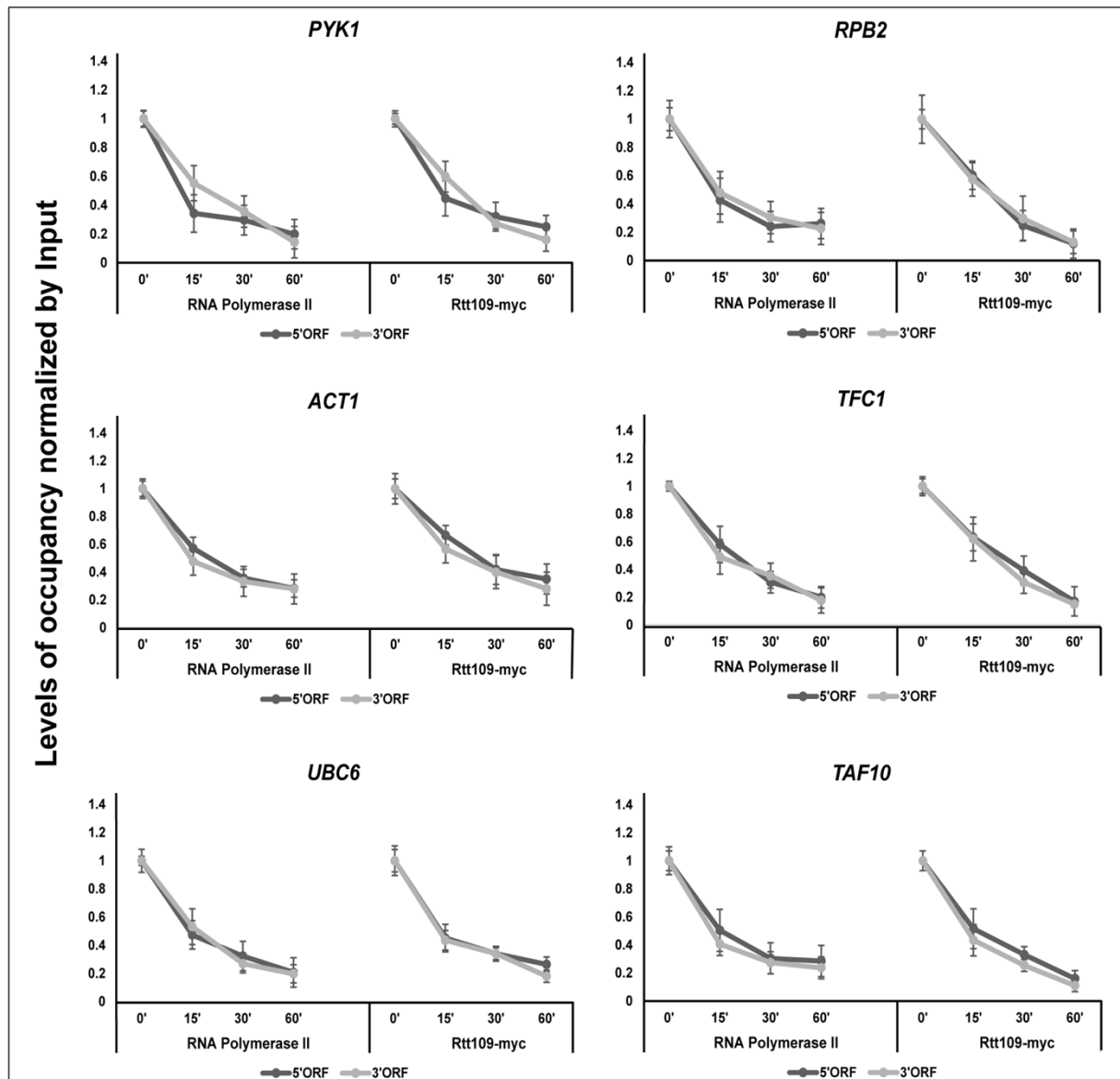


Figure C23. Comparative analyses of RNAPII and Rtt109-myc occupancy in the ORF of constitutive genes upon transcription inhibition. Chromatin isolated from wild type cells treated with or without 1,10-phenanthroline for 15, 30, and 60 min was subjected to immunoprecipitation with anti-RNAPII (8WG16) and anti-myc antibodies. The occupancy of RNAP II and Rtt109-myc in 1,10-phenanthroline treated and untreated (0 min) samples was normalized by input (1%), and occupancy under conditions of transcription inhibition was graphically plotted relative to the untreated (0 min) state in the 5'ORF and 3'ORF of PYK1, RPB2, ACT1, TFC1, UBC6, and TAF10 loci. The data represents the mean of three independent experiments with standard error of mean bars. (Taken from Khan et al., MCB 2023)

The observations revealed a rapid and significant reduction in RNAPII occupancy within 15 minutes of PH treatment across the 5' coding region and 3' coding region of constitutive genes (Figure C23). Further, this reduction intensified with prolonged PH treatment. Interestingly, the association of Rtt109-myc with the coding regions of constitutive genes also exhibited a

pronounced decrease in response to transcription inhibition by PH. Notably, the manner in which Rtt109-myc occupancy decreased in the ORF of constitutive genes strongly correlated with the dissociation of RNAPII upon PH treatment (Figure C23). These collective observations unequivocally suggest a close association between the acetylation machinery of H3K56 and active RNAPII. Hence, in coding regions, both H4K16 deacetylation and active transcription are essential for effective H3K56 acetylation—a crucial event for efficient RNAPII progression through the gene body.



Discussion

The dynamics of chromatin within the coding regions of active genes is crucial for precise regulation of gene expression. This importance stems from the unique challenge presented in the gene body, where maintaining a nucleosome-free state, as seen in gene promoters, is not feasible. Histone post-translational modifications within the gene body demand meticulous control. This strict regulation is essential because reduced nucleosome density in coding regions would carry the risk of initiating transcription from cryptic sites within the open reading frame (ORF), posing a potential threat to genomic integrity. Simultaneously, RNA polymerase II (RNAPII) must also be able to navigate and overcome the nucleosome barrier for effective elongation, adding another layer of complexity to the dynamic interplay within active coding regions. Thus, nucleosome dynamics within coding regions of active genes is critical for transcription regulation. As H3K56ac could critically regulate chromatin accessibility and nucleosome dynamics during NER, the next aim was to understand its function in regulating a vital process such as transcription when occurring in a chromatin environment. In *Saccharomyces cerevisiae*, H3K56 serves as a well-established marker of active transcription, and tightly regulate during transcription the dynamics of nucleosomes at promoter sites, disassembly of chromatin, and exchange of histones^{212,223,333-335}. The present study builds upon this knowledge, revealing within genes that are expressed constitutively a significant elevation of the levels of H3K56 acetylation within gene bodies in comparison to their promoters. Notably, this hyperacetylation pattern positively correlates with transcription levels, indicating a potential regulatory role for H3K56 acetylation. The study further underscores the importance of H3K56 acetylation by demonstrating that the absence of such acetylation, as seen in the H3K56R mutant, significantly obstructs the RNAPII occupancy, particularly in the active gene bodies. This aligns with earlier reports suggesting that H3K56 acetylation participates in facilitating the DNA unfolding at entry/exit sites, thereby enabling the translocation of RNAPII through nucleosomes²²⁰. Collectively, these observations not only support prior findings but also emphasize the positive role of H3K56 acetylation during transcription.

However, histone modifications rarely act in isolation; instead, they often engage in combinatorial interactions where the interplay of different modifications effectively contributes to a DNA dependent process. In a preceding study (refer to Background study), the impact of deacetylation of H4K16 on constitutive gene expression was explored. Interestingly, a reciprocal relationship was discovered between H4K16 acetylation and transcription, wherein a consistently deacetylated state of H4K16 was associated with enhanced gene expression. Furthermore, the deacetylation of H4K16 was noted to impact the acetylation status of the core domain residue of histone H3, H3K56, thereby exerting regulatory control over

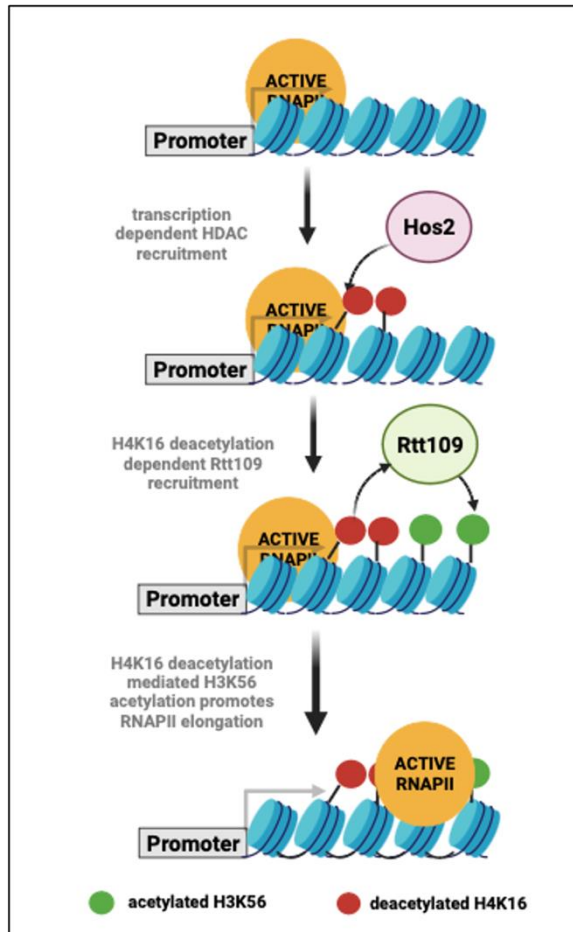
transcription²⁴⁵. In the present investigation, it was noted that the persistence of H4K16 deacetylation, in the absence of the HAT Sas2, fostered H3K56 hyperacetylation within the gene bodies of continually active loci. Conversely, the absence of Hos2, the histone deacetylase for H4K16 deacetylation, led to a substantial reduction in both the acetylation of H3K56 as well as RNAPII recruitment along the active loci. Previous observations in *B. bassiana* have corroborated these findings, demonstrating that the deletion of Hos2 results in a decrease in H3K56 acetylation³³⁶. Collectively, it strongly indicates the essentiality of deacetylation of H4K16 in order to acetylate H3K56. Given the positive correlation observed between both deacetylation of H4K16 and H3K56 acetylation with gene expression, this study primarily focussed on unravelling the interplay between H4K16 deacetylation and H3K56 acetylation and elucidating their collective impact on gene regulation. The intricate interplay between H4K16 deacetylation and H3K56 acetylation, revealed a nuanced regulatory mechanism in the transcriptional landscape. Notably, the study unveiled a remarkable observation in context to this: continuous acetylation of H3K56 even when H4K16 could not be deacetylated, as seen in the *Hos2ΔH3K56Q* mutant, was able to alleviate the transcription defect observed in the absence of H4K16 deacetylation. This intriguing finding suggested that while H4K16 deacetylation is positively correlated with transcription, its need could be circumvented if H3K56 was constantly acetylated.

The strength of this notion was further reinforced by the observations that the existence of constant acetylation of H3K56 enabled cells to override transcription inhibition irrespective of whether H4K16 was constantly acetylated or deacetylated. Subsequent analyses of the profiles of gene expression and the RNAPII occupancy levels in the double mutants provided further evidence that H3K56 acetylation played a crucial role in transcription. Particularly noteworthy was the finding that under situations where H3K56 acetylation was constantly present, as observed in cells with the H3K56Q mutation, the necessity for deacetylating H4K16 could be circumvented. This finding, indicating that the existence of persistent H3K56 acetylation rendered transcription independent of the acetylation status of H4K16, held significant implications. It suggested that H4K16 deacetylation could only aid transcription if H3K56 acetylation was present. Consequently, the transcriptional defect seen in H4K16Q cells could be rectified in the presence of constant H3K56 acetylation (H4K16QH3K56Q). This led to the fundamental question: What exactly is the function of H4K16 deacetylation in relation to H3K56 acetylation? The study delves into this question and dissects the mechanism by which H4K16 deacetylation operates. Interestingly, the findings suggest a reliance on the deacetylation of H4K16 for the chromatin binding of Rtt109 which is the principle HAT that

acetylates H3K56. This implies that H4K16 deacetylation plays a crucial role in generating a accommodating chromatin environment that allows the subsequent acetylation of H3K56 by facilitating recruitment of the acetyltransferase Rtt109. The N- and C-terminal tail acetylation of H3 and H4 lysine residues has long been associated with transcription activation, primarily due to their ability to facilitate the recruitment of histone acetyltransferases (HATs) via their bromodomains to transcribing loci³³⁷. However, Rtt109 presents a unique case among acetyltransferases as it lacks a bromodomain, a common feature in many acetyltransferases. Instead, the activation of Rtt109 depends on a histone chaperone, specifically either Vps75 (Vacuolar Protein Sorting 75) or Asf1 (Anti-silencing factor 1)³³⁸. The choice of chaperone, Vps75 or Asf1, determines which histone lysine residues are acetylated by Rtt109³³⁹. When Rtt109 associates with Asf1, it acetylates H3K56. Asf1 plays a crucial role by interacting with histone H4 and stabilizing the β strand at the extreme C-terminus of histone H4, which is a prerequisite for the acetylation of H3K56 by Rtt109³⁴⁰. Furthermore, a study has previously indicated that the lack of the N-terminal histone H3 and H4 tails hinders the Rtt109-mediated acetylation of H3K56²¹³. This implies that there exists a regulatory function of histone tails in the acetylation process of H3K56 by Rtt109. Although, Rtt109 lacks a bromodomain, HAT complexes containing bromodomains, such as Gen5, which are also known to associate with transcriptionally active loci preferentially bind to histones acetylated at H4K16^{341,342}. It is plausible that the binding of such large HAT complexes might lead to steric hindrance, potentially impeding the interaction of the machinery that acetylates H3K56 with its target residue. Hence, a plausible mechanism may be in play where the removal of acetyl groups from the N-terminal tail residue H4K16, may create a favourable environment for Rtt109 to effectively associate with H3 and acetylate the lysine 56 residue. Notably, the necessity for H3K56 acetylation extends beyond the sole prerequisite of H4K16 deacetylation. This interplay is intricately tied to the transcriptional process, as evidenced by the essential requirement for active RNAPII in facilitating H3K56 acetylation. In essence, both H4K16 deacetylation and H3K56 acetylation are contingent on the dynamics of active transcription, highlighting a reciprocal relationship between histone modifications and ongoing gene expression. Intriguingly, the fact that the association of the H3K56 HAT, Rtt109 with the ORF of genes that are constitutively active relies on RNAPII activity is a very important observation. The H3K56 residue, situated laterally on the histone octamer surface and typically shielded by nucleosomal DNA, was initially believed to undergo acetylation primarily on free histones before their deposition onto chromatin²¹³.

Fascinatingly, recent investigations have unveiled an interesting aspect of RNAPII when confronted with the nucleosome barrier. These studies propose the utilization of a peeling mechanism by RNAPII, involving the deliberate tearing off of DNA from the histone surface. This process exposes pivotal sites on the histones, providing access points for chromatin-modifying enzymes³⁴³. Drawing from this, the fact that recruitment of Rtt109 is dependent on RNAPII within the actively transcribing coding regions raise intriguing possibilities. Specifically, the observations suggest that transcription itself may serve as a mechanism that facilitates H3K56 acetylation, even in the context of nucleosomal histones. This implies that as RNAPII progresses through the gene, encountering nucleosomes, it initiates a process where DNA is peeled away from the histone surface. This peeling action exposes specific histone residues, such as H3K56, rendering them accessible for modification. The recruitment of Rtt109, a histone acetyltransferase responsible for H3K56 acetylation, in a transcription-dependent manner supports the notion that the transcriptional machinery actively participates in modifying the chromatin landscape. However, it remains intriguing to ascertain whether there is a direct interaction between RNAPII and Rtt109. Notably, in this study, attempts were made to capture a physical interaction of Rtt109 with RNAPII. However, no such interaction could be detected, either due to its absence or limitations in the experimental conditions employed. Nevertheless, the robust correlation observed between the recruitment of Rtt109 and the occupancy of RNAPII introduces an intriguing possibility. It suggests that the localized disruptions in chromatin induced by RNAPII, wherein histone-DNA contacts are weakened, may create favorable conditions for Rtt109 to access the H3K56 residue on chromatin, thereby facilitating its acetylation in a way that intricately relies on the deacetylated state of H4K16. This notion gains support from mammalian studies, where the nucleosome disruption by nucleosome-destabilization factors (NDF) has been demonstrated to enable p300-CBP to acetylate H3K56 on histones that are nucleosomal³⁴⁴. A comparable mechanism could potentially be operative that enables Rtt109 to bind and subsequently acetylate H3K56 during transcription on a chromatinized structure. Further studies in the future in this direction hold the promise of unveiling more about the underlying mechanisms. Regardless of how RNAPII guides Rtt109 to active regions, the study suggests that H3K56 acetylation is not merely a consequence of transcription; rather, it emerges as a fundamental driver of the transcriptional process. Without H3K56 acetylation, the elongation of RNAPII through the genome is hindered.

The current scenario as illustrated in the model (left-bottom panel) implies the existence of a feedforward mechanism where active RNAPII signals the recruitment of specific histone deacetylases (HDACs) for H4K16 deacetylation. Subsequently, this deacetylation promotes recruitment of histone acetyltransferase (HAT) Rtt109 for H3K56 acetylation, ultimately facilitating efficient translocation of RNAPII through the genome.



Schematic representing the transcription dependent crosstalk between H4K16 deacetylation and H3K56 acetylation that regulates efficient RNAPII-mediated elongation.

In essence, the proposed mechanism suggests a sophisticated regulatory loop, where the transcriptional machinery actively participates in shaping the chromatin landscape. The interplay between histone modifications and the transcriptional process is not merely a sequential event; rather, it reflects a dynamic and reciprocal relationship, where transcription both influences and is influenced by the chromatin environment. The study underscores the complexity of these regulatory networks and points towards the need for further investigations to unravel the intricate details of how histone modifications orchestrate and respond to the process of transcription.

SUMMARY AT A GLANCE

This study investigates the impact of H3K56 acetylation on chromatin dynamics using two DNA metabolic tools, namely Nucleotide Excision Repair (NER) and transcription.

- Utilizing H3K56 mutants (H3K56R and H3K56Q) the study reveals the importance of H3K56 acetylation in regulating early NER events.
- H3K56 acetylation is crucial for recruiting Rad16 and promoting H3 tail hyperacetylation during initial repair phases.
- H3K56 acetylation facilitates UV-induced chromatin oscillation, indicating its role in nucleosome dynamics and DNA accessibility during NER.
- Besides NER, the study reveals that H3K56 hyperacetylation is essential for RNA Polymerase II (RNAPII) recruitment and effective transcription of constitutively expressed genes.
- Hos2-dependent deacetylation of H4K16 is found to be a prerequisite for H3K56 acetylation and consequently RNAPII progression within gene bodies.
- Interestingly, H4K16 deacetylation is dispensable in the presence of constitutive H3K56 acetylation for effective transcription indicating that H4K16 deacetylation is an upstream event primarily required to promote H3K56 acetylation during transcription.
- Strikingly, H4K16 deacetylation and H3K56 acetylation are both dependent on active transcription. RNAPII activity is essential for recruitment of the H3K56 acetyltransferase Rtt109 to active regions thus indicating a feed forward mechanism of transcription maintenance in constitutively active loci.

In summary, the findings of this study underscore the significance of H3K56 acetylation not only in the specific context of Nucleotide Excision Repair (NER) but also in its broader role of shaping the chromatin environment and exerting a discernible influence on the outcomes of the process of transcription.



BIBLIOGRAPHY

- 1 Crick, F. Central Dogma of Molecular Biology. *Nature* **227**, 561-563, doi:10.1038/227561a0 (1970).
- 2 Jin, J. *et al.* In and out: histone variant exchange in chromatin. *Trends in biochemical sciences* **30**, 680-687, doi:10.1016/j.tibs.2005.10.003 (2005).
- 3 Bowman, G. D. & Poirier, M. G. Post-Translational Modifications of Histones That Influence Nucleosome Dynamics. *Chemical reviews* **115**, 2274-2295, doi:10.1021/cr500350x (2015).
- 4 Hübner, M. R. & Spector, D. L. Chromatin dynamics. *Annual review of biophysics* **39**, 471-489, doi:10.1146/annurev.biophys.093008.131348 (2010).
- 5 Grewal, S. I. & Moazed, D. Heterochromatin and epigenetic control of gene expression. *Science (New York, N.Y.)* **301**, 798-802, doi:10.1126/science.1086887 (2003).
- 6 Wegel, E. & Shaw, P. Gene activation and deactivation related changes in the three-dimensional structure of chromatin. *Chromosoma* **114**, 331-337, doi:10.1007/s00412-005-0015-7 (2005).
- 7 Saksouk, N., Simboeck, E. & Déjardin, J. Constitutive heterochromatin formation and transcription in mammals. *Epigenetics & Chromatin* **8**, 3, doi:10.1186/1756-8935-8-3 (2015).
- 8 Rego, A., Sinclair, P. B., Tao, W., Kireev, I. & Belmont, A. S. The facultative heterochromatin of the inactive X chromosome has a distinctive condensed ultrastructure. *Journal of cell science* **121**, 1119-1127, doi:10.1242/jcs.026104 (2008).
- 9 Gilbert, N. *et al.* Chromatin architecture of the human genome: gene-rich domains are enriched in open chromatin fibers. *Cell* **118**, 555-566, doi:10.1016/j.cell.2004.08.011 (2004).
- 10 Maeshima, K., Ide, S. & Babokhov, M. Dynamic chromatin organization without the 30-nm fiber. *Current opinion in cell biology* **58**, 95-104, doi:10.1016/j.ceb.2019.02.003 (2019).
- 11 Adolph, K. W., Cheng, S. M. & Laemmli, U. K. Role of nonhistone proteins in metaphase chromosome structure. *Cell* **12**, 805-816, doi:10.1016/0092-8674(77)90279-3 (1977).
- 12 Adolph, K. W., Cheng, S. M., Paulson, J. R. & Laemmli, U. K. Isolation of a protein scaffold from mitotic HeLa cell chromosomes. *Proceedings of the National Academy of Sciences of the United States of America* **74**, 4937-4941, doi:10.1073/pnas.74.11.4937 (1977).
- 13 Woodcock, C. L., Grigoryev, S. A., Horowitz, R. A. & Whitaker, N. A chromatin folding model that incorporates linker variability generates fibers resembling the native structures. *Proceedings of the National Academy of Sciences of the United States of America* **90**, 9021-9025, doi:10.1073/pnas.90.19.9021 (1993).
- 14 Woodcock, C. L. & Ghosh, R. P. Chromatin higher-order structure and dynamics. *Cold Spring Harbor perspectives in biology* **2**, a000596, doi:10.1101/cshperspect.a000596 (2010).
- 15 Horn, P. J. & Peterson, C. L. Molecular biology. Chromatin higher order folding--wrapping up transcription. *Science (New York, N.Y.)* **297**, 1824-1827, doi:10.1126/science.1074200 (2002).
- 16 Maeshima, K., Hihara, S. & Eltsov, M. Chromatin structure: does the 30-nm fibre exist in vivo? *Current opinion in cell biology* **22**, 291-297, doi:10.1016/j.ceb.2010.03.001 (2010).
- 17 Hansen, J. C. Conformational dynamics of the chromatin fiber in solution: determinants, mechanisms, and functions. *Annual review of biophysics and biomolecular structure* **31**, 361-392, doi:10.1146/annurev.biophys.31.101101.140858 (2002).
- 18 Hansen, J. C. *et al.* The 10-nm chromatin fiber and its relationship to interphase chromosome organization. *Biochemical Society transactions* **46**, 67-76, doi:10.1042/bst20170101 (2018).
- 19 Hancock, R. Structure of metaphase chromosomes: a role for effects of macromolecular crowding. *PloS one* **7**, e36045, doi:10.1371/journal.pone.0036045 (2012).
- 20 Maeshima, K., Imai, R., Tamura, S. & Nozaki, T. Chromatin as dynamic 10-nm fibers. *Chromosoma* **123**, 225-237, doi:10.1007/s00412-014-0460-2 (2014).
- 21 Luger, K., Mäder, A. W., Richmond, R. K., Sargent, D. F. & Richmond, T. J. Crystal structure of the nucleosome core particle at 2.8 Å resolution. *Nature* **389**, 251-260, doi:10.1038/38444 (1997).

- 22 Arents, G. & Moudrianakis, E. N. The histone fold: a ubiquitous architectural motif utilized in DNA compaction and protein dimerization. *Proceedings of the National Academy of Sciences of the United States of America* **92**, 11170-11174, doi:10.1073/pnas.92.24.11170 (1995).
- 23 Baldi, S., Korber, P. & Becker, P. B. Beads on a string—nucleosome array arrangements and folding of the chromatin fiber. *Nature structural & molecular biology* **27**, 109-118, doi:10.1038/s41594-019-0368-x (2020).
- 24 Robinson, P. J., Fairall, L., Huynh, V. A. & Rhodes, D. EM measurements define the dimensions of the "30-nm" chromatin fiber: evidence for a compact, interdigitated structure. *Proceedings of the National Academy of Sciences of the United States of America* **103**, 6506-6511, doi:10.1073/pnas.0601212103 (2006).
- 25 Robinson, P. J. & Rhodes, D. Structure of the '30 nm' chromatin fibre: a key role for the linker histone. *Current opinion in structural biology* **16**, 336-343, doi:10.1016/j.sbi.2006.05.007 (2006).
- 26 Finch, J. T. & Klug, A. Solenoidal model for superstructure in chromatin. *Proceedings of the National Academy of Sciences of the United States of America* **73**, 1897-1901, doi:10.1073/pnas.73.6.1897 (1976).
- 27 Widom, J. & Klug, A. Structure of the 300Å chromatin filament: X-ray diffraction from oriented samples. *Cell* **43**, 207-213, doi:10.1016/0092-8674(85)90025-x (1985).
- 28 Williams, S. P. *et al.* Chromatin fibers are left-handed double helices with diameter and mass per unit length that depend on linker length. *Biophysical journal* **49**, 233-248, doi:10.1016/s0006-3495(86)83637-2 (1986).
- 29 Sedat, J. & Manuelidis, L. A direct approach to the structure of eukaryotic chromosomes. *Cold Spring Harbor symposia on quantitative biology* **42 Pt 1**, 331-350, doi:10.1101/sqb.1978.042.01.035 (1978).
- 30 Maeshima, K. & Laemmli, U. K. A two-step scaffolding model for mitotic chromosome assembly. *Developmental cell* **4**, 467-480, doi:10.1016/s1534-5807(03)00092-3 (2003).
- 31 Strukov, Y. G., Wang, Y. & Belmont, A. S. Engineered chromosome regions with altered sequence composition demonstrate hierarchical large-scale folding within metaphase chromosomes. *The Journal of cell biology* **162**, 23-35, doi:10.1083/jcb.200303098 (2003).
- 32 Narwade, N. *et al.* Mapping of scaffold/matrix attachment regions in human genome: a data mining exercise. *Nucleic Acids Res* **47**, 7247-7261, doi:10.1093/nar/gkz562 (2019).
- 33 Banfalvi, G. Chromatin fiber structure and plectonemic model of chromosome condensation in *Drosophila* cells. *DNA and cell biology* **27**, 65-70, doi:10.1089/dna.2007.0671 (2008).
- 34 van Steensel, B. & Belmont, A. S. Lamina-Associated Domains: Links with Chromosome Architecture, Heterochromatin, and Gene Repression. *Cell* **169**, 780-791, doi:10.1016/j.cell.2017.04.022 (2017).
- 35 Matheson, T. D. & Kaufman, P. D. Grabbing the genome by the NADs. *Chromosoma* **125**, 361-371, doi:10.1007/s00412-015-0527-8 (2016).
- 36 Bizhanova, A. & Kaufman, P. D. Close to the edge: Heterochromatin at the nucleolar and nuclear peripheries. *Biochimica et Biophysica Acta (BBA) - Gene Regulatory Mechanisms* **1864**, 194666, doi:<https://doi.org/10.1016/j.bbagr.2020.194666> (2021).
- 37 Dixon, J. R., Gorkin, D. U. & Ren, B. Chromatin Domains: The Unit of Chromosome Organization. *Mol Cell* **62**, 668-680, doi:10.1016/j.molcel.2016.05.018 (2016).
- 38 Beagan, J. A. & Phillips-Cremins, J. E. On the existence and functionality of topologically associating domains. *Nature Genetics* **52**, 8-16, doi:10.1038/s41588-019-0561-1 (2020).
- 39 Li, G. & Reinberg, D. Chromatin higher-order structures and gene regulation. *Current opinion in genetics & development* **21**, 175-186, doi:10.1016/j.gde.2011.01.022 (2011).
- 40 Schwartz, U. *et al.* Characterizing the nuclease accessibility of DNA in human cells to map higher order structures of chromatin. *Nucleic Acids Res* **47**, 1239-1254, doi:10.1093/nar/gky1203 (2019).

- 41 Poirier, M. G., Bussiek, M., Langowski, J. & Widom, J. Spontaneous access to DNA target sites in folded chromatin fibers. *J Mol Biol* **379**, 772-786, doi:10.1016/j.jmb.2008.04.025 (2008).
- 42 Poirier, M. G., Oh, E., Tims, H. S. & Widom, J. Dynamics and function of compact nucleosome arrays. *Nature structural & molecular biology* **16**, 938-944, doi:10.1038/nsmb.1650 (2009).
- 43 Hihara, S. *et al.* Local nucleosome dynamics facilitate chromatin accessibility in living mammalian cells. *Cell reports* **2**, 1645-1656, doi:10.1016/j.celrep.2012.11.008 (2012).
- 44 Luger, K., Mäder, A. W., Richmond, R. K., Sargent, D. F. & Richmond, T. J. Crystal structure of the nucleosome core particle at 2.8 Å resolution. *Nature* **389**, 251-260, doi:10.1038/38444 (1997).
- 45 White, C. L., Suto, R. K. & Luger, K. Structure of the yeast nucleosome core particle reveals fundamental changes in internucleosome interactions. *The EMBO journal* **20**, 5207-5218, doi:10.1093/emboj/20.18.5207 (2001).
- 46 Richmond, T. J., Finch, J. T., Rushton, B., Rhodes, D. & Klug, A. Structure of the nucleosome core particle at 7 Å resolution. *Nature* **311**, 532-537, doi:10.1038/311532a0 (1984).
- 47 Simpson, R. T. Structure of the chromatosome, a chromatin particle containing 160 base pairs of DNA and all the histones. *Biochemistry* **17**, 5524-5531, doi:10.1021/bi00618a030 (1978).
- 48 Ramakrishnan, V., Finch, J. T., Graziano, V., Lee, P. L. & Sweet, R. M. Crystal structure of globular domain of histone H5 and its implications for nucleosome binding. *Nature* **362**, 219-223, doi:10.1038/362219a0 (1993).
- 49 Lohr, D. & Hereford, L. Yeast chromatin is uniformly digested by DNase-I. *Proceedings of the National Academy of Sciences of the United States of America* **76**, 4285-4288, doi:10.1073/pnas.76.9.4285 (1979).
- 50 Grunstein, M. Histone function in transcription. *Annual review of cell biology* **6**, 643-678, doi:10.1146/annurev.cb.06.110190.003235 (1990).
- 51 Godde, J. S. & Widom, J. Chromatin structure of *Schizosaccharomyces pombe*. A nucleosome repeat length that is shorter than the chromatosomal DNA length. *J Mol Biol* **226**, 1009-1025, doi:10.1016/0022-2836(92)91049-u (1992).
- 52 Patterson, H. G., Landel, C. C., Landsman, D., Peterson, C. L. & Simpson, R. T. The biochemical and phenotypic characterization of Hho1p, the putative linker histone H1 of *Saccharomyces cerevisiae*. *The Journal of biological chemistry* **273**, 7268-7276, doi:10.1074/jbc.273.13.7268 (1998).
- 53 Richmond, T. J. & Davey, C. A. The structure of DNA in the nucleosome core. *Nature* **423**, 145-150, doi:10.1038/nature01595 (2003).
- 54 Wang, D., Ulyanov, N. B. & Zhurkin, V. B. Sequence-dependent Kink-and-Slide deformations of nucleosomal DNA facilitated by histone arginines bound in the minor groove. *Journal of biomolecular structure & dynamics* **27**, 843-859, doi:10.1080/07391102.2010.10508586 (2010).
- 55 van Holde, K. & Zlatanova, J. Chromatin higher order structure: chasing a mirage? *The Journal of biological chemistry* **270**, 8373-8376, doi:10.1074/jbc.270.15.8373 (1995).
- 56 Simon, M. *et al.* Histone fold modifications control nucleosome unwrapping and disassembly. *Proceedings of the National Academy of Sciences of the United States of America* **108**, 12711-12716, doi:10.1073/pnas.1106264108 (2011).
- 57 Zhou, K., Gaullier, G. & Luger, K. Nucleosome structure and dynamics are coming of age. *Nature structural & molecular biology* **26**, 3-13, doi:10.1038/s41594-018-0166-x (2019).
- 58 Arents, G., Burlingame, R. W., Wang, B. C., Love, W. E. & Moudrianakis, E. N. The nucleosomal core histone octamer at 3.1 Å resolution: a tripartite protein assembly and a left-handed superhelix. *Proceedings of the National Academy of Sciences of the United States of America* **88**, 10148-10152, doi:10.1073/pnas.88.22.10148 (1991).
- 59 Baxeavanis, A. D., Arents, G., Moudrianakis, E. N. & Landsman, D. A variety of DNA-binding and multimeric proteins contain the histone fold motif. *Nucleic Acids Res* **23**, 2685-2691, doi:10.1093/nar/23.14.2685 (1995).

- 60 McGinty, R. K. & Tan, S. Nucleosome structure and function. *Chemical reviews* **115**, 2255-2273, doi:10.1021/cr500373h (2015).
- 61 Venkatesh, S. & Workman, J. L. Histone exchange, chromatin structure and the regulation of transcription. *Nature Reviews Molecular Cell Biology* **16**, 178-189, doi:10.1038/nrm3941 (2015).
- 62 Cutter, A. R. & Hayes, J. J. A brief review of nucleosome structure. *FEBS letters* **589**, 2914-2922, doi:10.1016/j.febslet.2015.05.016 (2015).
- 63 Walker, I. O. Differential dissociation of histone tails from core chromatin. *Biochemistry* **23**, 5622-5628, doi:10.1021/bi00318a037 (1984).
- 64 Smith, R. M. & Rill, R. L. Mobile histone tails in nucleosomes. Assignments of mobile segments and investigations of their role in chromatin folding. *The Journal of biological chemistry* **264**, 10574-10581 (1989).
- 65 Ausio, J., Dong, F. & van Holde, K. E. Use of selectively trypsinized nucleosome core particles to analyze the role of the histone "tails" in the stabilization of the nucleosome. *J Mol Biol* **206**, 451-463, doi:10.1016/0022-2836(89)90493-2 (1989).
- 66 Lee, D. Y., Hayes, J. J., Pruss, D. & Wolffe, A. P. A positive role for histone acetylation in transcription factor access to nucleosomal DNA. *Cell* **72**, 73-84, doi:10.1016/0092-8674(93)90051-q (1993).
- 67 Polach, K. J., Lowary, P. T. & Widom, J. Effects of core histone tail domains on the equilibrium constants for dynamic DNA site accessibility in nucleosomes. *J Mol Biol* **298**, 211-223, doi:10.1006/jmbi.2000.3644 (2000).
- 68 Vettese-Dadey, M., Walter, P., Chen, H., Juan, L. J. & Workman, J. L. Role of the histone amino termini in facilitated binding of a transcription factor, GAL4-AH, to nucleosome cores. *Mol Cell Biol* **14**, 970-981, doi:10.1128/mcb.14.2.970-981.1994 (1994).
- 69 Lee, K. M. & Hayes, J. J. The N-terminal tail of histone H2A binds to two distinct sites within the nucleosome core. *Proceedings of the National Academy of Sciences of the United States of America* **94**, 8959-8964, doi:10.1073/pnas.94.17.8959 (1997).
- 70 Lee, K. M. & Hayes, J. J. Linker DNA and H1-dependent reorganization of histone-DNA interactions within the nucleosome. *Biochemistry* **37**, 8622-8628, doi:10.1021/bi980499y (1998).
- 71 Wang, X., Moore, S. C., Laszczak, M. & Ausió, J. Acetylation increases the alpha-helical content of the histone tails of the nucleosome. *The Journal of biological chemistry* **275**, 35013-35020, doi:10.1074/jbc.M004998200 (2000).
- 72 Allan, J., Harborne, N., Rau, D. C. & Gould, H. Participation of core histone "tails" in the stabilization of the chromatin solenoid. *The Journal of cell biology* **93**, 285-297, doi:10.1083/jcb.93.2.285 (1982).
- 73 Schwarz, P. M. & Hansen, J. C. Formation and stability of higher order chromatin structures. Contributions of the histone octamer. *The Journal of biological chemistry* **269**, 16284-16289 (1994).
- 74 Dorigo, B., Schalch, T., Bystricky, K. & Richmond, T. J. Chromatin fiber folding: requirement for the histone H4 N-terminal tail. *J Mol Biol* **327**, 85-96, doi:10.1016/s0022-2836(03)00025-1 (2003).
- 75 Zheng, C., Lu, X., Hansen, J. C. & Hayes, J. J. Salt-dependent intra- and internucleosomal interactions of the H3 tail domain in a model oligonucleosomal array. *The Journal of biological chemistry* **280**, 33552-33557, doi:10.1074/jbc.M507241200 (2005).
- 76 Kan, P. Y., Caterino, T. L. & Hayes, J. J. The H4 tail domain participates in intra- and internucleosome interactions with protein and DNA during folding and oligomerization of nucleosome arrays. *Mol Cell Biol* **29**, 538-546, doi:10.1128/mcb.01343-08 (2009).
- 77 Pepenella, S., Murphy, K. J. & Hayes, J. J. A distinct switch in interactions of the histone H4 tail domain upon salt-dependent folding of nucleosome arrays. *The Journal of biological chemistry* **289**, 27342-27351, doi:10.1074/jbc.M114.595140 (2014).

- 78 Zheng, C. & Hayes, J. J. Structures and interactions of the core histone tail domains. *Biopolymers* **68**, 539-546, doi:10.1002/bip.10303 (2003).
- 79 Jenuwein, T. & Allis, C. D. Translating the histone code. *Science (New York, N.Y.)* **293**, 1074-1080, doi:10.1126/science.1063127 (2001).
- 80 Luger, K. & Hansen, J. C. Nucleosome and chromatin fiber dynamics. *Current opinion in structural biology* **15**, 188-196, doi:10.1016/j.sbi.2005.03.006 (2005).
- 81 Shogren-Knaak, M. *et al.* Histone H4-K16 acetylation controls chromatin structure and protein interactions. *Science (New York, N.Y.)* **311**, 844-847, doi:10.1126/science.1124000 (2006).
- 82 Sinha, D. & Shogren-Knaak, M. A. Role of direct interactions between the histone H4 Tail and the H2A core in long range nucleosome contacts. *The Journal of biological chemistry* **285**, 16572-16581, doi:10.1074/jbc.M109.091298 (2010).
- 83 Allahverdi, A. *et al.* The effects of histone H4 tail acetylations on cation-induced chromatin folding and self-association. *Nucleic Acids Res* **39**, 1680-1691, doi:10.1093/nar/gkq900 (2011).
- 84 Garcia-Ramirez, M., Rocchini, C. & Ausio, J. Modulation of chromatin folding by histone acetylation. *The Journal of biological chemistry* **270**, 17923-17928, doi:10.1074/jbc.270.30.17923 (1995).
- 85 Fletcher, T. M. & Hansen, J. C. Core histone tail domains mediate oligonucleosome folding and nucleosomal DNA organization through distinct molecular mechanisms. *The Journal of biological chemistry* **270**, 25359-25362, doi:10.1074/jbc.270.43.25359 (1995).
- 86 Tse, C., Sera, T., Wolffe, A. P. & Hansen, J. C. Disruption of higher-order folding by core histone acetylation dramatically enhances transcription of nucleosomal arrays by RNA polymerase III. *Mol Cell Biol* **18**, 4629-4638, doi:10.1128/mcb.18.8.4629 (1998).
- 87 Polach, K. J. & Widom, J. Mechanism of protein access to specific DNA sequences in chromatin: a dynamic equilibrium model for gene regulation. *J Mol Biol* **254**, 130-149, doi:10.1006/jmbi.1995.0606 (1995).
- 88 Anderson, J. D. & Widom, J. Sequence and position-dependence of the equilibrium accessibility of nucleosomal DNA target sites. *J Mol Biol* **296**, 979-987, doi:10.1006/jmbi.2000.3531 (2000).
- 89 Culkin, J., de Bruin, L., Tompitak, M., Phillips, R. & Schiessel, H. The role of DNA sequence in nucleosome breathing. *The European physical journal. E, Soft matter* **40**, 106, doi:10.1140/epje/i2017-11596-2 (2017).
- 90 Becker, P. B. Nucleosome sliding: facts and fiction. *The EMBO journal* **21**, 4749-4753, doi:10.1093/emboj/cdf486 (2002).
- 91 Bowman, G. D. & Deindl, S. Remodeling the genome with DNA twists. *Science (New York, N.Y.)* **366**, 35-36, doi:10.1126/science.aay4317 (2019).
- 92 Armeev, G. A., Kniazeva, A. S., Komarova, G. A., Kirpichnikov, M. P. & Shaytan, A. K. Histone dynamics mediate DNA unwrapping and sliding in nucleosomes. *Nature communications* **12**, 2387, doi:10.1038/s41467-021-22636-9 (2021).
- 93 Bilokapic, S., Strauss, M. & Halic, M. Structural rearrangements of the histone octamer translocate DNA. *Nature communications* **9**, 1330, doi:10.1038/s41467-018-03677-z (2018).
- 94 Sinha, K. K., Gross, J. D. & Narlikar, G. J. Distortion of histone octamer core promotes nucleosome mobilization by a chromatin remodeler. *Science (New York, N.Y.)* **355**, doi:10.1126/science.aaa3761 (2017).
- 95 Bowman, G. D. & Poirier, M. G. Post-translational modifications of histones that influence nucleosome dynamics. *Chemical reviews* **115**, 2274-2295, doi:10.1021/cr500350x (2015).
- 96 Fujisawa, T. & Filippakopoulos, P. Functions of bromodomain-containing proteins and their roles in homeostasis and cancer. *Nature reviews. Molecular cell biology* **18**, 246-262, doi:10.1038/nrm.2016.143 (2017).
- 97 Hyun, K., Jeon, J., Park, K. & Kim, J. Writing, erasing and reading histone lysine methylations. *Experimental & molecular medicine* **49**, e324, doi:10.1038/emm.2017.11 (2017).

- 98 Bannister, A. J. & Kouzarides, T. Regulation of chromatin by histone modifications. *Cell Research* **21**, 381-395, doi:10.1038/cr.2011.22 (2011).
- 99 Zhao, Y. & Garcia, B. A. Comprehensive Catalog of Currently Documented Histone Modifications. *Cold Spring Harbor perspectives in biology* **7**, a025064, doi:10.1101/cshperspect.a025064 (2015).
- 100 Strahl, B. D. & Allis, C. D. The language of covalent histone modifications. *Nature* **403**, 41-45, doi:10.1038/47412 (2000).
- 101 Lindroth, A. M. *et al.* Dual histone H3 methylation marks at lysines 9 and 27 required for interaction with CHROMOMETHYLASE3. *The EMBO journal* **23**, 4286-4296, doi:10.1038/sj.emboj.7600430 (2004).
- 102 Fuchs, S. M., Krajewski, K., Baker, R. W., Miller, V. L. & Strahl, B. D. Influence of combinatorial histone modifications on antibody and effector protein recognition. *Current biology : CB* **21**, 53-58, doi:10.1016/j.cub.2010.11.058 (2011).
- 103 Ruthenburg, A. J. *et al.* Recognition of a mononucleosomal histone modification pattern by BPTF via multivalent interactions. *Cell* **145**, 692-706, doi:10.1016/j.cell.2011.03.053 (2011).
- 104 Vermeulen, M. *et al.* Selective anchoring of TFIID to nucleosomes by trimethylation of histone H3 lysine 4. *Cell* **131**, 58-69, doi:10.1016/j.cell.2007.08.016 (2007).
- 105 Rando, O. J. Combinatorial complexity in chromatin structure and function: revisiting the histone code. *Current opinion in genetics & development* **22**, 148-155, doi:10.1016/j.gde.2012.02.013 (2012).
- 106 Rea, S. *et al.* Regulation of chromatin structure by site-specific histone H3 methyltransferases. *Nature* **406**, 593-599, doi:10.1038/35020506 (2000).
- 107 Castellano-Pozo, M. *et al.* R loops are linked to histone H3 S10 phosphorylation and chromatin condensation. *Mol Cell* **52**, 583-590, doi:10.1016/j.molcel.2013.10.006 (2013).
- 108 Fischle, W. *et al.* Regulation of HP1-chromatin binding by histone H3 methylation and phosphorylation. *Nature* **438**, 1116-1122, doi:10.1038/nature04219 (2005).
- 109 Tsai, W. W. *et al.* TRIM24 links a non-canonical histone signature to breast cancer. *Nature* **468**, 927-932, doi:10.1038/nature09542 (2010).
- 110 Otani, J. *et al.* Structural basis for recognition of H3K4 methylation status by the DNA methyltransferase 3A ATRX-DNMT3-DNMT3L domain. *EMBO reports* **10**, 1235-1241, doi:10.1038/embor.2009.218 (2009).
- 111 Eustermann, S. *et al.* Combinatorial readout of histone H3 modifications specifies localization of ATRX to heterochromatin. *Nature structural & molecular biology* **18**, 777-782, doi:10.1038/nsmb.2070 (2011).
- 112 Iwase, S. *et al.* ATRX ADD domain links an atypical histone methylation recognition mechanism to human mental-retardation syndrome. *Nature structural & molecular biology* **18**, 769-776, doi:10.1038/nsmb.2062 (2011).
- 113 Rajakumara, E. *et al.* PHD finger recognition of unmodified histone H3R2 links UHRF1 to regulation of euchromatic gene expression. *Mol Cell* **43**, 275-284, doi:10.1016/j.molcel.2011.07.006 (2011).
- 114 Rose, N. R. & Klose, R. J. Understanding the relationship between DNA methylation and histone lysine methylation. *Biochimica et biophysica acta* **1839**, 1362-1372, doi:10.1016/j.bbagr.2014.02.007 (2014).
- 115 Nakanishi, S. *et al.* Histone H2BK123 monoubiquitination is the critical determinant for H3K4 and H3K79 trimethylation by COMPASS and Dot1. *The Journal of cell biology* **186**, 371-377, doi:10.1083/jcb.200906005 (2009).
- 116 Worden, E. J., Zhang, X. & Wolberger, C. Structural basis for COMPASS recognition of an H2B-ubiquitinated nucleosome. *eLife* **9**, e53199, doi:10.7554/eLife.53199 (2020).
- 117 Klein, B. J. *et al.* Histone H3K23-specific acetylation by MORF is coupled to H3K14 acylation. *Nature communications* **10**, 4724, doi:10.1038/s41467-019-12551-5 (2019).

- 118 Bian, C. *et al.* Sgf29 binds histone H3K4me2/3 and is required for SAGA complex recruitment and histone H3 acetylation. *The EMBO journal* **30**, 2829-2842, doi:10.1038/emboj.2011.193 (2011).
- 119 Hung, T. *et al.* ING4 mediates crosstalk between histone H3 K4 trimethylation and H3 acetylation to attenuate cellular transformation. *Mol Cell* **33**, 248-256, doi:10.1016/j.molcel.2008.12.016 (2009).
- 120 Doyon, Y., Selleck, W., Lane, W. S., Tan, S. & Côté, J. Structural and functional conservation of the NuA4 histone acetyltransferase complex from yeast to humans. *Mol Cell Biol* **24**, 1884-1896, doi:10.1128/mcb.24.5.1884-1896.2004 (2004).
- 121 Taverna, S. D. *et al.* Yng1 PHD finger binding to H3 trimethylated at K4 promotes NuA3 HAT activity at K14 of H3 and transcription at a subset of targeted ORFs. *Mol Cell* **24**, 785-796, doi:10.1016/j.molcel.2006.10.026 (2006).
- 122 Crump, N. T. *et al.* Dynamic acetylation of all lysine-4 trimethylated histone H3 is evolutionarily conserved and mediated by p300/CBP. *Proceedings of the National Academy of Sciences of the United States of America* **108**, 7814-7819, doi:10.1073/pnas.1100099108 (2011).
- 123 Clouaire, T. *et al.* Cfp1 integrates both CpG content and gene activity for accurate H3K4me3 deposition in embryonic stem cells. *Genes & development* **26**, 1714-1728, doi:10.1101/gad.194209.112 (2012).
- 124 Zhang, T., Cooper, S. & Brockdorff, N. The interplay of histone modifications – writers that read. *EMBO reports* **16**, 1467-1481-1481, doi:<https://doi.org/10.15252/embr.201540945> (2015).
- 125 Keogh, M. C. *et al.* Cotranscriptional set2 methylation of histone H3 lysine 36 recruits a repressive Rpd3 complex. *Cell* **123**, 593-605, doi:10.1016/j.cell.2005.10.025 (2005).
- 126 Carrozza, M. J. *et al.* Histone H3 methylation by Set2 directs deacetylation of coding regions by Rpd3S to suppress spurious intragenic transcription. *Cell* **123**, 581-592, doi:10.1016/j.cell.2005.10.023 (2005).
- 127 Joshi, A. A. & Struhl, K. Eaf3 chromodomain interaction with methylated H3-K36 links histone deacetylation to Pol II elongation. *Mol Cell* **20**, 971-978, doi:10.1016/j.molcel.2005.11.021 (2005).
- 128 Pasini, D. *et al.* Characterization of an antagonistic switch between histone H3 lysine 27 methylation and acetylation in the transcriptional regulation of Polycomb group target genes. *Nucleic Acids Res* **38**, 4958-4969, doi:10.1093/nar/gkq244 (2010).
- 129 Vermeulen, M. *et al.* Quantitative interaction proteomics and genome-wide profiling of epigenetic histone marks and their readers. *Cell* **142**, 967-980, doi:10.1016/j.cell.2010.08.020 (2010).
- 130 Vardabasso, C. *et al.* Histone variants: emerging players in cancer biology. *Cellular and molecular life sciences : CMLS* **71**, 379-404, doi:10.1007/s00018-013-1343-z (2014).
- 131 Bönisch, C. & Hake, S. B. Histone H2A variants in nucleosomes and chromatin: more or less stable? *Nucleic Acids Res* **40**, 10719-10741, doi:10.1093/nar/gks865 (2012).
- 132 Corujo, D. & Buschbeck, M. Post-Translational Modifications of H2A Histone Variants and Their Role in Cancer. *Cancers* **10**, doi:10.3390/cancers10030059 (2018).
- 133 Foltz, D. R. *et al.* The human CENP-A centromeric nucleosome-associated complex. *Nature cell biology* **8**, 458-469, doi:10.1038/ncb1397 (2006).
- 134 Maze, I., Noh, K. M., Soshnev, A. A. & Allis, C. D. Every amino acid matters: essential contributions of histone variants to mammalian development and disease. *Nature reviews. Genetics* **15**, 259-271, doi:10.1038/nrg3673 (2014).
- 135 Wang, Y. *et al.* Histone variants H2A.Z and H3.3 coordinately regulate PRC2-dependent H3K27me3 deposition and gene expression regulation in mES cells. *BMC Biology* **16**, 107, doi:10.1186/s12915-018-0568-6 (2018).

- 136 Fan, J. Y., Rangasamy, D., Luger, K. & Tremethick, D. J. H2A.Z Alters the Nucleosome Surface to Promote HP1 α -Mediated Chromatin Fiber Folding. *Molecular Cell* **16**, 655-661, doi:<https://doi.org/10.1016/j.molcel.2004.10.023> (2004).
- 137 Tramantano, M. *et al.* Constitutive turnover of histone H2A.Z at yeast promoters requires the preinitiation complex. *eLife* **5**, e14243, doi:10.7554/eLife.14243 (2016).
- 138 Brunelle, M. *et al.* The histone variant H2A.Z is an important regulator of enhancer activity. *Nucleic Acids Research* **43**, 9742-9756, doi:10.1093/nar/gkv825 (2015).
- 139 Watanabe, S., Radman-Livaja, M., Rando, O. J. & Peterson, C. L. A histone acetylation switch regulates H2A.Z deposition by the SWR-C remodeling enzyme. *Science (New York, N.Y.)* **340**, 195-199, doi:10.1126/science.1229758 (2013).
- 140 Hammond, C. M., Strømme, C. B., Huang, H., Patel, D. J. & Groth, A. Histone chaperone networks shaping chromatin function. *Nature reviews. Molecular cell biology* **18**, 141-158, doi:10.1038/nrm.2016.159 (2017).
- 141 Li, Q. *et al.* Acetylation of histone H3 lysine 56 regulates replication-coupled nucleosome assembly. *Cell* **134**, 244-255, doi:10.1016/j.cell.2008.06.018 (2008).
- 142 Su, D. *et al.* Structural basis for recognition of H3K56-acetylated histone H3-H4 by the chaperone Rtt106. *Nature* **483**, 104-107, doi:10.1038/nature10861 (2012).
- 143 Tessarz, P. *et al.* Glutamine methylation in histone H2A is an RNA-polymerase-I-dedicated modification. *Nature* **505**, 564-568, doi:10.1038/nature12819 (2014).
- 144 Tyagi, M., Imam, N., Verma, K. & Patel, A. K. Chromatin remodelers: We are the drivers!! *Nucleus (Austin, Tex.)* **7**, 388-404, doi:10.1080/19491034.2016.1211217 (2016).
- 145 Mueller-Planitz, F., Klinker, H. & Becker, P. B. Nucleosome sliding mechanisms: new twists in a looped history. *Nature structural & molecular biology* **20**, 1026-1032, doi:10.1038/nsmb.2648 (2013).
- 146 Clapier, C. R., Iwasa, J., Cairns, B. R. & Peterson, C. L. Mechanisms of action and regulation of ATP-dependent chromatin-remodelling complexes. *Nature reviews. Molecular cell biology* **18**, 407-422, doi:10.1038/nrm.2017.26 (2017).
- 147 Längst, G. & Manelyte, L. Chromatin Remodelers: From Function to Dysfunction. *Genes* **6**, 299-324, doi:10.3390/genes6020299 (2015).
- 148 Narlikar, G. J., Sundaramoorthy, R. & Owen-Hughes, T. Mechanisms and functions of ATP-dependent chromatin-remodeling enzymes. *Cell* **154**, 490-503, doi:10.1016/j.cell.2013.07.011 (2013).
- 149 Kasten, M. *et al.* Tandem bromodomains in the chromatin remodeler RSC recognize acetylated histone H3 Lys14. *The EMBO journal* **23**, 1348-1359, doi:10.1038/sj.emboj.7600143 (2004).
- 150 Hauk, G., McKnight, J. N., Nodelman, I. M. & Bowman, G. D. The chromodomains of the Chd1 chromatin remodeler regulate DNA access to the ATPase motor. *Mol Cell* **39**, 711-723, doi:10.1016/j.molcel.2010.08.012 (2010).
- 151 Hassan, A. H. *et al.* Function and selectivity of bromodomains in anchoring chromatin-modifying complexes to promoter nucleosomes. *Cell* **111**, 369-379, doi:10.1016/s0092-8674(02)01005-x (2002).
- 152 Williams, S. K., Truong, D. & Tyler, J. K. Acetylation in the globular core of histone H3 on lysine-56 promotes chromatin disassembly during transcriptional activation. *Proceedings of the National Academy of Sciences* **105**, 9000-9005, doi:10.1073/pnas.0800057105 (2008).
- 153 Zeng, L. *et al.* Mechanism and regulation of acetylated histone binding by the tandem PHD finger of DPF3b. *Nature* **466**, 258-262, doi:10.1038/nature09139 (2010).
- 154 Chen, G., Li, W., Yan, F., Wang, D. & Chen, Y. The Structural Basis for Specific Recognition of H3K14 Acetylation by Sth1 in the RSC Chromatin Remodeling Complex. *Structure (London, England : 1993)* **28**, 111-118.e113, doi:10.1016/j.str.2019.10.015 (2020).
- 155 Sims, R. J., 3rd *et al.* Human but not yeast CHD1 binds directly and selectively to histone H3 methylated at lysine 4 via its tandem chromodomains. *The Journal of biological chemistry* **280**, 41789-41792, doi:10.1074/jbc.C500395200 (2005).

- 156 Huang, Y., Fang, J., Bedford, M. T., Zhang, Y. & Xu, R. M. Recognition of histone H3 lysine-4 methylation by the double tudor domain of JMJD2A. *Science (New York, N.Y.)* **312**, 748-751, doi:10.1126/science.1125162 (2006).
- 157 Anderson, J. D., Lowary, P. T. & Widom, J. Effects of histone acetylation on the equilibrium accessibility of nucleosomal DNA target sites. *J Mol Biol* **307**, 977-985, doi:10.1006/jmbi.2001.4528 (2001).
- 158 Brower-Toland, B. *et al.* Specific contributions of histone tails and their acetylation to the mechanical stability of nucleosomes. *J Mol Biol* **346**, 135-146, doi:10.1016/j.jmb.2004.11.056 (2005).
- 159 Lee, J. Y., Wei, S. & Lee, T. H. Effects of histone acetylation by Piccolo NuA4 on the structure of a nucleosome and the interactions between two nucleosomes. *The Journal of biological chemistry* **286**, 11099-11109, doi:10.1074/jbc.M110.192047 (2011).
- 160 Kouzarides, T. Chromatin modifications and their function. *Cell* **128**, 693-705, doi:10.1016/j.cell.2007.02.005 (2007).
- 161 Suganuma, T. & Workman, J. L. Signals and combinatorial functions of histone modifications. *Annual review of biochemistry* **80**, 473-499, doi:10.1146/annurev-biochem-061809-175347 (2011).
- 162 Simpson, R. T. Structure of chromatin containing extensively acetylated H3 and H4. *Cell* **13**, 691-699, doi:10.1016/0092-8674(78)90219-2 (1978).
- 163 Kraus, W. L. & Kadonaga, J. T. p300 and estrogen receptor cooperatively activate transcription via differential enhancement of initiation and reinitiation. *Genes & development* **12**, 331-342, doi:10.1101/gad.12.3.331 (1998).
- 164 Chahal, S. S., Matthews, H. R. & Bradbury, E. M. Acetylation of histone H4 and its role in chromatin structure and function. *Nature* **287**, 76-79, doi:10.1038/287076a0 (1980).
- 165 Kalashnikova, A. A., Porter-Goff, M. E., Muthurajan, U. M., Luger, K. & Hansen, J. C. The role of the nucleosome acidic patch in modulating higher order chromatin structure. *Journal of the Royal Society, Interface* **10**, 20121022, doi:10.1098/rsif.2012.1022 (2013).
- 166 Luger, K., Dechassa, M. L. & Tremethick, D. J. New insights into nucleosome and chromatin structure: an ordered state or a disordered affair? *Nature reviews. Molecular cell biology* **13**, 436-447, doi:10.1038/nrm3382 (2012).
- 167 Pepenella, S., Murphy, K. J. & Hayes, J. J. Intra- and inter-nucleosome interactions of the core histone tail domains in higher-order chromatin structure. *Chromosoma* **123**, 3-13, doi:10.1007/s00412-013-0435-8 (2014).
- 168 Tremethick, D. J. Higher-order structures of chromatin: the elusive 30 nm fiber. *Cell* **128**, 651-654, doi:10.1016/j.cell.2007.02.008 (2007).
- 169 Tropberger, P. & Schneider, R. Scratching the (lateral) surface of chromatin regulation by histone modifications. *Nature structural & molecular biology* **20**, 657-661, doi:10.1038/nsmb.2581 (2013).
- 170 North, J. A. *et al.* Regulation of the nucleosome unwrapping rate controls DNA accessibility. *Nucleic Acids Res* **40**, 10215-10227, doi:10.1093/nar/gks747 (2012).
- 171 Dai, J. *et al.* Probing nucleosome function: a highly versatile library of synthetic histone H3 and H4 mutants. *Cell* **134**, 1066-1078, doi:10.1016/j.cell.2008.07.019 (2008).
- 172 Hyland, E. M. *et al.* Insights into the role of histone H3 and histone H4 core modifiable residues in *Saccharomyces cerevisiae*. *Mol Cell Biol* **25**, 10060-10070, doi:10.1128/mcb.25.22.10060-10070.2005 (2005).
- 173 Fenley, A. T., Adams, D. A. & Onufriev, A. V. Charge state of the globular histone core controls stability of the nucleosome. *Biophysical journal* **99**, 1577-1585, doi:10.1016/j.bpj.2010.06.046 (2010).
- 174 Richards, E. J. & Elgin, S. C. Epigenetic codes for heterochromatin formation and silencing: rounding up the usual suspects. *Cell* **108**, 489-500, doi:10.1016/s0092-8674(02)00644-x (2002).

- 175 Grunstein, M. Histone acetylation in chromatin structure and transcription. *Nature* **389**, 349-352, doi:10.1038/38664 (1997).
- 176 Sterner, D. E. & Berger, S. L. Acetylation of histones and transcription-related factors. *Microbiology and molecular biology reviews : MMBR* **64**, 435-459, doi:10.1128/mmb.64.2.435-459.2000 (2000).
- 177 Narita, T. *et al.* Enhancers are activated by p300/CBP activity-dependent PIC assembly, RNAPII recruitment, and pause release. *Mol Cell* **81**, 2166-2182.e2166, doi:10.1016/j.molcel.2021.03.008 (2021).
- 178 Schiltz, R. L. *et al.* Overlapping but distinct patterns of histone acetylation by the human coactivators p300 and PCAF within nucleosomal substrates. *The Journal of biological chemistry* **274**, 1189-1192, doi:10.1074/jbc.274.3.1189 (1999).
- 179 Dancy, B. M. & Cole, P. A. Protein lysine acetylation by p300/CBP. *Chemical reviews* **115**, 2419-2452, doi:10.1021/cr500452k (2015).
- 180 Peña, C. *et al.* The expression levels of the transcriptional regulators p300 and CtBP modulate the correlations between SNAIL, ZEB1, E-cadherin and vitamin D receptor in human colon carcinomas. *International journal of cancer* **119**, 2098-2104, doi:10.1002/ijc.22083 (2006).
- 181 Goodman, R. H. & Smolik, S. CBP/p300 in cell growth, transformation, and development. *Genes & development* **14**, 1553-1577 (2000).
- 182 Gates, L. A. *et al.* Acetylation on histone H3 lysine 9 mediates a switch from transcription initiation to elongation. *The Journal of biological chemistry* **292**, 14456-14472, doi:10.1074/jbc.M117.802074 (2017).
- 183 Tropberger, P. *et al.* Regulation of Transcription through Acetylation of H3K122 on the Lateral Surface of the Histone Octamer. *Cell* **152**, 859-872, doi:<https://doi.org/10.1016/j.cell.2013.01.032> (2013).
- 184 Di Cerbo, V. *et al.* Acetylation of histone H3 at lysine 64 regulates nucleosome dynamics and facilitates transcription. *eLife* **3**, e01632, doi:10.7554/eLife.01632 (2014).
- 185 Dipta, S., Elias, T. F., Robert, S. I., Wendy, A. B. & Yatendra, K. Acetylation of H3K115 at the nucleosome dyad is associated with fragile nucleosomes at active regulatory sites. *bioRxiv*, 2023.2011.2010.566531, doi:10.1101/2023.11.10.566531 (2023).
- 186 Smeenk, G. & Mailand, N. Writers, Readers, and Erasers of Histone Ubiquitylation in DNA Double-Strand Break Repair. *Frontiers in genetics* **7**, 122, doi:10.3389/fgene.2016.00122 (2016).
- 187 Piekna-Przybylska, D., Bambara, R. A. & Balakrishnan, L. Acetylation regulates DNA repair mechanisms in human cells. *Cell Cycle* **15**, 1506-1517, doi:10.1080/15384101.2016.1176815 (2016).
- 188 Dhar, S., Gursoy-Yuzugullu, O., Parasuram, R. & Price, B. D. The tale of a tail: histone H4 acetylation and the repair of DNA breaks. *Philosophical transactions of the Royal Society of London. Series B, Biological sciences* **372**, doi:10.1098/rstb.2016.0284 (2017).
- 189 Hunt, C. R. *et al.* Histone modifications and DNA double-strand break repair after exposure to ionizing radiations. *Radiation research* **179**, 383-392, doi:10.1667/rr3308.2 (2013).
- 190 Banerjee, D. R., Deckard, C. E., 3rd, Zeng, Y. & Szczepanski, J. T. Acetylation of the histone H3 tail domain regulates base excision repair on higher-order chromatin structures. *Sci Rep* **9**, 15972, doi:10.1038/s41598-019-52340-0 (2019).
- 191 Horikoshi, N. *et al.* Pre-existing H4K16ac levels in euchromatin drive DNA repair by homologous recombination in S-phase. *Communications biology* **2**, 253, doi:10.1038/s42003-019-0498-z (2019).
- 192 Ogiwara, H. *et al.* Histone acetylation by CBP and p300 at double-strand break sites facilitates SWI/SNF chromatin remodeling and the recruitment of non-homologous end joining factors. *Oncogene* **30**, 2135-2146, doi:10.1038/onc.2010.592 (2011).
- 193 Gupta, A. *et al.* Involvement of human MOF in ATM function. *Mol Cell Biol* **25**, 5292-5305, doi:10.1128/mcb.25.12.5292-5305.2005 (2005).

- 194 Qian, M.-X. *et al.* Acetylation-Mediated Proteasomal Degradation of Core Histones during DNA Repair and Spermatogenesis. *Cell* **153**, 1012-1024, doi:<https://doi.org/10.1016/j.cell.2013.04.032> (2013).
- 195 Downs, J. A. *et al.* Binding of Chromatin-Modifying Activities to Phosphorylated Histone H2A at DNA Damage Sites. *Molecular Cell* **16**, 979-990, doi:<https://doi.org/10.1016/j.molcel.2004.12.003> (2004).
- 196 Murr, R. *et al.* Histone acetylation by Trrap-Tip60 modulates loading of repair proteins and repair of DNA double-strand breaks. *Nature cell biology* **8**, 91-99, doi:10.1038/ncb1343 (2006).
- 197 Bhaskara, S. *et al.* Deletion of histone deacetylase 3 reveals critical roles in S phase progression and DNA damage control. *Mol Cell* **30**, 61-72, doi:10.1016/j.molcel.2008.02.030 (2008).
- 198 Hsiao, K. Y. & Mizzen, C. A. Histone H4 deacetylation facilitates 53BP1 DNA damage signaling and double-strand break repair. *Journal of molecular cell biology* **5**, 157-165, doi:10.1093/jmcb/mjs066 (2013).
- 199 Tamburini, B. A. & Tyler, J. K. Localized histone acetylation and deacetylation triggered by the homologous recombination pathway of double-strand DNA repair. *Mol Cell Biol* **25**, 4903-4913, doi:10.1128/mcb.25.12.4903-4913.2005 (2005).
- 200 Ray, A., Khan, P. & Nag Chaudhuri, R. Regulated acetylation and deacetylation of H4 K16 is essential for efficient NER in *Saccharomyces cerevisiae*. *DNA repair* **72**, 39-55, doi:10.1016/j.dnarep.2018.09.009 (2018).
- 201 Davey, C. A., Sargent, D. F., Luger, K., Maeder, A. W. & Richmond, T. J. Solvent mediated interactions in the structure of the nucleosome core particle at 1.9 Å resolution. *J Mol Biol* **319**, 1097-1113, doi:10.1016/s0022-2836(02)00386-8 (2002).
- 202 Neumann, H. *et al.* A method for genetically installing site-specific acetylation in recombinant histones defines the effects of H3 K56 acetylation. *Mol Cell* **36**, 153-163, doi:10.1016/j.molcel.2009.07.027 (2009).
- 203 Fillingham, J. *et al.* Chaperone control of the activity and specificity of the histone H3 acetyltransferase Rtt109. *Mol Cell Biol* **28**, 4342-4353, doi:10.1128/mcb.00182-08 (2008).
- 204 Masumoto, H., Hawke, D., Kobayashi, R. & Verreault, A. A role for cell-cycle-regulated histone H3 lysine 56 acetylation in the DNA damage response. *Nature* **436**, 294-298, doi:10.1038/nature03714 (2005).
- 205 Shimko, J. C., North, J. A., Bruns, A. N., Poirier, M. G. & Ottesen, J. J. Preparation of fully synthetic histone H3 reveals that acetyl-lysine 56 facilitates protein binding within nucleosomes. *J Mol Biol* **408**, 187-204, doi:10.1016/j.jmb.2011.01.003 (2011).
- 206 Adams, C. C. & Workman, J. L. Binding of disparate transcriptional activators to nucleosomal DNA is inherently cooperative. *Mol Cell Biol* **15**, 1405-1421, doi:10.1128/mcb.15.3.1405 (1995).
- 207 Polach, K. J. & Widom, J. A model for the cooperative binding of eukaryotic regulatory proteins to nucleosomal target sites. *J Mol Biol* **258**, 800-812, doi:10.1006/jmbi.1996.0288 (1996).
- 208 Schneider, J., Bajwa, P., Johnson, F. C., Bhaumik, S. R. & Shilatifard, A. Rtt109 is required for proper H3K56 acetylation: a chromatin mark associated with the elongating RNA polymerase II. *The Journal of biological chemistry* **281**, 37270-37274, doi:10.1074/jbc.C600265200 (2006).
- 209 Driscoll, R., Hudson, A. & Jackson, S. P. Yeast Rtt109 Promotes Genome Stability by Acetylating Histone H3 on Lysine 56. *Science (New York, N.Y.)* **315**, 649-652, doi:10.1126/science.1135862 (2007).
- 210 Recht, J. *et al.* Histone chaperone Asf1 is required for histone H3 lysine 56 acetylation, a modification associated with S phase in mitosis and meiosis. *Proceedings of the National Academy of Sciences* **103**, 6988-6993, doi:10.1073/pnas.0601676103 (2006).
- 211 English, C. M., Maluf, N. K., Tripet, B., Churchill, M. E. A. & Tyler, J. K. ASF1 Binds to a Heterodimer of Histones H3 and H4: A Two-Step Mechanism for the Assembly of the H3-H4 Heterotetramer on DNA. *Biochemistry* **44**, 13673-13682, doi:10.1021/bi051333h (2005).

- 212 Kaplan, T. *et al.* Cell cycle- and chaperone-mediated regulation of H3K56ac incorporation in yeast. *PLoS genetics* **4**, e1000270, doi:10.1371/journal.pgen.1000270 (2008).
- 213 Han, J., Zhou, H., Li, Z., Xu, R. M. & Zhang, Z. The Rtt109-Vps75 histone acetyltransferase complex acetylates non-nucleosomal histone H3. *The Journal of biological chemistry* **282**, 14158-14164, doi:10.1074/jbc.M700611200 (2007).
- 214 Fazly, A. *et al.* Histone Chaperone Rtt106 Promotes Nucleosome Formation Using (H3-H4)₂ Tetramers*. *Journal of Biological Chemistry* **287**, 10753-10760, doi:<https://doi.org/10.1074/jbc.M112.347450> (2012).
- 215 Celic, I. *et al.* The sirtuins hst3 and Hst4p preserve genome integrity by controlling histone h3 lysine 56 deacetylation. *Current biology : CB* **16**, 1280-1289, doi:10.1016/j.cub.2006.06.023 (2006).
- 216 Maas, N. L., Miller, K. M., DeFazio, L. G. & Toczyski, D. P. Cell Cycle and Checkpoint Regulation of Histone H3 K56 Acetylation by Hst3 and Hst4. *Molecular Cell* **23**, 109-119, doi:<https://doi.org/10.1016/j.molcel.2006.06.006> (2006).
- 217 Celic, I., Verreault, A. & Boeke, J. D. Histone H3 K56 Hyperacetylation Perturbs Replisomes and Causes DNA Damage. *Genetics* **179**, 1769-1784, doi:10.1534/genetics.108.088914 (2008).
- 218 Brachmann, C. B. *et al.* The SIR2 gene family, conserved from bacteria to humans, functions in silencing, cell cycle progression, and chromosome stability. *Genes & development* **9**, 2888-2902, doi:10.1101/gad.9.23.2888 (1995).
- 219 Kim, J., Lee, J. & Lee, T. H. Lysine Acetylation Facilitates Spontaneous DNA Dynamics in the Nucleosome. *The journal of physical chemistry. B* **119**, 15001-15005, doi:10.1021/acs.jpcc.5b09734 (2015).
- 220 Huynh, M. T., Yadav, S. P., Reese, J. C. & Lee, T. H. Nucleosome Dynamics during Transcription Elongation. *ACS chemical biology* **15**, 3133-3142, doi:10.1021/acscchembio.0c00617 (2020).
- 221 Värnv, S. *et al.* Acetylation of H3 K56 is required for RNA polymerase II transcript elongation through heterochromatin in yeast. *Mol Cell Biol* **30**, 1467-1477, doi:10.1128/mcb.01151-09 (2010).
- 222 Topal, S., Vasseur, P., Radman-Livaja, M. & Peterson, C. L. Distinct transcriptional roles for Histone H3-K56 acetylation during the cell cycle in Yeast. *Nature communications* **10**, 4372, doi:10.1038/s41467-019-12400-5 (2019).
- 223 Rufiange, A., Jacques, P. E., Bhat, W., Robert, F. & Nourani, A. Genome-wide replication-independent histone H3 exchange occurs predominantly at promoters and implicates H3 K56 acetylation and Asf1. *Mol Cell* **27**, 393-405, doi:10.1016/j.molcel.2007.07.011 (2007).
- 224 Williams, S. K., Truong, D. & Tyler, J. K. Acetylation in the globular core of histone H3 on lysine-56 promotes chromatin disassembly during transcriptional activation. *Proceedings of the National Academy of Sciences* **105**, 9000, doi:10.1073/pnas.0800057105 (2008).
- 225 Xu, F., Zhang, K. & Grunstein, M. Acetylation in histone H3 globular domain regulates gene expression in yeast. *Cell* **121**, 375-385, doi:10.1016/j.cell.2005.03.011 (2005).
- 226 Etchegaray, J. P. *et al.* The Histone Deacetylase SIRT6 Restrains Transcription Elongation via Promoter-Proximal Pausing. *Mol Cell* **75**, 683-699.e687, doi:10.1016/j.molcel.2019.06.034 (2019).
- 227 McCullough, L. L. *et al.* Establishment and Maintenance of Chromatin Architecture Are Promoted Independently of Transcription by the Histone Chaperone FACT and H3-K56 Acetylation in *Saccharomyces cerevisiae*. *Genetics* **211**, 877-892, doi:10.1534/genetics.118.301853 (2019).
- 228 Durairaj, G. *et al.* Regulation of chromatin assembly/disassembly by Rtt109p, a histone H3 Lys56-specific acetyltransferase, in vivo. *The Journal of biological chemistry* **285**, 30472-30479, doi:10.1074/jbc.M110.113225 (2010).
- 229 Wurtele, H. *et al.* Histone H3 lysine 56 acetylation and the response to DNA replication fork damage. *Mol Cell Biol* **32**, 154-172, doi:10.1128/mcb.05415-11 (2012).

- 230 Fu, I., Geacintov, N. E. & Broyde, S. Molecular dynamics simulations reveal how H3K56 acetylation impacts nucleosome structure to promote DNA exposure for lesion sensing. *DNA repair* **107**, 103201, doi:<https://doi.org/10.1016/j.dnarep.2021.103201> (2021).
- 231 Clemente-Ruiz, M., González-Prieto, R. & Prado, F. Histone H3K56 Acetylation, CAF1, and Rtt106 Coordinate Nucleosome Assembly and Stability of Advancing Replication Forks. *PLoS genetics* **7**, e1002376, doi:10.1371/journal.pgen.1002376 (2011).
- 232 Prado, F., Cortés-Ledesma, F. & Aguilera, A. The absence of the yeast chromatin assembly factor Asf1 increases genomic instability and sister chromatid exchange. *EMBO reports* **5**, 497-502, doi:10.1038/sj.embor.7400128 (2004).
- 233 Muñoz-Galván, S., Jimeno, S., Rothstein, R. & Aguilera, A. Histone H3K56 Acetylation, Rad52, and Non-DNA Repair Factors Control Double-Strand Break Repair Choice with the Sister Chromatid. *PLoS genetics* **9**, e1003237, doi:10.1371/journal.pgen.1003237 (2013).
- 234 Xu, F., Zhang, Q., Zhang, K., Xie, W. & Grunstein, M. Sir2 deacetylates histone H3 lysine 56 to regulate telomeric heterochromatin structure in yeast. *Mol Cell* **27**, 890-900, doi:10.1016/j.molcel.2007.07.021 (2007).
- 235 Potoyan, D. A. & Papoian, G. A. Regulation of the H4 tail binding and folding landscapes via Lys-16 acetylation. *Proceedings of the National Academy of Sciences* **109**, 17857-17862, doi:10.1073/pnas.1201805109 (2012).
- 236 Shogren-Knaak, M. & Peterson, C. L. Switching on chromatin: mechanistic role of histone H4-K16 acetylation. *Cell cycle (Georgetown, Tex.)* **5**, 1361-1365, doi:10.4161/cc.5.13.2891 (2006).
- 237 Robinson, P. J. *et al.* 30 nm chromatin fibre decompaction requires both H4-K16 acetylation and linker histone eviction. *Journal of molecular biology* **381**, 816-825, doi:10.1016/j.jmb.2008.04.050 (2008).
- 238 Zhang, R., Erler, J. & Langowski, J. Histone Acetylation Regulates Chromatin Accessibility: Role of H4K16 in Inter-nucleosome Interaction. *Biophysical journal* **112**, 450-459, doi:10.1016/j.bpj.2016.11.015 (2017).
- 239 Millar, C. B., Kurdistani, S. K. & Grunstein, M. Acetylation of yeast histone H4 lysine 16: a switch for protein interactions in heterochromatin and euchromatin. *Cold Spring Harbor symposia on quantitative biology* **69**, 193-200, doi:10.1101/sqb.2004.69.193 (2004).
- 240 De Nadal, E. *et al.* The MAPK Hog1 recruits Rpd3 histone deacetylase to activate osmoresponsive genes. *Nature* **427**, 370-374, doi:10.1038/nature02258 (2004).
- 241 Wang, X. & Hayes, J. J. Acetylation mimics within individual core histone tail domains indicate distinct roles in regulating the stability of higher-order chromatin structure. *Molecular and cellular biology* **28**, 227-236, doi:10.1128/mcb.01245-07 (2008).
- 242 Dion, M. F., Altschuler, S. J., Wu, L. F. & Rando, O. J. Genomic characterization reveals a simple histone H4 acetylation code. *Proceedings of the National Academy of Sciences of the United States of America* **102**, 5501-5506, doi:10.1073/pnas.0500136102 (2005).
- 243 Liu, C. L. *et al.* Single-nucleosome mapping of histone modifications in *S. cerevisiae*. *PLoS biology* **3**, e328, doi:10.1371/journal.pbio.0030328 (2005).
- 244 Simoneau, A. *et al.* Interplay between histone H3 lysine 56 deacetylation and chromatin modifiers in response to DNA damage. *Genetics* **200**, 185-205, doi:10.1534/genetics.115.175919 (2015).
- 245 Ray, A., Khan, P. & Nag Chaudhuri, R. Deacetylation of H4 lysine16 affects acetylation of lysine residues in histone H3 and H4 and promotes transcription of constitutive genes. *Epigenetics* **16**, 597-617, doi:10.1080/15592294.2020.1809896 (2021).
- 246 Ferreira, H., Somers, J., Webster, R., Flaus, A. & Owen-Hughes, T. Histone tails and the H3 alphaN helix regulate nucleosome mobility and stability. *Mol Cell Biol* **27**, 4037-4048, doi:10.1128/mcb.02229-06 (2007).
- 247 Khan, P. & Chaudhuri, R. N. Acetylation of H3K56 orchestrates UV-responsive chromatin events that generate DNA accessibility during Nucleotide Excision Repair. *DNA repair* **113**, 103317, doi:10.1016/j.dnarep.2022.103317 (2022).

- 248 Ghosh-Roy, S., Das, D., Chowdhury, D., Smerdon, M. J. & Chaudhuri, R. N. Rad26, the transcription-coupled repair factor in yeast, is required for removal of stalled RNA polymerase-II following UV irradiation. *PloS one* **8**, e72090, doi:10.1371/journal.pone.0072090 (2013).
- 249 Khan, P., Singha, P. & Nag Chaudhuri, R. RNA Polymerase II Dependent Crosstalk between H4K16 Deacetylation and H3K56 Acetylation Promotes Transcription of Constitutively Expressed Genes. *Molecular and cellular biology* **43**, 596-610, doi:10.1080/10985549.2023.2270912 (2023).
- 250 Sobanski, M. A. & Dickinson, J. R. A simple method for the direct extraction of plasmid DNA from yeast. *Biotechnology Techniques* **9**, 225-230, doi:10.1007/BF00157083 (1995).
- 251 Zheng, L., Baumann, U. & Reymond, J. L. An efficient one-step site-directed and site-saturation mutagenesis protocol. *Nucleic acids research* **32**, e115, doi:10.1093/nar/gnh110 (2004).
- 252 Gietz, R. D. & Woods, R. A. Yeast transformation by the LiAc/SS Carrier DNA/PEG method. *Methods in molecular biology (Clifton, N.J.)* **313**, 107-120, doi:10.1385/1-59259-958-3:107 (2006).
- 253 Gardner, J. M. & Jaspersen, S. L. Manipulating the yeast genome: deletion, mutation, and tagging by PCR. *Methods in molecular biology (Clifton, N.J.)* **1205**, 45-78, doi:10.1007/978-1-4939-1363-3_5 (2014).
- 254 Yu, S. C., Kuemmel, F., Skoufou-Papoutsaki, M. N. & Spanu, P. D. Yeast transformation efficiency is enhanced by TORC1- and eisosome-dependent signaling. *MicrobiologyOpen* **8**, e00730, doi:10.1002/mbo3.730 (2019).
- 255 Bepalov, V. A., Conconi, A., Zhang, X., Fahy, D. & Smerdon, M. J. Improved method for measuring the ensemble average of strand breaks in genomic DNA. *Environmental and molecular mutagenesis* **38**, 166-174, doi:10.1002/em.1068 (2001).
- 256 Khan, P. & Chaudhuri, R. N. Acetylation of H3K56 orchestrates UV-responsive chromatin events that generate DNA accessibility during Nucleotide Excision Repair. *DNA repair* **113**, 103317, doi:<https://doi.org/10.1016/j.dnarep.2022.103317> (2022).
- 257 Yang, J. *et al.* The Histone Chaperone FACT Contributes to DNA Replication-Coupled Nucleosome Assembly. *Cell Reports* **14**, 1128-1141, doi:<https://doi.org/10.1016/j.celrep.2015.12.096> (2016).
- 258 Riles, L., Shaw, R. J., Johnston, M. & Reines, D. Large-scale screening of yeast mutants for sensitivity to the IMP dehydrogenase inhibitor 6-azauracil. *Yeast (Chichester, England)* **21**, 241-248, doi:10.1002/yea.1068 (2004).
- 259 Poramba-Liyanage, D. W. *et al.* Inhibition of transcription leads to rewiring of locus-specific chromatin proteomes. *Genome research* **30**, 635-646, doi:10.1101/gr.256255.119 (2020).
- 260 Grigull, J., Mnaimneh, S., Pootoolal, J., Robinson, M. D. & Hughes, T. R. Genome-Wide Analysis of mRNA Stability Using Transcription Inhibitors and Microarrays Reveals Posttranscriptional Control of Ribosome Biogenesis Factors. *Molecular and Cellular Biology* **24**, 5534-5547, doi:10.1128/MCB.24.12.5534-5547.2004 (2004).
- 261 Johnston, G. C. & Singer, R. A. RNA synthesis and control of cell division in the yeast *S. cerevisiae*. *Cell* **14**, 951-958, doi:10.1016/0092-8674(78)90349-5 (1978).
- 262 Khan, P., Singha, P. & Nag Chaudhuri, R. RNA Polymerase II Dependent Crosstalk between H4K16 Deacetylation and H3K56 Acetylation Promotes Transcription of Constitutively Expressed Genes. *Mol Cell Biol* **43**, 596-610, doi:10.1080/10985549.2023.2270912 (2023).
- 263 Dhanasekaran, S., Doherty, T. M. & Kenneth, J. Comparison of different standards for real-time PCR-based absolute quantification. *Journal of immunological methods* **354**, 34-39, doi:10.1016/j.jim.2010.01.004 (2010).
- 264 Sinha, R. P. & Häder, D. P. UV-induced DNA damage and repair: a review. *Photochemical & photobiological sciences : Official journal of the European Photochemistry Association and the European Society for Photobiology* **1**, 225-236, doi:10.1039/b201230h (2002).

- 265 Thoma, F. Repair of UV lesions in nucleosomes--intrinsic properties and remodeling. *DNA repair* **4**, 855-869, doi:10.1016/j.dnarep.2005.04.005 (2005).
- 266 Mohan, C., Das, C. & Tyler, J. Histone and Chromatin Dynamics Facilitating DNA repair. *DNA repair* **107**, 103183, doi:10.1016/j.dnarep.2021.103183 (2021).
- 267 Yu, Y. & Waters, R. Histone acetylation, chromatin remodelling and nucleotide excision repair: hint from the study on MFA2 in *Saccharomyces cerevisiae*. *Cell Cycle* **4**, 1043-1045, doi:10.4161/cc.4.8.1928 (2005).
- 268 Yu, S., Teng, Y., Waters, R. & Reed, S. H. How Chromatin Is Remodelled during DNA Repair of UV-Induced DNA Damage in *Saccharomyces cerevisiae*. *PLoS genetics* **7**, e1002124, doi:10.1371/journal.pgen.1002124 (2011).
- 269 Duan, M. R. & Smerdon, M. J. Histone H3 lysine 14 (H3K14) acetylation facilitates DNA repair in a positioned nucleosome by stabilizing the binding of the chromatin Remodeler RSC (Remodels Structure of Chromatin). *The Journal of biological chemistry* **289**, 8353-8363, doi:10.1074/jbc.M113.540732 (2014).
- 270 Masumoto, H., Hawke, D., Kobayashi, R. & Verreault, A. A role for cell-cycle-regulated histone H3 lysine 56 acetylation in the DNA damage response. *Nature* **436**, 294-298, doi:10.1038/nature03714 (2005).
- 271 Chen, C.-C. *et al.* Acetylated Lysine 56 on Histone H3 Drives Chromatin Assembly after Repair and Signals for the Completion of Repair. *Cell* **134**, 231-243, doi:<https://doi.org/10.1016/j.cell.2008.06.035> (2008).
- 272 Yuan, J., Pu, M., Zhang, Z. & Lou, Z. Histone H3-K56 acetylation is important for genomic stability in mammals. *Cell Cycle* **8**, 1747-1753, doi:10.4161/cc.8.11.8620 (2009).
- 273 Muñoz-Galván, S., Jimeno, S., Rothstein, R. & Aguilera, A. Histone H3K56 acetylation, Rad52, and non-DNA repair factors control double-strand break repair choice with the sister chromatid. *PLoS genetics* **9**, e1003237, doi:10.1371/journal.pgen.1003237 (2013).
- 274 Prakash, S. & Prakash, L. Nucleotide excision repair in yeast. *Mutation research* **451**, 13-24, doi:10.1016/s0027-5107(00)00037-3 (2000).
- 275 Guzder, S. N., Sung, P., Prakash, L. & Prakash, S. The DNA-dependent ATPase activity of yeast nucleotide excision repair factor 4 and its role in DNA damage recognition. *The Journal of biological chemistry* **273**, 6292-6296, doi:10.1074/jbc.273.11.6292 (1998).
- 276 Li, S. *et al.* The roles of Rad16 and Rad26 in repairing repressed and actively transcribed genes in yeast. *DNA repair* **6**, 1596-1606, doi:10.1016/j.dnarep.2007.05.005 (2007).
- 277 Verhage, R. *et al.* The RAD7 and RAD16 genes, which are essential for pyrimidine dimer removal from the silent mating type loci, are also required for repair of the nontranscribed strand of an active gene in *Saccharomyces cerevisiae*. *Mol Cell Biol* **14**, 6135-6142, doi:10.1128/mcb.14.9.6135-6142.1994 (1994).
- 278 Yu, S., Owen-Hughes, T., Friedberg, E. C., Waters, R. & Reed, S. H. The yeast Rad7/Rad16/Abf1 complex generates superhelical torsion in DNA that is required for nucleotide excision repair. *DNA repair* **3**, 277-287, doi:<https://doi.org/10.1016/j.dnarep.2003.11.004> (2004).
- 279 Yu, S., Teng, Y., Waters, R. & Reed, S. H. How chromatin is remodelled during DNA repair of UV-induced DNA damage in *Saccharomyces cerevisiae*. *PLoS genetics* **7**, e1002124, doi:10.1371/journal.pgen.1002124 (2011).
- 280 Teng, Y. *et al.* *Saccharomyces cerevisiae* Rad16 mediates ultraviolet-dependent histone H3 acetylation required for efficient global genome nucleotide-excision repair. *EMBO reports* **9**, 97-102, doi:10.1038/sj.embor.7401112 (2008).
- 281 van Eijk, P. *et al.* Nucleosome remodeling at origins of global genome-nucleotide excision repair occurs at the boundaries of higher-order chromatin structure. *Genome research* **29**, 74-84, doi:10.1101/gr.237198.118 (2019).
- 282 Yu, Y., Teng, Y., Liu, H., Reed, S. H. & Waters, R. UV irradiation stimulates histone acetylation and chromatin remodeling at a repressed yeast locus. *Proceedings of the National Academy*

- of Sciences of the United States of America **102**, 8650-8655, doi:10.1073/pnas.0501458102 (2005).
- 283 Green, C. M. & Almouzni, G. When repair meets chromatin. First in series on chromatin dynamics. *EMBO reports* **3**, 28-33, doi:10.1093/embo-reports/kvf005 (2002).
- 284 Duan, M.-R. & Smerdon, M. J. UV Damage in DNA Promotes Nucleosome Unwrapping*. *Journal of Biological Chemistry* **285**, 26295-26303, doi:<https://doi.org/10.1074/jbc.M110.140087> (2010).
- 285 Ramanathan, B. & Smerdon, M. J. Enhanced DNA Repair Synthesis in Hyperacetylated Nucleosomes. *Journal of Biological Chemistry* **264**, 11026-11034, doi:[https://doi.org/10.1016/S0021-9258\(18\)60422-3](https://doi.org/10.1016/S0021-9258(18)60422-3) (1989).
- 286 Battu, A., Ray, A. & Wani, A. A. ASF1A and ATM regulate H3K56-mediated cell-cycle checkpoint recovery in response to UV irradiation. *Nucleic Acids Research* **39**, 7931-7945, doi:10.1093/nar/gkr523 (2011).
- 287 Smerdon, M. J., Lan, S. Y., Calza, R. E. & Reeves, R. Sodium butyrate stimulates DNA repair in UV-irradiated normal and xeroderma pigmentosum human fibroblasts. *Journal of Biological Chemistry* **257**, 13441-13447, doi:[https://doi.org/10.1016/S0021-9258\(18\)33468-9](https://doi.org/10.1016/S0021-9258(18)33468-9) (1982).
- 288 Ozdemir, A. *et al.* Characterization of Lysine 56 of Histone H3 as an Acetylation Site in *Saccharomyces cerevisiae**. *Journal of Biological Chemistry* **280**, 25949-25952, doi:<https://doi.org/10.1074/jbc.C500181200> (2005).
- 289 Yu, S. *et al.* Global genome nucleotide excision repair is organized into domains that promote efficient DNA repair in chromatin. *Genome research* **26**, 1376-1387, doi:10.1101/gr.209106.116 (2016).
- 290 Cote, J. M. *et al.* Two factor authentication: Asf1 mediates crosstalk between H3 K14 and K56 acetylation. *Nucleic Acids Research* **47**, 7380-7391, doi:10.1093/nar/gkz508 (2019).
- 291 Teng, Y., Yu, Y. & Waters, R. The *Saccharomyces cerevisiae* histone acetyltransferase gcn5 has a role in the photoreactivation and nucleotide excision repair of UV-induced cyclobutane pyrimidine dimers in the MFA2 gene1 Edited by J. Karn. *Journal of Molecular Biology* **316**, 489-499, doi:<https://doi.org/10.1006/jmbi.2001.5383> (2002).
- 292 Bondarenko, V. A. *et al.* Nucleosomes can form a polar barrier to transcript elongation by RNA polymerase II. *Mol Cell* **24**, 469-479, doi:10.1016/j.molcel.2006.09.009 (2006).
- 293 Cole, H. A., Ocampo, J., Iben, J. R., Chereji, R. V. & Clark, D. J. Heavy transcription of yeast genes correlates with differential loss of histone H2B relative to H4 and queued RNA polymerases. *Nucleic Acids Res* **42**, 12512-12522, doi:10.1093/nar/gku1013 (2014).
- 294 Jamai, A., Imoberdorf, R. M. & Strubin, M. Continuous histone H2B and transcription-dependent histone H3 exchange in yeast cells outside of replication. *Mol Cell* **25**, 345-355, doi:10.1016/j.molcel.2007.01.019 (2007).
- 295 Kireeva, M. L. *et al.* Nucleosome remodeling induced by RNA polymerase II: loss of the H2A/H2B dimer during transcription. *Mol Cell* **9**, 541-552, doi:10.1016/s1097-2765(02)00472-0 (2002).
- 296 Filipovski, M., Soffers, J. H. M., Vos, S. M. & Farnung, L. Structural basis of nucleosome retention during transcription elongation. *Science (New York, N.Y.)* **376**, 1313-1316, doi:10.1126/science.abo3851 (2022).
- 297 Kwak, H. & Lis, J. T. Control of transcriptional elongation. *Annual review of genetics* **47**, 483-508, doi:10.1146/annurev-genet-110711-155440 (2013).
- 298 Venkatesh, S. & Workman, J. L. Histone exchange, chromatin structure and the regulation of transcription. *Nature reviews. Molecular cell biology* **16**, 178-189, doi:10.1038/nrm3941 (2015).
- 299 Smolle, M. & Workman, J. L. Transcription-associated histone modifications and cryptic transcription. *Biochimica et biophysica acta* **1829**, 84-97, doi:10.1016/j.bbagr.2012.08.008 (2013).

- 300 Ardehali, M. B. & Lis, J. T. Tracking rates of transcription and splicing in vivo. *Nature structural & molecular biology* **16**, 1123-1124, doi:10.1038/nsmb1109-1123 (2009).
- 301 Gaykalova, D. A. *et al.* A polar barrier to transcription can be circumvented by remodeler-induced nucleosome translocation. *Nucleic Acids Res* **39**, 3520-3528, doi:10.1093/nar/gkq1273 (2011).
- 302 Li, B., Carey, M. & Workman, J. L. The role of chromatin during transcription. *Cell* **128**, 707-719, doi:10.1016/j.cell.2007.01.015 (2007).
- 303 Burke, R. L., Tekamp-Olson, P. & Najarian, R. The isolation, characterization, and sequence of the pyruvate kinase gene of *Saccharomyces cerevisiae*. *The Journal of biological chemistry* **258**, 2193-2201 (1983).
- 304 Pearce, A. K. *et al.* Pyruvate kinase (Pyk1) levels influence both the rate and direction of carbon flux in yeast under fermentative conditions. *Microbiology (Reading, England)* **147**, 391-401, doi:10.1099/00221287-147-2-391 (2001).
- 305 Archambault, J. & Friesen, J. D. Genetics of eukaryotic RNA polymerases I, II, and III. *Microbiological reviews* **57**, 703-724, doi:10.1128/mr.57.3.703-724.1993 (1993).
- 306 Pruyne, D. & Bretscher, A. Polarization of cell growth in yeast. I. Establishment and maintenance of polarity states. *Journal of cell science* **113** (Pt 3), 365-375, doi:10.1242/jcs.113.3.365 (2000).
- 307 Swanson, R. N. *et al.* Isolation of TFC1, a gene encoding one of two DNA-binding subunits of yeast transcription factor tau (TFIIIC). *Proceedings of the National Academy of Sciences of the United States of America* **88**, 4887-4891, doi:10.1073/pnas.88.11.4887 (1991).
- 308 Parsons, M. C. & Weil, P. A. Cloning of TFC1, the *Saccharomyces cerevisiae* gene encoding the 95-kDa subunit of transcription factor TFIIIC. *The Journal of biological chemistry* **267**, 2894-2901 (1992).
- 309 Gilon, T., Chomsky, O. & Kulka, R. G. Degradation signals recognized by the Ubc6p-Ubc7p ubiquitin-conjugating enzyme pair. *Mol Cell Biol* **20**, 7214-7219, doi:10.1128/mcb.20.19.7214-7219.2000 (2000).
- 310 Sommer, T. & Jentsch, S. A protein translocation defect linked to ubiquitin conjugation at the endoplasmic reticulum. *Nature* **365**, 176-179, doi:10.1038/365176a0 (1993).
- 311 Klebanow, E. R., Poon, D., Zhou, S. & Weil, P. A. Isolation and characterization of TAF25, an essential yeast gene that encodes an RNA polymerase II-specific TATA-binding protein-associated factor. *The Journal of biological chemistry* **271**, 13706-13715, doi:10.1074/jbc.271.23.13706 (1996).
- 312 Uprety, B., Lahudkar, S., Malik, S. & Bhaumik, S. R. The 19S proteasome subcomplex promotes the targeting of NuA4 HAT to the promoters of ribosomal protein genes to facilitate the recruitment of TFIID for transcriptional initiation in vivo. *Nucleic Acids Res* **40**, 1969-1983, doi:10.1093/nar/gkr977 (2012).
- 313 Thayer, N. H. *et al.* Identification of long-lived proteins retained in cells undergoing repeated asymmetric divisions. *Proceedings of the National Academy of Sciences of the United States of America* **111**, 14019-14026, doi:10.1073/pnas.1416079111 (2014).
- 314 Henderson, K. A., Hughes, A. L. & Gottschling, D. E. Mother-daughter asymmetry of pH underlies aging and rejuvenation in yeast. *eLife* **3**, e03504, doi:10.7554/eLife.03504 (2014).
- 315 Bennetzen, J. L. & Hall, B. D. The primary structure of the *Saccharomyces cerevisiae* gene for alcohol dehydrogenase. *The Journal of biological chemistry* **257**, 3018-3025 (1982).
- 316 Jensen, L. T., Ajua-Alemanji, M. & Culotta, V. C. The *Saccharomyces cerevisiae* high affinity phosphate transporter encoded by PHO84 also functions in manganese homeostasis. *The Journal of biological chemistry* **278**, 42036-42040, doi:10.1074/jbc.M307413200 (2003).
- 317 Nishimura, K., Yasumura, K., Igarashi, K., Harashima, S. & Kakinuma, Y. Transcription of some PHO genes in *Saccharomyces cerevisiae* is regulated by spt7p. *Yeast (Chichester, England)* **15**, 1711-1717, doi:10.1002/(sici)1097-0061(199912)15:16<1711::aid-yea497>3.0.co;2-8 (1999).

- 318 Pokholok, D. K. *et al.* Genome-wide map of nucleosome acetylation and methylation in yeast. *Cell* **122**, 517-527, doi:10.1016/j.cell.2005.06.026 (2005).
- 319 Krogan, N. J. *et al.* Methylation of histone H3 by Set2 in *Saccharomyces cerevisiae* is linked to transcriptional elongation by RNA polymerase II. *Mol Cell Biol* **23**, 4207-4218, doi:10.1128/mcb.23.12.4207-4218.2003 (2003).
- 320 Zhao, W. *et al.* Investigating crosstalk between H3K27 acetylation and H3K4 trimethylation in CRISPR/dCas-based epigenome editing and gene activation. *Scientific Reports* **11**, 15912, doi:10.1038/s41598-021-95398-5 (2021).
- 321 Jung, I. *et al.* Global mapping of the regulatory interactions of histone residues. *FEBS letters* **589**, 4061-4070, doi:10.1016/j.febslet.2015.11.016 (2015).
- 322 Reines, D. in *Methods in Enzymology* Vol. 371 284-292 (Academic Press, 2003).
- 323 Shilatifard, A. The COMPASS family of histone H3K4 methylases: mechanisms of regulation in development and disease pathogenesis. *Annual review of biochemistry* **81**, 65-95, doi:10.1146/annurev-biochem-051710-134100 (2012).
- 324 Karam, C. S., Kellner, W. A., Takenaka, N., Clemmons, A. W. & Corces, V. G. 14-3-3 mediates histone cross-talk during transcription elongation in *Drosophila*. *PLoS genetics* **6**, e1000975, doi:10.1371/journal.pgen.1000975 (2010).
- 325 Li, J., Moazed, D. & Gygi, S. P. Association of the histone methyltransferase Set2 with RNA polymerase II plays a role in transcription elongation. *The Journal of biological chemistry* **277**, 49383-49388, doi:10.1074/jbc.M209294200 (2002).
- 326 Xiao, T. *et al.* Phosphorylation of RNA polymerase II CTD regulates H3 methylation in yeast. *Genes & development* **17**, 654-663, doi:10.1101/gad.1055503 (2003).
- 327 Govind, C. K. *et al.* Phosphorylated Pol II CTD recruits multiple HDACs, including Rpd3C(S), for methylation-dependent deacetylation of ORF nucleosomes. *Mol Cell* **39**, 234-246, doi:10.1016/j.molcel.2010.07.003 (2010).
- 328 Ng, H. H., Robert, F., Young, R. A. & Struhl, K. Targeted recruitment of Set1 histone methylase by elongating Pol II provides a localized mark and memory of recent transcriptional activity. *Mol Cell* **11**, 709-719, doi:10.1016/s1097-2765(03)00092-3 (2003).
- 329 Kim, T. & Buratowski, S. Dimethylation of H3K4 by Set1 recruits the Set3 histone deacetylase complex to 5' transcribed regions. *Cell* **137**, 259-272, doi:10.1016/j.cell.2009.02.045 (2009).
- 330 Grigull, J., Mnaimneh, S., Pootoolal, J., Robinson, M. D. & Hughes, T. R. Genome-wide analysis of mRNA stability using transcription inhibitors and microarrays reveals posttranscriptional control of ribosome biogenesis factors. *Mol Cell Biol* **24**, 5534-5547, doi:10.1128/mcb.24.12.5534-5547.2004 (2004).
- 331 Martin, B. J. E., Chruscicki, A. T. & Howe, L. J. Transcription Promotes the Interaction of the FAcilitates Chromatin Transactions (FACT) Complex with Nucleosomes in *Saccharomyces cerevisiae*. *Genetics* **210**, 869-881, doi:10.1534/genetics.118.301349 (2018).
- 332 Martin, B. J. E. *et al.* Transcription shapes genome-wide histone acetylation patterns. *Nature communications* **12**, 210, doi:10.1038/s41467-020-20543-z (2021).
- 333 Williams, S. K., Truong, D. & Tyler, J. K. Acetylation in the globular core of histone H3 on lysine-56 promotes chromatin disassembly during transcriptional activation. *Proceedings of the National Academy of Sciences of the United States of America* **105**, 9000-9005, doi:10.1073/pnas.0800057105 (2008).
- 334 Topal, S., Vasseur, P., Radman-Livaja, M. & Peterson, C. L. Distinct transcriptional roles for Histone H3-K56 acetylation during the cell cycle in Yeast. *Nature communications* **10**, 4372, doi:10.1038/s41467-019-12400-5 (2019).
- 335 Weiner, A. *et al.* High-resolution chromatin dynamics during a yeast stress response. *Mol Cell* **58**, 371-386, doi:10.1016/j.molcel.2015.02.002 (2015).
- 336 Cai, Q., Tong, S. M., Shao, W., Ying, S. H. & Feng, M. G. Pleiotropic effects of the histone deacetylase Hos2 linked to H4-K16 deacetylation, H3-K56 acetylation, and H2A-S129

- phosphorylation in *Beauveria bassiana*. *Cellular microbiology* **20**, e12839, doi:10.1111/cmi.12839 (2018).
- 337 Josling, G. A., Selvarajah, S. A., Petter, M. & Duffy, M. F. The role of bromodomain proteins in regulating gene expression. *Genes* **3**, 320-343, doi:10.3390/genes3020320 (2012).
- 338 D'Arcy, S. & Luger, K. Understanding histone acetyltransferase Rtt109 structure and function: how many chaperones does it take? *Current opinion in structural biology* **21**, 728-734, doi:10.1016/j.sbi.2011.09.005 (2011).
- 339 Tang, Y. *et al.* Structure of the Rtt109-AcCoA/Vps75 complex and implications for chaperone-mediated histone acetylation. *Structure (London, England : 1993)* **19**, 221-231, doi:10.1016/j.str.2010.12.012 (2011).
- 340 Zhang, L. *et al.* Multisite Substrate Recognition in Asf1-Dependent Acetylation of Histone H3 K56 by Rtt109. *Cell* **174**, 818-830.e811, doi:10.1016/j.cell.2018.07.005 (2018).
- 341 Owen, D. J. *et al.* The structural basis for the recognition of acetylated histone H4 by the bromodomain of histone acetyltransferase gcn5p. *The EMBO journal* **19**, 6141-6149, doi:10.1093/emboj/19.22.6141 (2000).
- 342 Hassan, A. H. *et al.* Selective recognition of acetylated histones by bromodomains in transcriptional co-activators. *The Biochemical journal* **402**, 125-133, doi:10.1042/bj20060907 (2007).
- 343 Kujirai, T. *et al.* Structural basis of the nucleosome transition during RNA polymerase II passage. *Science (New York, N.Y.)* **362**, 595-598, doi:10.1126/science.aau9904 (2018).
- 344 Fei, J. *et al.* NDF, a nucleosome-destabilizing factor that facilitates transcription through nucleosomes. *Genes & development* **32**, 682-694, doi:10.1101/gad.313973.118 (2018).



PUBLICATIONS



RESEARCH ARTICLE

RNA Polymerase II Dependent Crosstalk between H4K16 Deacetylation and H3K56 Acetylation Promotes Transcription of Constitutively Expressed Genes

Preeti Khan, Priyabrata Singha, Ronita Nag Chaudhuri

Department of Biotechnology, St Xavier's College, Kolkata, India

ABSTRACT Nucleosome dynamics in the coding region of a transcriptionally active locus is critical for understanding how RNA polymerase II progresses through the gene body. Histone acetylation and deacetylation critically influence nucleosome accessibility during DNA metabolic processes like transcription. Effect of such histone modifications is context and residue dependent. Rather than effect of individual histone residues, the network of modifications of several histone residues in combination generates a chromatin landscape that is conducive for transcription. Here we show that in *Saccharomyces cerevisiae*, crosstalk between deacetylation of the H4 N-terminal tail residue H4K16 and acetylation of the H3 core domain residue H3K56, promotes RNA polymerase II progression through the gene body. Results indicate that deacetylation of H4K16 precedes and in turn induces H3K56 acetylation. Effectively, recruitment of Rtt109, the HAT responsible for H3K56 acetylation is essentially dependent on H4K16 deacetylation. In Hos2 deletion strains, where H4K16 deacetylation is abolished, both H3K56 acetylation and RNA polymerase II recruitment gets significantly impaired. Notably, H4K16 deacetylation and H3K56 acetylation are found to be essentially dependent on active transcription. In summary, H4K16 deacetylation promotes H3K56 acetylation and the two modifications together work towards successful functioning of RNA polymerase II during active transcription.

KEYWORDS gene expression, H3K56, histone acetylation, H4K16, RNA polymerase II, transcription regulation

INTRODUCTION

For effective gene expression RNA polymerase II (RNAPII) is required to access DNA that is occluded by nucleosomes. In the promoter region of a locus while a stretch of nucleosome depleted region (NDR) is generated for RNAPII access, the coding region has localized disruption of nucleosomes that is enough for RNAPII to progress.^{1–6} The accessibility of nucleosomal DNA is critically regulated by post-translational modification of histones.^{7,8} Of the known post-translational histone modifications, acetylation of lysine residues is the most prevalent.⁹ Some of the prominent acetylation events involve residues of the histone H4 N-terminal tails, including that of H4K16. Being the only acetylatable residue present in the acidic patch binding region of histone H4 tail, H4K16 acetylation can directly influence higher order chromatin compaction-relaxation dynamics.^{10–13} The state of H4K16 acetylation is critically regulated and affects gene silencing, transcription, as well as DNA repair.^{14–19} Besides affecting local chromatin dynamics,²⁰ histone tail modifications primarily function to recruit chromatin effector proteins that in turn alter nucleosome structure and affect different stages of transcription.^{21–24} At the nucleosomal level, often more than the histone tail residues those

© 2023 Taylor & Francis Group, LLC

Supplemental data for this article can be accessed online at <https://doi.org/10.1080/10985549.2023.2270912>.

Address correspondence to Ronita Nag Chaudhuri, ronita.nc@sxccal.edu, ronita_7@yahoo.co.in.

Received 25 May 2023

Revised 14 August 2023

Accepted 5 October 2023

present on the globular core domain can directly influence interactions between the histone octamer and the nucleosomal DNA.^{25–27} H3K56 is a globular core residue located at the site where the nucleosomal DNA enters or leaves the histone octamer and its acetylation weakens the interaction at the DNA entry/exit site thereby promoting unwrapping of nucleosomal DNA.^{28–32} Thus far, acetylation of H3K56 is known to primarily occur on free histones, in a replication-dependent or independent manner, and is accomplished in yeast by a complex formed by the histone chaperone Asf1 and the HAT Rtt109.^{30,33–37} In *Saccharomyces cerevisiae*, H3K56 acetylation is a marker of active transcription that has been strongly associated with promoter-nucleosome dynamics, chromatin disassembly and histone exchange.^{35,38–41} By exposing the linker DNA region, H3K56 acetylation is known to maintain chromatin in a more poised state and facilitates recruitment of the SWI/SNF chromatin remodeling complexes.^{42–44} Furthermore, in heterochromatin loci, H3K56 acetylation can promote transcription elongation without affecting the formation of higher order chromatin structures.⁴⁵ In addition, histone H2A/H2B eviction and FACT mediated nucleosome assembly/disassembly is critically regulated by H3K56 acetylation.^{46,47} Recent in vitro studies have suggested that by unwrapping nucleosomal DNA H3K56 acetylation can shorten the pause duration of RNAPII.⁴⁸ Indeed, in mESCs, it has been reported that hyperacetylation of H3K56 facilitates promoter-proximal pause release and RNAPII progression within genes.⁴⁹ Thus, acetylation of histone tail and core domain residues confers distinct modes of chromatin regulation that alters nucleosomal DNA accessibility and affects processes like transcription. Often histone modifications do not act in isolation, but their deposition, recognition and influence on chromatin functions are dependent on the crosstalk with modifications on other histone residues.^{50,51} For instance, Set 1 mediated H3K4 trimethylation which is a hallmark of active transcription is dependent on H2B ubiquitination.^{52,53} Conversely, H3K9 acetylation is dependent on H3K4 trimethylation.^{54,55} In mammals for instance, H3K27 acetylation is required for H3K4 trimethylation, and H3K4 trimethylation alone cannot promote gene activation in absence of H3K27ac.⁵⁶ Although histone acetylation is often associated with active genes in yeast, role of H4K16 deacetylation has been found to be unique. Interestingly, presence of H4K16 deacetylation with H3K36me3 signals transcription elongation, while H4K16 deacetylation with H3K4me3 suppresses transcription initiation.⁵⁷ Thus, a particular histone modification may signal both activating and repressive functions based on its crosstalk with associated histone modifications. Often these histone modification cross talks are cotranscriptionally established on chromatin based on the RNAPII CTD phosphorylation status^{53,58–65} and serves to orchestrate an intricate array of signals that regulate distinct stages of transcription. Thus, understanding how RNAPII mediates the crosstalk between histone post-translational modifications serves as the basis for deciphering the exact histone code that effectively regulates transcription.

In this study, we elucidate a functional crosstalk between deacetylation of H4K16 and acetylation of H3K56 during transcription of constitutively expressed genes. We demonstrate that in *S. cerevisiae*, this cross talk is essentially dependent on active RNAPII with H4K16 deacetylation being an important prerequisite for H3K56 acetylation. Our work indicates that the RNAPII mediated crosstalk between H4K16 deacetylation and H3K56 acetylation is essential for efficient transcription in the gene body of constitutively expressed genes.

RESULTS

Hyperacetylation of H3K56 in the ORF region promotes expression of constitutively active genes. To understand the significance of H3K56 acetylation in regulating expression of constitutively active genes, we performed ChIP assay with antibody against acetylated H3K56. We observed that in the ORF of constitutively active genes H3K56 gets hyperacetylated, relative to the promoter region (Fig. 1A). To endorse that the observed H3K56 acetylation was actually related to active transcription, H3K56 acetylation levels in the transcriptionally silenced telomere locus (*TEL08R*),

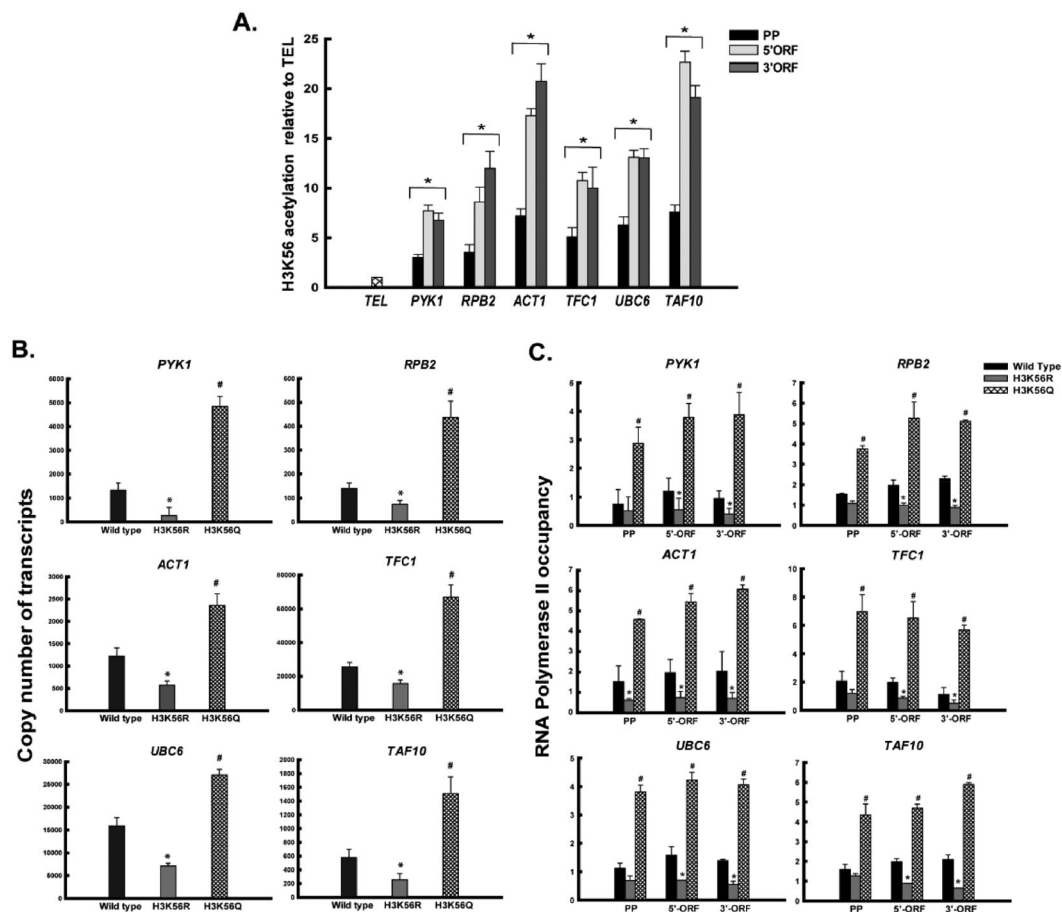


FIG 1 H3K56 acetylation is required for transcription of constitutively expressed genes. (A) ChIP qPCR analyses were performed to check H3K56 acetylation levels in the promoter (PP), 5'ORF and 3'ORF of *PYK1*, *RPB2*, *ACT1*, *TFC1*, *UBC6* and *TAF10* loci. H3K56 acetylation levels were normalized to ChIP data with anti-H3 antibody of the same regions and graphically represented relative to a nontranscribing control region of *TELO8R* denoted as *TEL*. (B) RNA was isolated from wild-type and H3K56 mutants followed by RT-qPCR analyses using absolute quantification method as described in Materials and Methods. The copy number of transcripts in wild-type and mutants, respectively are graphically plotted for the genes mentioned above. (C) ChIP analyses with anti-RNAPII (8WG16) antibody to check occupancy at the promoter (PP), 5'ORF and 3'ORF of *PYK1*, *RPB2*, *ACT1*, *TFC1*, *UBC6* and *TAF10* loci. The data normalized by 1% input was graphically plotted. Data represents the mean of three independent experiments with standard error of mean bars. * and # denote *t* test significant *P* values of <0.05.

was used as the control. To further correlate the role of H3K56 acetylation with transcription of active genes, we worked with two mutants – H3K56R, which mimics a state of constitutive deacetylation and H3K56Q, mimicking a state of constitutive acetylation. We performed RT-qPCR based comparative gene expression analyses between wild type and the two mutant strains of H3K56. Our results indicated that absence of H3K56 acetylation (H3K56R) caused significant reduction in gene expression levels, compared to wild-type. On the contrary, presence of constitutive acetylation of H3K56 (H3K56Q) resulted in significant upregulation of gene expression, relative to wild-type (Fig. 1B). It was further observed that, in H3K56Q mutants there was significantly higher recruitment of RNAPII in the promoter and ORF regions of the actively transcribing genes, while RNAPII recruitment was impaired in H3K56R mutants, compared to wild-type (Fig. 1C). To confirm that the observed effect of H3K56 acetylation on transcription of constitutively expressed genes, was a phenomenon that can be generalized for any housekeeping gene, the above results were confirmed for three more loci namely, *PMA1*, *ADH1* and *PHO84* (Fig. S1). Taken together, the above results indicated that acetylation of H3K56 was essential for recruitment of RNAPII during transcription of constitutively active genes.

H3K56 acetylation is dependent on H4K16 deacetylation. Previously we have reported that in constitutively active loci H4K16 deacetylation promotes H3K56

acetylation.¹⁹ In order to elucidate the correlation between H4K16 deacetylation and H3K56 acetylation, we deleted *Sas2*, the major HAT responsible for H4K16 acetylation.^{16,66,67} To validate the Δ *Sas2* mutant, we compared the levels of H4K16 acetylation in wild-type and the mutant and found that deletion of *Sas2* reduced H4K16 acetylation levels significantly in constitutively active genes (Fig. S2). Thereafter we compared the levels of H3K56 acetylation in wild-type and Δ *Sas2* mutant. Our results indicated that in all the constitutively active genes tested, H3K56 acetylation was significantly higher in Δ *Sas2* mutant, compared to wild-type (Fig. 2A). The telomeric region (*TEL08R*) was used as the nontranscribing region control, to confirm that the observed H3K56 acetylation pattern was a signature related to transcribing loci. In trying to corroborate this with transcription, we observed that RNAPII occupancy was also

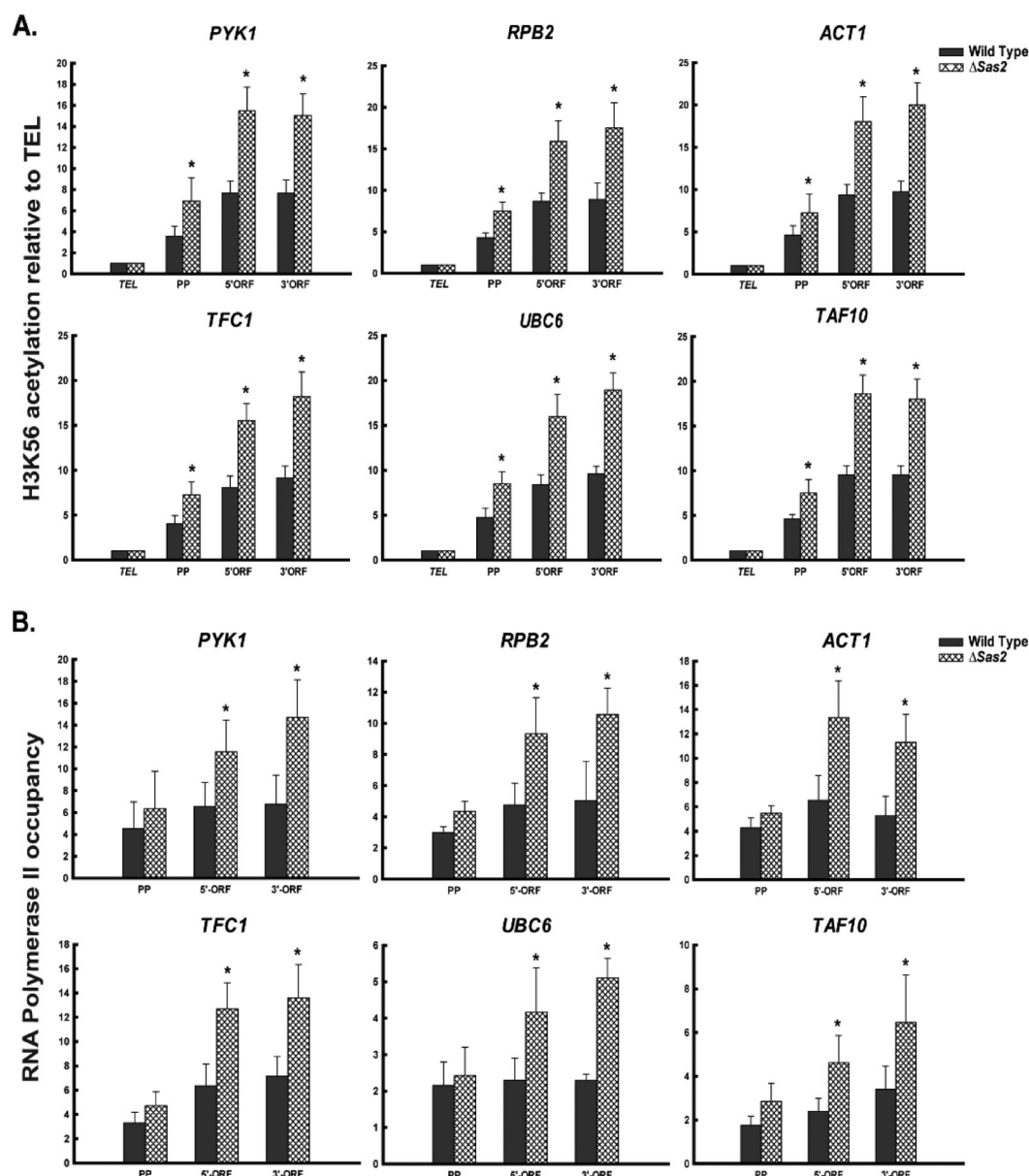


FIG 2 Comparative analyses of H3K56 acetylation levels and RNAP II occupancy in wild-type and Δ *Sas2* mutant. Chromatin of wild-type and Δ *Sas2* mutant was immunoprecipitated with (A) anti-H3K56ac antibody (B) anti-RNAPII (8WG16) antibody and the occupancy was thereafter monitored by qPCR at the promoter (PP), 5'-ORF and 3'-ORF of *PYK1*, *RPB2*, *ACT1*, *TFC1*, *UBC6* and *TAF10* loci. H3K56 acetylation levels were normalized to ChIP data with anti-H3 antibody of the same regions and graphically represented relative to a nontranscribing control region of *TEL08R* denoted as *TEL*. RNAPII occupancy was normalized by input (1%) and graphically represented. Data represents the mean of three independent experiments with standard error of mean bars and * denote *t* test significant *P* values of <0.05.

significantly higher in Δ Sas2 mutant, compared to wild-type (Fig. 2B). Notably, higher RNAPII recruitment was evident specifically in the ORF of the constitutively active genes that we tested. This was in consonance with previous reports that have indicated a negative correlation of Sas2 mediated H4K16 acetylation with RNAPII progression.⁶⁶ These results indicated that H4K16 deacetylation and the consequent higher H3K56 acetylation observed in the Δ Sas2 mutant possibly aid RNAPII recruitment along the ORF of the constitutively expressed genes.

To understand the direct impact of H4K16 deacetylation on H3K56 acetylation, we deleted Hos2, the HDAC responsible for deacetylation of H4K16 in the euchromatin region.⁶⁸ To validate that Hos2 targets deacetylation of H4K16 residue, acetylation level of H4K16 was checked in WT and *Hos2* Δ mutants. Results indicated that in absence of Hos2, acetylation levels of H4K16 were significantly higher compared to wild-type, in all loci tested (Fig. S2). Cell survival assay with *Hos2* Δ mutants showed that under control conditions they have growth comparable to wild-type. To further correlate this with transcription, we did cell survival assay in presence of the transcription elongation inhibitor 6-azauracil (6-AU). In presence of 6-AU the *Hos2* Δ mutant showed increased sensitivity compared to wild-type. In addition, it was interesting to note that, H3K56Q mutation in *Hos2* Δ background exhibited increased resistance to 6-AU, compared to wild-type (Fig. 3A). This implied that H4K16 deacetylation along with H3K56 acetylation generated a chromatin landscape conducive for transcription progression in the gene body. Furthermore, H3K56 acetylation levels were reduced in *Hos2* Δ mutant, compared to wild-type, suggesting dependence of H3K56 acetylation on H4K16 deacetylation (Fig. 3B). H3K56 acetylation levels at the telomeric region (*TEL08R*) was used as the nontranscribing locus control. Furthermore, lack of H4K16 deacetylation impaired recruitment of RNAPII across the promoter and gene body of the constitutively expressed genes tested, indicating its requirement for progression of RNAPII in transcriptionally active loci (Fig. 3C). Taken together, the above results indicate that H3K56 acetylation is dependent on Hos2-mediated H4K16 deacetylation, and these two events are essential for active transcription.

In presence of constitutive acetylation of H3K56 the requirement for H4K16 deacetylation can be evaded. To further understand the crosstalk between H3K56 acetylation and H4K16 deacetylation, we generated the following sets of double mutants: H4K16RH3K56Q, H4K16QH3K56Q, H4K16RH3K56R, H4K16QH3K56R. As shown in Fig. 4A, cell survival assay under control conditions indicated that the double mutants H4K16RH3K56R and H4K16QH3K56R have moderately reduced growth compared to wild-type, the single mutants, and the double mutants H4K16RH3K56Q or H4K16QH3K56Q. Interestingly, cell survival assay in presence of the transcription inhibitor 6-AU showed that any single or double mutant that bore H3K56Q mutation exhibited increased resistance to 6-AU (Fig. 4A-right panel). This implied that acetylation of H3K56 is a critical factor that regulates efficient transcription. In consonance, we further observed that H3K56Q bearing double mutants showed significantly higher gene expression levels, compared to wild-type (Fig. 4B). Notably, such enhanced gene expression was observed in H3K56Q double mutants irrespective of whether H4K16 was mutated to R or Q along with. In contrast, double mutants bearing H3K56R mutation showed significantly reduced gene expression levels compared to wild-type, irrespective of H4K16 mutated to R or Q along with. Furthermore, RNAPII occupancy was higher in the double mutants bearing H3K56Q mutation compared to wild-type, irrespective of H4K16 acetylation status (Fig. 4C). These results not only indicate that H3K56 acetylation is an important event involved in transcription, but interestingly also imply that in presence of constitutive acetylation of H3K56 (H3K56Q) H4K16 deacetylation may be bypassed.

H4K16 deacetylation is required for Rtt109 recruitment in constitutively expressed genes. Rtt109 is the major HAT that is known to acetylate H3K56.^{31,34,69,70}

To understand how H4K16 deacetylation influences H3K56 acetylation, we expressed Myc-tagged Rtt109 in WT, H4K16R and H4K16Q cells. Thereafter ChIP with anti-Myc antibody was done to check for Rtt109 recruitment in the constitutively expressed genes in WT and the H4K16 mutant cells. We observed that in H4K16Q cells, which

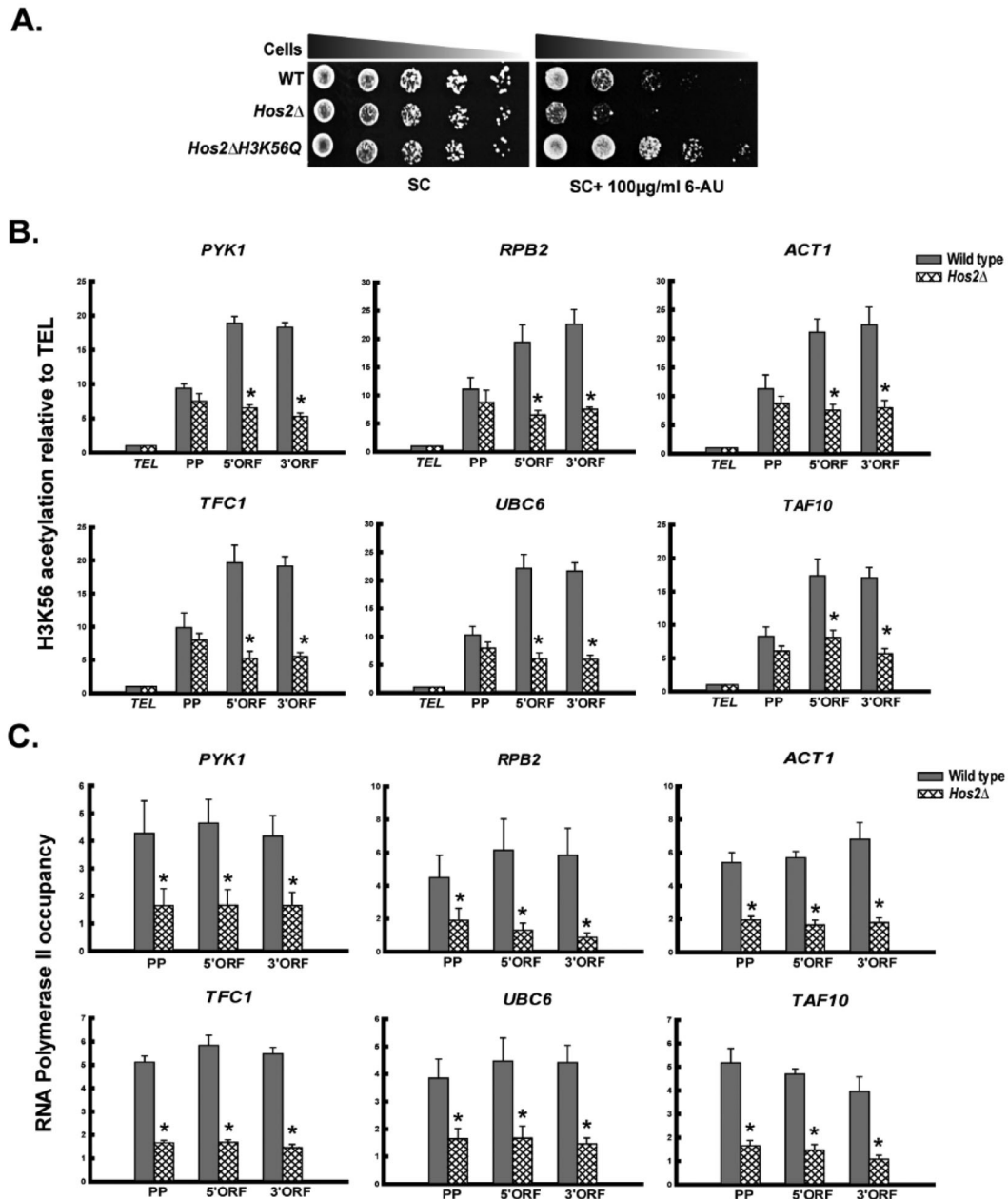


FIG 3 *Hos2* facilitates H3K56 acetylation during transcription. (A) Ten-fold serial dilutions of wild-type, *Hos2*Δ and *Hos2*Δ*H3K56Q* were spotted on SC agar plates with or without 100 μg/mL 6-AU and growth sensitivity was monitored following an incubation period of 2–4 days. (B) Comparative analysis of H3K56 acetylation levels in wild type and *Hos2*Δ at the promoter (PP), 5'ORF and 3'ORF of *PYK1*, *RPB2*, *ACT1*, *TFC1*, *UBC6* and *TAF10* loci. H3K56 acetylation levels were normalized to ChIP data with anti-H3 antibody of the same regions and graphically represented relative to a nontranscribing control region of *TELO8R* denoted as TEL. (C) Chromatin of wild-type and *Hos2*Δ was immunoprecipitated with anti-RNAPII (8WG16) antibody and occupancy was checked at the promoter (PP), 5'ORF and 3'ORF of the loci mentioned above. The data normalized by 1% input was graphically plotted. Data represents the mean of three independent experiments with standard error of mean bars and * denote *t* test significant *P* values of <0.05.

lacked H4K16 deacetylation and mimicked a state of constitutive acetylation, Rtt109 recruitment was significantly impaired compared to wild-type, in the constitutively transcribing loci (Fig. 5). On the contrary, in presence of constitutive deacetylation of H4K16 (H4K16R), Rtt109 recruitment was favored compared to wild-type. Collectively these results suggest that H4K16 deacetylation promotes H3K56 acetylation by aiding recruitment of Rtt109 to the transcriptionally active loci.

Acetylation of H3K56 is dependent on active transcription. It was further necessary to understand whether acetylation of H3K56 was associated with active transcription. For this we checked the H3K56 acetylation levels in presence of another

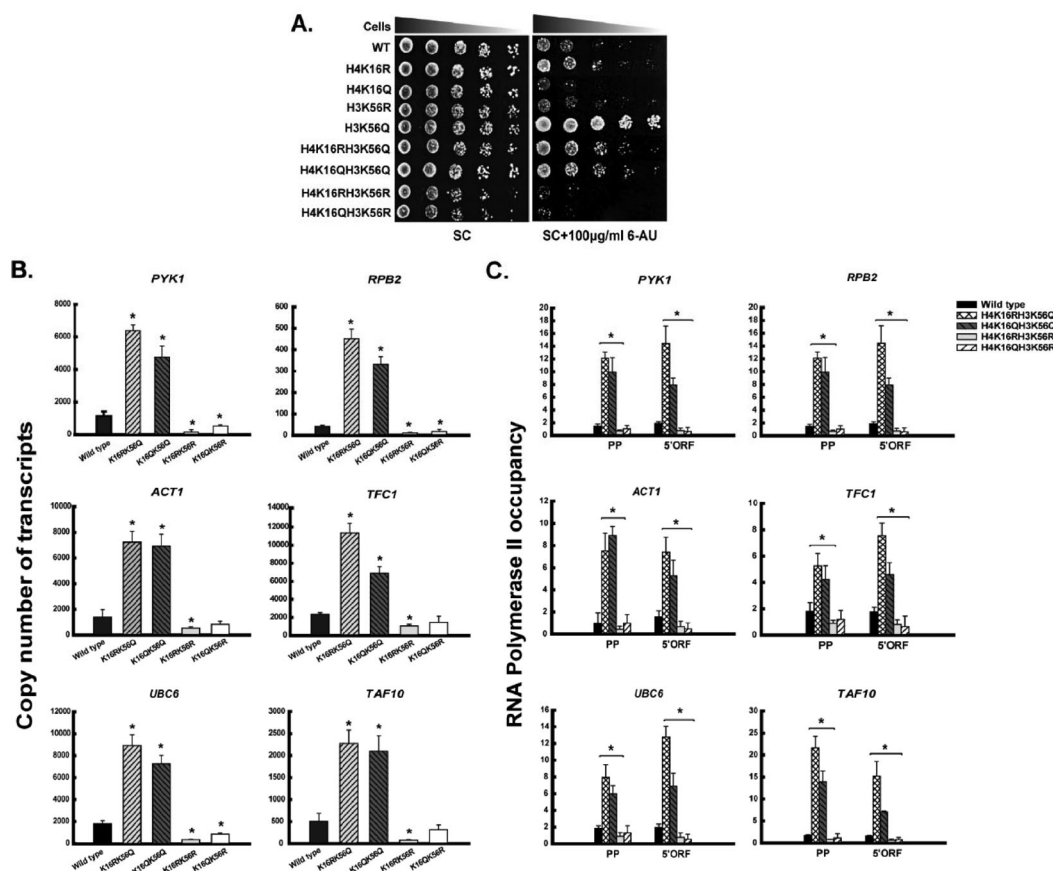
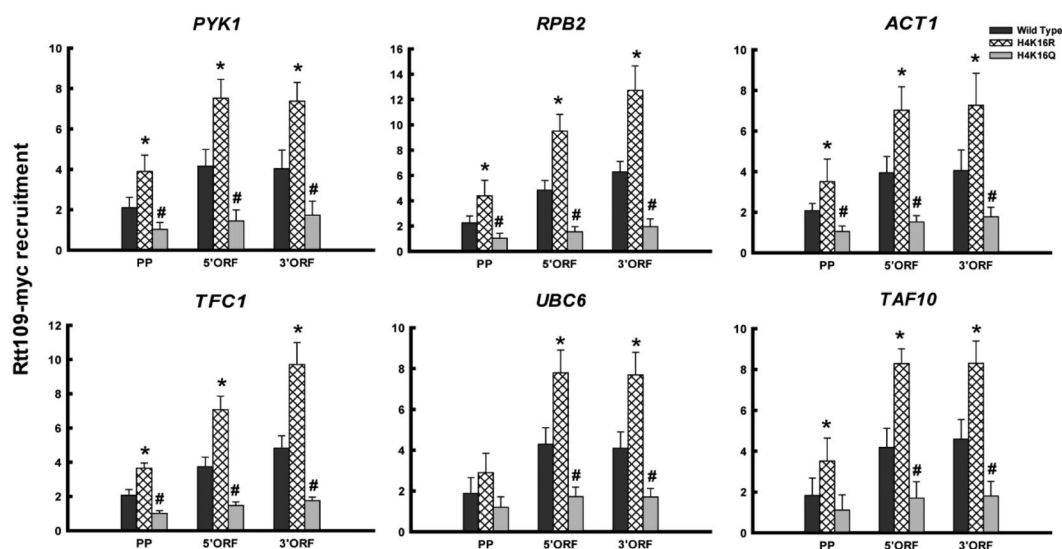


FIG 4 In H3K56Q mutant background H4K16 deacetylation can be bypassed. (A) Ten-fold serial dilutions of wild-type and mutants were spotted on SC agar plates with or without 100 µg/mL 6-AU and growth sensitivity was monitored following an incubation period of 2–4 days. (B) RNA was isolated from wild-type and mutants followed by RT-qPCR analyses using absolute quantification method as described in Materials and Methods. The copy number of transcripts of *PYK1*, *RPB2*, *ACT1*, *TFC1*, *UBC6* and *TAF10* in wild-type and mutants were graphically plotted. (C) ChIP analyses were done with anti-RNAPII (8WG16) antibody and occupancy was monitored at the promoter (PP) and 5'ORF of the loci mentioned above in wild-type and mutants. The data normalized by 1% input was graphically plotted. Data represents the mean of three independent experiments with standard error of mean bars and *denote *t* test significant *P* values of <0.05.



transcription inhibitor 1,10-phenanthroline or PH. PH is a metal chelator that is known to significantly inhibit transcription in yeast.^{71–75} Total cellular protein was isolated with or without PH treatment and immunoblotted with respective antibodies. To standardize PH treatment, we first performed immunoblot with antibody against H4K16 acetylation. Results indicated that, H4K16 acetylation levels increased upon inhibition of transcription, compared to when active transcription was present (Fig. 6A). This is in consonance with previous reports that have established negative

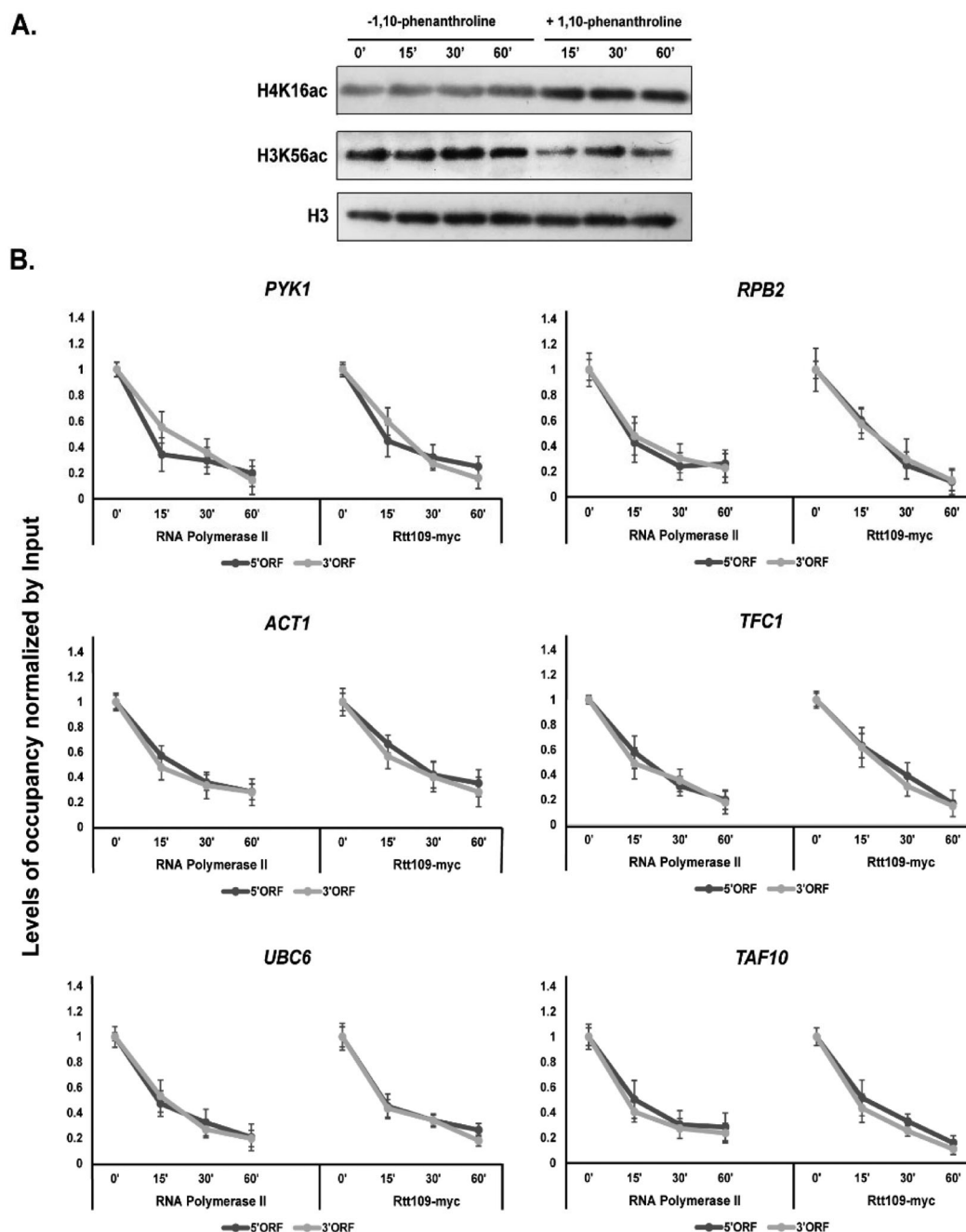


FIG 6 Transcription activity promotes H3K56 acetylation. (A) Equal amounts of whole cell extracts from wild-type cells treated with or without 1,10-phenanthroline for varying time periods as indicated were resolved on 16% SDS-PAGE and immunoblotted with anti-H4K16ac, anti-H3K56ac and anti-H3 antibody, respectively. (B) Chromatin isolated from wild-type cells treated with or without 1,10-phenanthroline for 15, 30, and 60 min, respectively were immunoprecipitated with anti-RNAPII (8WG16) and anti-myc antibodies. RNAP II and Rtt109-myc occupancy of 1,10-phenanthroline treated and untreated (0min) sample was normalized by input (1%) and occupancy under conditions of transcription inhibition were graphically plotted relative to untreated (0min), in the 5'ORF and 3'ORF of *PYK1*, *RPB2*, *ACT1*, *TFC1*, *UBC6*, and *TAF10* loci. Data represents the mean of three independent experiments with standard error of mean bars.

correlation between active transcription and H4K16 acetylation.^{15,19,40,66,68,76,77} Immunoblot using antibody against H3K56 acetylation indicated that inhibition of transcription by PH treatment, distinctly reduced H3K56 acetylation, compared to untreated samples. This implied that unlike H4K16, acetylation of H3K56 is positively associated with active transcription and absence of transcription decreases H3K56 acetylation at the cellular level. To further establish the correlation between active transcription and H3K56 acetylation, we performed ChIP experiments with or without PH treatment. Simultaneous ChIP with antibody against RNAPII (8WG16) and myc tagged Rtt109 indicated that, PH treatment led to reduction in RNAP II recruitment along with reduction in Rtt109-myc occupancy. Such a reduction in RNAPII recruitment and Rtt109-myc occupancy was observed across the ORF of all tested constitutively active loci upon PH treatment, compared to untreated controls (Fig. 6B). These observations clearly indicate that the acetylation machinery of H3K56 is closely associated with active RNA Polymerase II and inhibition of transcription impairs recruitment of Rtt109 and subsequent acetylation of H3K56.

DISCUSSION

Understanding chromatin dynamics in the coding region of a transcribing gene is critical to understanding how RNAPII makes its way through the nucleosomes during transcription. To understand the “histone code” that regulates chromatin dynamism during transcription we had previously reported the effect of H4K16 deacetylation on expression of constitutively active genes. H4K16 acetylation is known to have an anti-correlation with transcription^{15,19,40,58,66,68,76} and presence of constitutive deacetylation of H4K16 promote expression of constitutively active genes.¹⁹ Our earlier observation indicated that deacetylation of H4K16 promotes acetylation of H3K56 residue. H3K56 is known to be a crucial histone residue whose acetylation has not only been correlated with nucleosome disassembly during transcription activation,^{35,39,42} but also with transcription elongation.^{34,41,45,47–49} Presently we observed that H3K56 acetylation is significantly higher in the coding regions of constitutively expressed genes compared to their promoter. As evident, such hyperacetylation positively correlated with transcription (Fig. 1). Recent studies have reported that unwrapping of the DNA at the entry/exit site mediated by H3K56 acetylation enables RNAPII to translocate through nucleosomes.⁴⁸ In consonance, we observed that lack of H3K56 acetylation (H3K56R) significantly impeded recruitment of RNAPII, especially in the ORF of active genes. Collectively, our results indicated that H3K56 acetylation in the coding region is an important event during transcription of constitutively expressed genes. Strikingly, H3K56 acetylation pattern in constitutive genes (Fig. 1) is in negative correlation with the pattern of H4K16 acetylation which is significantly low in the coding region, compared to promoter.¹⁹ We further observed that, deacetylated state of H4K16 in Δ Sas2 mutant promotes acetylation of H3K56 in the coding region of constitutively active loci, suggesting the essentiality of H4K16 deacetylation for H3K56 acetylation. This, coupled with the presence of significantly higher levels of RNAPII in the coding regions of Δ Sas2 mutants, compared to wild-type, endorsed the fact that H4K16 deacetylation and effectively H3K56 acetylation influences RNAPII progression within the gene bodies (Fig. 2). In actively transcribing loci, H4K16 deacetylation is primarily catalyzed by the HDAC Hos2 for regulating gene activation.⁶⁸ The observation that in presence of transcription elongation inhibitor 6-AU, *Hos2* Δ mutants show increased growth sensitivity compared to wild-type, indicated a role of Hos2-mediated H4K16 deacetylation during transcription. Furthermore, in absence of Hos2, H3K56 acetylation and RNAPII recruitment along the active gene loci reduced significantly (Fig. 3). It therefore implied that Hos2 mediated H4K16 deacetylation is important for progression of RNAPII during transcription. Notably, constitutive acetylation of H3K56 in absence of Hos2 (*Hos2* Δ H3K56Q) could restore the growth sensitivity to 6-AU exhibited by *Hos2* Δ mutant. This implied that Hos2-mediated deacetylation of H4K16 is essential for H3K56 acetylation and that in presence of constitutive acetylation of H3K56, Hos2 function

can be bypassed. In consonance with our findings, it has been recently reported in *Beauveria bassiana* that Hos2 deletion leads to reduced acetylation of H3K56.⁷⁸ Collectively, our findings make it explicit that Hos2 mediated deacetylation of H4K16 is a pre-requisite for H3K56 acetylation, and these events are required for RNAPII mediated effective transcription.

Our observations on growth sensitivity to 6-AU clearly indicated that while constitutive acetylation of H4K16 (H4K16Q) has anticorrelation with transcription, constitutive acetylation of H3K56 (H3K56Q) promotes transcription. What is to be further noted is that presence of constitutive acetylation of H3K56 conferred resistance to 6-AU irrespective of the H4K16 acetylation status (Fig. 4). Subsequent, gene expression profiles and RNAPII occupancy with the double mutants further implied that H3K56 acetylation was vital for transcription and more importantly in presence of constitutive H3K56 acetylation requirement for H4K16 deacetylation could be evaded. Furthermore, the observation that presence of constitutive H3K56 acetylation (H3K56Q) made transcription independent of H4K16 acetylation status was significant. It implied that, H4K16 deacetylation can promote transcription only in presence of effective H3K56 acetylation. Thus, the transcription defect exhibited by H4K16Q could be restored in presence of constitutive acetylation of H3K56 (H4K16QH3K56Q). This further emphasizes that H3K56 acetylation is critical for transcription of constitutively active genes and that deacetylation of H4K16 is primarily required to promote acetylation of H3K56 during the process. Indeed, recruitment of Rtt109, the HAT for H3K56ac, was found to be dependent on H4K16 acetylation status. Presence of H4K16 deacetylation (H4K16R) promoted Rtt109 recruitment whereas constitutive acetylation of H4K16 (H4K16Q) significantly impeded Rtt109 recruitment in active genes (Fig. 5). This implied that H4K16 deacetylation must precede Rtt109 recruitment and the resultant H3K56 acetylation. In transcribing loci, several bromodomain containing HATs such as Gcn5^{79,80} are known to bind to H4K16 acetylated histones. It is possible that such binding hinders the association of H3K56 acetylation machinery with its target residue. H4K16 deacetylation may thus be a probable mechanism by which the respective HAT Rtt109, gets effectively recruited for H3K56 acetylation. Earlier it has been reported that absence of H3/H4 N-terminal tails compromises Rtt109 mediated acetylation of H3K56, indicating that H3/H4 tails have a regulatory role in H3K56 acetylation.^{33,36} Further investigations are required in this direction to understand how exactly H4K16 deacetylation promotes H3K56 acetylation.

It is known that Hos2 mediated H4K16 deacetylation is targeted to active genes by the RNAPII Ser 5 CTD.^{58,59,81} Active transcription is therefore required for H4K16 deacetylation. In consonance we observed that inhibition of transcription with 1,10 phenanthroline^{71,72} causes H4K16 hyperacetylation at the cellular level further indicating that deacetylation of H4K16 is transcription dependent (Fig. 6). In trying to understand whether the H4K16 deacetylation mediated H3K56 acetylation event was also dependent on active transcription, we observed that H3K56 acetylation was conspicuously reduced upon transcription inhibition at the cellular level. H3K56 residue is present on the lateral surface of the histone octamer which is embedded in nucleosomal DNA and thus far has been reported to be acetylated primarily on free histones.³³ However, in consonance with Schneider et al.³⁴ we observed that Rtt109 promotes H3K56 acetylation within the nucleosome dense coding regions of actively transcribing genes, raising a possibility that Rtt109 may acetylate nucleosomal H3, as well. Moreover, upon transcription inhibition, Rtt109 recruitment within coding regions of constitutive genes decreased in a manner that strongly correlated with RNAPII dissociation (Fig. 6). This implied that Rtt109 function was closely associated with the active form of RNAPII. However, we could not observe any direct physical interaction between RNAPII and Rtt109 either due to lack of any such interaction or maybe such interaction could not be captured under our experimental conditions. Interestingly, recent studies have suggested that the localized chromatin disruptions caused by RNAPII promotes recruitment of HATs to gene bodies.⁷⁵ In fact, in mammals it has been shown that, disruption

of nucleosomes by nucleosome-destabilization factor (NDF) allows p300-CBP mediated H3K56 acetylation even on nucleosomal histones.⁸² A similar mechanism might be involved in recruitment of Rtt109 and consequent acetylation of H3K56 during transcription in a chromatinized template. Future investigations in this regard would help to shed more light on the underlying mechanisms. However, the strong correlation between Rtt109 and RNAPII occupancy on chromatin clearly suggest that transcriptional activity in the coding region promotes Rtt109 recruitment and effectively H3K56 acetylation in a manner that is essentially dependent on H4K16 deacetylation.

In summary, our findings reveal that H3K56 acetylation is crucial for RNAPII progression in the gene body of actively transcribing genes. Hos2-mediated H4K16 deacetylation is dependent on active transcription and essentially directs H3K56 acetylation. This becomes evident as constitutive presence of H3K56 acetylation can alleviate the need for Hos2-mediated H4K16 deacetylation during transcription. H4K16 deacetylation along with H3K56 acetylation together generate a “histone code” that facilitates RNAPII passage through the gene body and forms a crucial combination of histone modifications required for successful transcription in active loci.

MATERIALS AND METHODS

Yeast strains. The procedure for generation of yeast strains has been previously discussed in detail.^{18,19,83} Briefly, both copies of genomic histone H3-H4 were deleted from *S. cerevisiae* strain WY121 bearing plasmid pJL001 (*CEN URA3 HHT2-HHF2*) as the only source of histone H3-H4 and *URA3* as the counter-selectable marker. Plasmid pEMH7 (*CEN TRP1 HHT2-HHF2*) containing one copy of H3-H4 with counter-selectable marker *TRP1* was transformed into WY121 followed by growth in presence of 5-FoA (5'-Fluoroorotic acid) consequently leading to the loss of plasmid pJL001 and the subsequent generation of wild type strain. The plasmids pEMH33, pEMH35 bearing H4K16R and H41K6Q point mutations in *HHF2* gene and plasmids pEMH129, pEMH108 bearing H3K56R and H3K56Q point mutations in *HHT2* gene, respectively, were isolated from *Escherichia coli* and transformed similarly into WY121 yeast strain followed by plasmid shuffling to generate histone H4 and H3 mutant strains H4K16R, H4K16Q, H3K56R and H3K56Q, respectively. The transformed plasmids were isolated from yeast cells and sequenced to confirm the presence of the desired mutations.

For the generation of double mutants, plasmids pEMH33 and pEMH35 bearing H4K16R and H41K6Q point mutations in *HHF2* gene were subjected to site-directed mutagenesis⁸⁴ to generate point mutations H3K56R and H3K56Q in the *HHT2* gene of the respective plasmids. After sequencing confirmations, the plasmids bearing point mutations H4K16RH3K56Q, H4K16QH3K56Q, H4K16RH3K56R and H4K16QH3K56R, respectively were transformed into WY121 followed by plasmid shuffling in presence of 5-FoA to generate the respective double mutant strains. WY121 strain and pEMH plasmids were gifts from Dr John Wyrick (Washington State University, USA) and Prof. J.D. Boeke (Johns Hopkins University School of Medicine, USA), respectively. Δ Sas2 mutant was generated as previously discussed.¹⁹ For this study, *Hos2* Δ and *Hos2* Δ H3K56Q strains were generated similarly by the PCR-based homologous recombination-mediated gene deletion method.⁸⁵ Plasmid pFA6-KANMX4 was a gift from Prof. Shubho Chaudhuri (Bose Institute, Kolkata, India).

For C-terminal myc-tagging of *RTT109* in wild type, H4K16R and H4K16Q strains, PCR based homologous recombination method was employed.⁸⁵ A linear DNA cassette containing the KANMX6 module and flanking regions homologous to regions immediately upstream and downstream of the stop codon of *RTT109* gene was amplified from shuttle vector, pFA6A-13myc-KANMX6 and used to transform wild-type, H4K16R and H4K16Q strains, respectively and allowed to grow on G418 for selection of positive transformants. The tagging of wild-type and H4K16 mutants was confirmed by Western blot analysis. Plasmid pFA6A-13myc-KANMX6 was procured from Addgene (Addgene plasmid # 39294; <http://n2t.net/addgene:39294>; RRID: Addgene_39294)

Gene expression analysis. Yeast cells grown till mid-log phase with an O.D₆₀₀ of ~0.7 (~1 × 10⁷ cells/mL) were collected to isolate RNA. 50 mL cell pellets were flash-frozen in liquid N₂. To the frozen cell pellet TRIzol[®] reagent was added and allowed to defrost on ice. Cell pellets were resuspended in TRIzol[®] reagent and transferred to 1.5 mL tubes containing DEPC treated acid-washed glass beads. The cells were disrupted by vortexing with 1 min rest in between cycles. Lysed cells were centrifuged at full speed for 15 min at 4 °C to pellet debris. The supernatant was subjected to chloroform extraction and subsequent precipitation of RNA pellets with isopropanol. Pellets were washed with 75% ethanol, air-dried, and dissolved in RNase free water. 20 µg of RNA was subjected to DNase I treatment followed by TRIzol[®], chloroform extraction and isopropanol precipitation. Five micrograms of total RNA was used for reverse transcription using Revertaid RT (Thermo Scientific) as per manufacturer's instructions. An absolute quantification method was employed to obtain the copy number of transcripts for every gene in wild-type and mutants which is equivalent to the mRNA copy numbers.^{19,86} For this, as previously described¹⁹, a standard curve was prepared from serial dilutions of the cDNA ranging from 1/101 to 1/109 to serve as template for qPCR with primers for the six constitutive genes and the C_T values were used to plot a standard curve depicting C_T values on the Y-axis for the corresponding number of amplicons (ng) on the X-axis for each primer set. Subsequently, qPCR was performed with undiluted cDNA

samples and the C_T values of the expressed genes were plotted on the standard curves to calculate the actual number of transcripts expressed for each gene using the standard formula: (amount of dsDNA in ng * Avogadro No.)/(Base pair size of dsDNA) * (330*2*D. F). The dilution factor (DF) was 109 and the amount of dsDNA present in ng was estimated as values of "x" from the standard curve plot: $y = m \cdot \ln(x) + c$ considering the C_T values of the expressed genes as "y." Triplicate qPCRs were performed twice for each biological replicate ($n = 3$) of every strain. To denote statistical significance of the difference in gene expression levels between wild-type and mutant strains a two-tailed independent Student's t test was performed and the results with P value of < 0.05 were significant.

6-AU sensitivity assay. Ten-fold serial dilutions of exponentially grown yeast cells OD_{600} of 0.6 - 0.7 ($\sim 0.9 \times 10^7$ cells/mL) in yeast extract-peptone-dextrose (YPD) were spotted on SC medium with or without 100 μ g/mL 6-AU (Sigma-A1757) and incubated at 30 °C. The control plates without 6-AU were incubated at 30 °C for 2 days and the 100 μ g/mL 6-AU treated plates were incubated for 4 days at 30 °C.

Phenanthroline treatment. For phenanthroline treatment, mid-log phase yeast cells with an OD_{600} of ~ 0.7 ($\sim 1 \times 10^7$ cells/mL) were used, an untreated sample (0 min) was separated, the rest of the cells were divided into two equal halves, one-half of the cells were treated with 200 μ g/mL 1,10-phenanthroline (Sigma- P9375) dissolved in 100% ethanol and the other half of the cells were simultaneously treated with 100% ethanol without 1,10-phenanthroline. The samples that were only subjected to 100% ethanol were simultaneously incubated with phenanthroline treated samples at 30 °C for a period of 15, 30, and 60 min, respectively. The phenanthroline treated and untreated cells were used for Western blot analysis and chromatin immunoprecipitation assay.

Western blot analysis. Whole cell extracts were prepared as per the protocol previously described.¹⁹ Protein concentration was measured by Bradford assay and equal amounts of protein (10 μ g) from each sample were electrophoresed on a 16% SDS-PAGE and transferred onto a PVDF membrane. The membrane was blocked with 5% NFD in 1X TBS and incubated overnight at 4 °C with the following primary antibodies: antihistone H4 Acetyl K16 (Cell Signaling Technology – E2B8W), antihistone H3 acetyl K56 (Abcam – ab195478), and antihistone H3 (Biobharati, India, BB-AB0055). Following an incubation with appropriate horseradish peroxidase (HRP) – conjugated secondary antibody, membrane was incubated with a chemiluminescent substrate (SuperSignal® West Pico Chemiluminescent Substrate by Thermo Scientific) and visualized on an autoradiographic film.

Chromatin immunoprecipitation. The detailed protocol of chromatin immunoprecipitation assay has been previously described.^{18,19,83} Briefly, cells were collected in their mid-log phase OD_{600} of ~ 0.7 ($\sim 1 \times 10^7$ cells/mL) and formaldehyde cross-linked to capture protein-DNA complexes. The antibodies used for ChIP assay were as follows: antihistone H3 acetyl K56 (Abcam – ab195478), anti-RNA polymerase II [8WG16] (Abcam – ab817), anti-myc tag [9E10] (Abcam- ab32) and antihistone H3 (Biobharati, India, BB-AB0055). For each ChIP, qPCR analysis was done as previously described.^{18,19,83} Histone modification levels were calculated by the formula $2^{(C_{T(\text{Input})} - C_{T(\text{IP})})}$ and normalized by the levels of histone H3. H3K56ac levels were graphically represented as relative to a nontranscribing control region of *TELO8R*. RNA polymerase II and Rtt109-myc occupancy were calculated as a percentage of input (1%) after extrapolating the input to 100%. The assay was performed in triplicates for every biological replicate ($n = 3$). Statistical significance was calculated using a two-tailed independent Student's t test and the results with P value of < 0.05 were significant.

ACKNOWLEDGEMENTS

We thank Prof. J.D. Boeke (Johns Hopkins University School of Medicine, USA) for kind gift of the pEMH series of plasmids and acknowledge Prof. Michael J. Smerdon, Washington State University, USA for kind donation of the plasmids. We also thank Prof. John Wyrick (Washington State University, USA) for sharing the WY121 strain.

AUTHOR'S CONTRIBUTION

RNC and PK designed and conceptualized the experiments. PK and PS performed the experiments. PK and RNC analyzed the data and wrote the manuscript. The manuscript has been read and approved by all authors.

FUNDING

This work was supported by Science and Engineering Research Board (SERB), India (Scheme #CRG/2018/000461) to Dr Ronita Nag Chaudhuri, Department of Biotechnology, St Xavier's College, Kolkata; CSIR fellowship [# 08/548(0009)/2019-EMR-I] to Ms Preeti Khan and by Department of Biotechnology, India Grant No. BT/INF/22/SP41296/2020 to St Xavier's College, Kolkata.

DATA AVAILABILITY STATEMENT

All strains, plasmids and reagents used in this study are available upon request. The authors confirm that all data supporting the findings of this study are available within

the main article or in the [supplementary material](#) and can also be found at figshare doi:10.6084/m9.figshare.23931501.

DISCLOSURE STATEMENT

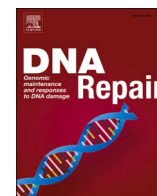
No potential conflict of interest was reported by the authors.

REFERENCES

- Kulaeva OI, Hsieh F-K, Chang H-W, Luse DS, Studitsky VM. Mechanism of transcription through a nucleosome by RNA polymerase II. *Biochim Biophys Acta*. 2013;1829:76–83. doi:10.1016/j.bbagr.2012.08.015.
- Arimura Y, Tachiwana H, Oda T, Sato M, Kurumizaka H. Structural analysis of the hexasome, lacking one histone H2A/H2B dimer from the conventional nucleosome. *Biochemistry*. 2012;51:3302–3309. doi:10.1021/bi300129b.
- Kireeva ML, Walter W, Tchernajenko V, Bondarenko V, Kashlev M, Studitsky VM. Nucleosome remodeling induced by RNA polymerase II: loss of the H2A/H2B dimer during transcription. *Mol Cell*. 2002;9:541–552. doi:10.1016/s1097-2765(02)00472-0.
- Gaykalova DA, Kulaeva OI, Volokh O, Shaytan AK, Hsieh F-K, Kirpichnikov MP, Sokolova OS, Studitsky VM. Structural analysis of nucleosomal barrier to transcription. *Proc Natl Acad Sci USA*. 2015;112:E5787–95. doi:10.1073/pnas.1508371112.
- Bintu L, Kopaczynska M, Hodges C, Lubkowska L, Kashlev M, Bustamante C. The elongation rate of RNA polymerase determines the fate of transcribed nucleosomes. *Nat Struct Mol Biol*. 2011;18:1394–1399. doi:10.1038/nsmb.2164.
- Kujirai T, Ehara H, Fujino Y, Shirouzu M, Sekine SI, Kurumizaka H. Structural basis of the nucleosome transition during RNA polymerase II passage. *Science*. 2018;362:595–598. doi:10.1126/science.aau9904.
- Bannister AJ, Kouzarides T. Regulation of chromatin by histone modifications. *Cell Res*. 2011;21:381–395. doi:10.1038/cr.2011.22.
- Bowman GD, Poirier MG. Post-translational modifications of histones that influence nucleosome dynamics. *Chem Rev*. 2015;115:2274–2295. doi:10.1021/cr500350x.
- Verdin E, Ott M. 50 years of protein acetylation: from gene regulation to epigenetics, metabolism and beyond. *Nat Rev Mol Cell Biol*. 2015;16:258–264. doi:10.1038/nrm3931.
- Zhang R, Erler J, Langowski J. Histone acetylation regulates chromatin accessibility: role of H4K16 in Inter-nucleosome Interaction. *Biophys J*. 2017;112:450–459. doi:10.1016/j.bpj.2016.11.015.
- Shogren-Knaak M, Ishii H, Sun JM, Pazin MJ, Davie JR, Peterson CL. Histone H4-K16 acetylation controls chromatin structure and protein interactions. *Science*. 2006;311:844–847. doi:10.1126/science.1124000.
- Shogren-Knaak M, Peterson CL. Switching on chromatin: mechanistic role of histone H4-K16 acetylation. *Cell Cycle*. 2006;5:1361–1365. doi:10.4161/cc.5.13.2891.
- Robinson PJJ, An W, Routh A, Martino F, Chapman L, Roeder RG, Rhodes D. 30 nm chromatin fibre decompaction requires both H4-K16 acetylation and linker histone eviction. *J Mol Biol*. 2008;381:816–825. doi:10.1016/j.jmb.2008.04.050.
- Oppikofer M, Kueng S, Martino F, Soeroes S, Hancock SM, Chin JW, Fischle W, Gasser SM. A dual role of H4K16 acetylation in the establishment of yeast silent chromatin. *Embo J*. 2011;30:2610–2621. doi:10.1038/emboj.2011.170.
- Reiter C, Heise F, Chung HR, Ehrenhofer-Murray AE. A link between Sas2-mediated H4 K16 acetylation, chromatin assembly in S-phase by CAF-I and Asf1, and nucleosome assembly by Spt6 during transcription. *FEMS Yeast Res*. 2015;15:fov073. doi:10.1093/femsyr/fov073.
- Suka N, Luo K, Grunstein M. Sir2p and Sas2p oppositely regulate acetylation of yeast histone H4 lysine16 and spreading of heterochromatin. *Nat Genet*. 2002;32:378–383. doi:10.1038/ng1017.
- Kayne PS, Kim UJ, Han M, Mullen JR, Yoshizaki F, Grunstein M. Extremely conserved histone H4 N terminus is dispensable for growth but essential for repressing the silent mating loci in yeast. *Cell*. 1988;55:27–39. doi:10.1016/0092-8674(88)90006-2.
- Ray A, Khan P, Nag Chaudhuri R. Regulated acetylation and deacetylation of H4 K16 is essential for efficient NER in *Saccharomyces cerevisiae*. *DNA Repair (Amst)*. 2018;72:39–55. doi:10.1016/j.dnarep.2018.09.009.
- Ray A, Khan P, Nag Chaudhuri R. Deacetylation of H4 lysine16 affects acetylation of lysine residues in histone H3 and H4 and promotes transcription of constitutive genes. *Epigenetics*. 2021;16:597–617. doi:10.1080/15592294.2020.1809896.
- Chen Y-JC, Koutelou E, Dent SYR. Now open: evolving insights to the roles of lysine acetylation in chromatin organization and function. *Mol Cell*. 2022;82:716–727. doi:10.1016/j.molcel.2021.12.004.
- Gates LA, Shi J, Rohira AD, Feng Q, Zhu B, Bedford MT, Sagum CA, Jung SY, Qin J, Tsai M-J, et al. Acetylation on histone H3 lysine 9 mediates a switch from transcription initiation to elongation. *J Biol Chem*. 2017;292:14456–14472. doi:10.1074/jbc.M117.802074.
- Jain N, Tamborini D, Evans B, Chaudhry S, Wilkins BJ, Neumann H. Interaction of RSC chromatin remodeling complex with nucleosomes is modulated by H3 K14 acetylation and H2B SUMOylation in vivo. *iScience*. 2020;23:101292. doi:10.1016/j.isci.2020.101292.
- Chen G, Li W, Yan F, Wang D, Chen Y. The structural basis for specific recognition of H3K14 acetylation by Sth1 in the RSC chromatin remodeling complex. *Structure*. 2020;28:111–118.e3. doi:10.1016/j.str.2019.10.015.
- Taverna SD, Li H, Ruthenburg AJ, Allis CD, Patel DJ. How chromatin-binding modules interpret histone modifications: lessons from professional pocket pickers. *Nat Struct Mol Biol*. 2007;14:1025–1040. doi:10.1038/nsmb1338.
- Cosgrove MS, Boeke JD, Wolberger C. Regulated nucleosome mobility and the histone code. *Nat Struct Mol Biol*. 2004;11:1037–1043. doi:10.1038/nsmb851.
- Fenley AT, Anandakrishnan R, Kidane YH, Onufriev AV. Modulation of nucleosomal DNA accessibility via charge-altering post-translational modifications in histone core. *Epigenetics Chromatin*. 2018;11:11. doi:10.1186/s13072-018-0181-5.
- Tessarz P, Kouzarides T. Histone core modifications regulating nucleosome structure and dynamics. *Nat Rev Mol Cell Biol*. 2014;15:703–708. doi:10.1038/nrm3890.
- Ozdemir A, Spicuglia S, Lasonder E, Vermeulen M, Campsteijn C, Stunnenberg HG, Logie C. Characterization of lysine 56 of histone H3 as an acetylation site in *Saccharomyces cerevisiae*. *J Biol Chem*. 2005;280:25949–25952. doi:10.1074/jbc.C500181200.
- Hyland EM, Cosgrove MS, Molina H, Wang D, Pandey A, Cottee RJ, Boeke JD. Insights into the role of histone H3 and histone H4 core modifiable residues in *Saccharomyces cerevisiae*. *Mol Cell Biol*. 2005;25:10060–10070. doi:10.1128/MCB.25.22.10060-10070.2005.
- Masumoto H, Hawke D, Kobayashi R, Verreault A. A role for cell-cycle-regulated histone H3 lysine 56 acetylation in the DNA damage response. *Nature*. 2005;436:294–298. doi:10.1038/nature03714.
- Tsubota T, Berndsen CE, Erkmann JA, Smith CL, Yang L, Freitas MA, Denu JM, Kaufman PD. Histone H3-K56 acetylation is catalyzed by histone chaperone-dependent complexes. *Mol Cell*. 2007;25:703–712. doi:10.1016/j.molcel.2007.02.006.
- Simon M, North JA, Shimko JC, Forties RA, Ferdinand MB, Manohar M, Zhang M, Fishel R, Ottesen JJ, Poirier MG, et al. Histone fold modifications control nucleosome unwrapping and disassembly. *Proc Natl Acad Sci USA*. 2011;108:12711–12716. doi:10.1073/pnas.1106264108.
- Han J, Zhou H, Li Z, Xu R-M, Zhang Z. The Rtt109-Vps75 histone acetyltransferase complex acetylates non-nucleosomal histone H3*. *J Biol Chem*. 2007;282:14158–14164. doi:10.1074/jbc.M700611200.
- Schneider J, Bajwa P, Johnson FC, Bhaumik SR, Shilatifard A. Rtt109 is required for proper H3K56 acetylation: a chromatin mark associated with the elongating RNA polymerase II. *J Biol Chem*. 2006;281:37270–37274. doi:10.1074/jbc.C600265200.
- Rufiange A, Jacques PE, Bhat W, Robert F, Nourani A. Genome-wide replication-independent histone H3 exchange occurs predominantly at promoters and implicates H3 K56 acetylation and Asf1. *Mol Cell*. 2007;27:393–405. doi:10.1016/j.molcel.2007.07.011.

36. Zhang L, Serra-Cardona A, Zhou H, Wang M, Yang N, Zhang Z, Xu R-M. Multisite substrate recognition in Asf1-dependent acetylation of histone H3 K56 by Rtt109. *Cell*. 2018;174:818–830.e11. doi:10.1016/j.cell.2018.07.005.
37. Fillingham J, Recht J, Silva AC, Suter B, Emili A, Stagljar I, Krogan NJ, Allis CD, Keogh M-C, Greenblatt JF, et al. Chaperone control of the activity and specificity of the histone H3 acetyltransferase Rtt109. *Mol Cell Biol*. 2008;28:4342–4353. doi:10.1128/MCB.00182-08.
38. Kaplan T, Liu CL, Erkmann JA, Holik J, Grunstein M, Kaufman PD, Friedman N, Rando OJ. Cell cycle- and chaperone-mediated regulation of H3K56ac incorporation in yeast. *PLoS Genet*. 2008;4:e1000270. doi:10.1371/journal.pgen.1000270.
39. Williams SK, Truong D, Tyler JK. Acetylation in the globular core of histone H3 on lysine-56 promotes chromatin disassembly during transcriptional activation. *Proc Natl Acad Sci U S A*. 2008;105:9000–9005. doi:10.1073/pnas.0800057105.
40. Weiner A, Hsieh T-HS, Appleboim A, Chen HV, Rahat A, Amit I, Rando OJ, Friedman N. High-resolution chromatin dynamics during a yeast stress response. *Mol Cell*. 2015;58:371–386. doi:10.1016/j.molcel.2015.02.002.
41. Topal S, Vasseur P, Radman-Livaja M, Peterson CL. Distinct transcriptional roles for histone H3-K56 acetylation during the cell cycle in yeast. *Nat Commun*. 2019;10:4372. doi:10.1038/s41467-019-12400-5.
42. Xu F, Zhang K, Grunstein M. Acetylation in histone H3 globular domain regulates gene expression in yeast. *Cell*. 2005;121:375–385. doi:10.1016/j.cell.2005.03.011.
43. Watanabe S, Resch M, Lilyestrom W, Clark N, Hansen JC, Peterson C, Luger K. Structural characterization of H3K56Q nucleosomes and nucleosomal arrays. *Biochim Biophys Acta*. 2010;1799:480–486. doi:10.1016/j.bbagr.2010.01.009.
44. Lee J, Lee T-H. How protein binding sensitizes the nucleosome to histone H3K56 acetylation. *ACS Chem Biol*. 2019;14:506–515. doi:10.1021/acscchembio.9b00018.
45. Värvi S, Kristjuhan K, Peil K, Lööke M, Mahlaköiv T, Paapsi K, Kristjuhan A. Acetylation of H3 K56 is required for RNA polymerase II transcript elongation through heterochromatin in yeast. *Mol Cell Biol*. 2010;30:1467–1477. doi:10.1128/MCB.01151-09.
46. McCullough LL, Pham TH, Parnell TJ, Connell Z, Chandrasekharan MB, Stillman DJ, Formosa T. Establishment and maintenance of chromatin architecture are promoted independently of transcription by the histone chaperone FACT and H3-K56 acetylation in *Saccharomyces cerevisiae*. *Genetics*. 2019;211:877–892. doi:10.1534/genetics.118.301853.
47. Durairaj G, Chaurasia P, Lahudkar S, Malik S, Shukla A, Bhaumik SR. Regulation of chromatin assembly/disassembly by Rtt109p, a histone H3 Lys56-specific acetyltransferase, in vivo. *J Biol Chem*. 2010;285:30472–30479. doi:10.1074/jbc.M110.113225.
48. Huynh MT, Yadav SP, Reese JC, Lee T-H. Nucleosome dynamics during transcription elongation. *ACS Chem Biol*. 2020;15:3133–3142. doi:10.1021/acscchembio.0c00617.
49. Etchegaray J-P, Zhong L, Li C, Henriques T, Ablondi E, Nakadai T, Van Rechem C, Ferrer C, Ross KN, Choi J-E, et al. The histone deacetylase SIRT6 restrains transcription elongation via promoter-proximal pausing. *Mol Cell*. 2019;75:683–699.e7. doi:10.1016/j.molcel.2019.06.034.
50. Lee JS, Smith E, Shilatifard A. The language of histone crosstalk. *Cell*. 2010;142:682–685. doi:10.1016/j.cell.2010.08.011.
51. Zhang T, Cooper S, Brockdorff N. The interplay of histone modifications - writers that read. *EMBO Rep*. 2015;16:1467–1481. doi:10.15252/embr.201540945.
52. Worden EJ, Zhang X, Wolberger C. Structural basis for COMPASS recognition of an H2B-ubiquitinated nucleosome. *Elife*. 2020;9:e53199. doi:10.7554/eLife.53199.
53. Bae HJ, Dubarry M, Jeon J, Soares LM, Dargemont C, Kim J, Geli V, Buratowski S. The Set1 N-terminal domain and Swd2 interact with RNA polymerase II CTD to recruit COMPASS. *Nat Commun*. 2020;11:2181. doi:10.1038/s41467-020-16082-2.
54. Bian C, Xu C, Ruan J, Lee KK, Burke TL, Tempel W, Barsyte D, Li J, Wu M, Zhou BO, et al. Sgf29 binds histone H3K4me2/3 and is required for SAGA complex recruitment and histone H3 acetylation. *Embo J*. 2011;30:2829–2842. doi:10.1038/emboj.2011.193.
55. Vermeulen M, Eberl HC, Matarese F, Marks H, Denissov S, Butter F, Lee KK, Olsen JV, Hyman AA, Stunnenberg HG, et al. Quantitative interaction proteomics and genome-wide profiling of epigenetic histone marks and their readers. *Cell*. 2010;142:967–980. doi:10.1016/j.cell.2010.08.020.
56. Zhao W, Xu Y, Wang Y, Gao D, King J, Xu Y, Liang F-S. Investigating cross-talk between H3K27 acetylation and H3K4 trimethylation in CRISPR/dCas-based epigenome editing and gene activation. *Sci Rep*. 2021;11:15912. doi:10.1038/s41598-021-95398-5.
57. Jung I, Seo J, Lee H-S, Stanton LW, Kim D, Choi JK. Global mapping of the regulatory interactions of histone residues. *FEBS Lett*. 2015;589:4061–4070. doi:10.1016/j.febslet.2015.11.016.
58. Govind CK, Qiu H, Ginsburg DS, Ruan C, Hofmeyer K, Hu C, Swaminathan V, Workman JL, Li B, Hinnebusch AG, et al. Phosphorylated Pol II CTD recruits multiple HDACs, including Rpd3C(S), for methylation-dependent deacetylation of ORF nucleosomes. *Mol Cell*. 2010;39:234–246. doi:10.1016/j.molcel.2010.07.003.
59. Kim T, Buratowski S. Dimethylation of H3K4 by Set1 recruits the Set3 histone deacetylase complex to 5' transcribed regions. *Cell*. 2009;137:259–272. doi:10.1016/j.cell.2009.02.045.
60. Xiao T, Kao C-F, Krogan NJ, Sun Z-W, Greenblatt JF, Osley MA, Strahl BD. Histone H2B ubiquitylation is associated with elongating RNA polymerase II. *Mol Cell Biol*. 2005;25:637–651. doi:10.1128/MCB.25.2.637-651.2005.
61. Krogan NJ, Dover J, Wood A, Schneider J, Heidt J, Boateng MA, Dean K, Ryan OW, Golshani A, Johnston M, et al. The Paf1 complex is required for histone H3 methylation by COMPASS and Dot1p: linking transcriptional elongation to histone methylation. *Mol Cell*. 2003;11:721–729. doi:10.1016/s1097-2765(03)00091-1.
62. Youdell ML, Kizer KO, Kisseleva-Romanova E, Fuchs SM, Duro E, Strahl BD, Mellor J. Roles for Ctk1 and Spt6 in regulating the different methylation states of histone H3 lysine 36. *Mol Cell Biol*. 2008;28:4915–4926. doi:10.1128/MCB.00001-08.
63. Govind CK, Zhang F, Qiu H, Hofmeyer K, Hinnebusch AG. Gcn5 promotes acetylation, eviction, and methylation of nucleosomes in transcribed coding regions. *Mol Cell*. 2007;25:31–42. doi:10.1016/j.molcel.2006.11.020.
64. Pinto D, Pagé V, Fisher RP, Tanny JC. New connections between ubiquitylation and methylation in the co-transcriptional histone modification network. *Curr Genet*. 2021;67:695–705. doi:10.1007/s00294-021-01196-x.
65. Fuchs G, Hollander D, Voicheck Y, Ast G, Oren M. Cotranscriptional histone H2B monoubiquitylation is tightly coupled with RNA polymerase II elongation rate. *Genome Res*. 2014;24:1572–1583. doi:10.1101/gr.176487.114.
66. Heise F, Chung H-R, Weber JM, Xu Z, Klein-Hitpass L, Steinmetz LM, Vingron M, Ehrenhofer-Murray AE. Genome-wide H4 K16 acetylation by SAS-I is deposited independently of transcription and histone exchange. *Nucleic Acids Res*. 2012;40:65–74. doi:10.1093/nar/gkr649.
67. Kimura A, Umehara T, Horikoshi M. Chromosomal gradient of histone acetylation established by Sas2p and Sir2p functions as a shield against gene silencing. *Nat Genet*. 2002;32:370–377. doi:10.1038/ng993.
68. Wang A, Kurdistan SK, Grunstein M. Requirement of Hos2 histone deacetylase for gene activity in yeast. *Science*. 2002;298:1412–1414. doi:10.1126/science.1077790.
69. Collins SR, Miller KM, Maas NL, Roguev A, Fillingham J, Chu CS, Schuldiner M, Gebbia M, Recht J, Shales M, et al. Functional dissection of protein complexes involved in yeast chromosome biology using a genetic interaction map. *Nature*. 2007;446:806–810. doi:10.1038/nature05649.
70. Han J, Zhou H, Horazdovsky B, Zhang K, Xu RM, Zhang Z. Rtt109 acetylates histone H3 lysine 56 and functions in DNA replication. *Science*. 2007;315:653–655. doi:10.1126/science.1133234.
71. Poramba-Liyanage DW, Korthout T, Cucinotta CE, van Kruisbergen I, van Welsem T, El Atmioui D, Ovaa H, Tsukiyama T, van Leeuwen F. Inhibition of transcription leads to rewiring of locus-specific chromatin proteomes. *Genome Res*. 2020;30:635–646. doi:10.1101/gr.256255.119.
72. Grigull J, Mnaimneh S, Pootoolal J, Robinson MD, Hughes TR. Genome-wide analysis of mRNA stability using transcription inhibitors and microarrays reveals posttranscriptional control of ribosome biogenesis factors. *Mol Cell Biol*. 2004;24:5534–5547. doi:10.1128/MCB.24.12.5534-5547.2004.
73. Martin BJE, Chruscicki AT, Howe LJ. Transcription promotes the interaction of the Facilitates Chromatin Transactions (FACT) complex with nucleosomes in *Saccharomyces cerevisiae*. *Genetics*. 2018;210:869–881. doi:10.1534/genetics.118.301349.
74. Johnston GC, Singer RA. RNA synthesis and control of cell division in the yeast *S. cerevisiae*. *Cell*. 1978;14:951–958. doi:10.1016/0092-8674(78)90349-5.
75. Martin BJE, Brind'Amour J, Kuzmin A, Jensen KN, Liu ZC, Lorincz M, Howe LJ. Transcription shapes genome-wide histone acetylation patterns. *Nat Commun*. 2021;12:210. doi:10.1038/s41467-020-20543-z.

76. Kurdistan SK, Tavazoie S, Grunstein M. Mapping global histone acetylation patterns to gene expression. *Cell*. 2004;117:721–733. doi:[10.1016/j.cell.2004.05.023](https://doi.org/10.1016/j.cell.2004.05.023).
77. Bell O, Wirbelauer C, Hild M, Scharf AND, Schwaiger M, MacAlpine DM, Zilbermann F, van Leeuwen F, Bell SP, Imhof A, et al. Localized H3K36 methylation states define histone H4K16 acetylation during transcriptional elongation in *Drosophila*. *Embo J*. 2007;26:4974–4984. doi:[10.1038/sj.emboj.7601926](https://doi.org/10.1038/sj.emboj.7601926).
78. Cai Q, Tong SM, Shao W, Ying SH, Feng MG. Pleiotropic effects of the histone deacetylase Hos2 linked to H4-K16 deacetylation, H3-K56 acetylation, and H2A-S129 phosphorylation in *Beauveria bassiana*. *Cell Microbiol*. 2018;20:e12839. doi:[10.1111/cmi.12839](https://doi.org/10.1111/cmi.12839).
79. Owen DJ, Ornaghi P, Yang JC, Lowe N, Evans PR, Ballario P, Neuhaus D, Filetici P, Travers AA. The structural basis for the recognition of acetylated histone H4 by the bromodomain of histone acetyltransferase gcn5p. *Embo J*. 2000;19:6141–6149. doi:[10.1093/emboj/19.22.6141](https://doi.org/10.1093/emboj/19.22.6141).
80. Hassan AH, Awad S, Al-Natour Z, Othman S, Mustafa F, Rizvi TA. Selective recognition of acetylated histones by bromodomains in transcriptional co-activators. *Biochem J*. 2007;402:125–133. doi:[10.1042/BJ20060907](https://doi.org/10.1042/BJ20060907).
81. Ng HH, Robert F, Young RA, Struhl K. Targeted recruitment of Set1 histone methylase by elongating Pol II provides a localized mark and memory of recent transcriptional activity. *Mol Cell*. 2003;11:709–719. doi:[10.1016/S1097-2765\(03\)00092-3](https://doi.org/10.1016/S1097-2765(03)00092-3).
82. Fei J, Ishii H, Hoeksema MA, Meitinger F, Kassavetis GA, Glass CK, Ren B, Kadonaga JT. NDF, a nucleosome-destabilizing factor that facilitates transcription through nucleosomes. *Genes Dev*. 2018;32:682–694. doi:[10.1101/gad.313973.118](https://doi.org/10.1101/gad.313973.118).
83. Khan P, Chaudhuri RN. Acetylation of H3K56 orchestrates UV-responsive chromatin events that generate DNA accessibility during Nucleotide Excision Repair. *DNA Repair (Amst)*. 2022;113:103317. doi:[10.1016/j.dnarep.2022.103317](https://doi.org/10.1016/j.dnarep.2022.103317).
84. Zheng L, Baumann U, Reymond J-L. An efficient one-step site-directed and site-saturation mutagenesis protocol. *Nucleic Acids Res*. 2004;32:e115–e115. doi:[10.1093/nar/gnh110](https://doi.org/10.1093/nar/gnh110).
85. Gardner JM, Jaspersen SL. Manipulating the yeast genome: deletion, mutation, and tagging by PCR. In Smith JS, Burke DJ, editors. *Methods in molecular biology*. Vol. 1205. USA: Springer; 2014. p. 45–78.
86. Dhanasekaran S, Doherty TM, Kenneth J. Comparison of different standards for real-time PCR-based absolute quantification. *J Immunol Methods*. 2010;354:34–39. doi:[10.1016/j.jim.2010.01.004](https://doi.org/10.1016/j.jim.2010.01.004).



Acetylation of H3K56 orchestrates UV-responsive chromatin events that generate DNA accessibility during Nucleotide Excision Repair

Preeti Khan, Ronita Nag Chaudhuri^{*}

Department of Biotechnology, St. Xavier's College, 30, Mother Teresa Sarani, Kolkata 700016, India

ARTICLE INFO

Keywords:

DNA damage
H3K56
Histone acetylation
Chromatin modification
Chromatin regulation
Nucleotide excision repair
Rad16

ABSTRACT

Histone modifications have long been related to DNA damage response. Nucleotide excision repair pathway that removes helix-distorting lesions necessitates DNA accessibility through chromatin modifications. Previous studies have linked H3 tail residue acetylation to UV-induced NER. Here we present evidences that acetylation of H3K56 is crucial for early phases of NER. Using H3K56 mutants K56Q and K56R, which mimic acetylated and unacetylated lysines respectively, we show that recruitment of the repair factor Rad16, a Swi/Snf family member is dependent on H3K56 acetylation. With constitutive H3K56 acetylation, Rad16 recruitment became UV-independent. Furthermore, H3K56 acetylation promoted UV-induced hyperacetylation of H3K9 and H3K14. Importantly, constitutive H3K56 acetylation prominently increased chromatin accessibility. During NER, lack of H3K56 acetylation that effectively aborted H3 tail residue acetylation and Rad16 recruitment, thus failed to impart essential chromatin modulations. The NER-responsive oscillation of chromatin structure observed in wild type, was distinctly eliminated in absence of H3K56 acetylation. *In vitro* assay with wild type and H3K56 mutant cell extracts further indicated that absence of H3K56 acetylation negatively affected DNA relaxation during NER. Overall, H3K56 acetylation regulates Rad16 redistribution and UV-induced H3 tail residue hyperacetylation, and the resultant modification code promotes chromatin accessibility and recruitment of subsequent repair factors during NER.

1. Introduction

In eukaryotic cells, the packaging of DNA into chromatin is crucial for maintenance of structural and functional fidelity of the genome. However, such wrapping up of DNA into “nucleosomes” makes the resultant chromatin architecture non-permissive to DNA dependent functions [1]. It poses a barrier for the nuclear machinery towards DNA accessibility during cellular metabolic processes such as replication, transcription and DNA repair [2–6]. Genomic stability and cellular integrity get continually challenged by several endogenous as well as exogenous agents that induce DNA damage. UV radiation is one such damaging agent that generates helix distorting lesions that can impair nuclear functions [7]. Consequently, intricate regulation of the chromatin architecture is of utmost importance in response to UV-induced DNA damage in order to maintain genomic stability and promote cell survivability. Nucleotide Excision Repair in eukaryotes involves large multi-protein complexes that participate in recognition, incision and excision of bulky UV-induced lesions such as cyclobutane-pyrimidine dimers (CPDs) and 6, 4-photoproducts. In placental mammals, failure

to activate the NER pathway leads to genetic disorders such as xeroderma pigmentosum, Cockayne syndrome and trichothiodystrophy that can make an organism susceptible to skin cancers and developmental defects [8]. According to the “Access-Repair-Restore” model a DNA repair pathway like NER, essentially involves the three basic steps: manipulation of the chromatin architecture to facilitate access to the damage site, removal of the damage and finally restoration of chromatin to pre-damaged state [9–12]. During NER, accessibility of the repair machinery to the site of damage requires almost a 100 bp of nucleosome free DNA [13]. Hence, in response to UV-mediated DNA damage, dynamic restructuring of chromatin is critical to generate a more conducive platform for accessibility of repair factors, which are otherwise occluded by nucleosomes [4,14].

Nucleotide Excision Repair can be carried out via two sub-pathways: Transcription-Coupled NER (TC-NER) and Global genome NER (GG-NER). While TC-NER participates in removal of damages incurred in the actively transcribing regions, GG-NER works primarily in the non-transcribing strand of active regions, in transcriptionally repressed as well as silent regions of the genome [15–17]. Removal of damage by the

^{*} Corresponding author.

E-mail address: ronita.nc@sxccal.edu (R.N. Chaudhuri).

<https://doi.org/10.1016/j.dnarep.2022.103317>

Received 14 November 2021; Received in revised form 25 February 2022; Accepted 7 March 2022

Available online 9 March 2022

1568-7864/© 2022 Elsevier B.V. All rights reserved.

GG-NER pathway is dependent on a protein complex consisting of Rad7/16 and Abf1 [18–20]. Genome wide removal of UV-damage by the GG-NER pathway is found to be defective in cells lacking Rad7 and Rad16 proteins [16–18,21]. Rad16 is a member of the SWI/SNF superfamily of ATPases [22] and participates in damage recognition via GG-NER pathway [21]. With the help of its inherent ATPase activity the Rad7/16 complex spans the genome and stalls upon encountering UV damage thereby enabling the recruitment of downstream NER factors [21]. Recently it has been shown that in absence of UV induced damage the GG-NER complex remains locked at specific sites within the genome by barrier nucleosomes and a UV responsive chromatin remodelling event leads to the redistribution of the Rad7/16 complex to the sites of damage [23,24]. The complex has also been linked to post-damage recognition stages in NER, wherein the super-helical torsion generated in the DNA primarily by Rad16 helps in efficient damage removal [25, 26]. Removal of damage by the GG-NER pathway is slower compared to TC-NER and primarily influenced by the architecture of the chromatin with more accessible regions of the genome being repaired preferentially faster than others [27]. Interestingly, Rad16 promotes chromatin remodelling facilitating recruitment of HATs that induce histone hyper-acetylation, leading to chromatin accessibility and thus paving the pathway for efficient damage removal [28,29].

Regulated chromatin accessibility during any metabolic event is aided by the interplay of histone post-translational modifications, histone variants, chromatin remodellers and histone chaperones. Amongst these, histone post-translational modifications (PTMs), particularly acetylation plays a pivotal role in modulating chromatin architecture in a most pervasive manner. Acetylation of histones lysine residues through neutralization of the positive charge can influence intra-nucleosomal histone-histone and histone-DNA interactions, inter-nucleosomal interactions as well as can regulate the recruitment of chromatin modifiers [30–35]. Structurally histones possess two distinct domains: the tails and the globular core domain. Histone tails are highly dynamic and accessible making them the most prominent hub for post-translational modifications. Previous studies have shown hyper-acetylation of histone H3 tail residues K9 and K14 during NER in yeast [29,36]. Earlier we have reported that acetylation of H4 N-terminal tail residue K16 regulates acetylation of other H4 and H3 N-terminal tail residues essential for efficient NER and gene transcription [37,38]. However, post-translational modifications of histones not only occur in the tails but also in residues within the core domain. While PTMs in the N-terminal tails regulate chromatin structure mainly by aiding binding of non-histone proteins to chromatin, globular core residues depending on their location, function through specific mechanisms that involve transformation of the nucleosome structure. The histone code generated by a combination of both tail and core residue modifications orchestrates chromatin structural and functional regulation during any DNA metabolic process [31,39]. An acetylatable residue within histone H3 core is K56 [40]. H3 K56 is distinct in its location being placed at a region where the nucleosomal DNA enters or leaves the histone core octamer. Acetylation status of H3 K56 is thus thought to critically influence the DNA wrapping/unwrapping dynamics [41–44]. In *Saccharomyces cerevisiae*, H3 K56 acetylation is known to be regulated by the HAT Rtt109 in complex with histone chaperones Asf1 or Vps75, that confers Rtt109 its substrate specificity [45–54]. In yeast, acetylation of H3 K56 has been implicated in replication, transcription, DNA damage repair and telomeric silencing [45–47,51,55–61]. Both overexpression of H3 K56 acetylation or a failure to acetylate H3K56 during replication renders cells sensitive to genotoxic agents indicating the need for regulated acetylation-deacetylation of H3K56 for proper chromatin functions [58, 62–65]. With this backdrop, it is relevant to say that despite insightful works on H3K56 acetylation and deacetylation during various DNA metabolic events, the exact role of H3 K56 acetylation during NER still remains elusive. Here we show that H3K56 acetylation in *Saccharomyces cerevisiae* is essential for regulating UV-induced H3 N-terminal tail acetylation, which promotes efficient NER. It was evident that lack of

H3K56 acetylation impairs chromatin flexibility and accessibility during NER. H3K56 acetylation occurs at a very early NER phase and triggers further histone modifications, recruitment of Rad16 factor, generates a chromatin landscape conducive for subsequent NER machinery recruitment, consequently allowing proficient removal of UV-induced DNA damage.

2. Results

2.1. Acetylation of histone H3K56 is required for NER in yeast

Despite previous studies indicating a relation of H3K56 acetylation to DNA damage response [58,60,66,67], specific role of H3K56 acetylation during NER has not been established yet. In trying to understand how H3K56 acetylation influences repair of UV-induced DNA damage, specifically through NER pathway, we generated two H3K56 mutants-H3K56R, that mimic constitutively deacetylated state of H3K56 residue and H3K56Q, that mimic constitutively acetylated state of the residue. For UV sensitivity assay the H3K56 mutant cells were irradiated with different doses of UV and cell survivability was assessed in comparison to wild type. Our results indicated that lack of H3K56 acetylation (H3K56R) leads to increased UV sensitivity, especially distinct at UV irradiations of 100 J/m² and 150 J/m² respectively, compared to wild type and H3K56Q cells (Fig. 1A & B). To further substantiate this observation, NER efficiency in wild type and the H3K56 mutants were checked after UV treatment. For this, the yeast strains were subjected to UV irradiation at 100 J/m² and repair incubated for various time periods. T4 endonuclease V assay followed by alkaline gel electrophoresis of genomic DNA was done to measure cyclobutane pyrimidine dimers (CPDs) and the rate of CPD removal was thereafter calculated, as indicated in the Materials and Methods section. It was evident from our results that, in H3K56R cells lacking K56 acetylation, rate of CPD removal were significantly reduced compared to wild type (Fig. 1C & D). Presence of constitutive acetylation of H3K56 (H3K56Q) on the other hand, made CPD removal in H3K56Q mutants as proficient as wild type cells with a moderately higher rate of CPD removal in the early NER phases (Fig. 1C & D).

As lack of H3K56 acetylation impeded NER functionality, hereafter checking H3K56 acetylation status during NER seemed imperative. H3K56 acetylation was tested in the two transcriptionally silent regions of *HML* and telomere, in the transcriptionally repressed *GAL10* and active *RPB2* loci, respectively, through ChIP assay using antibody specific to H3K56ac. Our results indicated that the residue undergoes significant levels of UV-induced hyperacetylation very early during NER (Fig. 2). Such UV-induced increased levels of H3K56 acetylation were maintained at least during first 60 min of NER. This observation underlines the fact that H3K56 acetylation is a requisite during the NER pathway and explains why H3K56R mutants that lacked such acetylation showed impaired rate of NER.

2.2. Recruitment of Rad16 during NER requires H3K56 acetylation

The Swi/Snf family member Rad16 is a crucial NER protein, which along with Rad7 is required at least for the excision step of the repair process [25,26]. It has been further implicated that histone H3 acetylation during NER is dependent on Rad16 and Rad7 [29]. Through ChIP assay using anti-Rad16 antibody, we observed that recruitment of Rad16 during NER is dependent on H3K56 acetylation (Fig. 3). Rad16 recruitment was checked in all the four loci mentioned above. Interestingly, our observations indicated that in all the loci tested, H3K56Q mutants have significantly higher levels of Rad16 recruitment with or without UV treatment, compared to wild type. As previously reported, while in wild type cells Rad16 recruitment is clearly NER-dependent, this requirement could be entirely bypassed in presence of constitutive H3K56 acetylation (Fig. 3). Absence of H3K56 acetylation on the other hand resulted in impaired Rad16 recruitment during NER, as no

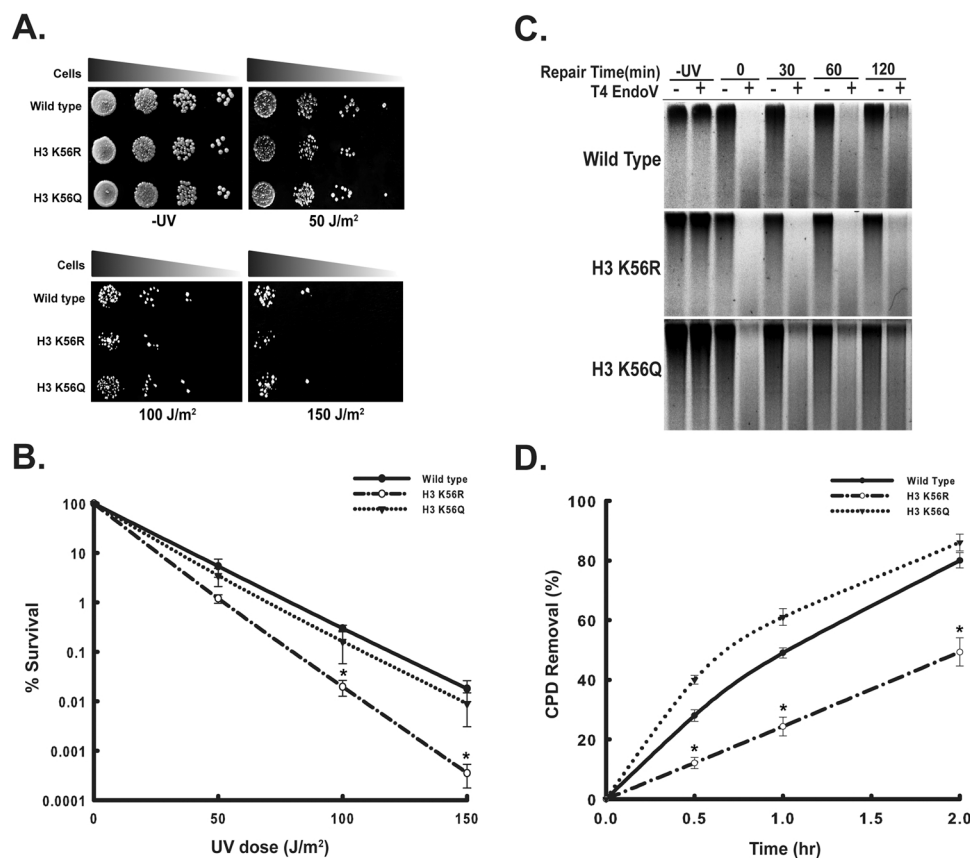


Fig. 1. H3K56 acetylation is required for efficient NER. Ten-fold serial dilutions of control or UV-treated cells of wild type and H3K56 mutants were either **A.** spotted or **B.** spread on YEA plates. For spread assay the colony forming units from triplicate sets were counted and the average was graphically plotted to represent percent cell survival in response to different doses of UV with respect to no UV control. Data represents the standard error of mean bars for three independent experiments and * indicates t-test significant P values < 0.05. **C.** Global genome NER study of wild type and H3K56 mutant cells treated without or with 100 J/m² of UV irradiation and repair incubated for various time periods. Genomic DNA isolated, treated with or without T4 endonuclease V and resolved in alkaline agarose gel. **D.** CPD removal of wild type and H3K56 mutants calculated and graphically represented. Data represents the mean for three independent experiments with standard error of mean bars and * indicates t-test significant P values < 0.05.

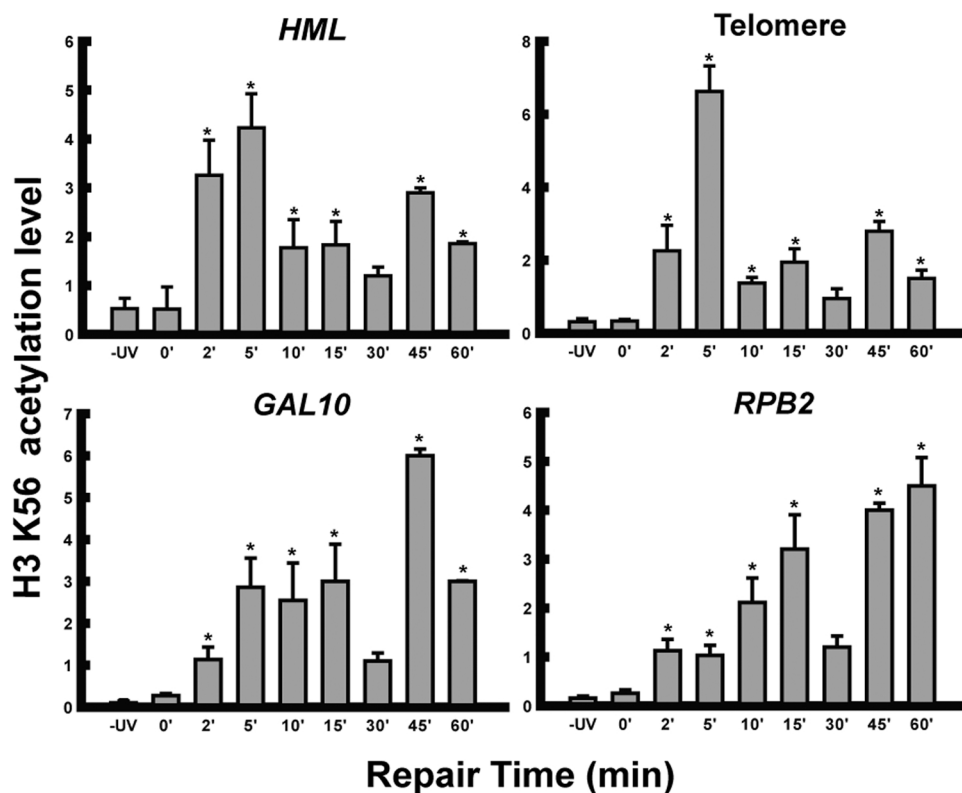


Fig. 2. Acetylation of H3K56 during NER. ChIP q-PCR analyses using anti-acetyl H3K56 antibody on chromatin isolated from wild type cells treated with or without UV irradiation at 100 J/m² followed by repair incubation for different time periods as indicated. Genomic DNA isolated following ChIP was subjected to qPCR using primers specific to *HML*, *GAL10*, *RPB2* and telomere regions. H3K56 acetylation levels were normalized to ChIP data of the same regions with anti-H3 antibody and graphically plotted for representation. Data represent the mean for three independent experiments with standard error of mean bars and * indicates t-test significant P values < 0.05.

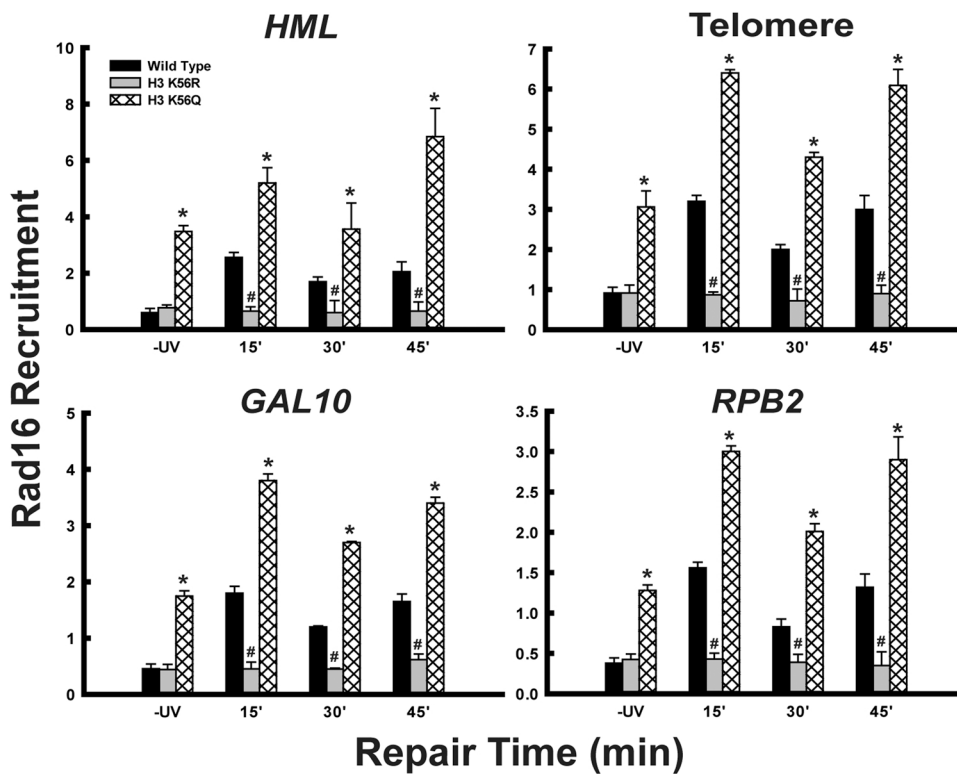


Fig. 3. Comparative recruitment of Rad16 in wild type and H3K56 mutants during NER. ChIP q-PCR analyses using anti-Rad16 antibody on chromatin isolated from wild type and H3K56 mutant cells treated with or without UV irradiation at 100 J/m² followed by repair incubation for different time periods as indicated. Genomic DNA was subjected to qPCR using primers specific to *HML*, *GAL10*, *RPB2* and telomere regions. For each strain, data represent the mean for three independent experiments with standard error of mean bars, * and # indicates t-test significant P values < 0.05 of H3K56Q and H3K56R cells respectively, relative to wild type.

significant levels of Rad16 enrichment could be observed even 45 min post-UV irradiation, in all the loci tested (Fig. 3). It is thus evident from our results that H3K56 acetylation is a pre-requisite for Rad16 recruitment during NER. Importantly, H3K56 acetylation seems to regulate Rad16 redistribution at sites of repair in an UV-dependent manner, and constitutive acetylation of H3K56 alleviates such regulation.

2.3. H3 N-terminal tail acetylation during NER requires H3K56 acetylation

UV-induced acetylation of H3 N-terminal tail residues like H3K9 and

K14 has been shown to be involved in DNA repair, especially through recruitment of chromatin remodeller to facilitate CPD removal [28,36, 68–70]. H3 acetylation is known to prevent DNA damage and in absence of the corresponding histone acetyltransferase enzymes like Gcn5 and Rtt109, cells are rendered sensitive to DNA damaging agents [71,72]. Next attempt therefore was to understand whether a crosstalk exists between acetylation of the H3 core residue H3K56 and acetylation of H3 tail residues like K9 or K14, during NER. For this, ChIP-qPCR based assays were done in all chromatin loci mentioned above, with wild type and H3K56 mutant cells treated or untreated with UV, using antibodies against H3K14ac and H3K9ac respectively. We observed that under

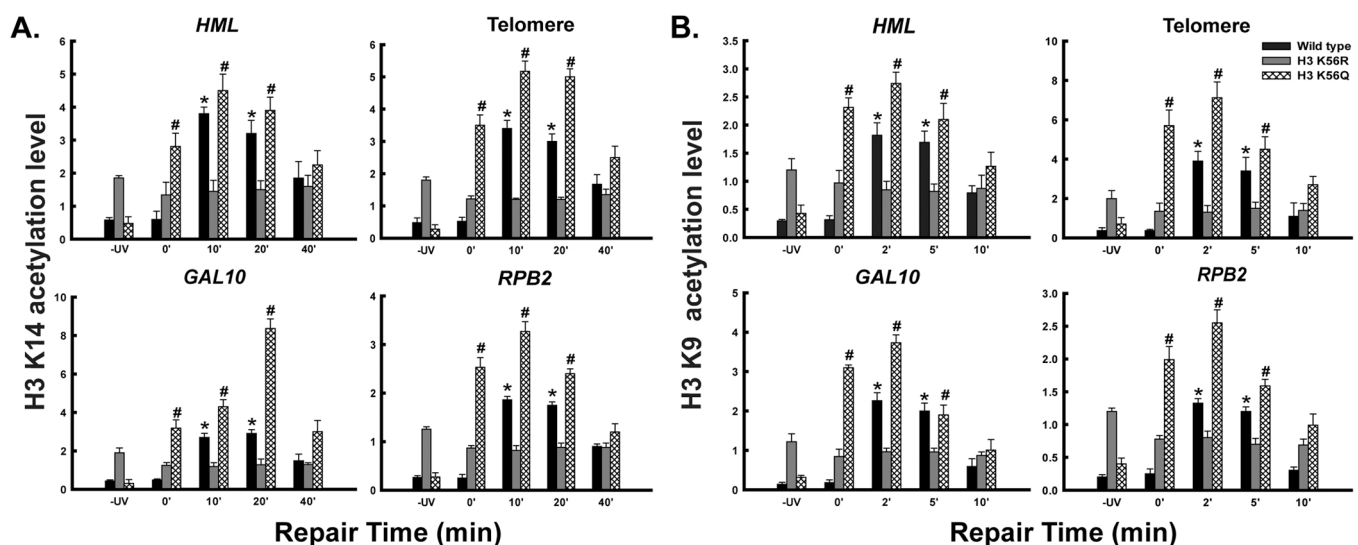


Fig. 4. H3K56 acetylation promotes H3 N-terminal tail residue acetylation during NER. ChIP q-PCR analyses using A. anti-acetyl H3K14 and B. anti-acetyl H3K9 antibody on chromatin isolated from wild type and H3K56 mutant cells treated with or without UV irradiation at 100 J/m² followed by repair incubation for different time periods as indicated. Genomic DNA was subjected to qPCR using primers specific to *HML*, *GAL10*, *RPB2* and telomere regions. For each strain, data represent the mean for three independent experiments with standard error of mean bars. * and # indicate t-test significant P values < 0.05.

control conditions, H3K14 acetylation in H3K56R mutants was significantly higher, compared to wild type and H3K56Q cells (Fig. 4A). During NER, distinct UV-induced hyperacetylation of H3K14 occurred in wild type and H3K56Q cells. Interestingly, while in wild type cells the hyperacetylation became significant around 10 min of repair, in H3K56Q cells significant hyperacetylation was observed immediately after UV irradiation (0 min). In contrast, no UV-induced increase in H3K14 acetylation was observed in H3K56R cells at least till first 40 min of NER (Fig. 4A). From these observations, it became evident that while under control conditions H3K14 acetylation was not dependent on H3K56 acetylation status, UV-induced hyperacetylation of H3K14 during NER requires H3K56 acetylation. This is further strengthened by the observation that constitutive H3K56 acetylation, as in H3K56Q cells, actually promoted H3K14 acetylation immediately after UV irradiation, even earlier than wild type cells. It has been previously reported that increased Gcn5 recruitment occurs in the silent *MFA2* locus within 0 min post UV irradiation [36]. Thus, it is possible that immediately after UV irradiation, Gcn5 recruitment occurs which in turn promotes H3 tail residue acetylation and the event is favoured in presence of constitutive H3K56 acetylation. It can therefore be concluded that UV-induced hyperacetylation of H3K14, essentially requires H3K56 acetylation. Subsequent ChIP assay with H3K9ac antibody showed a pattern similar to H3K14 acetylation in the H3K56 mutants, compared to wild type. Under control conditions, H3K9 acetylation in H3K56R mutants was found to be significantly higher compared to wild type and H3K56Q (Fig. 4B). Post UV-irradiation however, while NER-specific H3K9 hyperacetylation was observed for wild type and H3K56Q, no such increase in acetylation was observed for H3K56R mutant. Similar to H3K14 acetylation, H3K9 acetylation in H3K56Q cells increased immediately after UV irradiation, while in wild type hyperacetylation was observed within 2 min of repair. In conclusion, the above results clearly indicate that, in absence of UV, H3K9 and K14 acetylation events are independent of H3K56 acetylation, however post UV-irradiation, the

NER-responsive hyperacetylation of H3K9 and K14 is significantly dependent on H3K56 acetylation.

2.4. Regulation of chromatin accessibility during NER is impaired in absence of H3K56 acetylation

Chromatin reorganisation for DNA damage accessibility is an important aspect of NER. To understand the significance of H3K56 acetylation in modulating chromatin during NER, we performed micrococcal nuclease (MNase) digestion assay. MNase assay done under control conditions (-UV) showed clear difference in digestion profile between wild type and the H3K56Q mutant. When subjected to MNase digestion the chromatin of H3K56Q cells showed less distinct nucleosomal DNA bands, compared to wild type and H3K56R (Fig. 5A, left most panel; compare lanes of wild type, K56R and K56Q digested with 10 units of MNase), indicating a more accessible chromatin structure. The respective scans of the MNase digested chromatin of wild type, H3K56Q and H3K56R under control conditions also clearly indicate that at same MNase concentrations, presence of constitutive H3K56 acetylation (i.e., in H3K56Q), render cells with higher chromatin accessibility (Fig. 5B). It is evident from the scans that peak heights are greater in nuclease digested chromatin fractions of wild type and H3K56R cells, indicating presence of higher intensity nucleosomal DNA bands. The nucleosomal DNA in these cells is thus less accessible for MNase digestion. On the contrary, in H3K56Q cells the scan peaks are of lower heights indicating less distinct nucleosomal DNA bands. This clearly suggests that the nucleosomal DNA fraction in presence of constitutive H3K56 acetylation is more accessible to nuclease digestion. In consonance with our observations, it has been earlier shown that wild type and H3K56R mutants have more distinct nucleosomal fractions compared to H3K56Q, due to more extensive MNase digestions and higher chromatin accessibility in the latter [58].

To further our understanding, comparative MNase digestion profiles

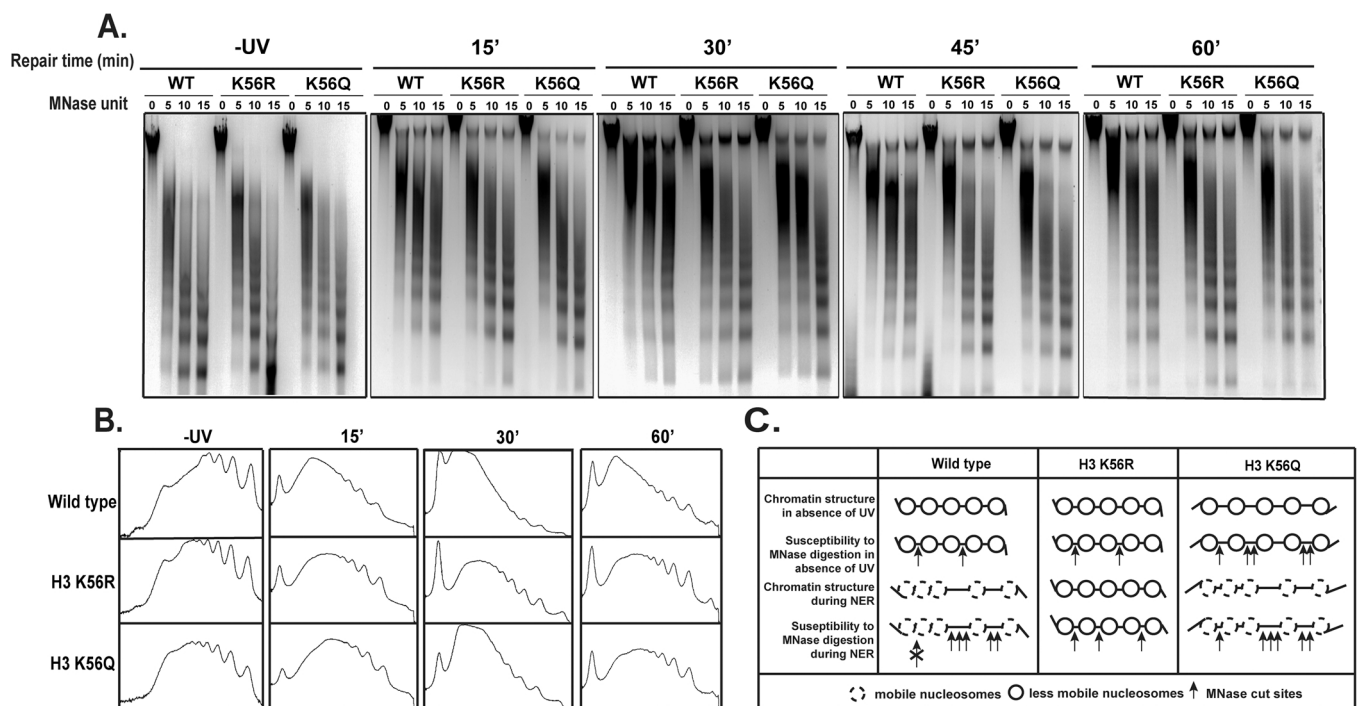


Fig. 5. H3K56 acetylation enhances chromatin accessibility. Equal amounts of cells of wild type and H3 K56 mutants were simultaneously treated without or with 100 J/m² UV irradiation followed by repair incubation for indicated time periods and subjected to various concentrations of MNase, genomic DNA isolated and resolved on 1.2% agarose gel. **A.** Representative gels showing digestion profile of bulk chromatin, stained with ethidium bromide **B.** Corresponding scans of 10 units of MNase (25 U/μl) digest gel lanes **C.** Schematic representation depicting how constitutive acetylation of H3K56 generates chromatin more accessible to MNase digestion, that in presence of UV irradiation aids chromatin switching between compacted and relaxed states, that essentially occurs in wild type in a NER-responsive manner. Three independent experiments were performed to analyse the chromatin accessibility dynamics during NER in wild type and H3K56 mutants.

were obtained during NER. Results indicated significant differences in chromatin accessibility during NER in presence and absence of H3K56 acetylation. As shown in Fig. 5A and the corresponding scans (Fig. 5B, third panel from the left), it is very evident that by 30 min of repair, wild type cells undergo perceptible chromatin rearrangements leading to generation of prominent higher order chromatin conformations resistant to nuclease digestion. Within 60 min of repair, the higher order chromatin peaks tend to reduce in wild type and lower order structures start to reappear (Fig. 5A & B). Such an oscillation between the higher and lower order chromatin states thus seems to be a signature for efficient NER. Constitutive H3K56 acetylation as seen in H3K56Q mutants, allowed similar oscillation between the chromatin states during NER (Fig. 5B, compare 30 min scan of wild type and H3K56Q). As further evident from the scans, by 60 min of NER H3K56Q cells still maintained a more open chromatin structure, compared to wild type (Fig. 5B, compare 60 min scan of wild type and H3K56Q). It thus became apparent that constitutive H3K56 acetylation generates a chromatin structure more accessible in nature. In contrast, lack of H3K56 acetylation led to a chromatin environment with lesser flexibility. Higher order chromatin states were less prominently formed in H3K56R mutants during NER and the distinct dynamism observed in wild type and H3K56Q was clearly absent (Fig. 5B, compare scans of wild type, H3K56Q and H3K56R at 30 min time point). Micrococcal nuclease digestion pattern of H3K56R obtained around 60 min of NER was almost comparable to that observed after 15 min of the repair process, indicating impaired oscillation between the chromatin states (Fig. 5A, compare 15 min gel picture of H3K56R with 60 min gel picture). In absence of H3K56 acetylation thus lack of such chromatin modulation during NER may hinder DNA damage accessibility and consequently challenge repair efficiency. It is known that in a chromatinized environment, nucleosomal rearrangement is an essential pre-requisite for the NER machinery to access the damaged site. The access step importantly involves posttranslational modification of histones in isolation or in concert with chromatin remodelling [29,36,69,70]. From our results it thus becomes evident that H3K56 acetylation is required for significant nucleosomal rearrangements during NER, as explained through the schematic in Fig. 5D. In wild type cells presence of H3K56 acetylation post UV irradiation, allows the chromatin to undergo essential compaction at some regions and relaxation at others, so that the damage sites get adequately exposed to the repair machinery. In presence of constitutive H3K56 acetylation (H3K56Q) such a NER conducive chromatin state is achieved as efficiently as in wild type cells, but lack of acetylation (H3K56R) impairs this prerequisite step for NER (Fig. 5D).

2.5. H3K56 acetylation maintains supercoiled DNA in relaxed state “in vitro”

It is known that as DNA wraps around the histone octamer it generates approximately one negative supercoil per core particle. Therefore, to substantiate the chromatin accessibility we studied the effect of

H3K56 acetylation on nucleosome wrapping dynamics during NER through plasmid supercoiling assay. For supercoiling assay, the plasmid was relaxed with Topoisomerase I and then incubated with total cellular extracts prepared from wild type, H3K56R and H3K56Q cells respectively, that were treated with or without UV and allowed to undergo NER for different time periods. From our results, it was evident that under control conditions, cell extracts from wild type maintained the plasmids primarily in the supercoiled state, while that from H3K56Q failed to generate such a state and kept the plasmid in a more relaxed configuration (Fig. 6). Extracts from cells bearing constitutive H3K56 acetylation thus tends to generate an open conformation of the DNA. On the contrary, cell extract from H3K56R mutant generated several conformations of the plasmid DNA between supercoiled and relaxed states, unlike wild type or H3K56Q. This indicated that lack of H3K56 acetylation neither generated a completely relaxed nor efficiently compacted DNA. Thus, simplistically speaking, H3K56Q mutant cell extract is completely defective and H3K56R mutant cell extract is partially defective in nucleosome assembly, in vitro. Interestingly, during NER the wild type cell extract caused a significant shift in the plasmid conformation and the DNA was maintained distinctly in the relaxed state. As seen in Fig. 6, such a state with or without UV treatment already existed in plasmids incubated with extracts from H3K56Q cells. This clearly substantiates the fact that H3K56 acetylation helps to maintain DNA in a more open and relaxed state and that probably confers an advantage during NER, especially when occurring in a chromatin environment. On the contrary, extracts from H3K56R cells did not allow such a distinct shift of the DNA molecule into a more relaxed state during NER. Unlike wild type and H3K56Q, when incubated with H3K56R cell extract treated with or without UV, the plasmid seems to maintain a conformation without a significant change during NER. It is thus evident that H3K56R cell extract lacks the ability to oscillate DNA between compact and relaxed conformation during the process of NER. This complements our MNase assay results (Fig. 5), which indicated that absence of H3K56 acetylation (H3K56R) impairs chromatin accessibility during NER. To sum up, lack of H3K56 acetylation, thus impedes pragmatic dynamics required in nucleosomal DNA during NER and consequently negatively impacts efficiency of process. Hence, H3K56 acetylation essentially regulates chromatin dynamics and consequently DNA accessibility during NER.

3. Discussion

Nucleotide excision repair is a complex process, especially when occurring in a chromatin environment. Successful NER requires coordination of several events which encompasses the basic essentialities of “Access-Repair-Restore” [10,11]. Apart from the obvious requirement of NER factors during the repair phase, access and restoration steps involve coordinated action of histone modifiers, histone chaperones and chromatin remodellers. Of the histone modifications involved, certain H3 and H4 N-terminal tail residues have been related to NER [28,36,37,68,

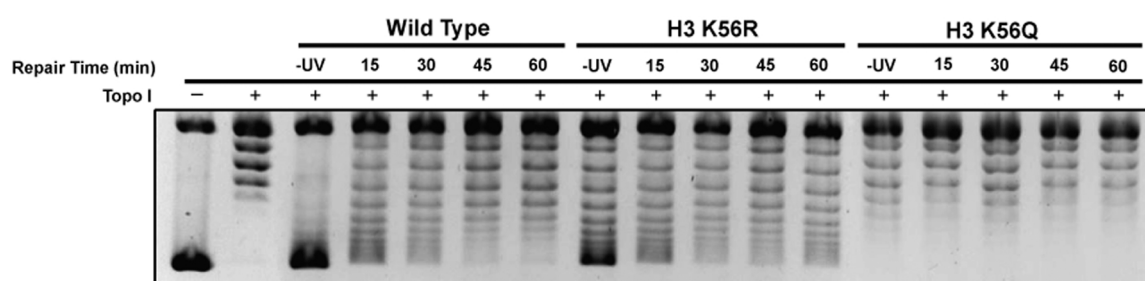


Fig. 6. Plasmid supercoiling assay with wild type and H3K56 mutant cell extract. Cell extracts were prepared from wild type and H3K56 mutants treated with or without UV irradiation followed by repair incubation for indicated time periods, as mentioned in Materials and methods. Negatively supercoiled plasmid DNA was treated with Topoisomerase I; the relaxed plasmid was incubated with wild type and H3K56 mutant cell extracts, DNA isolated after protein removal, resolved on an agarose gel and stained with ethidium bromide.

69]. H3K56, being a core histone residue located near the entry-exit point of the nucleosome, its acetylation weakens interaction between ends of the DNA and the histone octamer. This effectively has a role to play in nucleosomal DNA wrapping-unwrapping and eventual disassembly [1,40–44,58,73–75]. For a process such as NER, nucleosomal DNA accessibility to the large repair complex, is a rate limiting step. Thus, requirement of H3K56 acetylation for regulating nucleosomal DNA accessibility during NER, was a tempting speculation. While H3K56 acetylation has been related to DNA damage response, in a replication dependent or independent manner [40,47,55,58,60,63–66,76–80], sporadic information exists about specific role of H3K56 acetylation during UV-induced DNA repair, or more precisely during NER in yeast. From our observations here we found that lack of H3K56 acetylation (H3K56R) renders cell more sensitive to UV irradiation compared to wild type, more significantly when treated with high UV doses of 100 J/m² and 150 J/m². Notably few earlier works have reported no effect of H3K56 mutation on UV sensitivity, with UV irradiations done at 50 J/m² or even as low as 5 J/m² [58,75]. The increased UV sensitivity of H3K56R cells that we observed in comparison to wild type, however was very consistent at UV irradiation of 100 J/m² and 150 J/m². Mimicking constitutive H3K56 acetylation on the other hand, did not significantly alter UV sensitivity of cells compared to wild type. Taken together, it was apparent from our results that absence of H3K56 acetylation significantly affects UV-induced DNA damage response. As 100 J/m² is a UV dose generally used for NER studies in yeast cells [23,37,81–90] all our subsequent NER related experiments have been done using this dose. The observation that H3K56R mutant had much lower rate of CPD removal, compared to wild type and H3K56Q, made it further evident that H3K56 acetylation has a role to play during NER. Histone modifications may play a critical role in either one or both of the steps of access and restoration during any DNA metabolic process. Hence, it was necessary to understand the exact phase of NER which requires H3K56 acetylation. Our results on NER indicated that the H3K56Q mutants, with constitutive H3K56 acetylation, had a moderately enhanced CPD removal rate especially during the early phases (30 min, 1 h). Moreover, we observed that UV-induced H3K56 hyperacetylation occurs within 2 min of UV irradiation. This clearly indicated that H3K56 acetylation is required during the early phases of UV-induced NER and might be essential for triggering initial events of the process.

It has been previously reported that UV-induced H3 hyperacetylation is required for efficient DNA repair in yeast as well as in mammals [36,78,91,92]. In yeast, importance of UV-responsive acetylation of H3 tail residues like K9 and K14 has been well documented as initial NER events [36,37,70]. From our results we could further establish a correlation between H3K56 acetylation and H3 N-terminal tail residue modifications during NER. We found that UV-induced hyperacetylation of H3K9 and K14 was dependent on H3K56 acetylation. Intriguingly, presence of constitutive H3K56 acetylation (H3K56Q) provided cells with an added advantage and H3 tail residue acetylation was triggered immediately after UV irradiation. This evidently provided a better kick start to NER. The finding also importantly indicates a clear crosstalk between hyperacetylation of a H3 core residue (K56), with the H3 N-terminal tail residues (K9 and K14) in response to UV. Notably in absence of UV, acetylation of H3K9 and K14 residues was not dependent on H3K56 acetylation. Under control conditions absence of H3K56 acetylation, as seen in H3K56R cells, rather promoted H3K9 and K14 acetylation. Whether such increased acetylation of H3 N-terminal tail residues in absence of H3K56 acetylation is dependent or independent of the HAT Gcn5, will be an interesting avenue of future investigations. A previous study has already demonstrated that presence or absence of acetylation in certain H3 lysine residues can alter specificity of HAT complex like Rtt109-Vps75 towards its target residues, *in vitro* [54]. Additionally, what significantly emerges from our results is the fact that despite higher H3K9 and K14 acetylation in absence of UV, H3K56R cells have less efficient NER rate. This is possibly due to its inability to redistribute such

acetylation to target damage sites, in response to UV irradiation [23,24]. To sum up, our results indicate that a crosstalk exists between acetylation of the core residue H3K56 and the tail residues H3K9 and K14, and it is primarily an early NER event that stimulates successful removal of DNA lesions. In yeast, UV induced hyperacetylation of H3 tail residues is dependent on Gcn5 and partially on the chromatin remodeller Swi2, and it is essentially required for progression of NER in a refractory chromatin environment [29,36,69]. Furthermore, UV-induced hyperacetylation of H3 tail residues has been reported to be dependent on Rad16 activity and constitutive hyperacetylation of H3 can bypass the need for Rad16 and Rad7 during GG- NER, in specific chromatin loci [28,29]. At the whole genome level however, while Gcn5 deletion had insignificant effect on NER, Rad16 deletion distinctly reduced NER efficiency, compared to wild type [68]. In addition, we found that UV-induced H3 tail residue acetylation and recruitment of the repair factor Rad16 during NER, is significantly dependent on H3K56 acetylation status. Lack of H3K56 acetylation could not promote NER-responsive recruitment of Rad16, which is a natural event in wild type cells following UV irradiation. On the contrary, presence of constitutive H3K56 acetylation led to relatively higher Rad16 recruitment irrespective of presence or absence of UV. This is an important observation and indicates that H3K56 acetylation is required for Rad16 recruitment that effectively leads to efficient NER. Recent reports have established that the GG-NER complex, especially Rad16 and Rad7 are involved in redistribution of Gcn5 in response to UV irradiation [23]. As Gcn5 is a major HAT responsible for H3K9 and K14 acetylation, impaired Rad16 recruitment in absence of H3K56 acetylation, could negatively affect UV-induced tail residue acetylation and consequently NER, as observed in H3K56R cells. Additionally, during NER, Rad16 contributes towards generating a superhelical torsion that is essential for removal of the damaged oligonucleotide from DNA [25,26]. Taken together all these evidences suggest that inability to recruit Rad16 following UV damage affects NER proficiency, as observed in H3K56R cells. To summarize, during NER, H3K56 acetylation is a pre-requisite for regulation of downstream events such as, UV-induced redistribution of Rad16 and hyperacetylation of H3K9 and H3K14 residues. This coordination between H3K56 acetylation, Rad16 recruitment and, H3K9 and H3K14 hyperacetylation is essential for proficient NER.

Earlier studies have suggested the necessity of unwrapping nucleosomal DNA to promote accessibility of lesions within occluded regions of the genome [92,93]. Our results here show that, H3K56 acetylation is crucial for promoting chromatin accessibility in response to UV damage. It was evident that in absence of H3K56 acetylation, yeast cells lacked the chromatin dynamics observed in wild type cells during NER. In response to UV irradiation wild type cells exhibit significant chromatin rearrangements generating prominent higher order chromatin structure and fuzzier lower order structures during early NER phases. With progression of NER, lower order structures start to reappear indicating the need for a significant oscillation of chromatin between compact and relaxed structure for efficient repair. Our observations find further support from an earlier report which states that UV-responsive loss of regularly spaced nucleosomes occurs during early phases of NER subsequently generating more closely spaced nucleosomes [24], implying that an intense nucleosome rearrangement occurs during repair. Such chromatin modulation during NER must be a necessary step in promoting accessibility of the downstream repair factors to the site of DNA damage. A recent *in vitro* study demonstrates that acetylation of H3K56 aids in exposing helix distorting bulky lesions located in the nucleosomal DNA, by facilitating nucleosomal repositioning [94]. The fact that nucleosome remodelling and chromatin rearrangement during NER essentially requires H3K56 acetylation is further substantiated by our observations on plasmid supercoiling. It was evident that presence of H3K56 acetylation poised the DNA in a more relaxed and open state that is a requisite for NER, as seen in wild type and H3K56Q cells following UV irradiation. From comparison of pre-UV and post-UV plasmid conformation profile in wild type cells it became very apparent that with

progress of NER, the drastic shift in plasmid conformation from a highly supercoiled state to a more relaxed state was significant. This closely resembled the plasmid state observed with H3K56Q cell extract at pre-UV conditions. Such a state could not be achieved in absence of H3K56 acetylation and was the cause of reduced NER efficiency observed in H3K56R cells. This strongly validates the fact that in response to UV-induced NER, yeast cells tend to achieve a conducive chromatin configuration through H3K56 hyperacetylation, as one of the critical downstream events.

Presence of H3K56 acetylation thus significantly favours chromatin modulations to generate a landscape conducive for NER. Recent findings have suggested that GG-NER initiates around the boundaries of higher order chromatin domains, from where GG-NER complexes containing Rad16 and Rad7 get redistributed in response to UV irradiation [24]. This generates a platform further promoting H3 hyperacetylation, histone exchange and chromatin remodelling by SWI/SNF or RSC complex during NER [24,95]. In consonance, we observed that in absence of H3K56 acetylation (H3K56R), cells failed to recruit Rad16 in an UV-dependent manner, lacked H3 tail residue hyperacetylation and consequently effective chromatin modulation during NER was impaired. With constitutive H3K56 acetylation (H3K56Q) on the other hand, cells showed higher Rad16 occupancy with or without UV irradiation and immediate UV-responsive hyperacetylation of H3K9 and K14 residues and efficient chromatin remodelling during NER. While UV-responsive Rad16 recruitment was observed in H3K56Q cells and apparently favoured CPD removal, presence of significantly high levels of Rad16 even in the absence of UV damage indicates that a damage inducible response is mis-regulated in presence of constitutive H3 K56 acetylation. Another interesting observation was that despite more efficient NER process at least during early NER phases, H3K56Q cells showed a small but consistently higher UV sensitivity compared to wild type. While this might seem an apparent contradiction, such increased UV sensitivity in presence of constitutive H3K56 acetylation may be attributed to cell cycle defects. Previous studies have shown that H3 K56 acetylation specifically occurs during S-phase and is very tightly regulated by the HDACs hst3 and hst4 during the G2/M phase to facilitate unperturbed cell cycle. H3K56 acetylation in response to DNA damage is essential for triggering the necessary repair pathway and for cell cycle arrest to prevent passing of the damaged DNA to the daughter cells [64]. However, if H3K56 acetylation is not removed following DNA damage repair, cell cycle defect is manifested [63,96]. Thus, the slightly increased UV sensitivity in presence of constitutive H3K56 acetylation could possibly be a reflection of cell cycle defect post DNA damage removal, as no lack of NER proficiency was observed in H3K56Q cells.

To conclude, upon UV irradiation, wild type cells tend to achieve a state of flexible chromatin architecture with accessibility of the DNA damage site to the repair factors and associated chromatin modifiers. As summarized in the proposed model (Fig. 7), this is achieved through acetylation of the H3K56 residue, as an early NER event. Significant levels of H3K56 acetylation that manifests within minutes of UV irradiation, triggers a series of downstream occurrences including recruitment of the repair factor Rad16 and significant hyperacetylation of H3 tail residues like H3K9 and H3K14 in an UV responsive manner. A combination of the H3 acetylation events in the core and tail residues in response to UV exposure consequently induces chromatin plasticity, promotes recruitment of chromatin remodellers and finally generates DNA accessibility that favours efficient NER. This is the first ever report of involvement of H3K56 acetylation in the access step of NER and opens up further avenue for understanding the basis of histone code that forms the essential platform for understanding how a DNA metabolic event is regulated while occurring within a chromatin landscape.

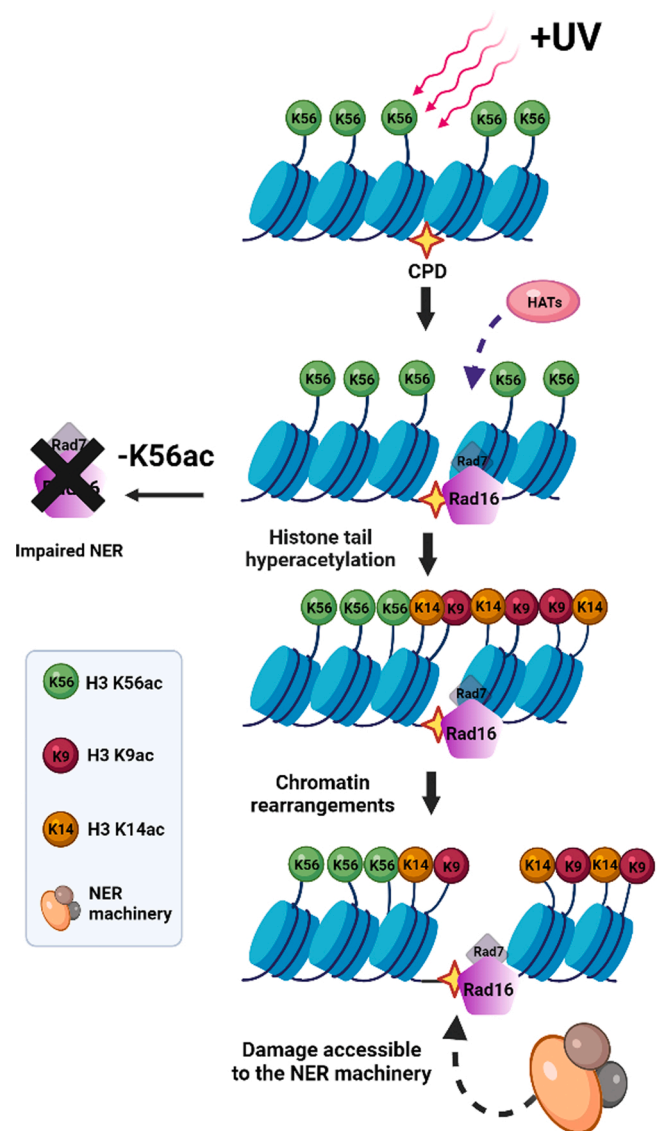


Fig. 7. Working model showing the involvement of H3K56 acetylation during early phases of NER. Exposure to UV rapidly induces H3K56 acetylation, which in turn triggers redistribution of NER factor Rad16 in complex with Rad7, followed by acetylation of H3 tail residues K9 and K14, subsequently conferring desired flexibility to chromatin architecture that promotes efficient NER for CPD removal.

4. Materials and methods

4.1. Yeast strains

The detailed procedure for generation of yeast strains has been previously described in Ray et al., 2018; 2020 [37,38]. *Saccharomyces cerevisiae* strain WY121 with both copies of genomic histone H3-H4 deleted and containing plasmid pJL001 (*CEN URA3 HHT2-HHF2*) as the only copy of H3-H4 with *URA3* counter-selectable marker was transformed with plasmid pEMH7 (*CEN TRP1 HHT2-HHF2*) containing one copy of H3-H4 with counter-selectable marker *TRP1*. Plasmid shuffling of transformed cells in presence of 5-FoA (5'-Fluoroorotic acid) led to the loss of plasmid pJL001 leading to the generation of the wild type strain. The plasmids pEMH129 and pEMH108 containing H3 K56R and H3 K56Q mutations in the *HHT2* gene respectively, were isolated from *E. coli* and similarly transformed into WY121 yeast strain followed by plasmid shuffling, to generate histone H3 mutant strains H3K56R and H3K56Q. The transformed plasmids were isolated from

yeast cells and sequenced to confirm the presence of the desired mutations.

4.2. UV sensitivity assay

The UV sensitivity assay was done as per the protocol described in Toussaint et al., 2006 [97] with minor modifications. Yeast cells were grown exponentially to an OD₆₀₀ of 0.6–0.7 ($\sim 0.9 \times 10^7$ cells/ml) in yeast extract-peptone-dextrose (YPD) and incubated overnight at 30 °C in shaking conditions. Following day, cells were collected by centrifugation, resuspended in sterile water to 0.9×10^7 cells/ml. 300 µl of 0.9×10^7 cells/ml of yeast cell suspension in sterile water was either treated without or with UV irradiation (254 nm) at a dose of 50, 100 or 150 J/m² respectively. 10-fold serial dilutions of the UV treated or untreated cells were either spotted or spread on YPD plate. The plates were incubated in the dark at 30 °C for 48–72 h. For spread assay, each serial dilution for the respective UV doses and the no UV control plate were spread in triplicates for each of the strains and the numbers of colony forming units were counted and the average data was plotted. For each strain, error bars indicate the standard error of mean of three technical replicates from three biological repeats each (n = 3).

4.3. Whole genome NER analyses

For the analysis of genome-wide NER rate, yeast cells were grown in YPD at 30 °C to mid-log phase with an OD₆₀₀ of ~ 0.7 ($\sim 1 \times 10^7$ cells/ml), an aliquot of cells was separated to serve as the no UV control and the remaining cells were collected, re-suspended in 1X PBS and treated with UV at a dose of 100 J/m² (254 nm). The UV treated cells were then harvested, re-suspended in pre-warmed YPD and allowed to repair for various time periods (0 h, 0.5 h, 1 h, 2 h) by incubation in the dark at 30 °C. Genomic DNA was isolated from the harvested cells as per the protocol described in Ray et al., 2018 [37]. Equal amounts of genomic DNA from each repair time point were either mock treated or treated with T4 Endonuclease V (NEB, USA, M0308S) for 2 h at 37 °C and electrophoresed under denaturing conditions in an alkaline gel without ethidium bromide (0.5 M NaCl, 0.01 M EDTA pH 8.0, 1.2% agarose). The gel was neutralized with neutralisation buffer (1 M Tris-Cl (pH 7.6), 1.5 M NaCl) followed by ethidium bromide staining and visualised. Repair rate was analysed using an extension of the DNA CPD quantification method described earlier [37,98]. For each time point of repair of each strain the approximate number of CPDs was calculated by normalisation of the band intensity of T4 endonuclease V treated samples by the mock treated ones. At every time points of repair the number of CPDs that were present for each strain was subsequently normalised to the number of CPDs present initially in that strain at 0 min of repair. The negative log of these values was plotted as the percentage of CPDs that were repaired. The percentage of CPD removal was obtained using the formula $100 - 100 * [-\ln(\text{CPD no. at repair time point } x) / -\ln(\text{CPD no. at 0 min of repair})]$. The T4 Endonuclease V assay was repeated thrice from each set of genomic DNA isolated from the three strains. The data obtained was plotted and graphically represented as the percentage of CPD removal. Error bars represent the standard error of mean between the three biological repeats (n = 3).

4.4. Chromatin accessibility assay

For chromatin accessibility assay protocol was followed as described in Ray et al., 2018, with brief modifications [37]. To check chromatin accessibility during NER equal amounts of wild type, H3K56R and H3K56Q cells at their mid-log phase O. D₆₀₀ ~ 0.7 ($\sim 1 \times 10^7$ cells/ml) were simultaneously harvested and an aliquot of cells were separated as

no UV control. The remaining cells were harvested, washed with 1X PBS and UV irradiated with a dose of 100 J/m² (254 nm). The wild type and H3K56 mutant cells were then harvested, re-suspended in pre-warmed YPD and allowed to repair in dark at 30 °C for 15, 30, 45, 60 min, respectively. The no UV control cells and the UV-treated cells for all the three strains were processed simultaneously as previously described in Ray et al., 2018 [37]. Briefly, the cell pellets were washed with 1 M sorbitol and harvested. Thereafter, cell pellets were gently and quickly resuspended in YLE buffer (10 mg/ml Zymolyase (MP Biomedicals, USA, Zymolyase 20 T) in 1 M sorbitol, 5 mM β-mercaptoethanol) and incubated at 22 °C for 30 min to allow the formation of spheroplasts. The spheroplasted cells were collected by centrifugation and washed twice with sorbitol wash buffer (1 M sorbitol, 2 mM β-mercaptoethanol, 1 mM PMSF) and resuspended in spheroplast digestion buffer (50 mM NaCl, 1 M Sorbitol, 5 mM MgCl₂, 10 mM Tris-Cl pH 7.5, 1 mM CaCl₂, 1 mM β-mercaptoethanol, and 0.075% v/v NP-40 and 0.5 mM spermidine). The cell suspension was then divided into equal aliquots and treated with varying concentrations of Micrococcal nuclease (Worthington, USA, LS004798) for 10 min at 37 °C. For studying chromatin accessibility during NER MNase concentrations (25 U/µl) of 5, 10, 15 units respectively, were used. The reactions were terminated with 0.1 volumes of stop solution (5% SDS, 250 mM EDTA pH 8.0) followed by Proteinase-K treatment for 2 h at 55 °C. Samples were extracted twice with phenol/chloroform, treated with 10 mg/ml of RNase A and precipitated with ethanol. DNA was re-suspended in TE buffer, electrophoresed on a 1.2% agarose gel containing ethidium bromide and visualised. Densitometric scans of the agarose gels were performed using Image J software to analyse chromatin accessibility of wild type and mutants. Gel profile of 10 unit of MNase digestion under control conditions and during the repair time points as indicated in Fig. 5B, was analysed for all the three strains. Peaks in the densitometric scans are representative of the intensity of nucleosomal DNA bands in the corresponding lanes mentioned above, for respective strains. Three independent experiments were performed to understand the chromatin accessibility dynamics during NER in wild type and H3K56 mutant cells.

4.5. Chromatin immunoprecipitation assay

Chromatin immunoprecipitation assay was performed as previously mentioned in Ray et al., 2018; 2020 [37,38]. Briefly, mid-log phase yeast cells with an OD₆₀₀ of ~ 0.7 ($\sim 1.0 \times 10^7$ cells/ml) were harvested and an aliquot of cells was separated for no UV control. The remaining cells were UV irradiated, harvested, and re-suspended in pre-warmed YPD to allow the cells to repair for various time periods in the dark at 30 °C. The time periods of repair incubation for studying H3K56 acetylation status during NER was 0, 2, 5, 10, 15, 30, 45, 60 min, respectively. H3K14 and H3K9 acetylation status in wild type, H3K56R and H3K56Q mutants was checked at the repair time points of 0, 10, 20, 40 min and 0, 2, 5, 10 min, respectively. Rad16 occupancy was checked at the repair time points of 15, 30, 45, 60 min, respectively. Both no UV control cells and cells incubated for various repair time periods were first cross-linked with 1% formaldehyde for 30 min at room temperature to capture protein-DNA complexes. The antibodies used for immunoprecipitation were as follows - anti-histone H3 acetyl K56 (Abcam – ab195478), anti-Rad16 (Abcam – ab21758), anti-histone H3 acetyl K9 (Abcam – ab10812), anti-histone H3 acetyl K14 (Abcam – ab52946) and anti-histone H3 (Biobharati, India- BB-AB0055). The assay was repeated thrice and triplicate qPCR were performed from each biological replicate using the following primers:

Primers	Sequence	
HML (YCL065)	F- 5' CATCGTCTTGCTCTTGTT 3'	R- 5' GTATATAGACAATGCAATCGTAC 3'
Telomere (YHR218)	F- 5' GGTAATAATTCAGAACTGGTGC 3'	R- 5' CTTGAAACAACGTGTAGACCA 3'
GAL10	F- 5' GGTAATTGACTGCTGGTGA 3'	R- 5' AAAGTGGGGATTTTGGG 3'
RPB2	F- 5' TGGTCACACAGGTAATAAACT 3'	R- 5' AAAATCTCTCTCGAACGATCGG 3'

4.6. Plasmid supercoiling assay

Yeast cells were grown to mid-log phase with an OD₆₀₀ of ~ 0.7 (~ 1 × 10⁷ cells/ml). An aliquot of the cells was separated to serve as the no UV control. The remaining cells were UV irradiated at a dose of 100 J/m² (254 nm) and allowed to repair for 15, 30, 45, 60 min, respectively and collected by centrifugation. The cell pellets were then processed for the preparation of yeast whole cell extracts as mentioned in Li et al., 2016 [99] with modifications. Briefly, the harvested cell pellets were washed in ice-cold distilled water and then resuspended in YEB extraction buffer (245 mM KCl, 2.5 mM DTT, 1 mM EDTA pH 8.0, 100 mM Hepes-KOH pH 7.9, 1 mM PMSF, 1 mg/ml protease inhibitor cocktail (SRE0055)) and flash frozen in liquid N₂. 700 µl of acid-washed glass beads was then added and the cells were vortexed at maximum speed for 30 s following which the sample tubes were placed in a mixture of ice and water for 30 s. The process was repeated 7–8 more times. Thereafter, the supernatant was collected by centrifugation and dialysed for 4 h at 4 °C in YDBI buffer (50 mM KCl, 0.05 mM EDTA pH 8.0, 1 mM DTT, 20 mM Hepes-KOH pH 7.9, 20% v/v glycerol, 0.1 mM PMSF). The cell extracts were then used for plasmid DNA supercoiling assay. For the supercoiling assay, 2 µg of negatively supercoiled plasmid pBSK (size 2.95 kb) [100] was first relaxed with Topoisomerase I (NEB, M0301S) at 30 °C for 1 h. The reaction mixture containing the relaxed plasmid in presence of Topoisomerase I was then incubated with 20 µg of whole cell extracts of no UV control samples and that of whole cell extracts from various repair time periods (15, 30, 45, 60 min) at 30 °C for 1.5 h. The reaction was stopped by 10 mM EDTA pH 8.0% and 0.05% SDS and incubated at 37 °C for 30 min. The reaction mix was then incubated with RNase A for 1 h at 37 °C and Proteinase K for 1 h at 55 °C in presence of 0.1% SDS. DNA was purified by phenol/chloroform extraction, precipitated with ethanol, resolved on a 1.2% agarose gel and visualized after staining with ethidium bromide.

4.7. Real time PCR and data analysis

ChIP experiments were analysed by Real time PCR (qPCR) using the Applied Biosystems 7500 Fast Real-Time PCR System (Thermo Fisher Scientific), Dynamo Colour Flash SYBR® Green QPCR Kit (Thermo Fisher Scientific) as previously mentioned in Ray et al., DNA Repair 2018, Ray et al., 2020 [37,38]. The levels of histone modifications were calculated by the formula $2^{(C_{T(\text{Input})} - C_{T(\text{IP})})}$ and normalised by the histone H3 levels. Rad16 occupancy was calculated as a percentage of input after extrapolating the input to 100% as the Input DNA was taken as 1% of the whole cell extract. For each ChIP experiment, qPCR was performed in triplicates for the three biological replicates (n = 3) and the data was plotted with standard error of mean bars. The statistical significance of the difference in levels of histone modifications was calculated by using two-tailed paired student's t-test and the statistical significance of the difference in the levels of Rad16 recruitment between wild type and mutants was checked using two-tailed independent student's t-test and results with a P value of < 0.05 were considered significant.

Funding statements

This work was supported by Science and Engineering Research Board (SERB), India (Scheme #CRG/2018/000461) to Dr. Ronita Nag Chaudhuri, Department of Biotechnology, St. Xavier's College, Kolkata; CSIR fellowship [# 08/548(0009)/2019-EMR-I] to Ms. Preeti Khan; fundings to St. Xavier's College, Kolkata by Department of Science and Technology, India [DST-FIST Grant No. SR/FST/COLLEGE-014/2010 (C)] and by Department of Biotechnology, India Grant No. BT/INF/22/SP41296/2020.

Acknowledgements

We thank Prof. JD Boeke (Johns Hopkins University School of Medicine, USA) for kind gift of the pEMH series of plasmids and our sincere acknowledgement to Prof. Michael J. Smerdon, Washington State University, USA for kind donation of the plasmids. We also sincerely thank Prof. John Wyrick (Washington State University, USA) for sharing the WY121 strain.

Author's contribution

RNC and PK designed the experiments, PK performed the experiments, RNC and PK analysed the results and wrote the paper.

Conflict of Interest

Contents of this manuscript are solely the responsibility of the authors and do not necessarily represent the official views of the funding agency.

References

- [1] K. Luger, A.W. Mäder, R.K. Richmond, D.F. Sargent, T.J. Richmond, Crystal structure of the nucleosome core particle at 2.8 Å resolution, *Nature* 389 (1997) 251–260.
- [2] C.H. Chang, D.S. Luse, The H3/H4 tetramer blocks transcript elongation by RNA polymerase II in vitro, *J. Biol. Chem.* 272 (1997) 23427–23434.
- [3] R. Hara, J. Mo, A. Sancar, DNA damage in the nucleosome core is refractory to repair by human excision nuclease, *Mol. Cell Biol.* 20 (2000) 9173–9181.
- [4] F. Thoma, Repair of UV lesions in nucleosomes—intrinsic properties and remodeling, *DNA Repair* 4 (2005) 855–869.
- [5] S.J. Petesch, J.T. Lis, Overcoming the nucleosome barrier during transcript elongation, *Trends Genet.* 28 (2012) 285–294.
- [6] W. Kobayashi, H. Kurumizaka, Structural transition of the nucleosome during chromatin remodeling and transcription, *Curr. Opin. Struct. Biol.* 59 (2019) 107–114.
- [7] R.P. Rastogi, Richa, A. Kumar, M.B. Tyagi, R.P. Sinha, Molecular mechanisms of ultraviolet radiation-induced DNA damage and repair, *J. Nucleic Acids* 2010 (2010), 592980.
- [8] S.-L. Yu, S.-K. Lee, Ultraviolet radiation: DNA damage, repair, and human disorders, *Mol. Cell. Toxicol.* 13 (2017) 21–28.
- [9] M.J. Smerdon, M.W. Lieberman, Nucleosome rearrangement in human chromatin during UV-induced DNA- repair synthesis, *Proc. Natl. Acad. Sci.* 75 (1978) 4238.
- [10] M.J. Smerdon, DNA repair and the role of chromatin structure, *Curr. Opin. Cell Biol.* 3 (1991) 422–428.
- [11] C.M. Green, G. Almouzni, When repair meets chromatin. First in series on chromatin dynamics, *EMBO Rep.* 3 (2002) 28–33.
- [12] G. Soria, S.E. Polo, G. Almouzni, Prime, repair, restore: the active role of chromatin in the DNA damage response, *Mol. Cell* 46 (2012) 722–734.


- [13] V. Mocquet, J.P. Lainé, T. Riedl, Z. Yajin, M.Y. Lee, J.M. Egly, Sequential recruitment of the repair factors during NER: the role of XPG in initiating the resynthesis step, *EMBO J.* 27 (2008) 155–167.
- [14] L. Guintini, R. Charton, F. Peyresaubes, F. Thoma, A. Conconi, Nucleosome positioning, nucleotide excision repair and photoreactivation in *Saccharomyces cerevisiae*, *DNA Repair* 36 (2015) 98–104.
- [15] C. Terleth, P. Schenk, R. Poot, J. Brouwer, P. van de Putte, Differential repair of UV damage in rad mutants of *Saccharomyces cerevisiae*: a possible function of G2 arrest upon UV irradiation, *Mol. Cell Biol.* 10 (1990) 4678–4684.
- [16] R. Verhage, A.M. Zeeman, N. de Groot, F. Gleig, D.D. Bang, P. van de Putte, J. Brouwer, The RAD7 and RAD16 genes, which are essential for pyrimidine dimer removal from the silent mating type loci, are also required for repair of the nontranscribed strand of an active gene in *Saccharomyces cerevisiae*, *Mol. Cell Biol.* 14 (1994) 6135–6142.
- [17] S. Li, B. Ding, D. LeJeune, C. Ruggiero, X. Chen, M.J. Smerdon, The roles of Rad16 and Rad26 in repairing repressed and actively transcribed genes in yeast, *DNA Repair* 6 (2007) 1596–1606.
- [18] Z. Wang, S. Wei, S.H. Reed, X. Wu, J.Q. Svestrup, W.J. Feaver, R.D. Kornberg, E. C. Friedberg, The RAD7, RAD16, and RAD23 genes of *Saccharomyces cerevisiae*: requirement for transcription-independent nucleotide excision repair in vitro and interactions between the gene products, *Mol. Cell Biol.* 17 (1997) 635–643.
- [19] S.H. Reed, M. Akiyama, B. Stillman, E.C. Friedberg, Yeast autonomously replicating sequence binding factor is involved in nucleotide excision repair, *Genes Dev.* 13 (1999) 3052–3058.
- [20] S. Yu, J.B. Smirnova, E.C. Friedberg, B. Stillman, M. Akiyama, T. Owen-Hughes, R. Waters, S.H. Reed, ABF1-binding sites promote efficient global genome nucleotide excision repair*, *J. Biol. Chem.* 284 (2009) 966–973.
- [21] S.N. Guzder, P. Sung, L. Prakash, S. Prakash, Yeast Rad7-Rad16 complex, specific for the nucleotide excision repair of the nontranscribed DNA strand, is an ATP-dependent DNA damage sensor, *J. Biol. Chem.* 272 (1997) 21665–21668.
- [22] D.D. Bang, R. Verhage, N. Goosen, J. Brouwer, P. van de Putte, Molecular cloning of RAD16, a gene involved in differential repair in *Saccharomyces cerevisiae*, *Nucleic Acids Res.* 20 (1992) 3925–3931.
- [23] S. Yu, K. Evans, P. van Eijk, M. Bennett, R.M. Webster, M. Leadbitter, Y. Teng, R. Waters, S.P. Jackson, S.H. Reed, Global genome nucleotide excision repair is organized into domains that promote efficient DNA repair in chromatin, *Genome Res.* 26 (2016) 1376–1387.
- [24] P. van Eijk, S.P. Nandi, S. Yu, M. Bennett, M. Leadbitter, Y. Teng, S.H. Reed, Nucleosome remodeling at origins of global genome-nucleotide excision repair occurs at the boundaries of higher-order chromatin structure, *Genome Res.* 29 (2019) 74–84.
- [25] S.H. Reed, Z. You, E.C. Friedberg, The yeast RAD7 and RAD16 genes are required for postincision events during nucleotide excision repair. In vitro and in vivo studies with rad7 and rad16 mutants and purification of a Rad7/Rad16-containing protein complex, *J. Biol. Chem.* 273 (1998) 29481–29488.
- [26] S. Yu, T. Owen-Hughes, E.C. Friedberg, R. Waters, S.H. Reed, The yeast Rad7/Rad16/Abf1 complex generates superhelical torsion in DNA that is required for nucleotide excision repair, *DNA Repair* 3 (2004) 277–287.
- [27] C. Han, A.K. Srivastava, T. Cui, Q.E. Wang, A.A. Wani, Differential DNA lesion formation and repair in heterochromatin and euchromatin, *Carcinogenesis* 37 (2016) 129–138.
- [28] Y. Teng, H. Liu, H.W. Gill, Y. Yu, R. Waters, S.H. Reed, *Saccharomyces cerevisiae* Rad16 mediates ultraviolet-dependent histone H3 acetylation required for efficient global genome nucleotide-excision repair, *EMBO Rep.* 9 (2008) 97–102.
- [29] S. Yu, Y. Teng, R. Waters, S.H. Reed, How chromatin is remodelled during DNA repair of UV-induced DNA damage in *Saccharomyces cerevisiae*, *PLoS Genet.* 7 (2011), e1002124.
- [30] D.J. Owen, P. Ornaghi, J.C. Yang, N. Lowe, P.R. Evans, P. Ballario, D. Neuhaus, P. Filetici, A.A. Travers, The structural basis for the recognition of acetylated histone H4 by the bromodomain of histone acetyltransferase gcn5p, *EMBO J.* 19 (2000) 6141–6149.
- [31] T. Agaloti, G. Chen, D. Thanos, Deciphering the transcriptional histone acetylation code for a human gene, *Cell* 111 (2002) 381–392.
- [32] M. Shogren-Knaak, H. Ishii, J.M. Sun, M.J. Pazin, J.R. Davie, C.L. Peterson, Histone H4-K16 acetylation controls chromatin structure and protein interactions, *Science* 311 (2006) 844–847.
- [33] T. Kouzarides, Chromatin modifications and their function, *Cell* 128 (2007) 693–705.
- [34] M.D. Shahbazian, M. Grunstein, Functions of site-specific histone acetylation and deacetylation, *Annu. Rev. Biochem.* 76 (2007) 75–100.
- [35] G.D. Bowman, M.G. Poirier, Post-translational modifications of histones that influence nucleosome dynamics, *Chem. Rev.* 115 (2015) 2274–2295.
- [36] Y. Yu, Y. Teng, H. Liu, S.H. Reed, R. Waters, UV irradiation stimulates histone acetylation and chromatin remodeling at a repressed yeast locus, *Proc. Natl. Acad. Sci. USA* 102 (2005) 8650.
- [37] A. Ray, P. Khan, R. Nag Chaudhuri, Regulated acetylation and deacetylation of H4 K16 is essential for efficient NER in *Saccharomyces cerevisiae*, *DNA Repair* 72 (2018) 39–55.
- [38] A. Ray, P. Khan, R. Nag Chaudhuri, Deacetylation of H4 lysine16 affects acetylation of lysine residues in histone H3 and H4 and promotes transcription of constitutive genes, *Epigenetics* 16 (2021) 597–617.
- [39] T. Jenuwein, C.D. Allis, Translating the histone code, *Science* 293 (2001) 1074–1080.
- [40] E.M. Hyland, M.S. Cosgrove, H. Molina, D. Wang, A. Pandey, R.J. Cottee, J. D. Boeke, Insights into the role of histone H3 and histone H4 core modifiable residues in *Saccharomyces cerevisiae*, *Mol. Cell Biol.* 25 (2005) 10060–10070.
- [41] H. Neumann, S.M. Hancock, R. Buning, A. Routh, L. Chapman, J. Somers, T. Owen-Hughes, J. van Noort, D. Rhodes, J.W. Chin, A method for genetically installing site-specific acetylation in recombinant histones defines the effects of H3 K56 acetylation, *Mol. Cell* 36 (2009) 153–163.
- [42] S. Watanabe, M. Resch, W. Lilestrom, N. Clark, J.C. Hansen, C. Peterson, K. Luger, Structural characterization of H3K56Q nucleosomes and nucleosomal arrays, *Biochim. Biophys. Acta* 1799 (2010) 480–486.
- [43] M. Simon, J.A. North, J.C. Shimko, R.A. Forties, M.B. Ferdinand, M. Manohar, M. Zhang, R. Fishel, J.J. Ottesen, M.G. Poirier, Histone fold modifications control nucleosome unwrapping and disassembly, *Proc. Natl. Acad. Sci.* 108 (2011) 12711.
- [44] J. Lee, T.-H. Lee, How protein binding sensitizes the nucleosome to histone H3K56 acetylation, *ACS Chem. Biol.* 14 (2019) 506–515.
- [45] J. Schneider, P. Bajwa, F.C. Johnson, S.R. Bhaumik, A. Shilatfard, Rtt109 is required for proper H3K56 acetylation: a chromatin mark associated with the elongating RNA polymerase II, *J. Biol. Chem.* 281 (2006) 37270–37274.
- [46] G. Durairaj, P. Chaurasia, S. Lahudkar, S. Malik, A. Shukla, S.R. Bhaumik, Regulation of chromatin assembly/disassembly by Rtt109p, a histone H3 Lys56-specific acetyltransferase, in vivo, *J. Biol. Chem.* 285 (2010) 30472–30479.
- [47] R. Driscoll, A. Hudson, S.P. Jackson, Yeast Rtt109 promotes genome stability by acetylating histone H3 on lysine 56, *Sci. (N. Y.)* 315 (2007) 649–652.
- [48] S. D'Arcy, K. Luger, Understanding histone acetyltransferase Rtt109 structure and function: how many chaperones does it take? *Curr. Opin. Struct. Biol.* 21 (2011) 728–734.
- [49] E. Radovani, M. Cadorin, T. Shams, S. El-Rass, A.R. Karsou, H.-S. Kim, C.F. Kurat, M.-C. Keogh, J.F. Greenblatt, J.S. Fillingham, The carboxyl terminus of Rtt109 functions in chaperone control of histone acetylation, *Eukaryot. Cell* 12 (2013) 654–664.
- [50] L. Zhang, A. Serra-Cardona, H. Zhou, M. Wang, N. Yang, Z. Zhang, R.-M. Xu, Multisite substrate recognition in Asf1-dependent acetylation of histone H3 K56 by Rtt109, *Cell* 174 (2018) 818–830.e811.
- [51] S. Topal, P. Vasseur, M. Radman-Livaja, C.L. Peterson, Distinct transcriptional roles for Histone H3-K56 acetylation during the cell cycle in yeast, *Nat. Commun.* 10 (2019) 4372.
- [52] T. Tsubota, C.E. Berndsen, J.A. Erkmann, C.L. Smith, L. Yang, M.A. Freitas, J. M. Denu, P.D. Kaufman, Histone H3-K56 acetylation is catalyzed by histone chaperone-dependent complexes, *Mol. Cell* 25 (2007) 703–712.
- [53] Y. Tang, M.A. Holbert, N. Delgosaie, H. Wurtele, B. Guillemette, K. Meeth, H. Yuan, P. Drogaris, E.-H. Lee, C. Durette, P. Thibault, A. Verreault, P.A. Cole, R. Marmorstein, Structure of the Rtt109-AcCoA/Vps75 complex and implications for chaperone-mediated histone acetylation, *Structure* 19 (2011) 221–231.
- [54] J.M. Cote, Y.-M. Kuo, R.A. Henry, H. Scherman, D.D. Krzizike, A.J. Andrews, Two factor authentication: Asf1 mediates crosstalk between H3 K14 and K56 acetylation, *Nucleic Acids Res.* 47 (2019) 7380–7391.
- [55] J. Han, H. Zhou, B. Horazdovsky, K. Zhang, R.M. Xu, Z. Zhang, Rtt109 acetylates histone H3 lysine 56 and functions in DNA replication, *Science* 315 (2007) 653–655.
- [56] Q. Li, H. Zhou, H. Wurtele, B. Davies, B. Horazdovsky, A. Verreault, Z. Zhang, Acetylation of histone H3 lysine 56 regulates replication-coupled nucleosome assembly, *Cell* 134 (2008) 244–255.
- [57] M. Clemente-Ruiz, R. González-Prieto, F. Prado, Histone H3K56 acetylation, CAF1, and Rtt106 coordinate nucleosome assembly and stability of advancing replication forks, *PLoS Genet.* 7 (2011), e1002376.
- [58] H. Masumoto, D. Hawke, R. Kobayashi, A. Verreault, A role for cell-cycle-regulated histone H3 lysine 56 acetylation in the DNA damage response, *Nature* 436 (2005) 294–298.
- [59] T. Kaplan, C.L. Liu, J.A. Erkmann, J. Holik, M. Grunstein, P.D. Kaufman, N. Friedman, O.J. Rando, Cell cycle- and chaperone-mediated regulation of H3K56ac incorporation in yeast, *PLoS Genet.* 4 (2008), e1000270.
- [60] C.C. Chen, J.J. Carson, J. Feser, B. Tamburini, S. Zabaronick, J. Linger, J.K. Tyler, Acetylated lysine 56 on histone H3 drives chromatin assembly after repair and signals for the completion of repair, *Cell* 134 (2008) 231–243.
- [61] S.K. Williams, D. Truong, J.K. Tyler, Acetylation in the globular core of histone H3 on lysine-56 promotes chromatin disassembly during transcriptional activation, *Proc. Natl. Acad. Sci. USA* 105 (2008) 9000–9005.
- [62] H. Wurtele, G.S. Kaiser, J. Bacal, E. St-Hilaire, E.-H. Lee, S. Tsao, J. Dorn, P. Maddox, M. Lisby, P. Pasero, A. Verreault, Histone H3 lysine 56 acetylation and the response to DNA replication fork damage, *Mol. Cell Biol.* 32 (2012) 154–172.
- [63] I. Celic, A. Verreault, J.D. Boeke, Histone H3 K56 hyperacetylation perturbs replisomes and causes DNA damage, *Genetics* 179 (2008) 1769–1784.
- [64] N.L. Maas, K.M. Miller, L.G. DeFazio, D.P. Toczyski, Cell cycle and checkpoint regulation of histone H3 K56 acetylation by Hst3 and Hst4, *Mol. Cell* 23 (2006) 109–119.
- [65] A. Simoneau, N. Delgosaie, I. Celic, J. Dai, N. Abshiru, S. Costantino, P. Thibault, J.D. Boeke, A. Verreault, H. Wurtele, Interplay between histone H3 lysine 56 deacetylation and chromatin modifiers in response to DNA damage, *Genetics* 200 (2015) 185–205.
- [66] J. Yuan, M. Pu, Z. Zhang, Z. Lou, Histone H3-K56 acetylation is important for genomic stability in mammals, *Cell Cycle (Georget. Tex.)* 8 (2009) 1747–1753.
- [67] S. Muñoz-Galván, S. Jimeno, R. Rothstein, A. Aguilera, Histone H3K56 acetylation, Rad52, and non-DNA repair factors control double-strand break repair choice with the sister chromatid, *PLoS Genet.* 9 (2013), e1003237.
- [68] Y. Teng, Y. Yu, R. Waters, The *Saccharomyces cerevisiae* histone acetyltransferase Gcn5 has a role in the photoreactivation and nucleotide excision repair of UV-

- induced cyclobutane pyrimidine dimers in the MFA2 gene, *J. Mol. Biol.* 316 (2002) 489–499.
- [69] R. Guo, J. Chen, D.L. Mitchell, D.G. Johnson, GCN5 and E2F1 stimulate nucleotide excision repair by promoting H3K9 acetylation at sites of damage, *Nucleic Acids Res.* 39 (2011) 1390–1397.
- [70] M.R. Duan, M.J. Smerdon, Histone H3 lysine 14 (H3K14) acetylation facilitates DNA repair in a positioned nucleosome by stabilizing the binding of the chromatin Remodeler RSC (Remodels Structure of Chromatin), *J. Biol. Chem.* 289 (2014) 8353–8363.
- [71] Q. Li, A.M. Fazly, H. Zhou, S. Huang, Z. Zhang, B. Stillman, The elongator complex interacts with PCNA and modulates transcriptional silencing and sensitivity to DNA damage agents, *PLoS Genet.* 5 (2009), e1000684.
- [72] R.J. Burgess, H. Zhou, J. Han, Z. Zhang, A role for Gcn5 in replication-coupled nucleosome assembly, *Mol. Cell* 37 (2010) 469–480.
- [73] C.A. Davey, D.F. Sargent, K. Luger, A.W. Maeder, T.J. Richmond, Solvent mediated interactions in the structure of the nucleosome core particle at 1.9 Å resolution, *J. Mol. Biol.* 319 (2002) 1097–1113.
- [74] T.J. Richmond, C.A. Davey, The structure of DNA in the nucleosome core, *Nature* 423 (2003) 145–150.
- [75] A. Ozdemir, S. Spicuglia, E. Lasonder, M. Vermeulen, C. Campsteijn, H. G. Stunnenberg, C. Logie, Characterization of lysine 56 of histone H3 as an acetylation site in *Saccharomyces cerevisiae*, *J. Biol. Chem.* 280 (2005) 25949–25952.
- [76] K.M. Miller, J.V. Tjeertes, J. Coates, G. Legube, S.E. Polo, S. Britton, S.P. Jackson, Human HDAC1 and HDAC2 function in the DNA-damage response to promote DNA nonhomologous end-joining, *Nat. Struct. Mol. Biol.* 17 (2010) 1144–1151.
- [77] R.K. Vempati, R.S. Jayani, D. Notani, A. Sengupta, S. Galande, D. Haldar, p300-mediated acetylation of histone H3 lysine 56 functions in DNA damage response in mammals, *J. Biol. Chem.* 285 (2010) 28553–28564.
- [78] A. Battu, A. Ray, A.A. Wani, ASF1A and ATM regulate H3K56-mediated cell-cycle checkpoint recovery in response to UV irradiation, *Nucleic Acids Res.* 39 (2011) 7931–7945.
- [79] J. Che, S. Smith, Y.J. Kim, E.Y. Shim, K. Myung, S.E. Lee, Hyper-acetylation of histone H3K56 limits break-induced replication by inhibiting extensive repair synthesis, *PLoS Genet.* 11 (2015), e1004990.
- [80] J. Chen, Z. Wang, X. Guo, F. Li, Q. Wei, X. Chen, D. Gong, Y. Xu, W. Chen, Y. Liu, J. Kang, Y. Shi, TRIM66 reads unmodified H3R2K4 and H3K56ac to respond to DNA damage in embryonic stem cells, *Nat. Commun.* 10 (2019) 4273.
- [81] R. Nag, F. Gong, D. Fahy, M.J. Smerdon, A single amino acid change in histone H4 enhances UV survival and DNA repair in yeast, *Nucleic Acids Res.* 36 (2008) 3857–3866.
- [82] R.E. Wellinger, F. Thoma, Nucleosome structure and positioning modulate nucleotide excision repair in the non-transcribed strand of an active gene, *EMBO J.* 16 (1997) 5046–5056.
- [83] M.J. Smerdon, J. Bedoyan, F. Thoma, DNA repair in a small yeast plasmid folded into chromatin, *Nucleic Acids Res.* 18 (1990) 2045–2051.
- [84] F. Gong, D. Fahy, M.J. Smerdon, Rad4-Rad23 interaction with SWI/SNF links ATP-dependent chromatin remodeling with nucleotide excision repair, *Nat. Struct. Mol. Biol.* 13 (2006) 902–907.
- [85] R. Nag, M. Kyriss, J.W. Smerdon, J.J. Wyrick, M.J. Smerdon, A cassette of N-terminal amino acids of histone H2B are required for efficient cell survival, DNA repair and Swi/Snf binding in UV irradiated yeast, *Nucleic Acids Res.* 38 (2010) 1450–1460.
- [86] Y. Yu, Y. Deng, S.H. Reed, C.B. Millar, R. Waters, Histone variant Htz1 promotes histone H3 acetylation to enhance nucleotide excision repair in Htz1 nucleosomes, *Nucleic Acids Res.* 41 (2013) 9006–9019.
- [87] L. Zhang, K. Jones, M.J. Smerdon, F. Gong, Assays for chromatin remodeling during nucleotide excision repair in *Saccharomyces cerevisiae*, *Methods (San. Diego Calif.)* 48 (2009) 19–22.
- [88] S. Yu, Y. Teng, N.F. Lowndes, R. Waters, RAD9, RAD24, RAD16 and RAD26 are required for the inducible nucleotide excision repair of UV-induced cyclobutane pyrimidine dimers from the transcribed and non-transcribed regions of the *Saccharomyces cerevisiae* MFA2 gene, *Mutat. Res./DNA Repair* 485 (2001) 229–236.
- [89] L.J. Long, P.H. Lee, E.M. Small, C. Hillyer, Y. Guo, M.A. Osley, Regulation of UV damage repair in quiescent yeast cells, *DNA Repair* 90 (2020), 102861.
- [90] A.J. Hodges, D.A. Plummer, J.J. Wyrick, NuA4 acetyltransferase is required for efficient nucleotide excision repair in yeast, *DNA Repair* 73 (2019) 91–98.
- [91] M.J. Smerdon, S.Y. Lan, R.E. Calza, R. Reeves, Sodium butyrate stimulates DNA repair in UV-irradiated normal and xeroderma pigmentosum human fibroblasts, *J. Biol. Chem.* 257 (1982) 13441–13447.
- [92] B. Ramanathan, M.J. Smerdon, Enhanced DNA repair synthesis in hyperacetylated nucleosomes, *J. Biol. Chem.* 264 (1989) 11026–11034.
- [93] M.R. Duan, M.J. Smerdon, UV damage in DNA promotes nucleosome unwrapping, *J. Biol. Chem.* 285 (2010) 26295–26303.
- [94] I. Fu, N.E. Geacintov, S. Broyde, Molecular dynamics simulations reveal how H3K56 acetylation impacts nucleosome structure to promote DNA exposure for lesion sensing, *DNA Repair* 107 (2021), 103201.
- [95] K.A. Bohm, A.J. Hodges, W. Czaja, K. Selvam, M.J. Smerdon, P. Mao, J.J. Wyrick, Distinct roles for RSC and SWI/SNF chromatin remodelers in genomic excision repair, *Genome Res.* 31 (2021) 1047–1059.
- [96] C.B. Brachmann, J.M. Sherman, S.E. Devine, E.E. Cameron, L. Pillus, J.D. Boeke, The SIR2 gene family, conserved from bacteria to humans, functions in silencing, cell cycle progression, and chromosome stability, *Genes Dev.* 9 (1995) 2888–2902.
- [97] M. Toussaint, G. Levasseur, J. Gervais-Bird, R.J. Wellinger, S.A. Elela, A. Conconi, A high-throughput method to measure the sensitivity of yeast cells to genotoxic agents in liquid cultures, *Mutat. Res.* 606 (2006) 92–105.
- [98] V.A. Bepalov, A. Conconi, X. Zhang, D. Fahy, M.J. Smerdon, Improved method for measuring the ensemble average of strand breaks in genomic DNA, *Environ. Mol. Mutagen.* 38 (2001) 166–174.
- [99] J. Yang, X. Zhang, J. Feng, H. Leng, S. Li, J. Xiao, S. Liu, Z. Xu, J. Xu, D. Li, Z. Wang, J. Wang, Q. Li, The histone chaperone FACT contributes to DNA replication-coupled nucleosome assembly, *Cell Rep.* 14 (2016) 1128–1141.
- [100] M.C. Schultz, D.J. Hockman, T.A.A. Harkness, W.I. Garinther, B.A. Altheim, Chromatin assembly in a yeast whole-cell extract, *Proc. Natl. Acad. Sci.* 94 (1997) 9034–9039.

RESEARCH PAPER



Deacetylation of H4 lysine16 affects acetylation of lysine residues in histone H3 and H4 and promotes transcription of constitutive genes

Anagh Ray , Preeti Khan, and Ronita Nag Chaudhuri

Department of Biotechnology, St. Xavier's College, Kolkata, India

ABSTRACT

Histone modification map of H4 N-terminal tail residues in *Saccharomyces cerevisiae* reveals the prominence of lysine acetylation. Previous reports have indicated the importance of lysine acetylation in maintaining chromatin structure and function. H4K16, a residue with highly regulated acetylation dynamics has unique functions not overlapping with the other H4 N-terminal acetylatable residues. The present work unravels the role of H4K16 acetylation in regulating expression of constitutive genes. H4K16 gets distinctly deacetylated over the coding region of constitutively expressed genes. Deacetylation of H4K16 reduces H3K9 acetylation at the cellular and gene level. Reduced H3K9 acetylation however did not negatively correlate with active gene transcription. Significantly, H4K16 deacetylation was found to be associated with hypoacetylated H4K12 throughout the locus of constitutive genes. H4K16 and K12 deacetylation is known to favour active transcription. *Sas2*, the HAT mutant showed similar patterns of hypoacetylated H3K9 and H4K12 at the active loci, clearly implying that the modifications were associated with deacetylation state of H4K16. Deacetylation of H4K16 was also concurrent with increased H3K56 acetylation in the promoter region and ORF of the constitutive genes. Combination of all these histone modifications significantly reduced H3 occupancy, increased promoter accessibility and enhanced RNAPII recruitment at the constitutively active loci. Consequently, we found that expression of active genes was higher in H4K16R mutant which mimic deacetylated state, but not in H4K16Q mimicking constitutive acetylation. To summarize, H4K16 deacetylation linked with H4K12 and H3K9 hypoacetylation along with H3K56 hyperacetylation generate a chromatin landscape that is conducive for transcription of constitutive genes.

ARTICLE HISTORY

Received 5 April 2020

Revised 2 July 2020

Accepted 24 July 2020

KEYWORDS

H4K16; histone acetylation; transcription; constitutive genes; H4K12; H3K56; H3K9

Introduction

Functional fidelity of an eukaryotic genome is essentially maintained by regulated dynamism in chromatin. Post translational modifications of histones play a vital role in contributing to the flexibility of chromatin structure and function. In this context 'histone code hypothesis' has long proposed how an interplay of different histone modifications in various combinations forms the platform for chromatin changes during a nuclear process [1–4]. The 'access-repair-restore' (ARR) model put forth decades back in context of DNA damage repair, holds true for any DNA metabolic process like transcription or replication [5]. It emphasizes how timely modulation in chromatin structure makes DNA accessible or refractory to nuclear factors during a DNA metabolic process. This is a critical parameter that decides the

proficiency of any DNA-dependent phenomenon like transcription, its initiation as well as regenerating the chromatin after completion of the process. An important modification that affects chromatin structure is acetylation of lysine residues that alters histone-DNA interactions and often facilitates recruitment of trans-factors that recognize acetylated lysines [4,6–10].

The histone H4 N-terminal tail has 4 acetylatable lysine residues, namely, lysine 5 (H4K5), lysine 8 (H4K8), lysine 12 (H4K12) and lysine 16 (H4K16). Of these residues only H4K16 is known not to get methylated by virtue of its position [11–13]. Lysine 16 of histone H4 N-terminal tail is a key player amongst the acetylatable histone residues that actively contributes to the fidelity of chromatin structure [9,14,15]. Consequently acetylation status of H4 K16 affects several nuclear functions such as gene silencing [16–21], DNA repair

[22,23] and transcription [24–30]. In yeast, Hos2 mediated deacetylation of H4K16 is known to be required for active transcription [29]. Earlier reports further indicate that deacetylation of H4K16 is a marker of human cancer and is correlated with reduced levels of DNA methylation [31].

The chromatin environment of constitutively transcribed genes and the mode of their expression regulation is still not well understood. The current definitions of genes as constitutive or inducible do not include their regulatory state with respect to their position in chromatin domains. In *Saccharomyces cerevisiae* based on their activity and design of regulatory elements, genes are broadly classified into ‘growth genes’ or ‘house-keeping’ genes, that have constant levels of expression, encode ribosomal proteins, rRNA-processing enzymes, glycolytic enzymes and other factors required for rapid biomass production and ‘stress genes’ that have low levels of transcription under normal conditions but are induced to express at high levels under any form of stress [32]. Transcription initiation in chromatin context is known to

be initiated by formation of the pre-initiation complex (PIC), comprising of RNA Pol II and general transcription factors (TFIID/A/B/E/H) at the core promoter element aided by binding of activators to enhancers and recruitment of adaptor complexes SAGA and/or Mediator [33–37]. Earlier classifications considered housekeeping genes to be lacking TATA boxes, having a well-defined NFR upstream of coding region and regulated by TFIID without aid of chromatin regulators like SAGA, while inducible genes contain TATA boxes and required the action of SAGA for access of TBP to promoters that remain occluded by nucleosomes [32,38,39]. SAGA dominated genes were thought to be predominantly inducible and TFIID was considered to have a more housekeeping role. Inducible gene promoters were known to have more extensive chromatin regulation for successful transcription under inducible conditions [32,40]. Parallel studies however, also depict that over 99% of the measurable genome is positively regulated by the overlapping involvement of both TFIID and SAGA [39,41]. Additionally SAGA seems to get recruited to both TFIID and SAGA

dominated promoters, irrespective of the presence of TATA box, signifying that SAGA acts as a general cofactor required for essentially all RNA polymerase II transcription [42,43]. The presence or absence of TATA box was rather found to affect the prevalence of histone modifications associated with transcription [44]. The above studies have brought into perspective a different mode of classification of constitutive and inducible gene regulation that does not depend solely on TFIID or SAGA recruitment or presence or absence of TATA box in the gene promoters.

With this backdrop study on transcription of constitutive genes based on the combination of histone modifications that aids the process in a chromatin environment becomes an important avenue of investigation. Here we show that in *Saccharomyces cerevisiae*, deacetylation of H4K16 enhances transcription of constitutively expressed genes. Loss of acetylation in H4K16 was found to affect acetylation status of neighbouring lysine residues in H4 N-terminal tail and in the tail and core residues of histone H3 which enhanced promoter accessibility and RNA Pol II recruitment. This work thus sheds light on how deacetylation of H4K16 positively correlates with constitutive gene expression, due to an overall combinatorial effect of associated histone modifications that favour the process of transcription in the chromatin milieu of an eukaryotic cell.

Results

To understand the role of H4 K16 acetylation in transcription, studies were done with two histone mutant strains of yeast. One mutant strain H4 K16R has K16 of H4 mutated to

arginine (R), to mimic the unacetylatable state of lysine 16. The other mutant strain H4 K16Q has K16 of H4 mutated to glutamine (Q), to mimic constitutively acetylated state of lysine. Thereafter comparative studies were done in wild type and the two H4K16 mutants to understand the effect of H4K16 acetylation and associated chromatin modifications on transcription of constitutively expressed genes.

For the present study, six genes located on different chromosomes and having different physiological functions were chosen such that their level

of expression would be constant throughout the cell cycle. *PYK1* (*YAL038 W*), on chromosome I codes for pyruvate kinase which catalyses the final step of glycolysis i.e., conversion of phosphoenolpyruvate to pyruvate [45–47]. *TFC1* (*YBR123 C*), on chromosome II codes for the transcription factor Tau, one of the six subunits of the RNA polymerase III transcription initiation complex (TFIIIC) [48,49]. *TAF10* (*YDR167W*), on chromosome IV codes for a TATA-binding-protein associated factor that is a subunit of the TFIID and the SAGA complex, both of which are required for the formation of the RNA polymerase II transcription initiation complex [34–37,50–52]. *UBC6* (*YER100W*), on chromosome V codes for a ubiquitin conjugating enzyme (E2) present on the cytosolic membrane of the endoplasmic reticulum (ER), which functions in the ER associated proteasomal degradation (ERAD) pathway of misfolded proteins [53,54]. *ACT1* (*YFL039C*), on chromosome VI encodes the single gene for the formation of yeast actin, which is a ubiquitous

structural protein, conserved for various cytoskeletal functions like polarization of cell growth [55,56]. *RPB2* (*YOR151 C*), on chromosome XV encodes the second largest subunit of the RNA polymerase II core enzyme, the absence or mutation of which leads to non-assembly of the core complex [57].

Deacetylation of H4K16 promotes transcription of constitutively expressed genes

To check the effect of H4K16 acetylation on expression of constitutive genes, RT- qPCR based study was done. Comparative transcription analyses of six genes, *PYK1*, *TFC1*, *TAF10*, *UBC6*, *ACT1* and *RPB2*, were done in wild type, H4K16R and H4K16Q cells. Results indicate that expression of these genes was significantly higher in H4K16R mutants, compared to wild type and H4K16Q (Figure 1(a)). In H4K16Q cells, level of gene expression was rather distinctly reduced compared to wild type. Previous studies have

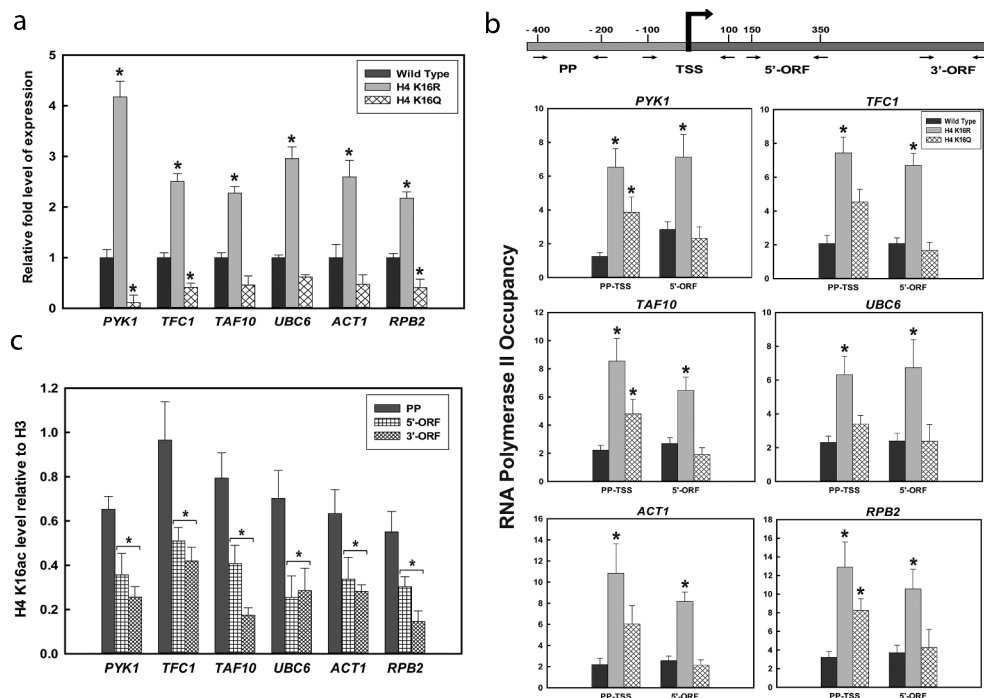


Figure 1. Constitutive Gene Expression in H4K16 mutants and the status of H4K16 acetylation during transcription. (a) RNA was isolated from wild type and H4 K16 mutant strains, followed by RT-qPCR to check expression of six constitutively active genes- *PYK1*, *TFC1*, *TAF10*, *UBC6*, *ACT1* and *RPB2*. ChIP analyses with (b) RNAPII antibody to check recruitment at the promoter, TSS (PP-TSS) and 5' end (5'-ORF) (c) anti-acetyl H4K16 antibody in wild type cells to check the level of acetylation at the promoter proximal region (PP), 5' end (5'-ORF) and 3' end (3'-ORF) of the constitutively transcribing genes mentioned above. The H4K16 acetylation levels were normalized to ChIP data of the same regions with anti-H3 antibody and graphically plotted. Data represent the mean for three independent experiments with standard error of mean bars and asterisks indicate *t*-test significant *P* values < 0.05.

shown that H4K16 acetylation in gene bodies is anticorrelated with transcription and presence of the mark towards 3'-ORF regions are transcription independent [58]. These observations suggest that deacetylation of H4K16 promotes active gene transcription and acetylation of the residue has a negative

correlation with the event. This was further correlated with RNAPII recruitment in the regions covering promoter and transcription start site (TSS) and 5'-ORF of the active genes, using specific antibody in a ChIP-based assay. It was very evident from our results that in the H4K16R mutant, both around the TSS and the 5' end of coding region RNAPII recruitment was significantly enhanced compared to wild type (Figure 1(b)). H4K16Q however had higher RNAPII recruitment than wild type in the promoter region but not in the 5'-ORF. This strengthens the earlier observation that transcription related events are favoured in absence of H4K16 acetylation. Thereafter, state of H4K16 acetylation was checked in wild type cells at the promoter proximal region and gene body of the above-mentioned loci using antibody against acetylated H4K16 followed by qPCR. Results indicated that H4K16 acetylation decreased significantly in the coding region of these genes compared to the promoter region (Figure 1(c)). This clearly indicate that reduction in H4K16 acetylation was required for transcription of the constitutively expressing genes. Our observations find support with the previous report that Hos2-mediated deacetylation of H4K16 is required for transcription activation [29]. Similar patterns of acetylated H4K16 at promoters followed by hypoacetylation at the gene body have also emerged from genome wide histone modification map of *Drosophila* [59]. From the above results it is thus evident that deacetylation of H4K16 promotes transcription of constitutively expressed genes.

Cellular levels of histone acetylation in wild-type and H4K16 mutants

With an aim to understand the effect of H4K16 deacetylation on transcription of constitutive genes, cellular level acetylation of certain histone residues was next checked. In the H4 N-terminal

tail, there are several acetylatable histone lysine residues neighbouring H4K16. Among these, acetylation of H4K8 and K12 has been related to transcription. Acetylation of H4K8 in mammals has been shown to be required for binding of bromodomain containing proteins which function as co-activators and aid in the process of transcription activation [60]. In actively transcribing genes Hos2-mediated deacetylation of H4K12 is known to occur predominantly at the coding region [29]. To check H4K8 and K12 acetylation in wild-type and H4K16 mutants at the whole cell level, immunoblot assays were done with protein extracted from wild type, H4K16R and K16Q cells. As shown in Figure 2, levels of H4K12 and K8 acetylation were similar in wild type and H4K16 mutants. When compared to the H3 levels in all the three strains, it was evident that H4 K8 and K12 acetylation levels had no significant difference between wild-type, H4K16R and K16Q mutants. The above observations indicate that constitutive acetylation or deacetylation of H4K16 do not differentially affect

H4K8 and K12 acetylation at cellular level. Hereafter, acetylation level of another lysine residue H3K9 was compared in wild type and H4K16 mutant cells. H3K9 acetylation is known to be enriched in the promoter and around the TSS region of actively transcribing genes and promotes mammalian RNA Pol II towards transcription elongation [43,61]. When cellular levels of H3K9 acetylation was checked in wild-type and H4K16 mutants, it was observed that acetylation was lower in H4K16R compared to wild type and H4K16Q (Figure 2). Such an observation indicated that deacetylation of H4K16 do not favour H3K9 acetylation. This observation is in consonance with an earlier report that has shown that Gcn5 the HAT responsible for acetylation of H3K9, prefers binding to acetylated H4K16 *in vitro* [62]. Notably, even with lower H3K9 acetylation levels transcription of constitutive genes was not impeded but was rather higher in H4K16R cells, compared to wild type and H4K16Q.

Deacetylated state of H4K16 affects H3K9 acetylation at gene level

To further investigate, acetylation level of H3K9 was thereafter checked in the six constitutively

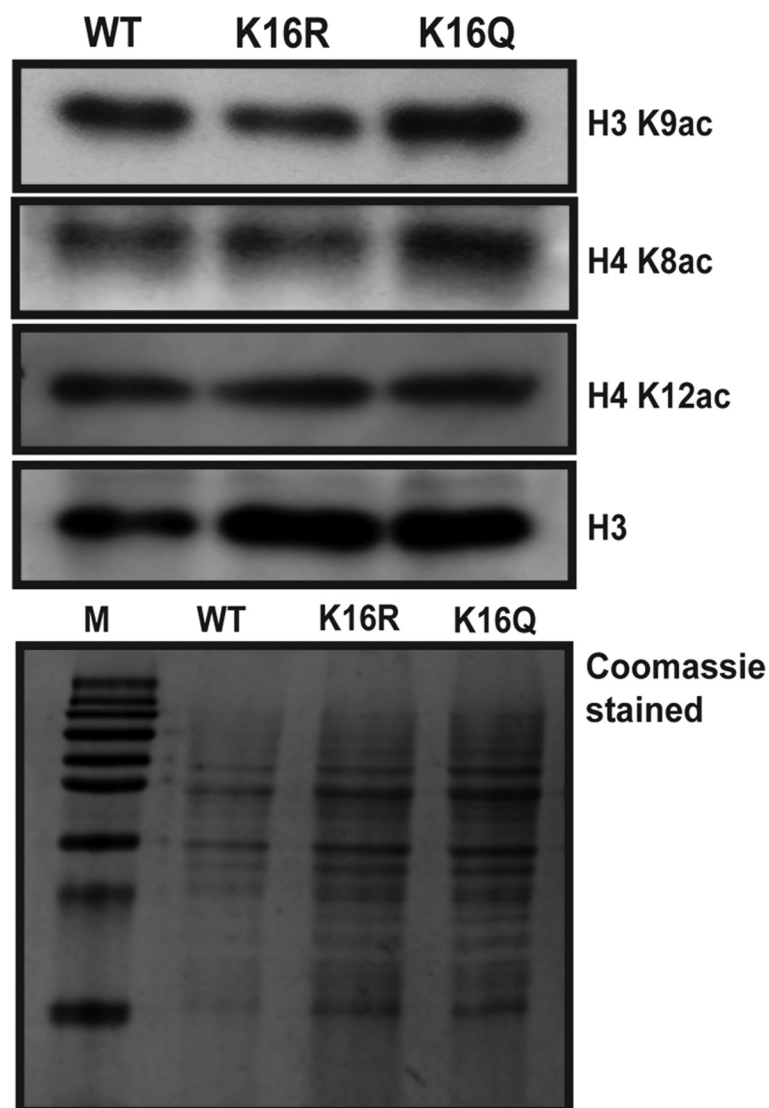


Figure 2. Cellular level acetylation of histone H3 and H4 residues. Total protein was isolated from wild type (WT) and H4K16 mutant (K16R and K16Q) cells. Equal amount of protein from each strain was resolved in 15% SDS-PAGE and immunoblotted with antibodies against H3K9ac, H4K8ac, H4K12ac and H3, respectively. Membrane was incubated with horseradish peroxidase (HRP) – conjugated secondary antibody, treated with a chemiluminescent substrate and exposed to autoradiograph film for visualization.

expressing genes namely, *PYK1*, *TFC1*, *TAF10*, *UBC6*, *ACT1* and *RPB2*, whose transcription was tested. For this, ChIP-qPCR was done using antibody against acetylated H3K9 and primers specific to promoter, TSS and ORF regions of the genes (Figure 3(a)). As shown in Figure 3(b), in all the six genes tested, H3K9 acetylation levels were found to be distinctly reduced in H4K16R mutant, compared to wild type and H4K16Q. Lower H3K9 acetylation was found in the promoter and TSS region as well in the ORF of the genes. This observation is in continuity with the reduced cellular levels of H3K9 acetylation found in H4K16R cells,

compared to wild type and H4K16Q (Figure 2). To further confirm that reduced H3K9 acetylation was an effect of deacetylation of H4K16 (as H4K16R represents a constitutively deacetylated state of H4K16), *Sas2* – a HAT responsible for acetylation of H4K16 residue was deleted. When tested, H3K9 acetylation level in H4K16R and *Sas2* mutant was found to be similarly reduced compared to wild type and H4K16Q cells (Figure 3(b)). Interestingly, these observations further indicate that in constitutively active loci despite reduced H3K9 acetylation, relatively higher levels of gene expression were found in H4K16R compared to

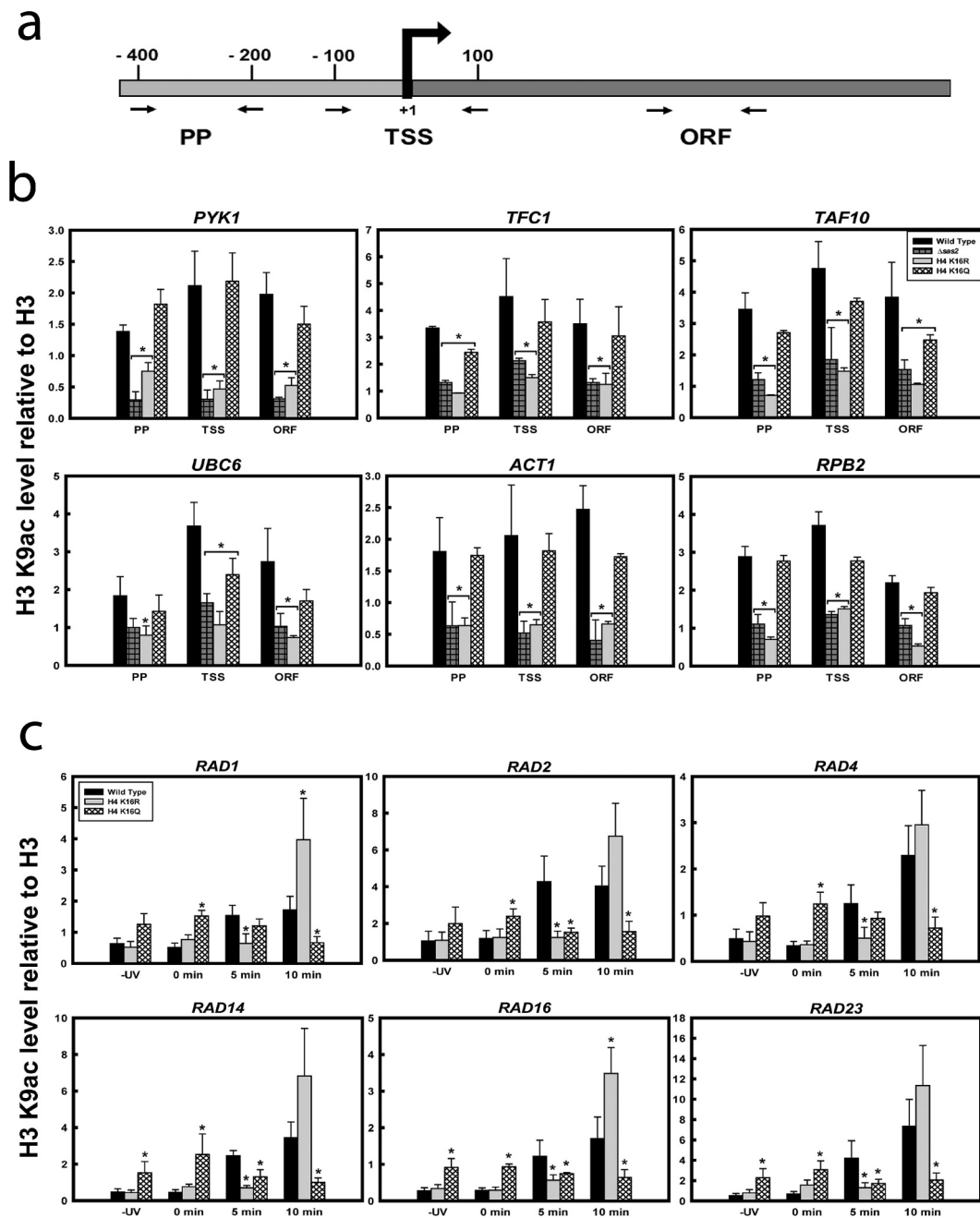


Figure 3. H3K9 acetylation in wild-type and H4K16 mutants at the gene level. ChIP q-PCR analyses on chromatin isolated from wild type and the H4K16 mutant strains treated with or without UV radiation at 100 J/m² followed by repair incubation for 5 or 10 min respectively, with anti-acetyl H3K9 antibody. (a) Schematic showing primers used for ChIP-qPCR, specific to promoter proximal region (PP), transcription start site (TSS) and mid ORF region (ORF) of genes. The levels of H3K9 acetylation in wild-type and H4K16 mutant cells were normalized to ChIP data of the same regions with anti-H3 antibody and graphically plotted to represent (b) constitutively expressing genes or (c) around the promoter and TSS region of UV-inducible genes. Data represent the mean for three independent experiments with standard error of mean bars and asterisks indicate *t*-test significant *P* values < 0.05.

wild type and H4K16Q. To further understand the correlation between transcription and H3K9 acetylation, modification level was checked in six UV responsive genes, *RAD1*, *RAD2*, *RAD4*, *RAD14*, *RAD16* and *RAD23* under inducible conditions. For this, chromatin was isolated from all three

kinds of cells treated with or without UV irradiations of 100 J/m² and allowed to repair for 5 min or 10 min, respectively, followed by immunoprecipitation with anti-acetyl H3K9 antibody. Earlier we had shown that expression of these UV-inducible NER responsive genes was reduced in H4K16 mutants

and the proteins showed a delayed recruitment at the NER site compared to wild type [23]. Present results indicate that at the six inducible loci during early transcription induction (5 min), H3K9 acetylation levels were low in H4K16R cells, compared to wild type. The acetylation levels however increased at later time points post-UV-irradiation (Figure 3(c)). In contrast, H3K9 acetylation levels did not vary in the H4K16Q cells pre- and post-induction. Notably, this was different from the pattern exhibited by wild type and H4K16R cells, both of which exhibited increased H3K9 acetylation following 5 min of transcription induction compared to the pre-induction level. Thus, in H4K16Q, H3K9 acetylation levels were higher than both wild type and H4K16R before transcription induction but reduced after UV irradiation. The exact reason for such constant H3K9 acetylation levels in H4K16Q cells before and after transcription induction needs to be further elucidated. A previous study [63] has reported that H4K16R mutation causes upregulation of genes, especially of those that are regulated by chromatin. As expression of inducible genes is more intricately controlled by chromatin regulation an increase in H3K9 acetylation may be essential for the process. Hence unlike constitutive genes, for inducible gene expression a delayed but distinct increase in H3K9 acetylation was observed in the H4K16R cells. A constitutive hypoacetylation of H3K9 in inducible loci would possibly have graver effect on transcription of such genes, compared to what was observed for constitutive genes. In this context it has been previously shown that transcription initiation from inducible promoters requires recruitment of SAGA, the complex that includes Gcn5- although such recruitment may or may not depend on HAT activity of the complex [64,65]. To sum up, it thus becomes evident that when H4K16 is constitutively deacetylated lower H3K9 acetylation levels do not affect expression of constitutive genes. However, constitutive deacetylation of H4K16 cannot evade the requirement of H3K9 acetylation for expression of inducible genes.

H4K16 acetylation state affects acetylation of other H4 N-terminal lysine residues

To further understand the correlation between H4K16 acetylation dynamics and chromatin

regulation during transcription of constitutively expressing genes, the acetylation levels of H4 N-terminal lysine residues 8 and 12, was next checked at the gene level. ChIP- qPCR was done using antibodies against H4K8ac and H4K12ac, respectively followed by qPCR with primers spanning the promoter region and ORF of the six constitutively active genes mentioned above. H4K8 acetylation in both the H4K16 mutants and *Sas2* was found to be higher compared to wild type, in the promoter region as well as over the gene body (Figure 4(a)). Previously, it has been reported that H4K8 is the second-most redundantly acetylated H4 N-terminal lysine residue which gets acetylated in a transcription independent manner in yeast [58,63]. H4K8 acetylation in the mid and 3'-ORF regions of genes have been found to be either uncorrelated or anticorrelated with transcriptional activity in yeast genome [27,58]. Our observation of higher levels of H4K8 acetylation in both H4K16R and H4K16Q cells compared to wild type are in corroboration with the earlier reports of redundant H4K8 acetylation. It seems that irrespective of the deacetylated state of H4K16(R) which promotes transcription or the acetylated state of H4K16(Q) where transcription is hindered, H4K8 is apparently independently acetylated in a redundant manner. Hereafter, H4K12 acetylation level was checked at the constitutive loci. As shown in Figure 4(b), for all the genes tested, H4K16R mutants have reduced level of H4K12 acetylation compared to wild type and H4K16Q. The difference was especially evident in the promoter region, where H4K12 acetylation in the H4K16R cells was significantly lower than wild type and H4K16Q. While in wild type H4K12 acetylation gradually reduced over the gene body compared to promoter region, in H4K16R mutants H4K12 acetylation levels were low even at the promoter region and remained hypoacetylated in the 5' ORF regions, as well. *Sas2* mutant showed a similar pattern of reduced H4K12 acetylation in the promoter region and 5'ORF, compared to wild type. Unlike H4K16R and *Sas2* mutants, H4K16Q cells did not show significantly reduced H4K12 acetylation level in the promoter or 5' ORF regions, compared to wild type. As deacetylated H4K12 has been correlated with transcriptional activity [29] increased H4K12

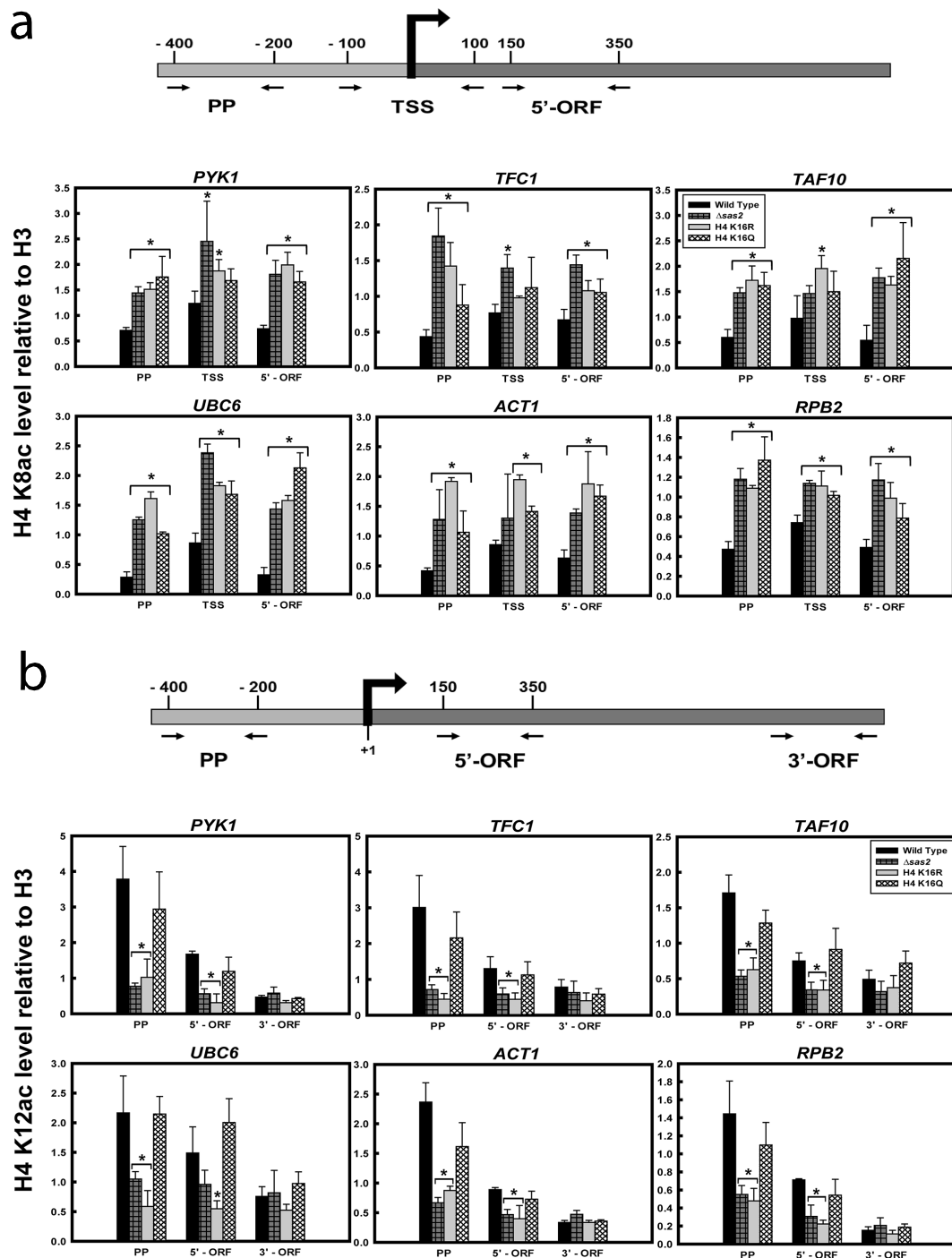


Figure 4. H4 K8 and K12 acetylation in wild type and H4K16 mutants at the gene level. ChIP-qPCR analyses with (a) anti-acetyl H4K8 antibody to check the level of acetylation at the promoter proximal region (PP), transcription start site (TSS) and 3' end of the ORFs (3'-ORF); (b) anti-acetyl H4K12 antibody to check the level of acetylation at the promoter proximal region (PP), 5' end (5'-ORF) and 3' end (3'-ORF) of the ORFs of the constitutively transcribing genes mentioned above. The values were normalized to ChIP data of the same regions with anti-H3 antibody and graphically plotted to represent levels of H4 K8 and K12 acetylation in wild type and H4K16 mutant cells. Data represent the mean for three independent experiments with standard error of mean bars and asterisks indicate t -test significant P values < 0.05 .

hypoacetylation in H4K16R than H4K16Q, especially at promoter region of constitutive genes may rationalize why gene expression is favoured in H4K16R compared to H4K16Q. Thus,

a differential level of H4K12 acetylation is evident not only between wild type and H4K16R cells, but also between the two H4K16 mutants. As Hos2 mediated deacetylation of H4 K16 and K12 is

essential for transcription activation, increased hypoacetylation of H4K12 in H4K16R mutants may provide a more conducive landscape for constitutive gene expression.

Deacetylation of H4K16 promotes acetylation of H3K56 residue

Acetylation of another histone H3 residue K56 is a hallmark for several DNA metabolic activities like replication, DNA damage repair and transcription that essentially involves nucleosome assembly and disassembly [66–75]. This residue located at the entry-exit point of the DNA in a nucleosome is preferentially acetylated at the expressing loci and has been implicated as a marker of transcription activation [71,72,74–76]. Next aim therefore was to understand whether H4K16 acetylation which contributes to chromatin structure and plays a

role in metabolic functions like DNA repair and gene expression, has any correlation with H3K56 acetylation. ChIP-qPCR results clearly indicated significantly enhanced levels of H3K56 acetylation in the H4K16R mutant compared to wild type (Figure 5). The higher levels of H3K56 acetylation in H4K16R was especially significant around the

promoter and TSS region and was also prominent over the gene body. H4K16Q on the other hand was found to have H3K56 acetylation levels similar to wild type. From the above results it therefore becomes apparent that H4K16 deacetylation is associated with increased levels of H3K56 acetylation as observed in H4K16R cells. Whether activity of Rtt109, the primary HAT involved in H3K56 acetylation in yeast [74,75], is directly linked with H4K16 acetylation status needs to be pursued in future.

H3 occupancy and promoter accessibility in H4K16R cells

Earlier works have reported that H3K56 acetylation promotes high rate of histone exchange, especially prevalent near the nucleosome-free regions found at promoter sequences of both housekeeping and inducible genes and also facilitates RNA Pol II distribution along the expressing locus [70,71,74,75]. It has been further shown that absence of Rtt109 – the designated HAT, negatively affects eviction of histone H3, resulting in reduced RNAPII recruitment and decreased gene expression [74,75]. In this context, we hereafter checked histone occupancy in the active loci of

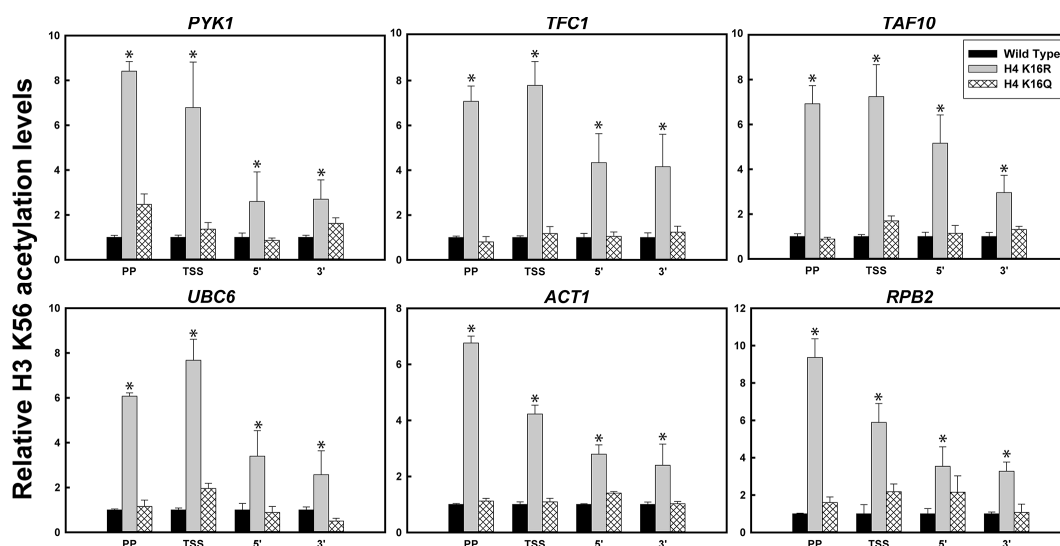


Figure 5. H3K56 acetylation pattern in H4K16 mutants. ChIP-qPCR analyses with anti-acetyl H3K56 antibody to check H3K56 acetylation pattern in transcriptionally active loci at the promoter proximal region (PP), transcription start site (TSS), 5' end (5'-ORF) and 3' end (3'-ORF) of the ORFs of the constitutively active genes. The values were normalized to ChIP data of the same regions with anti-H3 antibody and graphically plotted to represent levels of H3K56 acetylation in H4K16 mutant cells relative to wild type. Data represent the mean for three independent experiments with standard error of mean bars and asterisks indicate *t*-test significant *P* values < 0.05.

wild type and H4K16 mutant cells. ChIP assay with anti-H3 antibody followed by qPCR at the six constitutively expressing loci indicated that H4K16R cells have distinctly reduced H3 occupancy at the promoter region, compared to wild type and H4K16Q (Figure 6(a)). The difference was significant primarily in the promoter region and was not conspicuous over the gene body. This is consonance with previous reports that Rtt109 mediated acetylation of H3K56 is required for histone H3 eviction and RNAPII recruitment at the promoter region of active genes [74,75]. Overall, our results indicate that deacetylation of H4K16 residue is linked to increased acetylation of H3K56 which results in reduced H3 occupancy at the promoter regions of active genes.

The above observations of increased H3K56 acetylation and reduced H3 occupancy in H4K16R cells was thereafter complemented with chromatin accessibility assay in the promoter region of these genes. For this, DNase I digestion was done with chromatin from wild type, H4K16R and K16Q cells, for three different time points. Genomic DNA obtained following digestion reactions were subjected to qPCR using primers encompassing the promoter and TSS region of each of the genes. Logically, any differential chromatin accessibility in between the

three strains will be reflected as a difference in DNase I accessibility in the loci. Consequently, higher DNase I accessibility will result in lower PCR signals, or the reverse. For all the strains, the PCR signals obtained from each time point for each gene was normalized against the signals obtained from no DNase I digestion control and averaged thereafter. Values thus obtained were graphically plotted as normalized signal intensity to represent inverse function of DNase I digestion. As shown in Figure 6(b), it was found that for all the genes tested the PCR signals obtained from H4K16R cells was noticeably lower than those obtained from wild-type and H4K16Q cells. It is thus conclusive that promoter region of the genes tested had higher DNase I digestion kinetics in H4K16R cells, compared to wild type and H4K16Q. Therefore, in H4K16R cells the promoter region of the constitutively active genes has increased chromatin accessibility, compared to wild type. Interestingly, *in vitro* experiments done

earlier has shown that acetylation of H3K56 as found in H3K56Q cells, impedes nucleosome array oligomerization and is a probable mechanism for generating nucleosome free chromatin regions required for accessibility of trans factors during different DNA metabolic processes [76].

Discussion

Acetylation of H4K16 has been previously described as a modification that acts as a switch to maintain heterochromatin-euchromatin structure and functions in *S. cerevisiae* [16–20, 24–30]. In yeast, the modification dynamics of this particular residue is so critical that in addition to the common HAT (Esa1) and HDAC (Hos2) for the acetylatable residues in the H4 N-terminal tail, H4K16 has its own unique set of HAT (Sas2) and HDAC (Sir2) for maintaining its acetylation-deacetylation states [18,20,25,29,77]. Acetylated state of H4 N-terminal tail is known to affect transcription efficiency and more specifically Sas2-mediated acetylation of H4K16 holds an inverse correlation with transcription elongation and RNA Pol II occupancy [24,25,27,58,78]. Results from a whole genome transcriptional analysis done earlier concluded that of the four acetylatable lysine residues present at the H4 N-terminal tail, only mutation in H4K16 produced specific effects on transcription, while mutation of others was partially redundant [63]. In trying to further link H4K16 modification with transcription regulation, we deciphered how deacetylation state of H4K16 acts to promote expression of constitutive genes. The six genes tested were chosen from different yeast chromosomes with diverse functional roles. Additionally, four out of the six genes – *UBC6*, *ACT1*, *TAF10* and *TFC1* were without consensus TATA box sequences [TATA(A/T)A(A/T)(A/G)]; while two

genes *RPB2* and *PYK1* had consensus TATA box sequences within 100 bp upstream of TSS [38]. Our present observations are therefore of constitutively expressing genes from different chromosomal locations, with varied functions and irrespective of whether their promoters are TATA-less or TATA-containing. It was evident from our results that deacetylated state of H4K16, as found in the H4K16R mutant,

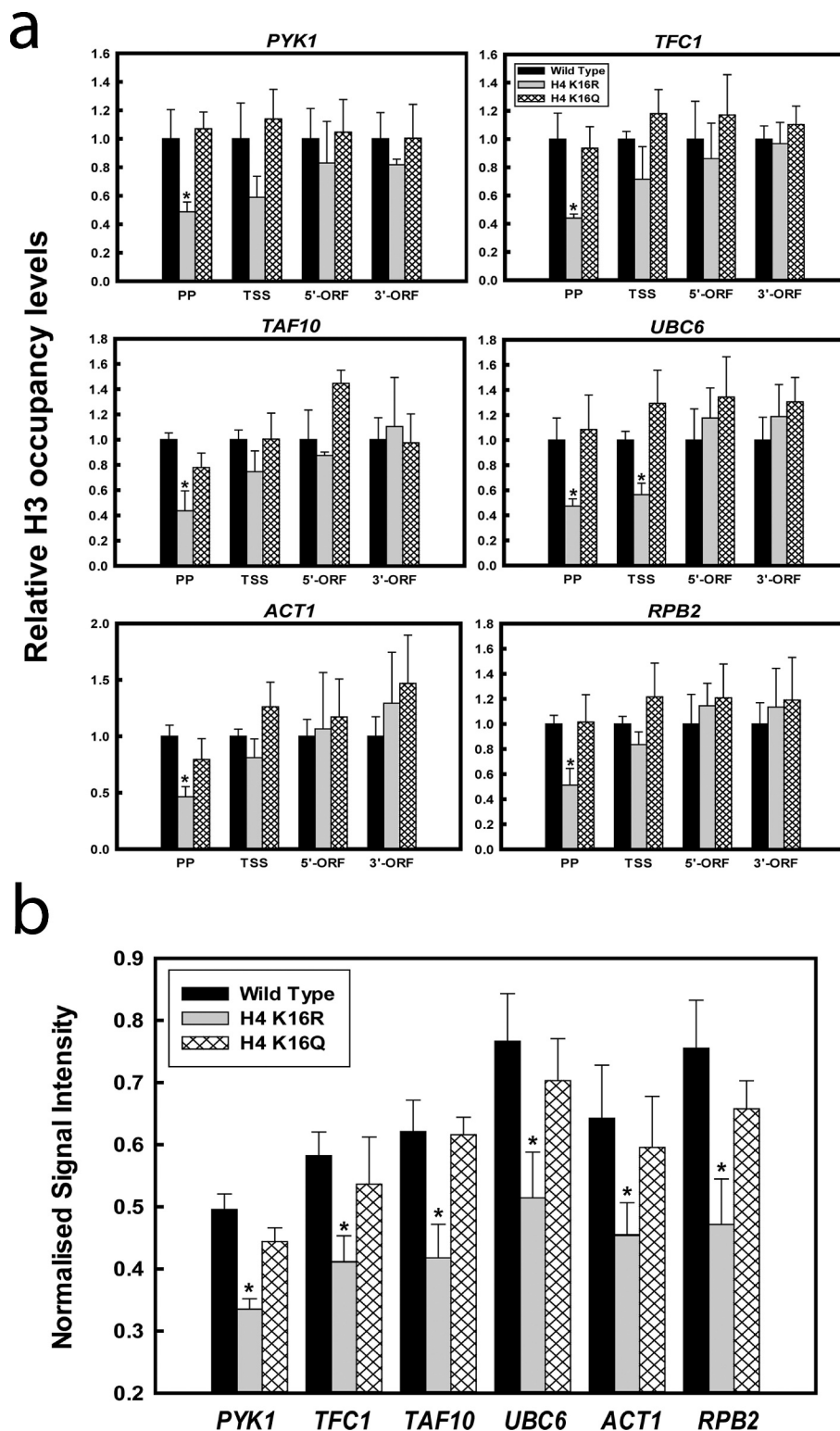


Figure 6. Comparative histone occupancy and chromatin accessibility between wild type and H4K16 mutants. (a) ChIP-qPCR analyses with anti-H3 antibody for checking H3 occupancy at the promoter proximal region (PP), transcription start site (TSS), 5' end (5'-ORF) and 3' end (3'-ORF) of the ORFs of transcriptionally active loci of wild type and H4K16 mutant cells. The values were calculated as percentage of input and graphically plotted to represent levels of H3 occupancy in H4K16 mutant cells relative to wild type. (b) DNase I digestion for different time points done with chromatin isolated from wild type and H4K16 mutant cells. Isolated DNA was subjected to qPCR with primers covering the promoter and TSS region. The amount of DNA amplified at each time point was normalized to the value of no digestion control. Normalized values from all the digestion time points was averaged and graphically plotted as normalized signal intensity for wild type and H4K16 mutants. Data represent the mean for three independent experiments with standard error of mean bars and asterisks indicate *t*-test significant *P* values < 0.05.

facilitates several fold higher expressions of constitutively active genes. In wild type cells it was seen that acetylation of H4K16 significantly decreased over the gene body compared to promoter region, consistently for all the constitutive genes tested. Thus, normally a dynamism between acetylated and deacetylated states of H4K16 exists for the process of transcription. It has been shown earlier that Esa1-mediated acetylation of H4 N-terminal tail is essential for recruitment of TFIID and absence of such acetylation hampers transcription initiation leading to reduced expression of genes [50,65]. Precisely, such acetylation at the H4K16 residue at the promoter region of constitutively active genes is required for binding of Bdf1 protein through direct interaction with histones and subsequently aids in recruitment of TFIID [79–81]. Since, TFIID is known to be required for expression of all mRNA in yeast [41] and acetylated H4 tails works to anchor TFIID to the promoter during the initial stages of transcription activation [82], the initial presence of acetylated H4K16 at the promoter region of the constitutive genes in wild type cells seems quite pertinent. Alongside, earlier experimental results have suggested that Sas2-mediated H4K16 acetylation poses an inhibitory effect on RNA Pol II travel over the gene body and consequently lower levels of H4K16 acetylation are found in genes that are frequently transcribed [25]. Hypoacetylation of H4K16 has been found to be most prominent at –1 and +1 nucleosomes, but this is not restricted to these marks [58]. Nucleosome mapping of PTMs on induction of stress has shown that H4K16 is acetylated on stress responsive genes at early time points but is eventually lost at later time points and deacetylated H4K16 is associated with the gene when transcriptional activity gets induced [83]. As H4K16 acetylation at gene bodies has not been related to transcription [58], rather deacetylation of H4K16 and H4K12 is shown to be required for transcription it is not surprising that in H4K16R where H4K12 acetylation is reduced expression of constitutive genes was higher compared to wild type. Notably, we also observed lower gene expression levels in H4K16Q cells compared to wild type, indicating that the lack of large-scale chromosome compaction observed in H4K16Q [84] and removing H4K16

hypoacetylation by mimicking acetylated form might not confer a transcriptional advantage. Our observations thus underscore the importance of H4K16 hypoacetylation for effective transcription of constitutive genes in yeast.

Various combinations of acetylation patterns in H4-N terminal tail lysine residues, with certain extent of redundancy, has been correlated with several cellular functions in yeast, including transcription of different groups of genes [27,58,63,78,85–87]. Our observation that elevated levels of H4K8 acetylation is present in the promoter and throughout the gene body of both H4K16 mutants in comparison to wild type, implied that acetylation of H4K8 and its role in transcription is independent of H4K16 acetylation status. On the contrary, the observation that the deacetylated state of H4K16 was distinctly associated with reduced levels of H4K12 acetylation was intriguing. Enrichment of hypoacetylated H4K12 in H4K16R and *Sas2* mutant cells was especially prominent at the promoter region, compared to wild-type and H4K16Q cells. In wild type and H4K16Q, H4K12 hypoacetylation was enriched primarily in the coding region, but for H4K16R and *Sas2* mutants hypoacetylated H4K12 was found throughout the active loci. These observations indicate a level of crosstalk between H4K16 and K12 residues in terms of acetylation and deacetylation during transcription. It is important to note in this context that NuA4 complex through its catalytic subunit Esa1 is responsible for acetylation of H4K12 along with H4K16, although abrogation of the HAT activity reduces H4K12 acetylation most strongly compared to all other substrates of Esa1 [88]. Rpd3 and Hos2 the two HDACs responsible for deacetylation of H4 N-terminal tail residues, also have distinct roles. Rpd3 is known to be associated with actively expressed genes and is recruited throughout inducible loci under conditions of both activation and repression [89–91]. Hos2 on the other hand, gets recruited only during transcription induction [29] and thus seems to be more specifically required for the process of transcription. It has been previously shown that Hos2 mediates deacetylation of both H4K12 and H4K16 and this is required for activation of gene transcription. Deacetylation by Hos2 can occur in the coding and promoter region of

actively transcribing genes and the transcription elongation factor Spt6 is known to specifically deposit deacetylated H4K16 on the ORFs during transcription [29,78]. Beyond *S. cerevisiae*, Hos2 in

U. maydis has also been shown to associate with the gene body, aid in transcription elongation and support maintenance of basal level gene expression [92]. It is thus evident that Hos2-regulated deacetylation of H4K12 and K16 in transcriptionally active loci, is essential for gene expression. It is worth mentioning here that in wild type cells, acetylation of both H4K16 and K12 was found in the promoter region and hypoacetylation was observed more prominently at the coding sequences. While this may aid in transcription activation through recruitment of TFIID or SAGA [41,64,65,93] – hypoacetylation of both H4K16 and K12 residues at the promoter region of genes, as found in H4K16R mutant, must confer an additional benefit in the process. Lack of deacetylation due to deletion of Hos2 and Rpd3 has been shown to severely

reduce RNAPII recruitment at the promoter region and consequently affect gene expression. It has been suggested that the deacetylation is required at a later stage of pre-initiation complex (PIC) formation and for multiple rounds of transcription initiation [94]. This theory gains further support from our observation that RNAPII recruitment around the TSS and 5'-ORF regions is prominently enhanced in the H4K16R mutant, compared to wild type. Whether presence of deacetylated H4K16 and K12 at the promoter region of H4K16R mutant better facilitates PIC formation during transcription initiation compared to wild type, may be an interesting avenue to elucidate in future. Taken together, it is relevant to conclude from the present work that acetylation states of histones H4K16 and H4K12 crosstalk during transcription and the cumulative effect of deacetylation of these two residues promotes expression of constitutively active genes.

Acetylation of K9 in histone H3 has been linked to transcription through its association with active promoters and enhancers [95]. Until recently direct functional role for H3K9ac during transcription was not known till it was shown that the acetylation was necessary to promote transcription elongation by recruitment of the super

elongation complex (SEC) and for RNA Pol II pause release post initiation [61]. It was further shown that lack of Gcn5 the HAT responsible for H3K9 acetylation, did not affect PIC formation [61] indicating that H3K9 acetylation was required downstream to initiation. As per our observations, H3K9 acetylation was found to be significantly reduced in the promoter, around the TSS and in the ORF of constitutively expressed genes in H4K16R and *Sas2* mutant cells. Notably previous *in vitro* studies have shown that, Gcn5 prefers acetylated H4K16 for binding and will not dock on the deacetylated residue [62]. From all these studies it is thus clear that deacetylated state of H4K16 do not promote acetylation of H3K9, possibly due to inefficiency in binding of Gcn5. The fact that despite such low levels of H3K9 acetylation, expression of constitutively active genes was favoured in H4K16R mutant implies that H3K9 acetylation might not be absolutely indispensable for expression of such genes. This suggests that a bypass mechanism possibly exists for crucial steps such as PIC formation, RNA Pol II pause release or elongation when deacetylated H4K16 might not allow Gcn5 to acetylate H3K9. Interestingly, as mentioned above while NuA4 mediated H4 N-terminal tail acetylation in the promoter region of active genes is required for TFIID recruitment, in absence of functional NuA4, SAGA is involved in TBP recruitment to the promoter, irrespective of its HAT activity [64,65]. SEC recruitment has also been shown to be H4K5 acetylation dependent [61] and H4K5ac is the most redundantly acetylated amongst all four lysine residues of the H4 N-terminal tail [63]. It is therefore evident

as to why lack of H4K16 acetylation at the promoter region, as found in the H4K16R cells, might not act as a stumbling block for constitutive gene expression. Thus, H4K16 acetylation-dependent and Gcn5-mediated H3K9 acetylation seems to be dispensable for transcription of constitutive genes. Our findings on enhanced constitutive gene expression in absence of H3K9 acetylation thus indicates a new avenue for analysing the requirement of histone acetylation during active transcription.

For inducible gene expression, however, H3K9ac seems to be necessary as even in

H4K16R mutant acetylation was observed with progress in time of induction. Under such circumstances H3K9 acetylation may be mediated by one or more HAT other than Gcn5, whose recruitment is not dependent on H4K16 acetylation state. Recent findings show that regulated acetylation and deacetylation of H3K9 is required for different repair pathways and that H3K9 acetylation by different HATs is required for different functions of H3K9 in diverse chromatin processes [23,83,96–99]. Rtt109 mediated acetylation of H3K9 has been found to be essential for tiding over the effects of genotoxic agents that block replication [98,100,101]. Regulatory role of acetylated H3K9 during transcription is possibly mediated by HAT/coactivator p300, apart from the general H3 HAT Gcn5 [99]. Thus, it is possible that other HATs capable of acetylating H3K9, whose recruitment and activity does not depend on H4K16 acetylation status, replace Gcn5 when H3K9 acetylation becomes absolutely necessary during transcription. This possibly explains why in H4K16R mutant delayed but distinct increase in H3K9 acetylation was observed for inducible gene expression.

Importantly, our present study shows a relation between acetylation of another histone H3 lysine residue with H4K16 acetylation state. Acetylation of the H3 core residue K56 was found to be significantly elevated when H4K16 was deacetylated. Enhanced H3K56 acetylation in H4K16 deacetylated cells was found throughout the loci, at the promoter region and throughout the gene body. Earlier it has been shown that during DNA damage response the effect of H3K56 hyperacetylation, can be suppressed by reducing H4K16 acetylation levels [102], thus indicating a probable crosstalk between these two histone modifications. Interestingly, *in vitro* studies have shown that Rtt109 when associated with Vps75 show HAT activity for H4 K12, but shows no such detectable activity for H4 residues as Rtt109-Asf1 complex [100]. This indicates a possibility that Rtt109 as a HAT may have an affinity for H4 N-terminal lysine residues in general or specifically through its association with H4K12. This may work as a rate limiting step for H3K56 acetylation. When both H4K16 and K12 residues remain predominantly deacetylated, as seen in H4K16R cells, Rtt109 may be more readily available for H3K56 acetylation. This could possibly explain why

enhanced levels of H3K56 acetylation was observed in constitutive loci of H4K16R cells, compared to wild type and H4K16Q. The direct correlation between these two modifications however remain to be established and needs further investigation. Furthermore, our observation that elevated levels of H3K56 acetylation in H4K16R cells was associated with significantly reduced H3 occupancy in the promoter region of all the constitutive tested genes is in agreement with the current understanding that H3K56 acetylation contributes during active transcription through its role in histone exchange and nucleosome disassembly [25,69–72,74,75,83,103–105]. While acetylated state of H3K56 has been distinctly correlated with nucleosome free region, it is well established that Rtt109-Asf1 mediated H3K56 acetylation although dispensable for PIC formation, is essential for histone eviction in transcriptionally active loci [70,74,76,106]. Therefore, deacetylated states of H4K16 and K12 along with highly acetylated H3K56 leads to reduced histone occupancy at the promoter region generating a chromatin landscape with increased accessibility. This is clearly evident from our DNase I accessibility assay results showing that chromatin around the promoter and TSS region of the constitutively active genes have higher accessibility in absence of H4K16 acetylation. The increased chromatin accessibility around the promoter region may have thus favoured transcription initiation while prevalence of H4K16 deacetylation in the coding region may have further promoted the process of transcription.

To summarize, our work here shows that deacetylation of H4K16 is a preferential histone modification for expression of constitutively active genes. Deacetylated state of H4K16 is part of a histone modification network that involves H4K12 deacetylation and H3K56 acetylation leading to a chromatin milieu with reduced H3 occupancy and increased DNA accessibility at the promoter region. The histone code so generated favours transcription of constitutive genes in yeast.

Materials and methods

Yeast strains

Saccharomyces cerevisiae strain WY121 was used as the parent strain to generate wild type, histone

mutant and deletion mutant strains. Both copies of genomic histone H3-H4 are deleted in WY121 and one copy of H3-H4 is provided by plasmid pJL001 (CEN URA3 HHT2-HHF2) with *URA3* as a counter-selectable marker. Plasmids pEMH7 (CEN TRP1 HHT2-HHF2), pEMH33 and pEMH35 with *TRP1* selection marker, containing one copy of either wild type H3-H4 or point mutations of H4K16R or H4K16Q in the *HHF2* gene coding for histone H4, were transformed into WY121 so that cells could now grow in synthetic $SC^{-TRP-URA}$ medium. Subsequently cells were grown in presence of 5'-FoA (5'-Fluoroorotic Acid) to shuffle out the *URA3* containing pJL001 plasmid. These cells now containing only one plasmid served as the WT (pEMH7), K16R (pEMH33) and K16Q (pEMH35) strains. The WY121 strain and the pEMH plasmids were kind gifts from Dr. John Wyrick (Washington State University, USA) and Prof. J.D. Boeke (Johns Hopkins University School of Medicine, USA) respectively.

For generation of the $\Delta sas2$ strain, a PCR based homologous recombination-mediated gene deletion technique was used [107]. Primers were designed for a selectable marker present on a shuttle vector, such that they had 5' – overhangs with ~ 40 bp of sequence homology to regions flanking the *SAS2* gene. The forward primer used was 5'- TCTAGTTGCTTTTGTTCCTCACTC GCAAAAAAATGGCAAGATCTCAGCTGAA-GC TTCGTACGC-3' and the reverse primer used was 5'- TCCTGAAATACATATGCCATTAA GTTACATCCTGAATAGATTCTAGCATAGGCC ACTAGTGGATCTG-3'. The 3' end of the primer was specific for the KANMX4 module conferring resistance to antibiotic geneticin (G418), from the vector plasmid pFA6-KANMX4. The plasmid was a kind gift from Prof. Shubho Chaudhuri (Bose Institute, India). The PCR amplified linear DNA cassette containing selectable marker KANMX4 flanked by regions homologous to *SAS2* was then transformed into WY121 cells using high efficiency yeast transformation protocol. The transformants were grown on G418 containing plates. Genomic DNA was isolated from colonies growing on G418 containing plates and subjected to PCR to confirm the deletion. PCR was done using forward primer corresponding to *SAS2* specific region and the reverse primer in either the

KANMX4 cassette or the *SAS2* gene to serve as positive and negative controls. The genotype of the $\Delta sas2$ strain was further confirmed by Southern blotting.

Gene expression

Mid-log phase yeast cells with an O.D₆₀₀ of ~ 0.7 (~ 1×10^7 cells/ml) were used to isolate RNA as previously described [23]. Briefly, cell pellets were treated with a modified YLE buffer (1 M Sorbitol, 0.1 M EDTA pH 7.4, 0.1% β -mercaptoethanol, 50 U Zymolyase/ 10^7 cells), washed with Sorbitol wash buffer (1 M Sorbitol, 1 mM PMSF, 2 mM β -mercaptoethanol) and vortexed

vigorously with Trizol® Reagent while keeping on ice. The mixture was then centrifuged at full speed for 10 minutes at 4°C to remove undissolved debris and the supernatant was used for chloroform extraction and subsequent precipitation of RNA pellets with isopropanol. 10 μ g of RNA was DNaseI treated by Trizol®: chloroform extraction and isopropanol precipitation again. 5 μ g of isolated RNA was used for reverse transcription using Revertaid RT (Thermo Scientific) as per manufacturer's instructions. The cDNA formed was then serially diluted from $1/10^1$ to $1/10^9$ to serve as template for qPCR with primers for the six constitutive genes and the C_T values obtained were used to plot a standard curve of C_T values to number of amplicons (ng) present for each primer set. Subsequently, the undiluted cDNA was used for qPCR and the C_T values of the expressed genes were then used on the standard curves to calculate the actual number of transcripts expressed for each gene using the standard formula: (amount of dsDNA in ng * Avogadro No.)/(Base pair size of dsDNA)*(330*2*D.F). The dilution factor (D.F) was taken as 10^9 and the amount of dsDNA present in ng was calculated as values of 'x' from the standard curve plot: $y = \ln(x) + c$ considering the C_T values of the expressed genes as 'y'. For each biological replicate ($n = 3$), triplicate qPCRs were repeated twice for each strain. The statistical significance of the difference in level of expression between wild type and mutant strains was tested using two-tailed independent student's t-test and the results having a *P* value of < 0.05 were considered to be significant.

Chromatin immunoprecipitation

Log phase yeast cells with an OD₆₀₀ of 0.9 ~ 1 (~ 1.5×10^7 cells/ml) were treated with 1% formaldehyde. For inducible genes, cells were treated or mock treated with 100 J/m² UV light (254 nm), allowed to repair in the dark at 30°C for different time intervals (0, 5 and 10 mins) and then cross-linked with 1% formaldehyde. These cross-linked were harvested and washed with Sorbitol wash buffer (1 M sorbitol, 1 mM PMSF, 2 mM β -mercaptoethanol). Subsequent digestion with 50 units of Micrococcal Nuclease as mentioned previously [21] was done, to generate 200–500 bp chromatin fragments and pre-cleared with pre-treated (50% slurry pre- absorbed with 0.1% BSA and 100 mg/ml of herring sperm DNA) Protein A-Sepharose beads at 4°C. 1% of the pre-cleared whole cell extract was kept as Input DNA and the rest was divided into equal aliquots and immunoprecipitated with 2–3 μ g of antibody overnight at 4°C. The antibodies used were anti-Histone H4 Acetyl K16 (Cell Signalling Technology – E2B8W), anti-Histone H3 Acetyl K9 (abcam – ab10812), anti-Histone H4 acetyl K8 (abcam – ab15823), anti-Histone H4 acetyl K12 (abcam – ab46983), anti-Histone H3 acetyl K56 (abcam – ab195478), anti-RNA polymerase II (abcam – ab817) and anti-Histone H3 (BioBharati LifeScience – BB-AB0055). The immunocomplexes were precipitated with Protein A-Sepharose beads (pre- treated 50% slurry), washed with lysis buffer (50 mM HEPES-KOH pH 7.5, 140 mM NaCl, 1 mM EDTA, 1% Triton X-100, 0.1% sodium deoxycholate, 1 mM PMSF), wash buffer 1 (Lysis buffer containing 500 mM NaCl), wash buffer 2 (10 mM Tris-Cl pH 8, 250 mM LiCl, 0.5% NP-40, 0.5% sodium deoxycholate, 1 mM EDTA) and TE buffer, and then treated with RNase

A. Immunocomplexes were then eluted from the beads using elution buffer (1% SDS, 0.1 M NaHCO₃), crosslinks were reversed by incubation at 65°C and the de-cross-linked samples were treated with Proteinase K at 55°C. The DNA was isolated by phenol: chloroform extraction and ethanol precipitation and used for analysis by qPCR. Levels of histone modification were calculated using the formula $2^{(C_T^{(Input)} - C_T^{(IP)})}$ and were normalized by the levels of H3 present at each of the regions tested. H3 and RNA Polymerase II occupancy levels were calculated as

a percentage of Input after extrapolating the 1% Input levels to 100%. For each ChIP, triplicate qPCRs were performed for three biological replicates ($n = 3$) and the data was plotted with standard error of mean bars. The statistical significance of the difference in levels of histone modifications between wild type and mutant strains was tested using two-tailed independent student's *t*-test and the results having a *P* value of < 0.05 were considered to be significant.

Western blot

Whole cell lysates were prepared as per described protocol [108], with brief modifications. Yeast cells were grown at 30°C in YPD to stationary phase with an O.D₆₀₀ of 0.9–1.5 (~ $2\text{--}5 \times 10^7$ cells/ml), harvested, washed in ice cold 1X PBS with 1X protease inhibitor cocktail and pelleted. Cell pellets were lysed by rigorous vortexing with acid-washed glass beads (Sigma, 425–600 μ m) in presence of ice-cold cell lysis buffer (50 mM HEPES pH 7.3, 200 mM NaCl, 1% Triton-X, 1X PIC, 1 mM PMSF). Samples were then centrifuged 15,000 *g* at 4°C for 15 minutes and the supernatant was used as whole cell extract (WCE). Protein concentration was estimated by Bradford Assay and 10 μ g WCE was electrophoresed on 15% SDS-PAGE to blot samples on a PVDF membrane. Membrane was blocked with 5% NFD milk in TBS (25 mM Tris-Cl pH 7.5, 137 mM NaCl, 2.7 mM KCl) and incubated with primary antibody to the protein of interest in 1X TBS overnight at 4°C. Next day membrane was washed with 1X TBST (1X TBS, 0.1% Tween-20) and incubated with appropriate horseradish peroxidase (HRP) – conjugated secondary antibody for 1–3 hr at RT. Membrane was washed several times in excess volumes of 1X TBST. The membrane was thereafter incubated with a chemiluminescent substrate (SuperSignal® West Pico Chemiluminescent Substrate by Thermo Scientific), exposed to autoradiograph film and developed to visualize.

DNase I accessibility

Mid-log phase yeast cells with an O.D₆₀₀ of ~ 0.7 (~ 1×10^7 cells/ml) were harvested and sphaeroplasted using YLE buffer (10 mg/ml Zymolyase 20 T in 1 M

Sorbitol, 5 mM β -mercaptoethanol) by incubation at 22°C for 30 min. Hereafter previously described method [109,110] was followed with brief modifications. The sphaeroplasts were centrifuged at 500 g for 5 mins at 4°C and resuspended in ice-cold RSB buffer (10 mM Tris-Cl pH 7.4, 10 mM NaCl, 3 mM MgCl₂) by flicking gently. Gentle lysis was done by addition of IGEPAL CA-360 at 0.05–0.1% final concentration followed by centrifugation at 500 g for 10 mins at 4°C. The white chromatin pellet thus obtained was resuspended in ice-cold RSB. Equal concentration of chromatin for each strain was determined based on Bradford Assay. Aliquots were taken and subjected to DNase I digestion using enzyme at a final concentration of 0.05 U/ μ l for increasing time points (0, 4, 8, 12 mins). Reactions were stopped by addition of 50 mM EDTA and heat inactivation at 65°C. DNA was isolated and subjected to qPCR with primers covering the promoter and TSS region. The amount of DNA amplified at each time point was normalized to the value of 0 min digestion control. Thereafter average of normalized values from all the time points was done. The average of the normalized values thus obtained was an inverse function of the accessibility to DNase I as lesser PCR signals indicated higher nuclease accessibility. Triplicate qPCRs were performed for three independent biological replicates ($n = 3$) and the data was plotted with standard error of mean bars. The statistical significance of the difference in accessibility to DNase I between wild type and mutant strains was tested using two-tailed independent student's *t*-test and the results having a *P* value of < 0.05 were considered to be significant.

Acknowledgements

We thank Prof. JD. Boeke (Johns Hopkins University School of Medicine, USA) for kind gift of the pEMH series of plasmids and our sincere acknowledgement to Prof. Michael J. Smerdon, Washington State University, USA for kind donation of the plasmids. We also sincerely thank Prof. John Wyrick (Washington State University, USA) for sharing the WY121 strain.

Authors' contribution

RNC and AR designed the experiments; AR and PK performed the experiments; RNC, AR and PK analysed the results and wrote the paper.

Disclosure statement

Contents of this manuscript are solely the responsibility of the authors and do not necessarily represent the official views of the funding agency.

Funding

This work was supported by Science and Engineering Research Board (SERB), India [Scheme #CRG/2018/000461] to Dr. Ronita Nag Chaudhuri, Department of Biotechnology, St. Xavier's College, Kolkata; CSIR fellowship [# 08/548-(0009)/2019-EMR-I] to Ms. Preeti Khan; by West Bengal DBT BOOST Grant No. [335/WBBD/CP-2/2013] to Department of Biotechnology, St. Xavier's College, Kolkata and by Department of Science and Technology, India [DST-FIST Grant No. SR/FST/COLLEGE-014/2010(C)] to St. Xavier's College, Kolkata.

ORCID

Anagh Ray  <http://orcid.org/0000-0002-2380-6467>

References

- [1] Bannister AJ, Kouzarides T. Regulation of chromatin by histone modifications. *Cell Res.* **2011**;21:381–395.
- [2] Jenuwein T, Allis CD. Translating the histone code. *Science.* **2001**;293:1074–1080.
- [3] Shukla A, Chaurasia P, Bhaumik SR. Histone methylation and ubiquitination with their cross-talk and roles in gene expression and stability. *Cell Mol Life Sci.* **2009**;66:1419–1433.
- [4] Strahl BD, Allis CD. The language of covalent histone modifications. *Nature.* **2000**;403:41–45.
- [5] Smerdon MJ. DNA repair and the role of chromatin structure. *Curr Opin Cell Biol.* **1991**;3:422–428.
- [6] Bannister AJ, Kouzarides T. The CBP co-activator is a histone acetyltransferase. *Nature.* **1996**;384:641–643.
- [7] Luger K, Mader AW, Richmond RK, et al. Crystal structure of the nucleosome core particle at 2.8 Å resolution. *Nature.* **1997**;389:251–260.
- [8] Millar CB, Kurdiani SK, Grunstein M. Acetylation of yeast histone H4 lysine 16: a switch for protein interactions in heterochromatin and euchromatin. *Cold Spring Harb Symp Quant Biol.* **2004**;69:193–200.
- [9] Shogren-Knaak M, Peterson CL. Switching on chromatin: mechanistic role of histone H4-K16 acetylation. *Cell Cycle.* **2006**;5:1361–1365.
- [10] Bhaumik SR, Smith E, Shilatifard A. Covalent modifications of histones during development and disease pathogenesis. *Nat Struct Mol Biol.* **2007**;14:1008–1016.
- [11] Fulton MD, Zhang J, He M, et al. Intricate effects of alpha-amino and lysine modifications on arginine

- methylation of the N-terminal tail of histone H4. *Biochemistry*. 2017;56:3539–3548.
- [12] Green EM, Mas G, Young NL, et al. Methylation of H4 lysines 5, 8 and 12 by yeast Set5 calibrates chromatin stress responses. *Nat Struct Mol Biol*. 2012;19:361–363.
 - [13] Green EM, Morrison AJ, Gozani O. New marks on the block: set5 methylates H4 lysines 5, 8 and 12. *Nucleus*. 2012;3:335–339.
 - [14] Shogren-Knaak M, Ishii H, Sun JM, et al. Histone H4-K16 acetylation controls chromatin structure and protein interactions. *Science*. 2006;311:844–847.
 - [15] Zhang R, Erler J, Langowski J. Histone acetylation regulates chromatin accessibility: role of H4K16 in inter-nucleosome interaction. *Biophys J*. 2017;112:450–459.
 - [16] Hecht A, Laroche T, Strahl-Bolsinger S, et al. Histone H3 and H4 N-termini interact with SIR3 and SIR4 proteins: a molecular model for the formation of heterochromatin in yeast. *Cell*. 1995;80:583–592.
 - [17] Johnson A, Li G, Sikorski TW, et al. Reconstitution of heterochromatin-dependent transcriptional gene silencing. *Mol Cell*. 2009;35:769–781.
 - [18] Kimura A, Umehara T, Horikoshi M. Chromosomal gradient of histone acetylation established by Sas2p and Sir2p functions as a shield against gene silencing. *Nat Genet*. 2002;32:370–377.
 - [19] Oppikofer M, Kueng S, Martino F, et al. A dual role of H4K16 acetylation in the establishment of yeast silent chromatin. *Embo J*. 2011;30:2610–2621.
 - [20] Suka N, Luo K, Grunstein M. Sir2p and Sas2p opposingly regulate acetylation of yeast histone H4 lysine16 and spreading of heterochromatin. *Nat Genet*. 2002;32:378–383.
 - [21] Kayne PS, Kim UJ, Han M, et al. Extremely conserved histone H4 N terminus is dispensable for growth but essential for repressing the silent mating loci in yeast. *Cell*. 1988;55:27–39.
 - [22] Bird AW, Yu DY, Pray-Grant MG, et al. Acetylation of histone H4 by Esa1 is required for DNA double-strand break repair. *Nature*. 2002;419:411–415.
 - [23] Ray A, Khan P, Nag Chaudhuri R. Regulated acetylation and deacetylation of H4 K16 is essential for efficient NER in *saccharomyces cerevisiae*. *DNA Repair (Amst)*. 2018;72:39–55.
 - [24] Durrin LK, Mann RK, Kayne PS, et al. Yeast histone H4 N-terminal sequence is required for promoter activation in vivo. *Cell*. 1991;65:1023–1031.
 - [25] Heise F, Chung HR, Weber JM, et al. Genome-wide H4 K16 acetylation by SAS-I is deposited independently of transcription and histone exchange. *Nucleic Acids Res*. 2012;40:65–74.
 - [26] Horikoshi N, Kumar P, Sharma GG, et al. Genome-wide distribution of histone H4 lysine 16 acetylation sites and their relationship to gene expression. *Genome Integr*. 2013;4:3.
 - [27] Kurdastani SK, Tavazoie S, Grunstein M. Mapping global histone acetylation patterns to gene expression. *Cell*. 2004;117:721–733.
 - [28] Taylor GC, Eskeland R, Hekimoglu-Balkan B, et al. H4K16 acetylation marks active genes and enhancers of embryonic stem cells, but does not alter chromatin compaction. *Genome Res*. 2013;23:2053–2065.
 - [29] Wang A, Kurdastani SK, Grunstein M. Requirement of Hos2 histone deacetylase for gene activity in yeast. *Science*. 2002;298:1412–1414.
 - [30] Yu Y, Teng Y, Liu H, et al. UV irradiation stimulates histone acetylation and chromatin remodeling at a repressed yeast locus. *Proc Natl Acad Sci U S A*. 2005;102:8650–8655.
 - [31] Fraga MF, Ballestar E, Villar-Garea A, et al. Loss of acetylation at Lys16 and trimethylation at Lys20 of histone H4 is a common hallmark of human cancer. *Nat Genet*. 2005;37:391–400.
 - [32] Rando OJ, Winston F. Chromatin and transcription in yeast. *Genetics*. 2012;190:351–387.
 - [33] Li B, Carey M, Workman JL. The role of chromatin during transcription. *Cell*. 2007;128:707–719.
 - [34] Lee TI, Causton HC, Holstege FC, et al. Redundant roles for the TFIID and SAGA complexes in global transcription. *Nature*. 2000;405:701–704.
 - [35] Bhaumik SR, Green MR. SAGA is an essential in vivo target of the yeast acidic activator Gal4p. *Genes Dev*. 2001;15:1935–1945.
 - [36] Bhaumik SR, Green MR. Differential requirement of SAGA components for recruitment of TATA-box-binding protein to promoters in vivo. *Mol Cell Biol*. 2002;22:7365–7371.
 - [37] Li XY, Bhaumik SR, Green MR. Distinct classes of yeast promoters revealed by differential TAF recruitment. *Science*. 2000;288:1242–1244.
 - [38] Basehoar AD, Zanton SJ, Pugh BF. Identification and distinct regulation of yeast TATA box-containing genes. *Cell*. 2004;116:699–709.
 - [39] Huisinga KL, Pugh BF. A genome-wide housekeeping role for TFIID and a highly regulated stress-related role for SAGA in *Saccharomyces cerevisiae*. *Mol Cell*. 2004;13:573–585.
 - [40] Nagai S, Davis RE, Mattei PJ, et al. Chromatin potentiates transcription. *Proc Natl Acad Sci U S A*. 2017;114:1536–1541.
 - [41] Warfield L, Ramachandran S, Baptista T, et al. Transcription of nearly all yeast RNA polymerase II-transcribed genes is dependent on transcription factor TFIID. *Mol Cell*. 2017;68:118–129 e115.
 - [42] Baptista T, Grunberg S, Minoungou N, et al. SAGA is a general cofactor for RNA polymerase II transcription. *Mol Cell*. 2017;68:130–143 e135.
 - [43] Bonnet J, Wang CY, Baptista T, et al. The SAGA coactivator complex acts on the whole transcribed

- genome and is required for RNA polymerase II transcription. *Genes Dev.* **2014**;28:1999–2012.
- [44] Natsume-Kitatani Y, Mamitsuka H. Classification of promoters based on the combination of core promoter elements exhibits different histone modification patterns. *PLoS One.* **2016**;11:e0151917.
- [45] Burke RL, Tekamp-Olson P, Najarian R. The isolation, characterization, and sequence of the pyruvate kinase gene of *Saccharomyces cerevisiae*. *J Biol Chem.* **1983**;258:2193–2201.
- [46] Fraenkel DG. The top genes: on the distance from transcript to function in yeast glycolysis. *Curr Opin Microbiol.* **2003**;6:198–201.
- [47] Pearce AK, Crimmins K, Groussac E, et al. Pyruvate kinase (Pyk1) levels influence both the rate and direction of carbon flux in yeast under fermentative conditions. *Microbiology.* **2001**;147:391–401.
- [48] Parsons MC, Weil PA. Cloning of TFC1, the *Saccharomyces cerevisiae* gene encoding the 95-kDa subunit of transcription factor TFIIC. *J Biol Chem.* **1992**;267:2894–2901.
- [49] Swanson RN, Conesa C, Lefebvre O, et al. Isolation of TFC1, a gene encoding one of two DNA-binding subunits of yeast transcription factor tau (TFIIC). *Proc Natl Acad Sci U S A.* **1991**;88:4887–4891.
- [50] Uprety B, Lahudkar S, Malik S, et al. The 19S proteasome subcomplex promotes the targeting of NuA4 HAT to the promoters of ribosomal protein genes to facilitate the recruitment of TFIID for transcriptional initiation in vivo. *Nucleic Acids Res.* **2012**;40:1969–1983.
- [51] Klebanow ER, Poon D, Zhou S, et al. Isolation and characterization of TAF25, an essential yeast gene that encodes an RNA polymerase II-specific TATA-binding protein-associated factor. *J Biol Chem.* **1996**;271:13706–13715.
- [52] Tora L. A unified nomenclature for TATA box binding protein (TBP)-associated factors (TAFs) involved in RNA polymerase II transcription. *Genes Dev.* **2002**;16:673–675.
- [53] Gilon T, Chomsky O, Kulka RG. Degradation signals recognized by the Ubc6p-Ubc7p ubiquitin-conjugating enzyme pair. *Mol Cell Biol.* **2000**;20:7214–7219.
- [54] Sommer T, Jentsch S. A protein translocation defect linked to ubiquitin conjugation at the endoplasmic reticulum. *Nature.* **1993**;365:176–179.
- [55] Pruyne D, Bretscher A. Polarization of cell growth in yeast. *J Cell Sci.* **2000**;113(Pt 4):571–585.
- [56] Pruyne D, Bretscher A. Polarization of cell growth in yeast. I. Establishment and maintenance of polarity states. *J Cell Sci.* **2000**;113(Pt 3):365–375.
- [57] Archambault J, Friesen JD. Genetics of eukaryotic RNA polymerases I, II, and III. *Microbiol Rev.* **1993**;57:703–724.
- [58] Liu CL, Kaplan T, Kim M, et al. Single-nucleosome mapping of histone modifications in *S. cerevisiae*. *PLoS Biol.* **2005**;3:e328.
- [59] Bell O, Wirbelauer C, Hild M, et al. Localized H3K36 methylation states define histone H4K16 acetylation during transcriptional elongation in *Drosophila*. *Embo J.* **2007**;26:4974–4984.
- [60] Gaucher J, Boussouar F, Montellier E, et al. Bromodomain-dependent stage-specific male genome programming by Brdt. *Embo J.* **2012**;31:3809–3820.
- [61] Gates LA, Shi J, Rohira AD, et al. Acetylation on histone H3 lysine 9 mediates a switch from transcription initiation to elongation. *J Biol Chem.* **2017**;292:14456–14472.
- [62] Owen DJ, Ornaghi P, Yang JC, et al. The structural basis for the recognition of acetylated histone H4 by the bromodomain of histone acetyltransferase gcn5p. *Embo J.* **2000**;19:6141–6149.
- [63] Dion MF, Altschuler SJ, Wu LF, et al. Genomic characterization reveals a simple histone H4 acetylation code. *Proc Natl Acad Sci U S A.* **2005**;102:5501–5506.
- [64] Shukla A, Bajwa P, Bhaumik SR. SAGA-associated Sgf73p facilitates formation of the preinitiation complex assembly at the promoters either in a HAT-dependent or independent manner in vivo. *Nucleic Acids Res.* **2006**;34:6225–6232.
- [65] Uprety B, Sen R, Bhaumik SR. Eaf1p is required for recruitment of NuA4 in targeting TFIID to the promoters of the ribosomal protein genes for transcriptional initiation in vivo. *Mol Cell Biol.* **2015**;35:2947–2964.
- [66] Bernier M, Luo Y, Nwokelo KC, et al. Linker histone H1 and H3K56 acetylation are antagonistic regulators of nucleosome dynamics. *Nat Commun.* **2015**;6:10152.
- [67] Hyland EM, Cosgrove MS, Molina H, et al. Insights into the role of histone H3 and histone H4 core modifiable residues in *Saccharomyces cerevisiae*. *Mol Cell Biol.* **2005**;25:10060–10070.
- [68] Maas NL, Miller KM, DeFazio LG, et al. Cell cycle and checkpoint regulation of histone H3 K56 acetylation by Hst3 and Hst4. *Mol Cell.* **2006**;23:109–119.
- [69] Masumoto H, Hawke D, Kobayashi R, et al. A role for cell-cycle-regulated histone H3 lysine 56 acetylation in the DNA damage response. *Nature.* **2005**;436:294–298.
- [70] Rufiange A, Jacques PE, Bhat W, et al. Genome-wide replication-independent histone H3 exchange occurs predominantly at promoters and implicates H3 K56 acetylation and Asf1. *Mol Cell.* **2007**;27:393–405.
- [71] Topal S, Vasseur P, Radman-Livaja M, et al. Distinct transcriptional roles for histone H3-K56 acetylation during the cell cycle in Yeast. *Nat Commun.* **2019**;10:4372.
- [72] Xu F, Zhang K, Grunstein M. Acetylation in histone H3 globular domain regulates gene expression in yeast. *Cell.* **2005**;121:375–385.
- [73] Yang J, Zhang X, Feng J, et al. The histone chaperone FACT contributes to DNA replication-coupled nucleosome assembly. *Cell Rep.* **2016**;14:1128–1141.
- [74] Schneider J, Bajwa P, Johnson FC, et al. Rtt109 is required for proper H3K56 acetylation: a chromatin

- mark associated with the elongating RNA polymerase II. *J Biol Chem.* **2006**;281:37270–37274.
- [75] Durairaj G, Chaurasia P, Lahudkar S, et al. Regulation of chromatin assembly/disassembly by Rtt109p, a histone H3 Lys56-specific acetyltransferase, in vivo. *J Biol Chem.* **2010**;285:30472–30479.
- [76] Watanabe S, Resch M, Lilyestrom W, et al. Structural characterization of H3K56Q nucleosomes and nucleosomal arrays. *Biochim Biophys Acta.* **2010**;1799:480–486.
- [77] Allard S, Utley RT, Savard J, et al. NuA4, an essential transcription adaptor/histone H4 acetyltransferase complex containing Esa1p and the ATM-related cofactor Tra1p. *Embo J.* **1999**;18:5108–5119.
- [78] Reiter C, Heise F, Chung HR, et al. A link between Sas2- mediated H4 K16 acetylation, chromatin assembly in S-phase by CAF-I and Asf1, and nucleosome assembly by Spt6 during transcription. *FEMS Yeast Res.* **2015**;15:fov073.
- [79] Jacobson RH, Ladurner AG, King DS, et al. Structure and function of a human TAFII250 double bromodomain module. *Science.* **2000**;288:1422–1425.
- [80] Matangkasombut O, Buratowski S. Different sensitivities of bromodomain factors 1 and 2 to histone H4 acetylation. *Mol Cell.* **2003**;11:353–363.
- [81] Pamblanco M, Poveda A, Sendra R, et al. Bromodomain factor 1 (Bdf1) protein interacts with histones. *FEBS Lett.* **2001**;496:31–35.
- [82] Martinez-Campa C, Politis P, Moreau JL, et al. Precise nucleosome positioning and the TATA box dictate requirements for the histone H4 tail and the bromodomain factor Bdf1. *Mol Cell.* **2004**;15:69–81.
- [83] Weiner A, Hsieh TH, Appleboim A, et al. High-resolution chromatin dynamics during a yeast stress response. *Mol Cell.* **2015**;58:371–386.
- [84] Hsieh TH, Weiner A, Lajoie B, et al. Mapping nucleosome resolution chromosome folding in yeast by micro-C. *Cell.* **2015**;162:108–119.
- [85] Goudarzi A, Zhang D, Huang H, et al. Dynamic competing histone H4 K5K8 acetylation and butyrylation are hallmarks of highly active gene promoters. *Mol Cell.* **2016**;62:169–180.
- [86] Ma XJ, Wu J, Altheim BA, et al. Deposition-related sites K5/K12 in histone H4 are not required for nucleosome deposition in yeast. *Proc Natl Acad Sci U S A.* **1998**;95:6693–6698.
- [87] Ruan K, Yamamoto TG, Asakawa H, et al. Histone H4 acetylation required for chromatin decompaction during DNA replication. *Sci Rep.* **2015**;5:12720.
- [88] Chang CS, Pillus L. Collaboration between the essential Esa1 acetyltransferase and the Rpd3 deacetylase is mediated by H4K12 histone acetylation in *Saccharomyces cerevisiae*. *Genetics.* **2009**;183:149–160.
- [89] De Nadal E, Zapater M, Alepuz PM, et al. The MAPK Hog1 recruits Rpd3 histone deacetylase to activate osmoresponsive genes. *Nature.* **2004**;427:370–374.
- [90] Kurdistani SK, Robyr D, Tavazoie S, et al. Genome-wide binding map of the histone deacetylase Rpd3 in yeast. *Nat Genet.* **2002**;31:248–254.
- [91] Robert F, Pokholok DK, Hannett NM, et al. Global position and recruitment of HATs and HDACs in the yeast genome. *Mol Cell.* **2004**;16:199–209.
- [92] Elias-Villalobos A, Helmlinger D, Ibeas JI. Histone deacetylases: revealing the molecular base of dimorphism in pathogenic fungi. *Microb Cell.* **2015**;2:491–493.
- [93] Ferdoush J, Sen R, Kaja A, et al. Two distinct regulatory mechanisms of transcriptional initiation in response to nutrient signaling. *Genetics.* **2018**;208:191–205.
- [94] Sharma VM, Tomar RS, Dempsey AE, et al. Histone deacetylases RPD3 and HOS2 regulate the transcriptional activation of DNA damage-inducible genes. *Mol Cell Biol.* **2007**;27:3199–3210.
- [95] Karmodiya K, Krebs AR, Oulad-Abdelghani M, et al. H3K9 and H3K14 acetylation co-occur at many gene regulatory elements, while H3K14ac marks a subset of inactive inducible promoters in mouse embryonic stem cells. *BMC Genomics.* **2012**;13:424.
- [96] Guo R, Chen J, Mitchell DL, et al. GCN5 and E2F1 stimulate nucleotide excision repair by promoting H3K9 acetylation at sites of damage. *Nucleic Acids Res.* **2011**;39:1390–1397.
- [97] Meyer B, Fabbri MR, Raj S, et al. Histone H3 lysine 9 acetylation obstructs ATM activation and promotes ionizing radiation sensitivity in normal stem cells. *Stem Cell Reports.* **2016**;7:1013–1022.
- [98] Chen Y, Zhang Y, Ye H, et al. Structural basis for the acetylation of histone H3K9 and H3K27 mediated by the histone chaperone Vps75 in *Pneumocystis carinii*. *Signal Transduct Target Ther.* **2019**;4:14.
- [99] Zhou W, Jiang D, Tian J, et al. Acetylation of H3K4, H3K9, and H3K27 mediated by p300 regulates the expression of GATA4 in cardiocytes. *Genes Dis.* **2019**;6:318–325.
- [100] Abshiru N, Ippersiel K, Tang Y, et al. Chaperone-mediated acetylation of histones by Rtt109 identified by quantitative proteomics. *J Proteomics.* **2013**;81:80–90.
- [101] Cote JM, Kuo YM, Henry RA, et al. Two factor authentication: Asf1 mediates crosstalk between H3 K14 and K56 acetylation. *Nucleic Acids Res.* **2019**;47:7380–7391.
- [102] Simoneau A, Delgosaie N, Celic I, et al. Interplay between histone H3 lysine 56 deacetylation and chromatin modifiers in response to DNA damage. *Genetics.* **2015**;200:185–205.
- [103] Tan Y, Xue Y, Song C, et al. Acetylated histone H3K56 interacts with Oct4 to promote mouse embryonic stem cell pluripotency. *Proc Natl Acad Sci U S A.* **2013**;110:11493–11498.
- [104] Williams SK, Truong D, Tyler JK. Acetylation in the globular core of histone H3 on lysine-56 promotes chromatin disassembly during transcriptional activation. *Proc Natl Acad Sci U S A.* **2008**;105:9000–9005.
- [105] Xie W, Song C, Young NL, et al. Histone h3 lysine 56 acetylation is linked to the core transcriptional

- network in human embryonic stem cells. *Mol Cell*. [2009](#);33:417–427.
- [106] Kaplan T, Liu CL, Erkmann JA, et al. Cell cycle- and chaperone-mediated regulation of H3K56ac incorporation in yeast. *PLoS Genet*. [2008](#);4:e1000270.
- [107] Gardner JM, Jaspersen SL. Manipulating the yeast genome: deletion, mutation, and tagging by PCR. *Methods Mol Biol*. [2014](#);1205:45–78.
- [108] Szymanski EP, Kerscher O. Budding yeast protein extraction and purification for the study of function, interactions, and post-translational modifications. *J Vis Exp*. [2013](#);80:e50921.
- [109] Song L, Crawford GE. DNase-seq: a high-resolution technique for mapping active gene regulatory elements across the genome from mammalian cells. *Cold Spring Harb Protoc*. [2010](#);2010: pdb prot5384.
- [110] Zhong J, Luo K, Winter PS, et al. Mapping nucleosome positions using DNase-seq. *Genome Res*. [2016](#);26:351–364.



Regulated acetylation and deacetylation of H4 K16 is essential for efficient NER in *Saccharomyces cerevisiae*

Anagh Ray, Preeti Khan, Ronita Nag Chaudhuri*

Department of Biotechnology, St. Xavier's College, 30, Mother Teresa Sarani, Kolkata, 700016, India

ARTICLE INFO

Keywords:

H4 K16
Histone acetylation
Nucleotide excision repair
Chromatin accessibility
Cyclobutane pyrimidine dimer removal

ABSTRACT

Acetylation status of H4 K16, a residue in the histone H4 N-terminal tail plays a unique role in regulating chromatin structure and function. Here we show that, during UV-induced nucleotide excision repair H4 K16 gets hyperacetylated following an initial phase of hypoacetylation. Disrupting H4 K16 acetylation-deacetylation by mutating H4 K16 to R (deacetylated state) or Q (acetylated state) leads to compromised chromatin functions. In the silenced mating locus and telomere region H4 K16 mutants show higher recruitment of Sir proteins and spreading beyond the designated boundaries. More significantly, chromatin of both the H4 K16 mutants has reduced accessibility in the silenced regions and genome wide. On UV irradiation, the mutants showed higher UV sensitivity, reduced NER rate and altered H3 N-terminal tail acetylation, compared to wild type. NER efficiency is affected by reduced or delayed recruitment of early NER proteins and chromatin remodeller Swi/Snf along with lack of nucleosome rearrangement during repair. Additionally UV-induced expression of *RAD* and *SNF5* genes was reduced in the mutants. Hindered chromatin accessibility in the H4 K16 mutants is thus non-conducive for gene expression as well as recruitment of NER and chromatin remodeller proteins. Subsequently, inadequate nucleosomal rearrangement during early phases of repair impeded accessibility of the NER complex to DNA lesions, in the H4 K16 mutants. Effectively, NER efficiency was found to be compromised in the mutants. Interestingly, in the transcriptionally active chromatin region, both the H4 K16 mutants showed reduced NER rate during early repair time points. However, with progression of repair H4 K16R repaired faster than K16Q mutants and rate of CPD removal became differential between the two mutants during later NER phases. To summarize, our results establish the essentiality of regulated acetylation and deacetylation of H4 K16 residue in maintaining chromatin accessibility and efficiency of functions like NER and gene expression.

1. Introduction

Eukaryotic DNA is compacted into chromatin, whose basic structural units the nucleosomes are comprised of histone proteins. Regulated dynamism in chromatin structure maintains the functional fidelity of the genome. A plethora of post-translational modifications in the histones contribute to chromatin plasticity [1,2]. The “histone code” hypothesis aims to explain how the myriads of different combinations of histone modifications lead to a specific output in terms of transcription, repair or replication [3–6]. Histone modifications can affect chromatin function through either alteration of higher-order chromatin structure by bringing about changes in inter-nucleosomal interactions or by targeting histone-DNA interactions at specific sites. Of the various post-translational modifications in histones, acetylation and deacetylation of lysine re-

sides mediated by histone acetyltransferases (HATs) and deacetylases (HDACs) respectively, is most pervasive [7]. Charge neutralization of the inherently positively charged lysine residues, caused by histone acetylation has several effects: firstly, it alters histone-DNA interactions or interaction with the acidic patches of the adjacent nucleosomes and secondly, it mediates recruitment of chromatin modifying proteins that recognize acetylation state of specific lysines [8–11]. Of the known acetylatable lysine residues, histone H4 N-terminal tail bears four lysines namely, lysine 5, 8, 12 and 16 (K5, K8, K12 and K16), whose modifications have proven significance in almost all species examined till date. Acetylation status of H4 K16 specifically has been found to have profound importance in regulating several nuclear processes such as gene silencing [12–17], transcription [18–23], chromatin compaction [10,11] and double-strand break repair [24]. In the transcriptionally silent re-

* Corresponding author.

E-mail address: ronita7@yahoo.co.in (R. Nag Chaudhuri).

<https://doi.org/10.1016/j.dnarep.2018.09.009>

Received 26 April 2018; Received in revised form 27 August 2018; Accepted 18 September 2018

1568-7864/ © 2018 Elsevier B.V. All rights reserved.

regions such as telomere and mating locus of yeast, which form a heterochromatinized structure, recruitment of the silencer proteins Sir2 and Sir3 depends on the H4 K16 acetylation status. Within the silenced chromatin domains while hypoacetylated H4 K16 is the preferred binding site for the silencer protein Sir3, the Sir2-4 complex shows affinity for acetylated H4 K16 [9,13,17,25]. Sir2, which is a NAD-dependent histone deacetylase is responsible for specifically deacetylating H4 K16 in the heterochromatin region, while Sas2, a HAT belonging to the MYST acetyltransferase family is primarily responsible for acetylation of H4 K16 in the entire genome [13–15,22]. In the transcriptionally active regions of the genome, H4 K16 acetylation shows a strong anti-correlation with gene expression and Hos2 mediated deacetylation of H4 K16 is essential for gene activation [19–23]. Thus, interplay between acetylation and deacetylation of H4 K16 residue by action of specific HATs and HDACs is an important factor in regulating the fidelity of chromatin structure and function.

Proficiency of DNA metabolic processes like DNA repair, transcription and replication is essentially dependent on dynamic chromatin landscape and its proper regulation to ensure DNA accessibility. Chromatin architecture of genes along with histone modifications and chromatin remodelling ensures correct spatio-temporal regulation of the transcription process [26–29]. Similarly, for DNA damage repair processes like nucleotide excision repair (NER) which involves large multiprotein complexes, packaging of DNA into chromatin hinders the accessibility of NER factors to the lesion [27,30]. For NER pathway, the repair proteins are known to form a large complex near the DNA adduct and require at least 100 base pairs of naked DNA for the excision process [28]. For NER to occur in a chromatin environment, histone modifications, chromatin accessibility and nucleosomal rearrangement at the damage site is thus a prerequisite. Chromatin structure and associated histone modifications regulate accessibility of NER machinery to the DNA lesion and can directly or indirectly affect efficiency of the repair process [4,20,23,29,31–33].

Previous studies have shown that histone acetylation, especially in the N-terminal lysine residues of histone H3 and H4, stimulates UV-induced DNA damage repair [34–38]. Genome-wide studies have further shown that histone hyperacetylation, specifically H3 K9 and/or K14 acetylation occurs in an UV-dependent manner during repair of a transcriptionally repressed yeast locus [37,39]. *In vitro* studies have also shown that Gcn5, the HAT required for the acetylation of H3 K9 and H3 K14 favourably binds to acetylated H4 K16 [40].

With this background, our aim was to study the effect of H4 K16 acetylation and deacetylation on UV-induced NER pathway. Till date no direct correlation between acetylation and deacetylation of H4 K16 residue and its effect on NER pathway has been elucidated. Therefore, study was done with two mutant strains, where H4 K16 has been mutated to arginine (H4 K16R) representing constitutively deacetylated form or to glutamine (H4 K16Q) representing constitutively acetylated form. Our work clearly demonstrates how loss of H4 K16 acetylation or deacetylation hinders chromatin accessibility during NER and consequently reduces NER proficiency.

2. Materials and methods

2.1. Yeast strains

Saccharomyces cerevisiae strain WY121, which has both copies of genomic histone H3-H4 deleted and contains plasmid pJL001 (*CEN*

URA3 HHT2-HHF2) to provide one copy of H3-H4 with *URA3* as a counter-selectable marker, was a kind gift from Dr. John Wyrick (Washington State University). Plasmid pEMH7 (*CEN TRP1 HHT2-HHF2*) containing one copy of H3-H4 and counter-selectable marker *TRP1* was isolated from bacteria and transformed into WY121 so that; it contained both plasmids pJL001 and pEMH7 when grown in SC^{-TRP-URA} medium. To shuffle out the pJL001 plasmid, the strains were grown in SC medium supplemented with 5'-FoA (5'-Fluoroorotic Acid). Yeast strains that are phenotypically Ura⁺ become Ura⁻ after selection. The strain in which histone H3-H4 was supplied only from the pEMH7 plasmid, henceforth served as the wild type yeast strain. The plasmids pEMH33 and pEMH35 contained H4 K16R and H4 K16Q mutations respectively in the *HHF2* gene coding for histone H4. These plasmids were similarly isolated from bacteria and transformed into WY121 instead of pEMH7 to generate histone H4 mutant strains H4 K16R and H4 K16Q. The plasmids were then isolated from yeast cells and sequenced to check the presence of the desired mutations. pEMH7, pEMH33 and pEMH35 were kind gifts from Prof. J.D. Boeke (Johns Hopkins University School of Medicine).

2.2. Chromatin immunoprecipitation

Log phase yeast cells with an OD₆₀₀ of 0.9 ~ 1 (~ 1.5 × 10⁷ cells/ml) were treated with 1% formaldehyde for 30 min at room temperature, pelleted and washed twice with Sorbitol wash buffer (1 M sorbitol, 1 mM PMSF, 2 mM β-mercaptoethanol). These cross-linked cells were then processed for MNase digestion as described in chromatin accessibility assay and digested with 50 units of MNase to generate 200–500 bp fragments. The reaction was terminated using stop solution and the reaction was diluted to a volume having < 0.3% SDS. 1 mM PMSF was added and this served as the whole cell extract which was pre-cleared with pre-treated (50% slurry pre-absorbed with 0.1% BSA and 100 mg/ml of herring sperm DNA) Protein A-Sepharose beads for 4 h at 4 °C. The whole cell extract was divided into equal aliquots and immunoprecipitated with 2–3 µg of antibody overnight at 4 °C. 1% of the aliquot volume was separated and stored as Input DNA to serve as the no antibody experimental control. For Sir binding studies, anti-Sir2 (Santa Cruz Biotechnology – sc-6666) and anti-Sir3 (Santa Cruz Biotechnology – sc-28552) antibodies were used. Anti-Rad23 (Santa Cruz Biotechnology – sc-15556), anti-Rad16 (abcam – ab21758), Ms pAb to Snf5 (abcam – ab24425-100), anti-Histone H3 Acetyl K9 (abcam – ab10812), anti-Histone H3 Acetyl K14 (abcam – ab52946), anti-Histone H4 Acetyl K16 (Cell Signaling Technology – E2B8W) and anti-Histone H3 antibody (abcam – ab1791) were used for other occupancy studies. The immunocomplexes were precipitated using 6 antibody volumes of Protein A-Sepharose beads (pre-treated 50% slurry) and subsequently washed with lysis buffer (50 mM HEPES-KOH pH 7.5, 140 mM NaCl, 1 mM EDTA, 1% Triton X-100, 0.1% sodium deoxycholate, 1 mM PMSF), wash buffer 1 (Lysis buffer containing 500 mM NaCl), wash buffer 2 (10 mM Tris-Cl pH 8, 250 mM LiCl, 0.5% NP-40, 0.5% sodium deoxycholate, 1 mM EDTA) and TE buffer, and then treated with RNase A in TE at 37 °C for 30 min. Chromatin was then eluted from the beads using elution buffer (1% SDS, 0.1 M NaHCO₃) and the crosslinks were reversed by incubation at 65 °C overnight. The de-cross-linked samples were treated with Proteinase K at 55 °C for 1 h, extracted with equal volume phenol: chloroform and precipitated. The purified DNA pellets were dissolved in TE and analysed by qPCR using the following primers:

Primers	Sequence	
YFR057 3'	F – 5' GGCAGTCCTTTCTATTTTCATT 3'	R – 5' TTGTTACGCTTGCACTTGA 3'
XC-1KB	F – 5' AGTATACAAATTGCAGGCAAA 3'	R – 5' CGCATACCTTTTTTTTTCTG 3'
XC-2KB	F – 5' TGCTGCCAACAGAAAGAA 3'	R – 5' TGCTTGGATATGATGTTGTGA 3'
XC-3KB	F – 5' AAACGTGGCTTACGTAACAG 3'	R – 5' AAAGGCTTCATCTGATCTAGG 3'
XC-4KB	F – 5' TGGATGATGAAGCAGATAATC 3'	R – 5' AGGAACGCAAGTAGATAAAGC 3'
XC-5KB	F – 5' TATCTCTTTGGCGCTATTGGC 3'	R – 5' TGTACTTCCATGGTCCCAGAA 3'
YCL073 5'	F – 5' TCTAGTGTGTTGTTGCTCCTCA 3'	R – 5' TCCAAACCCACATACAAACG 3'
YCL069 5'	F – 5' TCTGAGTCTCATTGGGGAAG 3'	R – 5' TCACGTCCATTGGTGATTTC 3'
YCL069 3'	F – 5' ATCTAGAGCCTTACGAAGGA 3'	R – 5' AAATTATCTTCTGCTGCTCG 3'
YCL065 3'	F – 5' CATCGTCTTGCTCTTGTT 3'	R – 5' GTATATAGACAATGCAATCGTAC 3'
I-500	F – 5' AGATTCAAGCTGAAACATTCTAAG 3'	R – 5' TCCTTACTAAGTGAAGAAAAGCAA 3'
CHA1 5'	F – 5' TCGATAGTCTACAATAAAACACCA 3'	R – 5' CATTACCGCCAGAACTAGC 3'
RPB2-1	F – 5' TGTCAGACCTTGCAAACTCAG 3'	R – 5' TTCGGTAGTATGTTGAGCCAA 3'
RPB2-2	F – 5' TGGTCACACAGGTAAAAAACT 3'	R – 5' CGGATGCTTCCATTAATCTC 3'

ChIP experiment was repeated three times for immunoprecipitation with each antibody for each strain.

2.3. Chromatin accessibility assay

Yeast cells were grown at 30 °C in YPD to late-log phase with an OD₆₀₀ of 0.9 ~ 1 (~ 1.5 × 10⁷ cells/ml), harvested and washed with 1 M sorbitol. Cells were then sphaeroplasted using YLE buffer (10 mg/ml Zymolyase in 1 M Sorbitol, 5 mM β-mercaptoethanol) by incubation at 22 °C for 30 min. The sphaeroplasts formed were washed twice with Sorbitol wash buffer (1 M sorbitol, 1 mM PMSF, 2 mM β-mercaptoethanol) and re-suspended in sphaeroplast digestion buffer (1 M Sorbitol, 50 mM NaCl, 10 mM Tris-Cl pH 7.5, 5 mM MgCl₂, 1 mM CaCl₂, 1 mM β-mercaptoethanol, 0.5 mM spermidine and 0.075% v/v NP-40). The mixture was divided into equal aliquots and digested with varying concentrations of Micrococcal Nuclease (25 U/μl) for 10 min at 37 °C. The 5 tubes contained 1.5, 3, 6, 9 and 12 units of enzyme respectively. The reactions were terminated with 0.1 volumes of stop solution (5% SDS, 250 mM EDTA) followed by proteinase-K treatment for 2 h at 55 °C. Samples were extracted twice with phenol/chloroform, treated with 10 mg/ml of RNase A and ethanol precipitated. DNA was re-suspended in TE, digested by restriction endonucleases to generate locus specific fragments, electrophoresed on 1.2% agarose gel, and southern blotted. For locus specific accessibility assay, *Bsp1286I*, *BsaAI* and *NruI* restriction endonucleases were used to generate a 2.38 kb fragment of the *HML* locus, a 2.24 kb fragment containing the telomere of chromosome VIII_R and a 3.4 kb fragment containing the *RPB2* gene, respectively. Southern blot analysis was done using specific probes for *HML* (PCR amplification product of 518 bp region encompassing the whole of *HMLa1* ORF; Forward Primer – 5'-ACTTTCGAAGCCTGCTTTCAA-3', Reverse Primer – 5'-AAGGCCAAATGTACAAACACA-3'), TEL-08R (PCR amplification product of 556 bp spanning the 3' end of ORF *YHR219W* and its adjacent region, close to the C_{1.3}A repeats which form the telosome TR1; Forward – 5' – CATTTCGGCAGAACTGGAA – 3', Reverse – 5' – CCTGTTCTTTAGCCCTACAGC – 3') and *RPB2* (*EcoRI* and *XhoI* digestion of plasmid pKS212) [41]. For whole chromatin accessibility studies, samples were electrophoresed on 1.2% agarose gel, visualized by staining in ethidium bromide, photographed on Gel Doc™ EZ Imager and scanned by densitometry using Image Lab™ Software to quantify intensities of digested chromatin fractions. These values were normalized by the total chromatin intensity values and plotted as undigested chromatin fractions. Higher concentrations of MNase would digest chromatin more and hence show lower values of undigested chromatin fraction. The averages of triplicate results were plotted for each locus and therefore the whole chromatin accessibility graph

reflects a pattern from 9 experimental repeats. Statistical significance was tested using two-tailed independent student's *t*-test and the results having a P value of < 0.05 were considered to be significant.

2.4. Southern blot analysis

Electrophoresed 1.2% agarose gels were de-purinated with 0.2 N HCl, equilibrated in alkaline transfer buffer (0.4 N NaOH, 1 M NaCl) and blotted on Hybond N + transfer membranes (Amersham, GE Healthcare). The membranes were neutralised with neutralisation buffer (0.5 M Tris-Cl pH 7.2, 1 M NaCl) and equilibrated with Pre-Hybridisation buffer (0.5 M Phosphate buffer (Na₂HPO₄·7H₂O + H₃PO₄ + H₂O) pH 7.2, 1 mM EDTA, 7% SDS, 1% BSA) at 65 °C. Probes were radiolabelled using [α³²P]dATP and DecaLabel DNA Labeling Kit (Thermo Fisher Scientific) and added to the Pre-Hybridisation buffer containing the membrane to hybridise overnight at 65 °C. The hybridised membrane was washed with buffer 1 (27.6 mM Na₂HPO₄, 12.4 M NaH₂PO₄, 1 mM EDTA, 5% SDS, 0.5% BSA), buffer 2 (27.6 mM Na₂HPO₄, 12.4 M NaH₂PO₄, 1 mM EDTA, 1% SDS), and scanned using PhosphorImager (Bose Institute, Kolkata, India) and ImageQuant Software (GE Healthcare Life Sciences).

2.5. UV sensitivity assay

Yeast cells were grown at 30 °C in YPD to mid-log phase with an OD₆₀₀ of 0.6 ~ 0.7 (~ 0.9 × 10⁷ cells/ml) and serial ten-fold dilutions of the cultures were either spotted or spread on YPD plates. The plates were irradiated with UV light (254 nm) at doses of 50, 100 and 150 J/m² for spot assay and at 50, 100, 150 and 200 J/m² for spread plate assay and incubated at 30 °C for 48 – 72 h in the dark along with UV untreated plates serving as control. Both the experiments were repeated at least thrice. For spread assay, each strain was spread thrice for every serial dilution. The number of colony forming units was counted, and the average results were plotted. The error bars for each strain represent the standard error of the mean of three technical replicates from three biological repeats each (n = 3).

2.6. Yeast genomic DNA isolation

Harvested and PBS washed yeast cells were dissolved in nuclei isolation buffer NIB (17% glycerol, 50 mM MOPS (pH 8.0), 150 mM potassium acetate, 2 mM MgCl₂, 0.5 mM spermine, 0.15 mM spermidine) and vortexed rigorously with 1.5 ml of acid-washed glass beads (Sigma, 425–600 μm) for ten to twelve 30 s pulses to break up the cells completely. The samples were then incubated with 700 μl of 10% SDS

at 65 °C for 3.5 h. After cooling to room temperature 1 ml TE and 2.5 ml saturated NaCl solution was added to the samples and centrifuged at 10,000 g, at room temperature, for 20 min and supernatant collected. The DNA was precipitated with isopropanol, washed with 70% ethanol, treated with RNase A and extracted with phenol/chloroform. After re-precipitation with 2.5 volumes of chilled ethanol and 0.1 volumes of sodium acetate (3 M) and 70% ethanol wash, the DNA was dissolved in TE and stored at -20 °C before use.

2.7. Locus specific NER analyses

Primers	Sequence	
HML-1	F – 5' GCTCAAGAGGTCCGCTAATT 3'	R – 5' CAGAGGACACCGGTTTACAAA 3'
HML-2	F – 5' CATCGTCTTGCTCTTGTT 3'	R – 5' GTATATAGACAATGCAATCGTAC 3'
TEL08R-1	F – 5' TTCAGGGACTTGCATCAGTTG 3'	R – 5' CCCAAGCTGATCATGCAATT 3'
TEL08R-2	F – 5' CATTCGGCAGAACTGGAA 3'	R – 5' CCTGTCTTTAGCCCTACAGC 3'

Yeast cells were grown in YPD at 30 °C to mid-log phase with an OD₆₀₀ of ~ 0.7 (~ 1 × 10⁷ cells/ml), harvested, re-suspended in 1X PBS and UV-treated with a dose of 100 J/m² (254 nm). The UV irradiated cells were then harvested, re-suspended in pre-warmed YPD and allowed to repair by incubation for various time periods (0 h, 0.5 h, 1 h, 2 h) in the dark at 30 °C. Genomic DNA was isolated and digested with *Bsp*1286I, *Bsa*AI and *Nru*I restriction endonucleases to generate a 2.38 kb fragment of the *HML* locus, a 2.24 kb fragment containing the telomere of chromosome VIIIIR and a 3.4 kb fragment of the *RPB2* gene, respectively. Equal amounts of digested DNA from each repair time point, were treated or mock treated with T4 Endonuclease V for 2 h at 37 °C and electrophoresed under denaturing conditions in an alkaline gel (0.5 M NaCl, 0.01 M EDTA, 1.2% agarose). The gel was neutralised with a neutralisation buffer (1 M Tris-Cl (pH 7.6), 1.5 M NaCl) and Southern blotted as mentioned above with the same probes used as chromatin accessibility studies above. For repair analyses, an extension of the DNA CPD quantification method [42] was used. The approximate number of CPDs for each time point of each strain was calculated by normalising the band intensity of T4 endonuclease V treated samples by the mock treated ones. The number of CPDs present at each time point of repair for each strain was then normalised to the initial number of CPDs present in that strain at 0 min repair. The negative log of these values was then plotted as the percentage of CPDs repaired. CPD removal % was calculated using the formula $100 - 100 * [-\ln(\text{CPD no. at repair time point } x) / -\ln(\text{CPD no. at 0 min repair})]$. The repair experiments were repeated three times and Southern blot analyses were done twice from each set of genomic DNA isolated from the three strains. The data obtained was plotted graphically to represent the percentage of CPD removal. Error bars represent standard error of mean between three biological repeats (n = 3).

2.8. Nucleosome occupancy assay

Mid-log phase yeast cells with an OD₆₀₀ of ~ 0.7 (~ 1 × 10⁷ cells/ml) were harvested and an aliquot of cells was separated for no UV control. The remaining cells were UV irradiated and incubated for repair time-points 15 min, 30 min and 60 min in the method mentioned above. The cells were formaldehyde cross-linked before harvesting and ChIP assay with anti-H3 antibody was done with these cells as mentioned above. The assay was repeated thrice and triplicate qPCR were performed from each biological replicate using the following primers.

H3 occupancy was checked with these primers that span two representative regions of each of the two loci which were studied for NER analyses. The data was graphically represented as the nucleosome occupancy levels of each strain at different repair time points with the values normalised to UV untreated control. Statistical significance was tested using two-tailed paired student's *t*-test and the results having a *P* value of < 0.05 were considered to be significant.

2.9. Gene expression analysis

Mid-log phase yeast cells with an OD₆₀₀ of ~ 0.7 (~ 1 × 10⁷ cells/ml) were treated or mock treated with 100 J/m² UV light (254 nm), allowed to repair in the dark at 30 °C for 1 h and harvested for RNA isolation. Taking necessary precautions, RNA was isolated from yeast cells by re-suspending unwashed cell pellets in a modified YLE buffer (1 M Sorbitol, 0.1 M EDTA pH 7.4, 0.1% β-mercaptoethanol, 50 U Zymolyase/107 cells) for 30 min at room temperature, washing with Sorbitol wash buffer (1 M Sorbitol, 1 mM PMSF, 2 mM β-mercaptoethanol) and vortexing vigorously with Trizol® Reagent. Samples from each strain were vortexed in pulses of 30 s, 8–10 times to completely disrupt cells and kept on ice, followed by centrifugation at full speed for 10 min at 4 °C to remove undissolved debris. The supernatant was used for chloroform extraction and subsequent precipitation of RNA pellets with isopropanol, which were washed with 75% ethanol and dissolved in DEPC treated water after drying. 10 µg of RNA was used for DNaseI treatment for 1 h at 37 °C followed by Trizol®: chloroform extraction and isopropanol precipitation again. 5 µg of isolated RNA was used for reverse transcription using Revertaid RT (ThermoScientific) as per manufacturer's instructions. The product was used to study expression of various genes by RT-qPCR using the following primers.

Primers	Sequence	
RAD1	F – 5' TATATGGTCTTCTCACCCCT 3'	R – 5' ACAGGTGCTTCAGGAACATCA 3'
RAD2	F – 5' TGTGTAATTTATGATGCGGA 3'	R – 5' CCATGACGCTAGGAAAATCA 3'
RAD4	F – 5' AATTGCGGAGGAAGAACTTA 3'	R – 5' TGTGTACAAAAGCGGAGGAAA 3'
RAD14	F – 5' AGAAAAGCCGAACCCCTCA 3'	R – 5' TTTCTTCAGTTTCTAGCC 3'
RAD16	F – 5' TAAATCCATTGTGTTTTCCCA 3'	R – 5' AGAACTGTAAATCAGCTGGCG 3'
RAD23	F – 5' GGACTGGGACAAGGTGAAGGT 3'	R – 5' GGCATGATCGCTGAATAGAA 3'
SNF5	F – 5' CAATGCTCCGAGTCCAGAAT 3'	R – 5' TAGTCAACAATGTCGCTTCGC 3'

RNA was isolated 3 times from each strain, treated or mock treated with UV irradiation.

2.10. Real time PCR and data analysis

Real-time PCR analyses (qPCR) of ChIP experiments were done using Applied Biosystems 7500 Fast Real-Time PCR System (Thermo Fisher Scientific), Dynamo Colour Flash SYBR® Green QPCR Kit (Thermo Fisher Scientific). The C_T values of the input samples were extrapolated to 100%, as the input DNA isolated was 1% of the whole cell extract and the C_T IP values were then plotted as a percentage of input using the formula $100 \times 2^{(C_{T(\text{Input})} - C_{T(\text{IP})})}$. For gene expression studies, absolute quantification using the standard curve method was done. cDNA template dilutions of 1/101 to 1/109 were used to perform qPCR with the respective primer sets and the C_T values obtained were used to plot a standard curve to find the amount of amplicons (ng) present for each primer set. The C_T values from the qPCR of the expressed genes were then used as values of “y” in the equation of the standard curve plot: $y = \ln(x) + c$. Thereafter x was calculated as the amount of amplicons (dsDNA) present in ng. The copy number of transcripts was then obtained using the standard formula: (amount of dsDNA in ng * Avogadro No.) / (Base pair size of dsDNA) * (330 * 2 * 109). For each set of templates, triplicate qPCR were repeated twice for each strain. For all experiments there were three sets of templates from three biological repeats (n = 3). The statistical significance was tested using either two-tailed independent or two-tailed paired student's t-test and the results having a P value of < 0.05 were considered to be significant.

3. Results

The acetylation status of H4 K16 is implicated as a switch which strictly regulates heterochromatin-euchromatin structure and function [9]. For the present study two H4 K16 mutants – H4 K16R and H4 K16Q have been used. As mentioned above, mutation of H4 lysine 16 to arginine (H4 K16R) represents a constitutively deacetylated state, while mutation to glutamine (H4 K16Q) causes charge neutralization and represents a state similar to constitutive acetylation [14,15,18,21]. These H4 K16 mutants therefore lack the dynamic acetylation and deacetylation states of the H4 K16 residue that is present in the wild type. The mutants were generated by plasmid shuffling into wild type yeast strain WY121, where both the chromosomal copies of H3 and H4 genes have been disrupted. The mutant yeast strains H4 K16R and H4 K16Q were confirmed by sequencing. Under normal growth condition at 30 °C, both the H4 K16 mutants grow at a rate comparable to wild type.

3.1. H4 K16 mutations affect binding of Sir proteins at the transcriptionally silent loci

In heterochromatin regions of the genome, acetylation-deacetylation status of H4 K16 residue is known to act as a recognition cue for binding of Sir proteins [9,13–15,17]. To characterize the effect of H4 K16R and K16Q mutations on Sir-mediated silencing, we first checked the level and extent of Sir protein binding in the mutant cells. Sir protein recruitment was tested in two regions: i) the sub-telomeric regions adjacent to telomere VIR (*TEL06R*) – starting from *YFR057* up to a distance of 5 kb from the X-core consensus element (Fig. 1A) and ii) *HML* adjacent regions (Fig. 1D), both of which are known to be silenced in a Sir-dependent manner. For the present study *TEL06R* was chosen because of its more simplistic features compared to other chromosomes in terms of heterochromatin-euchromatin structure [14,43]. Sir3 binding was found to be highest in the H4 K16R mutant compared to wild type and H4 K16Q. At *YFR057*, H4 K16R had 3-fold higher Sir3 recruitment compared to wild type (Fig. 1B). This is in consonance with the fact that unacetylated H4 N-terminal tail facilitates Sir3 binding [13,25,44,45]. H4 K16Q mutants also showed Sir3 binding at different

regions of the *TEL06R* locus - the binding was reduced compared to H4 K16R but was not less than wild type cells (Fig. 1B). Earlier reports indicate that amino acids 503–971 of Sir3 protein can bind to the acetylated form of H4 K16 residue and mutation of H4 K16 to Q does not reduce Sir3 binding if H4 K5, K8 and K12 are not mutated along with K16 [13,25,46]. Our observations with H4 K16Q support these findings and further indicate that isolated mutation of K16 residue to Q does not reduce Sir3 binding in telomere region compared to wild type. The most notable feature observed for both the H4 K16 mutants was extended binding of Sir3 protein beyond the designated silencing domains. Unlike wild type where Sir3 recruitment progressively decreased with increasing distance away from the X-core element, Sir3 binding in both H4 K16R and H4 K16Q mutants did not show such reduction, even at a distance of 5 kb away from the X-core element (Fig. 1B). It is known that at the telomere region recruitment of Sir3 proteins beyond 3 kb from the chromosome end leads to heterochromatinization spreading [15,43,47]. It is thus evident that increased Sir3 binding and heterochromatin spreading occurs in the H4 K16 mutants at the sub-telomeric region. Antagonistic activities of Sir2 and the histone acetyltransferase Sas2 are known to maintain the levels and extent of H4 K16 acetylation and consequently restrict the spreading of heterochromatinization [14,15]. When recruitment of Sir2 was checked at the *TEL06R* locus, it was observed that starting from *YFR057* up to 5 kb from the X-core, Sir2 recruitment was maximum in H4 K16Q cells compared to wild type and H4 K16R (Fig. 1C). This result corroborates with the earlier known fact that acetylated H4 K16 is preferred by Sir2 for initiation and spreading of silencing [16,17,48,49]. Additionally, while Sir2 binding in wild type cells reduced considerably at distances 4 and 5 kb away from the X-core, it continued to remain higher for both H4 K16Q and K16R mutant cells, indicating spreading of Sir2 proteins beyond the normal boundary (Fig. 1C). Taken together, these observations indicate that both the H4 K16 mutants have higher Sir protein binding and spreading to the telomere adjacent regions, which compared to wild type generates a more repressive chromatin structure in this region.

The *HML* region has more defined boundary elements, namely the E silencer and I silencer which restrict spreading of heterochromatinization [50,51]. For the *HML* region, as shown in Fig. 1D - Sir3 and Sir2 recruitment was checked within the *HML* locus bracketed between the E and I silencer, as well as up to 2 kb on either side away from the E and I silencers. Similar to the observations in the telomere region, increased Sir protein binding and spreading was observed in this region, as well. For example, at the *YCL065* 3' region, between the E and I-silencers, Sir3 recruitment was found to be highest for H4 K16R cells (Fig. 1E). Similarly, at the 3' end of *YCL069* which is 75 bp to the left of the E-silencer, Sir3 binding was highest in the H4 K16R cells, compared to wild type or H4 K16Q cells (Fig. 1E). While reduction in Sir3 recruitment was observed in wild type cells at *HML* distal regions [compare 5' end of *YCL069*, which is about 1.4 kb from the E-silencer and 500 bp right of I silencer (I-500)], Sir3 recruitment in H4 K16R cells remained about two-fold higher in these regions. This is in agreement with earlier findings where Sir3 binding in mating locus of H4 K16R mutants was found to be higher compared to wild type [45]. For H4 K16Q cells, Sir3 recruitment at the E-silencer region (*YCL069*) was lower than H4 K16R but not wild type and such high binding was found near and beyond the I-silencer region as well (Fig. 1E). Farther away from the *HML* Locus, near the 5' end of the inducible gene *CHA1* (*YCL064*), which is about 2 kb right of the I silencer and at the 5' end of another inducible gene *GEX1* (*YCL073*), which is about 3 kb left of the E silencer, Sir3 recruitment was reduced in both the H4 mutant cells and in wild type (Fig. 1E). When Sir2 recruitment was tested in the same regions of the *HML* locus, it was found that Sir2 binding was highest in the H4 K16Q cells, compared to H4 K16R and wild type (Fig. 1F). Sir2 binding reduced in regions distant from the silencer elements in wild type and H4 K16R cells but continued to remain higher in the H4 K16Q cells (Fig. 1F). To sum up, mutation in H4 K16 residue to R or Q disrupts the level and extent of Sir protein binding in both the silenced regions and

A: Sub - Telomeric Region (*TEL06R*)

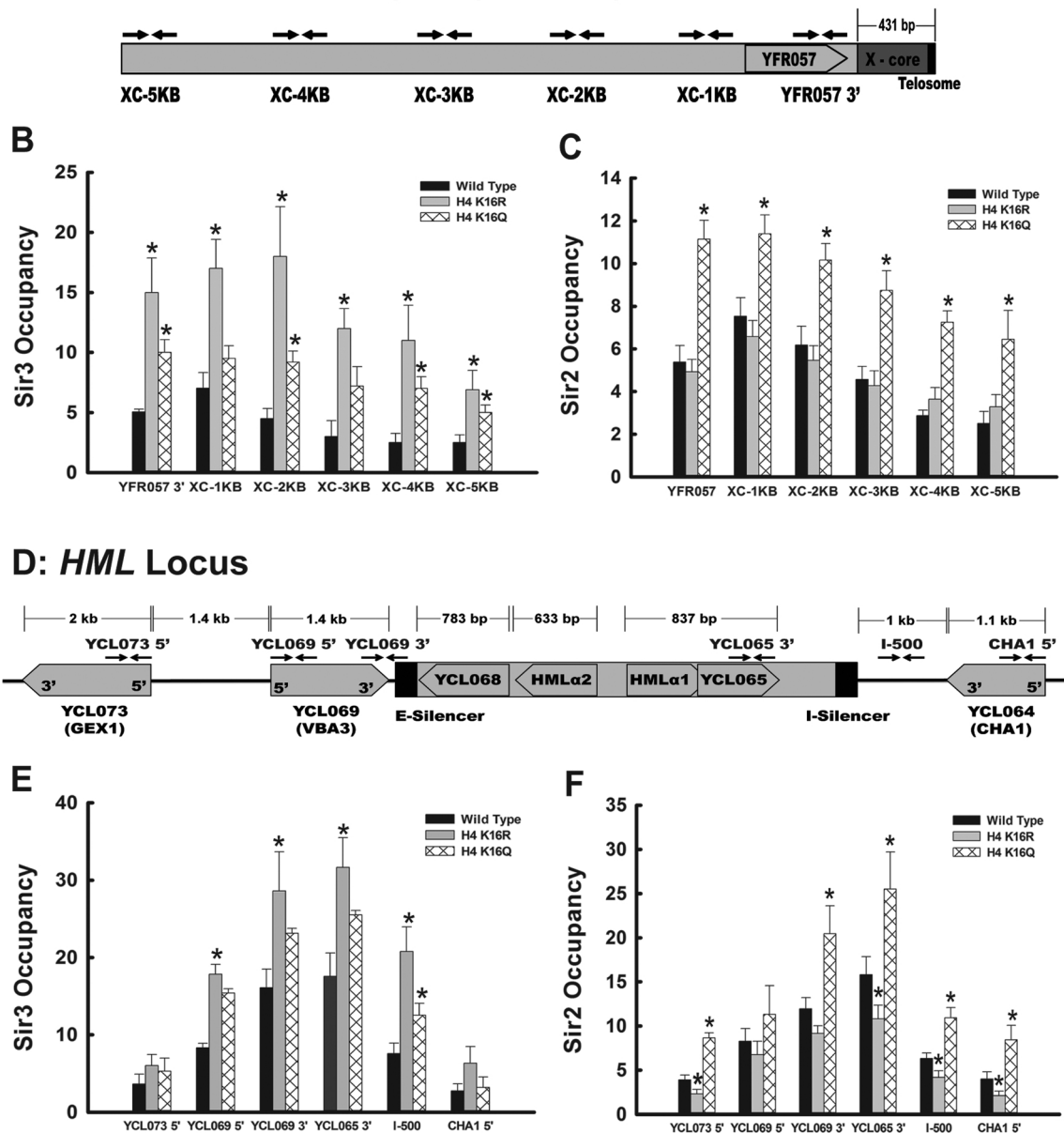


Fig. 1. Sir protein binding to the silenced *HML* locus and sub-telomeric region. ChIP analyses done either with anti-Sir3 or anti-Sir2 antibody followed by qPCR to check binding of Sir proteins. **A)** Schematic representation of sub-telomeric region, showing X-core consensus element, *YFR057* and different distances from the X-core element. Each arrow set represents primer pairs used for ChIP-qPCR of the specified regions. **B)** Sir3 occupancy and **C)** Sir2 occupancy in the above mentioned sub-telomeric regions. **D)** Schematic representation of the *HML* locus, showing the silenced regions between the E- and the I-silencer elements and the regions beyond the designated silencer elements. Each arrow set represents primer pairs used for ChIP-qPCR of the specified regions. **E)** Sir3 occupancy and **F)** Sir2 occupancy in the above-mentioned regions of the *HML* locus. For each strain, data represent the mean for three independent experiments with standard error of mean bars and asterisks indicate *t*-test significant P values < 0.05.

causes heterochromatin spreading beyond the designated boundary elements. The above results are in accordance with previous literature that elucidate the role of H4 K16 in silencing and further confirm that mutating H4 K16 to either R or Q is equivalent to disrupting regulation of H4 K16 mediated silencing and spreading of heterochromatin.

3.2. Mutation of H4 K16 causes alteration in chromatin accessibility

Crystal structure has shown that the H4 N-terminal tail of a nucleosome protrudes into the H2A/H2B patch of the neighbouring nucleosome and H4 K16 is a key player in such inter-nucleosomal interactions thus contributing to the higher order chromatin compaction [8,52]. So next aim was to investigate whether mutation of H4 K16

residue cause any alterations in the chromatin accessibility per se. For this, micrococcal nuclease (MNase) accessibility studies were done in H4 K16 mutant chromatin and compared to wild type (Fig. 2). MNase digestion profiles in the silent loci showed reduced MNase accessibility in the H4 K16 mutants compared to wild type, both in the *HML* and telomere region (Fig. 2A, B). As represented graphically, higher undigested chromatin fractions for the same enzyme concentration in a particular strain indicate reduced chromatin accessibility, compared to wild type. With the same enzyme concentration (12 units) while wild type chromatin showed more than 80% MNase digestion at these loci, the H4 K16 mutants exhibited only about 40–50% digestion. Additionally, when MNase digestion was done in whole chromatin both H4 K16R and K16Q cells showed similarly reduced accessibility

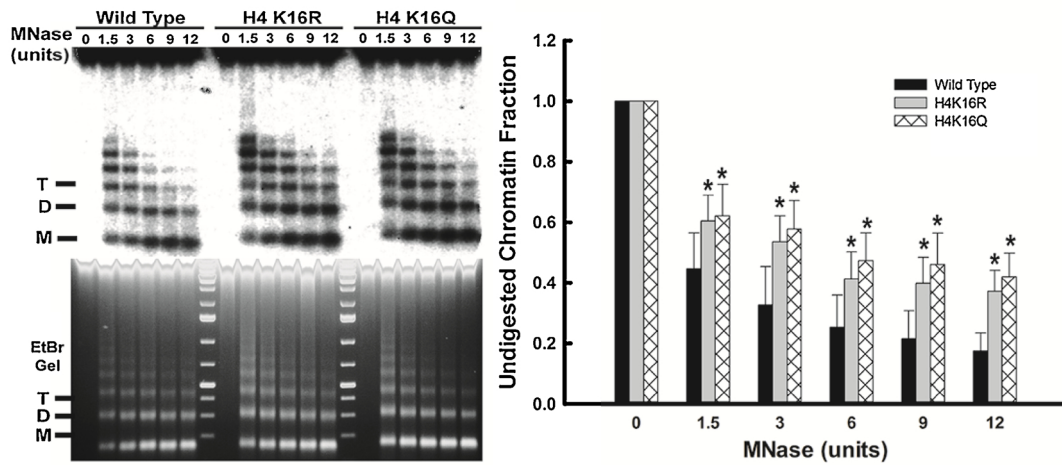
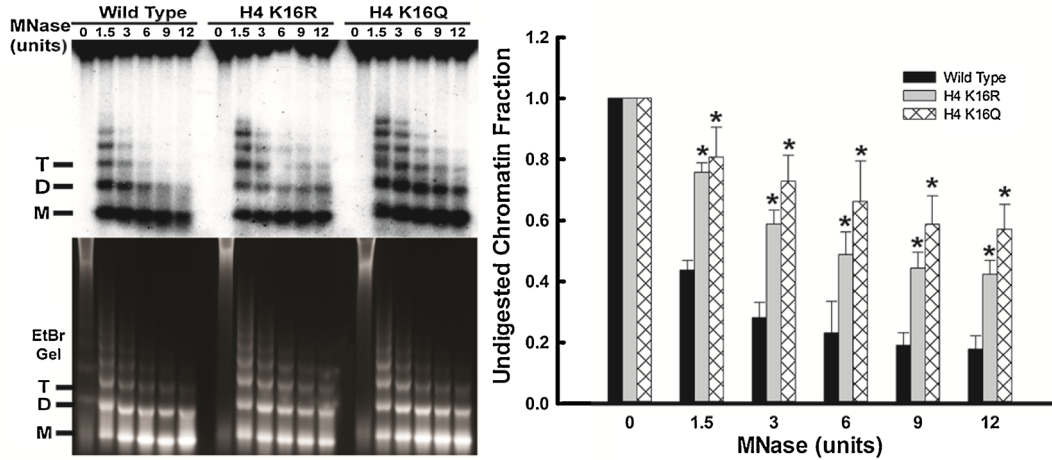
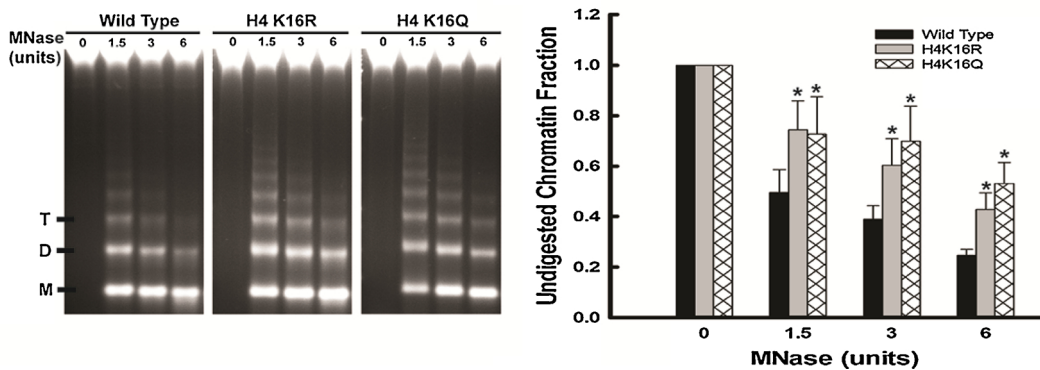
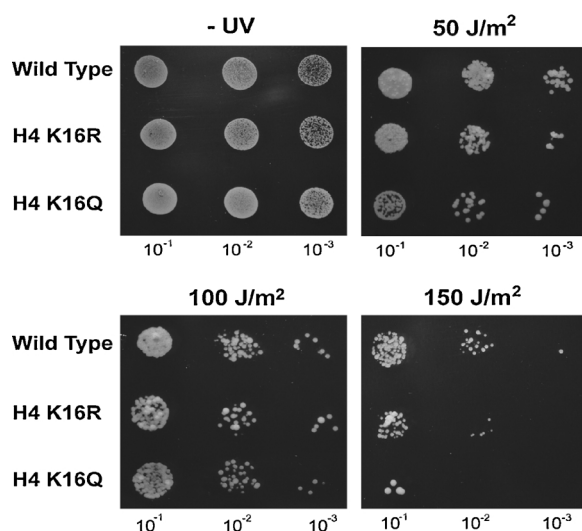
A: HML Locus**B: Telomere Region****C: Whole Chromatin**

Fig. 2. MNase digestion profile of wild type and H4 K16 mutant chromatin. Isolated spheroplasts from wild type and H4 K16 mutant cells were treated with various concentrations of MNase, as described in Materials and Methods, genomic DNA isolated and separated on 1.2% agarose gels. Southern hybridisation of gels done with probes specific to **A) HML** and **B) Telomere** regions; **C) Digestion** profile of whole chromatin stained with ethidium bromide. M, D and T denote positions of mono-, di- and tri-nucleosomal DNA populations, respectively. Undigested chromatin fraction was graphically plotted to represent comparative chromatin accessibility genome wide and in each locus. For each strain, data represent the mean for three independent experiments with standard error of mean bars and asterisks indicate *t*-test significant P values < 0.05.

A: Spot Assay



B: Spread Assay

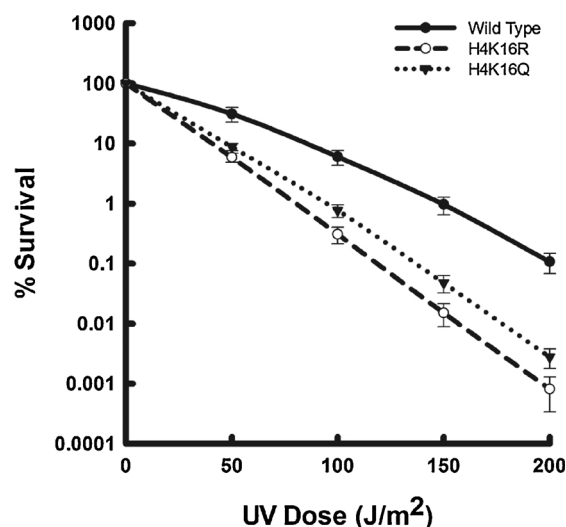


Fig. 3. UV sensitivity of wild type and H4 K16 mutants. Ten-fold serial dilutions of exponentially growing cultures were either A) spotted or B) spread on YEA plates with or without UV irradiation. Left panel shows differential UV sensitivity in spot assay. For spread assay the colony forming units were counted and graphically represented as percent cell survival with increasing doses of UV with respect to no UV control. For each strain, data represent the mean for three independent spread assays done, with standard error of mean bars.

compared to wild type especially at lower enzyme concentrations (Fig. 2C). It was observed that with 1.5 units of the enzyme while wild type cells showed 50% MNase digestion, the mutants showed less than 30%. Thus, mutation of H4 K16 to either R or Q results in hindered chromatin accessibility genome wide including the transcriptionally silenced mating locus and the telomere region.

3.3. H4 K16 mutants exhibit higher sensitivity to UV irradiation

Chromatin landscape is known to affect various nuclear processes. Changes in chromatin structure can influence NER efficiency and consequently UV sensitivity [29,33]. Therefore, aim was now to check whether the increased chromatin compaction observed in the H4 K16 mutants affects UV sensitivity or UV-induced NER efficiency. For this, the H4 K16 mutant strains were irradiated with different doses of UV and their cell survival was compared to wild type. Interestingly, after UV irradiation, both the H4 K16 mutants exhibited lower survival rate compared to wild type. As shown in Fig. 3, with increasing doses of UV, survival of the H4 K16 mutants became significantly lower compared to wild type. It is evident from these results that both H4 K16R and H4 K16Q cells have higher UV sensitivity compared to wild type.

3.4. H4 K16 mutation leads to reduced NER efficiency in heterochromatin regions of the genome

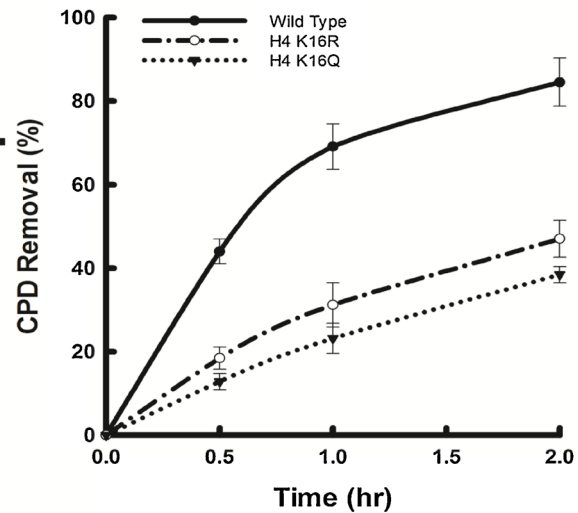
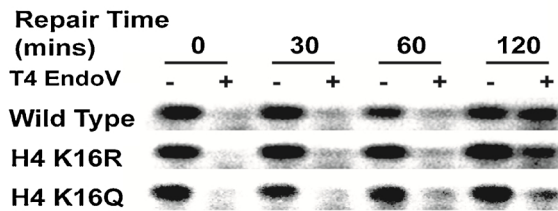
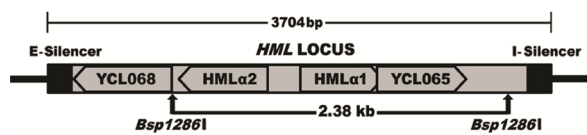
The higher UV sensitivity observed in the H4 K16 mutants could possibly be a reflection of reduced ability of the mutants to repair UV induced DNA damages. Altered chromatin structure or accessibility is often known to affect NER efficiency and consequently UV sensitivity [29,33]. So, nucleotide excision repair rate was next studied. For this, wild type and H4 mutant cells were irradiated with 100 J/m² of UV, followed by repair incubation for different time periods. T4 Endonuclease V cleaves DNA at the 5' end of an UV-induced CPD. T4 Endonuclease V digestion profile of UV induced and repair incubated samples was therefore used to estimate the number of CPDs present at each time point as mentioned in the Methods section [42]. The number of CPDs at each time point was calculated by normalising the signal intensity of the T4 Endonuclease V treated DNA samples to those of the

mock treated ones. Based on the number of CPDs present in each strain at 0 min of repair, the CPD removal percentage and hence the rate of NER for that strain was calculated using the formula: $100 - 100 * [-\ln(\text{CPD no. at repair time point } x) / -\ln(\text{CPD no. at 0 min repair})]$. NER was checked both at the *HML* and telomeric regions. As shown in Fig. 4A, CPD removal in the *HML* locus was much more efficient in the wild type cells compared to the H4 K16 mutants. By 60 min almost 70% CPDs were repaired in the wild type cells, compared to about 30% and 20% in the H4 K16R and K16Q mutants respectively (Fig. 4A). NER rate in the telomere region was checked in a completely heterochromatinized region of chromosome VIII. As shown in Fig. 4B, the telomere region of chromosome VIII contains all the characteristic elements present in a *Saccharomyces cerevisiae* telomere chromosome VIII which include, the conserved X-core consensus sequence, X element combinatorial repeats, telomeric repeat sequences and the Y' element. Even though Y'-telomeres do not contain the Sir proteins at the Y' elements, the region of *TEL08R* that was probed in this study for NER analyses is adjacent to the telomeric repeat sequences and silenced by enrichment of Sir proteins [53,54]. Similar to *HML* locus, in the telomeric region as well, NER rate in wild type cells was significantly higher compared to the mutants. As shown in the figure by 60 min of repair about 75% CPDs were removed in wild type, compared to only 30% and 25% CPD removal in H4 K16R and K16Q cells, respectively (Fig. 4B). To summarize, the above results indicate that UV-induced DNA damage repair is significantly compromised in the heterochromatinized regions of H4 K16 mutant cells.

3.5. Rad protein and Snf5 recruitment during NER is affected in the H4 K16 mutants

A successful repair pathway involves availability of NER proteins as well as proper accessibility of NER proteins to the lesion site. MNase digestion results indicated that the reduced chromatin accessibility in H4 K16 mutant cells possibly affects NER rate negatively. Next aim was therefore to check whether the mutant chromatin with hindered accessibility was refractory to recruitment of NER proteins during early steps of repair. Damage recognition during NER is the rate limiting step and in yeast cells Rad23 protein in complex with Rad4 is known to play

A. HML



B. Telomere

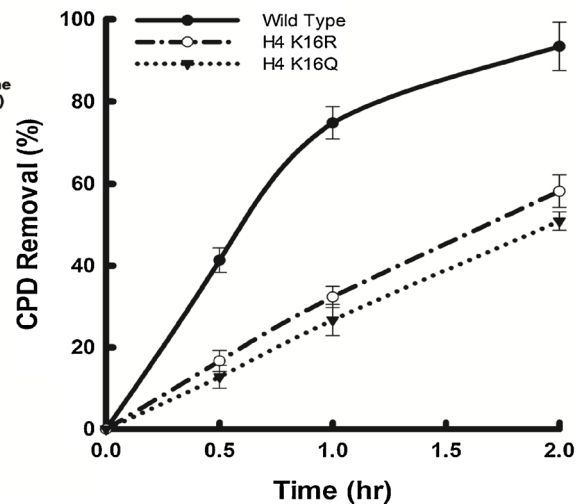
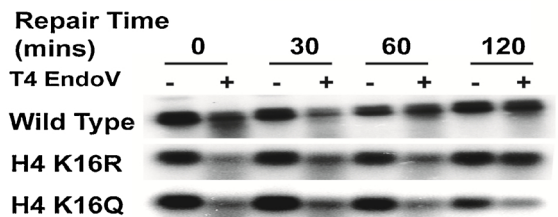
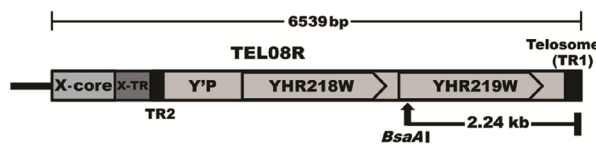


Fig. 4. NER in *HML* and Telomere region of wild type and H4 K16 mutants. Wild type and H4 K16 mutant cells were irradiated with a UV dose of 100 J/m², followed by repair incubation for different time periods. Genomic DNA was digested with locus specific restriction enzymes followed by digestion with or without T4 endonucleaseV, as mentioned in Material and Methods. Locus details and graphical representation of CPD removal from A) *HML* and B) Telomeric regions respectively are shown. For each strain, data represent the mean for three independent experiments with standard error of mean bars.

a role in damage recognition [55,56] Rad16 is another early NER protein which is a member of the SWI/SNF family of ATPases [57–59]. Recruitment of Rad23 and Rad16 occupancy was therefore checked at the *HML* and telomere regions, during NER. In the *HML* locus, Rad23 recruitment in wild type cells was observed within 10 min of repair. However, much delayed recruitment of Rad23 was observed in both the H4 K16 mutants (Fig. 5A). Similar pattern of Rad23 recruitment was observed in the telomere region where wild type cells recruited Rad23 protein within first 10 min. of repair, while the H4K16 mutants showed delayed recruitment (Fig. 5B). Such delayed Rad23 recruitment in the H4 K16 mutants suggest that initial damage recognition in the mutants is retarded, compared to wild type. Furthermore, Rad16 recruitment was also reduced in the H4 K16 mutants, compared to wild type during NER. As shown in the figure, level of Rad16 recruitment in the H4 K16 mutants during first 60 min of repair was significantly less compared to wild type, in both the *HML* and telomere regions (Fig. 5C & D). The above results make it clearly evident that the reduced chromatin accessibility in the H4 K16 mutants hinders recruitment of NER proteins during NER. Along with recruitment of NER proteins, chromatin remodelling is another crucial step during early NER and damage recognition proteins are known to interact with Swi/Snf complex during such repair process [60]. Comparative analysis of Swi/Snf recruitment

was thereafter done in the wild type and H4 K16 mutants during NER. For this, Snf5 recruitment was analysed in the H4 K16 mutants and wild type cells during first 60 min of NER, as mentioned above. As per our observations, in both the heterochromatin regions tested the level of Snf5 recruitment was significantly reduced in the H4 K16 mutants, compared to wild type (Fig. 5E & F). This indicates that chromatin remodelling required to make DNA lesions accessible to the repair machinery during early phases of NER, is compromised in the H4 K16 mutants. To summarize, our results clearly show that recruitment of NER proteins and chromatin remodelling complex Swi/Snf is hindered in both H4 K16R and K16Q mutants during initial phases of NER. Based on such observations it is logical to conclude that the reduced recruitment of the repair proteins and chromatin remodeller during NER is due to the more refractory chromatin in the H4 K16 mutants, compared to wild type and that has finally led to reduction in NER efficiency in the mutant cells.

3.6. H4 K16 mutation affects expression of NER genes

Reduced chromatin accessibility in the H4 K16 mutants may also affect efficiency of gene expression. In fact, previous reports have suggested that H4 K16 acetylation status can affect active transcription

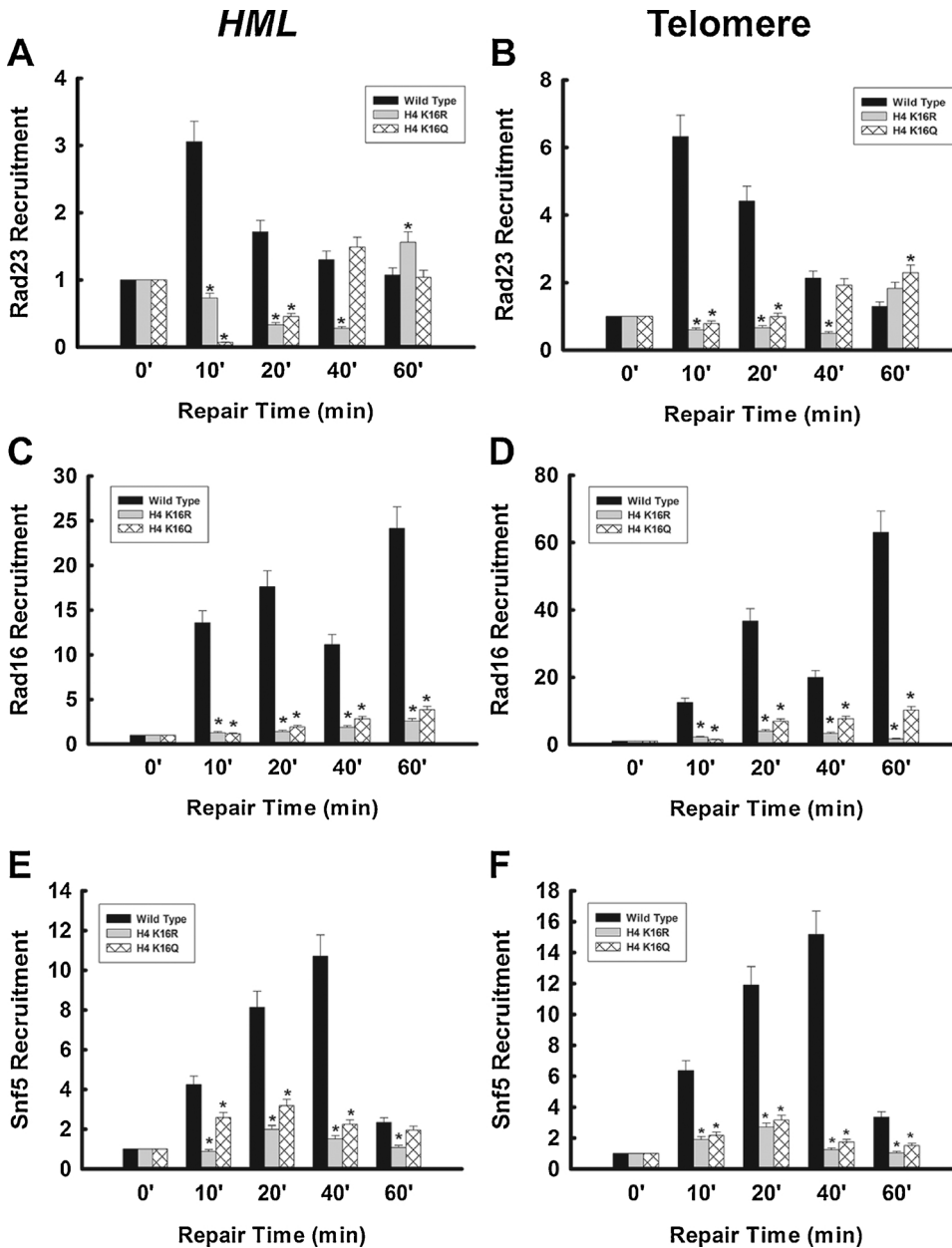


Fig. 5. Comparative recruitment of repair proteins and Snf5 in wild type and H4 K16 mutants during NER. Wild type, H4 K16R and H4 K16Q cells were subjected to UV irradiation at a dose of 100 J/m² followed by repair incubation for different time periods. ChIP analyses were done using antibodies against Rad23, Rad16 or Snf5 to check recruitment at A, C, E *HML* locus and B, D, F *Telomere* region. The data was calculated as percentage of input and plotted as relative fold change of recruitment over 0 min repair time point. For each strain, data represent the mean for three independent experiments with standard error of mean bars and asterisks indicate *t*-test significant P values < 0.05.

[19]. Thus, in addition to chromatin accessibility problem the observed inefficiency in recruitment of the Rad proteins and Swi/Snf complex during NER could also be due to decreased expression of the genes in the H4 K16 mutants during NER. Transcription of NER-responsive *RAD* genes and *Snf5* was therefore checked in the H4 K16 mutant cells. Expression of several NER-responsive genes functional during early and later phases of NER was checked and hence expression study was done within 60 min of UV irradiation. As per our observations during UV-induced repair, expression of the *RAD* genes that were tested namely, *RAD23*, *RAD4*, *RAD16*, *RAD1*, *RAD2* and *RAD14* genes, was significantly lower in both the H4 K16 mutants, compared to wild type. Similarly when *SNF5* expression was checked within 60 min of NER, both the H4 K16 mutants had lower levels of *SNF5* transcripts compared to wild type (Fig. 6). Since both the H4 K16 mutants have reduced chromatin accessibility genome wide (Fig. 2), it is therefore possible that the repressive chromatin structure in the mutants provides a refractory environment non-conducive for transcription leading to compromised expression of *RAD* and *SNF5* genes. Thus less accessible chromatin structure in the H4 K16 mutants causes reduced expression

of *RAD* and *SNF5* genes along with impaired recruitment of these proteins during NER, which together lead to less efficient repair in the mutants compared to wild type cells.

3.7. Nucleosome repositioning during NER is affected in the H4 K16 mutants

For NER to occur in chromatinized DNA, nucleosomal rearrangement or repositioning is an indispensable process that allows proper access of the huge NER complex to the DNA lesions [61–65]. It was reasoned that reduced recruitment of the NER proteins and Swi/Snf complex might also be associated with compromised nucleosome rearrangements in the H4 K16 mutants during NER. In view of this, nucleosome occupancy was checked in the H4 K16 mutants during NER. For this, H3 level was checked in both *HML* and *telomere* regions, during first 60 min of repair. To get a more accurate idea of nucleosome rearrangements at the two above mentioned loci during NER, H3 was measured in two physically separated regions of each locus. As per our results, nucleosome occupancy in wild type showed a steady decrease in

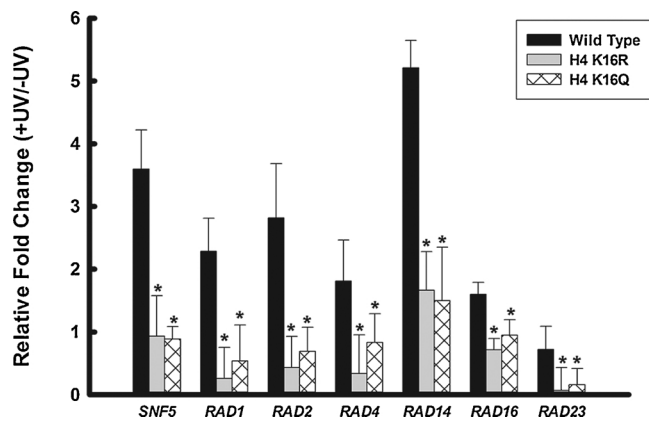


Fig. 6. Comparative expression of *SNF5* and *RAD* genes in wild type and H4 K16 mutants during UV induced NER. RNA was isolated from wild type and H4 K16 mutant cells without or with UV irradiation at a dose of 100 J/m² followed by 1 h of repair incubation. RT-qPCR was performed and the level of gene expression was plotted relative to UV untreated samples. For each strain, data represent the mean for three independent experiments with standard error of mean bars and asterisks indicate *t*-test significant P values < 0.05.

both loci within first 60 min of NER, compared to no UV control. However, no such significant reduction in nucleosome occupancy was found in the H4 K16 mutants during that period (Fig. 7). Therefore, it can be concluded that, lack of significant nucleosome repositioning in the H4 K16 mutants during initiation of NER, hinders accessibility of repair machinery to the DNA lesions. This strongly complements our NER results, where H4 K16 mutants have slower rate of repair, compared to wild type cells. Taken together our results indicate that K16 mutation to either R or Q impedes nucleosome repositioning during NER, which compromises NER efficiency in the mutants.

3.8. H4 K16 mutation also affects NER functions in euchromatin region of the genome

Our studies on micrococcal nuclease digestion profiles indicated that along with reduced accessibility in the heterochromatin regions, the H4 K16 mutants have genome wide reduced chromatin accessibility, compared to wild type (Fig. 2C). Therefore, we next wanted to check whether reduced NER efficiency and the associated altered chromatin functions in the H4 K16 mutants could be extended to the euchromatin regions of the genome, as well. For this, the transcriptionally active locus *RPB2* which codes for the second largest subunit of RNA polymerase II was chosen and subsequent studies were done in this locus as a representative euchromatin region (Fig. 8A). Chromatin accessibility studies showed that, at lower MNase concentrations both the H4 K16 mutants have reduced accessibility compared to wild type (Fig. 8B). However, with increasing MNase concentrations, accessibility of H4 K16R chromatin gradually increased and became comparable to wild type, while H4 K16Q continued to exhibit decreased access. This difference is noteworthy, as in the heterochromatin regions both the H4 K16 mutants exhibited similarly reduced chromatin accessibility in comparison to wild type. When NER rate was analysed at the *RPB2* locus, during early hours of repair the H4 K16 mutants removed CPD at a rate slower than wild type (Fig. 8C). Interestingly, however during later repair time points CPD removal rate in H4 K16R cells became much higher than H4 K16Q cells. As evident from the figure, by 2 h of repair H4K16R repaired more than 90% of CPDs, a rate almost comparable to wild type cells, while H4 K16Q cells repaired less than 70% CPDs. This indicates that in the euchromatin region, while H4 K16R cells shows a delay in CPD removal during early NER phases, unlike H4 K16Q cells, its repair rate enhances during later phases. As both the H4 K16 mutants show hindered chromatin accessibility even in the euchromatin region, initial steps of NER involving

damage recognition and accessibility is delayed in both the mutants. Once the initial accessibility hindrance is overcome, H4 K16R cells can remove CPDs faster than H4 K16Q. This is further substantiated by the observations that similar to the *HML* and telomere regions, recruitment of Rad23 and Rad16, the early repair proteins were also found to be delayed at the *RPB2* locus of both the H4 K16 mutants (Fig. 8D & E), compared to wild type. Thus, to summarize, in the euchromatin region while both the H4 K16 mutants have similarly compromised repair rate during initial phases of NER, during later phases they act in a somewhat differential manner. The reason for such differential behaviour between H4 K16R and K16Q mutants during NER in the euchromatin region will be an interesting avenue for future investigation.

3.9. Effect of H4 K16 mutation on UV-induced H3 N-terminal tail acetylation

Previous reports have shown that Gcn5-mediated histone H3 acetylation, more precisely H3 K9 and K14 acetylation occurs during NER [37,39,66]. Additionally, H4 K16 acetylation is known to influence Gcn5 binding to the H4 N-terminal tail [40]. Therefore, for the present study it was pertinent to check the status of H3 K9 and K14 acetylation during NER in the H4 K16 mutant cells. H3 acetylation was checked in the transcriptionally silent *HML* locus and active *RPB2* locus, during early NER time points. At the *HML* locus, UV-induced increase in acetylation of H3 K9 residue was observed early i.e., within 5 min of repair in both wild type and H4 K16Q mutant cells, compared to UV-untreated control. In H4 K16R mutants however, H3 K9 acetylation was delayed compared to wild type and H4 K16Q cells, and occurred after 10 min of UV irradiation (Fig. 9A). Similarly at the *RPB2* locus, increase in H3 K9 acetylation was found within 5 min of UV irradiation in both wild type and H4 K16Q cells, while maximal increase in H3 K9 acetylation in H4 K16R cells was observed during 10 min of repair (Fig. 9A). These findings support previous observations that in wild type yeast cells H3 K9 acetylation is known to occur very early during NER [67]. Findings were different for H3 K14 acetylation during NER. At the *HML* locus, increased H3 K14 acetylation in wild type cells was observed within 10 min of UV irradiation, while significant hyperacetylation in H4 K16Q cells was found only after 20 min of UV irradiation which increased further by 40 min. In comparison, H4 K16R cells showed further delay and significant H3 K14 acetylation was observed only after 40 min of UV irradiation (Fig. 9B). Similarly, at the *RPB2* locus, UV-induced increase in H3 K14 acetylation was observed in wild type cells within 10 min of UV irradiation, compared to untreated control. In H4 K16Q significant H3 K14 hyperacetylation was observed only after 20 min of UV treatment, levels of which increased further as NER progressed. However, in H4 K16R cells, a small increase in H3 K14 hyperacetylation was observed after 20 min of UV irradiation, which did not increase significantly by 40 min (Fig. 9B).

3.10. H4 K16 acetylation in response to UV-induced NER

The adverse effect of H4 K16 mutation, to either R or Q, on NER efficiency and NER associated events indicated that a regulated dynamism between acetylation and deacetylation states of H4 K16 is possibly important during the repair process. Acetylation status of H4 K16 during different phases of NER was therefore checked in wild type cells, in all the three loci where CPD removal was tested. At the transcriptionally active *RPB2* locus, no increase in H4 K16 acetylation was observed early during NER, compared to UV untreated cells. Significant hyper-acetylation of H4 K16 was observed only after 40 min. of repair, where after it increased further by 120 min of repair (Fig. 10A). For the transcriptionally silenced telomere and *HML* regions, observations were similar. Compared to UV untreated controls no increased acetylation of H4 K16 was observed during initial repair, followed by hyper-acetylation during later phases of NER. Similar to *RPB2* locus, maximum hyper-acetylation in both the silent loci was observed during 120 min of

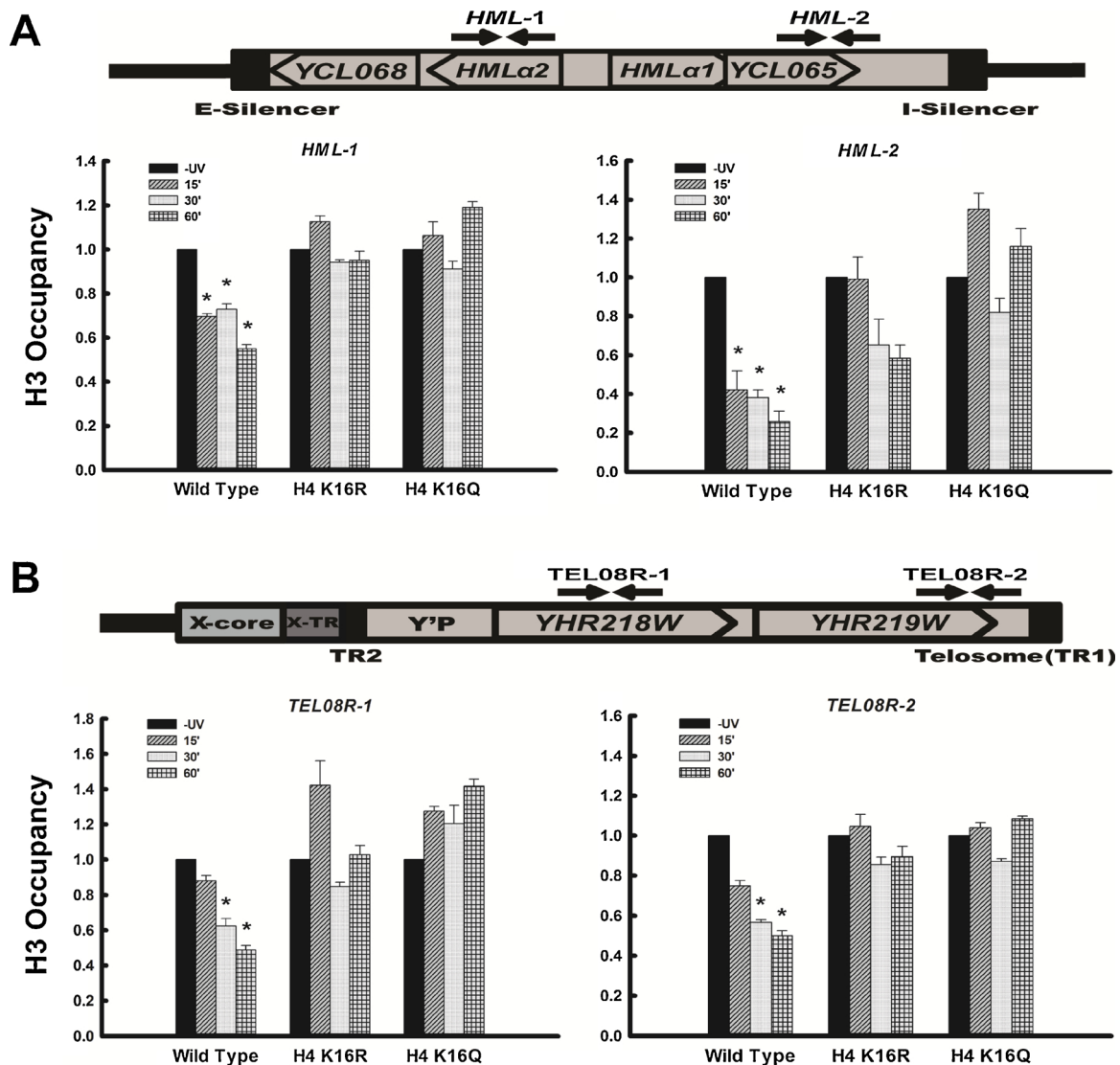


Fig. 7. Nucleosome occupancy during NER in wild type and H4 K16 mutants. Wild type, H4 K16R and H4 K16Q cells were irradiated with an UV dose of 100 J/m², followed by repair incubation for different time periods. ChIP analysis with anti-H3 antibody was done to check nucleosome occupancy at two regions representing A) *HML* and B) Telomeric loci, respectively. The data was calculated for H3 occupancy as a percentage of input for every time point and normalised against UV untreated samples. For each strain, data represent the mean for three independent experiments with standard error of mean bars and asterisks indicate *t*-test significant P values < 0.05.

NER (Fig. 10B & C). The above results clearly indicate that followed by an initial phase of hypoacetylation, hyperacetylation of H4 K16 occurs during later phases of NER. This regulated balance between the hypo- and hyperacetylated state of H4 K16 residue must be an essentiality during NER, which is maintained in wild type cells, but gets disturbed in both H4 K16R and K16Q mutant cells.

4. Discussion

H4 K16 acetylation status is known to regulate Sir mediated gene silencing at the heterochromatin regions [9,13–15,17]. When Sir protein occupancy was checked at the silent mating locus *HML* and the telomere region of H4 K16R and H4 K16Q mutants, increased binding of Sir3 and Sir2 and spreading of the proteins was observed beyond the designated boundaries. Thus, mutating H4 K16 to either a state of constitutive acetylation (Q) or to a state of constitutive deacetylation (R) disturbs the regulation and extent of Sir protein binding. This indicates that the dynamism between acetylation and deacetylation state of H4 K16 normally found in wild type cells is essential for regulated heterochromatinization. In H4 K16 mutants, the loss of acetylation-

deacetylation dynamism led to increased heterochromatinization and spreading of silencing and generated a less accessible chromatin compared to wild type cells. Interestingly this reduced chromatin accessibility in the H4 K16 mutants was not only found in the transcriptionally silenced regions but was observed genome wide. Thus, locking H4 K16 residue to a state of either acetylation or deacetylation reduces chromatin fluidity even in the euchromatin regions.

Chromatin landscape and its alterations are known to affect DNA metabolic functions like NER and consequently UV sensitivity of an organism [29,30,33]. H4 K16 mutation in fact rendered the mutants more sensitive to UV compared to wild type cells and NER was found to be compromised in the H4 K16 mutants at specific loci of both heterochromatin and euchromatin regions. Since the H4 K16 mutants exhibited reduced chromatin accessibility to small molecule like micrococcal nuclease, it can be reasoned that accessibility of a huge protein complex like the NER machinery, will also be hindered. Delayed recruitment of Rad23 protein observed in the H4 K16 mutants during early NER phases confirmed the above speculation. Among the proteins involved in NER, binding of Rad4-Rad23 complex to the damage site is one of the earliest steps of the repair pathway in yeast [55]. It is known

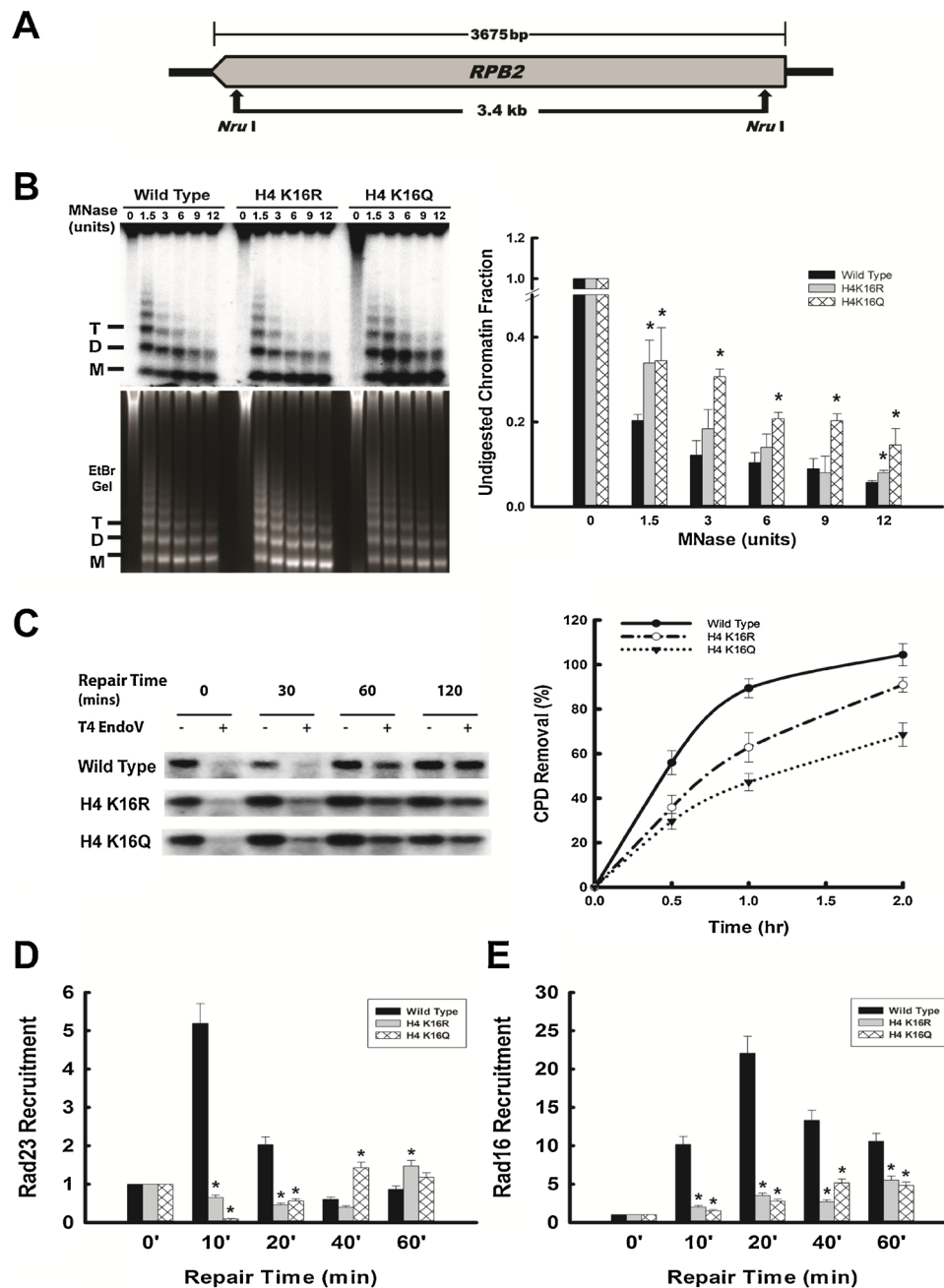
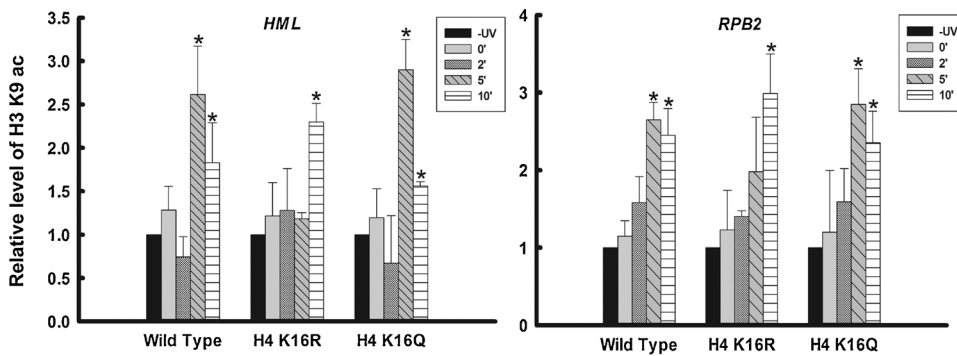


Fig. 8. Effect of H4 K16 mutation on transcriptionally active chromatin region. Transcriptionally active *RPB2* locus was used as a representative. **A)** Locus detail; **B)** MNase digestion profile; **C)** CPD removal, **D)** Rad23 and **E)** Rad16 recruitment during NER at the *RPB2* locus. For each strain, data represent the mean for three independent experiments with standard error of mean bars and asterisks indicate *t*-test significant *P* values < 0.05.

that absence of Rad23 disrupts Rad4 or XPC mediated damage recognition and impair NER in yeast and mammalian cells, respectively [68–70]. Since damage recognition is the rate limiting step of NER, reduced recruitment of Rad23 in the H4 K16 mutants have essentially affected NER efficiency in the mutant cells. Similarly, binding of another early NER factor Rad16 was also affected in the H4 K16 mutants. Since, heterodimerization of Rad16 with Rad7 and subsequent binding to DNA, is a crucial step in the process of GGR in yeast [57–59], it is evident that inefficient Rad16 recruitment would essentially reduce NER proficiency in the H4 K16 mutants. Thus, reduced chromatin accessibility in the H4 K16 mutants prevented efficient recruitment of two early NER proteins Rad23 and Rad16 during NER, which distinctly affected NER proficiency in the mutant cells. Furthermore, for NER to occur in a chromatinized environment, chromatin remodelling is an

essential event ([71]; [63] [32];). Swi/Snf mediated chromatin remodelling has been shown to be a crucial part of NER, especially in the silent chromatin regions [33,60,64]. In the H4 K16 mutants, Snf5 occupancy was found to be significantly reduced during NER in the transcriptionally silenced *HML* and telomere regions, compared to wild type. Thus, either constitutively acetylated or deacetylated state of H4 K16 hinders Swi/Snf recruitment to the transcriptionally silenced *HML* and telomere regions, during NER. Furthermore, apart from accessibility problem, reduced recruitment of Rad and Snf5 proteins in the mutant cells during NER was also a result of reduced expression of these genes during NER. As per our findings, the H4 K16 mutants have genome wide reduced accessibility and we reasoned that such a chromatin landscape can be refractory to the transcription machinery as it is to the NER machinery. In fact, UV-induced expression of the *RAD* and

A: H3 K9 Acetylation



B: H3 K14 Acetylation

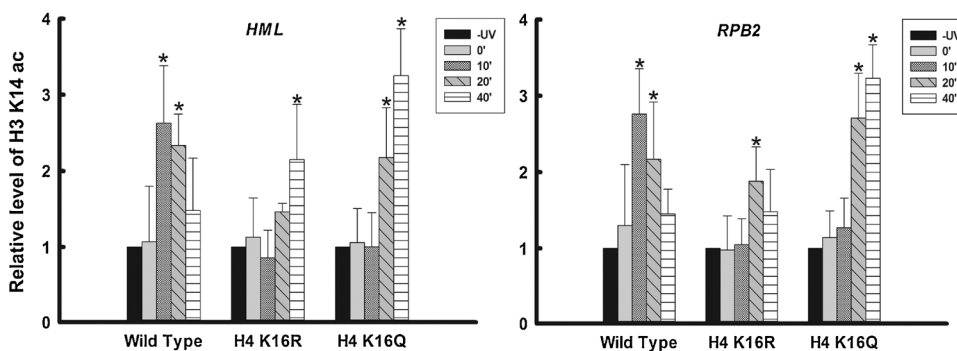


Fig. 9. H3 K9 and H3 K14 acetylation during NER. ChIP analyses were done using A) anti-H3 K9ac or B) anti-H3 K14ac antibody with cells treated without or with UV at a dose of 100 J/m² followed by repair incubation for various time points. Quantitative PCR was done to check H3 K9 or K14 acetylation status during NER at *RPB2* and *HML* loci, respectively. The data was normalised against H3 and plotted relative to UV untreated samples. For each strain, data represent the mean for three independent experiments with standard error of mean bars and asterisks indicate *t*-test significant P values < 0.05.

SNF5 genes was found to be significantly reduced in both the H4 K16 mutants, thus implying that mutation of H4 K16 to either R or Q generates a chromatin environment that is non-conducive for transcription of inducible genes. The impaired recruitment of Rad and Snf5 proteins observed in the H4 K16 mutants during NER is therefore a cumulative effect of hindered chromatin accessibility of the proteins and reduced UV-responsive inducibility of the genes. Repositioning of nucleosomes away from the lesion site for DNA accessibility of NER machinery is a crucial factor that affects NER efficiency [29,60]. In the H4 K16 mutants, inefficient Swi/Snf recruitment was coupled with lack of reduction in nucleosome occupancy during initial phases of NER. As the process of NER involves a large multiprotein complex, nucleosomal remodelling is essential for accessing DNA lesions in a chromatin context, *in vivo*. Here we find that, the inherent reduced accessibility of the H4 K16 mutant chromatin is associated with lack of proper recruitment of NER proteins and Swi/Snf, along with hindered nucleosomal repositioning during NER. All these aspects together led to improper access of the NER machinery to DNA lesions and adversely affected repair efficiency in the H4 K16 mutants.

Intriguingly, the scenario in transcriptionally active regions of the H4 K16 mutants gave a better insight into the chromatin accessibility features of the individual mutants. While in the heterochromatin regions, both the mutants showed similarly reduced chromatin accessibility, in the euchromatin region accessibility was differential between the two mutants. Increased nuclease accessibility in the H4 K16R mutants at higher MNase concentrations, compared to H4 K16Q cells, indicate that at the transcriptionally active regions, higher order chromatin structure gets more easily disrupted in the H4 K16R cells when exposed to high enzyme concentrations. This MNase digestion difference between H4 K16R and K16Q mutants further indicate a role of H4 K16 acetylation (H4 K16Q) in restricting chromatin accessibility in the euchromatin regions of the genome. It is thus logical to propose that the increased chromatin accessibility observed in the H4 K16R mutants compared to K16Q at the transcriptionally active region, could be due to the differentially modified chemical state of the K16 residue in the

two mutants. Similar to chromatin accessibility, NER rate in the *RPB2* region was also found to be more efficient in H4 K16R cells especially at later time points, compared to H4 K16Q.

Additionally, H4 K16 mutations also affected UV-induced acetylation of H3 N-terminal tail during NER. Following UV irradiation, hyperacetylation of H3 K14 at the *HML* and *RPB2* loci was distinctly delayed in both the H4 K16 mutants, compared to wild type. In between the two H4 K16 mutants, K16Q cells were preferred for hyperacetylation of H3 K14 and acetylation was found to be prolonged in these cells during NER. Furthermore, UV-induced H3 K9 hyperacetylation in H4 K16Q cells was similar to wild type cells at both the loci tested. Adverse effect was observed for H4 K16R cells, where H3 K9 acetylation was significantly delayed post UV irradiation. Previous *in vitro* assays have shown that binding of Gcn5 to H4 N-terminal tail is promoted by H4 K16 acetylation [40]. This may explain why among the two H4 K16 mutants, H4 K16Q mimicking a state of constitutive acetylation are less adversely affected for H3 N-terminal tail hyperacetylation, compared to H4 K16R cells. However the possibility remains that *in vivo*, along with modification of H4 K16 residue the charged state of other basic residues in H4 N-terminal tail also contribute to the phenomenon. Moreover, NER factor Rad16 is known to mediate H3 K9 and K14 acetylation [66]. It is thus possible that reduced or delayed hyperacetylation of H3 observed in the H4 K16 mutants is also an effect of reduced availability and recruitment of Rad16 in the H4 K16 mutants during NER. Interestingly, despite H4 K16Q having H3 K9 acetylation pattern similar to wild type cells during NER, the cells still show compromised NER efficiency due to several reasons discussed above. This indicates that apart from mere histone modifications, NER efficiency is largely dependent on parameters like chromatin structure, recruitment and availability of repair proteins and remodeller proteins, adequate nucleosomal rearrangements and finally accessibility of NER machinery to the DNA lesions.

Finally, most intriguing and conclusive was the observation that in wild type cells during initial phase of NER there is hypoacetylation of H4 K16, followed by hyperacetylation of the residue as NER proceeds.

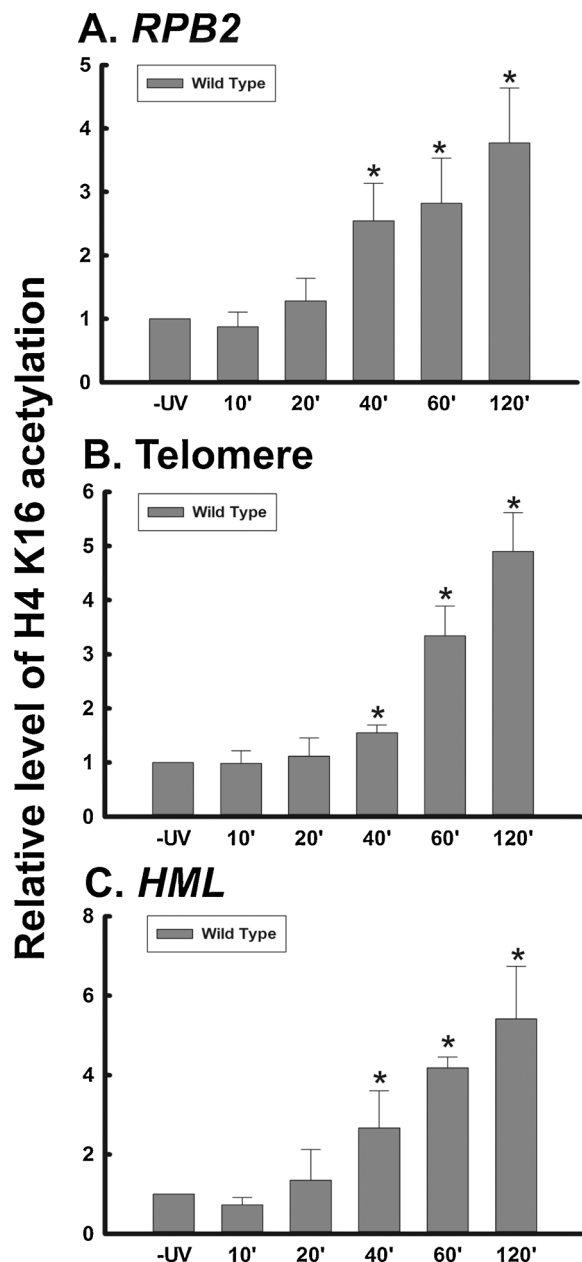


Fig. 10. H4 K16 acetylation during NER. ChIP analyses were done with anti-H4 K16ac antibody with cells treated without or with UV at a dose of 100 J/m² followed by repair incubation for various time points. Quantitative PCR was done to check H4 K16 acetylation status during NER at A) *RPB2*; B) Telomere and C) *HML* loci, respectively. The data was normalised against H3 and plotted relative to UV untreated samples. For each strain, data represent the mean for three independent experiments with standard error of mean bars and asterisks indicate *t*-test significant *P* values < 0.05.

This clearly indicates that for efficient NER and NER-related processes, H4 K16 residue oscillates between a state of hypoacetylation and hyperacetylation following UV irradiation. Our observation is in consonance with a previous work which has shown that UV-induced acetylation of H4 N-terminal tail occurs in yeast cells [37]. During early phases of NER, it is possible that a hypoacetylated state of H4 K16 is preferred for recruitment of NER factors and remodelling complexes. In fact, *in vivo* studies have indicated that recruitment of bromodomain-containing proteins like Bdf1 have anti-correlation with acetylation of H4 K16 [20]. However, future studies in this direction are required for reaching such conclusion for sure. Furthermore, our results on NER efficiency with two different H4 K16 mutants clearly imply that a

dynamism between states of acetylation and deacetylation of H4 K16 residue (as found in wild type cells) is essential for proper chromatin regulation during DNA metabolic functions in different genomic regions. Neither a constitutively acetylated form of H4 K16, nor a constitutively deacetylated form of the residue allows such regulated but dynamic chromatin accessibility and consequently affects efficiency of chromatin functions like NER and gene expression.

5. Conclusion

To summarize, H4 K16 is a unique H4 N-terminal residue whose acetylation-deacetylation status is under tight regulation. Conclusions from this work consolidate how mutation in H4 K16 residue affects chromatin accessibility and consequently DNA metabolic functions in the overall genome, *i.e.*, both in heterochromatin and euchromatin regions. It further emphasizes the need for efficient chromatin regulation and accessibility for DNA processes like damage repair. NER is a complex process dependent on several parameters including DNA accessibility in different chromatin domains, recruitment of NER proteins and their expression, chromatin remodelling and nucleosome rearrangements during NER. These processes can occur efficiently only when spatiotemporal modulation of the chromatin occurs in a faithful manner. Fidelity in chromatin accessibility is thus the underlying basis of such DNA-dependent functions. In yeast chromatin landscape is greatly influenced by the correct balance between acetylated and deacetylated state of H4 K16 residue. During NER, H4 K16 residue shows hypoacetylation during early NER phases followed by hyperacetylation as NER progresses. Thus, cells locked in a state of constant acetylation (H4 K16Q) or deacetylation (H4 K16R) of H4 K16 residue, exhibited altered chromatin regulations. UV-induced hyperacetylation of H3 N-terminal tail, chromatin decompaction, chromatin remodelling by Swi/Snf, nucleosomal rearrangements during early steps of NER and consequently accessibility of NER machinery to DNA lesions were thus distinctly affected in the H4 K16 mutants. In effect, NER efficiency was significantly compromised in the H4 K16 mutant cells. Our work thus consolidates the fact that regulated balance between the acetylated and deacetylated states of H4 K16 residue is essential for proper functioning of NER in all chromatin domains of *Saccharomyces cerevisiae*. In fact, in any living system mutation in such crucial residues may have disastrous effect on cellular fidelity and may lead to serious consequences and disease manifestation.

Author contributions

RNC and AR designed the experiments, AR and PK performed the experiments, RNC and AR analysed the results and wrote the paper.

Conflict of interest

Contents of this manuscript are solely the responsibility of the authors and do not necessarily represent the official views of the funding agency.

Acknowledgement

This work was supported by Science and Engineering Research Board (SERB), India [DST-Fast track Grant No. SR/FT/LS-145/2009] to Dr. Ronita Nag Chaudhuri, West Bengal DBT BOOST Grant No. [335/WBBD/CP-2/2013] to Department of Biotechnology, St. Xavier's College, Kolkata and by Department of Science and Technology, India [DST-FIST Grant No. SR/FST/COLLEGE-014/2010(C)] to St. Xavier's College, Kolkata. We sincerely acknowledge Prof. Michael J. Smerdon, Washington State University for kind donation of the plasmids. We also offer our sincere acknowledgement to Dr. Shubho Chaudhuri, Bose Institute for critical reading of the manuscript and for his scientific advices.

References

- [1] R.D. Kornberg, Y. Lorch, Twenty-five years of the nucleosome, fundamental particle of the eukaryote chromosome, *Cell* 98 (1999) 285–294.
- [2] B.M. Turner, Histone acetylation and an epigenetic code, *Bioessays* 22 (2000) 836–845.
- [3] B.D. Strahl, C.D. Allis, The language of covalent histone modifications, *Nature* 403 (2000) 41–45.
- [4] S.K. Kurdastani, M. Grunstein, Histone acetylation and deacetylation in yeast, *Nat. Rev. Mol. Cell Biol.* 4 (2003) 276–284.
- [5] A.E. Ehrenhofer-Murray, Chromatin dynamics at DNA replication, transcription and repair, *Eur. J. Biochem.* 271 (2004) 2335–2349.
- [6] A.J. Bannister, T. Kouzarides, Regulation of chromatin by histone modifications, *Cell Res.* 21 (2011) 381–395.
- [7] A.J. Bannister, T. Kouzarides, The CBP co-activator is a histone acetyltransferase, *Nature* 384 (1996) 641–643.
- [8] K. Luger, A.W. Mader, R.K. Richmond, D.F. Sargent, T.J. Richmond, Crystal structure of the nucleosome core particle at 2.8 Å resolution, *Nature* 389 (1997) 251–260.
- [9] C.B. Millar, S.K. Kurdastani, M. Grunstein, Acetylation of yeast histone H4 lysine 16: a switch for protein interactions in heterochromatin and euchromatin, *Cold Spring Harb. Symp. Quant. Biol.* 69 (2004) 193–200.
- [10] M. Shogren-Knaak, C.L. Peterson, Switching on chromatin: mechanistic role of histone H4-K16 acetylation, *Cell Cycle* 5 (2006) 1361–1365.
- [11] R. Zhang, J. Erler, J. Langowski, Histone acetylation regulates chromatin accessibility: role of H4K16 in inter-nucleosome interaction, *Biophys. J.* (2016).
- [12] P.S. Kaye, U.J. Kim, M. Han, J.R. Mullen, F. Yoshizaki, et al., Extremely conserved histone H4 N terminus is dispensable for growth but essential for repressing the silent mating loci in yeast, *Cell* 55 (1988) 27–39.
- [13] A. Hecht, T. Laroche, S. Strahl-Bolsinger, S.M. Gasser, M. Grunstein, Histone H3 and H4 N-termini interact with SIR3 and SIR4 proteins: a molecular model for the formation of heterochromatin in yeast, *Cell* 80 (1995) 583–592.
- [14] A. Kimura, T. Umehara, M. Horikoshi, Chromosomal gradient of histone acetylation established by Sas2p and Sir2p functions as a shield against gene silencing, *Nat. Genet.* 32 (2002) 370–377.
- [15] N. Suka, K. Luo, M. Grunstein, Sir2p and Sas2p oppositely regulate acetylation of yeast histone H4 lysine16 and spreading of heterochromatin, *Nat. Genet.* 32 (2002) 378–383.
- [16] A. Johnson, G. Li, T.W. Sikorski, S. Buratowski, C.L. Woodcock, et al., Reconstitution of heterochromatin-dependent transcriptional gene silencing, *Mol. Cell* 35 (2009) 769–781.
- [17] M. Oppikofer, S. Kueng, F. Martino, S. Soeroes, S.M. Hancock, et al., A dual role of H4K16 acetylation in the establishment of yeast silent chromatin, *EMBO J.* 30 (2011) 2610–2621.
- [18] L.K. Durrin, R.K. Mann, P.S. Kaye, M. Grunstein, Yeast histone H4 N-terminal sequence is required for promoter activation in vivo, *Cell* 65 (1991) 1023–1031.
- [19] A. Wang, S.K. Kurdastani, M. Grunstein, Requirement of Hos2 histone deacetylase for gene activity in yeast, *Science* 298 (2002) 1412–1414.
- [20] S.K. Kurdastani, S. Tavazoie, M. Grunstein, Mapping global histone acetylation patterns to gene expression, *Cell* 117 (2004) 721–733.
- [21] M.F. Dion, S.J. Altschuler, L.F. Wu, O.J. Rando, Genomic characterization reveals a simple histone H4 acetylation code, *Proc. Natl. Acad. Sci. U. S. A.* 102 (2005) 5501–5506.
- [22] F. Heise, H.R. Chung, J.M. Weber, Z. Xu, L. Klein-Hitpass, et al., Genome-wide H4 K16 acetylation by SAS-1 is deposited independently of transcription and histone exchange, *Nucleic Acids Res.* 40 (2012) 65–74.
- [23] C. Reiter, F. Heise, H.R. Chung, A.E. Ehrenhofer-Murray, A link between Sas2-mediated H4 K16 acetylation, chromatin assembly in S-phase by CAF-1 and Asf1, and nucleosome assembly by Spt6 during transcription, *FEMS Yeast Res.* (2015) 15.
- [24] A.W. Bird, D.Y. Yu, M.G. Pray-Grant, Q. Qiu, K.E. Harmon, et al., Acetylation of histone H4 by Esa1 is required for DNA double-strand break repair, *Nature* 419 (2002) 411–415.
- [25] A.A. Carmen, L. Milne, M. Grunstein, Acetylation of the yeast histone H4 N terminus regulates its binding to heterochromatin protein SIR3, *J. Biol. Chem.* 277 (2002) 4778–4781.
- [26] J.L. Workman, R.E. Kingston, Alteration of nucleosome structure as a mechanism of transcriptional regulation, *Annu. Rev. Biochem.* 67 (1998) 545–579.
- [27] F. Gong, Y. Kwon, M.J. Smerdon, Nucleotide excision repair in chromatin and the right of entry, *DNA Repair (Amst.)* 4 (2005) 884–896.
- [28] V. Mocquet, J.P. Laine, T. Riedl, Z. Yajin, M.Y. Lee, et al., Sequential recruitment of the repair factors during NER: the role of XPG in initiating the resynthesis step, *EMBO J.* 27 (2008) 155–167.
- [29] R. Nag, F. Gong, D. Fahy, M.J. Smerdon, A single amino acid change in histone H4 enhances UV survival and DNA repair in yeast, *Nucleic Acids Res.* 36 (2008) 3857–3866.
- [30] R. Nag, M.J. Smerdon, Altering the chromatin landscape for nucleotide excision repair, *Mutat. Res.* 682 (2009) 13–20.
- [31] M.J. Smerdon, A. Conconi, Modulation of DNA damage and DNA repair in chromatin, *Prog. Nucleic Acid Res. Mol. Biol.* 62 (1999) 227–255.
- [32] A. Groth, W. Rocha, A. Verreault, G. Almouzni, Chromatin challenges during DNA replication and repair, *Cell* 128 (2007) 721–733.
- [33] R. Nag, M. Kyriss, J.W. Smerdon, J.J. Wyrick, M.J. Smerdon, A cassette of N-terminal amino acids of histone H2B are required for efficient cell survival, DNA repair and Swi/Snf binding in UV irradiated yeast, *Nucleic Acids Res.* 38 (2010) 1450–1460.
- [34] M.J. Smerdon, S.Y. Lan, R.E. Calza, R. Reeves, Sodium butyrate stimulates DNA repair in UV-irradiated normal and xeroderma pigmentosum human fibroblasts, *J. Biol. Chem.* 257 (1982) 13441–13447.
- [35] B. Ramanathan, M.J. Smerdon, Changes in nuclear protein acetylation in u.v.-damaged human cells, *Carcinogenesis* 7 (1986) 1087–1094.
- [36] B. Ramanathan, M.J. Smerdon, Enhanced DNA repair synthesis in hyperacetylated nucleosomes, *J. Biol. Chem.* 264 (1989) 11026–11034.
- [37] Y. Yu, Y. Teng, H. Liu, S.H. Reed, R. Waters, UV irradiation stimulates histone acetylation and chromatin remodeling at a repressed yeast locus, *Proc. Natl. Acad. Sci. U. S. A.* 102 (2005) 8650–8655.
- [38] M.R. Duan, M.J. Smerdon, Histone H3 lysine 14 (H3K14) acetylation facilitates DNA repair in a positioned nucleosome by stabilizing the binding of the chromatin Remodeler RSC (Remodels Structure of Chromatin), *J. Biol. Chem.* 289 (2014) 8353–8363.
- [39] Y. Teng, Y. Yu, R. Waters, The *Saccharomyces cerevisiae* histone acetyltransferase Gcn5 has a role in the photoreactivation and nucleotide excision repair of UV-induced cyclobutane pyrimidine dimers in the MFA2 gene, *J. Mol. Biol.* 316 (2002) 489–499.
- [40] D.J. Owen, P. Ornaghi, J.C. Yang, N. Lowe, P.R. Evans, et al., The structural basis for the recognition of acetylated histone H4 by the bromodomain of histone acetyltransferase gcn5p, *EMBO J.* 19 (2000) 6141–6149.
- [41] K.S. Sweder, P.C. Hanawalt, Preferential repair of cyclobutane pyrimidine dimers in the transcribed strand of a gene in yeast chromosomes and plasmids is dependent on transcription, *Proc. Natl. Acad. Sci. U. S. A.* 89 (1992) 10696–10700.
- [42] V.A. Bepalov, A. Conconi, X. Zhang, D. Fahy, M.J. Smerdon, Improved method for measuring the ensemble average of strand breaks in genomic DNA, *Environ. Mol. Mutagen.* 38 (2001) 166–174.
- [43] S. Strahl-Bolsinger, A. Hecht, K. Luo, M. Grunstein, SIR2 and SIR4 interactions differ in core and extended telomeric heterochromatin in yeast, *Genes Dev.* 11 (1997) 83–93.
- [44] B. Yang, A.L. Kirchmaier, Bypassing the catalytic activity of SIR2 for SIR protein spreading in *Saccharomyces cerevisiae*, *Mol. Biol. Cell* 17 (2006) 5287–5297.
- [45] B. Yang, J. Britton, A.L. Kirchmaier, Insights into the impact of histone acetylation and methylation on Sir protein recruitment, spreading, and silencing in *Saccharomyces cerevisiae*, *J. Mol. Biol.* 381 (2008) 826–844.
- [46] M. Altav, R.T. Utley, N. Lacoste, S. Tan, S.D. Briggs, et al., Interplay of chromatin modifiers on a short basic patch of histone H4 tail defines the boundary of telomeric heterochromatin, *Mol. Cell* 28 (2007) 1002–1014.
- [47] H. Renaud, O.M. Aparicio, P.D. Zierath, B.L. Billington, S.K. Chhablani, et al., Silent domains are assembled continuously from the telomere and are defined by promoter distance and strength, and by SIR3 dosage, *Genes Dev.* 7 (1993) 1133–1145.
- [48] G.J. Hoppe, J.C. Tanny, A.D. Rudner, S.A. Gerber, S. Danaie, et al., Steps in assembly of silent chromatin in yeast: Sir3-dependent binding of a Sir2/Sir4 complex to silencers and role for Sir2-dependent deacetylation, *Mol. Cell Biol.* 22 (2002) 4167–4180.
- [49] L.N. Rusche, A.L. Kirchmaier, J. Rine, Ordered nucleation and spreading of silenced chromatin in *Saccharomyces cerevisiae*, *Mol. Biol. Cell* 13 (2002) 2207–2222.
- [50] X. Bi, M. Braunstein, G.J. Shei, J.R. Broach, The yeast HML I silencer defines a heterochromatin domain boundary by directional establishment of silencing, *Proc Natl Acad Sci U S A* 96 (1999) 11934–11939.
- [51] X. Bi, Domains of gene silencing near the left end of chromosome III in *Saccharomyces cerevisiae*, *Genetics* 160 (2002) 1401–1407.
- [52] B. Dorigo, T. Schalch, K. Bystrycky, T.J. Richmond, Chromatin fiber folding: requirement for the histone H4 N-terminal tail, *J. Mol. Biol.* 327 (2003) 85–96.
- [53] D.M. Thurtle, J. Rine, The molecular topography of silenced chromatin in *Saccharomyces cerevisiae*, *Genes Dev.* 28 (2014) 245–258.
- [54] A. Ellahi, D.M. Thurtle, J. Rine, The Chromatin and Transcriptional Landscape of Native *Saccharomyces cerevisiae* Telomeres and Subtelomeric Domains, *Genetics* 200 (2015) 505–521.
- [55] L.E. Jansen, R.A. Verhage, J. Brouwer, Preferential binding of yeast Rad4/Rad23 complex to damaged DNA, *J. Biol. Chem.* 273 (1998) 33111–33114.
- [56] M.J. Mone, T. Bernas, C. Dinant, F.A. Goedvree, E.M. Manders, et al., In vivo dynamics of chromatin-associated complex formation in mammalian nucleotide excision repair, *Proc. Natl. Acad. Sci. U. S. A.* 101 (2004) 15933–15937.
- [57] R. Verhage, A.M. Zeeman, N. de Groot, F. Gleig, D.D. Bang, et al., The RAD7 and RAD16 genes, which are essential for pyrimidine dimer removal from the silent mating type loci, are also required for repair of the nontranscribed strand of an active gene in *Saccharomyces cerevisiae*, *Mol. Cell Biol.* 14 (1994) 6135–6142.
- [58] S.N. Guzder, P. Sung, L. Prakash, S. Prakash, Synergistic interaction between yeast nucleotide excision repair factors NEF2 and NEF4 in the binding of ultraviolet-damaged DNA, *J. Biol. Chem.* 274 (1999) 24257–24262.
- [59] S. Prakash, L. Prakash, Nucleotide excision repair in yeast, *Mutat. Res.* 451 (2000) 13–24.
- [60] F. Gong, D. Fahy, M.J. Smerdon, Rad4-Rad23 interaction with SWI/SNF links ATP-dependent chromatin remodeling with nucleotide excision repair, *Nat. Struct. Mol. Biol.* 13 (2006) 902–907.
- [61] M.J. Smerdon, DNA repair and the role of chromatin structure, *Curr. Opin. Cell Biol.* 3 (1991) 422–428.
- [62] S. Tanaka, M. Livingstone-Zatchej, F. Thoma, Chromatin structure of the yeast URA3 gene at high resolution provides insight into structure and positioning of nucleosomes in the chromosomal context, *J. Mol. Biol.* 257 (1996) 919–934.
- [63] R. Hara, J. Mo, A. Sancar, DNA damage in the nucleosome core is refractory to repair by human excision nuclease, *Mol. Cell Biol.* 20 (2000) 9173–9181.
- [64] C.M. Green, G. Almouzni, When repair meets chromatin. First in series on chromatin dynamics, *EMBO Rep.* 3 (2002) 28–33.

- [65] F. Thoma, Repair of UV lesions in nucleosomes–intrinsic properties and remodeling, *DNA Repair (Amst.)* 4 (2005) 855–869.
- [66] Y. Teng, H. Liu, H.W. Gill, Y. Yu, R. Waters, et al., *Saccharomyces cerevisiae* Rad16 mediates ultraviolet-dependent histone H3 acetylation required for efficient global genome nucleotide-excision repair, *EMBO Rep.* 9 (2008) 97–102.
- [67] R. Guo, J. Chen, D.L. Mitchell, D.G. Johnson, GCN5 and E2F1 stimulate nucleotide excision repair by promoting H3K9 acetylation at sites of damage, *Nucleic Acids Res.* 39 (2011) 1390–1397.
- [68] S.N. Guzder, P. Sung, L. Prakash, S. Prakash, The DNA-dependent ATPase activity of yeast nucleotide excision repair factor 4 and its role in DNA damage recognition, *J. Biol. Chem.* 273 (1998) 6292–6296.
- [69] S.N. Guzder, P. Sung, L. Prakash, S. Prakash, Affinity of yeast nucleotide excision repair factor 2, consisting of the Rad4 and Rad23 proteins, for ultraviolet damaged DNA, *J. Biol. Chem.* 273 (1998) 31541–31546.
- [70] S. Bergink, W. Toussaint, M.S. Luijsterburg, C. Dinant, S. Alekseev, et al., Recognition of DNA damage by XPC coincides with disruption of the XPC-RAD23 complex, *J. Cell Biol.* 196 (2012) 681–688.
- [71] U. Schieferstein, F. Thoma, Site-specific repair of cyclobutane pyrimidine dimers in a positioned nucleosome by photolyase and T4 endonuclease V in vitro, *EMBO J.* 17 (1998) 306–316.